



Characterisation of the cross-linking and calcification associated with glutaraldehyde-treated cardiac bioprostheses.

DELOGNE, Christophe.

Available from the Sheffield Hallam University Research Archive (SHURA) at:

<http://shura.shu.ac.uk/19550/>

A Sheffield Hallam University thesis

This thesis is protected by copyright which belongs to the author.

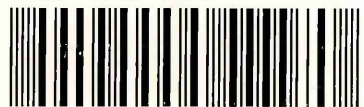
The content must not be changed in any way or sold commercially in any format or medium without the formal permission of the author.

When referring to this work, full bibliographic details including the author, title, awarding institution and date of the thesis must be given.

Please visit <http://shura.shu.ac.uk/19550/> and <http://shura.shu.ac.uk/information.html> for further details about copyright and re-use permissions.

CITY CAMPUS, HOWARD STREET
SHEFFIELD S1 1WB

101 715 900 9



REFERENCE

ProQuest Number: 10694431

All rights reserved

INFORMATION TO ALL USERS

The quality of this reproduction is dependent upon the quality of the copy submitted.

In the unlikely event that the author did not send a complete manuscript and there are missing pages, these will be noted. Also, if material had to be removed, a note will indicate the deletion.



ProQuest 10694431

Published by ProQuest LLC (2017). Copyright of the Dissertation is held by the Author.

All rights reserved.

This work is protected against unauthorized copying under Title 17, United States Code
Microform Edition © ProQuest LLC.

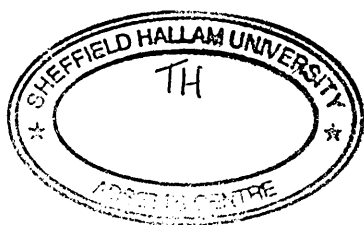
ProQuest LLC.
789 East Eisenhower Parkway
P.O. Box 1346
Ann Arbor, MI 48106 – 1346

CHARACTERISATION OF THE CROSS-LINKING
AND CALCIFICATION ASSOCIATED WITH
GLUTARALDEHYDE-TREATED CARDIAC
BIOPROSTHESES

MR CHRISTOPHE DELOGNE

A thesis submitted in partial fulfilment of the requirements of
Sheffield Hallam University
for the degree of Doctor of Philosophy

October 2002



Abstract

Around 170000 patients worldwide receive cardiac valve substitutes each year. Valve replacement with mechanical or bioprosthetic devices enhances patient survival and quality of life. Bioprosthetic valves have a significant advantage over mechanical valves: they do not necessarily require long-term anticoagulant therapy however, dystrophic calcification can lead to early failure. The actual mechanism of calcification is still poorly understood despite several established possible factors associated with it. Amongst these is the glutaraldehyde pre-treatment of the valves during their manufacture. Glutaraldehyde has been used for the treatment of bioprosthetic valves for the last thirty years, as a cross-linking agent and a sterilant. Whilst it is assumed to introduce stable inter- and intra-fibrillar collagen cross-links, which contribute to the durability of these valves, the specific chemistry of the fixation process is not fully understood. Additionally, glutaraldehyde is thought to be involved somehow in the process of dystrophic calcification of these same bioprosthetic valves.

The primary aim of this study was to gain a greater understanding of the chemistry involved in the treatment of collagenous valve tissue with glutaraldehyde. Amino acids, peptides and proteins were thus used to mimic the effect of the glutaraldehyde treatment and to model potential reactions involved in such treatment. Techniques such as MALDI-TOF MS, ESI MS, NMR, FTIR-ATR and Raman spectroscopy were utilised to study the products of the glutaraldehyde reaction and their relationship with the calcification process. Data obtained from the products of the reactions between glutaraldehyde and model compounds showed the presence of: aldol and aldol/Michael condensation products of glutaraldehyde, Schiff base moieties (including cross-links) and various cyclisation products incorporating pyridinium and dihydropyridine ring structures. Some of these structures are in agreement with the literature, whilst others are essentially new structures that have never been proposed.

Glutaric acid, used to mimic the oxidation of glutaraldehyde that can occur in-vivo, was shown to have the ability to form complexes with cations such as calcium in-vitro. A similar result was found with aqueous dilute solutions of glutaraldehyde (similar concentrations to the ones used in valve manufacture), thus leading to the hypothesis of its strong role in the initiation of calcification in-vivo. However, an extrapolation of these results to the role of the nucleophilic groups of amino acids or peptides, that could behave as the collagen macromolecule, was difficult to assess using FTIR because of the complex infrared spectra. However some findings corroborated the hypothesis that amino acids of the collagen tissue may also play a role in the initiation of calcification.

Secondly, methodology was developed to allow successful analysis of tissue calcification using environmental scanning electron microscopy (ESEM). This is thought to be an important step in the analysis of tissues in their native state. Investigation of the calcification process with samples from clinical investigations (explanted human calcified valves), in-vivo screening (rat subcutaneous implantation model) and in-vitro screening (pericardial tissue incubated in metastable calcification solution) was thus undertaken using ESEM, along with other techniques such as FTIR-ATR, Raman, XRD spectroscopy and ICP-OES. The data revealed both similarities and differences between in-vivo and in-vitro calcification, although the process is unequivocally different. Late calcific deposits were assigned to poorly crystalline hydroxyapatite with high Ca/P ratios due to the probable presence of carbonate and possibly cations such as silicon and magnesium. A picture of the onset of mineralisation was hypothesised involving precursors, containing various amounts of calcium and phosphate, along with the incorporation of magnesium and silicon. These precursor phases evolved with time of implantation to the poorly crystalline form of hydroxyapatite found in the late stage of calcification.

This work has provided an insight into how glutaraldehyde reacts with valve tissue and a possible explanation as to why valves fail by non-calcific or calcific mechanisms. A new approach to the study of calcified valve tissue has also been developed using ESEM methodology.

Acknowledgments

In particular, I would like to thank my supervisors, Dr Carolan Vikki, Dr Lawford Patricia, Dr Herbert Hughes, Dr Clench Malcolm and Prof Yarwood Jack for their advice.

I would also like to thank the following people from Sheffield Hallam University: Barry Christian for the great discussions we had while he was running samples on the NMR instrument, Joan Hague for carrying out for me some ESI-MS samples, Paul Collins for taking some of his time to give me some training on the ICP-OES, Brian Lewis for showing me how to use the XRD unit, and Stephen Habesch for all the time spent together in the ESEM lab.

Thanks to the project students for the good work they achieved with some MALDI-TOF MS samples, especially Ms Hema Patel, Katrina Finucane, and Celine Chollet.

Thanks to Gerry Screaton for providing explanted and un-implanted human bioprosthetic valves, along with pericardial tissue obtained from the Doncaster abattoir (given by Peter Warren), and to provide some useful information on these bioprosthetic valves.

I also have to thank the Materials Research Institute for providing the studentship and for the provision of some facilities for this thesis.

Additionally, I am extremely grateful to my friends that were always present and/or in contact with me through the years, although the large distance sometimes.

Finally, I would like to thank particularly my girlfriend, my aunt and a few other members of my family, and to dedicate this thesis to my grandparents.

Which is closer to us,
Our achievements or ourselves?
Which is more precious,
Ourselves or our possessions?
What is the greatest sadness,
To gain them or to lose them?
That is why he who aspires the highest,
Always has most to lose.

LAO-TSEU

Qu' est-ce qui nous touche de plus près,
De notre gloire ou de notre personne?
Qu' est-ce qui est le plus précieux,
De notre personne ou de nos richesses?
Quel est le plus grand malheur,
De les acquérir ou de les perdre?
C' est pourquoi celui qui a de grandes passions,
Est nécessairement exposé à de grands sacrifices.

LAO-TSEU

A mes grands parents

Contents

Abstract	i
Acknowledgments	ii
Poem	iii
Chapter 1 Bioprosthetic heart valves and their pathological calcification	
1.1 Introduction	1
1.2 Replacement heart valves	2
1.2.1 Introduction	2
1.2.2 The ideal valve replacement	3
1.2.3 Bioprosthetic valves	4
1.3 Pathological considerations after cardiac valve replacement	10
1.3.1 Introduction	10
1.3.2 Calcification	11
1.4 Type of tissue used in valve manufacture	12
1.4.1 The porcine valve	12
1.4.2 Pericardium	13
1.5 Tissue treatment	15
1.5.1 Introduction	15
1.5.2 Elastin	15
1.5.3 Collagen	17
1.5.4 Induced cross-linking by chemical and physical methods	22
1.6 Calcification: pathology and prevention	23
1.6.1 Introduction	23
1.6.2 Non-pathological calcification	24
1.6.3 Pathological calcification	25
1.6.4 The formation of hydroxyapatite (HAP) and its derivatives	30
1.6.5 Use of in-vivo and in-vitro models	35
1.7 Factors influencing mineralisation	40
1.7.1 Host factors	40
1.7.2 Tissue factors	44
1.7.3 Conclusion	50
1.8 Prevention of calcification with anticalcification treatments	51
1.9 Outline of the project	52
Chapter 2 Glutaraldehyde	
2.1 Introduction	75
2.1.1 History	75
2.1.2 The fixation process	76
2.2 Chemistry of glutaraldehyde	82
2.2.1 Glutaraldehyde in solution	82
2.2.2 Review of the various structures of glutaraldehyde in aqueous solutions	86

2.2.3 Factors affecting the reaction between glutaraldehyde and proteins	92
2.2.4 Types of reactions occurring between glutaraldehyde and proteins	97
2.3 Conclusion	109
 Chapter 3 Techniques: theory and applications	
3.1 Introduction	118
3.2 Methods	119
3.2.1 Freeze-drier	119
3.2.2 Environmental Scanning Electron Microscopy (ESEM)	120
3.2.3 ICP-OES (inductively coupled plasma-optical emission spectroscopy)	123
3.2.4 X-Ray Powder Diffraction (XRD)	125
3.2.5 Fourier transform infrared-attenuated total reflectance (FTIR-ATR) spectroscopy	127
3.2.6 Raman spectroscopy	137
3.2.7 The complementarity of FTIR and Raman spectroscopy	142
3.2.8 Nuclear magnetic resonance (NMR) spectroscopy	142
3.2.9 Electrospray ionisation-mass spectrometry (ESI-MS)	145
3.2.10 MALDI-TOF MS (matrix assisted laser desorption ionisation-time of flight mass spectrometry)	147
 Chapter 4 Investigation of the behaviour of glutaraldehyde in solution, at various pH values	
4.1 Introduction	159
4.2 Materials and methods	160
4.2.1 Materials	160
4.2.2 Sample preparation	161
4.2.3 Freeze-drier	161
4.2.4 FTIR-ATR analyses	162
4.2.5 Raman analyses	163
4.2.6 ESI-MS analyses	163
4.2.7 MALDI-TOF MS analyses	163
4.2.8 NMR analyses	164
4.3 Results and discussion	164
4.3.1 ESI-MS	164
4.3.2 MALDI-TOF MS	172
4.3.3 NMR	176
4.3.4 Raman and FTIR-ATR analyses	187
4.3.5 Overall discussion of data obtained	194
4.4 Conclusion	198
 Chapter 5 Investigation of the cross-linking occurring in glutaraldehyde-treated valve tissue	
5.1 Introduction	203
5.2 Materials and methods	205
5.2.1 Materials	205
5.2.2 Sample preparation	205

5.2.3 Freeze-drier	206
5.2.4 FTIR-ATR analyses	207
5.2.5 Raman analyses	207
5.2.6 NMR analyses	207
5.2.7. ESI-MS analyses	207
5.2.8 MALDI-TOF MS analyses	207
5.3 Results and discussion	208
5.3.1 Determination of optimum molar ratio	208
5.3.2 General characteristics of the reactions of model compounds with glutaraldehyde	211
5.3.3 Study of the reaction of glutaraldehyde with small amines and peptides	213
5.3.4 Study of the reaction of glutaraldehyde with proteins (cytochrome C and lysosyme)	234
5.3.5 Overall discussion of data obtained	241
5.4 Conclusion	245
 Chapter 6 Infrared spectroscopy in the evaluation of the calcification potential of molecular models	
6.1 Introduction	251
6.2 Materials and methods	256
6.2.1 Calcification studies	256
6.2.2 Freeze-drier	258
6.2.3 Infrared spectroscopy	258
6.3 Results and discussion	258
6.3.1 Calcification of glutaraldehyde	258
6.3.2 Calcification of glutaric acid	261
6.3.3 Calcification of an amino acid and peptide	263
6.3.4 Calcification of glut-treated amino acids and peptide	266
6.3.5 Overall discussion of data obtained	266
6.4 Conclusion	268
 Chapter 7 Characterisation of the calcification of cardiac valve bioprotheses by environmental scanning electron microscopy, x-ray diffraction and vibrational spectroscopy	
7.1 Introduction	274
7.2 Materials and methods	276
7.2.1 Materials	276
7.2.2 Low Energy Radiography	277
7.2.3 Electron Microscopy	277
7.2.3 X-ray diffraction (XRD)	280
7.2.4 Fourier-transform infrared (FTIR) spectroscopy	281
7.2.5 Raman spectroscopy	281
7.2.6 Inductively coupled plasma-optical emission spectroscopy (ICP-OES)	281
7.3 Results and discussion	282
7.3.1 ESEM imaging	282
7.3.2 Energy dispersive X-ray (EDS) analysis	291
7.3.3 X-ray diffraction (XRD) analysis	295

7.3.4 FTIR-ATR and Raman analyses	297
7.3.5 ICP-OES analysis	306
7.4 Conclusion	307
 Chapter 8 In-vitro and in-vivo calcification of pericardial tissue characterised by environmental scanning electron microscopy	
8.1 Introduction	314
8.2 Materials and methods	315
8.2.1 Materials	315
8.2.2 Tissue fixation	316
8.2.3 <i>In-vitro</i> Calcification Study	316
8.2.4 <i>In-vivo</i> Calcification Studies	316
8.2.5 Low Energy Radiography	318
8.2.6 ICP-OES (Inductively Coupled Plasma-Optical Emission Spectroscopy)	318
8.2.7 Histological study	319
8.2.8 ESEM	319
8.2.9 XRD	320
8.3 Results and discussion	320
8.3.1 Low energy radiography	320
8.3.2 ESEM analysis	321
8.3.3 ICP-OES analysis	341
8.3.4 Light microscopy analysis	343
8.3.5 XRD analysis	343
8.4 Conclusion	344
 Chapter 9 General conclusion and suggested future work	
9.1 General conclusion	347
9.2 Suggested future work	353
9.2.1 High Performance Liquid Chromatography-Matrix Assisted Laser Desorption Ionisation Mass Spectrometry (HPLC-MALDI MS)	353
9.2.2 Atomic Force Microscopy (AFM)	353
9.2.3 Scanning Tunnelling Microscopy (STM)	354
9.2.4 Circular Dichroism (CD)	355
9.2.5 X-ray Photoelectron Spectroscopy	355
9.2.6 Time of Flight-Secondary Ion Mass Spectrometry (TOF-SIMS)	355
9.2.7 Surface Enhanced Raman Spectroscopy (SERS)	356
 Appendix I Investigation of the in-vitro calcification potential of type I collagen films by FTIR microscopy	I
 Appendix II Investigation of the reaction products of glutaraldehyde-treated model compounds using TLC-MALDI-TOF MS	VIII

**Appendix III Hypothetical molecular structures present in
glutaraldehyde solutions**

XVII

**Appendix IV Hypothetical molecular structures present in solutions
of glutaraldehyde-treated model compounds**

XXIII

Chapter 1

1 Bioprosthetic heart valves and their pathological calcification.

1.1 Introduction

On Monday 2 July 2001, the first artificial self-sufficient heart (called the AbioCor) was successfully implanted by Drs Laman Gray and Robert Dowling¹ in an American patient at the Jewish Hospital of Louisville in Kentucky. Without doubt, this represents a gigantic achievement in prosthetic replacement advances and showed how much both science and technology have accomplished since the first total artificial heart replacement implanted in Dr Barney Clark two decades ago in 1982. Nevertheless, many aspects of cardiovascular research require further understanding and improvements. Such is the case for cardiac valve replacement. In the past four decades, countless models of valve substitutes have been designed and improved. However, an ideal valve replacement device has not yet been achieved.

Approximately 200,000 artificial heart valves are implanted annually worldwide², from which it is estimated that 60% are mechanical and 40% are tissue (bioprosthetic), with an increasing interest towards the use of tissue valves over the last 10 years³. This represents a worldwide market of \$600,000,000.

The UK Heart Valve Registry (UKHVR) was established in 1986⁴ to provide data and information for professionals in cardiology and legitimate patients' interests. From the UK Heart Valve Registry 2000 report⁵, around 7000 patients received heart valve replacements in the UK, 37% of these being bioprosthetic valves. The number of bioprosthetic heart valves used has risen steadily over the last decade from 24% to 36%⁵, in comparison to the use of mechanical valves. This clinical popularity is the

Chapter 1

result of many improvements and factors that will be discussed in the following sections of this chapter.

Cardiac valve replacement with mechanical or bioprosthetic devices enhances greatly patient survival and quality of life. However, even the latest designs have a finite life-span. Furthermore, prosthesis associated complications are frequent. Bioprosthetic heart valves have better hemodynamic efficiency and thromboresistance than mechanical valves; trileaflet tissue valves have a central orifice analogous to natural human valves.

For patients with mechanical valves, the most common and important problems are thrombus and thromboembolic complications, necessitating chronic anticoagulation⁶ treatment. In contrast, patients with a bioprosthetic valve, composed essentially of chemically-treated animal tissue (bovine or porcine), in general, do not require long-term anticoagulant therapy.

Bioprosthetic valves tend to fail by progressive tissue deterioration, especially that involving cusp calcification. Thus, tissue valves are superior to mechanical valves with respect to lack of thromboembolic complications and better hemodynamic characteristics, however, their long-term durability is questionable⁷.

1.2 Replacement heart valves

1.2.1 Introduction

The human heart has four cardiac valves (see figure 1.1). These respond passively to pressure and flow changes within the heart and function as loose flaps that seal the valvular orifices against regurgitation of blood when closed but fold out of the way when the valve is open, to provide an obstruction-free orifice. They open and close around 38 million times a year and are capable of withstanding pressure differences in excess of 100 mmHg (greater than this in hypertension). The left side of the heart must impart more energy to the blood to overcome the higher resistance of the systemic circulation. This is reflected in higher pressures and higher stresses on the valves. This in turn results in a higher incidence of valve disease in the left than in the right side of the heart.

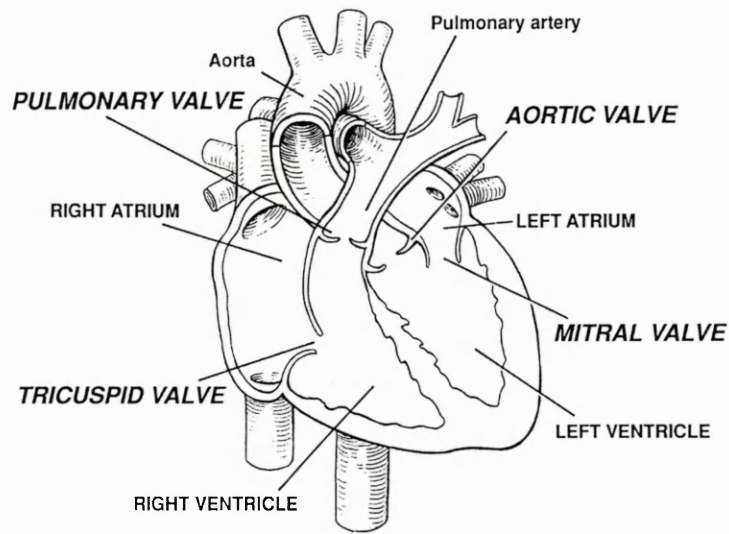


Figure 1.1. Schematic diagram of the human heart showing the four valves.

For the detailed anatomy of the heart, readers are invited to refer to publications such as those by Schoen⁸ and Marks and Marks⁹.

There are numerous different replacement valves available. The principal types of cardiac prostheses include mechanical, polymeric, bioprosthetic, and tissue-engineered valves, although the latter are still in their infancy. The following sections give an overview of the type of bioprosthetic valves available over the past 25 years.

Bioprostheses are intended for use in patients whose aortic or mitral valve disease is sufficiently advanced to warrant replacement of their natural valve with a prosthetic one. They may also be used to replace a failing aortic or mitral valve prosthesis.

In the presence of conditions affecting calcium metabolism or when calcium-containing chronic drug therapies are used, the use of mechanical prostheses is preferred. This is also true for patients under 20 years of age, those on a high calcium diet and for patients who are on maintenance hemodialysis. This is due to high risk of calcification of bioprosthetic valves in these patient groups¹⁰⁻¹².

1.2.2 The ideal valve replacement

The ideal valve replacement would meet the following criteria:

- Be easy to implant
- Not yield thrombus or thromboemboli

- Be quickly and permanently incorporated into the heart by host tissues
- Present minimal resistance to forward flow and allow insignificant regurgitation
- Not damage cellular and molecular blood components
- Undergo minimal wear or other degradative change following long-term implantation
- Not be excessively noisy or cause other discomfort to the patient¹³

Despite almost 50 years of this type of surgery, there are many questions that remain to be answered. The search for the optimal replacement device continues.

1.2.3 Bioprosthetic valves

1.2.3.1 Introduction:

Tissue valves, with low intrinsic thrombogenicity, are an attractive alternative to mechanical prosthetic valves when anticoagulation is contraindicated or undesirable. However, despite their superficial resemblance to natural valves, contemporary bioprostheses are non-viable and hence non-self renewing. (Re-endothelialisation of porcine bioprosthetic valve cusps has been reported. However this is only focal and far from complete¹⁴. Re-endothelialisation has not been demonstrated with pericardial bioprosthetic valves). They undergo structural degenerative changes during function, leading to progressive tissue deterioration with time (this includes both calcific and non-calcific damage). Whilst the rate of progression of degeneration varies from patient to patient, bioprostheses are generally reported to have a functional life span of 10-15 years. Glutaraldehyde-treated xenografts are an excellent choice for the elderly patient (greater than 70 years of age) or patients with an expected life span of less than 10 years¹⁵⁻¹⁹. Beyond this time, mineralisation and calcification are major disadvantages of the devitalised valve tissue, being particularly a problem in younger patients²⁰. Consequently, limitations of durability have been the major impediment to the wider use of bioprostheses, undermining their attractiveness as valve substitutes of choice for many patient groups²¹⁻²⁷. This has resulted in a swing back to the use of mechanical valves²⁸ until very recently. The statistics quoted earlier indeed suggest that the use of bioprostheses is increasing.

Certain patient groups necessitate special considerations when choosing suitable valve treatment. For children, a durable valve substitute with a low valve-related mortality is essential. The frequent need for prosthesis of small size demands maximum hemodynamic efficiency to minimise the need for replacement as the child continues to grow. Elimination of a requirement for systemic anticoagulants would avoid the risk of hemorrhage due to normal childhood activities. Bioprostheses were initially believed to be ideal for children, but accelerated calcific degeneration has made these valves an undesirable selection for young patients. Many clinicians favour bioprosthetic heart valves for women of child-bearing age. There are a number of reasons for this; warfarin anticoagulation has been shown to be teratogenic and is associated with increased spontaneous abortion also, anticoagulation is difficult to manage during pregnancy²⁹. Unfortunately, there is evidence to suggest that pregnancy might potentiate calcification of porcine bioprostheses³⁰ so the appropriate choice in this situation is by no means clear.

1.2.3.2 Stented porcine aortic valves:

1.2.3.2.1 The various valve generations:

For the last 25 years, stented porcine valves (stented bioprosthetic valves are mounted on a supporting frame or stent) have been the most widely used biological valves and as such represent a standard for measuring the performance of newer biological valve designs.

In the mid-sixties, hearts from a number of different animals (calves, pigs and sheep) were studied and it was found that the size of the pig heart was the closest to that of the human³¹. This was where the interest in using porcine aortic valves as stented xenograft prostheses emerged³². First-generation porcine aortic valves^{33,34}, such as the Hancock I bioprosthesis and the Carpentier-Edwards Standard bioprosthesis³⁵ were introduced in the early 1980s. Second-generation porcine valves incorporated improvements namely a better configuration to reduce transvalvular gradients and an optimised stent flexibility to reduce tissue stress³⁶⁻³⁸. Data on second-generation porcine valves such as the porcine SJM Biocor (see figure 1.2 below), the Intact³⁹, the Hancock II^{40,41} and the Carpentier Edwards Supra-Annular bioprosthesis⁴² suggest that the mechanical properties of cusps are improved when fixation occurs in an isotonic glutaraldehyde solution. These second-generation valves are

manufactured using quality control measures such as muscle bar-devoided leaflets thus eliminating potential calcification sites and the possible obstruction of the orifice.

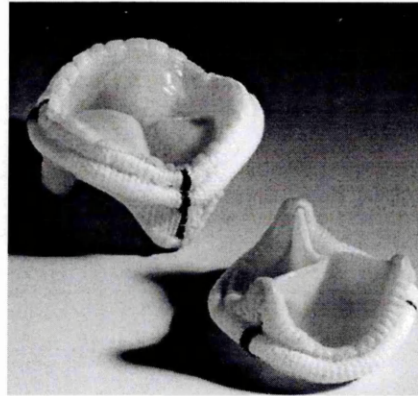


Figure 1.2: An unimplanted trileaflet porcine SJM bioprosthetic heart valve from St. Jude Medical.

1.2.3.2.2 Failure of porcine aortic valve bioprostheses:

Cuspal tears and calcification^{43,44} of the cusps are the most common causes of valve dysfunction^{45,46} and failure in stented porcine valves⁴⁷. The most frequent clinicopathological failure mode of porcine valves is regurgitation caused by a combination of calcification and leaflet tearing⁴³. Pure stenosis occurs less frequently. In contrast the primary mode of failure of pericardial valves, is calcification⁴⁸. Stenosis is often due to stiffening because of dystrophic calcification. Cuspal tears or perforations of tissue unrelated to either calcification or endocarditis can also lead to valve failure. Non-calcific tissue tears probably reflect mechanical failure of collagen architecture during function; the incidence of such structural valve deterioration may occur virtually anytime post-operatively and is more frequently seen with valves implanted in the mitral position rather than in the aortic position^{49,50}.

Calcific deposits are found predominantly at the cuspal commissures and basal attachments and are visible by the naked eye as nodular grey/white masses (predominantly found in the spongiosa in porcine valves⁵¹), which frequently ulcerate through the cuspal tissue. Calcification of the aortic wall is less frequent than that of the corresponding cusps⁵².

In spite of these problems, the durability of porcine valves appears to be improving. This is due in part to patient selection, especially with regard to age, but is also due to improved valve design⁵³.

1.2.3.3 Stentless porcine aortic valves:

The replacement of diseased heart valves with non-stented xenografts is a relatively recent development⁵⁴. Non-stented porcine aortic valve bioprostheses comprise glutaraldehyde-pretreated pig aortic root and valve cusps, and have no supporting stent^{55,56}. They are thus very similar to homograft valves (homografts are cadaveric human valves transplanted to unrelated recipients) in appearance and method of insertion. Compared to their stented counterparts, they differ slightly in overall configuration: the glutaraldehyde pretreatments conditions used, in design (they do not contain a true sewing ring) and, particularly, in the amount of aortic wall included. Stentless porcine valves were first designed essentially to improve the hemodynamic performance of porcine aortic valves and to enhance their durability^{57,58}.

The main advantage of the stentless design is that a larger bioprosthesis can be implanted for a given size of aortic root. This results in enhanced hemodynamics⁵⁸ and patient survival⁵⁹ when compared to stented porcine valves. In the latter, the stent and sewing ring take up space within the recipient aortic root, lowering the orifice area.

The disadvantage of using a stentless valve is the surgical skill required to implant such a device. Predilation of the valve root during the fixation at manufacture helps to produce valves with improved hydrodynamic performance. This is because the glutaraldehyde-treatment reduces the extensibility of the root, resulting in a lowering of biomechanical function compared to the fresh root⁶⁰. Several types of stentless valves are clinically available: they differ considerably in terms of design, tissue preservation and anticalcification treatment. Morphologically, this type of valve is similar to the native aortic valve⁶¹. Their longevity is expected to be similar to or better than the stented bioprosthetic valves (greater than 10-15 years life span)⁶².

1.2.3.4 Bovine pericardial valves:

Recently, there has been a renewed interest in bovine pericardial valves⁶³.

1.2.3.4.1 The various valve generations:

The first commercially available pericardial bioprosthesis, the Ionescu-Shiley pericardial valve, was developed by Marion Ionescu⁶⁴. This first-generation valve type was used from 1976 to 1987. As these valves were fashioned from sheets of pericardial tissue, they could be made in a wide range of sizes. Despite early favourable reports and excellent hemodynamic performance, they were withdrawn from clinical use because of a high potential for structural valve dysfunction and failure^{65,66}. This was later found to be due to design-related tissue preparation/mounting techniques⁶⁷: a suture which secured the leaflets to the stent post was associated with leaflet tears causing regurgitation^{68,69} and wearing against the fabric stent cover caused leaflet abrasion^{70,71}.

In consequence, second-generation pericardial valves, such as the Carpentier-Edwards Perimount valve, were developed with substantial design modifications⁷² (especially the improved tissue preservation without pressure in glutaraldehyde, the computer-aided design for optimal leaflet-to-stent matching, and no stent-post sutures as used with first-generation valves). These were introduced into clinical use in the early 1980s⁷³. Many types of second-generation pericardial bioprostheses are on the market. Such valves show excellent results, especially in patients over 60 years of age⁷⁴, and provide satisfactory hemodynamic results with low thrombogenicity and structural deterioration^{63,75}. However, leaflet degeneration is still a problem in patients under the age of 60 years. Recent data, from a study of many bioprostheses, show that stented bovine valves seem to be as good as stentless porcine valves, whilst being superior to conventional stented porcine bioprostheses with regard to leaflet calcification⁷⁶. Other obvious advantages of stented types of valves are their relative ease of insertion and the predictable hemodynamic performance⁷⁷.

1.2.3.4.2 Failure of bovine pericardial bioprostheses:

Calcific and non-calcific degeneration failures of pericardial bioprostheses have been frequently reported for both adults and children^{69,78-80}. Contemporary valves appear to have superior performance and durability to those of previous pericardial valves^{38,53,81}, but their ultimate mode of failure is mainly because of primary dystrophic calcification. In general, the performance of pericardial bioprostheses is

superior to that of porcine bioprostheses at 10 years in terms of freedom from structural valve deterioration⁴⁸, but they suffer from calcification.

1.2.3.5 Autologous tissue/Autografts/Homografts:

Historically, allografts (valves from different human individuals) were obtained from cadavers, but now they are also harvested from hearts removed from cardiac transplant recipients. However, as with all organ-donor situations, the availability of such grafts is severely limited, restricting the number of procedures that can be carried out.

The use of an aortic homograft valve in the subcoronary position was reported as early as 1962^{82,83}, and the technique is still in use today. It involves a normal human aortic valve removed at post-mortem examination and treated with appropriate antibiotics so that it can be transplanted into a suitable host. The first pulmonary autograft was described in 1967⁸⁴. This type of surgery involves replacement of the aortic valve or root by the patient's own pulmonary valve and is a common procedure^{85,86}. The removed pulmonary valve is usually replaced by a human pulmonic valve allograft.

Over the same period, other types of autologous tissues and allografts were investigated to try to eliminate some of the possible valve-related factors that were thought to be responsible for tissue calcification (inflammatory response and foreign tissue components). Valves were made of pericardium⁸⁷, dura mater⁸⁸ and fascia lata^{89,90} (fascia lata valve was developed in 1966⁹¹ and constructed at the time of operation using the patient's own living tissue, but its use was discontinued by 1978, whilst dura mater is also no longer used these days). Unfortunately, in practice, none of these grafts have been very successful. Failure rates have been high due to cuspal thickening, fibrosis with shrinkage, endocarditis and loss of graft pliability^{90,92-94}. Autologous materials were used fresh. Failure was due to the behaviour of the untreated tissue and the time-consuming, non-standardised methods used to construct such a valve. This led to problems after implantation.

A new approach was developed to rapidly construct intra-operatively a stent-mounted glutaraldehyde-fixed autologous pericardial valve in a standardised fashion⁹⁵. After successful in-vitro and in-vivo testing, the first clinical trials were described in the early 1990s⁹⁶. Autologous pericardium was excised, fixed in

glutaraldehyde for a short period of time (5 to 15 min) during surgery, cut into leaflet shapes by means of a special die and subsequently mounted on a stent⁹⁷. The brief glutaraldehyde treatment enhances the mechanical properties of the tissue. But following glutaraldehyde treatment, the tissue has been shown to calcify, showing a glutaraldehyde-dependent calcification pattern in the implants^{98,99}. However, if the treatment is too short (less than 10 minutes), elongation of the tissue after implantation and reduction in strength have been observed¹⁰⁰. Since the initial studies, almost five hundred autologous briefly-glutaraldehyde-treated bovine pericardium valves have been used throughout Europe¹⁰¹. Unfortunately, the selection and preparation of the autologous pericardium can make this type of valve graft problematic. Mechanical properties of the tissue can vary from patient to patient and brief glutaraldehyde treatment is sometimes insufficient for mechanical stability¹⁰². However, the low level of calcification generally observed by either X-ray analysis or by macroscopical or histological examination, and the possibility of nearly complete re-endothelialisation of the smooth outflow surface and rare endothelial in-growth on the rough inflow sides are encouraging for these types of valvular grafts¹⁰¹.

The advantage of using stent-mounted allografts made of autologous tissue is that they can be used to replace the mitral valve, while unmounted allografts (homograft) can only be used as aortic valve replacements (mechanical and stented bioprosthetic valves can be used in either site). It is also well accepted that the time course of failure of allografts is slower than that for other tissue valves, especially in a young population¹⁰³. Thus, the potential benefit of this difficult surgical technique is to provide a hemodynamically superior and potentially viable valve that might grow with somatic growth of children or adolescents for whom there is unfortunately no real satisfactory alternative.

1.3 Pathological considerations after cardiac valve replacement

1.3.1 Introduction

Re-operation and replacement of a prosthesis is to be avoided as it is associated with significant risk of mortality, hence anything which extends the life of a prosthesis is

of benefit. Early mortality of patients (within a few weeks of operation) for a first valve replacement is low (less than 10%). Early deaths are due mainly to complications associated with pre-existing pathological conditions, such as pulmonary hypertension, coronary artery disease and left ventricular myocardial degenerative changes. As late survival is enhanced and as an increasing number of younger patients undergo valve replacement, the frequency of re-operation for valve related problems is likely to increase. Late mortality (one month or more post-operatively) results from residual or associated cardiac defects or prosthesis-associated complications. These latter cause approximately half of late deaths^{26,104,105}. Leaflet deterioration¹⁰⁶ may be due to infection, calcification, tissue overgrowth, tissue degeneration, suture abrasion or trauma caused by the placement during surgery. The most common complications associated with replacement valves are thromboembolic complications, endocarditis, paravalvular leak, non-calcific valvular deterioration and calcification. As the current work is involved with calcification of bioprostheses, this is discussed further.

1.3.2 Calcification

The major cause of bioprosthetic valve dysfunction is primary tissue failure, especially related to cuspal calcification^{33,107,108}. Regurgitation through tears forming adjacent to calcific nodules is the most frequent failure mode. The amount of calcification seen after long-term implantation is very variable. Although mineralisation is observed in almost all porcine aortic valve bioprostheses after 4 years of implantation, valves with minimal or, in some cases, no calcification are found occasionally after 10 years of implantation. Pericardial prostheses also suffer from this problem, however non-calcific cuspal perforations and tears frequently cause failure of these valves, depending on the valve generation^{109,110}.

As stated before, patient age is certain to affect mineralisation, with the process being accelerated in children, adolescents and young adults^{79,111,112}. This increase in incidence of failure is reported up to the age of 35 years¹¹³.

Calcific deposits are composed of calcium phosphates, closely related to physiologic bone mineral (hydroxyapatite). These form predominantly at the cuspal commissures and basal attachments of the leaflets. In the initial stages, calcific deposits are often

found in association with connective tissue cells as well as collagen^{51,114}. Details of calcification can be found in section 1.6.

1.4 Type of tissue used in valve manufacture

1.4.1 The porcine valve

The porcine valve shows most resemblance to the human valve with regard to its dimensions and anatomical features¹¹⁵. In porcine bioprosthetic valves, the natural cuspal attachment to the aortic wall is retained. Since in pigs (not humans) the interventricular wall extends to the base of the right coronary cusp¹¹⁶, the base of the cusp is supported by strip of septal myocardium “the muscle shelf” (see figure 1.4 below). The muscular part of this cusp can be weakened by trimming, leading to stretching and subsequent prolapse of the valve. A slight asymmetry of the stent with a flattened part corresponding to the right coronary cusp makes it possible to cover and so to incorporate the muscular part of the right coronary cusp into the stent.

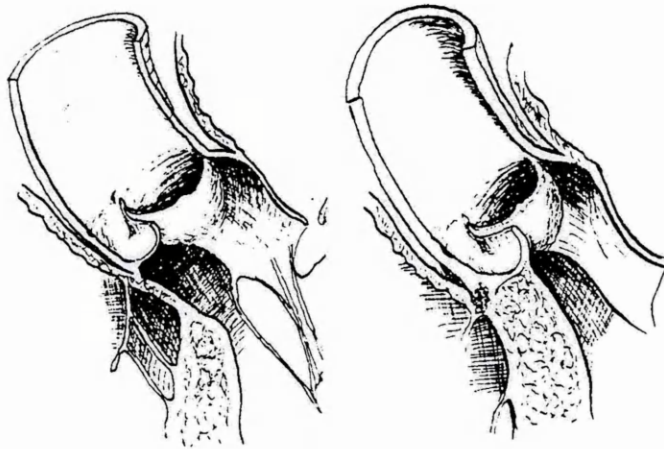


Figure 1.4: Comparative configuration of the human (*left*) and the porcine (*right*) aortic valves showing the difference of extension of the inter-ventricular wall along with the difference of support brought by the septal muscle myocardium. Adapted from Carpentier¹¹⁶.

Porcine aortic valve cusps are structurally non-homogeneous, having three well-defined structural layers (see figure 1.5 below) very much like the natural human cardiac valves: the ventricularis, near the inflow surface, is predominantly collagenous with some small amounts of elastin; the central spongiosa is a viscous

gelatinous layer made of loosely arranged collagen and contains abundant mucopolysaccharides¹¹⁷ such as proteoglycans; and the fibrosa has densely packed collagen and faces the outflow surface¹¹⁸. Blood vessels are absent except at the base of the leaflet. The collagen of porcine aortic valves is heterogeneous, being largely type I but a significant amount of type III is present, probably in a ratio of approximately 70% to 30%¹¹⁹. The elastin component of the ventricularis expands when the cusps stretch under backpressure. This increases the coaptation area and this improves competence. The elastin recoils to make the cusp smaller in the open phase^{120,121}. Shear stresses caused by the differential movement of the layers and the shock of valve closure are dissipated by the spongiosa. Hydrophilic glycosaminoglycans (GAGs) in this layer readily absorb water, swell to form a gel and resist compression forces.

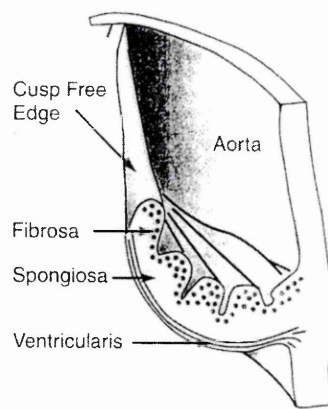


Figure 1.5: Schematic drawing of the leaflet and its aortic wall showing the three distinctive layers where the fibrosa appear as a folded sheet which can unfold when the leaflet stretches (adapted from Vesely¹²¹).

1.4.2 Pericardium

The cusps of pericardial valves are formed from glutaraldehyde-treated pericardium. The pericardium is attached to a frame. The various designs differ in the way the tissue is mounted on the frame.

The major structural protein of pericardium is type I collagen¹²², a small amount of low-molecular-weight dermatan proteoglycan^{123,124} and elastin has been demonstrated microscopically¹²⁵. Native porcine pericardium is thinner than bovine and thicker than human pericardium, and is used sometimes for heart valve bioprotheses¹²⁶, although bovine pericardium is more common. The thickness of

Chapter 1

bovine pericardium used for valve manufacture is approximately 0.4 mm. The tissue is heterogeneous and has been commonly selected for uniformity of thickness, absence of blood vessels, etc, rather than for its mechanical characteristics. Recently, it has been acknowledged that collagen fibre architecture is an important parameter for both the characterisation of mechanical behaviour and the material selection for fabrication of bioprostheses. The intrinsic structural and mechanical variability¹²⁷⁻¹²⁹ of pericardium is now recognised as a drawback. However, whilst the pericardial sac has regions which are “highly variable”^{128,130} areas have been identified which have the prerequisite properties for bioprosthetic heart valve fabrication or for other biomaterial applications.

Pericardium has been described as a pliant biological composite with three or more layers of laminated or interwoven collagen fibres embedded in an amorphous matrix^{127,131}. Unstressed, the collagen fibres are arranged in wavy bundles with small numbers of elastin fibres that are usually arranged at right angles to the collagen. In contrast to porcine tissue, pericardium tissue is as a relatively homogenous sheet of laminated collagen¹³², with frequent blood vessels in the plane of the tissue. However, in addition to the lamellar structure, the bovine pericardial collagen consists of three layers that can be identified in cross section; i) a smooth serosal surface, covered by mesothelial cells ii) fibrosa (which constitutes almost the entire thickness) which contains collagen, elastic fibres such as elastin, nerves and blood vessels and iii) rough epipericardial connective tissue consisting of loosely arranged collagen and elastin^{132,133} and containing fat and numerous blood vessels. The rough epipericardial layer of the pericardium is removed during tissue preparation^{132,133}. The smooth side of the pericardium (formerly the serosal surface, facing the pericardial space) is usually used as the cuspal outflow aspect; the rough surface forms the inflow side of the cusp. This rougher surface will be well-washed with blood flow following implantation. This is thought to reduce the possibility of thrombosis².

1.5 Tissue treatment

1.5.1 Introduction

As discussed in section 1.4, many tissue components contribute to the function of the valve. The major structural component is collagen, with elastin representing a small but relatively important contribution to tissue properties. Further consideration of the components (collagen and elastin) of valve tissue is required before the treatments and chemistry of the valve tissue can be considered further.

1.5.2 Elastin

Elastin, a structural protein of the extracellular matrix is a major component of elastic fibres in connective tissue with a unique elasticity and tensile strength. Heart valve cusps contain approximately 50% collagen, but also 13% elastin by dry weight¹³⁴ (as measured by hydroxyproline assay).

In common with most elastomers, elastin consists of randomly coiled polymer chains, joined together by cross-links into an extensible, three-dimensional network¹³⁵. Historically, it was thought that elastin consisted of an amorphous system of peptide chains covalently cross-linked at intervals¹³⁶, to account for its elastic properties and insolubility. These unknown probable cross-links were investigated and thus it led to the isolation (from bovine ligamentum nuchae elastin¹³⁷ and later from elastin of different tissues and species¹³⁸) of the amino acids named desmosine and isodesmosine. Desmosine is 4-(4-amino-4-carboxybutyl)-1-(5-amino-5-carboxypentyl)-3,5-bis(3-amino-3-carboxypropyl)pyridinium and isodesmosine is 2-(4-amino-4-carboxybutyl)-1-(5-amino-5-carboxypentyl)-3,5-bis(3-amino-3-carboxypropyl)pyridinium. It is worth noting that these two cross-linking structures are not found in naturally cross-linked collagen. As each compound has a strongly basic quaternary pyridinium nucleus and four α -amino and α -carboxylic groups, they are capable of cross-linking four lysine residues in different polypeptide chains, resulting in the tridimensional polymerisation of tropoelastin and the formation of the characteristic cross-links of mature elastin. It has been reported that each isodesmosine and desmosine molecule can cross-link two polypeptide chains¹³⁹. Several other lysine-derived amino acids have since been isolated, most of them being intermediates in the formation of desmosine and isodesmosine. These are

lysionorleucine¹⁴⁰, dehydrolysionorleucine (imine from allysine and lysine)¹⁴¹, mero- and dehydromerodesmosine (α,β -unsaturated imine)¹⁴², allysine (also known as α -aminoadipic acid δ -semialdehyde)¹⁴³, and a dehydrated aldol condensation product of allysine¹⁴⁴. Although lysionorleucine and merodesmosine are other possible cross-links, desmosine and isodesmosine are thought to be the primary inter-molecular cross-links responsible for the elastomeric properties of elastin¹⁴⁵. The other cross-links require only two lysine residues (not four) and are thus hypothesised to be involved in intra-molecular (bridges) cross-links while desmosine and isodesmosine-like cross-links are considered as “knots” rather than bridges. A mechanism for the formation of desmosine and isodesmosine was postulated and proposed^{146,147}. The process of cross-linking starts with the alignment of lysine pairs in the tropoelastin precursor¹³⁵, which are turned into allysine residues by the action of lysyl oxidase action (oxidative deamination of the 6-amino group of the lysine residue) and then go through the appropriate aldol and Schiff base condensation reactions (see figure 1.6). It has also been reported¹⁴⁸ that elastin, in addition to desmosine and isodesmosine, contains high levels of intermediates of higher reduction state: their respective cyclic dehydrodesmopiperidine precursors (dihydrodesmosines and dihydroisodesmosine that can be oxidised spontaneously to the respective (iso)-desmosines). The cross-links render elastin a highly hydrophobic, insoluble and elastic protein¹⁴⁹. The elastin in heart valves is not confined primarily to the ventricularis, as suggested in the past^{150,151}, but is widely distributed throughout the aortic valve in what appears to be a highly functional fashion¹²⁰. The mechanical role of elastin in heart valves has been largely ignored due to its low content and its limited stiffness. But the importance of elastin (even when present as a minor component) in proper mechanical function indicates that any disruption of elastin through disease or other means could be the reason for mechanical failure of a valve¹⁵².

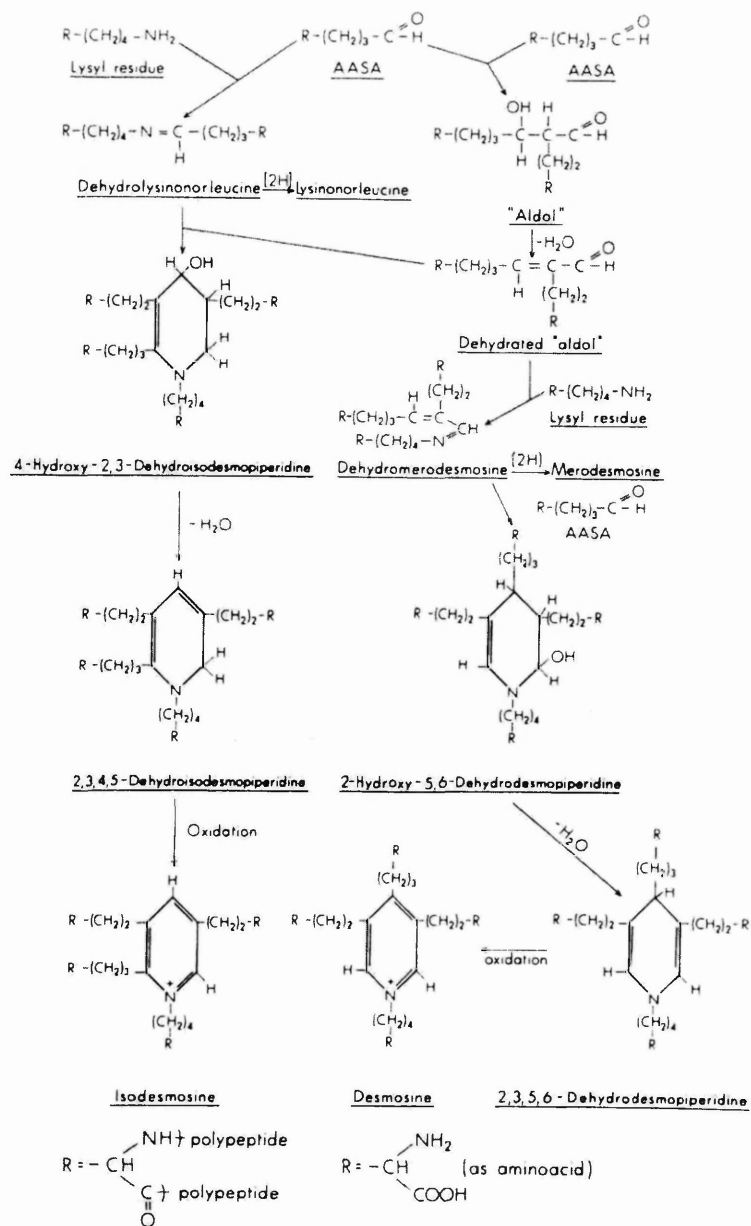


Figure 1.6: Proposed reactions for the formation of cross-links in elastin (AASA is α-amino adipic acid). Adapted from Paz et al¹⁴⁸.

1.5.3 Collagen

There are 16 distinct types of collagen^{153,154}. Amongst these, type I collagen is the most abundant and the most important with respect to biomaterials. Three types of collagen have been isolated and identified from bovine heart valves. These are; type I (the predominant component of heart valve tissue), type III and V. Type I collagen consists of three left-handed, helical α-chains (each chain contains 1050 amino acids) aggregated to form a right-handed triple helix. Every third residue in the chain

is the amino acid glycine. Other major amino acids are proline, lysine and hydroxylysine. The primary structure of collagen is a repeating amino acid triplet of the form (Gly-Pro-X)_n, where X can be any amino acid. Several amino acids present in the sequence contain potentially reactive groups. For examples the oxygen-containing groups would tend towards nucleophilicity, whereas the basic nitrogen-containing groups would tend towards electrophilicity. The triple helix is stabilised by hydrogen bonding. Non-helical terminal regions are thought to contain hydroxylysine residues. These are involved in natural inter-molecular cross-linking and further stabilise the structure. Such triple helices are assembled into ordered polymers called fibrils (100-300 nm in diameter) or fibres of several microns in diameter. When viewed by electron microscopy, collagen fibrils exhibit a characteristic banding pattern due to the staggered arrangement of the component tropocollagen molecules. For a more detailed review of collagen, the reader is invited to refer to some excellent publications in this area¹⁵⁴⁻¹⁵⁶.

1.5.3.1 Collagen for medical applications:

Collagen-based biomaterials are employed in numerous medical applications. Whilst a detailed description of the full range of applications is outside the scope of this thesis, however it is worth mentioning a few such as channels for nerve regeneration¹⁵⁷, tissue reconstruction^{158,159}, tissue augmentation^{160,161}, burn and wound dressings¹⁶²⁻¹⁶⁴, drug delivery systems¹⁶⁵⁻¹⁶⁷, soft contact lenses and ocular surfaces¹⁶⁸, urinary tract surgery^{169,170} and urinary incontinence in the exstrophy/epispadias complex¹⁷¹, closure of the pericardial sac after open-heart surgery¹⁷², vascular grafts^{173,174}, valved conduits⁹⁹ and ligament replacement¹⁷⁵. The materials most widely used are those derived from bovine, porcine and equine pericardium, all of which are or have been employed in the construction of cardiac prostheses.

1.5.3.2 Natural cross-linking of collagen:

In normal biological tissues, the collagen fibrils are stabilised and strengthened by covalent inter- and intra-molecular cross-links. Cross-linking also provides fibres with an adequate degree of tensile strength and visco-elasticity^{176,177}. Native cross-links, within the tropocollagen molecule (intra-molecular cross-links) and between different molecules (inter-molecular cross-links), are formed predominantly between

lysine and hydroxylysine residues. Intra-molecular cross-links in tropocollagen are formed between lysine residues located in the non-helical region near the amino terminal. Inter-molecular cross-links are formed by the joining of two hydroxylysine residues and one lysine residue. These cross-links are formed between residues near the amino terminal of one tropocollagen molecule and the carboxyl terminal of another. Three natural cross-linking reaction pathways occurring in type I collagen can be found in the literature. The allysine-derived pathway¹⁷⁸ (with two alternatives); the hydroxyallysine-derived pathway¹⁷⁸; and the formation of pyrrolic cross-links^{179,180}. A common feature in these natural cross-linking mechanisms is a requirement for the enzyme lysyl monoamine oxidase (a copper metalloenzyme). This initiates the cross-linking by specifically oxidatively deaminating some 6-amino groups of lysine and hydroxylysine into aldehydes. Thus lysine and hydroxylysine residues are turned into allysine and hydroxyallysine respectively. These can then undergo a series of condensation and imine formation reactions to form the intra- and inter-molecular cross-links involving mainly lysine, hydroxylysine and histidine residues. It has been proposed that aldehyde formation occurs by the enzyme binding to the carboxy-terminal telopeptide region of fibrillar collagen¹⁸¹, although there are reports that suggest the enzyme can act on lysine and hydroxylysine residues located in the helical regions¹⁸².

1.5.3.2.1 The allysine-derived cross-links (a)

Two allysines undergo an aldol condensation forming an intra-molecular cross-link between two chains in the N-terminal non-helical region of the same collagen molecule. A histidine residue reacts with this aldol condensation product by a Michael-type addition to form a dehydro-aldolhistidine. This, in turn, reacts with hydroxylysine to form a reducible dehydro-histidinohydroxymerodesmosine (deH-HHMD) cross-link¹⁷⁸. The histidinohydroxymerodesmosine is shown in figure 1.7 below.

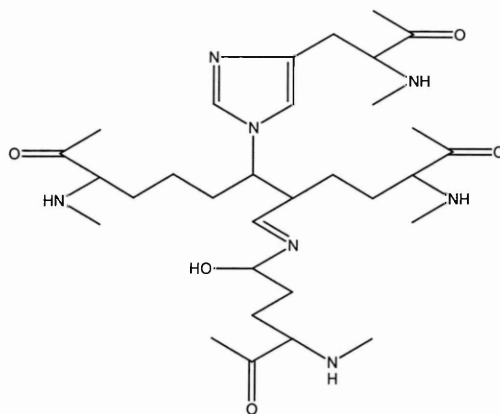


Figure 1.7: The structure of histidinohydroxymerodesmosine

1.5.3.2.2 The allysine-derived cross-links (b)

Allysines in the C- and N-terminal regions condense with 6-amino groups of specific helical peptidyl residues of lysine or hydroxylysine to form a reducible Schiff base inter-molecular cross-link (dehydro-hydroxylysinonorleucine). A histidine residue subsequently reacts to form a stable non-reducible histidinohydroxylysinonorleucine (HHL) inter-molecular cross-link¹⁷⁸. The histidinohydroxylysinonorleucine is shown in figure 1.8 below.

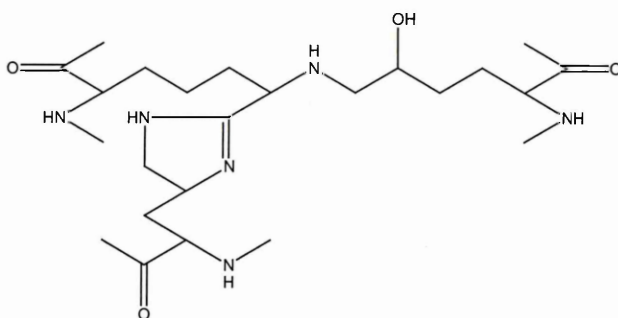


Figure 1.8: The structure of histidinohydroxylysinonorleucine

1.5.3.2.3 The hydroxyallysine-derived cross-links

Hydroxyallysine in the non-helical regions condenses with hydroxylysine to form reducible Schiff base cross-links (dehydro-dihydroxylysinonorleucine). The Schiff base undergoes an Amadori rearrangement forming stable ketoamine cross-links. The ketoamine undergoes a series of reactions with a further ketoamine or a hydroxyallysine to form a non-reducible pyridinoline inter-molecular cross-link¹⁷⁸. There are reports, however, which suggest that some of the cross-links remain in the

unstable Schiff base form¹⁸³. The pyrodinoline cross-link can be seen in figure 1.9 below.

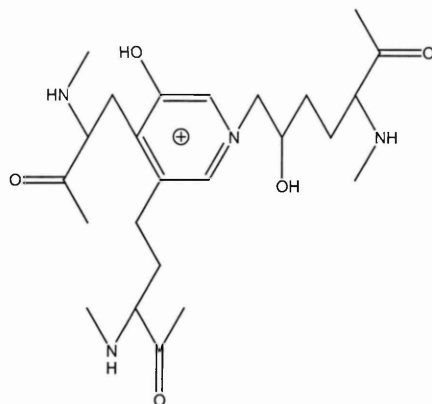


Figure 1.9: The pyrodinoline cross-link

1.5.3.2.4 The pyrrolic cross-links

Kemp and Scott¹⁷⁹ proposed the presence of pyrrolic cross-links, involving Ehrlich chromogens (EC) in collagen. In 1992, Kuypers et al¹⁸⁰ provided strong evidence that the collagen-associated EC is a major cross-link involving primarily the C-terminal helical cross-link region of the $\alpha 2(1)$ chain in bovine type I collagen. They proposed that the EC is a trisubstituted pyrrole formed from allysine reacting with hydroxylysino-5-oxonorleucine to form a Schiff base, which leads to a trisubstituted pyrrole. Such a trisubstituted pyrrole can be seen in figure 1.10 below.

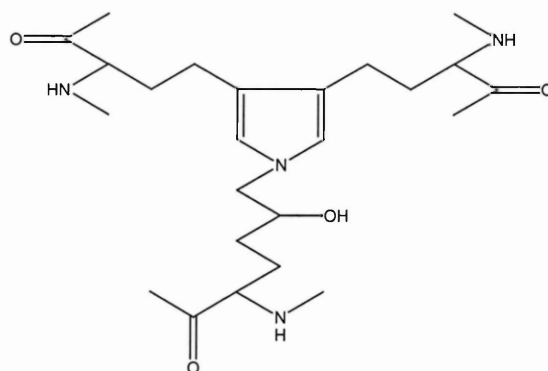


Figure 1.10: The structure of a trisubstituted pyrrole

To further stabilise collagen fibres in biological tissue, exogenous cross-links may be added to a tropocollagen molecule within its individual helical strands (intra-molecular cross-links), between adjacent tropocollagen molecules (inter-molecular

cross-links) or between tropocollagen and other molecular species, using cross-linking agents, as will be discussed in the following section.

1.5.4 Induced cross-linking by chemical and physical methods

1.5.4.1 Introduction:

As already mentioned, collagenous tissue degrades quite quickly once harvested. For clinical devices, this deterioration must be delayed or prevented and hence there is a need for stabilising by chemical or physical cross-linking techniques. To allow the exploitation of tissue, its structural and mechanical integrity has to be enhanced and maintained. In addition, the tissue's antigenic properties have to be neutralised while maintaining sterility and cross-linking indeed helps to abolish or minimise antigenicity¹⁸⁴. Additionally, there is a decrease in the concentration of naturally occurring cross-linking in explanted tissue compared with non-implanted tissue¹⁸⁵. This means that naturally occurring cross-links break down during implantation. Preparatory methods for collagen tissue are thus mainly concerned with the enhancement of mechanical stability by creating additional bonds. Thereby increasing the numbers of intra-molecular and inter-molecular cross-links¹⁸⁶ increases the mechanical strength of the tissue and its stability during implantation⁷⁸. Currently there are two different approaches to improving the properties of biological biomaterials: chemical and physical procedures, although some have their limitations.

1.5.4.2 Physical procedures:

Methods such as dehydrothermal treatment, photo-oxidation and UV irradiation, are primarily designed to avoid introducing potentially toxic chemical agents (there is no use of foreign substance). However the physical methods of cross-linking generally provide a low density of cross-links¹⁷⁶ and are out of the scope of this thesis.

1.5.4.3 Chemical procedures:

Chemical cross-linkers include hexamethylene diisocyanate¹⁸⁷, epoxy resins^{188,189}, carbodiimides¹⁷⁶, acyl azide¹⁹⁰ and genipin^{191 192}. Although some of these cross-linking agents seem to be preferable in terms of the reduced cytotoxicity, they cannot equal glutaraldehyde in terms of its ability to stabilise collagen¹⁹³. All current valve manufacturers employ glutaraldehyde at some stage of their tissue treatment

processes. Glutaraldehyde also has many other applications in various fields. A major hurdle to the introduction of a new cross-linking agent for valve stabilisation is the requirement for approval of the resulting product by the US Food and Drug Administration (FDA) and/or the EU Regulatory Agencies for implantation in humans. Due to the time associated with such a process and hence its cost, valve manufacturers have placed their research investments in the development of a more robust valve whilst retaining glutaraldehyde as the fixative, rather than adopting the radical approach of employing another agent.

Due to its importance in the manufacturing process in the valve industry and also because of its importance regarding the theme of this thesis, chapter 2 is dedicated to glutaraldehyde including its applications (particularly its use in the valve fixation process), toxicity and complex chemistry in solution and with proteins.

1.6 Calcification: pathology and prevention

1.6.1 Introduction

Calcification remains a major cause of clinical failure of glutaraldehyde-treated heart valves. Approximately 30% of bioprosthetic valves fail within 10 years of implantation¹⁹⁴. Almost half of these, display mineralisation that can lead to irreversible damage to the valve, such as leaflet rupture. Such a calcified valve can be seen in figure 1.11. Unfortunately, an incomplete understanding of the factors leading to mineralisation hampers the development of a prosthesis that is resistant to calcific failure.

In the following section, an insight into the process of non-pathological calcification will be given. This is followed by a discussion of the factors influencing the pathological calcification and the mechanism of calcification found in bioprosthetic heart valves.

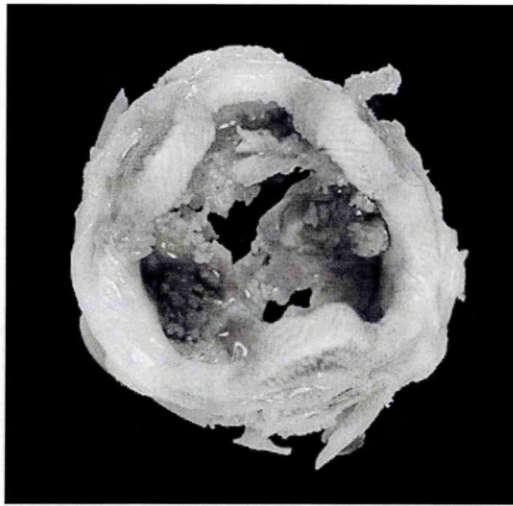


Figure 1.11: Explanted tissue valve exhibiting significant calcification.

1.6.2 Non-pathological calcification

Deposition of calcium in tissues can be part of a normal process, for example mineralisation of osteoid during endochondral bone formation, or formation of dentin and tooth enamel¹⁹⁵. In general, normal calcification essentially equates with bone formation. The mineral deposited initially in normal calcification is predominantly a poorly crystalline form of hydroxyapatite $[\text{Ca}_{10}(\text{PO}_4)_6(\text{OH})_2]$, often substituted in carbonate^{196,197}. This is insoluble in body fluids. Once formed, the calcific deposits tend to proliferate at the levels of calcium and phosphate found in serum, with initial crystals serving as nuclei or templates for the precipitation of new crystals. Under normal conditions, the concentrations of calcium and phosphate ions present in biological fluids are in a metastable state (their concentrations are too low for the spontaneous precipitation of hydroxyapatite to occur), however, physiological levels of these ions are sufficient to support the growth of crystals once precipitation is initiated¹⁹⁸. In early studies, it was suggested that collagen was capable of nucleating hydroxyapatite from a metastable solution because of a specific molecular stereoconformation that would have high affinity for cations¹⁹⁹. More recently, collagen has been hypothesised to play a role in mineralisation in bone^{200,201} and to orientate the newly formed crystals²⁰². Although many hypotheses have been postulated regarding the initiation of calcification, there is support for the hypothesis that the normal mineralisation process is initiated by extracellular matrix vesicles, which are rich in lipids and phospholipids²⁰³⁻²⁰⁵. The earliest hydroxyapatite crystals detected were reported to occur in association with extracellular matrix vesicles^{206,207}. The matrix vesicles are reported to form templates where salt

precipitation can take place in an ordered manner²⁰⁸. In the early phase of calcification, crystals are formed inside the matrix vesicle. Acidic phospholipids (phosphatidyl serine), present in matrix vesicles²⁰⁹, are known to possess a high affinity for calcium²¹⁰ and could act by trapping calcium ions, hence acting as initiator sites. Moreover, proteolipids have been reported to be able to nucleate both normal and pathological calcification²¹¹⁻²¹³. Furthermore, due to the action of energy-requiring transmembrane enzymes such as ATPase or phosphatases concentrated in the matrix vesicles, concentrations of calcium and phosphate are elevated to the point of spontaneous nucleation of calcium phosphate mineral²¹⁴. Additionally, pyrophosphate, a natural inhibitor of hydroxyapatite, can be hydrolysed by inorganic pyrophosphatase and alkaline phosphatase²¹⁵, which are both found in abundance at calcification sites, thus also providing phosphate for the nascent mineral formation. At the earliest stage, a mixture of calcium complexes may lead to the formation of calcified deposit mineral precursors. The complexes could then interact with phosphate ions to form calcium phosphate precursor nuclei, although the product could still be co-ordinately bound to the organic fraction²¹⁶. Once formed, apatite crystals are insoluble and tend to be self-propagating.

1.6.3 Pathological calcification

Calcium deposition can lead to functional anomalies (such as atherosclerotic plaques, tendon and joint dysfunction and failure of implantable prostheses including heart valve prostheses) when it takes place at ectopic sites, that is, sites other than within normal mineralised tissue such as bone or dental mineral¹⁹⁵. It is also worth mentioning that calcification in natural human aortic valves is found in about 2.9% of the elderly population, giving rise to calcific aortic stenosis. The risk increases with age^{217,218}. This is the most common form of valvular heart disease²¹⁹. In addition, such calcification is enhanced in damaged valves, such as those with congenital anomalies or those affected by rheumatic valvulitis.

Pathological calcification in-vivo has been classified in three categories:

Heterotopic calcification: This formation of true bone is quite commonly found after hip replacement and in association with the deposition of cartilage and generation of new osteoblasts, but the initial stimulus for this mineralisation remains unknown.

Metastatic calcification: This occurs when the plasma concentrations of calcium and/or phosphate ions rise above critical levels leading to deposits of apatite crystals, usually in association with a local rise in pH. It is often associated with renal disease and can be prevented by reducing plasma phosphate with ingested aluminium hydroxide.

Dystrophic calcification: It is defined as mineralisation that occurs in tissues other than teeth or bones in the absence of a systemic mineral imbalance²²⁰. Dystrophic calcification is a common response to injury in soft tissues and can have devastating effects when it occurs in soft tissues such as artificial heart valves and arteries. It is also a common detrimental consequence of implantation of many biomaterials, prostheses and other medical devices. Dystrophic calcification can be either intrinsic (i.e. directly associated with the biomaterial, for example in valves it is found with collagen bundles or connective tissue cells as well as at the commissures of the valve cusps); or extrinsic (i.e. superficial to the biomaterial and in association with debris attached to the surface of the material, for example with valves it can be found in association with thrombus, cell debris or vegetations²²¹).

Although the process of mineralisation of hard tissues has been extensively investigated throughout the last four decades^{207,222-224}, it is not yet fully understood. Pathologic calcification in calcific disease²⁰³ (e.g. degenerative calcific aortic stenosis of aged aortic valves²²⁵, atherosclerotic plaque²²⁶, arthritis, dental calculus and calcification of implanted medical devices) and the normal calcification of skeletal and dental tissues share important features. Deposits of calcium phosphate salts in bioprosthetic valves are chemically and crystallographically very similar to bone mineral²²⁷⁻²²⁹, resembling hydroxyapatite crystals $[\text{Ca}_{10}(\text{PO}_4)_6(\text{OH})_2]$ in composition and structure. The initial mineral deposits are poorly crystalline apatic mineral, highly insoluble in body fluids at physiological pH but able to proliferate in serum concentrations of calcium and phosphate. Cell and collagen crystal deposits are present ultimately, and initial crystal formation is believed to occur on cell membranes, usually in the form of extracellular vesicles^{202,203,225,226,230}. Similarly, mineral initiation in developing bones, in the dentin of teeth and in the epiphyseal growth plate cartilage of long bones results from the deposition of apatite crystals within and upon extracellular matrix vesicles. These structures have a high concentration of calcium-binding acidic phospholipids within their membranes and

exhibit high phosphatase activity, especially alkaline phosphatase^{202,203,230}. Alkaline phosphatase, an enzyme critical to bone mineral nucleation, is present in both fresh and fixed bioprosthetic tissue and has been identified at sites where early mineralisation occurs^{231,232}. In normal bone calcification, the growth of apatite crystals is regulated by several non-collagenous matrix proteins, including osteopontin (an acidic calcium-binding phosphoprotein with high affinity to hydroxyapatite that is abundant in the foci of cardiovascular calcification^{233,234}), osteonectin (known as secreted protein acidic rich in cysteine (SPARC)), and osteocalcin proteins, such as matrix glycosaminoglycan protein (MGP)^{235,236}. Osteopontin has been shown to inhibit calcification²³⁷ it has also been identified in calcified bioprosthetic and native heart valves removed from patients^{238,239}. Recent studies suggest that both physiologic and pathologic calcification are genetically controlled by inhibitory molecules^{237,240-242} and that calcification occurs passively when inhibitors are absent.

1.6.3.1 Calcification of valves:

Both experimental^{243,244} and clinical studies²⁴⁵ of valve bioprostheses have demonstrated that mineralisation occurs by deposition of crystalline calcium phosphate, namely hydroxyapatite, predominantly deep in the valve tissue. Calcification has been demonstrated to proceed in two major phases, the nucleation and then propagation of crystals²⁴⁶.

1.6.3.1.1 Nucleation phase:

This first phase of calcification is very critical because in normal biological fluids, calcium and phosphate levels are found in insufficient concentrations to allow spontaneous precipitation of hydroxyapatite from their possible preliminary compounds, namely amorphous calcium phosphate and octacalcium phosphate. Once hydroxyapatite is formed however, the reaction is irreversible as the product is insoluble. At the site of calcification, a localised micro-environment occurs in which concentrations of calcium and phosphate are elevated to the point of apatite precipitation. The initiation site has never been established conclusively. In a normal environment, calcium exists in metastable equilibrium with dissolved phosphate species²⁴⁷. This equilibrium is dependent on the pH, temperature or serum concentrations of the dissolved chemical species and can easily be changed in the

presence of foreign substances such as trace impurities or surface changes²⁴⁸. The subsequent shift of equilibrium may result in the spontaneous precipitation of calcium phosphate crystals at lower levels of super-saturation than those encountered physiologically²⁴⁷. Furthermore, it has been demonstrated that the presence of other ions can also promote the precipitation of calcium phosphate²⁴⁹. This may explain why calcification seems to result from the formation of calcium phosphate crystals with substantial incorporation of sodium, magnesium and carbonate that, by subsequent crystal aggregation, grow to form the calcified nodules that result in valve dysfunction and failure²⁵⁰. In contrast to bone formation, a non-energy-requiring Ca^{2+} trap has been postulated to occur in dystrophic mineralisation as a result of the presence of phospholipid complexes (e.g. phosphatidyl-serine), which can nucleate mineral phases from metastable calcium and phosphate^{198,210}. It has also been demonstrated that the initial calcium-forming event in bioprosthetic valve involves calcium diffusion into the phosphorus-rich ultrastructure of glutaraldehyde-devitalised cells^{232,251}. In viable cells there is a 10000 fold gradient of calcium across the plasma membrane. Low intra-cellular calcium concentrations are maintained by energy-dependent pumps in the cell membranes. In cells rendered non-viable by glutaraldehyde fixation, the mechanisms for calcium exclusion are no longer functional (the calcium pumps are impaired) and calcium passively diffuses into the cytoplasm where it can react with phospholipids of the plasma membrane and membrane bound organelles such as mitochondria^{122,252}. Cell debris, consisting of nuclear membrane and organelle fragments, is known to be a potential primary site for calcification^{122,253}. Recent studies in cultured cells suggest that calcification does not occur in dead cells, but in chemically-injured cells. This suggests that the calcium influx into the injured/dead cells is not passive but may be regulated at a cellular level in-vitro and at an organic level in-vivo²⁵⁴. More recently, results from a study of porcine valve fibroblasts agreed with the fact that mineralisation is initiated in cells but suggested that glutaraldehyde fixation causes a massive cytosolic calcium increase along with a concomitant increase in phosphorus concentration²⁵⁵. It was also recently reported that cells initiate calcification and extracellular matrix serves as a substrate for the subsequent growth of apatite in glutaraldehyde-treated vascular tissue²⁵⁶. Findings by others support the concept that valve calcification is not a random passive, degenerative process, but an active regulated process

Chapter 1
involving either a transformation of the human valve fibroblast cell to an osteoblast-like phenotype or the recruitment of osteoblast precursor cell in the inflamed area²⁵⁷.

The presence of endogenous or host proteins, the host's immune response, the fixative used and other parameters may be other possible factors in the explanation of consistent intrinsic calcification²⁵⁸ and these will be discussed later in this chapter.

1.6.3.1.2 Propagation phase:

Once nucleation has occurred, the concentration of calcium and phosphate in metastable fluids is sufficient to allow for crystal propagation. Precipitation may then proceed through the formation of unstable precursor phases since the various calcium phosphates have thermodynamically different solubilities. This is followed by the accumulation of calcium phosphate crystals. These are usually associated with the collagen fibrils of glutaraldehyde-treated valve tissues. The deposits increase in terms of size and number with time of implantation, finally obliterating implant architecture (cells, collagen) with subsequent nodule eruption through the tissue surface^{122,243}.

1.6.3.2 The calcification of elastin and collagen:

Calcification of collagen²⁵⁹ and elastin occurs by independent yet poorly understood mechanisms. Elastin-associated calcification was first reported in the calcification of aortic wall in the early 1970s²⁶⁰ and was later observed in aortic wall allografts²⁶¹ and glutaraldehyde-treated heterologous vascular grafts²²⁹ implanted subcutaneously in rats. Mineralisation within elastin fibres has been reported to occur independently of cross-linking whilst in collagen some alteration to the collagen molecule such as aldehyde cross-linking is required²⁶². Moreover, vascular elastin fibres have a tendency to calcify but cuspal elastin fibres do not²⁶³. This would suggest that the mineralisation capability (and also possibly the cross-linking capability) of elastin fibers of one tissue differs from that of others. It has been demonstrated that elastin fibres might be the principal site of calcification of biological vascular grafts when implanted in animals^{229,261}. A decrease in the degree of natural cross-linkage was found in the elastin in calcified atherosclerotic plaques within the aortic wall²⁶⁴. It

has been suggested that space within the macromolecular cross-linking of elastin may provide a nucleation site for mineralisation²⁶⁵.

1.6.3.3 The mineralisation of valves of different origin:

Data from a recent study shows that pericardial valves appear less prone to calcification than porcine valves, although further tests with a greater number of samples are required to prove this finding since many factors, such as tissue or manufacturing differences, or even the tissue source, must be taken into account²⁶⁶. Nevertheless, as already discussed earlier in this chapter, several reports support the finding that the performance of pericardial valves currently in clinical use is equal or superior to that of porcine valves^{53,81}.

Bovine pericardium has, however, been shown to calcify with pathological features and mechanisms of mineralisation identical to those of porcine aortic valves, despite differences in infrastructure¹²². Calcific deposits in either porcine valves or bovine pericardial tissue can be seen morphologically in residual connective-tissue cells of the bioprosthetic tissue (intrinsic calcification) within 48 h following subcutaneous implantation^{122,243}. Calcification can also occur within adherent thrombi or infective vegetations (extrinsic calcification)^{51,202,267}, but this is not relevant to this present work.

1.6.4 The formation of hydroxyapatite (HAP) and its derivatives

It has already been mentioned that the deposits of calcium phosphate salts found in bioprosthetic valves are chemically and crystallographically very similar to bone mineral²²⁷⁻²²⁹ and resemble apatite crystallites in composition and structure. The term “apatite” refers to a structural type that can be represented by the formula $[A_4B_6(MO_4)_6X_2]$. In bone, A and B are mostly calcium ions in two kinds of site, MO_4 is a PO_4 group (possibly with some substitutions) and X_2 are mostly OH^- ions. Hard vertebrate tissues are composites primarily composed of impure, calcium deficient hydroxyapatite (HAP) and collagen. The main product of calcification in bone is usually considered to be a variant of HAP^{216,268}. The formula for stoichiometric HAP is $[Ca_{10}(PO_4)_6(OH)_2]$, the unit cell of the crystal containing all eighteen ions of the formula. A detailed account of its structure can be found in the literature²⁶⁹. Stoichiometric HAP contains constitutional water, in the form of OH^- ions; this water can be driven off by high temperature treatment (e.g. ashing), first

producing a partially dehydrated HAP and then disproportionating according to the following reaction²⁶⁹:



Additionally, various proposals for non-stoichiometric apatites have been reported and include H_2O in place of hydroxide ions²⁷⁰, H_2O or H_3O^+ in place of Ca^{2+} ²⁷¹, water as $(\text{CO}_3+\text{H}_2\text{O})^{2-}$ substituting for PO_4^{3-} ²⁶⁹, interstitial H^+ as hydrogen bonds between oxygens of the phosphate ions²⁷² or even water hydration in octacalcium phosphate (OCP) ($\text{Ca}_8\text{H}_2(\text{PO}_4)_6 \cdot 5\text{H}_2\text{O}$) interlaid with HAP²⁷³. Indeed, HAP compound has a range of composition that may be characterised in terms of Ca/P ratios. The Ca/P ratio of stoichiometric HAP is generally reported as being 1.670, but stable compositions (assuming that no ionic substitution has taken place in the apatic structure) may have ratios extending down to approximately 1.500. This corresponds to a defective structure $[\text{Ca}_9(\text{HPO}_4)(\text{PO}_4)_5\text{OH}]$ created by the removal of a mole of CaO from the stoichiometric HAP²⁷⁴. It is widely known that low Ca/P ratios result from the presence of calcium vacancies, with charge compensation achieved by incorporation of protons interstitially, as HPO_4^{2-} or H_3O^+ ions, or by protonating OH^- ions to form H_2O ^{272,275}. Furthermore, the apparent presence of octacalcium phosphate (OCP $\text{Ca}_8\text{H}_2(\text{PO}_4)_6 \cdot 5\text{H}_2\text{O}$), brushite (dicalcium phosphate dihydrate DCPD $\text{CaHPO}_4 \cdot 2\text{H}_2\text{O}$) and possibly monetite (dicalcium phosphate anhydrous DCPA CaHPO_4) and “amorphous” calcium phosphate (ACP) as phases which are separate from the apatic mineral in bone has been cited as a possible cause for the observed variations in the Ca/P ratios²⁶⁹, associated with the maturation and aging of biological apatites^{276,277}. In fact the most commonly proposed precursors to HAP have been these same compounds, amorphous calcium phosphate (ACP)²⁷⁸⁻²⁸⁰, brushite (DCPD)²⁸¹, and octacalcium phosphate (OCP)²⁸². However, other researchers have stated that there is no evidence for the presence of a precursor phase with only the presence of apatite as the single mineral component being observed²⁸³⁻²⁸⁵. Thus, it is thought that a few of the compounds are worthy of further consideration.

Amorphous calcium phosphate (ACP): It has been reported that as much as half of the mineral in bone²⁸⁶ is in the form of ACP, although the same group later stated that fully developed bone mineral could not contain more than 10% ACP²⁸⁷. ACP

has been reported as the precursor to the formation of apatite²⁶⁹. ACP has been observed to represent the major solid CaP phase in the very earliest mineral deposits²⁸⁷⁻²⁸⁹. The Ca/P of ACP does not vary as much as the one of crystalline hydroxyapatite: it varies only from 1.200 to 1.500 where the structural unit is thought to be $\text{Ca}_9(\text{PO}_4)_6$ ²⁹⁰.

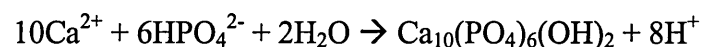
Octacalcium phosphate (OCP): The possible role of OCP as a precursor was reported as early as 1957²⁹¹. The structural composition of OCP ($\text{Ca}_8\text{H}_2(\text{PO}_4)_6 \cdot 5\text{H}_2\text{O}$) has been reported²⁶⁹ to be closely related to the one of HAP, with similar unit cell lengths b and c and also the enclosed angle alpha. The OCP structure thus consists of an apatitic layer almost identical in structure to HAP but also a hydrated layer that differs totally in its composition and structure from that of HAP. In-vitro at ambient temperatures, OCP crystals grow more rapidly than do HAP crystals (even in the presence of serum, where crystal growth poisons are reported to greatly hinder the formation of HAP but not that of OCP²⁹²), additionally it was reported that this process of fast crystal growth was probably taking place too in-vivo during bone growth²⁹³. It was reported that the initial bone crystallites appeared to be mostly thin plates, several Angstroms long, nearly as wide and about 50 Å thick, with a lack of hexagonal symmetry but a pronounced platy crystal morphology typical of octacalcium phosphate²⁶⁹. Because of the similarity in the structures of OCP and HAP, which can lead to the formation of epitaxial overgrowths of one on the other²⁷³, OCP is also thought to be the basis for the formation of non-stoichiometric apatites, by the presence of OCP as a separate phase²⁹³, by an incomplete hydrolysis of OCP to HAP²⁷³ or by the presence of half an OCP unit cell transition layer on crystallites resulting in lowering of the Ca/P ratio down to about 1.550 or even 1.400²⁹⁴. It has also been suggested that microdomains with an atomic arrangement different from that of apatite may exist²⁷³ and a plausible model involving the interlayering of OCP and HAP was evoked for the nucleating entity of bone and enamel²⁹⁵, and is referred to as octacalcium phosphate hydrolysate (OCPH). Such mixed crystals were reported to generate a slightly distorted but nevertheless apatite-like XRD pattern, explaining the failure to detect a phase other than apatite. Their composition would also account for the nonstoichiometry of biological apatite. Moreover, it is thought that apatitic biominerals are formed through a precursor mechanism in which OCP precipitates first and then hydrolyses irreversibly to a

transition product intermediate to OCP and HAP, which is OCPH¹⁹⁷. The hydrolysis of OCP has been studied in-vitro and was showed to yield a calcium-deficient apatite, providing good evidence also that OCP may be a precursor phase in the formation of pathological calcified deposits and normal biomineral which appear to be a complex hydrolysate of OCP²⁹⁶. The characterisation of biominerals in cardiovascular deposits showed that OCPH was the most likely compound according to many characteristics such as the presence of water and the incorporation of CO_3^{2-} , Na^+ and Mg^{2+} ²⁹². The same study showed the presence of carbonate in these biominerals and it is known that when OCP hydrolyses in the presence of carbonate ions it incorporates them, while a similar situation does not exist for hydroxyapatite prepared under the same conditions²⁹⁷.

Whitlockites: Whitlockite is β -tricalcium phosphate (β -TCP $\text{Ca}_3(\text{PO}_4)_2$). Whitlockites have been identified in-vitro²⁹⁸, but also in-vivo, associated with apatites and/or other calcium phosphates in pathological calcifications e.g.. soft tissue calcification^{299,300}, in human dental calculus³⁰¹⁻³⁰³ occasionally in human urinary calculi³⁰⁴, and also in synthetic systems³⁰⁵. It has been reported that biological whitlockites show a partial substitution of magnesium for calcium ions³⁰⁵ and such biological whitlockite is referred to as magnesium-substituted TCP or β -TCMP. β -TCMP was reported to be present when some species of bone^{306,307} or amorphous calcium phosphate³⁰⁸ were calcined at temperatures around 700-800°C. Such transformations from calcium-deficient apatite to β -tricalcium phosphate have been extensively studied because of their importance in calcium phosphate ceramics³⁰⁹ and problems with their differentiation³¹⁰. For example, the expected Ca/P ratio for β -TCP is 1.500, while that for amorphous calcium phosphate can approach a similar value of 1.520. However, a comparative study of the Raman spectra of both HAP and β -TCP reported recently allowed their differentiation³¹¹.

Now, regarding the process of calcification, it has been observed that the first crystals to form are the least stable but most rapidly growing ($\text{CaHPO}_4 \cdot 2\text{H}_2\text{O}$). This salt then hydrolyses, first to $\text{Ca}_8\text{H}_2(\text{PO}_4)_6 \cdot 5\text{H}_2\text{O}$ and then to $\text{Ca}_5(\text{PO}_4)_3\text{OH}$ ²⁷³, sometimes also forming monetite CaHPO_4 ³¹² as an intermediate. All these products may account for some of the observed variations from the amorphous calcium

phosphate Ca/P ratio of 1.500²⁶⁹. Afterwards, the $\text{Ca}_5(\text{PO}_4)_3\text{OH}$ converts slowly to crystalline apatite by an autocatalytic mechanism³¹³ associated with an increased in the Ca/P ratio reaching the ideal pure crystalline HAP phase with a ratio of 1.670. This amorphous calcium phosphate was hypothesised to be able to change somehow to a tricalcium phosphate, while according to others³¹⁴, HPO_4^{2-} ions are deposited and then quickly lose H^+ at the crystal surface. In either case, the overall reaction can be described by the following equation:



If the ions equivalent to the formation of a single HAP unit cell are to form a mineral nucleus, the eight corresponding protons must somehow be removed from the reaction sites. Unless the pH is raised or if no protons acceptors are made available, then the reaction tends to reverse and the crystal nuclei desintegrates instead of growing. The protons scavengers are thought to be organic compounds, possibly some combination of proteins and polysaccharides, possibly with some lipids²¹⁶ (as in the case of atherosclerotic plaques, where natural proton acceptors are made available). The inability of the environmental fluid (containing proteins, polysaccharides, lipids etc.) to remove from the calcifying tissue all the protons released by the formation of hydroxyapatite may explain the several-stage formation of some bone²¹⁶.

The understanding of naturally occurring calcification, leading to the formation of hydroxyapatite, was investigated mostly with the help of in-vitro experimentations. Collagenous matrices were first found to induce apatite formation from a soluble phase comparable to serum with respect to pH, ionic strength, calcium and phosphate concentration^{315,316}. It was hypothesised that matrix-induced calcification occurs by a multistep process^{316,317}, similar qualitatively to the spontaneous precipitation system leading to hydroxyapatite formation³¹⁸. The majority of information on CaP crystal phases comes from studies of calcium phosphate ceramics used in tissue/bone engineering^{319,320}. However, although in the majority of the cases no CaP mineral phase other than apatite is detected in the crystals, it is not possible to rule out the possibility that a very transient non-apatite CaP solid phase is the initial CaP species formed, which very rapidly undergoes phase transformation to purely crystalline apatite. For instance, the hypothesis involving octacalcium phosphate as a precursor

phase, either as a solution aggregate or as a distinct solid crystalline phase, formed as a precursor of the subsequent formation of poorly crystalline apatite crystals^{285,321,322} is supported by a research group in many of their studies; although as they postulated, the transition may be so rapid that no significant concentration of a solid crystalline phase allow its detection by XRD, or FTIR^{323,324}. Thus, the formation of hydroxyapatite-like structures in calcified tissue, is hypothesised to involve precursors such like OCP (octacalcium phosphate $\text{Ca}_8\text{H}_2(\text{PO}_4)_6 \cdot 5\text{H}_2\text{O}$), DCPD (dicalcium phosphate dihydrate or brushite $\text{CaHPO}_4 \cdot 2\text{H}_2\text{O}$), DCPA (dicalcium phosphate anhydrous CaHPO_4), α - or β -TCP (tricalcium phosphate $\text{Ca}_3(\text{PO}_4)_2$), TTCP (tetracalcium phosphate $\text{Ca}_4(\text{PO}_4)_2\text{O}$), CaO (calcium oxide), $\text{Ca}(\text{OH})_2$ (calcium hydroxide).

It is thought that the various hydroxyapatite structures formed may incorporate cations such as carbonate, magnesium, sodium etc, which may come from the surrounding blood plasma. Plasma contains approximately the following: Na^+ 142 mM, K^+ 5 mM, Ca^{2+} 2.5 mM, Mg^{2+} 1.5 mM, HCO_3^- 4.2 mM, Cl^- 148 mM, HPO_4^{2-} 1 mM, and SO_4^{2-} 0.5 mM³²⁵. Magnesium is the fourth most abundant cation in the body and, after potassium, the most abundant intra-cellular metal. A 70 kg man contains 1.18 kg calcium, 146 g potassium, 104 g sodium and 24 g magnesium³²⁶. Approximately 60% of total body magnesium is in the skeleton, either as an integral component of the hydroxyapatite (bone mineral) lattice (40%) or in an exchangeable fraction (20%) adsorbed to apatite and in equilibrium with the extracellular fluid. In contrast, only 1% of total bone calcium is considered to be readily exchangeable³²⁷. Plasma magnesium like plasma calcium exists either bound to serum proteins such as albumin³²⁷, complexed to organic anions such as citrate³²⁸ or as a free ion³²⁹, which has the greatest biological activity³³⁰. Biological apatites (inorganic phases of enamel, dentin, cementum, bone and some pathological calcifications) are reported to be associated with magnesium³³¹⁻³³³. Bioapatites are generally known to contain relatively high levels of ions, (CO_3^{2-} , Na^+ , Mg^{2+} , H^+ , Cl^- and others³³⁴), and lattice defects compared to the synthetic analogue hydroxyapatite. In relation to this, data have shown that during the hydrolysis of OCP, impurities and defects were incorporated into the structure of the non-stoichiometric apatitic product³³⁵. Furthermore, it is well known for example that Ca^{2+} can be replaced by different cations in the hydroxyapatite structure^{336,337}. It has been reported that sodium but not

Chapter 1

potassium was able to interchange with calcium on the surface of the crystals³³⁸ and that other ions such as Mg^{2+} , CO_3^{2-} , HCO_3^- , or pyrophosphate could be strongly adsorbed and affect the surface charge of apatites³³⁹. For instance hydroxyapatite can incorporate carbonate: the type-B carbonated HAP is an HAP with some replacement of PO_4^{3-} by CO_3^{2-} in its structure^{340,341}. Only about one half of the carbonate associated with carbonate-containing apatite is exchangeable, the remainder is presumed to be in the lattice³⁴².

1.6.5 Use of in-vivo and in-vitro models

Preclinical evaluation in a variety of animal models is used to evaluate the functionality of a valve design and assess its resistance to calcification. Models are useful to screen putative anticalcification therapies, study graft calcification and test new treatments. Clinical data in comparison to in-vivo and in-vitro models take many years to amass and are cost effective.

Calcification studies are commonly conducted in two types of animal model: the subcutaneous (static in-vivo) and the circulatory model (dynamic in-vivo). In both models, the biochemistry, morphology, host and implant determinants of bioprosthetic valve calcification²⁶⁷ are similar to those observed clinically but with accelerated kinetics¹²². In-vivo models (subdermal implantation under rat skin and orthotopic implantation in sheep), although used routinely, show variability in calcification due to individual host factors³⁴³. It is often difficult to extrapolate such data to the long-term results that could be experienced in humans or to determine the primary factors involved in mineralisation. A lengthy period of implantation is often necessary to assess calcification rate.

1.6.5.1 Subcutaneous models (static in-vivo):

Subcutaneous implant models have been developed using small animals of young age such as rabbits^{122,344}, mice or rats^{243,345,346} (the latter being the most commonly used animal). They provide convenient, inexpensive and relatively well-controlled models, with accelerated rates of calcification. Results obtained in the rat model are comparable to those obtained in the sheep circulatory model^{202,347} and display histological and chemical features consistent with failed clinical implants^{348,349}.

Although the samples are not in contact with circulating blood (proteins, lipids and cells can all potentially affect the mineralisation²) and do not experience the mechanical stresses imposed by implantation into the heart, the rat subcutaneous model is used as routine tool to screen candidate materials^{190,350} before continuing to the expense of larger animal studies. The validity of this test has been questioned as some anticalcification strategies have been found to be effective in the subcutaneous model, but later proved ineffective in a circulatory model³⁵¹. Reasons for this are numerous as, within the subcutaneous model itself, there are many variations in how the implanted tissues are fixed, along with the age, sex and species of animal in which tissue is implanted. If one takes the rat model as an example, there are potentially large variations of age, strain and sex of the animals from one study to another. Animal age is critical since tissue implanted into juvenile animals calcifies more rapidly than tissue implanted into older animals³⁴⁶. This behaviour is known to be analogous to the clinically-observed accelerated calcification of bioprosthetic valves in children/adolescents relative to adults. The use of different sexes and strains of rats³⁵² can also result in differences in the rate of calcification, although the reason for this is unclear. If the mineralisation process is considered as exponential with time, then a small difference in the number of nucleation sites could produce a large difference in mineralisation after a few weeks. The appropriate control of other factors, such as pH and temperature, must also be carefully monitored³⁵³, as these may affect the degree of calcification. Any comparison made between individual studies has to be carried out with caution.

1.6.5.2 Circulatory models (dynamic in-vivo):

In large animal circulatory models^{253,259,354} the valve or tissue is implanted into the aortic or mitral position of sheep^{355,356} or calves^{93,357}. Occasionally dogs³⁵⁸ or goats³⁵⁹ are used. Bioprosthetic valve implantation in juvenile sheep³⁶⁰ are most frequently used to test the in-vivo durability and calcification characteristics of bioprosthetic valves. Such models can display an accelerated mineralisation within a few months that would take several years to develop in patients³⁶¹. For example, calcification can occur within a few months in valves implanted in young, growing sheep. However, such experiments are technically difficult because the animals need to be maintained for a relatively long period of time (i.e. 200 days) and are very

expensive because of the extracorporeal circulation, the long-term housing of the animal and the high mortality rate (over 50%)^{362,363}.

The overall predictive capacity of these models suffers from the differences between lipoprotein blood content and accelerated calcium metabolism when compared to humans. They do not take into account the different human coagulation pathways, or the effects of cardiovascular disease. Furthermore, since some of the reported results show differences between the subcutaneous and the circulatory models, different mechanisms may apply. Despite these concerns, implantation in an animal is an essential step in the evaluation of any prosthetic valve prior to initial clinical evaluation and represents the only way of studying the effect of biological processes such as calcification, thrombosis and tissue ingrowth.

1.6.5.3 In-vitro model:

Several in-vitro methods have been developed for studying the calcification of isolated molecules such as proteins, as well as bioprosthetic valve materials. As in-vivo calcification occurs relatively rapidly, it is difficult to produce controlled, low levels of calcification for investigation of the early stages of the process. However in-vitro systems can theoretically achieve this. In the in-vitro system calcium phosphate is randomly deposited (in the biomaterial and the environment) in contrast to specific pathological calcification³⁶⁴, thus this method can only be used as first line screening for rapid evaluation of mechanisms of calcification or testing anticalcification strategies. Also, the amount of calcium phosphate available for precipitation is limited as it depends on concentrations of the initial working solution. For example, an early report of an in-vitro system described the mineralisation (formation of hydroxyapatite) of many gels, including type I collagen, using a cross-product of Ca and P of over 32 mM to ensure spontaneous mineralisation³⁶⁵. A smaller cross-product of 2.4 mM was used by Bernacca et al^{366,367}, which still allowed tissue to calcify. Earlier studies showed that calcium phosphate formation within 20 h was achieved with a calcium concentration of 2 mM and a phosphate concentration of 1.14 mM³⁶⁸. Mineral deposition also occurred within 24 h from a balanced salt solution³⁶⁹ containing 1.71 mM calcium and 1.18 mM phosphate at pH 7.4, with these concentrations being close to the values found in serum and rat dorsal interstitial fluid³⁷⁰. In contrast to in-vitro tests, body

homeostasis generates relatively unlimited amounts of calcium phosphate. Thus, the crystalline mineral phase in the in-vitro system is almost completely unpredictable and may not bear any resemblance to that occurring in-vivo.

In-vitro models of calcification may be static or dynamic. Calcium-rich solutions³⁷¹ can be applied to bioprosthetic valves placed into a fatigue system which opens and closes the valve at a variety of frequencies³⁷²⁻³⁷⁴ (dynamic in-vitro test); or placed in (shaken or not) tubes (static in-vitro test). Bernacca et al, using both static³⁶⁶ and dynamic^{375,376} in-vitro systems, investigated several calcium/phosphate media including bovine plasma and succeeded in producing calcification patterns in pericardial tissue similar to the ones seen in clinical explants by histological examination. The retained solution consisted of 135 mM NaCl, 2 mM $\text{CaCl}_2 \cdot 2\text{H}_2\text{O}$, 1.2 mM KH_2PO_4 in a 0.05 mM MOPS buffer, and was based on previously reported work³¹⁸. This solution produced calcification of 14.22 mg/g with a standard deviation of 21.78 mg/g after 21 days³⁷⁵. Many other metastable solutions were investigated³⁷⁷, all with varying concentrations of salts to mimic factors³⁴³ such as ion concentration, pH, temperature and condition of the calcium solution can be critical when studying in-vitro calcification³⁷⁸. Other groups performed extensive studies of in-vitro calcification of various bioprostheses^{374,379} and demonstrated, with the help of soft X-ray analysis and holographic interferometry, that mineralisation was initially minimal and then increased exponentially.

Although some authors reported patterns similar to those seen in clinical explants, the limitation of this technique is not the ability to produce calcification but difficulties in correlating the histologic and ultrastructural manifestation of this calcification to that seen in animal models and in human explants. In-vitro, at the earliest stage of the calcification process, a mixture of calcium complexes may lead to the formation of calcified deposit mineral precursors. These complexes may then interact with inorganic phosphate ions to form the calcium phosphate precursor nucleus, however, the product could still be coordinately bound to the organic fraction²¹⁶. At first, the atomic molar ratio of calcium and phosphorus is high, due to the incorporation of sodium, magnesium and carbonate in the crystal formation. It then decreases with time, finally approaching a value between those of OCP and HAP (e.g. 1.83 in 14 days³⁸⁰ and 2.16 at 14 days³⁸¹). Unfortunately, no in-vitro test system has yet been developed which reproduces the calcification rates seen in-vivo,

or the morphological characteristics of in-vivo models and clinical explants³⁸⁰. Although in-vitro models give reproducible data with respect to the end products of mineral deposition, their contribution to the understanding of the mechanisms of calcification and the role of different factors in each step of the process is quite limited. In fact, some studies report a poor correlation between the results of in-vitro and in-vivo methods³⁸². On the contrary a recent study³⁸³ found that in-vitro results compared relatively well with rat subcutaneous implant data, whilst the dynamic in-vitro model, studying valve mineralisation, showed promise in accelerating the screening of valves (which may ultimately reduce the cost and need for animal model experiments).

Histological staining is widely used as a qualitative technique to assess calcification, for example Von Kossa staining enables the calcification to be identified within the tissue, whereas Ca-analysis techniques, such as inductively-coupled plasma optical emission spectrometry (ICP-OES), may give quantitative data. However, Von Kossa staining is not very sensitive to early deposition and it only stains the phosphate of the calcium phosphate mineral to brown-black, cell nuclei in red, and cytoplasm in pink³⁸⁴.

In summary, no single model is able to determine the propensity of a bioprosthetic heart valve to calcify. However, the different test methods complement each other and the use of multiple models, along with an understanding of their differences and limitations, can help to build a fuller picture of the process of calcium deposition and the factors important to its promotion.

1.7 Factors influencing mineralisation

Several factors have been identified which promote calcification. These include glutaraldehyde treatment, tissue devitalisation, the quality of the biological material, mechanical stress and the presence of phospholipids. The extent and progression of calcification also depend on host factors such as age, the presence of renal disease, or pregnancy. Although many factors have been identified, the mechanism of calcification remains incompletely understood and other factors are under investigation. The often conflicting data and studies, previously discussed, serve to

underline the complexity of the calcification process and emphasise the multiplicity of pathways by which calcification can be initiated³⁸⁵. The following sections are designed to give a succinct overview of the separate “host” and “tissue” factors involved. These are, in reality, closely correlated.

1.7.1 Host factors:

1.7.1.1 Age:

Bioprosthetic tissue calcification is dependent on metabolic factors in the recipient, the most important host factor being age³⁸⁶⁻³⁸⁸. The clinically observed accelerated calcification in the young is simulated in the rat subcutaneous model as discussed previously. Calcification was reported as being associated with both³⁴⁶ high serum phosphate³⁸⁹ and osteocalcin levels³⁹⁰, as well as the enhanced parathyroid hormone and vitamin D metabolism³⁹¹ seen in the young. However, no direct correlation was found between individual serum phosphate or osteocalcin levels and calcium, phosphate or osteocalcin content in the valves³⁴⁶. Some recent in-vitro calcification results have shown that calcium accumulation is also dependent on the initial calcium concentration in the medium³⁹², thus explaining the extensive calcification of bioprostheses in children who have a high metabolic turnover of calcium with high peak serum concentrations. Another hypothesis lies with the role of alkaline phosphatase (see later) because children (and young rats), have higher serum levels of alkaline phosphatase than adults^{393,394}.

1.7.1.2 Renal failure linked to phosphate and calcium metabolism:

Patients with renal failure are reported to suffer from early degeneration of their biological implants³⁹⁵. A recent study showed the prognostic implication of cardiac valve calcification in long-term dialysis patients³⁹⁶. It has been suggested that the availability of phosphate ions could determine the rate of calcification, since calcification develops earlier in patients undergoing hemodialysis who have increased levels of serum phosphates³⁹⁷. Indeed, patients with chronic renal disease

also have a high rate of calcium turnover with rapid changes in their serum calcium concentrations³⁹⁸.

1.7.1.3 Deposition of proteins and circulating cells:

The deposition of extrinsic proteins³⁹⁹ from the host (adsorption of calcium-binding proteins) and circulating cells after implantation is thought to be a factor in valve mineralisation^{400,401}. It is hypothesised that proteins which normally contribute to bone matrix calcification may be involved, since serum proteins are known to be taken up in mineralised tissue⁴⁰². It was reported that calcification was associated with increased content of calcium-binding non-collagenous proteins containing γ -carboxyglutamic acid (Gla) residues⁴⁰³ within the tissue. These may serve as an initiator of calcification in the rat model³⁴⁵ and also in clinical studies in humans^{388,404}. It has been proposed that pre-adsorbed proteins and cells on biomaterial surfaces could induce local redistribution of the calcium fraction on the material surface and subsequently might act as the initial nuclei of calcification⁴⁰⁵. Others, however, refuted these findings^{195,346}. In particular, one study reports no correlation between Gla and calcium deposition, suggesting that although Gla may be adsorbed onto the forming calcium deposits it does not contribute to the calcification process⁴⁰⁶.

1.7.1.4 Anticoagulation treatment/Antiplatelet treatment:

Anticoagulants may be able to retard bioprosthetic valve calcification but this is a controversial subject. Vitamin K-dependent blood coagulation factors were the first proteins discovered to contain the γ -carboxyglutamic acid (Gla)-containing calcium-binding proteins⁴⁰⁷. Anticoagulant drugs, such as warfarin, inhibit Gla synthesis, resulting in a loss of calcium binding and anticoagulation⁴⁰⁸. An inhibitory effect of sodium warfarin on mineralisation was thus suggested⁴⁰⁹ because a number of Gla-containing proteins have been demonstrated to be associated with normal⁴¹⁰ and pathological calcification^{345,411,412}. However, the inhibition of Gla protein synthesis⁴⁰⁰, with the vitamin K antagonist warfarin, reduced the level of Gla but calcification was not significantly reduced. Other studies have also failed to demonstrate an effect of warfarin on calcification⁴¹³. They concluded that the Gla-containing protein was probably adsorbed onto the mineral from the blood and so did

not play an active role. This was later confirmed⁴⁰⁶ as they found no correlation between calcium and Gla concentration in explanted valves.

Calcium is required for most forms of platelet aggregation, and it is believed that cyclic adenosine monophosphate functions in platelets by directing the uptake of calcium⁴¹⁴. It is thus possible that the calcium influx (mineralisation) is due to cellular components such as the platelets or involves plasma proteins such as fibrinogen molecules. It was recently strongly hypothesised that cellular components (platelet activation and adhesion) and plasma proteins (fibrinogen) on biomaterial surfaces can affect salt precipitation, determining somehow the propensity of the implant to calcify⁴¹⁵.

Antiplatelet agents inhibit platelet activation and adhesion to biomaterials and reduce calcium deposition⁴¹⁵. Since human platelets possess membrane receptors for, for example, fibrinogen and collagen, it seems conceivable that these may modify, mask or prevent the expression of binding sites for adhesive proteins and cause reduction of platelet densities on the surfaces. Studies show that the deposition of calcium on glutaraldehyde-treated bovine pericardium⁴¹⁶ can be inhibited by very low levels of antiplatelet drugs, possibly by modifying the pericardial surface. Nevertheless, further studies are required to assess the definite involvement of cellular components and plasma proteins in tissue-associated mineralisation⁴¹⁵.

1.7.1.5 Host immune reaction:

The immunological reaction has been considered by some to be responsible for the calcific degeneration of cross-linked bioprosthetic heart valves^{417,418}. It has been suggested that rejection of the graft may play a significant role in calcium accumulation⁴¹⁹. However, some studies showed a positive correlation between an active immune response and bioprosthetic tissue degeneration⁴²⁰ despite the fact that they found no obvious relationship between immunogeneity (T-cell activation) and bioprosthetic calcification^{421,422}. Also, it was reported that neither non-specific inflammation nor specific immunologic responses appeared to mediate bioprosthetic tissue calcification and that no mineral deposition nor resorption were associated with inflammation⁴²³. However, recently, there has been a renewed interest in the contribution of immune response to the inflammation of tissue valves⁴²⁴ and their calcific degeneration⁴²⁵.

It was also demonstrated that the inflammatory reaction is inversely related to the extent of glutaraldehyde cross-linking of tissue^{426,427}, and a theory developed to link valve degeneration with immune response was that of sub-optimally masked antigenicity. Additionally, a number of studies have provided evidence that contemporary heart valve prostheses are insufficiently cross-linked⁴²⁸⁻⁴³⁰. It was shown possible to decrease calcification by 90% by increasing the density of these cross-links⁴²⁴. It is thought by some that glutaraldehyde cross-linking, provides some protection against calcification, although it is agreed that short-fixation has a tendency to produce a greater calcification than longer fixation treatments, even though low fixation is sufficient to alter the immunogenicity of bioprostheses⁴³¹. In addition, it is hypothesised that the diffusion of plasma between the collagen meshwork is favoured after long-term implantation when the cross-links may be lost⁴⁰⁶. These low-density cross-linked valves can therefore allow protein insudation and elicit an immune reaction⁴³² that may contribute largely to degeneration.

Thus, the contribution of immune responses to tissue mineralisation could probably be more important than initially thought, although the role of cross-links must be taken into account too.

1.7.2 Tissue factors:

1.7.2.1 Tissue as a potential initiation site/factor for calcification:

Collagen and bovine pericardium can bind calcium and phosphate in-vitro in the absence of host factors^{198,318,375}. It has been reported that collagen has potential calcium-binding sites (e.g. amino, carbonyl, carboxylic groups) and therefore may have a natural tendency to calcify⁵¹; these sites may normally be protected by glycosaminoglycans and proteoglycans that are subsequently lost during the glutaraldehyde treatment process. In addition, elastin has been reported as a predominant site of calcification in aortic tissue²⁶¹; the concept of “neutral binding site/charge neutralisation” has been proposed to explain the calcification of aortic elastin, suggesting that the binding sites for calcium are carbonyl oxygens of the peptide backbone⁴³³. In addition, glutaraldehyde cross-linking is reported to enhance the affinity of collagen tissue for calcium binding⁴³⁴. Thus, a likely candidate for a general calcification mechanism is cation chelation by groups present in the material containing lone pairs of electrons susceptible to interactions with electron-deficient

species (e.g. carbonyl oxygens from the collagen backbone or glutaraldehyde species). It is hypothesised that phosphate would be carried along in this process as the accompanying anion to maintain charge neutrality. Such a mechanism could explain both intrinsic and extrinsic calcification, since cellular debris could potentially provide similar binding sites.

1.7.2.2 Matrix and associated proteins:

Early mineral deposits have been reported in transplanted connective tissue cells but also involve extracellular collagen fibres¹¹⁴. Cells and their remnants can be found in the collagen/elastin matrix. Decellularisation of the tissue has been employed as a calcification mitigation strategy⁴³⁵. Matrix vesicles and proteolipids are thought to be involved in the initiation of hydroxyapatite deposition⁴³⁶. A recent study stated that the presence of matrix metalloproteinases may contribute to the in-vivo degradability of pericardium-based cardiac valves⁴³⁷. Acidic phospholipids are recognised as being involved in the initiation of both calcification in bone and dystrophic calcification⁴³⁸⁻⁴⁴⁰. Intrinsic phospholipids (and also proteolipids²¹²) have been considered to be an initial source of phosphorus in the initial stages of heart valve mineralisation due to phospho-ester hydrolysis^{202,349}, possibly due to electrostatic attraction between phospholipids in the connective tissue and calcium introduced into the system^{441,442}. The role of these phospholipids has recently been reconsidered as a potential nucleation source⁴⁴³ and a relatively recent dynamic in-vitro study also found a positive correlation of calcification with lipid deposits³⁷⁴. Infrared spectroscopy has helped to show that lipids may play a significant role in the first steps of the mineralisation process in the subcutaneous implant model, the lipid (phospholipids or triglycerides) content of the samples being directly correlated with the duration of implantation and preceding the appearance of phosphate⁴⁴⁴. Cholesterol (inherent or adsorbed during implantation) is also thought to be involved in intra-cellular pathologic calcification of bioprosthetic heart valves although the exact mechanism of this is not understood⁴⁴⁵. Furthermore, membrane-bound phospholipids have also been associated with calcification nucleation due to alkaline phosphatase hydrolysis²⁰². Alkaline phosphatase activity was found in both fresh and glutaraldehyde-treated bioprosthetic tissue²³¹.

1.7.2.3 Enzymatic activity:

It is believed that tissues treated with glutaraldehyde are rendered “non viable”^{446,447}. However, some enzymatic activity has been shown to be retained in various cellular fractions^{446,448}. In particular, it has been demonstrated that most hydrolases¹⁷⁷, in particular, proteases^{449,450}, are not inhibited by glutaraldehyde. It was suggested that tissue failure might be due to proteolytic enzymes originating from intrinsic (immobilised tissue proteases derived from devitalised cells) or extrinsic (infiltrating plasma and phagocytes) sources⁴⁵¹.

Early studies failed to find any correlation between enzyme activity (particularly alkaline phosphatase) and the mineralisation process in bioprosthetic valves⁴⁵²⁻⁴⁵⁴. However, it was subsequently reported that alkaline phosphatase was still active in cells within bioprosthetic bovine pericardial heart valves despite glutaraldehyde treatment²³¹ and that its distribution was correlated with the sites of early calcific deposits. In addition, the presence of alkaline phosphatase together with calcium-binding phosphoproteins was later shown to be associated with crystal formation in mineralising tissues⁴⁵⁵⁻⁴⁵⁷. Alkaline phosphatase can hydrolyse ATP and lead to the possible deposition of calcium and phosphate by matrix vesicles.

1.7.2.4 Mechanical stress factors:

Calcification in bioprosthetic valve tissue in association with mechanical stress is a controversial matter.

In-vivo bioprostheses are subjected to high levels of mechanical stress during each cardiac cycle, their leaflets undergoing cyclic loading and unloading with reversal of leaflet curvature and an extreme degree of flexion in the narrow zone of leaflet attachment⁴⁵⁸. This causes fatigue and flexion failure of the tissue resulting in loss of function⁴⁵⁹. In porcine valves, calcification initially occurs in the commissural regions where the stress is the highest and then later in the basal region (the middle of the leaflet, where a significant amount of flexion is observed).

Mechanical stress plays a role in the breakdown of collagen¹¹⁸ and it has been suggested that damaged collagen could be associated with focal calcification in-vitro^{367,375,376}. The calcification patterns, obtained from valves placed in a metastable calcium solution under dynamic loading, appear to be correlated with areas of sharp leaflet flexure where the mechanical stress is the greatest. It has been proposed that a likely mechanism of initiation of calcification is the breakdown of collagen resulting

from high local mechanical stress, which exposes calcium-binding sites previously protected by the intact surface, or the products of breakdown that can initiate calcification⁴⁶⁰.

Several other groups also postulated a close connection between the mechanical stress applied to a bioprosthetic heart valve and the process of calcification, although there was some uncertainty as to whether mechanical stress initiated calcification or vice versa⁴⁶¹. In another study, it was reported that dynamic stress may promote calcification but it is not essential, as subcutaneous implants, which are not subjected to mechanical deformation, also calcify³⁴³.

1.7.2.5 Cross-linking:

Glutaraldehyde remains the reagent of choice for bioprosthetic valve fabrication, because it improves biostability and structural integrity of treated-tissue³⁴⁶ and allows the treated-tissue to exhibit useful properties such as superior stability and tissue thromboresistance²⁰⁸. However, there is evidence to suggest that glutaraldehyde pre-treatment plays a critical role in calcification^{259,462} and subsequent mechanical degeneration of bioprosthetic heart valves in-vivo⁹⁸. The specific mechanisms by which glutaraldehyde fixation facilitates calcification are not fully understood¹²². It is ironic that the glutaraldehyde treatment itself, presently used in commercial valve processing, might be a calcification initiator. Glutaraldehyde cross-linking is thought to potentiate mineral deposition^{423,463,464}, possibly due to other structural deterioration of collagen, or by affecting the mechanical behaviour of the valves, with the tissue becoming stiffer and less flexible over time due to the extent of the glutaraldehyde process. Such findings suggest that the fundamental mechanisms of tissue mineralisation may depend on specific chemical modifications to the microstructural components of the tissue induced by the cross-linking agent. Untreated, type I collagen is resorbed within 3 weeks after implantation in the rat model without any sign of calcification³⁴⁶. Such implants are associated with a classic foreign body reaction, primarily composed of macrophages^{45,346}. Implanted aldehyde-treated purified type I collagen sponges, calcify in the absence of a foreign body reaction or cell-mediated mineral deposition^{259,465}, revealing the role of glutaraldehyde in decreasing the antigenicity of xenogeneic tissue as well as in calcification.

The glutaraldehyde process is also thought to alter the tissue by extracting some extracellular proteins (e.g. glycosaminoglycans (GAGs))⁴⁶⁶⁻⁴⁶⁸. It has been suggested that phosphate can form covalent bonds connecting inorganic and organic components via the 6-amino groups of lysine and hydroxylysine in collagen and that glycoproteins and proteoglycans (GAGs on protein back-bone), which would normally block these sites, are lost during processing of the tissue by glutaraldehyde⁵¹. This could initiate the mineralisation process. Additionally, this extraction mechanism may also create voids and cavities that form physical niches for calcification¹⁹⁰ and the morphologic equivalent of this loss is an abundance of water spaces in the tissue, which is associated with a high propensity for calcification^{170,466}. It has also been postulated that mineralisation is nucleated in the cells²⁴³ because of their devitalisation and the inactivation of their ion pumps by the glutaraldehyde process⁴⁶⁹. This would allow calcium to passively diffuse into the phosphate rich cells and accumulate leading to hydroxyapatite formation¹²². This mode of action would be analogous to the matrix vesicle theory of normal calcification (see section 1.6.2). Normal intra-cellular phosphorus levels are relatively high. Phosphate is incorporated in many proteins, lipids and the nucleus is especially prevalent within plasma and organellar membranes in the form of phospholipids. Schoen¹³, using electron energy loss spectrometry (EELS), demonstrated high concentrations of intra-cellular phosphorus in unimplanted, glutaraldehyde-preserved porcine aortic valves and bovine pericardium. He also showed the early entry of calcium ions at these sites following implantation.

In contrast, certain findings do not support the involvement of glutaraldehyde. Tissue stored in glutaraldehyde for more than 1 year are resistant to calcification⁴⁷⁰. In addition, valves treated with high concentrations of glutaraldehyde show diminished calcification⁴²⁸. Furthermore, contrary to the Schoen's hypothesis, glutaraldehyde cross-linking of an intact cell membrane may "freeze" the membrane-bound ion pumps rather than causing membrane breakdown, rendering it impermeable to sodium, potassium and calcium^{471,472}.

Another aspect of the effect of the cross-linking process is the loss of endothelial coverage. The aldehyde treatment also inhibits endothelial regrowth following implantation⁴⁷³. This is due to the toxicity of glutaraldehyde. This has been demonstrated in cell culture, where concentrations as low as 3 ppm^{427,474} or even 1

ppm⁴⁷⁵ were found to be toxic. The natural heart valve is totally covered by a confluent layer of endothelial cells¹⁵⁰, this prevents plasma insudation and fibrin and platelet aggregation⁴⁷⁶ and must in part be responsible for the absence of thrombosis on the surface of normal heart valves. The lack of cell growth on the bioprosthesis surface may decrease biocompatibility. Loss of endothelial cells are implicated in calcification, inflammation, an increase in surface thrombogenicity and degeneration of bioprosthetic heart valves⁴⁷³.

Glutaraldehyde-treated bioprostheses are known to slowly release glutaraldehyde over time, possibly by the partial hydrolytic degradation and reversibility of some cross-links^{163,477,478} (for example, Schiff bases possess a N=CH group which represents the hydrolysis-sensitive site⁴⁷⁹). It is also possible that unreacted glutaraldehyde is released from tissue or from the decomposition of its derivatives such as large molecular weight polymers (α,β -unsaturated polymers and acetal polymers-see chapter 2-) that can serve as a reservoir for the ongoing cytotoxic release of glutaraldehyde^{474,478}. It has been postulated that the glutaraldehyde measured might represent the degradation of only a fraction of all cross-links, most of which are thought to be stable⁴⁷⁵. It has also been postulated that this slow release of residual glutaraldehyde or free aldehyde moieties on the surface of the bioprosthesis tissue may play a role in calcification^{480,481}. It is also believed that unreacted glutaraldehyde can leach out into the body causing side effects, with its reaction products being cytotoxic^{427,482} and resulting in the deposition of cellular debris³⁴⁴. It was reported that hydrolysis is the main mechanism for glutaraldehyde being released at cytotoxic levels from glutaraldehyde cross-linked tendons for up to 6 months, even after extensive rinsing of the tendons⁴⁸³. It has also been speculated that it is polymerised hemi-acetals rather than the actual stable cross-links that cause calcification⁴²⁸.

The slow release of glutaraldehyde within tissue being a potential initiator for calcification, is supported by the fact that mineralisation is prevented by the use of binding agents that react with residual or free glutaraldehyde moieties⁴⁸². This basic idea of removing the unreacted glutaraldehyde residues by various methods, such as blocking with amino compounds has the potential to decrease calcification. Not all amino compounds are equally effective in preventing calcification⁴⁸⁰. This was suggested to be possibly related to the different "bridging effect" of the various

amino compounds (for example how many amino termini are available to react with the free aldehyde groups)⁴⁸⁰, although other reasons behind these discrepancies in the results remain unknown.

Tissue valve calcification has been hypothesised to correlate with the calcium-binding ability of glutaraldehyde polymers that are present on the surface of treated tissue⁴⁸⁴. That is, the final form of the cross-linked tissue tends to contain nucleophilic residues such as carbonyl oxygens^{485,486}. The reaction of glutaraldehyde with lysine side chains (lysyl and hydroxylysyl residues of collagenous tissue) may lead to an impaired balance between positively and negatively charged functional groups in the collagenous tissue, thus favouring calcium ion deposition⁴⁸⁷⁻⁴⁹⁰. Many reports have suggested a role for aldehyde-induced intra- and inter-molecular collagen cross-links in initiating tissue mineralisation^{190,491-493}. Quaternary pyridinium-type cross-links found in both elastin and collagen are also thought to serve as a nucleation point for calcification⁴⁹⁴. Moreover, a dipyridine structure was suggested to account for the high stability of the cross-links as well as being involved in calcification of glutaraldehyde-cross-linked collagen¹⁷⁰. This hypothesis was also confirmed by others⁴⁹⁵, who showed the possible involvement of cyclic cross-links. Additionally, it has been postulated that glutaraldehyde may cause calcification directly by the oxidation of free unreacted aldehyde groups (formyl), which might result in some carboxylic residues on the surface of the implant to attract and trap the host plasma calcium and contribute toward initiating calcification during implantation^{427,480,483}. It is easy to hypothesise that glutaraldehyde may oxidise to formylbutanoic acid since the air oxidation of aldehydes to carboxylic acids has been reported^{496,497}. Others agreed with this theory and proposed that blockage of the formyl groups should be effective in reducing calcification^{190,208,498}. However, this hypothesis has also been partially refuted⁴⁹⁵ in a report stating that neither NH₂ nor COOH groups seem to be involved in calcification in-vitro. They showed that cross-linking with hexamethylene diisocyanate, which only links with amino groups, did not induced calcification of the collagen. Furthermore all dermal sheep collagen were sterilised by ethylene oxide, which should block the remaining amino groups. In addition, cross-linking by acyl azide, which should block carboxyl residues, clearly reduced calcification of collagen, however, they believed that this is

not due to blockage of the carboxylic residues and that COOH groups are not involved in calcification.

In conclusion, in the production of commercial bioprosthetic heart valves, although cross-linking is necessary to minimise antigenicity and increase mechanical stability, the cross-linking process fails to prevent autolytic tissue degradation and extracellular component deprivation, and may, in fact, induce calcification.

1.7.3 Conclusion:

It is suggested that host metabolic and implant factors are responsible for the inherent propensity of bioprosthetic tissue to calcify⁴⁹⁹. The dynamic environment and exposure to blood promote but are not required for nucleation and growth of calcific deposits. Many factors potentially influencing mineralisation are still under active investigation. This thesis focuses on tissue and cross-linking factors.

1.8 Prevention of calcification with anticalcification treatments

The preclinical determination of the efficacy and safety of an anticalcification agent includes four stages: i) initial qualification using heterotopic implantation (rat model...), ii) hydrodynamic/durability testing (pulse simulator), iii) morphologic studies of unimplanted material to assess treatment-induced degradation and iv) valve replacement (orthotopic implantation) in an animal model (sheep). The durability of valves treated with such agents can only be assessed with certainty by long-term clinical follow-up (>10years).

Until now, the predominant chemical treatment for biological tissues has been cross-linking with glutaraldehyde. To date there has been no clinically proven effective strategy for preventing the calcification of bioprosthetic heart valves, or a successful replacement for glutaraldehyde. One reason for this is that the exact mechanism of induction and propagation of calcification is not well defined and thus a method to prevent it remains unclear. Various strategies for prevention of bioprosthetic valve mineralisation involve modification of either the implant or its local environment. These include (i) blocking the free aldehyde groups left after the glutaraldehyde treatment to avoid subsequent reactions; (ii) removal of potentially calcifiable materials from the tissue; (iii) inhibiting the mineral growth; (iv) altering the overall

surface charge; or (v) using alternative cross-linking agents in tandem with glutaraldehyde fixation.

The fundamental mechanisms of tissue mineralisation depend on specific biochemical modifications (such as glutaraldehyde fixation) to implant microstructural components induced by aldehyde or other pre-treatment. It was suggested in the early 1980s that reduced-calcification would possibly be attained using alternative cross-linking agents¹⁷⁶. Therefore, many alternative cross-linking methods^{208,500,501} were sought. Multifactorial approaches have been suggested⁵⁰². These approaches include careful removal of non-covalently bound glutaraldehyde or labile-associated non-bifunctionally unreacted residues of glutaraldehyde by thorough rinsing or neutralisation before implantation, removal of lipids and non-collagenous proteins (ideally including the antigenic nonhelical collagen telopeptides), along with a treatment which would interfere with potential crystal growth (such as a biphosphonate) in order to prevent the accumulation of any mineral in the tissue. This approach is valid, although a definitive treatment is difficult to achieve. More research is needed in order to understand the process of mineralisation and its co-factors.

1.9 Outline of the project

The reactions of glutaraldehyde with collagen remain incompletely understood. A number of studies have investigated the reactions of glutaraldehyde with a range of model compounds, from the simplest amino acids to complex collagenous tissue. A number of structures have been proposed for reactions products (see chapter 2) but at present there is no definitive understanding of the processes that take place. An understanding of the interactions between glutaraldehyde and tissue is essential in order if we are to comprehend why bioprostheses calcify and ultimately fail. Furthermore, the exact mechanism of calcification is unknown. Previous work approached this issue in an empirical fashion, due to the lack of specific knowledge regarding the mechanism of calcification. It is likely that the mechanism involves, amongst other factors, a contribution from both the tissue and the aldehyde fixative (glutaraldehyde) used routinely in the manufacturing process.

The aims of the present study are as follows:

- To study the behaviour of glutaraldehyde in solution to further our understanding of the nature of this compound in aqueous solution.
- To study the reactions between glutaraldehyde and amines, peptides and proteins, to determine the structures of the likely reaction products, and to extrapolate these to those occurring during the glutaraldehyde pre-treatment of bioprosthetic valves.
- To investigate the possible involvement of glutaraldehyde and the collagenous tissue itself in the calcification mechanism, by mimicking the effect of the glutaraldehyde treatment using various amino acids, peptides and protein models, in order to investigate the relationship between the products and the calcification process.
- To develop a methodology to investigate the calcification of bioprosthetic heart valves using an environmental scanning electron microscope (ESEM).
- To apply this methodology to allow the study of the dystrophic calcification process using calcified clinical explants, in-vivo screening (rat subcutaneous implantation model) and in-vitro screening (pericardial tissue incubated in metastable calcification solution). Additionally, to compare the results obtained in-vitro and in-vivo and assess any similarities.

1. Anonymous. Une premiere dans un hopital de Louisville, au Kentucky: Un coeur artificiel entierement autonome. In: *Le Figaro Journal*. Paris; 2001:1/12.
2. Schoen FJ, Levy RJ. Tissue heart valves: current challenges and future research perspectives. *Journal of Biomedical Materials Research*. 1999;47:439-465.
3. Schoen FJ. Approach to the analysis of cardiac valve prostheses as surgical pathology or autopsy specimens. *Cardiovascular Pathology*. 1995;4:241-255.
4. Edwards MB, Taylor KM. A profile of valve replacement surgery in the UK (1986-1997): a study from the UK heart valve registry. *Journal of Heart Valve Disease*. 1999;8:697-701.
5. Edwards MB, Taylor KM. The UK Heart Valve Registry Report. Collated data up to 1998. *2000 Report*. 2000.
6. Istvan O, Laszlo M, Erika N, Ersebet N. Experience in the care of patients with artificial heart valves. *Orvosi-Hetilap*. 1994;135:2523-2526.
7. Black MM, Cochrane T, Drury PJ, Lawford PV. Artificial heart valves: past performance and future prospects. *Cardiovascular Reviews and Reports*. 1987;8:40-45.
8. Schoen FJ. The Heart. In: Cotran RS, Kumar V, Robbins SL, Schoen FJ, eds. *Pathologic Basis of Disease*. 5th ed. London: W.B. Saunders Company; 1994:517-582.
9. Marks C, Marks PH. In: *Fundamentals of Cardiac Surgery*. London: Chapman and Hall Medical; 1993:3-115.
10. Jamieson WRE, Burr LH, Munro AI. Cardiac valve replacement in the ederyly: clinical performance of biological prosthesis. *Annals of Thoracic Surgery*. 1989;48:173-185.

11. Jamieson WRE, Tyers GF, Miyagishima RT. Carpentier-Edwards porcine bioprosthesis. Comparison of standard and supra-annular prosthesis at 7 years. *Circulation*. 1991;suppl.3:145-152.
12. Jamieson WRE, Tyers GF, Janusz MT. Age as a determinant for selection of porcine bioprosthesis for cardiac valve replacement: experience with Carpentier-Edwards standard bioprosthesis. *Canadian Journal of Cardiology*. 1991;7:181-188.
13. Schoen FJ. Cardiac valve prostheses: pathological and bioengineering considerations. *Journal of Cardiac Surgery*. 1987;2:65-108.
14. Ishihara T, Ferrans VJ, Jones M. Occurrence and significance of endothelial cells in implanted porcine bioprosthetic valves. *American Journal of Cardiology*. 1981;48:443-452.
15. Logeais Y, Langanay T, Leguerrier A, Rioux C, Chaperon J, Coutte MB. Aortic Carpentier-Edwards supraannular porcine bioprosthesis: a twelve-year experience. *Annals of Thoracic Surgery*. 1999;68:421-425.
16. Legarra JJ, Llorens R, Catalan M. Eighteen-year follow-up after Hancock II bioprosthesis insertion. *Journal of Heart Valve Disease*. 1999;8:16-24.
17. Neville PH, Aupart MR, Diemont FF, Sirinelli AL, Lemoine EM, Marchand MA. Carpentier-Edwards pericardial bioprosthesis in aortic or mitral position: a twelve year experience. *Annals of Thoracic Surgery*. 1998;66:143-147.
18. Fiane AE, Saatvedt K, Svennevig JL. Carpentier-Edwards bioprosthesis: experience of 17 years with analysis of risk factors of early mortality. *Scandinavian Cardiovascular Journal*. 1997;31:39-44.
19. Hurle A, Meseguer J, Llamas P, Casillas JA. Clinical experience with the Carpentier-Edwards supraannular porcine bioprosthesis implanted in the aortic position. *Journal of Heart Valve Disease*. 1998;7:331-335.
20. Jamieson WRE, Munro AI, Miyagishima RT, Allen P, Burr LH, Tyers GF. Carpentier-Edwards standard porcine bioprosthesis: clinical performance to seventeen years. *Annals of Thoracic Surgery*. 1996;60:999-1007.
21. Grunkemeier GL, Rahimtoola SH. Artificial Heart Valves. *Annual Review in Medicine*. 1990;41:251-263.
22. Jamieson WR. Modern cardiac valve-devices-bioprostheses and mechanical prostheses: state of the art. *Journal of Cardiac Surgery*. 1993;8:89-98.
23. Schoen FJ, Levy RJ, Piehler HR. Pathological considerations in replacement cardiac valves. *Cardiovascular Pathology*. 1992;1:29-52.
24. Turina J, Hess OM, Turina M, Krayenbuehl HP. Cardiac bioprostheses in the 1990's. *Circulation*. 1993;88:775-781.
25. Vongpatanasin W, Hillis D, Lange RA. Prosthetic heart valves. *New England Journal of Medicine*. 1996;335:407-416.
26. Bloomfield P, Wheatley DJ, Prescott RJ, Miller HC. Twelve-year comparison of a Bjork-Shiley mechanical heart valve with porcine bioprostheses. *New England Journal of Medicine*. 1991;324:573-579.
27. Hammermeister KE, Sethi GK, Henderson WG. A comparison of outcomes in men 11 years after heart-valve replacement with mechanical valve or bioprosthesis. *New England Journal of Medicine*. 1993;328:1289-1296.
28. Black MM. Artificial heart valves: past performance and future trends. *Biomedical Polymers*. 1988;3:1-4.
29. Salazar E, Zajarias AN, Iturbe I. The problem of cardiac valve prostheses, anticoagulants, and pregnancy. *Circulation*. 1984;74:1-169.
30. Bortolotti U, Milano A, Mazzucco A. Pregnancy in patients with a porcine valve bioprosthesis. *American Journal of Cardiology*. 1982;50:1051-1060.
31. Carpentier A. Utilisation d' heterogreffes dans le traitement des liaisons valvulaires aortiques. In: Paris: Foulon; 1966.
32. Kaiser GA, Hancock WD, Lukban SB, Salvador BL, Litwack RS. Clinical use of a new design stented xenograft heart valve prosthesis. *Surgical Forum*. 1969;20:137-138.
33. Jamieson WRE, Allen P, Miyagishima RT. The Carpentier-Edwards standard porcine bioprosthesis: a first generation tissue valve with excellent long term clinical performance. *Journal of Thoracic and Cardiovascular Surgery*. 1990;99:543-561.
34. Bernal JM, Rabasa JM, Cagigas JC, Echevarria JR, Carrion MF, Revuelta JM. Valve related complications with the Hancock I porcine bioprosthesis. *Journal of Thoracic and Cardiovascular Surgery*. 1991;101:871-880.

35. Carpentier A, Dubost C, Lane E. Continuing improvements in valvular prostheses. *Journal of Thoracic and Cardiovascular Surgery*. 1982;83:27-42.
36. Torka MC, Salefsky BE, Hacker RW. Intermediate clinical results after cardiac valve replacement with the Carpentier-Edwards pericardial bioprosthesis. *Annals of Thoracic Surgery*. 1995;60:S311-S315.
37. Pellerin M, Mihaileanu S, Couetil JP, Relland JY, Deloch A, Fabiani JN, Carpentier AF. Carpentier-Edwards pericardial bioprosthesis in the aortic position: long-term follow up 1980-1994. *Annals of Thoracic Surgery*. 1995;60:S292-S295.
38. Aupart MR, Sirinelli AL, Diemont FF, Meurisse YA, Dreyfus XB, Marchand MA. The last generation of pericardial valves in the aortic position: ten year follow-up in 589 patients. *Annals of Thoracic Surgery*. 1996;61:615-620.
39. Williams MA. The Intact bioprosthesis: early results. *Journal of Cardiac Surgery*. 1988;3:347-351.
40. Oury JH, Angell WW, Koziol JA. Comparison of Hancock I and Hancock II bioprostheses. *Journal of Cardiac Surgery*. 1988;3:375-381.
41. David TE, Ivanov J, Armstrong S, Feindel CM, Cohen G. Late results of heart valve replacement with the Hancock II bioprosthesis. *Journal of Thoracic and Cardiovascular Surgery*. 2001;121:268-278.
42. Jamieson WRE, Burr LH, Tyers GF, Munro AI. Carpentier-Edwards standard and supraannular porcine bioprostheses: ten year comparison of structural valve deterioration. *Journal of Heart Valve Disease*. 1994;3:59-65.
43. Schoen FJ, Levy RJ. Bioprosthetic heart valve failure: pathology and pathogenesis. *Cardiology Clinics*. 1984;2:717-739.
44. Schoen FJ, Kujovich JL, Webb CL, Levy RJ. Chemically determined mineral content of explanted porcine aortic valve bioprostheses: correlation with radiographic assessment of calcification and clinical data. *Circulation*. 1987;76:1061-1066.
45. Schoen FJ, Hobson CE. Anatomic analysis of removed prosthetic heart valves: causes of failure of 33 mechanical valves and 58 bioprostheses 1980 to 1983. *Human Pathology*. 1985;16:549-558.
46. Bortolotti U, Milano A, Mazzucco A. Results of reoperation for primary tissue failure of porcine bioprostheses. *Journal of Cardiovascular Surgery*. 1985;90:564-573.
47. Butany J, Yu W, Silver MD, David TE. Morphologic findings in explanted Hancock II porcine bioprostheses. *Journal of Heart Valve Disease*. 1999;8:4-15.
48. Jamieson WRE, Marchand MA, Pelletier CL, Norton R, Pellerin M, Dubiel TW, Aupart MR, Daenen WJ, Holden MP, David TE, Ryba EA, Anderson JWN. Structural valve deterioration in mitral valve replacement surgery: comparison of Carpentier-Edwards supraannular and Perimount pericardial. *Journal of Thoracic and Cardiovascular Surgery*. 1999;118:297-305.
49. Burdon TA, Miller DC, Oyer PE. Durability of porcine valves at fifteen years in a representative north American patient population. *Journal of Thoracic and Cardiovascular Surgery*. 1992;103:238-252.
50. Sarris GE, Robbins RC, Miller DC. Randomised, prospective assessment of bioprosthetic valve durability. *Circulation*. 1993;88:55-64.
51. Ferrans VJ, Boyce SW, Billingham ME, Jones M, Ishihara T, Roberts WC. Calcific deposits in porcine bioprostheses: structure and pathogenesis. *American Journal of Cardiology*. 1980;46:721-734.
52. Biedrzycki LM, Lerner E, Levy RJ, Schoen FJ. Differential calcification of cusps and aortic wall of failed stented porcine bioprosthetic valves. *Journal of Biomedical Materials Research*. 1997;34:411-415.
53. Grunkemeier GL, Bodnar E. Comparative assessment of bioprosthesis durability in the aortic position. *Journal of Heart Valve Disease*. 1995;4:49-55.
54. Jin XY, Pepper JR. Do stentless valves make a difference? *European Journal of Cardio-Thoracic Surgery*. 2002;22:95-100.
55. David TE, Feindel CM, Scully HE, Bos J, Rakowski H. Aortic valve replacement with stentless porcine aortic valves: a ten-year experience. *Journal of Heart Valve Disease*. 1998;7:250-254.
56. Westaby S, Jin XY, Katsuma T, Arifi A, Baidley P. Valve replacement with a stentless bioprosthesis: versatility of the porcine aortic root. *Journal of Thoracic and Cardiovascular Surgery*. 1998;116:477-484.
57. David TE, Ropchan GC, Butany JW. Aortic valve replacement with stentless porcine bioprostheses. *Journal of Cardiac Surgery*. 1988;3:501-505.

58. David TE, Pollick C, Bos J. Aortic valve replacement with stentless porcine aortic bioprosthesis. *Journal of Thoracic and Cardiovascular Surgery*. 1990;99:113-118.
59. David TE, Puschman R, Ivanov J, Bos J, Armstrong S, Feindel CM, Scully HE. Aortic valve replacement with stentless and stented porcine valves: a case-match study. *Journal of Thoracic and Cardiovascular Surgery*. 1998;116:236-241.
60. Lockie KJ, Fisher J, Juster NP, Davies GA, Watterson K. Biomechanics of glutaraldehyde-treated porcine aortic roots and valves. *Journal of Thoracic and Cardiovascular Surgery*. 1994;108:1037-1042.
61. Walther T, Falk V, Autschbach R. Hemodynamic assessment of the stentless Toronto SPV bioprosthesis by echocardiography. *Journal of Heart Valve Disease*. 1994;3:657-665.
62. Hazekamp MG, Goffin YA, Huysmans HA. The value of the stentless biovalve prosthesis, an experimental study. *European Journal of Cardio-Thoracic Surgery*. 1993;7:514-519.
63. Frater RWB, Salomon NW, Rainer WG, Cosgrove DM, Wickham E. The Carpentier-Edwards pericardial valve: intermediate results. *Annals of Thoracic Surgery*. 1992;53:764-771.
64. Ionescu MI, Tandon AP. The Ionescu-Shiley pericardial xenograft heart valve. In: Ionescu MI, ed. *Tissue Heart Valves*. London: Butterworths; 1979:201-253.
65. Daenen WJ, Noyez L, Lasaffre E. The Ionescu-Shiley pericardial valve: results in 473 patients. *Annals of Thoracic Surgery*. 1988;46:536-541.
66. Gallo I, Nistal F, Revuelta JM, Garcia-Statue E, Artinano E, Duran CG. Incidence of primary valve failure with the Ionescu-Shiley pericardial valve. *Journal of Thoracic and Cardiovascular Surgery*. 1985;90:278-280.
67. Leandri J, Bertrand P, Mazzucotelli JP, Loisanse D. Mode of failure of the Mitroflow pericardial valve. *Journal of Heart Valve Disease*. 1992;1:225-231.
68. Gabbay S, Bortolotti U, Wasserman F, Tindel N, Factor SM, Frater RWM. Long-term follow-up of the Ionescu-Shiley mitral pericardial xenograft. *Journal of Thoracic and Cardiovascular Surgery*. 1984;88:758-763.
69. Brais MP, Bedard JP, Goldstein W, Koshal A, Keon WJ. Ionescu-Shiley pericardial xenografts: follow-up of up to six years. *Annals of Thoracic Surgery*. 1985;39:105-114.
70. Walley VM, Keon CA, Khalili M, Moher D, Campagna M, Keon WJ. Ionescu-Shiley valve failure I. Experience with 125 standard-profile explants. *Annals of Thoracic Surgery*. 1992;54:111-116.
71. Walley VM, Keon CA, Khalili M, Moher D, Campagna M, Keon WJ. Ionescu-Shiley valve failure II. Experience with 25 low-profile explants. *Annals of Thoracic Surgery*. 1992;54:117-123.
72. Fisher J, Wheatley DJ. An improved pericardial bioprosthetic heart valve: design and laboratory evaluation. *European Journal of Cardio-Thoracic Surgery*. 1987;1:71-79.
73. Baxter International Inc. Carpentier-Edwards Perimount Pericardial Bioprosthesis Model 2700. *Clinical Communique*. 1998.
74. Frater RWB, Furlong P, Cosgrove DM, Okies JE, Colburn LQ, Katz AS, Lowe NL, Ryba EA. Long-term durability and patient functional status of the Carpentier-Edwards Perimount pericardial bioprosthesis in the aortic position. *Journal of Heart Valve Disease*. 1998;7:48-53.
75. Aupart M, Neville P, Dreyfus X. The Carpentier-Edwards pericardial aortic valve: intermediate results in 420 patients. *European Journal of Cardio-Thoracic Surgery*. 1994;8:277-280.
76. Deiwick M, Glasmacher B, Pettenazzo E, Hammel D, Castellon W, Thiene G, Reul H, Berendes E, Scheld HH. Primary tissue failure of bioprostheses: new evidence from in-vitro tests. *Journal of Thoracic and Cardiovascular Surgery*. 2001;49:78-83.
77. Hacker RW, Urbanski P, Jachmann U, Schneider A. Clinical comparison between the Toronto SPV valve and the Carpentier-Edwards Perimount valve. *11th International Symposium of the Denton A. Cooley Cardiovascular Surgical Society Meeting*. 1998;August 1-5:20-21.
78. Ionescu MI, Smith DR, Hasen SS. Clinical durability of the pericardial xenograft valve: ten years experience with mitral replacement. *Annals of Thoracic Surgery*. 1982;34:265-277.
79. Reul GJ, Cooley DA, Duncan JM. Valve failure with the Ionescu-Shiley bovine pericardial bioprosthesis: analysis of 2680 patients. *Journal of Vascular Surgery*. 1985;2:192-204.
80. Nistal F, Garcia-Statue E, Artinano E. Comparative study of primary tissue failure between Ionescu-Shiley pericardial and Hancock porcine valves in the aortic position. *American Journal of Cardiology*. 1986;57:161-170.

81. Cosgrove DM, Lytle BW, Taylor PC, Camacho MT, Stewart RW, McCarthy PM, Miller DP, Piedmont MR, Loop FD. The Carpentier-Edwards pericardial aortic valve: ten-year results. *Journal of Thoracic and Cardiovascular Surgery*. 1995;110:651-662.
82. Ross DN. Homograft replacement of the aortic valve. *The Lancet*. 1962;2:487-492.
83. Barratt-Boyes BG. A method for preparing and inserting a homograft aortic valve. *British Journal of Surgery*. 1965;52:847-855.
84. Ross DN. Replacement of the aortic and mitral valve with a pulmonary autograft. *The Lancet*. 1967;2:956.
85. Kouchoukos NT, Davila-Roman VG, Spray TL, Murphy SF, Perrillo JB. Replacement of the aortic root with a pulmonary autograft in children and young adults with aortic-valve disease. *New England Journal of Medicine*. 1994;330:1-6.
86. Chambers JC, Somerville J, Stone S, Ross DN. Pulmonary autograft procedure for aortic valve disease: long-term results of the pioneer series. *Circulation*. 1997;96:2206-2214.
87. Bjork VO, Hultquist G. Teflon and pericardial aortic valve prosthesis. *Journal of Thoracic Surgery*. 1964;47:693-701.
88. Osinowo O, Monro JL, Ross JK. The use of glycerol-preserved homologous dura mater grafts in cardiac surgery: the Southampton experience. *Annals of Thoracic Surgery*. 1985;39:367-370.
89. Senning A. Fascia lata replacement of aortic valves. *Journal of Thoracic and Cardiovascular Surgery*. 1967;54:465-470.
90. Silver MD, Hudson REB, Trimble AS. Morphologic observations on heart valve prostheses made of fascia lata. *Journal of Thoracic and Cardiovascular Surgery*. 1975;70:360-369.
91. Senning A. Aortic valve replacement with fascia lata. *Acta Chirurgica Scandinavica*. 1966;365B:17-20.
92. Carpentier A, Lemaigre G, Rober L, Carpentier S, Dubost C. Biological factors affecting long-term results of valvular heterografts. *Journal of Thoracic and Cardiovascular Surgery*. 1969;58:467-483.
93. Yarborough J, Roberts WC, Reis RL. Structural alterations in tissue cardiac valves implanted in patients and in calves. *Journal of Thoracic and Cardiovascular Surgery*. 1973;65:364-373.
94. Hisatomi K, Isomura T, Sato T, Kosuga K, Ohishi K, Katoh H. Mitral valve repair for regurgitation with ventricular septal defect in children. *Annals of Thoracic Surgery*. 1996;62:1773-1777.
95. Love JW, Calvin JH, Phelan RF, Love CS. Rapid intraoperative fabrication of an autologous tissue heart valve: a new technique. In: Bodnar E, Yacoub M, eds. *Proceedings of the Third International Symposium on Cardiac Bioprotheses*. New York: Yorke Medical Books; 1986:691-698.
96. Love CS, Love JW. The autologous tissue heart valve: current status. *Journal of Cardiac Surgery*. 1991;6:499-507.
97. Love JW, Schoen FJ, Breznock EM, Shermer SP, Clove CS. Experimental evaluation of an autologous tissue heart valve. *Journal of Heart Valve Disease*. 1992;1:232-241.
98. Liao K, Frater RWM, LaPietra A, Ciuffo G, Ilardi CF, Seifter E. Time-dependent effect of glutaraldehyde on the tendency to calcify of both autografts and xenografts. *Annals of Thoracic Surgery*. 1995;60:S343-S347.
99. Kumar MN, Prabhakar G, Kumar N, Shahid M, Becker AE, Duran CMG. Autologous glutaraldehyde-treated pericardial valved conduit: an experimental study. *Annals of Thoracic Surgery*. 1995;60:S200-S204.
100. Haluck RS, Richenbacher WE, Myers JL, Miller CA, Wise RK, Waldhausen JA. Pericardium as a thoracic aortic patch: glutaraldehyde-fixed and fresh autologous pericardium. *Journal of Surgical Research*. 1990;48:611-614.
101. Gross C, Simon P, Grabenwoger M, Mair R, Sihorsch K, Grimm M, Brucke P. Midterm results after aortic valve replacement with the autologous tissue cardiac valve. *European Journal of Cardio-Thoracic Surgery*. 1999;16:533-539.
102. Hiester ED, Sacks MS. Optimal bovine pericardial tissue selection sites I. Fiber architecture and tissue thickness measurements. *Journal of Biomedical Materials Research*. 1998;39:207-214.
103. Salles CA, Buffolo E, Andrade JC, Palma JH, Silva RRP, Santiago R, Casagrande IS, Consolacao M, Moreira V. Mitral valve replacement with glutaraldehyde preserved aortic allografts. *European Journal of Cardio-Thoracic Surgery*. 1998;13:135-143.

104. Schoen FJ, Titus JL, Lawrie GM. Autopsy-determined causes of death after cardiac valve replacement. *Journal of the American Medical Association*. 1983;249:899-902.
105. Schoen FJ, Titus JL, Lawrie GM. Bioengineering aspects of heart valve replacement. *Annals of Biomedical Engineering*. 1982;10:97-106.
106. Edmunds LH, Clark RE, Cohn LH, Miller DC, Weisel RD. Guidelines for reporting morbidity and mortality after cardiac valvular operations. *Journal of Thoracic and Cardiovascular Surgery*. 1988;96:351-353.
107. Foster AH, Greenberg GJ, Underhill DJ, McIntosh CL, Clark RE. Intrinsic failure of Hancock mitral bioprostheses: 10 to 15 years experience. *Annals of Thoracic Surgery*. 1987;44:568-577.
108. Milano AD, Bortolotti U, Mazzucco A. Performance of the Hancock porcine bioprosthesis following aortic valve replacement: considerations based on a 15 year experience. *Annals of Thoracic Surgery*. 1988;46:216-222.
109. Walley VM, Keon WJ. Patterns of failure in Ionescu-Shiley bovine pericardial bioprosthetic valves. *Journal of Thoracic and Cardiovascular Surgery*. 1987;93:925-933.
110. Bortolotti U, Milano A, Guerra F. Failure of Hancock pericardial xenografts: is prophylactic bioprosthetic replacement justified? *Annals of Thoracic Surgery*. 1991;51:430-437.
111. Kopf GS, Geha AS, Hellenbrandt WE, Kleinman CS. Fate of left-sided cardiac bioprosthesis valves in children. *Archives of Surgery*. 1986;121:488-490.
112. Schoen FJ, Fernandez J, Gonzales-Lavin L, Cernaianu A. Causes of failure and pathologic findings in surgically removed Ionescu-Shiley standard bovine pericardial heart valve bioprostheses: emphasis on progressive structural deterioration. *Circulation*. 1987;76:618-627.
113. Magilligan DJ, Lewis JW, Tilley B, Peterson E. The porcine bioprosthetic valve: twelve years later. *Journal of Thoracic and Cardiovascular Surgery*. 1985;89:499-507.
114. Valente M, Bortolotti U, Thiene G. Ultrastructural substrates of dystrophic calcification in porcine bioprosthetic valve failure. *American Journal of Pathology*. 1985;119:12-21.
115. Sands MP, Rittenhouse EA, Mohri H, Merendino KA. An anatomical comparison of human, pig, calf and sheep aortic valves. *Annals of Thoracic Surgery*. 1969;8:407-414.
116. Carpentier A. From valvular xenograft to valvular bioprosthesis (1965-1977). *Medical Instrumentation*. 1977;11:98-101.
117. Minns RJ, Soden PD, Jackson DS. The role of fibrous components and ground substance in the mechanical properties of biological tissues: a preliminary investigation. *Journal of Biomechanics*. 1973;6:153-165.
118. Ferrans VJ, Spray TC, Billingham ME, Roberts WC. Structural changes in glutaraldehyde-treated porcine heterografts used as substitute cardiac valves. Transmission and scanning electron microscopy observation in 12 patients. *American Journal of Cardiology*. 1978;41:1159-1184.
119. Mannschott P, Herbage D, Weiss M. Collagen heterogeneity in pig heart valves. *Biochimica et Biophysica Acta*. 1976;434:177-183.
120. Scott MJ, Vesely I. Morphology of porcine aortic valve cusp elastin. *Journal of Heart Valve Disease*. 1996;5:464-471.
121. Vesely I. The role of elastin in aortic valve mechanisms. *Journal of Biomechanics*. 1998;31:115-123.
122. Schoen FJ, Tsao JW, Levy RJ. Calcification of bovine pericardium used in cardiac valve bioprostheses. Implications for the mechanism of bioprosthetic tissue mineralisation. *American Journal of Pathology*. 1986;123:134-145.
123. Simionescu D, Alper R, Kefalides NA. Partial characterisation of a low molecular weight proteoglycan isolated from bovine parietal pericardium. *Biochemical and Biophysical Research Communications*. 1988;151:480-486.
124. Simionescu D, Iozzo RV, Kefalides NA. Bovine pericardial proteoglycan, biochemical, immunological and ultrastructural studies. *Matrix*. 1989;9:301-310.
125. Trowbridge EA, Roberts KM, Crofts CE, Lawford PV. Pericardial heterografts, towards quality control of the mechanical properties of glutaraldehyde-fixed leaflets. *Journal of Thoracic and Cardiovascular Surgery*. 1986;92:21-28.
126. Fentie IH, Allen DJ, Schenck MH, Didio LJ. Comparative electron microscopic study of bovine, porcine and human parietal pericardium, as materials for cardiac valve bioprostheses. *Journal of Submicroscopic Cytology*. 1986;18:53-65.
127. Trowbridge E. Mechanical characteristics of pericardial tissue and their relevance to bioprosthetic design. *Critical Review of Biocompatibility*. 1989;5:105-172.

128. Crofts CE, Trowbridge EA. Local variation in the tearing strength of chemically modified pericardium. *Biomaterials*. 1989;10:230-234.
129. Lee JM, Haberer SA, Boughner DR. The bovine pericardial xenograft I. Effect of fixation in aldehydes without constraint on the tensile properties of bovine pericardium. *Journal of Biomedical Materials Research*. 1989;23:457-475.
130. Simionescu D, Simionescu A, Deac R. Mapping of glutaraldehyde-treated bovine pericardium and tissue selection for bioprosthetic heart valves. *Journal of Biomedical Materials Research*. 1993;27:697-704.
131. Trowbridge EA, Black MM, Daniel CL. The mechanical response of glutaraldehyde fixed bovine pericardium to uniaxial load. *Journal of Materials Science*. 1985;20:114-140.
132. Ishihara T, Ferrans VJ, Jones M. Structure of bovine parietal pericardium and of unimplanted Ionescu-Shiley pericardial valvular bioprostheses. *Journal of Thoracic and Cardiovascular Surgery*. 1981;81:747-757.
133. Ishihara T, Ferrans VJ, Jones M, Boyce SW, Kawanami O, Roberts WC. Histologic and ultrastructural features of normal human parietal pericardium. *American Journal of Cardiology*. 1980;46:744-753.
134. Bashey RI, Torii S, Angrist A. Age-related collagen and elastin content of human heart valves. *Journal of Gerontology*. 1967;22:203-208.
135. Anwar RA, Gerber GE, Baig KM. Studies on crosslinked regions of elastin. *Advances of Experimental Medical Biology*. 1977;86:709-727.
136. Partridge SM. Elastin. *Advances in Protein Chemistry*. 1962;17:227.
137. Thomas J, D.F. E, Partridge SM. Degradation products from elastin. *Nature*. 1963;200:651-652.
138. Anwar RA. Comparison of elastins from various sources. *Canadian Journal of Biochemistry*. 1966;44:725.
139. Foster JA, Rubin L, Kagan HM, Franzblau C, Bruenger E, Sandberg LB. Isolation and characterisation of cross-linked peptides from elastin. *Journal of Biological Chemistry*. 1974;249:6191-6196.
140. Franzblau C, Sinex FM, Faris B, Lampidis R. Identification of a new crosslinking amino acid in elastin. *Biochemica et Biophysica Research Communication*. 1965;21:575.
141. Lent RW, Franzblau C. Studies on the reduction of bovine elastin: evidence for the presence of delta6,7-dehydrolysinorleucine. *Biochemical and Biophysical Research Communications*. 1967;26:43-50.
142. Starcher BC, Partridge SM, Elsdén DF. Isolation and partial characterisation of a new amino acid from reduced elastin. *Biochemistry Journal*. 1967;6:2425.
143. Miller EJ, Pinnell SR, Martin GR, Schiffman E. Investigation of the intermediates involved in desmosine biosynthesis. *Biochemica et Biophysica Research Communication*. 1967;26:132.
144. Lent RW, Smith B, Salcedo LL, Faris B, Franzblau C. Studies on the reduction of elastin II. Evidence for the presence of alpha-amino adipic acid delta-semialdehyde and its aldol condensation product. *Biochemistry Journal*. 1969;8:2837.
145. Sandberg LB, Weissman N, Gray WR. Structural features of tropoelastin related to the sites of crosslinks in aortic elastin. *Biochemistry Journal*. 1971;10:52-56.
146. Partridge SM, Elsdén DF, Thomas J, Dorfman A, Telser A, Ho PL. Incorporation of labelled lysine into the desmosine crossbridges in elastin. *Nature*. 1966;209:399.
147. Davies NR, Anwar RA. On the mechanism of formation of desmosine and isodesmosine crosslinks of elastin. *Journal of the American Chemical Society*. 1970;92:3778-3782.
148. Paz MA, Gallop PM, Blumenfeld OO, Henson E, Seifter S. The presence in elastin of possible cyclic precursors of desmosine and isodesmosine. *Biochemical and Biophysical Research Communications*. 1971;43:289-297.
149. Jacob MP, Robert L. Isolation, characterisation and biochemical properties of elastin. In: Robert L, Hornberck W, eds. *Elastin and Elastases*. Boca Raton: CRC Press; 1989:49-66.
150. Clark RE, Finke EH. Scanning and light microscopy of human aortic leaflets in stressed and relaxed states. *Journal of Thoracic and Cardiovascular Surgery*. 1974;67:792-804.
151. Christie GW. Anatomy of aortic heart valve leaflets: the influence of glutaraldehyde fixation on function. *European Journal of Cardio-Thoracic Surgery*. 1992;6:S25-S33.
152. Oxlund H, Manschot J, Viidik A. The role of elastin in the mechanical properties of skin. *Journal of Biomechanics*. 1988;21:213-218.
153. Kuhn K. The classical collagens: type I, II, III. In: Mayne R, Burgeson RE, eds. *Structure and Function of Collagen Types*. New York: Academic Press; 1987:1-42.

154. In: Smith CA, Wood EJ, eds. *Cell Biology*. London: Chapman et Hall; 1996:252-283.
155. In: Darnell J, Lodish H, Baltimore D, eds. *Molecular Cell Biology*. New York: Scientific American Books; 1990:906-915.
156. Nimni ME, Harkness RD. Molecular structures and functions of collagen. In: Nimni ME, ed. *Collagen*. Boca Raton: CRC Press; 1988:1-77.
157. Colin W, Donoff RB. Nerve regeneration through collagen tubes. *Journal of Dental Research*. 1984;63:987-993.
158. Harriger MD, Supp AP, Warden GD, Boyce ST. Glutaraldehyde crosslinking of collagen substrates inhibits degradation in skin substitutes grafted to athymic mice. *Journal of Biomedical Materials Research*. 1997;35:137-145.
159. Goissis G, Marcantonio E, Marcantonio RAC, Lia RCC, Cancian DCJ, Carvalho WM. Biocompatibility studies of anionic collagen membranes with different degree of glutaraldehyde crosslinking. *Biomaterials*. 1999;20:27-34.
160. Burke KE, Naughton G, Waldo E, Cassai N. Bovine collagen implant: histologic chronology in pig dermis. *Journal of Dermatology and Surgical Oncology*. 1983;9:889-895.
161. DeLustro F, Smith ST, Sundsmo J, Salem G, Kincaid S, Ellingsworth L. Reaction to injectable collagen: results in animal models and clinical use. *Plastic Reconstruction Surgery*. 1987;79:581-592.
162. Yannas IV, Burke JF. Design of an artificial skin I. Basic design principles. *Journal of Biomedical Materials Research*. 1980;14:65-81.
163. Chvapil M. Considerations on manufacturing principles of a synthetic burn dressing: a review. *Journal of Biomedical Materials Research*. 1982;16:245-263.
164. Pruitt BA, Levine NS. Characteristics and uses of biologic dressings and skin substitute. *Archives of Surgery*. 1984;119:312-322.
165. Bradley WG, Wilkes GL. Some mechanical property considerations of reconstituted collagen for drug release supports. *Biomaterials, Medical Devices and Artificial Organs*. 1977;5:159-175.
166. Weiger AL, Carpenter-Green SS, Soehgen EC, Lenk RP, Popescu MC. Liposome-collagen gel matrix: a novel sustained drug delivery system. *Journal of Pharmaceutical Science*. 1985;74:922-925.
167. O'Brien TP, M.R. S, Dick JJ, Hamburg TR, Gottch JD. Use of topical tobramycin. *Journal of Cataract and Refractive Surgery*. 1988;14:505-507.
168. Geggel HS, Friend J, Thoft RA. Collagen gel for ocular surface. *Investigative Ophthalmology and Visual Science*. 1985;26:901-905.
169. Tanner JC, Marcucci MA, Bradly WH, Morgan JW. Partial nephrectomy and use of collagen graft for renal wound closure. *Journal of Urology*. 1968;109:710-712.
170. Nimni ME, Cheung DT, Strates BS, Kodama M, Sheikh K. Chemically modified collagen: a natural biomaterial for tissue replacement. *Journal of Biomedical Materials Research*. 1987;21:741-771.
171. Caione P, Lais A, De Gennaro M, Capozza N. Glutaraldehyde crosslinked bovine collagen in exstrophy/epispadias complex. *Journal of Urology*. 1993;150:631-633.
172. Chvapil M, Kronenthal RL, Van Winkle JW. Medical surgical applications of collagen. In: Hall DA, Jackson DS, eds. *International Review of Connective Tissue Research*. London: Academic Press; 1970:1-61.
173. Menasche P, Flaud P, Huc CA, Piwnica A. Collagen vascular grafts: a step towards improved compliance in small calibre by-pass surgery: preliminary report. *Life Support Systems*. 1984;2:233-237.
174. Weinberg CP, Bell E. A blood vessel model constructed from collagen and cultured vascular cells. *Science*. 1986;231:397-400.
175. Huguet D, Delecrin J, Passuti N, Daculsi G. Ovine anterior cruciate ligament reconstruction using a synthetic prosthesis and a collagen inductor. *Journal of Materials Science*. 1997;8:67-73.
176. Weadock K, Olson RM, Silver FH. Evaluation of collagen crosslinking techniques. *Biomaterials, Medical Devices and Artificial Organs*. 1983-84;11:293-318.
177. Gottschalk N, Jaeincke R. Chemically crosslinked lactate dehydrogenase: stability and reconstruction after glutaraldehyde fixation. *Biotechnology and Applied Biochemistry*. 1987;9:389-400.
178. Yamauchi M, Mechanic G. Cross-Linking of Collagen. In: Nimni ME, ed. *Collagen*. Boca Raton: CRC Press; 1988:157-172.

179. Kemp PD, Scott JE. Ehrlich chromogens, probable crosslinks in elastin and collagen. *Journal of Biochemistry*. 1988;252:387-393.
180. Kuypers R, Tyler M, Kurth LB, Jenkins ID, Horgan DJ. Identification of the Loci of the collagen-associated Ehrlich chromogen in type I collagen confirms its role as a trivalent crosslink. *Journal of Biochemistry*. 1992;283:129-136.
181. Fukae M, Mechanic GL. Maturation of collagenous tissue, temporal sequence of formation of peptidyl lysine derived crosslinked aldehydes and crosslinks in collagen. *Journal of Biological Chemistry*. 1980;255:6511.
182. Cronlund AL, Smith BD, Kagan HM. Binding of lysyl oxidase to fibrils of type I collagen. *Connective Tissue Research*. 1985;14:109.
183. Mechanic GL, Kuboki Y, Shimokawa H, Sasaki S, Kawanishi Y. Collagen crosslinks: direct quantitative determination of stable structural crosslinks in bone and dentin collagens. *Biochemical and Biophysical Research Communications*. 1974;60:756.
184. Murayama Y, Satoh S, Oka T, Imanishi J, Noishiki Y. The antigenicity of vascular xenografts. *Japanese Journal of Artificial Organs*. 1988;17:550-552.
185. Hugues H, Colwell A, McClurg WM, Lawford PV. Explanted bioprosthetic heart valves: crosslinks and calcium analysis. *Journal of Pathology*. 1997;181:A31.
186. Suh H. Fundamental concepts for the tissue engineering. *Biomaterials Research*. 1998;2:1-7.
187. Naimark WA, Pereira CA, Tsang K, Lee JM. HMDC crosslinking of bovine pericardial tissue: a potential role of the solvent environment in the design of bioprosthetic materials. *Journal of Materials Science. Materials in Medicine*. 1995;6:235-241.
188. Masuoka M, Nakamura M. Effect of catalysts on epoxy tannage. *Leather Chemistry [Japan]*. 1985;30:223-232.
189. Noishiki Y, Koyanagi H, Miyata T, Furuse M. Bioprosthetic Valve. In: *Patent EP0306256A2*. Japan; 1988.
190. Bernacca GM, Dimitri WR, Fischer AC, Mackay TG, Wheatley DJ. Chemical modification of bovine pericardium and its effect on calcification in the rat subdermal model. *Biomaterials*. 1992;13:345-352.
191. Fujikawa S, Yokota T, Koga K, Kumada J. The continuous hydrolysis of geniposide to genipin using immobilised B-glucosidase on calcium alginate gel. *Biotechnology Letters*. 1987;9:697-702.
192. Tsai TH, Westly J, Lee TF, Chen CF. Identification and determination of geniposide, genipin, gardenoside, and geniposidic acid from herbs by HPLC/photodiode array detection. *Journal of Liquid Chromatography*. 1994;17:2199-2205.
193. Rault I, Frei V, Herbage D, Abdul-Malak N, Huc A. Evaluation of different chemical methods for crosslinking collagen gel, films and sponges. *Journal of Materials Science. Materials in Medicine*. 1996;7:215-221.
194. Lawford PV, Kenyon C, Rodgers S, Black MM. Understanding valve/host interactions through experimental valve analysis. *Journal of Medical Engineering and Technology*. 1992;16:23-26.
195. Nimni ME, Bernick S, Cheung DT, Ertl DC, Nishimoto SK, Paule WJ, Salka C, Strates BS. Biochemical differences between dystrophic calcification of cross-linked collagen implants and mineralisation during bone induction. *Calcified Tissue International*. 1988;42:313-320.
196. Posner AS. The mineral of bone. *Clinical Orthopaedics*. 1985;200:87-99.
197. Tomazic BB, Etz ES, Brown WE. Nature and properties of cardiovascular deposits. *Scanning Microscopy*. 1987;1:95-105.
198. Anderson HC. Normal and abnormal mineralisation in mammals. *American Society Artificial Internal Organs Transaction*. 1981;27:702-708.
199. Glimcher MJ. Molecular biology of mineralised tissue with particular reference to bone. *Reviews of Modern Physics*. 1959;31:3.
200. Glimcher MJ. On the form and function of bone: from molecules to organs. In: Veis A, ed. *The Chemistry and Biology of Mineralised Connective Tissues*. Amsterdam: Elsevier; 1981:617-673.
201. Glimcher MJ. The role of collagen and phosphoproteins in the calcification of bone and other collagenous tissues. In: Rubin RP, Weiss GB, Putney JW, eds. *Calcium in Biological Systems*. New York: Plenum; 1985:607-616.
202. Schoen FJ, Harasaki H, Kim KM, Anderson C, Levy RJ. Biomaterials-associated calcification: pathology, mechanisms, and strategies for prevention. *Journal of Biomedical Materials Research: Applied Biomaterials*. 1988;22:11-36.

203. Anderson HC. Calcific diseases: a concept. *Archives of Pathological and Laboratory Medicine*. 1983;107:341-348.
204. Kim KM. Role of membranes in calcification. *Survey and Synthesis of Pathology Research*. 1983;2:215-228.
205. Anderson HC. Mineralisation by matrix vesicles. *Scanning Electron Microscopy*. 1984;2:953-964.
206. Anderson HC. Electron microscopic studies of induced cartilage development and calcification. *Journal of Cell Biology*. 1967;35:81-101.
207. Bonucci E. Fine structure of early cartilage calcification. *Journal of Ultrastructural Research*. 1967;20:33-50.
208. Pereira CA, Lee JM, Haberer SA. Effect of alternative crosslinking methods on the strain rate viscoelastic properties of bovine pericardial bioprosthetic material. *Journal of Biomedical Materials Research*. 1990;24:345-361.
209. Peress N, Sajdera SW, Anderson HC. The lipids of matrix vesicles from bovine fetal epiphyseal cartilage. *Calcified Tissue Research*. 1974;14:275-281.
210. Irving JT, Wuthier RE. Histochemistry and biochemistry of calcification with special reference to the role of lipids. *Clinical Orthopaedics*. 1968;56:237-260.
211. Ennever J, Riggan LJ, Vogel JJ. Proteolipid and collagen calcification in-vitro. *Cytobios*. 1984;39:151-157.
212. Ennever J, Vogel JJ, Riggan LJ. Calcification by proteolipid from atherosclerotic aorta. *Atherosclerosis*. 1980;35:209-213.
213. Ennever J, Boyan-Salyers B, Riggan LJ. Proteolipid and bone matrix calcification in-vitro. *Journal of Dental Research*. 1977;56:967-970.
214. Robison R. The possible significance of hexose phosphoric esters in ossification. *Journal of Biochemistry*. 1923;17:286.
215. Matsuzawa T, Anderson HC. Phosphatases of epiphyseal cartilage studied by electron microscopic cytochemical methods. *Journal of Histochemistry and Cytochemistry*. 1971;19:801.
216. Samachson J. Basic requirements for calcification. *Nature*. 1969;221:1247-1248.
217. Sell S, Scully RE. Aging changes in the aortic and mitral valves: histological and histochemical studies, with observations on the pathogenesis of calcific aortic stenosis and calcification of the mitral annulus. *American Journal of Pathology*. 1965;46:345-365.
218. Lindroos M, Kupari M, Heikkilä J, Tilvis R. Prevalence of aortic valve abnormalities in the elderly: an echocardiographic study of a random population sample. *Journal of the American College of Cardiology*. 1993;21:1220-1225.
219. Schoen FJ, Sutton MSJ. Contemporary issues in the pathology of valvular heart disease. *Human Pathology*. 1987;18:568-576.
220. Russel RGG, Kanis JA. Ectopic calcification and ossification. In: Nordin BEG, ed. *Metabolic Bone Disease*. New York: Churchill Livingstone; 1984:344-365.
221. Levy RJ, Schoen FJ, Golomb G. Bioprosthetic heart valve calcification: clinical features, pathobiology and prospects for prevention. In: William DF, ed. *Critical Reviews in Biocompatibility*: CRC Press; 1986:147-187.
222. Strates B, Neuman WF. On the mechanism of calcification. *Proceedings of the Society for Experimental Biology and Medicine*. 1958;97:688-693.
223. Howell DS. Current concepts of calcification. *Journal of Bone Joint Surgery*. 1971;53a:250-260.
224. Ali SY. Mechanism of calcification. In: Owens R, Goodfellow P, Bullough P, eds. *Scientific Foundations of Orthopaedics and Traumatology*. Philadelphia: Saunders, W.B.; 1980:175.
225. Kim KM, Valigorsky JM, Mergner WJ. Aging changes in the human aortic valve in relation to dystrophic calcification. *Human Pathology*. 1976;7:47-60.
226. Tanimura A, McGregor DH, Anderson HC. Matrix vesicles in atherosclerotic calcification. *Proceedings of the Society for Experimental Biology and Medicine*. 1983;172:173-177.
227. Carlstrom D, Engfeldt B, Engstrom A, Ringertz N. Studies on the chemical composition of normal and abnormal blood walls. *Laboratory Investigation*. 1953;2:325-332.
228. Weissman G, Weissman S. X-ray diffraction studies of human aortic elastic residues. *Journal of Clinical Investigation*. 1960;39:1657-1661.
229. Paule WJ, Bernick S, Strates BB, Nimni ME. Calcification of implanted vascular tissues associated with elastin in an experimental animal model. *Journal of Biomedical Materials Research*. 1992;26:1169-1177.

230. Anderson HC. Mechanism of mineral formation in bone. *Laboratory Investigation*. 1989;60:320-330.
231. Maranto AR, Schoen FJ. Alkaline phosphatase activity of glutaraldehyde-treated bovine pericardium used in bioprosthetic cardiac valves. *Circulation Research*. 1988;63:844-848.
232. Levy RJ, Schoen FJ, Flowers WB, Staelin ST. Inhibition of mineralisation in bioprosthetic heart valves: studies of alkaline phosphatase activity and its inhibition by $AlCl_3$ or $FeCl_3$ preincubations. *Journal of Biomedical Materials Research*. 1991;25:905-935.
233. McKee MD, Nanci A. Osteopontin: an interfacial extracellular matrix protein in mineralised tissues. *Connective Tissue Research*. 1996;35:197-205.
234. Giachelli CM, Scatena M, Wada T. Osteopontin: potential roles in vascular function and dystrophic calcification. *Journal of Bone and Mineral Metabolism*. 1997;15:179-183.
235. Hauschka PV, Lian JB, Cole DE, Gundberg CM. Osteocalcin and matrix Gla proteins: vitamin K-dependent proteins in bone. *Physiological Reviews*. 1989;69:990-1047.
236. Boskey AL. Matrix proteins and mineralisation: an overview. *Connective Tissue Research*. 1996;35:357-363.
237. Wada T, McKee MD, Steitz S, Giachelli CM. Calcification of vascular smooth muscle cell cultures: inhibition by osteopontin. *Circulation Research*. 1999;84:166-178.
238. O'Brien KD, Kuusisto J, Reichenbach DD, Ferguson M, Giachelli CM, Alpers CE, Otto CM. Osteopontin is expressed in human aortic valvular lesions: evidence that aortic valve calcification may be actively regulated. *Circulation*. 1995;92:2163-2168.
239. Srivatsa SS, Harrity PJ, Maercklein PB, Kleppe L, Veinot J, Edwards WD, Johnson CM, Fitzpatrick LA. Increased cellular expression of matrix proteins that regulate mineralisation is associated with calcification of native human and porcine xenograft bioprosthetic heart valves. *Journal of Clinical Investigation*. 1997;99:996-1009.
240. Parhami F, Bostrom K, Watson K, Demer LL. Role of molecular regulation in vascular calcification. *Journal of Atherosclerosis Thrombosis*. 1996;3:90-94.
241. Ducy P, Desbois C, Boyce B, Pinero G, Story B, Dunstan C, Smith E, Bonadio J, Goldstein S, Gunberg C, Bradley A, Karsenty G. Increased bone formation in osteocalcin-dependent mice. *Nature*. 1996;382:448-452.
242. Scinke T, McKee MD, Karsenty G. Extracellular matrix calcification: where is the action? *Nature Genetics*. 1999;21:150-151.
243. Schoen FJ, Levy RJ, Nelson AC, Bernhard WF, Nashef A, Hawley M. Onset and progression of experimental bioprosthetic heart valve calcification. *Laboratory Investigation*. 1985;52:523-532.
244. Schoen FJ. Biomaterial-associated infection, neoplasia and calcification: clinicopathologic features and pathophysiologic concepts. *American Society Artificial Internal Organs Transaction*. 1987;33:8-18.
245. Fishbein MC, Gissen SA, Collins JJJ, Barsamian EM, Cohn LH. Pathologic findings after cardiac valve replacement with glutaraldehyde-fixed porcine valves. *American Journal of Cardiology*. 1977;40:331-337.
246. Majno G, Joris I. In: *Cells, tissues and disease: principles of general pathology*. Cambridge: Blackwell Science; 1996:229.
247. Thoma RJ. Poly(ether)urethane reactivity with metal-ion in calcification and environmental stress cracking. *Journal of Biomaterials Applications*. 1987;90:449-486.
248. Wika KE, Utoh J, Brown J, Harasaki H. Quantification of the edge effect in calcified bioprosthetic tissues. *Journal of Biomedical Materials Research*. 1993;27:1293-1299.
249. Wouters LHG, Rousseau EPM, Van Steenhoven AA, German AL. An experimental set up for the in-vitro analysis of polyurethane calcification. In: *Proceedings of the Second International Conference on Polyurethanes in Biomedical Engineering*. Germany: Fellbach; 1986.
250. Tomazic BB, Brown WE, Schoen FJ. Physicochemical properties of calcific deposits isolated from porcine bioprosthetic heart valves removed from patients following 2-13 years function. *Journal of Biomedical Materials Research*. 1994;28:35-47.
251. Webb CL, Schoen FJ, Flowers WE, Alfrey AC, Horton C, Levy RJ. Inhibition of mineralisation of glutaraldehyde-pretreated bovine pericardium by $AlCl_3$: mechanism and comparisons with $FeCl_3$, $LaCl_3$ and $Ga(NO_3)_3$ in rat subdermal model studies. *American Journal of Pathology*. 1991;138:971-981.
252. Giddens DP, Yoganathan AP, Schoen FJ. Prosthetic cardiac valves. *Cardiovascular Pathology*. 1993;2:167S-177S.

253. Schoen FJ, Hirsch D, Bianco RW, Levy RJ. Onset and progression of calcification in porcine aortic bioprosthetic valves implanted as orthotopic mitral valve replacements in juvenile sheep. *Journal of Thoracic Cardiovascular Surgery*. 1994;108:880-887.
254. Chanda J, Kondoh K, Ijima K, Matsukawa M, Kuribayashi R. In-vitro and in-vivo calcification of vascular bioprostheses. *Biomaterials*. 1998;19:1651-1656.
255. Kim KM, Herrera GA, Battarbee HD. Role of glutaraldehyde in calcification of porcine aortic valve fibroblasts. *American Journal of Pathology*. 1999;154:843-852.
256. Kim KM. Cells, rather than extracellular matrix, nucleate apatite in glutaraldehyde-treated vascular tissue. *Journal of Biomedical Materials Research*. 2002;59:639-645.
257. Rajamannan NM, Subramaniam M, Rickard D, Stock S, Donovan JL, Fullerton D, Orszulak T, Tajik AJ, Bonow R, Spelsberg T. Human aortic valve calcification is accompanied by a transition to an osteoblast phenotype. *Journal of Bone Mineral Research*. 2002;17:5400.
258. Mako WJ, Vesely I. Regional distribution of calcification in aortic valve cusps: an in-vivo study. *American Society Artificial Internal Organs Journal*. 1996;42:M365-M367.
259. Levy RJ, Schoen FJ, Sherman FS, Nichols J, Hawley MA, Lund SA. Calcification of subcutaneously implanted type I collagen sponges: effects of glutaraldehyde and formaldehyde pretreatments. *American Journal of Pathology*. 1986;122:71-82.
260. Urry DW. On the molecular basis for vascular calcification. *Perspectives in Biology and Medicine*. 1974;18:68.
261. Webb CL, Nguyen NM, Schoen FJ, Levy RJ. Calcification of allograft aortic wall in a rat subdermal model: pathophysiology and inhibition by aluminium and aminodiphosphonate preincubations. *American Journal of Pathology*. 1992;141:487-496.
262. Vyavahare N, Ogle M, Schoen FJ, Levy RJ. Elastin calcification and its prevention with aluminium chloride pre-treatment. *American Journal of Pathology*. 1999;155:973-982.
263. Chanda J, Kuribayashi R, Abe T. Calcification prevention of glutaraldehyde-treated porcine aortic and pulmonary valves. *Annals of Thoracic Surgery*. 1997;64:1063-1066.
264. Yu SY. Crosslinking of elastin in human atherosclerotic aortas I. A preliminary study. *Laboratory Investigation*. 1971;25:121-125.
265. Partridge SM. Biosynthesis and nature of elastin structures. *Federation Proceedings*. 1966;25:1023-1029.
266. Glasmacher B, Reul H, Schnepferschoff S, Schrek S, Rau G. In-vitro calcification of pericardial bioprostheses. *Journal of Heart Valve Disease*. 1998;7:415-418.
267. Schoen FJ, Levy RJ. Pathophysiology of bioprosthetic heart valve calcification in biologic and bioprosthetic valves. In: Bodnar E, Yacoub M, eds. *Biologic and Bioprosthetic Valves*. New York: Yorke Medical Books; 1986:418-429.
268. Posner AS. The structure of bone mineral. *Clinical Orthopaedics*. 1957;9:5-15.
269. Brown WE, Chow LC. Chemical properties of bone mineral. *Annual Review of Materials Science*. 1976;6:213-236.
270. Hendricks SB, Hill WL. The nature of bone and phosphate rock. *Proceeding of the National Academy of Sciences of the USA*. 1950;36:731-737.
271. Neuman WF, Neuman MW. In: *The Chemical Dynamics of Bone Mineral*. Chicago: Chicago University Press; 1958.
272. Bett JAS, Christner LG, Hall WK. Studies of hydrogen held by solids XII. Hydroxyapatite catalysts. *Journal of the American Chemical Society*. 1967;89:5535-5541.
273. Brown WE, Lehr JR, Smith JP, Frazier AW. Crystallographic and chemical relations between octacalcium phosphate and hydroxyapatite. *Nature*. 1962;196:1050-1055.
274. Fulmer MT, Martin RI, Brown PW. Formation of calcium deficient hydroxyapatite at near-physiological temperature. *Journal of Materials Science. Materials in Medicine*. 1992;3:299-305.
275. Posner AS. Crystal chemistry of bone mineral. *Physiological Reviews*. 1969;49:760-792.
276. Legros R, Balmain N, Bonel G. Structure and composition of the mineral phase of periosteal bone. *Journal of Chemical Research. Synopses*. 1986;1:8-9.
277. Pellegrino ED, Biltz RM. Mineralisation in the chick embryo I. Monohydrogen phosphate and carbonate relationship during maturation of the bone crystal complex. *Calcified Tissue Research*. 1972;10:128-135.
278. Termine JD, Posner AS. Amorphous/crystalline interrelationship in bone mineral. *Calcified Tissue International*. 1966;6:335-342.
279. Eanes ED, Termine JD, Posner AS. Amorphous calcium phosphate in skeletal tissue. *Clinical Orthopaedics*. 1967;53:223-235.

280. Termine JD, Posner AS. Infrared analysis of rat bone: age dependency of amorphous and crystalline mineral fractions. *Science*. 1966;153:1523-1525.
281. Francis MD, Webb NC. Hydroxyapatite formation from a hydrated calcium monohydrogen phosphate precursor. *Calcified Tissue Research*. 1971;6:335-342.
282. Brown WE. Crystal growth of bone mineral. *Clinical Orthopaedics*. 1966;44:205-220.
283. Roufosse AH, Aue WB, Roberts JE, Glimcher MJ, Griffin RJ. Investigation of the mineral phase of bone by solid state phosphorus magic angle sample spinning nuclear magnetic resonance. *Biochemistry Journal*. 1984;23:6115-6120.
284. Grynblas MD, Bonar LC, Glimcher MJ. XRD radial distribution function of bone mineral and synthetic calcium phosphates. *Journal of Materials Science*. 1984;19:723-736.
285. Grynblas MD, Bonar LC, Glimcher MJ. Failure to detect amorphous calcium phosphate solid phase in bone mineral: a radial distribution function study. *Calcified Tissue International*. 1984;36:291-309.
286. Harper RA, Posner AS. Measurement of non-crystalline calcium phosphate in bone mineral. *Proceedings of the Society for Experimental Biology and Medicine*. 1966;122:137-142.
287. Posner AS, Betts F. Synthetic amorphous calcium phosphate and its relation to bone mineral structure. *Accounts of Chemical Research*. 1975;8:273-281.
288. Aoba T, Moriwaki Y, Doi Y, Okasaki N, Takahashi J, Yagi T. Diffuse-X-ray scattering from apatite crystals and its relation to amorphous bone mineral. *Journal of Osaka University Dental School*. 1980;20:81-90.
289. Glimcher MJ, Bonar LC, Grynblas MD, Landis WJ, Roufosse AH. Recent studies of bone mineral: Is the amorphous calcium phosphate theory valid? *Journal of Crystal Growth*. 1981;53:100-119.
290. Eanes ED, Gillespie IH, Posner AS. Intermediate states in the precipitation of hydroxyapatite. *Nature*. 1965;208:365-367.
291. Brown WE, Lehr JR, Smith JP, Frazier AW. Crystallography of octacalcium phosphate. *Journal of the American Chemical Society*. 1957;79:5318-5319.
292. Brown WE, Eidelman N, Tomazic B. Octacalcium phosphate as a precursor in biomineral formation. *Advances in Dental Research*. 1987;1:306-313.
293. Munzenberg KJ, Gebhardt M. *Clinical Orthopaedics*. 1973;90:271-273.
294. Wallace BM, Mattamal GJ, Brown WE. *Journal of Dental Research*. 1973;52:86.
295. Brown WE, Schroeder LW, Ferris JS. Interlayering of crystalline octacalcium phosphate and hydroxyapatite. *Journal of Physical Chemistry*. 1979;83:1385-1388.
296. Tomazic BB, Tung MS, Gregory TM, Brown WE. Mechanism of hydrolysis of octacalcium phosphate. *Scanning Microscopy*. 1989;3:119-127.
297. Chickerur NS, Tung MS, Brown WE. A mechanism for incorporation of carbonate into apatite. *Calcified Tissue International*. 1980;32:55-62.
298. Rowles SL. The precipitation of whitlockite from aqueous solutions. *Bulletin de la Societe Chimique de France*. 1968:1797-1802.
299. Gatter RZ, McCarthy DJ. Pathological calcification in man. *Archives of Pathology*. 1967;84:346-353.
300. Ali SY, Griffiths S. Formation of calcium phosphate crystals in normal and osteoarthritic cartilage. *Annals of the Rheumatic Diseases*. 1983;42:45-48.
301. Legeros RZ. Variations in the crystalline components of human dental calculus I. Crystallographic and spectroscopic methods of analyses. *Journal of Dental Research*. 1974;53:35-40.
302. Legeros RZ, Orly I, LeGeros JP, Gomez C, Kazimiroff K. Scanning electron microscopy and electron probe microanalyses of the crystalline components of human and animal dental calculi. *Scanning Microscopy*. 1988;2:345-356.
303. Jensen AT, Rowles SL. Magnesium whitlockites: a major constituent of dental calculus. *Acta Odontologica Scandinavica*. 1957;16:121-139.
304. Sutor DJ, Scheidt S. Identification standards for human urinary calculus components using crystallographic methods. *British Journal of Urology*. 1968;40:20-28.
305. LeGeros RZ, Daculsi G, Kijkowska R, Kerebel B. The effect of magnesium on the formation of apatites and whitlockites. In: Itokawa Y, Kerebel B, eds. *Magnesium in Health and Disease*. New York: John Libbey and Co.; 1989:11-19.
306. Sakae T, Okuda A. Crystallographical analysis of tooth enamel using milligram samples. *Journal of Ultrastructural Research*. 1985;91:77-81.
307. Trautz O, Fessenden E, Newton M. Magnesium whitlockite in ashed dental tissue: an identification by X-ray diffraction. *Journal of Dental Research*. 1954;33:687.

308. LeGeros RZ, Contigugulia SR, Alfrey AC. Pathological calcification associated with uremia: two types of calcium phosphate deposits. *Calcified Tissue Research*. 1973;13:173-185.
309. Ji H, Ponton CB, Marquis PM. Microstructural characterisation of hydroxyapatite coating on titanium. *Journal of Materials Science. Materials in Medicine*. 1992;3:283-287.
310. Gibson IR, Rehman I, Best SM, Bonfield W. Characterisation of the transformation from calcium deficient apatite to beta-tricalcium phosphate. *Journal of Materials Science. Materials in Medicine*. 2000;11:533-539.
311. Cusco R, Guitian F, De Aza S, Artus L. Differentiation between hydroxyapatite and beta-tricalcium phosphate by means of micro Raman spectroscopy. *Journal of European Ceramic Society*. 1998;18:1301-1305.
312. Shear MJ, Washburn M, Kramer B. Composition of bone VII. Equilibration of serum solutions with dicalcium phosphate. *Journal of Biological Chemistry*. 1929;83:697-720.
313. Termine JD, Posner AS. Infrared determination of the percentage of crystallinity in apatic calcium phosphates. *Nature*. 1966;211:268-270.
314. Samachson J. Mechanism of exchange of inorganic phosphate with bone material and its relation to the mechanism of calcification. *Nature*. 1968;218:1262.
315. Thomas WCJ, Tomita A. Mineralisation of human and bovine tissues in-vitro. *American Journal of Pathology*. 1967;51:621-628.
316. Wadkins CL, Luben R, Thomas M, Humphrey R. Physical biochemistry of calcification. *Clinical Orthopaedics*. 1974;99:246-266.
317. Luben RA, Sherman JK, Wadkins CL. Studies of the mechanism of biological calcification IV. Ultrastructural analysis of calcifying tendon matrix. *Calcified Tissue Research*. 1973;11:39-55.
318. Wadkins CL, Luben RA. Effects of fluoride on in-vitro calcification of tendon matrix. *Calcified Tissue Research*. 1978;26:51-59.
319. Hollinger JO, Battistone GC. Biodegradable bone repair materials. *Clinical Orthopaedics and Related Research*. 1986;831:427-437.
320. Friedman CD, Costantino PD, Tagaki S, Chow LC. Bone source hydroxyapatite cement: a novel biomaterial for craniofacial skeletal tissue engineering and reconstruction. *Journal of Biomedical Materials Research. Applied Biomaterials*. 1998;43:428-432.
321. Gotoh Y, Gerstenfeld LC, Glimcher MJ. Identification and characterisation of the major chicken bone phosphoprotein. Analysis of its synthesis by cultured embryonic chick osteoblasts. *European Journal of Biochemistry*. 1990;187:49-58.
322. Rey C, Glimcher MJ. Short range organisation of the Ca-P mineral phase in bone and enamel: changes with age and maturation. In: Slavkin H, Price P, eds. *Chemistry and Biology of Mineralised Tissues*. Amsterdam: Elsevier; 1992:5-18.
323. Kim HM, Rey C, Glimcher MJ. Isolation of calcium-phosphate crystals of mature bovine bone by reaction with hydrazine at low temperature. In: Brown PW, Constantz B, eds. *Hydroxyapatite and Related Materials*. Boca Raton: CRC Press; 1994:331-337.
324. Kim HM, Rey C, Glimcher MJ. Isolation of calcium-phosphate crystals of bone by non-aqueous methods at low temperature. *Journal of Bone Mineral Research*. 1995;10:1589-1601.
325. Nagano M, Nakamura T, Kokubo T, Tanashi M, Ogawa M. Differences of bone bonding ability and degradation behaviour in-vivo between amorphous calcium phosphate and highly crystalline hydroxyapatite coating. *Biomaterials*. 1996;17:1771-1777.
326. Rude RK, Singer FR. Magnesium deficiency and excess. *Revista de Medicina/Revista Medica*. 1981;32:245-259.
327. Neuman MW. Blood: bone equilibrium. *Calcified Tissue International*. 1982;34:382-385.
328. Speich M, Bousquet B, Nicolas G. Reference values for ionised, complexed, and protein-bound plasma magnesium in men and women. *Clinical Chemistry*. 1981;27:246-248.
329. Peach MJ. Cations: calcium, magnesium, barium. Lithium and ammonium. In: Goodman G, ed. *Pharmacological Basis of Therapeutics*. New York: Macmillan; 1975:782-797.
330. Wians FH, Krech KE, Hauschka PV. Effects of magnesium and calcium on osteocalcin adsorption to hydroxyapatite. *Magnesium*. 1983;2:83-92.
331. LeGeros RZ, LeGeros JP. Phosphate minerals in human tissues. In: Nilagu J, Moore P, eds. *Phosphate Minerals*. Berlin: Springer-Verlag; 1984:351-385.
332. LeGeros RZ. Apatites in biological systems. *Progress in Crystal Growth and Characterisation of Materials*. 1981;4:1-45.

333. LeGeros RZ. Incorporation of magnesium in synthetic and biological apatites: a preliminary report. In: Fearnhead RW, Suga S, eds. *Tooth Enamel*. New York: Elsevier Publishers; 1984:32-36.
334. Derise NL, Ritchey SJ. Mineral composition of normal human enamel and dentin and the relation of composition to dental caries. II. Microminerals. *Journal of Dental Research*. 1974;53:853-858.
335. Tomazic BB, Mayer I, Brown WE. Ion incorporation into octacalcium phosphate hydrolysates. *Journal of Crystal Growth*. 1991;108:670-682.
336. Van Raemdonck W, Ducheyne P, Meester P. In: *Metal and Ceramic in Biomaterials*. New York: CRC Press; 1984:143.
337. Yamashita K, Kanasawa T. In: *Inorganic Phosphate Materials*. Amsterdam: Elsevier; 1989:71.
338. Posner AS. Bone mineral on the molecular level. *Federation Proceedings*. 1973;32:1933-1937.
339. Gilbert IGF. Surface properties of bone mineral. *Biochemica et Biophysica Acta*. 1961;54:489-494.
340. Termine JD, Lundy DR. Vibrational spectra of some phosphate salts amorphous to X-ray diffraction. *Calcified Tissue Research*. 1974;15:55-70.
341. LeGeros RZ. Calcium phosphates in oral biology and medicine. In: Myers HM, ed. *Monographs in Oral Science*. Basel: Karger; 1991:81-129.
342. Neuman WF, Mulryan BJ. *Calcified Tissue Research*. 1966;1:94-104.
343. Mako WJ, Vesely I. In-vivo and in-vitro models of calcification in porcine aortic valve cusps. *Journal of Heart Valve Disease*. 1997;6:316-323.
344. Levy RJ, Schoen FJ, Anderson HC, Harasaki H, Koch TH, Brown W. Cardiovascular implant calcification: a survey and update. *Biomaterials*. 1991;12:707-714.
345. Fishbein MC, Levy RJ, Ferrans VJ, Dearden LC, Nashef A, Goodman AP, Carpentier A. Calcification of cardiac valve bioprostheses: biochemical, histological, and ultrastructural observations in a subcutaneous implantation model system. *Journal of Thoracic Cardiovascular Surgery*. 1982;83:602-609.
346. Levy RJ, Schoen FJ, Levy JT, Nelson AC, Howard SL, Oshry LJ. Biological determinants of dystrophic calcification and osteocalcin deposition in glutaraldehyde-preserved porcine aortic valve leaflets implanted subcutaneously in rats. *American Journal of Pathology*. 1983;113:143-155.
347. Vyavahare N, Hirsch D, Lerner E, Baskin JZ, Schoen FJ, Bianco R, Kruth HS, Zand R, Levy RJ. Prevention of bioprosthetic heart valve calcification by ethanol preincubation: efficacy and mechanisms. *Circulation*. 1997;95:479-488.
348. Schoen FJ, Golomb G, Levy RJ. Calcification of bioprosthetic heart valves: a perspective on models. *Journal of Heart Valve Disease*. 1992;1:110-114.
349. Schoen FJ, Levy RJ. Heart valve bioprostheses: antimineralisation. *European Journal of Cardiothoracic Surgery*. 1992;6:S91-S94.
350. Liao K, Seifter E, Hoffman D, Yellin EL, Frater RWM. Bovine pericardium versus porcine aortic valve: comparison of tissue biological properties as prosthetic valves. *Artificial Organs*. 1992;16:361-365.
351. Carpentier SM, Carpentier AF, Chen L, Shen M, Quintero LJ, Witzel TH. Calcium mitigation in bioprosthetic tissues by iron pre-treatment: the challenge of iron leaching. *Annals of Thoracic Surgery*. 1995;60:S332-S338.
352. Herrero EJ, Fernandez P, De La Torre N, Escudero C, Garcia-Paez JM, Bujan J, Castillo-Olivares JL. Inhibition of the calcification of porcine valve tissue by selective lipid removal. *Biomaterials*. 1994;15:815-820.
353. Tsao JW, Levy RJ, Schoen FJ. Compressive mechanical deformation inhibits calcification of bovine pericardium used in cardiac valve bioprostheses. *Proceedings of the 13th Annual Meeting for the Society of Biomaterials*. 1987:180.
354. Barnhart GR, Jones M, Ishihara T, Chavez AM. Bioprosthetic valvular failure. Clinical pathological observations in an experimental animal model. *Journal of Thoracic and Cardiovascular Surgery*. 1982;83:618-631.
355. Jones M, Barnhart GR, Chavez AM. Experimental evaluation of bioprosthetic valves in sheep. In: Cohn LH, Gallucci V, eds. *Cardiac Bioprostheses*. New York: Yorke Medical Books; 1982:275-292.

356. Gott JP, Chih P, Dorsey LMA, Jay JL, Jett GK, Schoen FJ, Girardot JM, Guyton RA. Calcification of porcine valves: a successful new method of antimineralisation. *Annals of Thoracic Surgery*. 1992;53:207-216.
357. Levy R, J., Zenker JA, Bernhard WF. Porcine bioprosthetic valve calcification in bovine left ventricle-aorta shunts: studies of the deposition of vitamin K-dependent proteins. *Annals of Thoracic Surgery*. 1983;36:187-196.
358. Okamura K, Yuge I, Kawazoe H, Kitamura N, Imamura E, Konno S. A comparative study between glutaraldehyde preserved aortic and pulmonary heterograft valves in dogs. *Journal of Cardiovascular Surgery*. 1976;17:178-186.
359. Melver AG, Howarth WS. The fate of prosthetic leaflet hart valves implanted in animals. In: Williams D, ed. *Biocompatibility of Implant Materials*. London: Sector Publishing; 1985:211-215.
360. Ali ML, Kumar SP, Bjornstad K, Duran CMG. The sheep as an animal model for heart valve research. *Journal of Cardiovascular Surgery*. 1996;4:543-549.
361. Barnhart GR, Jones M, Ishihara T, Rose DM, Chavez AM, Ferrans VJ. Degeneration and calcification of bioprosthetic cardiac valves. Bioprosthetic tricuspid valve implantation in sheep. *American Journal of Pathology*. 1982;106:136-139.
362. Gott JP, Girardot MN, Girardot JMD, Hall JD, Whitlark JD, Horsley WS, Dorsey LMA, Levy RJ, Chen W, Schoen FJ, Guyton RA. Refinement of the alpha-aminooleic acid bioprosthetic heart valve anticalcification technique. *Annals of Thoracic Surgery*. 1997;64:50-58.
363. Thiene G, Laborde F, Valente M, Gallix P, Talenti E, Calabrese F, Piwnica A. Morphological survey of a new pericardial valve prosthesis (Pericarbon): long-term animal experimental model. *European Journal of Cardio-Thoracic Surgery*. 1989;3:65-74.
364. Golomb G, Wagner D. Development of a new in-vitro model for studying implantable polyurethane calcification. *Biomaterials*. 1991;12:387-405.
365. Hunter GK, Nyburg SC, Pritzker KPH. Hydroxyapatite formation in collagen, gelatin and agarose gels. *Collagen and Related Research*. 1986;6:229-238.
366. Bernacca GM, Mackay TG, Wheatley DJ. In-vitro calcification of bioprosthetic heart valves: report of a novel method and review of the biochemical factors involved. *Journal of Heart Valve Disease*. 1992;1:115-130.
367. Bernacca GM, Fischer AC, Wilkinson R, Mackay TG, Wheatley DJ. Calcification and stress distribution in bovine pericardial heart valves. *Journal of Biomedical Materials Research*. 1992;26:959-966.
368. Howell DS, Pita JC, Marquez JF, Gatter RA. Demonstration of macromolecular inhibitors of calcification and nucleational factors in fluid from calcifying sites in cartilage. *Journal of Clinical Investigation*. 1969;48:630-641.
369. Termine JD, Eanes ED. Calcium phosphate deposition from balanced salt solutions. *Calcified Tissue Research*. 1974;15:81-84.
370. Rasmussen P. The concentration of calcium, inorganic phosphate and protein in the interstitial fluid of rats during hypercalcaemic conditions. *Calcified Tissue Research*. 1972;9:200-206.
371. Glasmacher B, Deiwick M, Reul H, Rau G. In-vitro calcification of bioprosthetic heart valves: a new in-vitro test method. *Journal of Artificial Organs*. 1996;19:535.
372. Fisher AC, Bernacca GM, Mackay TG, Dimitri WR, Wilkinson R, Wheatley DJ. Calcification modelling in artificial heart valves. *International Journal of Artificial Organs*. 1992;15:284-288.
373. Kapos J, Mavrilas D, Missirlis Y, Koutsoukos PG. Model experimental system for investigation of heart valve calcification in-vitro. *Journal of Biomedical Materials Research*. 1997;38:183-190.
374. Glasmacher B, Deiwick M, Reul H, Knesch H, Keus D, Rau G. A new in-vitro test method for calcification of bioprosthetic heart valves. *The International Journal of Artificial Organs*. 1997;20:267-271.
375. Bernacca GM, Fisher AC, Mackay TG, Wheatley DJ. A dynamic in-vitro method for studying bioprosthetic heart valve calcification. *Journal of Materials Science. Materials in Medicine*. 1992;3:293-298.
376. Bernacca GM, Tobasnick G, Wheatley DJ. Dynamic in-vitro calcification of porcine aortic valves. *Journal of Heart Valve Disease*. 1994;3:684-687.

377. Kokuno T, Kushitani H, Sakka S. Solutions able to reproduce in-vivo surface-structure changes in bioactive glass ceramic A-W3. *Journal of Biomedical Materials Research*. 1990;24:721-734.
378. In: Ratner BD, Hoffman AS, Schoen FJ, Lemons JE, eds. *Biomaterials Science: An Introduction to Materials in Medicine*. San Diego: Academic Press; 1996:272-280.
379. Deiwick M, Glasmacher B, Zarubin AM, Reul H, Geiger A, Von Bally G. Quality control of bioprosthetic heart valves by means of holographic interferometry. *Journal of Heart Valve Disease*. 1996;5:441-447.
380. Park JC, Hwang YS, Han DW, Suh H. A novel in-vitro assessment of tissue valve calcification by a continuous flow type method. *Artificial Organs*. 2000;24:156-164.
381. Suh H, Park JC. Evaluation of calcification in porcine valves treated by ultraviolet ray and glutaraldehyde. *Materials Science and Engineering C*. 2000;13:65-73.
382. Tingfei X, Jiazhen M, Wenhua T, Xuehui L, Shuhui L, Baoshu X. Prevention of tissue calcification on bioprosthetic heart valve by using epoxy compounds: a study of calcification tests in-vitro and in-vivo. *Journal of Biomedical Materials Research*. 1992;26:1241-1251.
383. Pettenazzo E, Deiwick M, Thiene G, Molin G, Glasmacher B, Martignano F, Bottio T, Reul H, Valente M. Dynamic in-vitro calcification of bioprosthetic porcine valves: evidence of apatite crystallisation. *Journal of Thoracic Cardiovascular Surgery*. 2001;121:500-508.
384. In: Sheenan DC, Hrapchak BB, eds. *Theory and Practice of Histotechnology*. Detroit: Lipshaw; 1980:227.
385. Gross JM. Calcification of bioprosthetic heart valves and its assessment. *Journal of Thoracic and Cardiovascular Surgery*. 2001;121:428-430.
386. Geha AS, Laks HH, Stansel HCJ, Cornhill JF, Kilman JW, Buckley MJ, Roberts WC. Late failure of porcine valve heterografts in children. *Journal of Thoracic and Cardiovascular Surgery*. 1979;78:351-364.
387. Thandroyen FT, Whitton ID, Pirie D, Rogers MA, Mitha AS. Severe calcification of glutaraldehyde-preserved porcine xenografts in children. *American Journal of Cardiology*. 1980;45:690-696.
388. Sanders SP, Levy R, J., Freed MD, Norwood WI, Castaneda AR. Use of Hancock porcine xenografts in children and adolescents. *American Journal of Cardiology*. 1980;46:429-438.
389. Round MJ. Plasma calcium, magnesium, phosphorus, and alkaline phosphatase in normal British school children. *British Medical Journal*. 1972;3:137-142.
390. Gunbeg CM, Cole DEC, Lian JB, Reade TM, Gallop PM. Serum osteocalcin in the treatment of inherited rickets with 1,25-dihydroxyvitamin D3. *Journal of Endocrinology Metabolism*. 1983;56:1063-1069.
391. DeLuca HF, Shoenes HK. Metabolism and mechanism of action of vitamin D. *Annual Review of Biochemistry*. 1973;45:1063-1082.
392. Dahm M, Dohmen G, Prufer D, Krummenauer F, Hafner G, Oelert H. Determinants of calcium uptake of bovine pericardium for heart valve replacement: results of in-vitro studies. *Journal of Heart Valve Disease*. 1998;7:170-173.
393. Cherian AG, Hill JG. Age dependence of serum enzymatic activities (alkaline phosphatase, apatite aminotransferase, and creatine kinase) in healthy children and adolescents. *American Journal of Clinical Pathology*. 1978;70:783.
394. Wolferd ST, Schroer RA, Gallo PO. Age-related changes in serum chemistry and haematology values in normal Sprague-Dawley rats. *Fundamentals of Applied Toxicology*. 1987;8:80.
395. Cohn LH, Koster JK, Mee RBB, Collins JJ. Long-term follow-up of the Hancock bioprosthetic heart valve: a six-year review. *Circulation*. 1979;60:87-92.
396. Wang AY-M, Wang M, Woo J, Lam CW-K, Li PK-T, Lui S-F, Sanderson JE. Cardiac valve calcification as an important predictor for all-cause mortality and cardiovascular mortality in long-term peritoneal dialysis patients: a prospective study. *Journal of the American Society of Nephrology*. 2003;14:159-168.
397. Kutsche LM, Oyer P, Shumway N, Baum D. An important complication of Hancock mitral valve replacement in children. *Circulation*. 1979;60:98-103.
398. Fann JI, Miller DC, Moore KA, Mitchell RS, Oyer PE, Stinson EB, Robbins RC, Reitz BA, Shumway NE. Twenty year experience with porcine bioprostheses. *Annals of Thoracic Surgery*. 1996;62:1301-1311.
399. Shen M, Farge D, Daudon M, Carpentier S, Pellerin M, Lacour B, Chen L, Martinet B, Carpentier A. Proteins and bioprosthetic calcification in the rat model. *Journal of Heart Valve Disease*. 1996;5:50-57.

400. Levy RJ, Schoen FJ, Anderson HC. The identification of the vitamin K-dependent bone protein, osteocalcin, as one of the gamma-carboxyglutamic acid containing proteins present in calcified atherosclerotic plaque and mineralised heart valves. *Atherosclerosis*. 1983;46:49-56.
401. Shen M, Marie P, Farge D, Carpentier S, De Pollak C, Hott M, Chen L, Martinet B, Carpentier A. Osteopontin is associated with bioprosthetic heart valve calcification in humans. *Comptes rendus de l'Academie des Sciences Paris. Sciences de la Vie*. 1997;320:49-57.
402. Gura TA, Wright KL, Veis A, Webb CL. Identification of specific calcium binding noncollagenous proteins associated with glutaraldehyde preserved bovine pericardium in the rat subdermal model. *Journal of Biomedical Materials Research*. 1997;35:483-495.
403. Dunn JM, Marmon L. Mechanisms of calcification of tissue valves. *Cardiology Clinics*. 1985;3:385-396.
404. Levy RJ, Zenker JA, Lian JB. Vitamin K-dependent calcium binding proteins in aortic valve calcification. *Journal of Clinical Investigation*. 1980;65:563-566.
405. Rosanova IB, Lanskaya IM, Sevastianov VI. Calcium-binding capacity of serum proteins after contact with biomaterials. *Biomaterial - Living System Interactions*. 1993;1:13-18.
406. Hughes H, Tipton LS, Feuchuk D, Prabhakar G, Aboul-Enein HY, Duran CMG. Glutaraldehyde, gamma-carboxyglutamic acid and calcium in explanted bioprosthetic heart valves. *Journal of Heart Valve Disease*. 1994;3:111-116.
407. Stenflo J, Fermlund P, Egan W, Roepstorff P. Vitamin-K dependent modifications of glutamic acid residues in prothrombin. *Proceedings of the National Academy of Sciences of the U.S.A.* 1977;71:2730-2733.
408. Suttie JW, Jackson CM. Prothrombin: structure, activation and biosynthesis. *Physiological Reviews*. 1977;57:1-70.
409. Stein PD, Riddle JM, Kemp SR. Effect of warfarin on calcification of spontaneously degenerated porcine bioprosthetic valves. *Journal of Thoracic and Cardiovascular Surgery*. 1985;90:119-128.
410. Hauschka PV. Quantitative determination of gamma-carboxyglutamic acid in proteins. *Analytical Biochemistry*. 1977;80:212-223.
411. Lian JB, Skinner M, Glimcher MJ, Gallop PM. The presence of carboxyglutamic acid in the proteins associated with ectopic calcification. *Biochemica et Biophysica Research Communication*. 1976;71:349-355.
412. Gallop PM, Lian JB, Hauschka PV. Carboxylated calcium-binding proteins and vitamin K. *New England Journal of Medicine*. 1980;302:1460-1469.
413. Lian JB, Levy RJ, Bernhard W. LVAD mineralisation of gamma-carboxyglutamic acid containing proteins in normal and pathologically mineralised tissue. *American Society Artificial Internal Organs Transaction*. 1981;27:683-692.
414. Packham MA. Platelet function inhibitors. *Thrombosis and Haemostasis*. 1983;50:610-619.
415. Chandy T, Das GS, Wilson RF, Rao GHR. Surface-immobilised biomolecules on albumin modified porcine pericardium for preventing thrombosis and calcification. *The International Journal of Artificial Organs*. 1999;22:547-558.
416. Vasudev SC, Chandy T, Sharma CP. Glutaraldehyde treated bovine pericardium: changes in calcification due to vitamins and platelet inhibitors. *Artificial Organs*. 1997;21:1007-1013.
417. Tector AJ, Boyd WC, Korn ME. Aortic valve allograft rejection. *Journal of Thoracic and Cardiovascular Surgery*. 1971;62:592-601.
418. Talbert WM, Wright P. Acute aortic stenosis of a porcine valve heterograft apparently caused by graft rejection. *Texas Heart Institute Journal*. 1982;9:225-229.
419. Lupinetti FM, Cobb SM, Kioschos HC, Thomson SA, Walters KS, Moore KC. Effect of immunological differences on rat aortic valve allograft calcification. *Journal of Cardiac Surgery*. 1992;7:65-70.
420. Noera G, Fattori G, Gatti MA. Early alteration of bioprosthetic cardiac valves in sheep: influence of the immunological status. *Journal of Thoracic and Cardiovascular Surgery*. 1989;37:207-212.
421. Gong G, Seifter E, Lyman WD, Factor SM, Blau S, Frater RWM. Bioprosthetic cardiac valve degeneration: role of inflammatory and immune response reactions. *Journal of Heart Valve Disease*. 1993;2:684-693.
422. Levy RJ, Schoen FJ, Howard SL. Mechanism of calcification of porcine bioprosthetic aortic valve cusps: role of T-lymphocytes. *American Journal of Cardiology*. 1983;52:629-631.

423. Gong G, Ling Z, Seifter E, Factor SM, Frater RWM. Aldehyde tanning: the villain in bioprosthetic calcification. *European Journal of Cardio-Thoracic Surgery*. 1991;5:288-293.
424. Human P, Zilla P. Characterisation of the immune response to valve bioprostheses and its role in primary tissue failure. *Annals of Thoracic Surgery*. 2001;71:S385-S388.
425. Vincentelli A, Latremouille C, Zegdi R. Does glutaraldehyde induce calcification of bioprosthetic tissue? *Annals of Thoracic Surgery*. 1998;66:S255-S288.
426. Meade KR, Silver FH. Immunogenicity of collagenous implants. *Biomaterials*. 1990;11:176-180.
427. Gendler E, Gendler S, Nimni ME. Toxic reactions evoked by glutaraldehyde-fixed pericardium and cardiac valve tissue bioprosthesis. *Journal of Biomedical Materials Research*. 1984;18:727-736.
428. Zilla P, Weissenstein C, Bracher M, Zhang Y, Koen W, Human P, Von Oppell U. High glutaraldehyde concentrations reduce rather than increase the calcification of aortic wall tissue. *Journal of Heart Valve Disease*. 1997;6:502-509.
429. Weissenstein C, Human P, Bezuidenhout D, Zilla P. Glutaraldehyde detoxification on top of enhanced amine crosslinking dramatically reduces bioprosthetic tissue calcification in the rat model. *Journal of Heart Valve Disease*. 2000;9:230-240.
430. Zilla P, Weissenstein C, Human P, Dower T, Von Oppell UO. High glutaraldehyde concentrations mitigate bioprosthetic root calcification in the sheep model. *Annals of Thoracic Surgery*. 2000;70:2091-2095.
431. Mirzaie M, Meyer T, Saalmuller A, Dalichau H. Influence of glutaraldehyde fixation on the detection of SLA-I and SLA-II antigens and calcification tendency in porcine cardiac tissue. *Scandinavian Cardiovascular Journal*. 2000;34:589-592.
432. Human P, Zilla P. Inflammatory and immune response processes: the neglected villain of bioprosthetic degeneration? *Journal of Long-Term Effects of Medical Implants*. 2001;11:199-220.
433. Long MM, Urry DW. On the molecular mechanism of elastic fiber calcification. *American Society Artificial Internal Organs Transaction*. 1981;27:690-696.
434. Ciesliga BL, Barkasi LD, Webb CL. Glutaraldehyde crosslinking enhances calcium binding to type I collagen in-vitro. *American Journal of Cardiology*. 1991;68:421.
435. O'Brien MF, Golstein S, Walsh S, Black KS, Elkins R, Clarke D. The SynerGraft valve: a new acellular (non glutaraldehyde-fixed) tissue heart valve for autologous recellularisation: first experimental studies before clinical implantation. *Seminar of Thoracic and Cardiovascular Surgery*. 1999;11:194-200.
436. Dmitrovsky E, Boskey AL. Calcium-acidic phospholipids-phosphate complexes in human atherosclerotic aortas. *Calcified Tissue International*. 1985;37:121-125.
437. Calero P, Jorge-Herrero E, Turnay J, Olmo N, Lopez De Silanes I, Lizarbe MA, Maestro MM, Arenaz B, Castillo-Olivares JL. Gelatinases in soft tissue biomaterials. Analysis of different crosslinking agents. *Biomaterials*. 2002;23:3473-3478.
438. Boskey AL, Posner AS. Extraction of calcium-phospholipid-phosphate complex from bone. *Calcified Tissue Research*. 1976;19:273.
439. Kim KM. Lipid matrix of dystrophic calcification and urinary stone. *Scanning Electron Microscopy*. 1983:1275.
440. Boskey AL. The role of calcium-phospholipid-phosphate complex in tissue mineralisation. *Metabolic Bone Disease and Related Research*. 1978;1:137.
441. Rossi MA. Lipid extracion attenuates the calcific degeneration of bovine pericardium used in cardiac valve bioprostheses. *Journal of Experimental Pathology*. 1990;71:187-196.
442. Herrero HJ. Inhibition of bovine pericardium calcification. *Journal of Materials Science. Materials in Medicine*. 1991;2:86-88.
443. Dunmore BJ, Boughner DR, Macris N, Vesely I. A comparison of macroscopic lipid content within porcine pulmonary and aortic valves. Implications for bioprosthetic valves. *Journal of Thoracic and Cardiovascular Surgery*. 1995;110:1756-1761.
444. Shen M, Lajos PS, Farge D, Daudon M, Carpentier SM, Chen L, Martinet B, Carpentier AF. Infrared spectroscopy in the evaluation of the process of calcification of valvular bioprostheses. *Annals of Thoracic Surgery*. 1998;66:S236-S239.
445. Gleason M, Medow M, Tulenko T. Excess membrane cholesterol alters calcium movements, cystolic calcium levels, and membrane fluidity in arterial smooth muscle cells. *Circulation Research*. 1991;69:216-227.
446. Hopwood D. Theoretical and practical aspects of glutaraldehyde fixation. *Histochemistry*. 1972;4:267-303.

447. Hopwood D. Cell and tissue fixation: 1972-1982. *Histochemical Journal*. 1985;17:389-442.
448. Sabatini DD, Bensch KG, Barnnett RJ. Cytochemistry and electron microscopy: the preservation of cellular ultrastructure and enzymatic activity by aldehyde fixation. *Journal of Cell Biology*. 1963;17:19-38.
449. Simionescu D, Simionescu A, Deac R. Detection of remnant proteolytic activities in unimplanted glutaraldehyde-treated bovine pericardium and unexplanted cardiac bioprostheses. *Journal of Biomedical Materials Research*. 1993;27:821-829.
450. Rajput YS, Gupta MN. Preparation of heterozyme conjugates: trypsin-chymotrypsin and trypsin-alkaline phosphatase. *Biotechnology Applied Biochemistry*. 1989;10:242-250.
451. Simionescu D, Simionescu A, Deac R. Biochemical pathways of tissue degeneration in bioprosthetic cardiac valves: the role of matrix metalloproteinases. *American Society Artificial Internal Organs Journal*. 1996;42:M561-M567.
452. Nijweide PJ, Kawailarang-DeHaas EWM, Wassenaar AM. Alkaline phosphatase and calcification: correlated or not? *Metabolic Bone Disease Related Research*. 1981;3:61-66.
453. Farley JR, Puzas JE, Baylink DJ. Effect of skeletal alkaline phosphatase inhibitors on bone cell proliferation in-vitro. *Mineral and Electrolyte Metabolism*. 1982;7:316-323.
454. Register TC, Warner GP, Wuthier RE. Effect of L- and D-tetramisole on 32P and 45Ca uptake and mineralisation by matrix vesicle-enriched fractions from chicken epiphyseal cartilage. *Journal of Biological Chemistry*. 1984;259:922-928.
455. Gehron RP. The biochemistry of bone. *Endocrinology and Metabolism Clinics of North America*. 1989;18:858-902.
456. Boskey AL. Non-collagenous matrix proteins and their role in mineralisation. *Journal of Bone and Mineral Research*. 1989;6:111-123.
457. Gehron RP, Bianco P, Termine JD. The cellular biology and molecular biochemistry of bone formation. In: Coe FL, Favus MJ, eds. *Disorders of Bone and Mineral Metabolism*. New York: Raven Press; 1992:241-263.
458. Thubrikar M, Skinner JR, Aouad J, Finkelmeier B, Nolan SP. Analysis of the design and dynamics of aortic valvular bioprostheses in-vivo. *Journal of Thoracic and Cardiovascular Surgery*. 1982;84:282-290.
459. Thubrikar M, Skinner JR, Eppink RT, Nolan SP. Stress analysis of porcine bioprosthetic heart valves in-vivo. *Journal of Biomedical Materials Research*. 1982;16:811-826.
460. Deck JD, Thubrikar MJ, Nolan SP, Aouad J. Role of mechanical stress in calcification of bioprostheses. In: Cohn LN, Gallucci V, eds. *Cardiac Bioprostheses*. New York: Yorke Medical Books; 1982:293-305.
461. Broom ND. Fatigue-induced damage in glutaraldehyde-preserved heart valve tissue. *Journal of Thoracic and Cardiovascular Surgery*. 1978;76:202-211.
462. Grabenwoger M, Grimm M, Eybl E. New aspects of the degeneration of bioprosthetic heart valve failure: pathology and pathogenesis. *Cardiology Clinics*. 1984;2:717-739.
463. Golomb G, Schoen FJ, Smith MS, Linden J, Dixon M, Levy RJ. The role of glutaraldehyde-induced cross-links in calcification of bovine pericardium used in cardiac valve bioprostheses. *American Journal of Pathology*. 1987;127:122-130.
464. Levy RJ. Glutaraldehyde and the calcification mechanism of bioprosthetic heart valves. *Journal of Heart Valve Disease*. 1994;3:101-104.
465. Sherman FS, Schoen FJ, Hawley MA, Nichols J, Levy RJ. Collagen crosslinks: a critical determinant of bioprosthetic heart valve calcification. *American Society Artificial Internal Organs Transaction*. 1984;30:577-581.
466. Blumenthal NC, Posner AS, Silverman LD. Effect of proteoglycans on in-vitro hydroxyapatite formation. *Calcified Tissue International*. 1979;27:75-79.
467. Grabenwoger M, Sider J, Fitzal F, Zelenka C, Windberger U, Grimm M, Moritz A, Bock P, Wolner E. Impact of glutaraldehyde on calcification of pericardial bioprosthetic heart material. *Annals of Thoracic Surgery*. 1996;62:772-777.
468. Grabenwoger M, Brock P, Fitzal F, Schmidberger A, Grimm M, Laufer G, Bergmeister H, Wolner E. Acidic glycoproteins accumulate in calcified areas of bioprosthetic tissue. *Journal of Heart Valve Disease*. 1998;7:229-234.
469. Schoen FJ, Levy RJ, Piehler HR. Pathological considerations in replacement heart valves. *Cardiovascular Pathology*. 1992;4:69-73.
470. Schryer PJ, Tomasek ER, Starr A, Wright JT. Anticalcification effect of glutaraldehyde-preserved valve tissue stored for increasing time in glutaraldehyde. In: Bodnar E, Yacoub M, eds. *Proceedings of the Third International Symposium on Biologic and Bioprosthetic Valves*. New York: Yorke Medical Books; 1986:471-477.

471. Elbers PF. Ion permeability of the egg of *Limnaea stagnalis* L. on fixation for electron microscopy. *Biochimica et Biophysica Acta*. 1966;112:318-329.
472. Bone Q, Denton EJ. The osmotic effects of electron microscope fixatives. *Journal of Cell Biology*. 1971;49:571-581.
473. Hoffman D, Gong G, Liao K, Macaluso F, Nikolic SD, Frater RWM. Spontaneous host endothelial growth on bioprostheses: influence of fixation. *Circulation*. 1992;86:II75-II79.
474. Speer DP, Chvapil M, Eskelson CD, Ulreich J. Biological effects of residual glutaraldehyde in glutaraldehyde-tanned collagen biomaterials. *Journal of Biomedical Materials Research*. 1980;14:753-764.
475. Wiebe D, Megerman J, L' Italien GJ, Abbott WM. Glutaraldehyde release from vascular prosthesis of biologic origin. *Surgery*. 1988;104:26-33.
476. Form DM, Pratt BM, Madri JA. Endothelial cell proliferation during angiogenesis. *Laboratory Investigation*. 1986;55:521-530.
477. Chvapil M, Speer D, Mora W, Eskelson CD. Effect of tanning agent on tissue reaction to tissue implanted collagen sponge. *Journal of Surgical Research*. 1983;35:402-409.
478. Eybl E, Griesmacher A, Grimm M, Wolner E. Toxic effects of aldehydes released from fixed pericardium on bovine aortic endothelial cells. *Journal of Biomedical Materials Research*. 1989;23:1355-1365.
479. Van Luyn MJA, Van Wachem PB, Olde Damink LHH, Dijkstra PJ, Feijen J, Nieuwenhuis P. Relations between in-vitro cytotoxicity and crosslinked dermal sheep collagen. *Journal of Biomedical Materials Research*. 1992;26:1091-1110.
480. Chanda J. Prevention of calcification of heart valve bioprostheses: an experimental study in rat. *Annals of Thoracic Surgery*. 1995;60:S339-S342.
481. Chanda J. Post-treatment with amino compounds effective in prevention of calcification of glutaraldehyde-treated pericardium. *Journal of Artificial Organs*. 1994;18:408-410.
482. Zilla P, Fullard L, Trescony P, Meinhart J, Bezuidenhout D, Gorlitzer M, Human P, Von Oppell U. Glutaraldehyde detoxification of aortic wall tissue: a promising perspective for emerging bioprosthetic valve concept. *Journal of Heart Valve Disease*. 1997;6:510-520.
483. Huang-Lee LHH, Cheung DT, Nimni ME. Biochemical changes and cytotoxicity associated with the degradation of polymeric glutaraldehyde derived cross-links. *Journal of Biomedical Materials Research*. 1990;24:1185-1201.
484. Thoma RJ, Phillips RE. The role of material surface chemistry in implant device calcification: a hypothesis. *Journal of Heart Valve Disease*. 1995;4:214-221.
485. Cheung DT, Nimni ME. Mechanism of crosslinking of proteins by glutaraldehyde I. Reaction with model compounds. *Connective Tissue Research*. 1982;10:187-199.
486. Cheung DT, Nimni ME. Mechanism of crosslinking of proteins by glutaraldehyde II. Reaction with monomeric and polymeric collagen. *Connective Tissue Research*. 1982;10:201-216.
487. Bowes JH, Cater CW. The reaction of glutaraldehyde with proteins and other biological materials. *Journal of the Royal Microscopical Society*. 1966;85:193-200.
488. Bowes JH, Cater CW. The interaction of aldehydes with collagen. *Biochimica et Biophysica Acta*. 1968;168:341-352.
489. Chvapil M. Reconstituted collagen. In: Viidik A, Vuust J, eds. *Biology of Collagen*. London: Academic; 1980:313-324.
490. Golomb G, Ezra V. Prevention of bioprosthetic heart valve tissue calcification by charge modification: effects of protamine binding by formaldehyde. *Journal of Biomedical Materials Research*. 1991;25:85-98.
491. Angell WW, Angell JD, Kosek JC. Twelve-year experience with glutaraldehyde-preserved porcine xenografts. *Journal of Thoracic and Cardiovascular Surgery*. 1982;83:493-502.
492. Schoen FJ, Collins JJ, Cohn LH. Long-term failure rate and morphologic correlations in porcine bioprosthetic heart valves. *American Journal of Cardiology*. 1983;51:957-966.
493. Imamura E, Sawatani O, Koyanagi H, Noishiki Y, Miyaya T. Epoxy compounds as a new crosslinking agent for porcine aortic leaflets: subcutaneous implant studies in rats. *Journal of Cardiac Surgery*. 1989;4:50-57.
494. Olde Damink LHH. Structure and properties of crosslinked dermal sheep collagen. In: Twente, The Netherlands: University of Twente; 1992:93-111.
495. Van Luyn MJA, Van Wachem PB, Dijkstra PJ, Olde Damink LHH, Feijen J. Calcification of subcutaneously implanted collagens in relation to cytotoxicity, cellular interactions and crosslinking. *Journal of Materials Science. Materials in Medicine*. 1995;6:288-296.

496. Niclaude M, Lemaire J, Letort M. The kinetics and mechanism of photochemical oxidation of aldehydes by molecular oxygen. In: *Advances in Photochemistry*. New York: Wiley and Sons; 1966:25-48.
497. Larkin DR. The role of catalysts in the air oxidation of aliphatic aldehydes. *Journal of Organic Chemistry*. 1990;55:1563-1568.
498. Petite H, Rault I, Huc A, Menasche P, Herbage D. Use of the acyl azide method for crosslinking collagen-rich tissues such as pericardium. *Journal of Biomedical Materials Research*. 1990;24:179-187.
499. Levy RJ, Schoen FJ, Howard JL, Levy JL. Calcification of cardiac valve bioprostheses: host and implant factors. In: Rubin RP, Weiss GB, Putney JB, eds. *Calcium in Biological Systems*. New York: Plenum Press; 1985:661.
500. Vasudev SC, Chandy T. Effect of alternative crosslinking techniques on the enzymatic degradation of bovine pericardia and their calcification. *Journal of Biomedical Materials Research*. 1997;35:357-360.
501. Vyavahare NR, Chen W, Joshi RR, Lee CH, Hirsch D, Levy J, Schoen FJ, Levy RJ. Current progress in anticalcification for bioprosthetic and polymeric heart valves. *Cardiovascular Pathology*. 1997;6:219-229.
502. Nimni ME, Myers D, Ertl D, Han B. Factors which affect the calcification of tissue derived bioprostheses. *Journal of Biomedical Materials Research*. 1997;35:531-537.

Chapter 2

2 Glutaraldehyde.

2.1 Introduction

Glutaraldehyde (1,5-pentanedialdehyde CAS111-30-8) is a bifunctional reagent containing two aldehyde groups. It has been the most extensively used cross-linking agent for the treatment of bioprosthetic devices for over thirty years¹⁻³. It is readily available, inexpensive and its aqueous solutions can effectively cross-link collagenous tissues in a relatively short period⁴. The first isolation and characterisation of glutaraldehyde, from the ozonolysis of cyclopentene, was reported in 1908⁵. The traditional process for the preparation of glutaraldehyde (a two-step process, converting acrolein via an ethoxy dihydro pyran to glutaraldehyde by acid hydrolysis)⁶ involved relatively expensive raw materials and drastic reaction conditions⁷. Thus, an improved method is now used in industry, giving a better yield and employing moderate reaction conditions⁸. The process involves hydrogenation of the raw material cyclopentadiene to cyclopentene, which is then oxidised to glutaraldehyde by hydrogen peroxide with tungstic acid as catalyst and t-butanol as solvent, whilst stirring at room temperature for 24 hours.

2.1.1 History

Glutaraldehyde was reported to be an excellent tanning agent for the leather industry in the early 1950s⁹, producing fairly good leather of a light tan colour over a very wide pH range. It was also more stable to washing processes and alkaline solutions than other tanning agents such as formaldehyde¹⁰. In 1963, glutaraldehyde was first introduced as a fixative for electron microscopy and electron histochemistry¹¹. Due to the instability and subsequent failure of formaldehyde-treated valve bioprostheses¹²⁻¹⁴, other aldehydes, including glutaraldehyde, were investigated for

their cross-linking properties. It was found that glutaraldehyde introduced more stable cross-links into collagen¹⁵ compared to other aldehydes investigated. Glutaraldehyde treatment resulted in enhanced mechanical properties of treated tissue-derived materials and also seemed to introduce chemically stable cross-links that are resistant to biologic degradation. Furthermore, it appeared to be the most effective agent for decreasing the antigenicity and increasing the stability of the tissue. Glutaraldehyde pre-treatment of bioprosthetic tissue was thus adopted in 1968 as the method of choice in preparation of tissue valves¹. Current commercial bioprosthetic valves are treated exclusively with glutaraldehyde; its concentrations are kept low and vary between 0.2% v/v (Hancock valve) and 0.625% v/v (Carpentier-Edwards valve). These low concentrations are considered to be insufficient for efficient sterilisation but higher concentrations lead to unwanted stiffening of the valve leaflets¹⁶. After primary fixation by glutaraldehyde, the valves are normally stored in either glutaraldehyde or formaldehyde to ensure a better sterilisation. The successful use of thousands of glutaraldehyde-treated bioprosthetic implants over the last decades, indicates its effectiveness and clinical acceptability despite its cytotoxicity^{3,17,18}.

2.1.2 The fixation process

The glutaraldehyde treatment used in the industrial production of valves is intended to reduce the immunogenicity of the material, increase its resistance to degradation by both the host and bacterial enzymes and sterilise the tissue¹⁹. In the valve industry, cross-linking is presently carried out in large containers, which unfortunately introduces impurities that can have a detrimental effect on the fixation procedure²⁰. Delay in the fixation, due to the distance between abattoirs and fixation/production plants, may also have an effect on the resulting bioprostheses. Other factors such as temperature, reagent concentration, pH etc. can also be important as will be discussed below. Additionally, before implantation in a patient, valves are stored in buffered aldehydes (formaldehyde or glutaraldehyde depending on the valve manufacture) for varying lengths of time. Manufactures also advise storage between 5 and 25° C, avoidance of exposure to sun or UV light and storage for less than 36 months. An optimal fixation procedure, to preserve the ultrastructural integrity and stability of contemporary manufactured bioprosthetic heart valves, has been investigated^{21,22} and the conditions are discussed below.

2.1.2.1 Temperature:

On raising the cross-linking temperature, two events occur: faster glutaraldehyde penetration and tissue reaction, as well as an accelerated autolytic process. At 37°C, it was found that there is faster penetration of glutaraldehyde into the tissue and that the tissue damage caused by autolysis is less severe than found at room temperature (the relationship between autolysis and cross-linking is not linear). The best ultrastructural tissue preservation is found at 4°C, whilst the worst results are found at room temperature (22°C), although room temperature cross-linking of commercial tissue has been used experimentally in many cases and the fact that the industrial fixation of valves is carried out at room temperature.

Glutaraldehyde commercial solutions and valves stored in buffered glutaraldehyde solutions tend to become darker and more yellow in colour especially after 23-32 months²¹; although no apparent changes are seen when stored at refrigerated temperature. It is assumed that the colour formation may be due to polymerisation of glutaraldehyde mechanism, forming oligomeric and polymeric products that might react with the valve tissue to produce this yellower colour (analogous to a Schiff base colour)²¹. It is known that glutaraldehyde polymerisation increases exponentially with temperature²³ and that the rate of glutaraldehyde polymerisation is influenced by many factors including concentration, pH, and temperature²⁴. The storage temperature, but not the length of storage, was shown to have a significant effect on some mechanical properties of the valves²¹ that may influence their long-term in-vivo performance.

2.1.2.2 pH/solvents:

The pH of the glutaraldehyde solution remains constant at refrigerator (4°C) temperature, but at room temperature the pH tends to drop significantly with time^{21,25}. The pH of stored valves is usually kept as similar as possible to the pH of blood (7.4), by the use of phosphate-buffered glutaraldehyde solutions, without any control of the temperature. Some studies have indicated that the higher the pH and the lower the temperature of the glutaraldehyde incubation solution, the greater the amount of glutaraldehyde bound to bovine pericardial valve tissue²⁶, thus glutaraldehyde uptake was enhanced at a temperature of 4°C and pH of 10. The glutaraldehyde fixation always takes place in water-based phosphate buffered

solutions in the valve industry, as it has been found that the use of other solvents can yield materials with mechanical properties not useful for heart valve leaflets²⁷.

2.1.2.3 Delayed fixation:

There is conflicting evidence in the literature relating to the effect of delayed fixation. Whilst some report no major effect of a delay²⁸, other studies report that immediately after slaughter signs of cell damage appear, and that immediate fixation rather than after two days of storage on ice, decreased aortic wall calcification in rats by 25%²⁹.

2.1.2.4 Concentration of glutaraldehyde:

For fear of stiffness and tissue toxicity, “sub-optimal” concentrations of cross-linking agents (glutaraldehyde) were chosen, and thus the resultant low immunogenicity³⁰, alkaline phosphatase activity³¹ and protease activity³² had to be accepted along with a known risk of calcification. Calcification has been related to the amount of glutaraldehyde introduced into the collagen^{33,34}, hence the use of a low concentration of glutaraldehyde in the manufacture of bioprostheses. Initially, residual antigenicity was not considered to be a major contributing factor to bioprosthetic tissue degeneration, however more recent studies have shown a correlation between antigenicity and calcification^{35,36}.

The actual concentrations of glutaraldehyde used commercially range from 0.2% to 0.65% v/v. Collagen cross-linked with a glutaraldehyde concentration as low as 0.0075% demonstrated a significantly better resistance to proteolytic degradation than non-cross-linked material³⁷. However, glutaraldehyde-treated tissue was shown to retain significant antigenicity when a 0.2% concentration was used³⁸, but it has also been shown that short-term exposure to such low concentrations of glutaraldehyde optimally preserved the natural structure of pericardial valves³⁹. Cross-linking can also be undertaken at slightly higher concentrations. For example, it was shown that a significant improvement in structural preservation occurred at a concentration of 1%²² compared to lower concentrations and that no inflammatory reactions to implants were seen when a concentration of 2.5% was used⁴⁰. However, at a concentration of 4%, a tissue-hardening phenomenon was observed⁴¹. Increased exposure to glutaraldehyde⁴² has been shown to reduce calcification (see later in this section) and it has also been shown that higher glutaraldehyde concentrations

(increasing concentration from 0.2% to 3%) can reduce (by almost one third) rather than increase tissue calcification in both the rat^{29,43} and sheep model⁴⁴. This finding is valid for porcine valve leaflets, pericardial tissue and also for aortic wall tissue. A further benefit of higher glutaraldehyde concentrations has been stated to be improvement in the ultra structural tissue preservation²², a reduction in the macrophage activation⁴⁵ and suppression of the immune response³⁶. However, the fact that the calcification sites remained the same after fixation at higher concentrations of glutaraldehyde, whereas overall calcification diminished, suggests that improved cross-linking only mitigates rather than alters the calcification mechanism⁴⁴.

2.1.2.5 Physical state of the glutaraldehyde cross-linker:

Glutaraldehyde is used as a solution buffered with phosphate at pH 7.4, in the valve industry and in the majority of studies reported in the literature. However, it has been reported that the use of glutaraldehyde vapour would improve the resistance of the treated tissue to degradation (collagenase tested in-vitro), increase the uniformity of the treatment and minimise the homopolymerisation of the cross-linking agent⁴⁶. The cross-linking could also be better controlled, as it would not be influenced by the ionic strength of the reaction medium, pH or concentration. The glutaraldehyde vapour, obtained from an 8% aqueous solution, was at a very low concentration in the gaseous phase owing to its small vapour pressure, however it was demonstrated to efficiently cross-link soluble collagen films⁴⁷.

2.1.2.6 Duration of fixation:

The variation in fixation methods used by different valve manufacturers lies mainly in the duration of fixation: valve tissues have been reported as having been fixed for periods of time ranging from a few hours to several months. Whilst some authors have reported complete glutaraldehyde uptake by bioprosthetic tissue within 24 hours of incubation⁴⁸, others have observed that complete glutaraldehyde uptake did not occur even one month after the onset of treatment when the bioprosthesis was preserved in glutaraldehyde solution of a particular concentration⁴⁹. Long-term storage of collagen or collagenous tissues in glutaraldehyde has been reported as being essential for optimal cross-linking to occur⁵⁰ because the polymerisation reaction of glutaraldehyde and lysine is found to be fast initially but continues to

proceed slowly with time. It has also been mentioned that long-term fixation (bovine and porcine pericardial tissue stored in glutaraldehyde for 15 months) might decrease susceptibility to calcification⁵¹. The authors reported inverse linear-relationships between the time in glutaraldehyde and the amount of extractable calcium in both types of tissue and also between duration of storage and shrinkage temperature. They concluded that the decrease in calcification was related to a decline in the number of glutaraldehyde cross-links within the tissue. Others presume that, whether prolonged or short-term, fixation probably does not change the features of calcification of the bioprosthesis when only glutaraldehyde treatment is used⁵². Such a discrepancy in the literature shows that, although various duration of fixation are used in valves industry for over 40 years, the important factor that represents the duration of fixation still requires further research, which is impeded by the lack of communication between the valve manufacturers.

2.1.2.7 Storage of valves in aldehydes:

After the initial glutaraldehyde fixation and before implantation in a patient, valves are stored in buffered aldehydes (formaldehyde or glutaraldehyde) for varying lengths of time. This is because the concentration of glutaraldehyde used routinely for fixation is not considered sufficient to ensure valve sterility. Formaldehyde was mainly used in the 1980s as a storage solution^{16,53,54}, while nowadays both glutaraldehyde and formaldehyde are used, depending mainly on the valve manufacturing protocol. It has been shown that tissue samples taken from valves stored for prolonged periods of time in formaldehyde failed to calcify in the rat subcutaneous implant model⁵⁵. Schryer et al have also demonstrated the benefit of long-term storage in glutaraldehyde on resistance against calcification⁵¹. Additionally, it has been shown that prolonged storage (>5 years) in glutaraldehyde can reduce the levels of calcification occurring in porcine aortic valves in the rat subcutaneous model⁵⁶. Also, valves stored in a glutaraldehyde solution for an extended period of time were shown by Girardot et al to resist calcification better than those that had been fixed for a short term⁵⁷. They found that cuspal calcification decreased significantly in the rat subcutaneous model after 12 months storage in glutaraldehyde. However, if prior to implantation, the valves were re-exposed to a similar glutaraldehyde solution at the end of the 12 months storage period, the cusps displayed high levels of calcification. It was thus proposed that re-exposure to

glutaraldehyde forms new Schiff bases and re-introduces free aldehydes that may have been converted during storage and so may have a key function in cuspal calcification. A more recent dynamic in-vitro study showed variation in calcification between similarly glutaraldehyde-stored valves (two months and four years): the valves with the shorter storage period calcified to the highest degree⁵⁸. In fact, fixation/storage time has been an uncontrolled variable in many studies and has thus made comparison of calcification rates between studies difficult.

Another matter arises when treated-valves are stored in aldehydes. Although many authors seem to assume that the formaldehyde incubation step (storage/sterilisation) does not alter the glutaraldehyde incorporated into the tissue during cross-linking^{3,54,59} and that formaldehyde is not retained within the tissue, it appears that formaldehyde, due to its smaller molecular size, can be incorporated into the glutaraldehyde-fixed tissue and may replace Schiff base bonded glutaraldehyde⁵⁵. Formaldehyde is thus displacing some of the glutaraldehyde from the treated-porcine or bovine tissue, and is also reacting with further free 6-amino lysyl groups that were stereochemically inaccessible to the larger glutaraldehyde molecules⁶⁰. This displacement of glutaraldehyde by formaldehyde is ruled out theoretically by organic chemistry principles that dictate that if a second aldehyde is added to the glutaraldehyde-treated tissue, substitution of the original aldehyde in the Schiff base may occur, depending on the concentration of this second aldehyde^{61,62}. It is hypothesised that formaldehyde condensation and crossed-Cannizzaro reactions can occur in the presence of an excess of formaldehyde, reducing the formyl groups and forming methylol groups⁶³. The authors also suggested that long-term storage in formaldehyde may be significantly better than glutaraldehyde, since at neutral pH (pH 7.4) formaldehyde is more reactive than glutaraldehyde and physically smaller, thus the formaldehyde aldol/crossed-Cannizzaro reactions might proceed at a much higher rate.

2.1.2.8 Washing:

Generally, prior to implantation, valves are washed with phosphate-buffered saline solutions to remove any unbound cytotoxic glutaraldehyde moieties. Tissues fixed in glutaraldehyde exhibit ranging degrees of toxicity due to the presence of glutaraldehyde (while untreated collagen is compatible with cell growth⁶⁴), the level

of which depends upon the storage solution and method of washing⁶⁵. The toxic effects of glutaraldehyde are apparent at very low concentrations (>10-25ppm)⁶⁶. It has been reported that glutaraldehyde-treated tissues washed in a glycine buffer showed less toxicity than simply glutaraldehyde-treated tissues, with the amino groups reacting with the excess free aldehydes that are responsible for the cytotoxicity⁶⁵. The effectiveness of the usual rinse with phosphate-buffered buffer was reported limited, because the glutaraldehyde reactivity could persist for a long period of time in the interstices of the tissues⁵⁰.

2.2 Chemistry of glutaraldehyde

2.2.1 Glutaraldehyde in solution

2.2.1.1 Introduction:

The chemical composition of glutaraldehyde solutions is not simple and is still in the process of being clearly defined (one aim of this thesis). A simple formula of five carbons with two carbonyl groups (monomeric glutaraldehyde) was first attributed to glutaraldehyde in solution and is still accepted these days by some authors. However, if such a formula was true, reaction of the aldehyde with the amino groups of proteins would lead to the formation of a Schiff base. This reaction would be reversible (pure principle of organic chemistry) and the product would not withstand reported treatments with acids, urea, semicarbazide and heat⁶⁷⁻⁶⁹. In fact, it appears that glutaraldehyde is actually a mixture of monomeric dialdehydes with varying amounts of “impurities”^{24,66} (including glutaric acid, acrolein, glutaraldoxime and polymers of glutaraldehyde)^{20,70}, along with mono- and di-hydrated monomeric glutaraldehyde, oligomers, monomeric and polymeric cyclic hemiacetals, various aldol condensation products (such as the α,β -unsaturated polymers)⁷¹ and probably other kinds of impurities not yet reported. The oxidation of aldehyde in solution to form carboxylic acids (glutaric acid being the dicarboxylic acid of glutaraldehyde) has been reported in the literature^{72,73}. A relatively recent analysis of the glutaraldehyde vapour by GC-FTIR revealed six main components, which three has been characterised as being methanol, butyraldehyde and likely what they refer to as monomeric glutaraldehyde⁷⁴. The presence of methanol being explained by the fact that the addition of methanol in glutaraldehyde solutions has been recommended to

enable them to be kept for longer periods through the formation of a hemi-acetal⁷⁵. In aqueous solution, it is believed that all these chemical species are in equilibrium but if a change in conditions occurs (e.g. pH or temperature) then the equilibrium will be displaced and the concentrations of the various species will be altered. However, the actual content of the “impurities” of glutaraldehyde is quite controversial. For example, it has been reported that the impurities of glutaraldehyde are not likely to be due to the accumulation of glutaric acid, because of the absence of the UV absorbance of glutaric acid in the absorbance of glutaraldehyde solutions⁷⁶. Also, while extensive polymerisation is often reported to be present, there is no consensus on the mechanism and nature of the polymerisation process^{23,24}. However, most of these “impurities” are thought to have a major impact on the phenomenon of cross-linking proteins with glutaraldehyde²⁴. Because of the many contradictory statements found in the literature over the last 40 years, and also because of the importance of the composition of glutaraldehyde solution for this thesis, a more complete assessment of all the molecular structures of glutaraldehyde in solution will be reviewed in section 2.2.2.

2.2.1.2 Purification methods:

Glutaraldehyde used in electron microscopy and for fixation in the valve industry is referred to as EM grade, distillation purified. This grade is supposed to provide a highly pure glutaraldehyde solution, free from polymers and other contaminants, sealed under dry nitrogen. However, it is known that repeated defrosting and recapping of a solution will promote the polymerisation of glutaraldehyde, shown by the production of an ultraviolet absorption peak at 235nm rather than at 280nm, as seen with pure EM grade glutaraldehyde. (The carbonyl peak at 280nm is due to monomeric glutaraldehyde, whereas the peak at 235nm is attributed to the presence of polymeric products⁷⁷). Indeed, purified glutaraldehyde was reported⁷⁸ to be unstable over time in aqueous solution at pH 7.4, since a freshly purified solution (1%) after 1h of equilibrium at room temperature showed limited polymerisation measured at 235nm, while after 24h extensive polymerisation was observed. The glutaraldehyde solution used in our work (25% glutaraldehyde solution EM grade Merck, UK) was reported to be stable for at least three days when refrigerated at 4°C⁷⁹. Various methods have been suggested to remove the polymeric impurities. For example, a method of vacuum distillation has been proposed⁸⁰, as has

purification by fractionation on Sephadex G-10⁸¹ or by the use of activated charcoal²⁰. However, even after five purifications with activated charcoal, some impurities were still observed. The two main UV peaks found in commercial glutaraldehyde solutions (the carbonyl peak at 280nm and the peak at 235nm) are commercially used to assess the purity of the solution.

2.2.1.3 Effects of temperature, pH and concentration:

Generally, pH is considered to be an important factor that fundamentally controls the molecular state of glutaraldehyde⁸², although sometimes contradicted⁸³. Polymerisation of glutaraldehyde is known to be enhanced at high concentration (>0.5%) and at alkaline pH. Temperature is also a factor, which can affect the molecular structure of glutaraldehyde in solution²⁴. For example, increasing monomer concentration and decreasing hemiacetal concentration is seen when the temperature is raised⁸³. Polymerisation has also been reported to be independent of light and oxygen, and almost independent of temperature in the range 1-25°C⁸⁴. However, in contrast, although no polymerisation was reported to occur when a solution of glutaraldehyde was stored for 5 months at -14°C, there was a slight increase with storage at 4°C and a rapid increase with storage around 20°C which continued with increasing temperature²³. Other workers have shown that glutaraldehyde solutions equilibrated at various increasing temperatures (25-40°C) did not induced new components when compared to a room temperature solution but the concentration of the components was reported to increase⁷⁴. Yokota et al have reported the structure of glutaraldehyde in solution be temperature dependent between -60°C and 40°C⁸⁵: between -60°C and 0°C up to 80% of glutaraldehyde is in form A (see figure 2.1 below), while at temperatures above 0°C form B predominates, along with traces of form A.

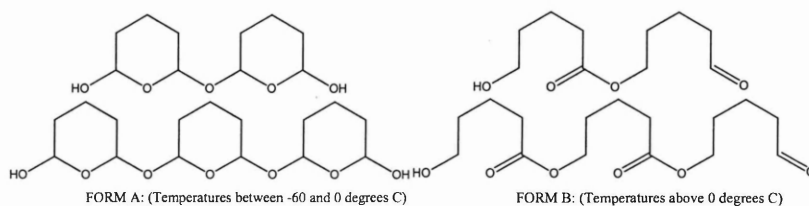


Figure 2.1: Two forms of glutaraldehyde oligomers present in solution in function of the temperature factor as reported by Yokota et al⁸⁵.

The formation of glutaraldehyde monomers from polymeric forms was reported to be enhanced by heating for a short time (less than 1 hour) below 90°C, although heating for longer periods or heating at temperatures higher than 90°C could also enhance the formation of glutaraldehyde polymers⁸⁶. It has been reported also that the concentration of free glutaraldehyde will rise from 4% at room temperature to 35% at 50°C⁸³. Ruijgrok et al have reported that high temperature promoted the cross-linking of collagen by glutaraldehyde, allowing the use of lower glutaraldehyde concentrations⁸⁷. In the same study, microwave irradiation was showed to be more effective in enhancing the cross-linking process compared with conventional heating. An even distribution of cross-links was thought to have been achieved by pre-soaking the tissue in glutaraldehyde at low temperature with subsequent short-time high temperature homogeneous heating in a microwave, also enhancing the speed of fixation. The process of glutaraldehyde polymerisation in function of temperature has been a matter of discussion and disagreement since it was reported to increase linearly⁷⁶, or exponentially with temperature²³.

The effect of pH on glutaraldehyde was also investigated by Rasmussen and Albrechtsen²³. They reported that the polymerisation rate of glutaraldehyde increased when the pH was slightly acidic or basic, whilst the rate of polymerisation decreased somewhat on addition of buffers. Changes in the pH of commercial glutaraldehyde solutions have also been reported to lead to an increase in the amount of glutaraldehyde polymers⁸⁸. The polymers formed in aqueous acidic solutions are thought to be largely of the acetal-like structure type⁸⁹. While acidic solutions of glutaraldehyde stored at room temperature in a closed system remain stable (below pH 5 polymerisation is reported to be very slow⁹⁰), polymerisation occurs rapidly above pH 8.0 (and even above pH 6.5²³) with observable reductions in the free aldehyde^{15 91}. In basic solutions, glutaraldehyde was reported to form long α,β -unsaturated polymers⁸² that may include up to eight elementary molecules of glutaraldehyde⁷¹. Glutaraldehyde concentrations, in freshly prepared alkaline solutions, have been shown to fall by approximately 45% in 14 days, indicating polymers formation. The rate of polymerisation was reported to be rapid in alkaline solutions even at 4°C⁹². Such polymers have been hypothesised to give long and flexible cross-links with proteins chains that increased molecular mobility and improved the accessibility of other amino (lysyl) groups⁹³. It has been suggested that

a polymer chain longer than the five carbons glutaraldehyde monomer is necessary to bridge the gap between appropriate amino acids in the collagen molecule. In the valve industry, it has also long been believed that at least some glutaraldehyde polymer should be present for effective cross-linking^{77,94}. This statement was later reiterated by reporting that during the cross-linking reaction, polymerisation was needed to bridge larger gaps between two reaction sites⁹⁵. Excessive polymerisation, on the other hand, is considered undesirable since the number of available aldehyde groups is greatly reduced⁹⁴. Additionally, under strong alkaline conditions or in the presence of sodium hydroxide, Cannizzaro reaction can take place⁹⁶ which enables the aldehyde groups in polymers of glutaraldehyde to be converted into a carboxyl and a hydroxyl group as can be seen in figure 2.2.

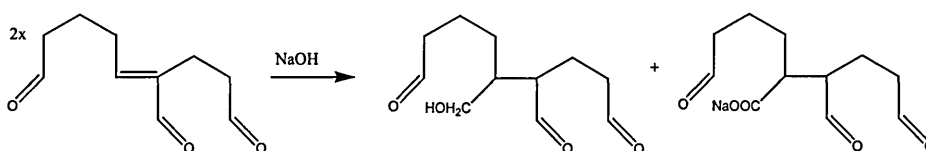


Figure 2.2: Cannizzaro reaction taking place under strong alkaline conditions (or under the presence of sodium hydroxide) on an aldol condensation dimer product.

2.2.2 Review of the various structures of glutaraldehyde in aqueous solutions

2.2.2.1 Hemiacetal formation and polymerisation:

It was found from a ^1H NMR study of a solution of glutaraldehyde that it undergoes rapid hydration in water to form an equilibrium between monomeric glutaraldehyde, its mono- and di-hydrates, and the cyclic hemiacetal form, in which equilibrium the hydrates were thought to predominate⁸⁹ (see figure 2.3 below). The dihydrate can cyclise to form a hemiacetal⁹⁷, whilst the formation of a poly-cyclic hemiacetal was possibly first proposed by Aso and Aito^{98,99}, although the structure given was not exactly the one later proposed by Yokota et al⁸⁵ and then also by Hardy et al⁸⁹, which is now well accepted (see figure 2.3 below). A later UV and ^1H NMR study showed that glutaraldehyde in a 70% v/v solution at 20°C is mostly present as an equilibrium between the monomeric glutaraldehyde (<15%), the cyclic hemiacetal and their oligomers ($n>2$) (both accounting for about the last 85%)⁷¹. They also reported a limited presence of glutaraldehyde hydrates, in contrast to the earlier work. A ^{13}C NMR study almost corroborated these results by proposing the following relative composition for glutaraldehyde solution at 23°C: 4% free glutaraldehyde, 16%

monohydrate, 9% dihydrate, 35% each of cis and trans isomers of the cyclic hemiacetal⁸³, which subsequently polymerises as shown in figure 2.3. They also attributed a minor contribution to the oligomers postulated by Korn et al⁷¹ and a major one to the hemiacetal structures. Additionally, they reported that the composition varied slightly with concentration and pH, whilst temperature had a profound effect. The above composition was slightly refined by a later FTIR and NMR study⁸², where it was demonstrated that at 25°C, a 25% v/v commercial glutaraldehyde solution (at pH~3) contains 3% monomeric glutaraldehyde, 79% water and 18% hydrated molecules in the form of the unstable cyclic hemiacetal and its oligomers ($n \geq 2$), in rapid reversible temperature-dependent equilibria with one another. It was reported in a relatively recent UV and light scattering study over the pH range 3-8, that a 2-20% v/v glutaraldehyde solution at room temperature consisted of 10.8% monomeric glutaraldehyde, 10.4% monohydrate, 2.5% dihydrate, 76% cyclic hemiacetal and very little hemiacetal polymers¹⁰⁰. In contrast, these authors in the same study reported that a 70% v/v solution of glutaraldehyde consisted of 7.5% of monomeric glutaraldehyde, 6.8% monohydrate, 1.7% dihydrate, and 85% in total of mono and polymeric cyclic hemiacetal.

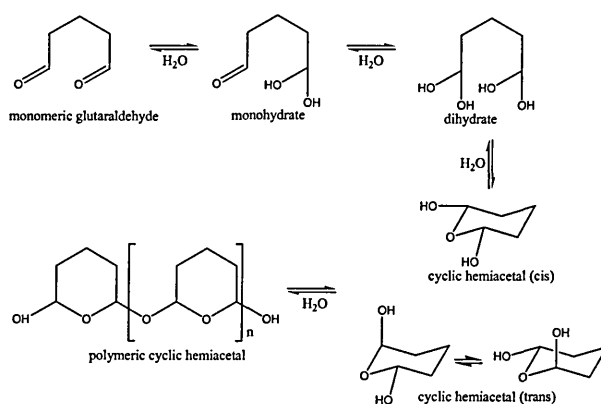


Figure 2.3: Hydrated states and cyclic hemiacetal formation of glutaraldehyde as first proposed by Hardy et al⁸⁹; the existence of the two isomers of the cyclic hemiacetal first mentioned by Korn et al⁷¹ and first characterised by Whipple and Ruta⁸³; and the formation of cyclic hemiacetal polymers as first proposed by Yokota et al⁸⁵.

Others oligomers have been isolated from aqueous solutions of glutaraldehyde and characterised by chemical ionisation-mass spectrometry^{101,102}. They include para-glutaraldehyde, which is a trimer and the principal trioxane derivative, along with the

pentamer and heptamer, which was found in small amounts (see figure 2.4 below). Similar compounds consisting of trioxane polymers (oligomers of the trimer) were later found in a 2% alkaline commercial sterilising solution of glutaraldehyde (pH7-11)¹⁰³.

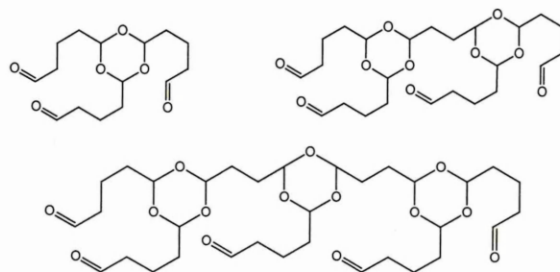


Figure 2.4: Trioxane-derivative oligomers of glutaraldehyde proposed by Tashima et al¹⁰¹⁻¹⁰³.

2.2.2.2 Aldol condensation polymerisation:

Polymerisation of glutaraldehyde molecules in aqueous solution with observable reductions in free aldehyde have been reported^{15,104}. It was concluded from early ¹H NMR data in D₂O that glutaraldehyde solutions contain polymers formed through aldol additions that dehydrate to give α,β -unsaturated aldehydes¹⁰⁵, known as aldol condensation products¹⁰⁶. (These products can also partially cyclise, as shown in figure 2.5 below). Others⁷¹, however, did not notice the presence of such unsaturated polymers using UV and NMR, while Hardy et al stated that unsaturated structures could only be a very minor component of the solutions⁸⁹ (see figure 2.6 below for the structures of the proposed condensation products). Glutaraldehyde solutions have nevertheless been reported to contain precipitates that result from aldol condensation⁸² and, in the pH range 4-8 and above, the free aldehyde is thought to undergo base-catalysed aldol condensation followed by dehydration to form α,β -unsaturated oligomers. The dimer, formed by an aldol condensation, is said to be the principal polymer in commercial (pH~3) solutions¹⁰⁷, an hypothesis that was corroborated by infrared and mass spectrometric data revealing the presence of both the dimer (MW 182) and trimer (MW 264)⁸² (both dimer and trimer are shown in figure 2.6 below). In contrast, others reported that aldol condensation products could only be present in a very small amount (far below 0.1% by weight), although they agreed that polyaldol structures would be likely involved in cross-linking and that the presence of amino groups would catalyse the glutaraldehyde polymerisation, thus

forming the aldol polymers involved in cross-linking⁹⁵. The statement that the polymerisation of glutaraldehyde could be catalysed by the amino groups of the collagen was later reiterated¹⁰⁰.

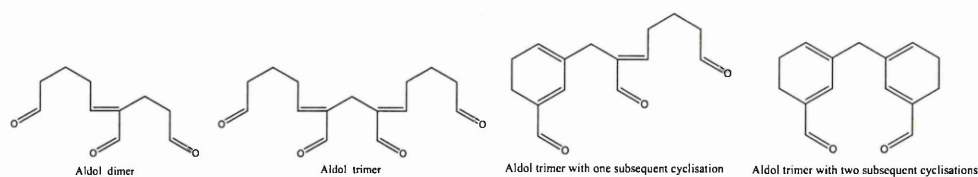


Figure 2.5: Aldol condensation products of glutaraldehyde as proposed by Richards and Knowles¹⁰⁵.

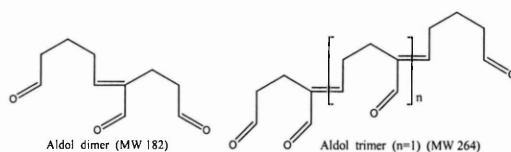


Figure 2.6: Aldol condensation products of glutaraldehyde as proposed by Hardy et al⁸⁹.

The aldol condensation can be both acid and base catalysed¹⁰⁶, as can be seen from figures 2.7 and 2.8 below, and thus can theoretically occur at all pH values.

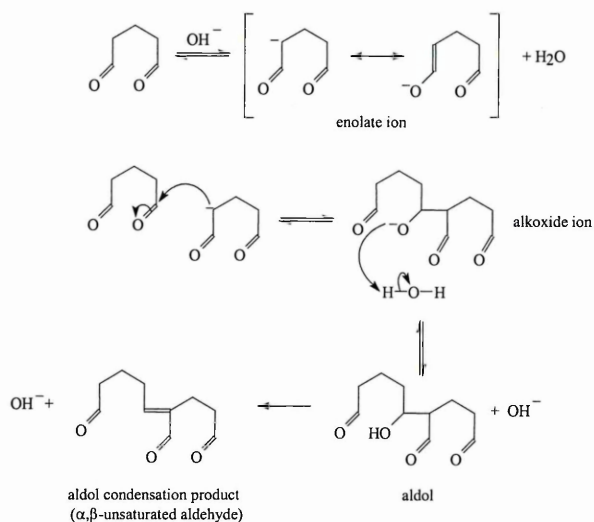


Figure 2.7: Mechanism of the base catalysed aldol condensation of glutaraldehyde showing a deprotonation by the base of an alpha carbon of a glutaraldehyde molecule forming a carbanion, followed by the nucleophilic attack of an enol form of another glutaraldehyde molecule by the carbanion thus forming an alkoxide ion, which then rearrange through a protonation and dehydration step.

When the aldol reaction is base catalysed, the base abstracts a proton from the α -carbon of one molecule of glutaraldehyde to give a resonance-stabilised enolate ion. The enolate ion participates in a nucleophilic attack on the carbonyl carbon of a second molecule of glutaraldehyde producing an alkoxide ion. The alkoxide ion then removes a proton from a molecule of water to form the aldol. The addition product in this case readily dehydrates to form the aldol condensation product, which is an α,β -unsaturated aldehyde. Dehydration occurs readily because of the acidity of the remaining α -hydrogens and because the product is stabilised by having conjugated double bonds¹⁰⁸. For clarity, throughout this thesis, α,β -unsaturated aldehydes will be referred to as aldol condensation products.

When the aldol reaction is acid catalysed, the first step of the reaction is the protonation of the carbonyl group, which attacks the α -carbon of the enol form of the molecule. After rearrangement through a loss of proton and a dehydration step, the resulting reaction product is an α,β -unsaturated polymer of glutaraldehyde (the formation of a dialdol condensation product is seen in figure 2.8 below).

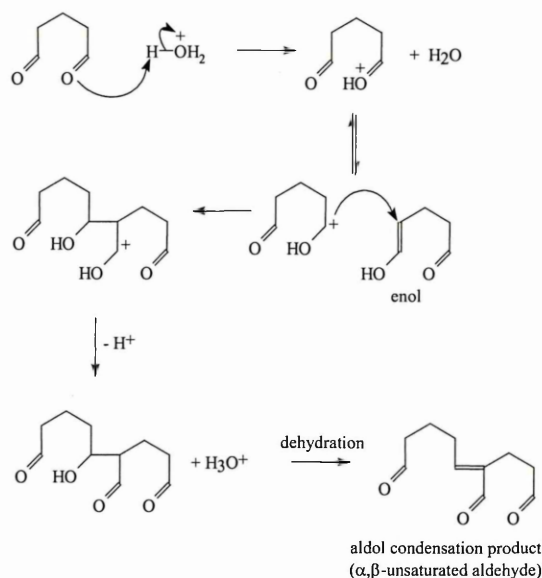


Figure 2.8: Mechanism of an acid catalysed aldol condensation of glutaraldehyde showing the protonation of the carbonyl of a glutaraldehyde molecule, followed by the attack of the α -carbon of the enol form of the glutaraldehyde molecule and rearrangement through a deprotonation and dehydration step.

Some authors also proposed the chemical structure given below in figure 2.9 (A), as a possible structure for poly-glutaraldehyde. From FTIR and UV studies of

glutaraldehyde solutions prepared at pH 7-13.5, hydroxyl groups were identified, have indicating that dehydration may not occurred at every consecutive step of the aldol condensation reaction¹⁰⁹. Such semi-dehydrated aldol condensation products have also been found by Tashima et al in a commercial sterilising solution of glutaraldehyde using chemical ionisation-mass spectrometry¹⁰³, and their presence was also later agreed¹¹⁰ and reported¹¹¹ by others. It is worth noting that some pendant aldehyde groups of the structures shown below (figure 2.9 (B)) could be barely hydrated¹⁰⁰ since the carbonyl form is stabilised by conjugation.

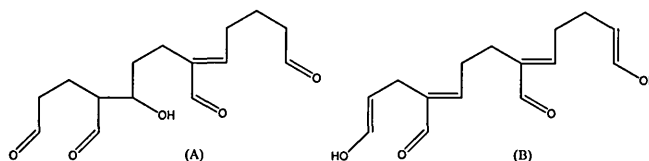


Figure 2.9: aldol condensation product where the consecutive dehydration step did not always occurred (A), as proposed by Margel and Rembaum¹⁰⁹ or where pendant non-conjugated aldehyde groups are in their hydrated forms (B), as proposed by Kawahara et al¹⁰⁰.

Other types of polymers have been characterised, using UV, IR and NMR spectroscopy along with gas chromatography-mass spectrometry, as dimers from an aqueous alkaline solution of glutaraldehyde¹¹². Such dimers (see figure 2.10 below) are formed by a dimolecular aldol condensation and may exist in equilibrium with their cyclic hemiacetal forms.

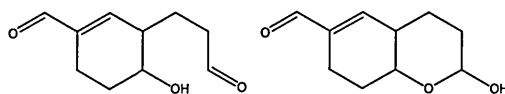


Figure 2.10: The dimer and its cyclic hemiacetal formed from a dimolecular aldol condensation of glutaraldehyde, as proposed by Tashima et al¹¹².

2.2.2.3 Michael reactions:

As well as undergoing aldol condensations along with cyclisation and hydration, glutaraldehyde can also undergo Michael reactions with aldol condensation products¹¹³. The Michael addition is a base-catalysed reaction. The first step of the mechanism involves the abstraction of an activated hydrogen from glutaraldehyde to

form a carbanion. Conjugate addition of the carbanion to the aldol condensation product subsequently occurs, followed by acceptance of a proton¹¹³. The mechanism of this process is shown below in figure 2.11.

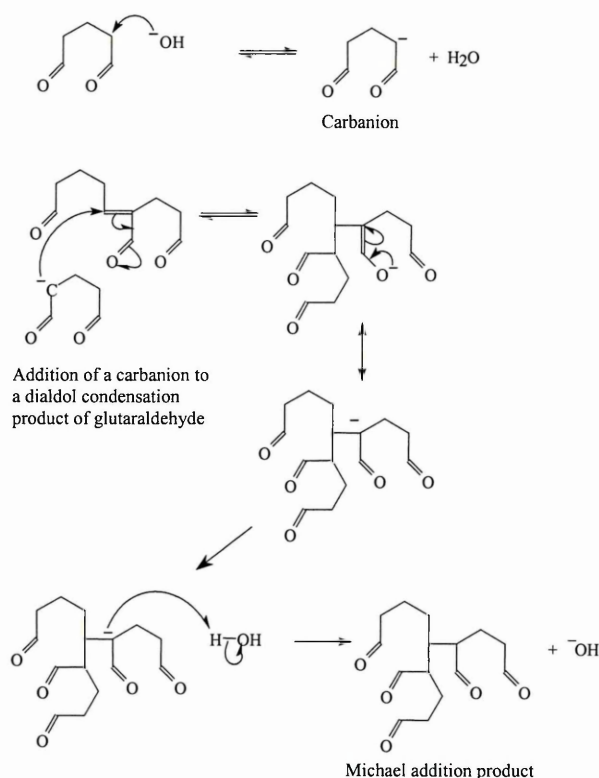


Figure 2.11: Mechanism of a Michael addition of glutaraldehyde to an aldol condensation product (dimer).

2.2.3 Factors affecting the reaction between glutaraldehyde and proteins

2.2.3.1 Introduction:

Historically, only the interactions of glutaraldehyde with the amine groups of collagen have been studied. The lysine residues in proteins appear to be the only amino acid clearly implicated in the reactions with glutaraldehyde (although various authors have speculated on the reaction of glutaraldehyde with other amino acids)^{15,69,114}. More specifically, it is the 6-(or ϵ -) amino groups of lysine residues, which react^{18,34,115}. Indeed, unlike formaldehyde and glyoxal, glutaraldehyde reacts apparently only with lysyl groups to a significant extent⁸². However, other groups such as the guanido group of arginine have been found to react particularly at alkaline pH, tyrosine was found to react slightly, whilst no reaction was observed between glutaraldehyde and histidine⁶⁹. Other authors partially contradicted this, by stating that glutaraldehyde can react with the amino acids tyrosine, tryptophan and

phenylalanine¹¹⁶ however the most reactive groups reported were the α -amino groups of glycine, and the α - and ϵ -amino groups of lysine (although some reported¹¹⁷ that there was no evidence for the participation of the α -amino group of lysine). Other groups, meanwhile, were found to be less reactive, for example the sulphhydryl group of cysteine, the phenolic group of tyrosine and the imidazole group of histidine, where the presence of a free amino group seemed to be necessary for glutaraldehyde to react with the imidazole group¹¹⁸. Work by Munton and Russell has indicated that glutaraldehyde could react with arginine, glutamine, phenylalanine, serine and threonine⁹⁷, whilst reactions may also occur at alkaline pH.

Later studies showed specifically that the aldehyde groups of glutaraldehyde react with amino acid residues of the polypeptide chains of collagen, such as the 6-amino group of lysine and hydroxylysine and also the carboxylic group of aspartic acid and glutamic acid^{17,95,119}, to give rise to cross-links¹²⁰ between the collagen molecules. Recently, it was suggested that stable cross-linking with glutaraldehyde could occur through hemiacetalisation between hydroxyl groups of hyaluronic acid (and other polyols) and aldehyde groups of glutaraldehyde¹²¹. Glutaraldehyde can also react with carboxy, amido and other groups of proteins^{15,122}. The order of reactivity of glutaraldehyde with other compounds was reported as follows: I^{ary} amines>peptides>guanidines>II^{ary} amines>hydroxyl groups³. However, the reaction of glutaraldehyde with amines and carboxylic acid (Mannich-type addition) was even briefly described.

Complete chemical analysis of the cross-linking entities formed by reaction of amines with glutaraldehyde has not been successfully achieved because the reaction products are extremely heterogeneous and varying the reaction conditions can affect the products formed¹²³. Therefore, although the reaction of glutaraldehyde with proteins has been extensively studied, it is still not fully understood.

2.2.3.2 Effects of pH:

The reaction between glutaraldehyde and proteins is known to be affected by pH^{116,124}. The incorporation of glutaraldehyde into tissue is dependent upon pH, the amount incorporated being lower at acidic pH than at neutral and basic pH³⁴. It has been shown that the reaction rate of glutaraldehyde with proteins is inversely proportional to the square root of the hydrogen ion concentration¹²⁵, which is in

keeping with others findings which showed that glutaraldehyde tanned more rapidly with increased pH levels^{118,126,127}. An early study on the application of glutaraldehyde for tanning showed that in 24 h, 50% of glutaraldehyde reacted at pH 4, 90% reacted at pH 4-5, 90 to 97% reacted at pH 6-6.5 and that 50% of glutaraldehyde was destroyed in 3 hours, possibly because of the pH¹²⁸.

At acidic pH, the proteins' binding sites are thought to be present in the acid form and the amino terminus would be an ammonium residue, which would not readily react with aldehyde groups of glutaraldehyde^{26,68}. The reaction of glutaraldehyde with collagen has been shown to be rapid at neutral pH, but fairly slow at acidic pH¹²⁹; however the data did indicate that effective cross-linking could be achieved at low pH. The rate of Schiff base formation between aldehydes and primary amines has been shown to be the highest at slightly acidic pH of approximately pH 4.5¹³⁰ because the second step in the formation of imine, namely the protonation of the carbinolamine intermediate and subsequent dehydration, is catalysed by mild acidity. If, however, the solution is too acidic, protonation of the amine renders it incapable of nucleophilic attack (the first step in the reaction). The maximum number of cross-links introduced during tanning with glutaraldehyde was found at pH 6.5⁶⁸. Also, at about pH 6.5, a change in the gel filtration properties of glutaraldehyde was observed and it was suggested that intra- and inter-molecular changes were occurring⁸¹.

At high pH, the proteins' binding sites are hypothesised to be present as the basic form of the lysine and hydroxylysine²⁶. It was also reported that alkalination may modify the glutaraldehyde molecule⁹⁷ and that polymerisation may¹³¹ or may not¹³² occur under these conditions. In other studies, glutaraldehyde was reported to undergo rapid polymerisation forming oligomers¹⁵ at pH levels greater than 8. It is thought that the increased tendency of the aldehyde to polymerise at pH 8 may limit the desired reaction from taking place⁶⁸ and that too alkaline a solution would lead to a loss of reagent through Cannizzaro-type reactions¹³³. It was even recently reported that a glutaraldehyde reaction with collagen membranes was "inhibited" simply by exposing the membranes to a pH 9 glycine/borate buffer solution¹³⁴.

2.2.3.3 Molar ratio:

By studying UV absorbance, loss of lysine residues and loss of glutaraldehyde from the solution, it has been shown in-vitro that approximately 4 moles of glutaraldehyde

are taken up per lysine residue¹¹⁷. However, not all these glutaraldehyde molecules seem to be firmly bound and an elemental analysis of the reaction products of glutaraldehyde-treated collagen has suggested a ratio of three glutaraldehyde molecules per lysine residue. This loss of protein-bound glutaraldehyde was also observed in-vivo²⁶.

Various molar ratios of glutaraldehyde to amino acids have also been reported, such as 1:1^{135,136}, 1:3¹³⁶, 2:1^{95,137,138}, 3:1^{17,139}, 3:2¹⁴⁰, 4:1^{71,95,114}, 5:1¹³⁹, suggesting the complexity and difficulty in assessing an exact molar ratio. These differences may be explained by the different availability of the appropriate reactive groups of the proteins involved in the various studies; for instance, the lysine residues in collagen may not all be accessible to glutaraldehyde, in comparison to those of a model compound in solution. Nevertheless, all these molar ratios lead to the conclusion that large structures containing many glutaraldehyde molecules are unlikely to be involved in cross-linking.

2.2.3.4 Kinetics of the reaction:

The reaction of glutaraldehyde with various proteins (including bovine serum albumin, lysozyme, ovalbumin and α -chymotrypsinogen) in solution has been followed by UV spectroscopy¹²⁵. It was concluded that the reaction kinetics were pseudo first-order, that the rate of formation of glutaraldehyde-protein links per protein molecule is about $1 \text{ sec}^{-1} \text{ mol}^{-1}$, that the rates of the reactions increased with increasing pH and that the rate of the reversible reaction was negligible. The observed kinetics were thus reported to be different from those of Schiff's base formation, which is commonly believed to be the likely reaction product of the reaction of glutaraldehyde with proteins. Another study of bovine pericardium found a linear relationship between the logarithm of initial glutaraldehyde concentration and incubation time, indicating first-order reaction kinetics⁴⁸. The various cross-linking reactions of glutaraldehyde with proteins have also been demonstrated to have different rates¹²², whilst the reactions were reported to be able to proceed for days (rearrangements leading to a greater degree of cross-linking)¹⁴¹.

2.2.3.5 The effect of concentration and penetration:

Although glutaraldehyde reacts rapidly with amino groups, it tends to penetrate slowly into tissues^{24,95}. Hence, cross-linking of the core regions of densely packed

molecules, such as collagen tissue fibres, often presents concern when fixing tissues for electron microscopy or for use as bioprotheses. Inadequate or heterogeneous cross-linking may indeed lead to enhanced enzymatic biodegradation, antigenicity and loss of mechanical function¹²⁰.

Low concentrations of glutaraldehyde reacted with dilute solutions of collagen were found to form only intra-molecular cross-links, while higher concentrations formed cross-links between two distant groups, including inter-molecular cross-links⁹⁵. This suggested that there were no cross-links formed between 6-amino functions of lysine from different molecules at low concentrations and that the cross-links formed only bridged short distances.

At higher concentrations, glutaraldehyde forms long polymeric chains of inter-molecular cross-links¹⁴² and the reaction is reversible. Cheung et al have shown that the rate of formation of these high molecular weight glutaraldehyde polymers is very fast and that they are able to generate an inter-molecular network of cross-linking¹¹⁹. The authors also demonstrated that low concentrations of glutaraldehyde have a better but slower bulk-cross-linking action than high concentrations. This is thought to promote rapid surface cross-linking of the tissue with rapid glutaraldehyde polymerisation at the site, preventing further diffusion into the bulk of the tissue¹¹⁹. It was also shown that treatment of collagen fibres by high concentration of glutaraldehyde led to an increase in the molecular length of the glutaraldehyde polymers (extending from the initial glutaraldehyde and lysyl residue reaction sites), rather than an increase in the actual number of cross-linking sites. It was suggested that glutaraldehyde would primarily fix to the surface of the tissue creating a polymeric network, which sterically prevents further cross-linking of the interstitium of the fibre^{95,119}. Since the physical properties of glutaraldehyde-treated tissue are of concern when making bioprotheses¹⁴³, the effect of glutaraldehyde concentration upon its penetration and the cross-links formation is of importance.

2.2.3.6 Duration of exposure:

The extent of cross-linking is also influenced by the duration of exposure to glutaraldehyde^{120,144}. Insufficient glutaraldehyde cross-linking can result in loss of xenograft strength¹⁴⁵, whilst prolonged exposure to glutaraldehyde has the advantages of sterilising xenografts as well as increasing their tensile strength.

2.2.3.7 Extent of completion:

It has been estimated that 18% of the lysine residues in collagen remain unreacted¹¹⁷. It was suggested that these lysine residues lie in the overlap zone of the collagen structure and are inaccessible due to steric constraints.

2.2.3.8 Cross-linking process:

It is postulated from studies of the reaction between glutaraldehyde and collagen, that formation of cross-links starts with the reaction of a (likely) lysyl residue with glutaraldehyde, followed by subsequent addition of glutaraldehyde molecules onto this nucleating site, generating polymeric chains^{95,123}. This process can have two negative effects, i.e. steric hindrance of other possible reactive sites (lysyl residues or others) and the depletion of glutaraldehyde from the solution, due to polymerisation catalysed by free amino groups⁹⁵. This view is supported by Kawahara et al who also stated that glutaraldehyde polymerisation could be catalysed by the presence of amino groups¹⁰⁰. Recently, Lusty hypothesised that cross-linking would take place in two steps: the first would be the formation of a reversible Michaelis complex (refer to the enzyme-substrate-like complex) and the second would be an irreversible reaction covalently linking glutaraldehyde to the protein¹⁴⁶.

2.2.3.9 Optimum treatment:

The actual amount of glutaraldehyde retained in the tissues and the nature and distribution of the cross-links formed in tissues are of vital importance because the less glutaraldehyde that is introduced, the less chance there is for inflammation and calcification to occur. In addition, if glutaraldehyde is not uniformly distributed throughout the collagen, the sites of the matrix with fewer cross-links will be subject to faster degradation. Therefore, it is important to minimise the amount of glutaraldehyde introduced into the implant but also to attain a homogeneous distribution of cross-links throughout the thickness of the collagen. For this purpose, a more complete understanding of the nature of glutaraldehyde and its behaviour when reacted with collagen may provide important information for future approaches to limiting calcification.

2.2.4 Types of reactions occurring between glutaraldehyde and proteins

2.2.4.1 Introduction:

The reaction of glutaraldehyde with proteins has been extensively studied by various analytical techniques. Among them, HPLC was reported to be suitable to follow the extent of protein cross-linking with formaldehyde, glyoxal or glutaraldehyde⁹³. UV spectroscopy was used in early studies and showed the irreversible fixation of collagen by glutaraldehyde and the appearance of a characteristic absorption maximum at 265nm in the hydrolysate of leather with the likely formation of aromatic compounds^{147,148}. Wet chemistry tests were also used in early studies, in order to characterise the cross-links between glutaraldehyde and proteins. These revealed that the primary amine was converted to a tertiary amine, which was then incorporated into heterocyclic compounds and/or polymer formation¹²⁴.

Small amines, peptides and proteins have been used to model the reaction of glutaraldehyde with the 6-amino functions of lysine and hydroxylysine present in collagen. This approach has been adopted by a number of authors and species include: glycine^{123,149}, α -aminoglutaric acid¹⁵⁰, 6-amino-n-caproic acid^{50,117,123,137,140,151}, N- α -acetyl-L-lysine^{82,137}, isopropylamine⁸², lysine⁸², poly-lysine^{71,117,136}, cytochrome C^{152,153}, lysosyme^{125,154}, bovine serum albumin^{118,125,152,155}, ovalbumin^{118,125,156,157}, gelatin^{158,159}, collagen fibres and collagen solution⁹⁵ and bovine pericardium¹¹⁹. Overall, despite the extensive range of publications relating to reactions between glutaraldehyde and various proteins, many of the reaction products formed when glutaraldehyde reacts with collagen remain unknown and thus to be characterised.

2.2.4.2 Formation of Schiff bases:

Note that imines are often referred to as Schiff bases since Schiff first discovered the reaction in 1864.

The most obvious potential product from the reaction of an aldehyde with a protein is a Schiff base, formed by the reaction of an amino terminus of the protein with an aldehyde group of glutaraldehyde^{66,117,160}. One reason for this deduction is the observation that solutions of protein, (if not already pigmented) reacted with glutaraldehyde have a yellow colour, which is attributed to Schiff base (aldimine)

formation^{158,161}. Upon reduction with sodium borohydride the colour is lost, thus confirming the aldimine linkage. Also, during study of the reaction of glutaraldehyde with various proteins in solution by UV spectroscopy, it was postulated that this coloration might be due to the formation of Schiff bases or azomethine^{125,162}. Glutaraldehyde was thus extensively reported to be capable of reacting with amino acid side chains, particularly with the lysine ϵ -amino group, to form Schiff bases^{163,164}. A similar yellow colour and strong blue-white fluorescence has been identified with elastin, indicating that glutaraldehyde-treated proteins may form similar cross-links to the cross-links of elastin¹⁶⁵. Such hypothetical molecular structures could be similar to the desmosine and isodesmosine structures containing quaternary pyridinium structures found in cross-linked elastin (see chapter 1 section 1.6.2).

Although the formation of an imine is acid catalysed, Schiff bases formed between monomeric glutaraldehyde and primary amines have been found relatively stable in alkaline media¹⁶⁶, but were reported to be hydrolytically unstable under acidic conditions. Thus, Schiff bases may not account for the stability of cross-links following treatment with acids¹⁶⁷. Imine formation is known to be affected by pH and is relatively slow at very low and high pH. Indeed, Schiff bases are known to be relatively unstable at neutral pH and can even revert to the free amine and aldehyde upon an increase in temperature or a decreased in pH⁶⁶. Some authors claim that imines (Schiff bases) are formed as unstable intermediates that are almost immediately transformed into more stable chemical structures^{20,117,168}. Others also stated that Schiff bases are regarded as the central intermediates from which subsequent reactions may occur before a cross-link is formed¹⁴⁰.

Nevertheless, the Schiff base can be stabilised (changed into a more stable reduced moiety) with the use of typically 0.01M NaBH₄¹⁶⁹ but the use of such a reducing agent might be inappropriate in cases where disulfide bridges in the proteins are responsible for maintaining structural integrity and reactivity¹¹⁰. The existence of simply a Schiff base from the interaction between glutaraldehyde and an amino group is thought precluded because Schiff base formation is reversible and such compounds would not survive the laboratory conditions used to assess cross-links formed, such as the acid hydrolysis¹⁶⁷ for amino acid analysis and over such a wide range of pH and temperature¹⁰⁵. Furthermore, it is well known that proteins

immobilised with glutaraldehyde are sufficiently stable to confirm that the Schiff base cannot be operative⁶⁹, although some authors however, suggest that Schiff bases are formed as a stable final linkage under the cross-linking conditions used in valve industry^{95,123}.

Therefore the formation of further molecular species had to be considered. For instance the reaction of ϵ -amino groups of lysine with glutaraldehyde has been found to proceed well beyond the stage of a Schiff base⁶⁹. The authors indicated that no lysine derivatives were found in hydrolysates of cross-linked material, suggesting the possibility of multiple side reactions and various possible products. It has also been observed that at reaction times over 24 hours, all initially formed Schiff bases have reacted and hydrolysis is blocked¹⁷. Additionally, it was found that, only after stabilisation of the initially formed hydrolysable Schiff base, cross-links were introduced into the glutaraldehyde-treated collagen matrix. Some recent UV data recently have suggested that fast formation of Schiff bases at the beginning of the reaction initiates aldol condensation of the carbonyl group of glutaraldehyde to give polymeric products¹⁵⁰.

The proposed mechanism¹⁷⁰ for the formation of a Schiff base from reaction of glutaraldehyde with an amino group is shown in figure 2.12. First, the amine adds to a carbonyl group of the glutaraldehyde to form a dipolar tetrahedral intermediate. A proton transfer from the nitrogen to oxygen occurs to form an amino-alcohol. (It is worth noting that this amino-alcohol was recently proposed as a final structure involved in the reaction between glutaraldehyde and leather¹¹¹). A subsequent loss of water leads to the formation of the imine (Schiff base), which can undergo a tautomeric shift forming an enamine and subsequently cyclise to form a pyridinium compound¹⁷¹. Some of the Schiff bases formed are thought to undergo cyclisation reactions, forming dihydropyridine derivatives, which can undergo oxidation and further condensation^{156,172}.

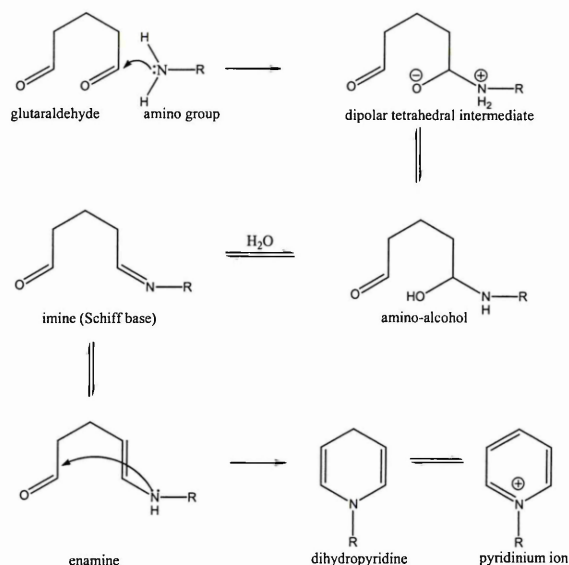


Figure 2.12: Mechanism to show the formation of a Schiff base, followed by its cyclisation into 1-(5-amino-5-carboxypentyl)-1,4-dihydropyridine, and subsequent oxidation to the corresponding pyridinium compound as proposed by Hardy et al^{156,172}.

The formation of N-alkyl-2,6-dihydroxy piperidine (see figure 2.13 below) was also reported¹⁷³ and later agreed by others¹⁵⁹. Its formation mechanism, although never reported, is thought to start from the formation of the amino-alcohol structure (see figure 2.12 above), which would then undergo an intra-rearrangement by starting from an attack of the electronic doublet of the nitrogen atom onto the available carbonyl group of the molecule, subsequently forming the cyclic aminal.

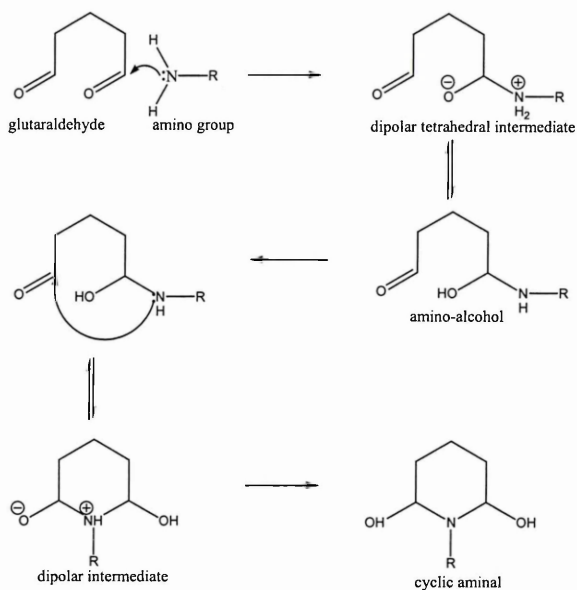


Figure 2.13: Formation of the N-alkyl-2,6-dihydroxy piperidine (cyclic aminal)

A Mannich-type reaction, between a protonated Schiff base and a glutaraldehyde-related enol, has also been proposed⁶⁶, resulting in the formation of a secondary amine (see figure 2.14 (A) below). Further reactions of these Mannich-type reaction products with glutaraldehyde through aldol condensations, and with amino groups (Schiff base), have been reported¹⁷ to lead to the formation of aliphatic cross-links such as the one shown in figure 2.14 (B) below.

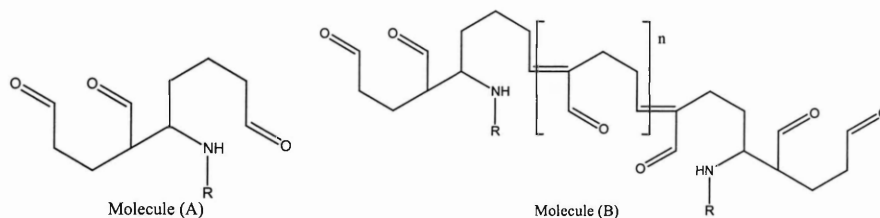


Figure 2.14: Mannich type reaction product from reaction of a Schiff base with an enol form of glutaraldehyde (A) proposed by Woodroof⁶⁶; and a molecule resulting from the further reaction of (A) with amino groups and glutaraldehyde molecules (B) proposed by Olde Damink et al¹⁷.

2.2.4.3 Formation of hemiacetal oligomeric structures:

It has been reported that monomeric glutaraldehyde, or one of its hydrated forms (likely hemiacetals), is responsible for protein cross-linking^{76,89}. Wet chemistry tests on the precipitate obtained from the reaction of glutaraldehyde with a protein (noradrenaline) showed the likely presence of such hemiacetal structures (*o*-dihydroxy grouping)¹²⁴. Some reactions involving other proteins and glutaraldehyde under acidic or neutral conditions have also been proposed to involve the oligomeric hemiacetal compounds of glutaraldehyde¹¹⁰. Such compounds would not require a further reduction step to obtain stable products (e.g. the one shown in the figure 2.15 below), in contrast to Schiff base formation that requires such a reduction step to give a stable product.

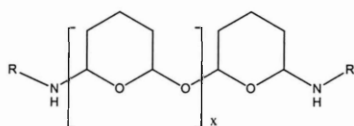


Figure 2.15: Possible reaction product (hemiacetal) from the reaction of glutaraldehyde with proteins under acidic or neutral conditions.

Indeed, hemiacetal polymers were also suggested^{110,159} to undergo Schiff base formation through the addition of a monomeric glutaraldehyde molecule. This type of product from the reaction between gelatin (protein) and glutaraldehyde is seen in figure 2.16 below.

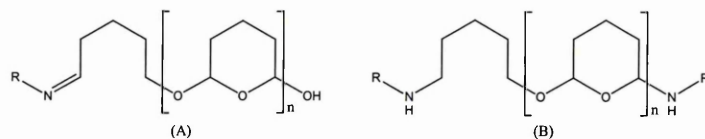


Figure 2.16: Reaction products (hemiacetal) from the reaction between glutaraldehyde polymeric hemiacetal and a protein as proposed by Matsuda et al¹⁵⁹ (structure A), and Walt et al¹¹⁰ (structure B).

Based on spectral data, Aso and Aito⁹⁹ have reported the formation of another possible compound with a hemiacetal polymer-like structure (see figure 2.17 below). They suggested that glutaraldehyde polymerises as a chain of six-membered pyranose rings joined by ether linkages (α -oxypyran rings formed giving tetramers and pentamers). This indicated that small oligomers were formed, which on average contained three glutaraldehyde residues and one free aldehydic group. It was later hypothesised by others that these types of structures may occur in the glutaraldehyde cross-links¹⁷⁴.

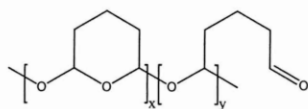


Figure 2.17: α -oxypyran ring polymers, where the ratio of x to y is said to be about six to sixteen, as proposed by Aso and Aito⁹⁹.

The formation of α -oxo-N-alkyl piperidine cross-links (see figure 2.18 below), after condensation of the N-alkyl-2,6-dihydroxy piperidine with a cyclic monohydrated glutaraldehyde, has also been suggested¹⁷³.

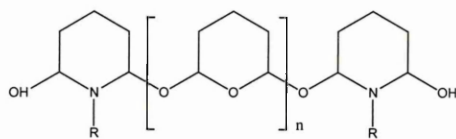


Figure 2.18: α -oxo-N-alkyl piperidine cross-link, suggested as a possible product formed by the condensation of the N-alkyl-2,6-dihydroxy piperidine with a cyclic mono-hydrated glutaraldehyde¹⁷³.

2.2.4.4 Schiff base and Michael-type addition involving aldol condensation products

Cross-links involving aldol condensation products through Schiff base formation have been reported^{89,159} (see figure 2.19 (A) below). It has also been suggested, from infrared spectroscopic data, that amino groups react with α,β -unsaturated aldol condensation products formed at alkaline or even at slightly acidic conditions, to form stabilised conjugated imino bonds by a resonance effect^{82,93} (see figure 2.19 (B) below). This may account for the observed increased stability of cross-links, because the equilibrium constant is usually unfavourable for non-conjugated imine formation in aqueous solution¹⁷⁵. Furthermore, the incorporation of several moles of glutaraldehyde per mole of lysine/hydroxylysine residue indicates that oligomeric rather than monomeric glutaraldehyde compounds are involved in the cross-linking reaction⁷¹. It was suggested that aldol condensates formed with up to 8 glutaraldehyde molecules could easily establish a bridge between two lysine residues⁸².

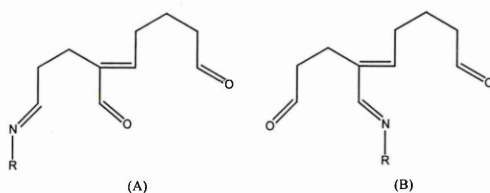


Figure 2.19: Imine formed from an aldol condensation product (A) as proposed by Hardy et al⁸⁹ and Matsuda et al¹⁵⁹; and a conjugated imine (more stable) formed from an aldol condensation product (B) as proposed by Monsan et al⁸², and Marquie et al⁹³.

Other mechanistic pathways leading to stable products have also been suggested, such as the one involving a Michael-type addition of side-chain amino groups to aldol condensation molecules¹⁰⁵. These Michael-type addition products are thought to be stable even under acid hydrolysis. Some cross-links between glutaraldehyde

and amino groups have been shown to be of the aldol condensation product form, with five carbon atoms in a chain between the two nitrogen atoms from the uptake of amino acids¹⁰⁵ (see figure 2.20 below). The same authors also hypothesised that these aldol condensation products could also react at one end by Michael-type addition and at the other by reversible Schiff base formation (see figure 2.20 below). Others then suggested that the unsaturated aldol-type polymers of glutaraldehyde are likely candidates for protein cross-linking reactions in alkaline solutions⁸⁹, although the cross-linking reaction was apparently not dependent on the initial presence of unsaturated compounds. The involvement of dimers characterised by Tashima et al¹¹², formed by a dimolecular aldol condensation and that may exist in equilibrium with their cyclic hemiacetal forms, have also been proposed¹¹⁰ to be formed in cross-linking through Michael-type addition and Schiff base reaction (see figure 2.21 below).

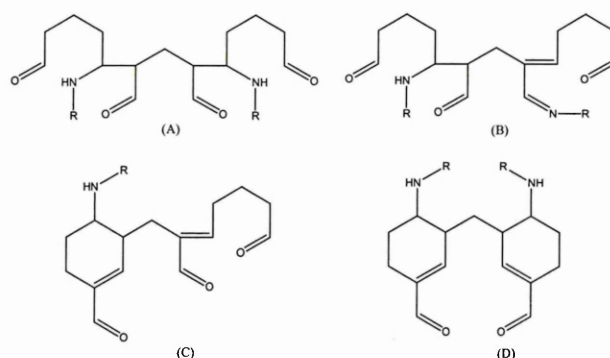


Figure 2.20: Stable cross-links formed by the Michael-type addition of amines with aldol condensation products, as proposed by Richards and Knowles¹⁰⁵ (note that further Schiff base formation can still occur with all the above-molecules (A-D), and Michael-type additions can still occur in the molecules C and D).

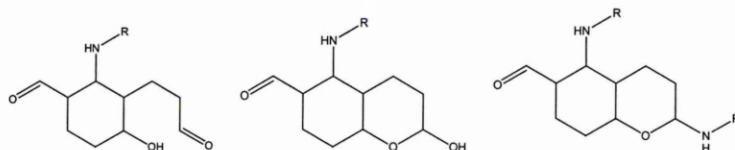


Figure 2.21: Cross-links formed by the Michael-type addition of amines to aldol condensation products, as proposed by Walt and Agayn¹¹⁰ (note that further Schiff base formation can still occur in all these above-molecules).

However, because of the presence of a resonance-stabilised ethylenic double bond with the imino bond formed from the reaction of an aldol condensate and an amino

acid (such an example can be found above in figure 2.20 (B)), these relatively stable molecular compounds are thought not to allow Michael-type addition reactions to take place⁸². The aldol condensation mechanism with the Michael addition postulated by Richards and Knowles¹⁰⁵ (yielding molecular compounds such as the ones found above in figure 2.20 (A-D)) was also reported to occur under the influence of the protein immediately prior to cross-linking and to represent only a minor contribution to the overall cross-linking^{164,168}.

The mechanism for the conjugate addition (Michael-type addition) of an amine to an aldol condensation product is shown in Figure 2.22 below. The initial step involves nucleophilic attack by the lone pair of electrons of the nitrogen on the β -carbon atom of an α,β -unsaturated carbonyl acceptor, forming an enolate as the product. The enolate then rearranges to give the more stable keto-form by abstracting a proton, from the solvent or from the starting nucleophile, to yield the final addition product^{176,177}.

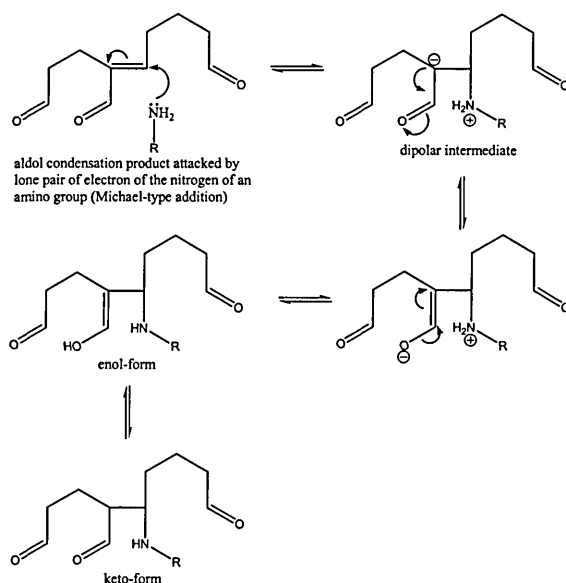


Figure 2.22: Mechanism for the conjugate addition of an amine to an aldol condensation product (dimer).

2.2.4.5 Formation of quaternary dihydropyridine compounds:

It has been known for some time that the reaction of an aldehyde with an amine can lead to the formation of a dihydropyridine that then leads to pyridinium salts¹⁷⁸⁻¹⁸⁰. The principal product of the condensation of an aliphatic aldehyde with an aliphatic aldimine is a 1,2,3,5-tetraalkyldihydropyridine¹⁸¹ (which has a similar structure to

that of isodesmosine found in elastin, see chapter 1). Under appropriate conditions, pyridines are the major reaction products of aldehyde-amine reactions^{180,182}. Some findings based on IR, UV and ¹H NMR data^{156,168}, confirming the previous findings of others¹¹⁷, indicated the possible formation of a quaternary pyridinium system (1,3,4,5-tetrasubstituted pyridinium salts as shown in figure 2.23 below) analogous to the 1,3,4,5-substitution pattern of desmosine, which is found in acid hydrolysates of elastin. They also suggested the likely formation of the 1,2,3,5-substitution (isodesmosine analogs). The UV absorption maximum observed for such pyridinium structures being at 265nm¹⁵⁶, was consistent with the original observation of Bowes and Cater¹¹⁷ who first reported the appearance of this UV absorption peak following the reaction of glutaraldehyde with amine compounds. It has also been suggested that pyridine products represent one of many possible irreversible cross-links created by the action of glutaraldehyde with proteins¹⁶⁸. They later isolated^{157,172} a 3-(2-piperidyl) pyridinium derivative (shown in figure 2.23 below) from the acid hydrolysates of glutaraldehyde-treated protein (ovalbumin), the structure being confirmed by UV, ¹H and ¹³C NMR in D₂O, and later named anabilysine (shown in figure 2.23 below) This pyridinium derivative was the first cross-linking entity to be isolated from a glutaraldehyde-treated protein.

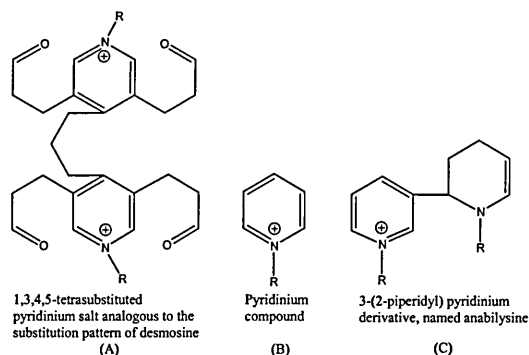


Figure 2.23: Quaternary pyridinium structures proposed by Hardy et al^{156,157,168,172}, where it can be seen that the molecular structures of the 1,3,4,5-tetrasubstituted pyridinium salt (substitution pattern similar to desmosine (A)), anabilysine (C) and even the pyridinium compound, (which is formed from the cyclisation of a Schiff base reaction of an amino group with a monomeric form of glutaraldehyde (see mechanism in figure 2.12)), all form stable cross-links.

More recently, other theoretical chemical structures (see figure 2.24 below) have also been proposed¹⁸³ including a cyclic imminium ion (A), dihydropyridine (B) and (C) pyridine-containing molecules.

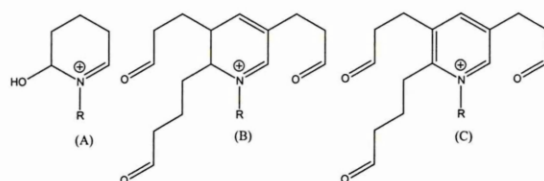


Figure 2.24: Cyclic imminium ion (A), dihydropyridine (B) and pyridine (C) structures proposed by Johnson¹⁸³.

Those same dihydropyridine structures are also thought to possibly condense with each other, instead of with additional glutaraldehyde, to form polymers of dihydropyridine (see figure 2.25 (A)), which can lead to the formation of pyridine polymers by oxidation (see figure 2.25 (B) below).

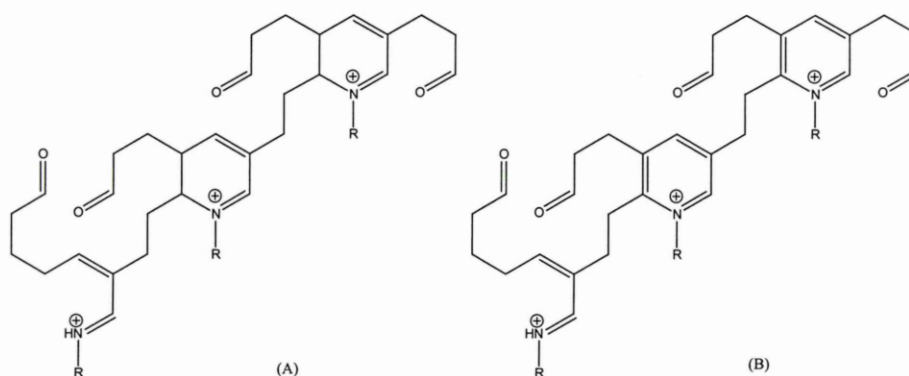


Figure 2.25: Polydihydropyridine (A) and polypyridine (B) structures proposed by Johnson¹⁸³.

In addition, quite a recent study¹⁵¹ of the reaction between glutaraldehyde and 6-aminohexanoic acid, using gel filtration and UV spectroscopy, showed that one of the separated products by SP-Sephadex corresponded to a pyridinium structure, which would be in agreement with the previous work of Hardy et al¹⁶⁸. However, from their UV data, they concluded that the structure suggested by Hardy et al (1,3,4,5-tetrasubstituted-pyridinium-type, similar to desmosine (see earlier figure 2.23) is quite different to the one they had characterised despite being of similar type. Therefore, they proposed a single large polymeric structure molecule with multiple pyridinium rings and an average molecular weight of 20000 (MW 5000-80000). A new chemical structure was not proposed however, but they referred back

to a chemical structure proposed previously by Hardy et al¹⁶⁸ (see figure 2.26 below).

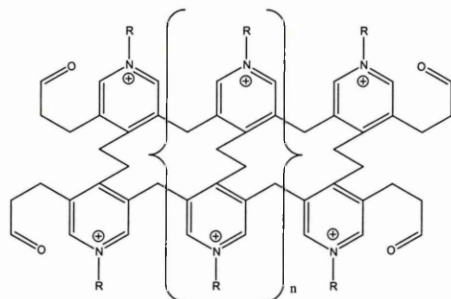


Figure 2.26: Chemical structure postulated by Hardy et al¹⁶⁸ for a purified product obtained from the reaction of glutaraldehyde and amino-containing model compounds (R is the radical of the corresponding protein or amino acid).

2.3 Conclusion

As a conclusion, it appears that the chemistry of glutaraldehyde in solution is quite complex and not yet clearly defined, and additionally there is sufficient evidence that the reaction between glutaraldehyde and protein is not simple, and although the characterisation of many structures have already been attempted, there are probably still as many to be characterised. Additionally, because of the many contradictions in the literature about a consensus of current opinion for the nature of glutaraldehyde in solutions and also for the nature of the products from the reaction between proteins and glutaraldehyde, this area has been studied in detail in this work and the results and discussion of these features can be found respectively in chapters 4 and 5.

1. Carpentier A, Lemaigre G, Rober L, Carpentier S, Dubost C. Biological factors affecting long-term results of valvular heterografts. *Journal of Thoracic and Cardiovascular Surgery*. 1969;58:467-483.
2. Woodroof EA. The chemistry and biology of aldehyde treated tissue heart valve xenografts. In: Ionescu MI, ed. *Tissue Heart Valves*. London: Butterworth; 1979:347-362.
3. Jayakrishnan A, Jameela SR. Glutaraldehyde as a fixative in bioprostheses and drug delivery matrices. *Biomaterials*. 1996;17:471-484.
4. Kohr E. Methods for the treatment of collagenous tissues for bioprostheses. *Biomaterials*. 1997;18:95-105.
5. Harries C, Tank L. Über die Aufspaltung des Cyclopentens zum Halbaldehyde der Glutarsäure bzw. Zum Glutardialdehyd. *Berichte der Deutschen Chemischen Gesellschaft*. 1908;41:1701-1711.
6. Smith CW, Ballard SA. Production of glutaraldehyde and substituted glutaraldehyde from dihydropyrans. In. United States: Shell Development Co.; 1951.

7. Hess LG, Kurtz AN, Stanton DB. In: Mark HF, Thmer DF, Overberger CG, Seaborg GT, eds. *Kirk-Othmer Encyclopaedia of Chemical Technology*. New York: John Wiley and Sons; 1978:277.
8. Dai W, Huang X, CHen H, Deng J. Kinetics and mechanism of the catalytic oxidation of cyclopentene to glutaraldehyde with aqueous hydrogen peroxide. *Indian Journal of Chemistry*. 1997;36B:583-589.
9. Seligsberger L, Sadlier C. New developments in tanning with aldehydes. *Journal of the American Leather Chemical Association*. 1957;52:2-16.
10. Cater CW. Glutaraldehyde tannages. *Journal of the Society Leather Trade Chemists*. 1967;52:239-249.
11. Sabatini DD, Bensch KG, Barnnett RJ. Cytochemistry and electron microscopy: the preservation of cellular ultrastructure and enzymatic activity by aldehyde fixation. *Journal of Cell Biology*. 1963;17:19-38.
12. Rose AG. Pathology of the formalin-treated heterograft porcine aortic valve in the mitral position. *Thorax*. 1972;27:401-410.
13. Stephen BJ, O'Brien MF. Pathology of xenografts in aortic valve replacement. *Pathology*. 1972;4:167-176.
14. Bortolotti U, Talenti E, Milano A, Thiene G, Gallucci V. Formaldehyde-versus glutaraldehyde processed porcine bioprostheses in the aortic valve position: long-term follow up. *American Journal of Cardiology*. 1984;54:681-682.
15. Bowes JH, Cater CW. The reaction of glutaraldehyde with proteins and other biological materials. *Journal of the Royal Microscopical Society*. 1966;85:193-200.
16. Estes MS, Komatsu SK, Koorjan S, Lane E, Nashref A, Steed D. Microbiology and biochemical data associated with the Carpentier-Edwards bioprosthesis. *American Edwards Laboratories Literature*. 1978.
17. Olde Damink LHH, Dijkstra PJ, Van Luyn MJA, Van Wachem PB, Nieuwenhuis P, Feijen J. Glutaraldehyde as a crosslinking agent for collagen-based biomaterials. *Journal of Materials Science. Materials in Medicine*. 1995;6:460-472.
18. Speer DP, Chvapil M, Eskelson CD, Ulreich J. Biological effects of residual glutaraldehyde in glutaraldehyde-tanned collagen biomaterials. *Journal of Biomedical Materials Research*. 1980;14:753-764.
19. Hopwood D. Theoretical and practical aspects of glutaraldehyde fixation. *Histochemistry*. 1972;4:267-303.
20. Anderson PJ. Purification and quantitation of glutaraldehyde and its effect on several enzyme activities in skeletal muscle. *Journal of Histochemistry and Cytochemistry*. 1967;15:652-661.
21. Julien M, Letouneau DR, Marois Y, Cardou A, King AW, Guidoin R, Chachra D, Lee JM. Shelf-life of bioprosthetic heart valves: a structural and mechanical study. *Biomaterials*. 1997;18:605-612.
22. Zilla P, Zhang Y, Human P, Koen W, Von Oppell U. Improved ultrastructural preservation of bioprosthetic tissue. *Journal of Heart Valve Disease*. 1997;6:492-501.
23. Rasmussen KE, Albrechtsen J. Glutaraldehyde: the influence of pH, temperature, and buffering on the polymerisation rate. *Histochemistry*. 1974;38:19-26.
24. Hayat MA. Aldehydes. In: Thubrican M, ed. *Fixation for Electron Microscopy*. New York: Academic Press; 1981:64-129.
25. Trelstad RL. The effect of pH on the stability of purified glutaraldehyde. *Journal of Histochemistry and Cytochemistry*. 1969;17:756-757.
26. Webb CL, Schoen FJ, Levy RJ. Covalent binding of aminopropanehydroxydiphosphonate to glutaraldehyde residues in pericardial bioprosthetic tissue: stability and calcification inhibition studies. *Experimental and Molecular Pathology*. 1989;50:291-302.
27. Gratzner PF, Pereira CA, Lee JM. Solvent environment modulates effects of glutaraldehyde crosslinking on tissue-derived biomaterials. *Journal of Biomedical Materials Research*. 1996;31:533-543.
28. Maranto AR, Schoen FJ. Effect of delay between tissue harvest and glutaraldehyde pretreatment on mineralisation of bovine pericardium used in bioprosthetic heart valves. *Journal of Biomedical Materials Research*. 1988;22:819-825.
29. Zilla P, Weissenstein C, Bracher M, Zhang Y, Koen W, Human P, Von Oppell U. High glutaraldehyde concentrations reduce rather than increase the calcification of aortic wall tissue. *Journal of Heart Valve Disease*. 1997;6:502-509.

30. Dahm M, Lyman WD, Schwell AB, Factor S, Frater RWM. Immunogenicity of glutaraldehyde-tanned bovine pericardium. *Journal of Thoracic Surgery*. 1990;99:1082-1090.
31. Maranto AR, Schoen FJ. Alkaline phosphatase activity of glutaraldehyde-treated bovine pericardium used in bioprosthetic cardiac valves. *Circulation Research*. 1988;63:844-848.
32. Simionescu D, Simionescu A, Deac R. Biochemical pathways of tissue degeneration in bioprosthetic cardiac valves: the role of matrix metalloproteinases. *American Society Artificial Internal Organs Journal*. 1996;42:M561-M567.
33. Levy RJ, Schoen FJ, Sherman FS, Nichols J, Hawley MA, Lund SA. Calcification of subcutaneously implanted type I collagen sponges: effects of glutaraldehyde and formaldehyde pretreatments. *American Journal of Pathology*. 1986;122:71-82.
34. Golomb G, Schoen FJ, Smith MS, Linden J, Dixon M, Levy RJ. The role of glutaraldehyde-induced cross-links in calcification of bovine pericardium used in cardiac valve bioprostheses. *American Journal of Pathology*. 1987;127:122-130.
35. Vincentelli A, Latremouille C, Zegdi R. Does glutaraldehyde induce calcification of bioprosthetic tissue? *Annals of Thoracic Surgery*. 1998;66:S255-S288.
36. Human P, Bracher M, Zilla P. The immune response to bioprosthetic tissue: influence of crosslink density. *Cardiovascular Pathology*. 1998;7:334.
37. McPherson JM, Ledger JP, Sawarana PW, Conti A, Wade S, Reihanian H, Wallace DG. The preparation and physicochemical characterisation of an injectable form of reconstituted glutaraldehyde crosslinked, bovine corium collagen. *Journal of Biomedical Materials Research*. 1986;20:79-92.
38. Nimni ME. The crosslinking and structure modification of the collagen matrix in the design of cardiovascular prosthesis. *Journal of Cardiac Surgery*. 1988;3:523-533.
39. Chachques JC, Vasseur B, Perier P, Balansa J, Chauvaud S, Carpentier A. A rapid method to stabilise biological materials for cardiovascular surgery. *Annals. New York Academy of Sciences*. 1988;529:184-186.
40. Ketharnathan V, Christie BA. Glutaraldehyde-tanned ovine collagen conduits as vascular xenografts in dogs. *Archives of Surgery*. 1980;115:967-969.
41. Chambers RW, Bowling MC, Grimley PM. Glutaraldehyde fixation in routine histopathology. *Archives of Pathology*. 1968;85:18-30.
42. Lawford PV, Kenyon CJ, Rogers S, Black MM. Inhibition of calcification of porcine bioprostheses by prolonged glutaraldehyde fixation. *Cardiovascular Science and Technology Conference AAMI/NIH*. 1993;Dec:10-12.
43. Weissenstein C, Human P, Bezuidenhout D, Zilla P. Glutaraldehyde detoxification on top of enhanced amine crosslinking dramatically reduces bioprosthetic tissue calcification in the rat model. *Journal of Heart Valve Disease*. 2000;9:230-240.
44. Zilla P, Weissenstein C, Human P, Dower T, Von Oppell UO. High glutaraldehyde concentrations mitigate bioprosthetic root calcification in the sheep model. *Annals of Thoracic Surgery*. 2000;70:2091-2095.
45. Dower T, Adler U, Davids L, Zilla P. Increasing crosslinking efficiency mitigates activation on bioprosthetic tissue. *Cardiovascular Pathology*. 1998;7:295-299.
46. Yannas IV, Kirk FJ. In: United States: Patent 448718; 1984.
47. Barbani N, Giusti P, Lazzeri L, Polacco G, Pizzirani G. Bioartificial materials based on collagen I. Collagen crosslinking with gaseous glutaraldehyde. *Journal of Biomaterials Science Polymer Edition*. 1995;7:461-469.
48. Schoen FJ, Tsao JW, Levy RJ. Calcification of bovine pericardium used in cardiac valve bioprostheses. Implications for the mechanism of bioprosthetic tissue mineralisation. *American Journal of Pathology*. 1986;123:134-145.
49. Chanda J. Anticalcification treatment of pericardial prostheses. *Biomaterials*. 1994;15:465-469.
50. Huang-Lee LHH, Cheung DT, Nimni ME. Biochemical changes and cytotoxicity associated with the degradation of polymeric glutaraldehyde derived cross-links. *Journal of Biomedical Materials Research*. 1990;24:1185-1201.
51. Schryer PJ, Tomasek ER, Starr A, Wright JT. Anticalcification effect of glutaraldehyde-preserved valve tissue stored for increasing time in glutaraldehyde. In: Bodnar E, Yacoub M, eds. *Proceedings of the Third International Symposium on Biologic and Bioprosthetic Valves*. New York: Yorke Medical Books; 1986:471-477.
52. Chanda J, Rao SB, Mohanty M. Calcification prevention of tissue valve. *Artificial Organs*. 1994;18:752-757.

53. Komatsu S, Lowery G, Nashef A, Parks L, Stegwell MJ. The improved sterilisation process for Carpentier-Edwards bioprostheses. *American Edwards Laboratories Literature*. 1982.
54. Koorajian S, Frugard G, Stegwell MJ. Sterilisation of tissue valves. In: Sebening F, Klovekorn WP, Meisner H, Struck E, eds. *Bioprosthetic Cardiac Valves*. Munchen: Deutsches Herzsentrum; 1979:373-378.
55. McClurg WM, Rogers S, Lawford PV, Hughes H. Acid hydrolysable aldehydes in long term stored commercial bioprosthetic heart valves: implications for calcification. *Cardiovascular Pathology*. 1998;7:233-237.
56. Roger S, Lawford PV, Kenyon C, Wain WH, Black MM. Prolonged fixation in glutaraldehyde retards/inhibits mineralisation in bioprosthetic valve tissue. *Journal of Pathology*. 1993;170:228a.
57. Girardot MN, Torrianni M, Dillehay D, Girardot JM. Role of glutaraldehyde in calcification of porcine heart valves: comparing cusp and wall. *Journal of Biomedical Materials Research*. 1995;29:793-801.
58. Glasmacher B, Reul H, Schnepferschoff S, Schrek S, Rau G. In-vitro calcification of pericardial bioprostheses. *Journal of Heart Valve Disease*. 1998;7:415-418.
59. Ferrans VJ, Hilbert SL, Jones M. Biomaterials. In: Bodnar E, ed. *Replacement Cardiac Valves*. New York: Pergamon Press; 1991:49-77.
60. McClurg WM, Lawford PV, Hughes H, Rogers S. Formaldehyde replaces glutaraldehyde in porcine bioprosthetic heart valves. *Journal of Heart Valve Disease*. 1996;5:343-347.
61. Patai S. In: *The Chemistry of Double Bonded Functional Groups*. New York: John Wiley and Sons; 1989:600-614.
62. Patai S. In: *The Chemistry of the Carbon-Nitrogen Double Bond*. New York: John Wiley and Sons; 1970:64-83.
63. Southern LJ. Identification of glutaraldehyde-induced structures in bioprosthetic heart valves using mass spectrometry: an insight into valve failure. In. Sheffield: University of Sheffield; 2001.
64. Dpeer DP, Chvapil M, Volz R, Holmes M. Enhancement of healing of osteochondral defects by collagen sponge implants. *Clinical Orthopaedics*. 1979;144:326-335.
65. Gendler E, Gendler S, Nimni ME. Toxic reactions evoked by glutaraldehyde-fixed pericardium and cardiac valve tissue bioprosthesis. *Journal of Biomedical Materials Research*. 1984;18:727-736.
66. Woodroof EA. Use of glutaraldehyde and formaldehyde to process tissue heart valves. *Journal of Bioengineering*. 1978;2:1-9.
67. Avrameas S, Ternynck T. The cross-linking of proteins with glutaraldehyde and its use for the preparation of immunoadsorbents. *Immunochemistry*. 1969;6:53-66.
68. Cater CW. The evaluation of aldehydes and other difunctional compounds as crosslinking agents for collagen. *Journal of the Society of Leather Trades Chemists*. 1963;47:259-272.
69. Quiocho FA, Richards FM. The enzymic behaviour of carboxypaptidase-A in the solid state. *Biochemistry Journal*. 1966;5:4062-4076.
70. Bovallius A, Anas P. Surface decontamination action of glutaraldehyde in the gas-aerosol phase. *Applied Environmental Microbiology*. 1977;34:129-134.
71. Korn AH, Fairheller SH, Filachione EM. Glutaraldehyde: nature of the reagent. *Journal of Molecular Biology*. 1972;65:525-529.
72. Niclaude M, Lemaire J, Letort M. The kinetics and mechanism of photochemical oxidation of aldehydes by molecular oxygen. In: *Advances in Photochemistry*. New York: Wiley and Sons; 1966:25-48.
73. Larkin DR. The role of catalysts in the air oxidation of aliphatic aldehydes. *Journal of Organic Chemistry*. 1990;55:1563-1568.
74. Scobbie E, Groves JA. An investigation of the composition of the vapour evolved from aqueous glutaraldehyde solutions. *Annals of Occupational Hygiene*. 1995;39:63-78.
75. Morel C, Reynier M, Cavigneaux A, Protois JC. Glutaraldehyde. *Cahiers Notes Documentation*. 1982;108:449-451.
76. Gillett R, Gull K. Glutaraldehyde: Its purity and stability. *Histochemie*. 1972;30:162-167.
77. Ranly DM. Glutaraldehyde purity and stability: implications for preparation, storage and use as a pulpotomy agent. *Pediatric Dentistry*. 1984;6:83-87.
78. Goissis G, Yoshioka SA, Braille DM, Ramirez VDA. The chemical protecting group concept applied in crosslinking of natural tissues with glutaraldehyde acetals. *Artificial Organs*. 1998;22:210-214.

79. Menet MC, Gueylard D, Fievet MH, Thuillier A. Fast specific separation and sensitive quantification of bactericidal and sporicidal aldehydes by HPLC. *Journal of Chromatography B*. 1996;692:79-86.
80. Fahimi HD, Drochmans P. Essai de standardisation de la fixation au glutaraldehyde I. Purification et determination de la concentration du glutaraldehyde. *Journal of Microscopie*. 1965;4:725-736.
81. Hopwood D. The behaviour of various glutaraldehyde on Sephadex G-10 and some implications for fixation. *Histochemie*. 1967;II:289-295.
82. Monsan P, Puzo G, Mazarguil H. Etude du mecanisme d'etablissement des liaisons glutaraldehyde-proteines. *Biochimie*. 1975;57:1281-1292.
83. Whipple EB, Ruta M. Structure of aqueous glutaraldehyde. *Journal of Organic Chemistry*. 1974;39:1666-1668.
84. Frigerio NA, Shaw MJ. A simple method for the determination of glutaraldehyde. *Journal of Histochemistry and Cytochemistry*. 1968;17:176-181.
85. Yokota K, Suzuki Y, Ishii Y. Temperature dependence of the polymerisation modes of glutaraldehyde. *Chemical Abstracts*. 1965;65:13835.
86. Robertson EA, Schultz RL. The impurities in commercial glutaraldehyde and their effects on the fixation of brain. *Journal of Ultrastructural Research*. 1970;30:275-287.
87. Ruijgrok JM, De Wijn JR, Boon ME. Optimising glutaraldehyde crosslinking of collagen: effects of time, temperature and concentrations as measured by shrinkage temperature. *Journal of Materials Science. Materials in Medicine*. 1994;5:80-87.
88. Blass J, Verriest C, Leau A, Weiss M. Monomeric glutaraldehyde as an effective crosslinking reagent for proteins. *Journal of the American Leather Chemists Association*. 1976;71:121-132.
89. Hardy PM, Nicholls AC, Rydon HN. The nature of glutaraldehyde in aqueous solution. *Journal of Chemical Society Chemical Communications*. 1969;10:565-566.
90. Prento P. Glutaraldehyde for electron microscopy: a practical investigation of commercial glutaraldehydes and glutaraldehyde-storage conditions. *Histochemical Journal*. 1995;27:906-913.
91. Trowbridge EA, Crofts EA. The standardisation of gauge length: its influence on the relative extensibility of natural and chemically modified pericardium. *Journal of Biomechanics*. 1986;19:1023-1033.
92. Gorman SP, Scott EM. Potentiation and stabilisation of glutaraldehyde biocidal activity utilising surfactant-divalent cation combinations. *International Journal of Pharmaceutics*. 1979;4:57-65.
93. Marquie C, Tessier AM, Aymard C, Guilbert S. HPLC determination of the reactive lysine content of cottonseed protein films to monitor the extent of crosslinking by formaldehyde, glutaraldehyde, and glyoxal. *Journal of Agricultural and Food Chemistry*. 1997;45:922-926.
94. Angell WW, Angell JD. Porcine valves. *Progress in Cardiovascular Diseases*. 1980;23:141-166.
95. Cheung DT, Nimni ME. Mechanism of crosslinking of proteins by glutaraldehyde II. Reaction with monomeric and polymeric collagen. *Connective Tissue Research*. 1982;10:201-216.
96. Okubo M, Takahashi M. Production of submicron size monodisperse polymer particles having aldehyde groups by the seeded aldol condensation polymerisation of glutaraldehyde II. *Colloid and Polymer Science*. 1994;272:422-426.
97. Munton TJ, Russell AD. Aspects of the action of glutaraldehyde on Escherichia Coli. *Journal of Applied Bacteriology*. 1970;33:410-419.
98. Aso C, Aito Y. Intramolecular-intermolecular polymerisation of glutaraldehyde. *Bulletin of the Chemical Society of Japan*. 1962;35:1426.
99. Aso C, Aito Y. Studies on the polymerisation of bifunctional monomers II: Polymerisation of glutaraldehyde. *Makromolekulare Chemie*. 1962;58:195-203.
100. Kawahara JI, Ohmori T, Ohkubo T, Hattori S, Kawamura M. The structure of glutaraldehyde in aqueous solution determined by ultraviolet absorption and light scattering. *Analytical Biochemistry*. 1992;201:94-98.
101. Tashima T, Kawakami U, Harada M, Sakata T, Satoh N, Nakagawa T, Tanaka H. Isolation and identification of new oligomers in aqueous solution of glutaraldehyde. *Chemical Pharmaceutical Bulletin*. 1987;35:4169-4180.

102. Tashima T, Kawakami U, Satoh N, Nakagawa T, Tanaka H. Detection of impurities in aqueous solution of glutaraldehyde by HPLC with a multichannel photodiode array UV detector. *Journal of Electron Microscopy*. 1987;36:136.
103. Tashima T, Kawakami U, Harada M, Imai M, Satoh N, Nakagawa T, Tanaka H. Polymerisation reaction in aqueous solution of glutaraldehyde containing trioxane-type oligomers under sterilising conditions. *Chemical Pharmaceutical Bulletin*. 1989;37:377-381.
104. Nimni ME, Cheung DT, Strates BS, Kodama M, Sheikh K. Bioprosthesis derived from crosslinked and chemically modified collagenous tissues. In: Nimni ME, ed. *Collagen*. Boca Raton Florida: CRC Press; 1988:1-38.
105. Richards FM, Knowles JR. Glutaraldehyde as a protein crosslinking reagent. *Journal of Molecular Biology*. 1968;37:231-233.
106. Mukaiyama T. The directed aldol condensation reaction. In: *Organic Reactions*. New York: John Wiley and Sons; 1983:203-332.
107. Robertson EA, Schultz L. The impurities of commercial glutaraldehyde and their effect on the fixation of the brain. *Journal of Histochemistry and Cytochemistry*. 1970;15:652-661.
108. Solomons TWG. The aldol reaction: the addition of enolate ions to aldehydes and ketones. In: *Organic Reactions*. 6th ed. New York: John Wiley and Sons; 1996:762-763.
109. Margel S, Rembaum A. Synthesis and characterisation of polyglutaraldehyde. A potential reagent for protein immobilisation and cell separation. *Macromolecules*. 1980;13:19-24.
110. Walt DR, Agayn VI. The chemistry of enzyme and protein immobilisation with glutaraldehyde. *Trends in Analytical Chemistry*. 1994;13:425-430.
111. Shan ZH. Glutaraldehyde and modified glutaraldehyde used in leather making. *Leather Science and Engineering*. 1999;9:30-33.
112. Tashima T, Imai M. Structure of a new oligomer of glutaraldehyde produced by aldol condensation reaction. *Journal of Organic Chemistry*. 1991;56:694-697.
113. Bergmann ED, Ginsbury D, Pappo R. The Michael reaction. In: *Organic Reactions*. New York: John Wiley and Sons; 1959:179-556.
114. Happich WF, Taylor MH, Fairheller SH. Amino acid composition of glutaraldehyde-stabilised wool. *Textile Research Journal*. 1970;40:768-769.
115. Tomimatsu Y, Jansen EF, Gaffield W, Olson AC. Physical chemical observations on the alpha-chymotrypsin glutaraldehyde system during formation of an insoluble derivative. *Journal of Colloid and Interface Science*. 1971;36:51-64.
116. Hopwood D. Some aspects of fixation by glutaraldehyde and formaldehyde. *Journal of Anatomy*. 1968;103:581.
117. Bowes JH, Cater CW. The interaction of aldehydes with collagen. *Biochimica et Biophysica Acta*. 1968;168:341-352.
118. Habeeb AFSA, Hiramoto R. Reactions of proteins with glutaraldehyde. *Archives of Biochemistry and Biophysics*. 1968;126:16-26.
119. Cheung DT, Perelman N, Ko EC, Nimni ME. Mechanism of crosslinking of proteins by glutaraldehyde III. Reactions with collagen in tissues. *Connective Tissue Research*. 1985;13:109-115.
120. Nimni ME, Cheung DT, Strates BS, Kodama M, Sheikh K. Chemically modified collagen: a natural biomaterial for tissue replacement. *Journal of Biomedical Materials Research*. 1987;21:741-771.
121. Tomihata K, Ikada Y. Crosslinking of hyaluronic acid with glutaraldehyde. *Journal of Polymer Science Part A-1*. 1997;35:3553-3559.
122. Blauer G, Harmatz D, Meir E, Swenson MK, Zvilichovsky B. The interaction of glutaraldehyde with poly(α ,L-lysine), N-butyl amine and collagen. I. The primary proton release in aqueous medium. *Biopolymers*. 1975;14:2585-2598.
123. Cheung DT, Nimni ME. Mechanism of crosslinking of proteins by glutaraldehyde I. Reaction with model compounds. *Connective Tissue Research*. 1982;10:187-199.
124. Coupland RE, Hopwood D. The mechanism of the differential staining reaction for adrenaline- and noradrenaline-storing granules in tissues fixed in glutaraldehyde. *Journal of Anatomy*. 1966;100:227-243.
125. Hopwood D, Allen CR, McCabe M. The reactions between glutaraldehyde and various proteins. An investigation of their kinetics. *Histochemical Journal*. 1970;2:137-150.
126. Bowes JH, Cater CW, Ellis MJ. Determination of formaldehyde and glutaraldehyde bound to collagen by carbon-14 assay. *Journal of the American Leather Chemists Association*. 1965;60:275-285.

127. Bowes JH, Cater CW. Crosslinking of collagen. *Journal of Applied Chemistry*. 1965;15:296-304.
128. Fein ML, Harris EHJ, Naghski J, Filachione EM. Tanning with glutaraldehyde I. Rate studies. *Journal of the American Leather Chemists Association*. 1959;54:488-502.
129. Casagrande F, Werkmeister JA, Ramshaw JAM, Ellender G. Evaluation of alternative glutaraldehyde stabilisation strategies for collagenous biomaterials. *Journal of Materials Science. Materials in Medicine*. 1994;5:332-337.
130. In: Wade LGJ, ed. *Organic Chemistry*. 3rd ed. Englewood Cliffs: Prentice-Hall; 1995:839-841.
131. Stonehill AA, Krop S, Borick PM. Buffered glutaraldehyde. *American Journal of Hospital Pharmacy*. 1963;20:458.
132. Rubbo SD, Gardner JF, Webb AL. Biocidal activities of glutaraldehyde and related compounds. *Journal of Applied Bacteriology*. 1967;30:78.
133. Sabatini DD, Miller F, Barrnett RJ. Aldehyde fixation for morphological and enzyme histochemical studies with the electron microscope. *Journal of Histochemistry and Cytochemistry*. 1964;12:57-71.
134. Goissis G, Marcantonio E, Marcantonio RAC, Lia RCC, Cancian DCJ, Carvalho WM. Biocompatibility studies of anionic collagen membranes with different degree of glutaraldehyde crosslinking. *Biomaterials*. 1999;20:27-34.
135. Bowes JH, Kenten RH. The effect of deamination and esterification on the reactivity of collagen. *Journal of Biochemistry*. 1949;44:147-152.
136. Swenson MK, Meir E, Yanai P, Zvilichovsky B, Blauer G. The interaction of glutaraldehyde with poly(α ,L-lysine), N-butyl amine and collagen. II. Hydrodynamic, electron microscopic, and optical investigations on the reaction products. *Biopolymers*. 1975;14:2599-2612.
137. Hardy PM, Nicholls AC, Rydon HN. The nature of the crosslinking of proteins by glutaraldehyde I. Interaction of glutaraldehyde with the amino-groups of 6-aminohexanoic acid and of N-acetyl-lysine. *Journal of Chemical Society Perkin Transaction I*. 1976:958-962.
138. Griffiths G. In: *Fine Structure Immuno-Cytochemistry*. Berlin: Springer Verlag; 1993.
139. Kuznetsova NP, Gudkin LR, Mishaeva RN. Oligomerisation of bifunctional aldehyde in reactions with bipolar ions. *Russian Journal of Applied Chemistry*. 2002;75:974-979.
140. Okuda K, Urabe I, Yamada Y, Okada H. Reaction of glutaraldehyde with amino and thiol compounds. *Journal of Fermentation and Bioengineering*. 1991;71:100-105.
141. Swenson MK, Meir E, Zvilichowsky B, Blauer G. The interaction of glutaraldehyde with poly-L-lysine, N-butylamine and collagen II. Hydrodynamic, electron microscopic and optical investigations on reactions products. *Biopolymers*. 1975;14:2599-2612.
142. Weadock K, Olson RM, Silver FH. Evaluation of collagen crosslinking techniques. *Biomaterials, Medical Devices and Artificial Organs*. 1983-84;11:293-318.
143. Lee JM, Pereira CA, Kan LWK. Effect of molecular structure of poly(glycidyl ether) reagents on crosslinking and mechanical properties of bovine pericardial xenograft materials. *Journal of Biomedical Materials Research*. 1994;28:981-992.
144. McMaster WC, Kouzelos J, Liddle S, Waugh TR. Tendon grafting with glutaraldehyde fixed material. *Journal of Biomedical Materials Research*. 1976;10:259-271.
145. Madden KN, Johnson KA, Howlett CR. Resorbable and nonresorbable augmentation devices for tenorrhaphy of xenografts in extensor tendon deficits: twelve week study. *Biomaterials*. 1997;18:225-234.
146. Lusty CJ. A gentle vapor diffusion technique for crosslinking of protein crystals for cryocrystallography. *Journal of Applied Crystallography*. 1999;32:106-112.
147. Filachione EM, Korn AH, Ard JS. The UV absorption of protein-bound glutaraldehyde. *Journal of the American Leather Chemists Association*. 1967;62:450-453.
148. Korn AH, Filachione EM. The direct determination of bound glutaraldehyde in glutaraldehyde-tanned collagen. *Journal of the American Leather Chemists Association*. 1967;62:507-520.
149. Kuznetsova NP, Mishaeva RN, Gudkin LR. Oligomerisation of glutaraldehyde in the course of its condensation with glycine. *Russian Journal of Applied Chemistry*. 1999;72:1236-1241.
150. Gudkin LR, Kuznetsova NP. Features of reaction of glutaraldehyde with glutamic acid. *Russian Journal of Applied Chemistry*. 1997;70:782-785.
151. Ishii T, Sorita A, Sawamura M, Kusunose H, Ukeda H. Determination of the reaction product of glutaraldehyde and amine based on the binding ability of coomassie brilliant blue. *Analytical Sciences*. 1997;13:5-9.

152. Weston PD, Avrameas S. Proteins coupled to polyacrylamide beads using glutaraldehyde. *Biochemical and Biophysical Research Communications*. 1971;45:1574-1580.
153. Reichlin M. Use of glutaraldehyde as a coupling agent for proteins and peptides. *Methods in Enzymology*. 1980;70:159-165.
154. Wang F, Hayter J, Wilson LJ. Salt-induced aggregation of lysosyme studied by crosslinking with glutaraldehyde: implications for crystal growth. *Acta Crystallographica Section D Biological Crystallography*. 1996;52:901-908.
155. Luft JH. Fixation for biological ultrastructure I. A viscometric analysis of the interaction between glutaraldehyde and bovine serum albumin. *Journal of Microscopy*. 1992;167:247-258.
156. Hardy PM, Hughes GJ, Rydon HN. Formation of quaternary pyridinium compounds by the action of glutaraldehyde on proteins. *Journal of Chemical Society Chemical Communications*. 1976;5:157-158.
157. Hardy PM, Hughes GJ, Rydon HN. The nature of the crosslinking of proteins by glutaraldehyde II. The formation of quaternary pyridinium compounds by the action of glutaraldehyde on proteins and the identification of a 3-(2-piperidyl)-pyridinium derivative, anabylisine, as a crosslinking entity. *Journal of the Chemical Society Perkin Transaction I*. 1979;9:2282-2288.
158. Chatterji PR. Gelatin with hydrophylic/hydrophobic grafts and glutaraldehyde crosslinks. *Journal of Applied Polymer Science*. 1989;37:2203-2212.
159. Matsuda S, Iwata H, Se N, Ikada Y. Bioadhesion of gelatin films crosslinked with glutaraldehyde. *Journal of Biomedical Materials Research*. 1999;45:20-27.
160. Reeves RL. In: Patai S, ed. *Chemistry of the Carbonyl Group*. London: Interscience; 1966:567-619.
161. Quijcho FA, Richards FM. Intermolecular crosslinking of a protein in the crystalline state: carboxypeptidase A. *Proceedings of the National Academy of Sciences of the U.S.A.* 1964;52:833-839.
162. Tramezzani JH, Chiocchio S, Wassermann GF. A technique for light and electron microscopic identification of adrenalin and noradrenaline storing cells. *Journal of Histochemistry and Cytochemistry*. 1964;12:890-899.
163. Means GE, Feeney RE. Reductive alkylation of amino groups in proteins. *Biochemistry Journal*. 1968;7:2192-2201.
164. Peters K, Richards FM. Chemical crosslinking: reagents and problems in studies of membrane structure. *Annual Review of Biochemistry*. 1977;46:523-551.
165. Franzblau C, Lent RW. Studies on the chemistry of elastin. Structure, function and evaluation in proteins. *Brookhaven Symposia in Biology*. 1968;21:358-377.
166. Shainoff J. Zonal immobilisation of proteins. *Biochemical and Biophysical Research Communications*. 1980;95:690-695.
167. Zilla P, Fullard L, Trescony P, Meinhardt J, Bezuidenhout D, Gorlitzer M, Human P, Von Oppell U. Glutaraldehyde detoxification of aortic wall tissue: a promising perspective for emerging bioprosthetic valve concept. *Journal of Heart Valve Disease*. 1997;6:510-520.
168. Hardy PM, Nicholls AC, Rydon HN. The nature of the crosslinking of proteins by glutaraldehyde I. Interaction of glutaraldehyde with the amino-groups of 6-amino-hexanoic acid and N-acetyl-L-lysine. *Journal of the Chemical Society Perkin Transaction I*. 1976:958-962.
169. Lee WK, Park KD, Kim YH, Suh H, Park JC, Lee JE, Sun K, Baek MJ, Kim HM, Kim SH. Improved calcification resistance and biocompatibility of tissue patch grafted with sulphonated PEO or heparin after glutaraldehyde fixation. *Journal of Biomedical Materials Research. Applied Biomaterials*. 2001;58:27-35.
170. Layer RW. The chemistry of imines. *Chemical Reviews*. 1963;63:489-510.
171. March J. In: *Advanced in Organic Chemistry*. 3rd ed. New York: John Wiley and Sons; 1985:784-786.
172. Hardy PM, Hughes GJ, Rydon HN. Identification of a 3-(2-piperidyl) pyridinium derivative (anabylisine) as a crosslinking entity in a glutaraldehyde-treated protein. *Journal of Chemical Society Chemical Communications*. 1977;21:759-760.
173. Lubig R, Kusch P, Roper K, Zahn H. On the mechanism of protein crosslinking with glutaraldehyde. *Monatshefte für Chemie*. 1981;112:1313-1323.
174. Cater CW. Investigation into the efficiency of dialdehydes and other compounds as crosslinking agents for collagen II. *Journal of the Society Leather Trade Chemists*. 1965;49:455-469.

175. Jenks WP. In: Cohen SG, Streitwieser A, Taft RW, eds. *Progress in Physical Organic Chemistry*. New York: Interscience; 1964:63.
176. Rouvier E, Giacomoni JC, Cambon A. Amines presentant un autre groupement fonctionnel I. Reactivite des amines primaires et secondaires sur quelques olefines actives. *Bulletin de la Societe Chimique de France*. 1971;5:1717-1723.
177. Solomons TWG. Aldehydes and ketones: additions to alpha,beta-unsaturated aldehydes and ketones. In: *Organic Chemistry*. 6th ed. New York: John Wiley and Sons; 1996:777.
178. Tschittschibabin A. Uber die Synthese von Pyridinbasen aus Aldehyden gesattigten Charakters und Ammoniak. *Chemisches Zentral-Blatt*. 1906;77:1438-1439.
179. Craig D, Schaeffer L, Tyler WP. N-phenyl-3,5-diethyl-2-propyl-1,4-dihydropyridine. *Journal of the American Chemical Society*. 1948;70:1624-1629.
180. Charman HB, Rowe JM. Condensations of aldehydes with ammonium salts to give substituted pyridines. *Chemical Communications*. 1971:476-477.
181. Patrick TM. The reaction of aldehydes with aldimines. *Journal of the American Chemical Society*. 1952;74:2984-2986.
182. Peracchia C. Structural changes after uncoupling procedures. *Journal of Cell Biology*. 1977;22:628-641.
183. Johnson TJA. Glutaraldehyde fixation chemistry: oxygen-consuming reactions. *European Journal of Cell Biology*. 1987;45:160-169.

Chapter 3

3 Techniques: theory and applications.

3.1 Introduction

When making a chemical analysis, it is rather difficult to draw definitive conclusions from the data obtained from one single technique; but more conclusive data can be obtained when several techniques are applied to a problem. For example, making definitive assumptions on molecular structure from mass spectrometry (MS) is not possible without the help of other techniques such as nuclear magnetic resonance (NMR), infrared (IR) or ultraviolet (UV) spectroscopy. Therefore, for this study, it was decided to use a large range of techniques in order to be able to draw realistic conclusions.

A primary aim of this study was to gain a greater understanding of the chemistry involved in the treatment of collagenous valve tissue with glutaraldehyde. Amino acids, peptides and proteins were thus used to model potential reactions involved in glutaraldehyde treatment of valve tissue. The following techniques were used to investigate the reactions and subsequent products: Nuclear Magnetic Resonance (NMR), Fourier-Transform Infra-Red (FTIR) and Raman spectroscopy, ElectroSpray Ionisation (ESI-MS) and Matrix Assisted Laser Desorption Ionisation-Time-of-Flight Mass Spectrometry (MALDI-TOF MS).

The second main aim of this study was to develop a successful method for observing the surface morphology of calcified tissue in its native wet state by using the Environmental Scanning Electron Microscopy (ESEM) coupled with analysis by Energy Dispersive X-ray (EDS). The developed methods were then applied to samples from clinical investigations (explanted human calcified valves), in-vivo screening (rat subcutaneous implantation model) and in-vitro screening (pericardial

tissue incubated in a metastable calcification solution) to investigate the calcification process. In order to further define the identity of the calcified structures, various spectroscopic techniques were used, such as XRD, FTIR-ATR and Raman spectroscopy. The quantitative determination of calcium and other metal ions present in these calcified tissues was carried out by ICP-OES analysis.

Each technique is only briefly discussed in this section for the sake of the length of the thesis, but particular details and relevant applications are given where applicable and the reader is directed to more detailed publications.

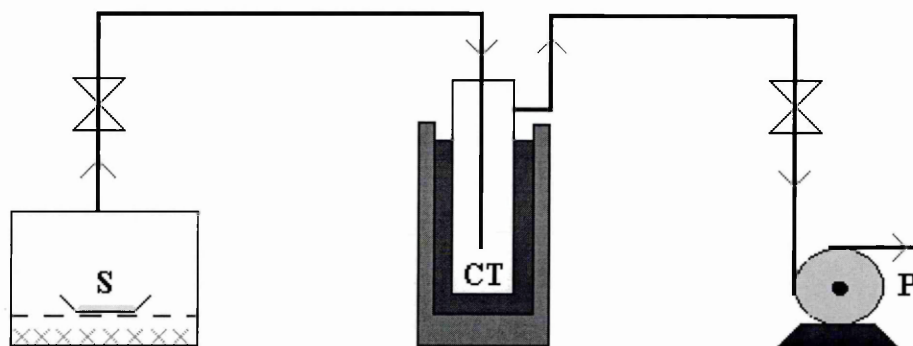
3.2 Methods

3.2.1 Freeze-drier

3.2.1.1 Theory and methodology:

The basics and theory of the freeze-drying lies in a commonly known-physical process, which is the sublimation process.

All samples subjected to freeze-drying (aqueous solutions or wet tissues for instance) were frozen for a few hours in an air environment in a -20°C fridge or immersed and swirled for a few minutes in liquid nitrogen with the help of a round-bottomed-flask. The frozen samples were then quickly removed and placed in the specimen chamber of the freeze drier. The frozen samples in the sample chamber were thus allowed to warm spontaneously, while the vacuum pump was facilitating a sublimation process. A cold trap (or condensing chamber) filled with liquid nitrogen prevented any solvent vapour from reaching the vacuum pump (two stages Edwards pump, Crawley, UK) where they might condense and cause the cavitation of the pump. The freeze-drying process only removed the solvent (water in this study) without altering the nature of the diluted species or the wet tissue. A laboratory-built freeze-drier was used for these studies. Occasionally, a “Cold Trap 1000” freeze-drier (UK) was also used to freeze-dry cardiac valves and pericardial tissue. The laboratory-built freeze-drier is illustrated in figure 3.1 below.



S: Sample Chamber.

CT: Cold Trap filled with liquid nitrogen.

P: Edwards Vacuum Pump.

Figure 3.1: "Laboratory-built" freeze-drier set up.

3.2.1.2 Applications related to this study:

The freeze-drying technique is widely used in the food industry (lyophilised products) and in the pharmaceutical industry in order to store products in a reliable stable phase. The process however is not yet fully understood. The development of a freeze-drying process used for cardiac valves has also been reported¹.

The freeze-drying process allows the analysis of solid reaction products resulting from an aqueous chemical reaction. The range of concentrations employed in this study was relatively low. To increase spectral intensity, samples were freeze-dried prior to analysis. To ensure species were unaffected by this process, all unreacted species used were first submitted to analysis as a freeze-died aqueous solution and as neat compounds. The overall conclusion was that all model compounds (amino acids, peptides and proteins) gave the same spectra from a freeze-dried sample as from the pure compound.

Also, freeze-dried samples can be readily diluted in other solvents if necessary. This can be particularly useful for concentrating the solution or for dissolving the sample in another solvent (especially useful in the case of mass spectrometry and nuclear magnetic resonance spectroscopy sample preparation).

3.2.2 Environmental Scanning Electron Microscopy (ESEM)

3.2.2.1 Theory:

The ESEM has been described in an extensive survey by its principal developer, Danilatos G.D.². In comparison to conventional SEM, which requires a high vacuum and stable samples at very low pressures and thus prevents wet, moist or dirty samples from being imaged, the ESEM uses a vacuum gradient to maintain high vacuum conditions at the primary electron source while permitting sample chamber pressures to be varied. A schematic representation of the ESEM sample chamber can be found below in figure 3.2.

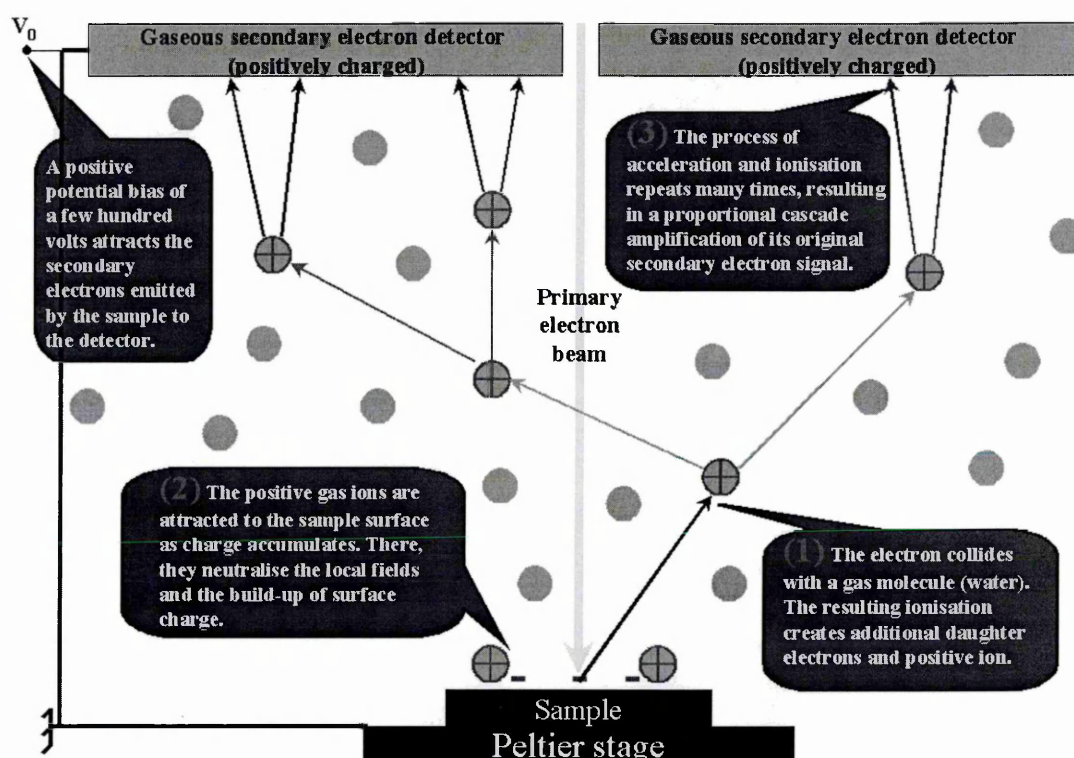


Figure 3.2: Schematic representation of the simplified "cascade process" occurring in the ESEM sample chamber

In the ESEM, an incoming primary electron beam is oriented towards the sample surface. When this primary electron beam hits the sample, secondary and backscattered electrons are emitted from the sample. The gaseous environment of the ESEM sample chamber is then ionised by secondary electrons derived from the sample. The resulting ionisation creates additional daughter electrons and positive ions. Electrons from ionising gas molecules precipitate a cascade multiplication of

the imaging current that is monitored by the detector³ (thus the name of “cascade process”). A positive bias applied to the detector electrode above the sample attracts the secondary electrons from the sample and accelerates them sufficiently to create a cascade of ion-electron pairs and to yield considerable amplification before they are collected. The positive ions produced upon ionisation of the gas molecules in the sample chamber neutralise charges on the sample surface. The elimination of charging allows insulators to be observed without the need for conducting coatings, unlike the conventional SEM. For further insight into the theory of ESEM, the reader is invited to refer to articles by Danilatos⁴⁻⁶ and Phillips and Toth⁷.

3.2.2.2 Applications related to this study:

The applications of ESEM are numerous although the number of publications is, as yet, relatively low. Applications include colloid characterisation⁸, bio-corrosion⁹, a study of ice films to simulate stratospheric clouds¹⁰, imaging of ink on paper¹¹, imaging of albumen photographs¹², real-time etching of dental enamel¹³ and studies of micro-organisms¹⁴.

Most electron microscopic studies of the calcification process have been limited to the study of thin sections of material (cut embedded specimen block), by both scanning electron microscopy (SEM) and transmission electron microscopy (TEM), thus focusing on calcific deposition within the structures of pericardium such as cells and collagen molecules^{15,16}. However, there has been little study of the deposition of calcium phosphate on pericardial surfaces and the insides of tissue in the early stages of calcification, using SEM and TEM. Moreover, the use of such techniques necessitates a particular sample preparation, e.g. transfer over several days from aqueous solution to methanol to ensure complete dehydration of the samples, followed by critical point drying. Samples have to be mounted on metallic surfaces and sputter coated with gold, carbon, etc. to facilitate good conduction. Gold coating permits study of the surface with minimal tissue damage in electron microscopy, however for the analysis of phosphorus, it can give very poor results because of the proximity of the phosphorus K- α and gold L X-ray peaks. Carbon coating, however, does not interfere in the X-ray spectrum but even after 4-5 coatings gives poor overall results because of the discontinuous conducting surface in comparison to gold. This leads to charging effects, causing poor imaging quality and such samples

can also be damaged quite easily by the primary beam. Additionally, exposure to the high vacuum and electron bombardment of calcified tissue is likely to decompose the hydrated calcium phosphate salts (making them appear amorphous) or cause disproportionation into a more stable mixture of salts¹⁷.

Although there are no publications reporting the application of ESEM to the analysis of valve tissue and calcified-tissue valves, the use of ESEM has been reported in studies of interest to this work. For example, Fulmer et al have reported the use of ESEM in the study of the morphologies of the reaction products, (mostly calcium deficient hydroxyapatite ($\text{Ca}_9(\text{HPO}_4)(\text{PO}_4)_5\text{OH}$)), which was formed by the reaction of tetracalcium phosphate ($\text{Ca}_4(\text{PO}_4)_2\text{O}$), monetite (CaHPO_4), brushite ($\text{CaHPO}_4 \cdot 2\text{H}_2\text{O}$) and calcium hydroxide ($\text{Ca}(\text{OH})_2$)¹⁸. The advantage of using ESEM when studying such samples is emphasised when it is reported that the use of a high vacuum environment in SEM or TEM can potentially cause the release of hydrogen and the further conversion of hydroxyapatite to a α -tricalcium phosphate structure¹⁹. ESEM has also been reported in the analysis of the viability of cells on different polymer scaffolds for valve tissue engineering purposes²⁰. The same technique was also described in the study of the morphology of cacodylic acid-fixed tissue fabricated in-vitro and was capable of showing the attachment of cells on the polymer scaffold²¹. Recently, the same group described the construction of a trileaflet heart valve scaffold for tissue engineering, which leads to successful cell proliferation and collagen formation. The subsequent evaluation of the leaflet surface and valve conduit implanted in-vivo in a lamb model was carried out with the help of ESEM^{22,23}.

3.2.3 ICP-OES (inductively coupled plasma-optical emission spectroscopy)

3.2.3.1 Theory:

The inductively coupled plasma is a flame, which exceeds temperatures normally attained by a conventional combustion flame. Its high temperature and stability eliminates interferences often associated with conventional flames. A radio frequency field generates the plasma within a flow of argon gas. When an aerosol of the sample solution is injected into the plasma through a stream of argon, excitation from ground state to the excited electronic state occurs. The ICP was found to be the most effective electrodeless excitation source^{24,25}. Atoms will relax to their ground

states emitting radiation of characteristic wavelengths. Photomultipliers are used to detect those wavelengths and convert them into an electrical signal. To be more specific, there are two parts for the detection line that can be used simultaneously if required, and thus many wavelengths of varying sensitivity are available for the determination of one element. The simultaneous part of the detector consists of a bank of six photomultipliers that are fixed at certain wavelengths for most common analysed elements (Mg, Na, Ni, Fe, Pb, Cu...). The other part of the detector (sequential part) consists of one photomultiplier that scans over a range of wavelengths, allowing the analysis of theoretically all elements at once. The detection limits are in the order of parts per million with a good linear range. Solid samples have to be digested using ultra pure acids and either a microwave (homogeneous heating) or a hotplate to aid digestion. For a much more detailed consideration of the theory of ICP-OES, the reader is invited to refer to specialised publications²⁶⁻²⁸.

3.2.3.2 Applications related to this study:

In valve calcification studies, calcium determination has generally been carried out by atomic absorption spectroscopy at a wavelength of 315.18 nm^{29,30}. Phosphorus has been determined by spectrophotometry of the reduction of phosphovanadomolybdic acid complex³¹ or another complexing method with ascorbic acid³². However, in order to detect the presence of many metal ions at once, the use of ICP-OES is ideal and was only recently reported for quantitative analysis of calcium and phosphorous deposits on valve leaflets in a canine in-vivo model³³ and an in-vitro model³⁴. The amounts of calcium and phosphorus accumulated on retrieved glutaraldehyde-treated bovine pericardium from canine vascular implantation for 40 days were respectively of $13.8 \pm 2.3 \mu\text{g}$ of Ca/mg of tissue and $19.3 \pm 4.3 \mu\text{g}$ of P/mg of tissue in the aorta implantation site, and $6.7 \pm 0.7 \mu\text{g}$ of Ca and $12.6 \pm 3.4 \mu\text{g}$ of P in the pulmonary artery implantation site³³. They reported that these values were rather low when compared with other reports. On the other hand, a static in-vitro assessment of tissue valve calcification (relatively similar model to the one used for these studies) exhibited $\sim 200 \mu\text{g}$ of Ca/mg of tissue and less than a few μg of P/mg of tissue (exact values not given)³⁴. These authors observed a difference between the results from dynamic in-vitro and static in-vitro testing to study calcification. Additionally, they reported a remarkable difference between the results from their in-

vitro calcification study and in-vivo methods. Apart from calcium and phosphorus, the measurement of silicon in biological fluids, which is of relevance for these studies, was also reported^{35,36}.

3.2.4 X-Ray Powder Diffraction (XRD)

3.2.4.1 Theory:

In modern XRD instruments, the production of X-rays occurs in an evacuated chamber containing a metal target (e.g. Cu), which is struck by incident high-speed electrons from a heated filament. The accelerated electrons strike the inner, more tightly bound, electrons of the target and knock them out of their orbital positions, away from the influence of the nucleus. This produces electron vacancies, which are filled by higher orbit electrons dropping inwards to fill the vacancy. This drop involves the production of an X-ray photon, the energy of which is proportional to the difference between the energy levels of the orbitals. This energy difference is dependent on the number of protons in the nucleus attracting the electrons. The X-rays produced are directed at the sample over a range of angles. X-rays are electromagnetic waves characterised by an electric field, the strength of which varies sinusoidally with time at any point in the beam. This oscillating electric field exerts a force on the electrons of an atom causing any electron it encounters to oscillate about its mean position. This accelerating and decelerating electron emits electromagnetic radiation and it is in this sense that the electron is said to scatter X-rays. The scattered beam is simply the beam radiated by the electron under the action of the incident beam and has the same frequency as the incident beam. Thus, the scattering of X-rays by matter occurs. Scattering of X-rays is proportional to the size of the atom, providing that the dimensions of that atom are less than the X-ray wavelength. If Bragg's law is obeyed, diffraction will occur at an angle θ , if a beam of X-rays falls on a series of atom bearing planes within the sample, each a distance d apart. Bragg's law states that $n\lambda = 2d\sin\theta$, where λ is the wavelength of the X-ray and n is an integer. During an experiment, both the detector and the sample are rotated (with the help of a goniometer) in order to reach the required angle. The intensity of the scattered X-rays obeying Bragg's law is measured as a function of the diffraction angle (degree 2θ or $^{\circ}2\theta$) and the orientation of the sample. By rearranging Bragg's equation, the d spacing of a mineral can be obtained by $d = n\lambda / 2\sin\theta$. For further

insight into the theory, the reader is invited to refer to the publication by Skoog et al³⁷.

Although quantitative analysis is possible using XRD, reproducibility is dependent upon many key factors including sample thickness, alignment of crystals, homogeneity and also the quality of the standards used³⁸. Hence, because of the small amounts of inorganic material available to be analysed, the studies reported in this thesis are strictly qualitative.

3.2.4.2 Applications related to this study:

XRD has been reported for use in the study of cross-linked collagen, showing its amorphous nature and suggesting that the process of aldehyde-cross-linking decreases the crystallinity of collagen³⁹. However, traditionally, XRD is the technique of choice for identification and characterisation of apatite-like minerals. Hence, the use of XRD is extensively reported in the literature for the determination and for the confirmation of the presence and the crystallinity of calcium phosphate crystals in calcified (in-vitro or in-vivo) tissues^{40,41}. Usually, XRD shows well-separated, relatively sharp peaks and discloses the presence of diffraction peaks, which are consistent with apatite. Such characterisation is usually hampered by the overwhelming presence of large amounts of organic components from the collagen matrix that tend to obscure spectral analyses due to the high background radiation⁴²⁻⁴⁴. Additionally, the minimum mass fraction of a calcium phosphate phase that can be detected by XRD is about 3%, rendering the analysis of poorly calcified samples difficult, especially for example the early stages of calcification. Furthermore, the low crystallinity and extremely small size of particles prevent a complete three-dimensional structural analysis by X-ray or even electron diffraction⁴⁵. Nevertheless, XRD is a useful tool, commonly employed for the analysis of solid powder mixtures. However, the broadening of the XRD do not generally allow precise determination of the unit cell dimensions in the case of bone or even synthetic apatite-like samples⁴⁶.

The analysis of hydroxyapatite (HAP $\text{Ca}_{10}(\text{PO}_4)_6(\text{OH})_2$) by XRD has received much attention⁴⁷: Reports have shown that the major reflections of the hexagonal hydroxyapatite phase correspond⁴⁸ to (200), (111), (002 2θ range $24.5\text{-}27^\circ$ ⁴⁹), (102), (210), (211), (112), (300), (202), (212) and (310 2θ range $37.5\text{-}42^\circ$ ⁴⁹). The region of

highest intensity (2θ range 30-35°) consists of four unresolved peaks with unmeasurable overlapping breadths⁴⁹. It was reported that if the (300) reflection, which is strong for apatite phases, is diffuse and poorly resolved, then it indicates low crystallinity and that the crystal may contain cations such as carbonate, sodium or potassium⁵⁰.

The major dicalcium phosphate dihydrate (DCPD $\text{CaHPO}_4 \cdot 2\text{H}_2\text{O}$) peaks correspond⁵¹ to (121), (020 $\theta=5.82^{52}$), (021 $\theta=10.46^{52}$), (110), (111), (112), (230) and (200).

Another important candidate as a possible precursor in cardiovascular mineralisation is octacalcium phosphate (OCP $\text{Ca}_8\text{H}_2(\text{PO}_4)_6 \cdot 5\text{H}_2\text{O}$)⁵³. However, although crystalline OCP has several diffraction peaks that are distinct from those of hydroxyapatite, poorly crystallised OCP and partially hydrolysed OCP (OCPH) have diffraction patterns that resemble that of hydroxyapatite⁵³ and it is usually difficult to distinguish between them.

3.2.5 Fourier transform infrared-attenuated total reflectance (FTIR-ATR) spectroscopy

3.2.5.1 Theory:

For a detailed account of the theory of FTIR-ATR spectroscopy, the reader is directed to several excellent publications⁵⁴⁻⁵⁶.

Reflectance spectroscopy is commonly used for obtaining infrared spectra of samples that are difficult to deal with by standard infrared techniques, for example solids, powders and films that require grinding to produce nujol mulls or KBr discs. Attenuated Total Reflectance (ATR) is particularly useful for the surface analysis of such samples and is reported as being a powerful technique in the analysis of biopolymers both for chemical identification and for molecular structure determinations⁵⁷. ATR is the only infrared technique that allows the study of proteins on surfaces in contact with aqueous medium and hence was chosen for use in this study. A simplified FTIR-ATR experimental set-up can be found below in figure 3.3.

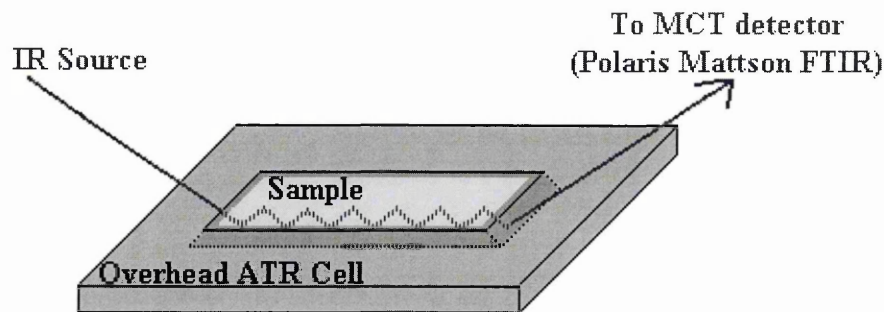


Figure 3.3: FTIR-ATR experimental set-up (simplified)

In FTIR-ATR, an infrared beam passes from a denser medium (ATR crystal with a high refractive index, such as zinc selenide, which is represented as a trapezoidal orange crystal in figure 3.3) to a less dense (sample) medium and reflection occurs. The fraction of the incident beam that is reflected increases as the angle of incidence becomes larger and beyond a certain critical angle internal reflectance is complete. It has been shown that during the reflectance process the beam acts as if it penetrates a small distance into the less dense medium before reflection occurs. The depth of penetration, which can vary from a fraction of a wavelength (micron scale) up to several wavelengths, depends upon the wavelength of the infrared beam, the index of refraction of the two materials (ATR crystal and sample) and the angle of the incident beam (usually 45°) with respect to the interface. The penetrating radiation is called the evanescent wave. If the less dense medium absorbs the evanescent radiation, attenuation of the beam occurs at the wavelengths of the absorption bands⁵⁸. Internal reflectance spectra are similar to ordinary absorption spectra as the same peaks occur but the relative intensities differ. The internal reflectance spectra absorbance, although dependent upon the angle of incidence, are independent of the sample thickness because the radiation penetrates only a few micrometers into the sample.

3.2.5.2 Applications related to this study:

3.2.5.2.1 Analysis of model compounds:

FTIR can provide information such as the composition, structure and crystallinity of the sample. FTIR is widely applied in clinical sciences⁵⁹ and these applications have been reviewed by Putzig et al⁶⁰. FTIR has been reported for the analysis of various

proteins⁶¹, some of relevance to these studies such as cytochrome C⁶², or collagenous tissue (human skin^{63,64}). Glutaraldehyde-treated proteins were also investigated by infrared spectroscopy such as cotton cellulose⁶⁵, chitosan⁶⁶ and gelatin⁶⁷. The respective data from these studies only revealed the presence of imine (Schiff base C=N) and ethylenic (C=C) bonds while the presence of imine bonds-stabilised by resonance with adjacent ethylenic bonds was thus suggested. A similar conclusion was drawn from studies of glutaraldehyde-treated amino acids (isopropylamine⁶⁸, 6-aminohexanoic acid and N-acetyl-L-lysine⁶⁹). Additionally, the analysis of glutaraldehyde was reported by Monsan et al⁶⁸ who postulated the presence of aldol condensation glutaraldehyde polymers containing aldehydes, conjugated aldehydes and ethylenic functions. Margel and Rembaum⁷⁰ hypothesised from their FTIR study of glutaraldehyde, the presence of similar polymers of glutaraldehyde but where the dehydration step of the aldol condensation reaction did not always occurred resulting in the presence of hydroxyl. This finding was later corroborated by Tashima et al^{71,72} who reported that glutaraldehyde included hydroxyl, carboxyl and α,β -unsaturated formyl groups but the exact structures could not be determined. All these studies are thus of particular relevance because one aim of this thesis is to model potential reactions and investigate the reactions and subsequent products involved in glutaraldehyde treatment of valve tissue by using various amino acids, peptides and proteins but also to determine the true nature of glutaraldehyde solutions.

3.2.5.2.2 Analysis of valve tissue:

FTIR-ATR is a sensitive technique and has been reported as being especially suitable for surface analysis⁵⁷. Tissue samples such as aortic valve tissue are a few tenths of microns thick and thus are not sufficiently transparent for transmission infrared analysis. This necessitates the use of an ATR accessory to obtain infrared spectra. The application of FTIR-ATR was thus reported for the study and characterisation of a new series of polyurethane replacement cardiac valves and their calcification⁷³; for the study of aortic wall tissue⁷⁴ and also for studying the effect of ethanol pre-incubation as an anti-calcification agent on glutaraldehyde-cross-linked porcine aortic valves⁷⁵. Additionally, cross-linked collagen membranes were also investigated with FTIR-ATR³⁹. This is of some relevance to studies of this thesis, since bioprosthetic heart valve tissue and its calcification is investigated.

3.2.5.2.3 Analysis of the calcification of valve tissue:

FTIR is most commonly employed for the analysis of solid mixtures along with XRD, except that XRD, (although a technique of choice for the identification of apatitic minerals), does not reveal spatial variations in the mineral structure of biological tissue specimens⁷⁶, while FTIR spectroscopy has been used to explore the spatial variations in mineral properties⁷⁷⁻⁷⁹. Note that “apatitic minerals “ refer to materials that have characteristics of apatites such as hydrolysed-octacalcium phosphate (OCPH) and hydroxyapatite (HAP). Additionally, the infrared study of inorganic powder samples uses only a few milligrams of sample, while the X-ray method requires at least twenty five to fifty times as much. In addition, the time for the infrared analysis is much shorter than that required for X-ray diffraction analysis⁸⁰.

The infrared spectra of many pure inorganic compounds can be found in the literature⁸¹. FTIR can provide information on the structure, the near-neighbour environment of carbonate and phosphate groups of the mineral phase, and an estimate of the degree of crystallinity of the crystal, as well as the organic matrix contribution expressed as amide bands^{82,83}. The complex phenomenon of crystal maturation (or aging) was studied in both in-vivo and in-vitro systems^{46,78,84-87} and it is known to be manifested through changes in the short range order of the crystals and the concentration and location of highly labile, reactive CO_3^{2-} and HPO_4^- groups. Such distinctive markers of bone mineral maturation are an increase in CO_3^{2-} and a decrease of labile CO_3^{2-} and HPO_4^- ions^{46,86,87}. Indeed, bone-type mineral was reported considered as a calcium-deficient apatite containing HPO_4^{2-} and CO_3^{2-} ions⁸⁸. The following paragraphs present various CaP-rich inorganic phases that are likely to be encountered in the analysis of calcific deposits in bioprosthetic valves.

a) Amorphous calcium phosphate (ACP):

Determining the presence of amorphous calcium phosphate (ACP) is not an easy task. However FTIR was reported to be useful in determining the percentage of crystallinity in a mixture of amorphous and apatitic calcium phosphates. The infrared spectrum of amorphous calcium phosphate presents limited or no splitting of the 600 cm^{-1} infrared band ($\nu_4(\text{PO}_4^{3-})$ region)⁸⁹ that one would expect for crystalline hydroxyapatite⁹⁰. Additionally, infrared spectra of the solids formed in the conversion

of amorphous calcium phosphate to crystalline hydroxyapatite were reported and showed a gradual splitting of the 600 cm^{-1} anti-symmetric bending band ($\nu_4(\text{PO}_4^{3-})$ region) from a broad singlet for amorphous CaP to a well-defined doublet for the fully crystalline solid⁸⁰.

b) Calcium-deficient apatite ($\text{Ca}_9(\text{HPO}_4)(\text{PO}_4)_5\text{OH}$)

Calcium-deficient apatite typical bands are⁹¹: hydroxyl band at 3569 cm^{-1} ; carbonate peaks at $1647, 1454, 1412\text{ cm}^{-1}$ ($\nu_3(\text{CO}_3^{2-})$ bands $1650\text{-}1400\text{ cm}^{-1}$) and phosphate peaks at $1092\text{ cm}^{-1}, 1030\text{ cm}^{-1}$ (intense $\nu_3(\text{PO}_4^{3-})$ bands-almost obscuring the ν_1 carbonate band⁹²), 960 cm^{-1} ($\nu_1(\text{PO}_4^{3-})$ band) and $629, 602, 563\text{ cm}^{-1}$ (intense $\nu_4(\text{PO}_4^{3-})$ bands $630\text{-}560\text{ cm}^{-1}$) and weak $\nu_2(\text{PO}_4^{3-})$ band at 473 cm^{-1} .

The bands of calcium-deficient apatite (or non stoichiometric apatite) are quite similar in fact to the ones of stoichiometric apatite, but are generally characterised by additional bands similar to those found in most biological apatites⁸⁶ ($1020, 1100\text{ cm}^{-1}$) and sometimes a typical band of HPO_4^- (1143 cm^{-1}) can be found along in these apatite-like structures⁹³.

c) α - and β -tricalcium phosphate⁹¹ (TCP $\text{Ca}_3(\text{H}_2\text{P}_2\text{O}_7)_2$):

A strong band at 970 cm^{-1} is usually quite characteristic of the presence or not of TCP⁸⁶. Furthermore, it is worth noting that this band is not observed in most biological samples and in poorly crystalline synthetic apatites.

d) Octacalcium phosphate (OCP $\text{Ca}_8(\text{H}_2\text{P}_2\text{O}_7)_2$):

The OCP spectra, (A and B forms), are somehow similar to the ones of apatite structure and a complete assignment of the infrared bands of both A and B form of OCP can be found in the literature⁹⁴. Note that the A and B OCP forms correspond respectively to carbonate ions occupying two different sites (respectively Cl^- or OH^- for the A site and PO_4^{2-} for the B site) in apatitic structures. Nevertheless, there are specific phosphate bands at 1138 cm^{-1} and another for the OCP structure at $913\text{-}917\text{ cm}^{-1}$ ⁹⁴, although this band was attributed later to components of the organic matrix⁸⁴. Additionally, it has been shown that OCP presents two non-equivalent HPO_4^{2-} ions⁹⁵, one attributed in the “apatitic layer” and the other in the “hydrated layer”⁴⁶.

3.2.5.2.4 Major vibrational spectroscopic regions of inorganic CaP-rich phases:

Because the calcific deposits, found in calcified human explanted valves, are composed of calcium phosphates, closely related to physiologic bone mineral (see chapter 1 in sections 1.4.2 and 1.7), and because no review yet exists, the following paragraphs present the major vibrational spectroscopic regions encountered in the analysis of bone, enamel and calcific deposits by infrared spectroscopy.

Inorganic orthophosphate ions (HPO_4^{2-}) and (PO_4^{3-}):

Two inorganic orthophosphate ions were reported to occur in biological apatites present in mineralised tissue: PO_4^{3-} and HPO_4^{2-} .

Hydrogenophosphate ions (HPO_4^{2-}):

The HPO_4^{2-} ion can be considered to be distorted PO_4^{3-} tetrahedron, which exhibits bands at almost the same frequencies as for the PO_4^{3-} ions (see section below dealing with phosphate (PO_4^{3-}) vibrational modes). However, the stretching vibration of the P-OH band (ν_3 mode) appears generally as a pronounced band⁹⁶ at a lower frequency (around $860\text{-}872\text{ cm}^{-1}$), where it may be overlapped by the strong $\nu_2(\text{CO}_3^{2-})$ band in biological apatites and cannot generally be observed. The P-O-H stretching can also give a broad band, between 2400 cm^{-1} and 3200 cm^{-1} that was not reported in the biological apatites. The ν_4 mode was reported to give two main bands at 600 and 560 cm^{-1} and a shoulder at 575 cm^{-1} , generally superimposed on a broad absorption band from the components of the organic matrix⁴⁶. The presence of HPO_4^{2-} can also be identified by two low-wave number bands⁹⁷ at $520\text{-}530\text{ cm}^{-1}$ and at $540\text{-}550\text{ cm}^{-1}$, a very broad band⁹⁷ that culminates at 730 cm^{-1} and also by other bands at $1133\text{-}1150\text{ cm}^{-1}$ ⁹⁷, and at 1217 cm^{-1} ⁹⁷.

Phosphate ions (PO_4^{3-}):

Theoretically, there are four vibrational modes present for phosphate PO_4^{3-} ions (ν_1 - ν_4). All these modes are both infrared and Raman active.

$\nu_1(\text{PO}_4^{3-})$ region: Only a band at 960 cm^{-1} was reported in the literature for this region.

$\nu_2(\text{PO}_4^{3-})$ region: Only a band at 473 cm^{-1} was reported in the literature for this region¹⁷.

$\nu_3(\text{PO}_4^{3-})$ region: Although weak $\nu_3(\text{CO}_3^{2-})$ bands can slightly obscure this region⁸⁶, the $\nu_3(\text{PO}_4^{3-})$ region consists of an intense broad absorption band generally split into two main components. The first is seen at 1170-1085 cm^{-1} with several bands generally around 1100, 1110, 1125, and 1145 cm^{-1} . The band (usually a broad shoulder) at about 1145 cm^{-1} exists in HPO_4^- -containing apatites and in several non-apatitic phosphates such as OCP (1138 cm^{-1}), or TCP (1144 cm^{-1})⁸⁶. The bands at 1110 cm^{-1} and 1125 cm^{-1} do not tend to appear clearly in the spectra of well-crystallised synthetic apatites and were considered to be representative of phosphate environments in poorly crystalline apatitic calcium phosphates⁸⁶. For instance, a clear band can be observed at 1125 cm^{-1} in the spectrum of the mineral of young enamel⁸⁶, while a shoulder would indicate lability of crystals ions.

The second component, that is generally the most intense, is seen at 1085-970 cm^{-1} , with two main maxima at 1020 cm^{-1} and 1030 cm^{-1} ⁸⁶. These two bands are present in most phosphate salts with an apatitic or non-apatitic structure. The 1030 cm^{-1} band was reported to occur in stoichiometric apatite whereas the 1020 cm^{-1} band was dominant in non-stoichiometric apatites containing HPO_4^- or CO_3^{2-} ions, and was interpreted as an indication of the persistence of vacancies. A splitting of the 1030 cm^{-1} band was reported to reveal a less stable environment of the phosphate ions.

$\nu_4(\text{PO}_4^{3-})$ region: This region (500-650 cm^{-1}) appears more complex than the ν_3 region⁸⁶. It is composed of five major apatitic bands⁴⁶ at 534, 560, 578-585 cm^{-1} , and two bands at 600-625 cm^{-1} , including a faint one and one generally encountered at 617 cm^{-1} . The absence of splitting on the 560 cm^{-1} band was reported to be characteristic of amorphous calcium phosphates⁸⁰, and in early calcific deposits this band presents an abnormal low intensity⁴⁶. In addition to HPO_4^{2-} , the mineral can also exhibit a non-apatitic PO_4^{3-} environment. The non-apatitic phosphate environment detected in poorly crystalline apatite was reported to be characterised by two bands near 560 cm^{-1} and 610 cm^{-1} ⁴⁶. The concentration of non-apatitic phosphate ions was also reported to increase during the early stages of mineralisation of calcified cartilage, but then to decrease as the mineral content steadily rose until full mineralisation was achieved⁹⁸.

Carbonate ions (CO_3^{2-}):

Carbonate ions are the third most abundant constituents of bone and tooth mineral after calcium and phosphate and were reported to play an important role in several of the biological processes concerned with calcification^{99,100}. It has been reported¹⁰¹ that as much as 22% carbonate (about three CO_3^{2-} ions per unit cell) can be incorporated into the structure of carbonate-hydroxyapatite. Infrared spectroscopy is more sensitive than X-ray diffraction for the detection of calcium carbonate salts¹⁰². Carbonate ions possess four vibrational modes (ν_1 - ν_4), three of which are observed in the infrared spectrum⁹²: the $\nu_2(\text{CO}_3^{2-})$ and $\nu_3(\text{CO}_3^{2-})$ vibrational modes are observed in the infrared spectra while the $\nu_4(\text{CO}_3^{2-})$ bands have very low intensity and are seldom seen in the infrared spectrum⁹⁷. Only ν_2 and ν_3 have really been extensively described in the literature (see below for more details). The $\nu_1(\text{CO}_3^{2-})$ region is not observable as this region is obscured by phosphate absorption bands⁹⁷. Additionally, although the ν_4 region occurs in a region un-obscured by strong phosphate absorption bands, only very weak IR carbonate bands arise and are barely noticeable in apatites with average carbonate content⁹⁷. The ν_4 region has thus been mostly roughly described in the literature^{102,103}, however some authors gave a proper assignment of the bands⁹⁷.

Carbonate ions can occupy two different sites in apatitic structures (A and B sites). The carbonate in apatites can be located in the monovalent anionic A sites which are located in channels along the c-axis of the hexagonal structure (and which are generally occupied by Cl^- ¹⁰⁴, or OH^- ¹⁰⁵), and mainly on trivalent anionic B sites (on which the phosphate ions, PO_4^{3-} , are located)¹⁰⁶. Carbonate located in monovalent A sites have been reported to represent only a minority of the carbonate present in apatitic structures, although no quantitative data is available¹⁰⁷. However, the charge balance due to these substitutions involves complex vacancy formations or cationic replacements^{108,109}. Additionally the occurrence of different environments of carbonate ions in apatites was reported to result also from the orientation of the ion in the site¹⁰⁴ and with the heterogeneities of distribution in the solid^{106,110}. Carbonate ions associated with apatites have been observed in bones¹¹¹, and also in fully mineralised dental enamel¹⁰⁵. Well-crystallised apatite samples are reported to show two sets of bands corresponding to the A (1545, 1450 and 880-890 cm^{-1}) and B

(1465, 1412 and 873 cm^{-1}) types of carbonate ions^{101,112-114}. These reported results are slightly different than the ones for bones, although these two sets of bands have been reported not to fully account for the overall spectra¹¹⁵, as discussed below.

$\nu_1(\text{CO}_3^{2-})$ region: No assignment was reported in the literature for this region. It is usually almost obscured by the intense $\nu_3(\text{PO}_4^{3-})$ bands⁹².

$\nu_2(\text{CO}_3^{2-})$ region: The out-of-plane bend $\nu_2(\text{CO}_3^{2-})$ FTIR domain (800-900 cm^{-1}) is not obscured by the organic matrix or by the phosphate absorption bands¹¹⁰, and it shows three carbonate bands observed in apatite and bone mineral at 879, 871, 868-866 cm^{-1} ^{110, 87}, which may be assigned to three different locations of the ion in the mineral. The second distinct peak at 879 cm^{-1} has been assigned to type A carbonate¹¹⁰; the most intense band around 871 cm^{-1} (866-873 cm^{-1})¹¹⁶ has been assigned to type B carbonate^{46,110}; the shoulder at 866 cm^{-1} (C band corresponding to carbonates in unstable locations) was assigned to loosely structured carbonate in either an amorphous calcium phosphate-like or surface environment¹¹¹ and was later hypothesised to be due to labile carbonates species in non-apatitic environments¹¹⁰. The occupancy of the ν_2 A sites is thus considered to occur competitively between the OH^- and CO_3^{2-} groups at the interface of growing crystal, while the occupancy of the B sites depends on competition between PO_4^{2-} , HPO_4^- and CO_3^{2-} ⁸⁷. The intensity ratio of the 879 cm^{-1} and 871 cm^{-1} bands was reported to remain constant in bone of any age, and the intensity ratio of the 866 cm^{-1} band to the 871 cm^{-1} band, was found to vary directly and decrease with the age of the mineral⁸⁷.

$\nu_3(\text{CO}_3^{2-})$ region: The $\nu_3(\text{CO}_3^{2-})$ infrared region shows peaks in the region of 1650-1300 cm^{-1} ¹¹⁶. However, this region is sometimes obscured by several absorption bands of proteins (CH, amide II, COO^-) or glycosaminoglycans (NH)¹¹⁷. The ν_3 vibrational mode is split into three main peaks centred around 1638, 1453 and 1412 cm^{-1} and the distribution of the carbonate ν_3 sites depends on the maturation and formation of apatite crystals. The occupancy of the ν_3 sites depends on competition between the phosphate and carbonate ions^{115,116}. The position of peaks around 1410-1420 cm^{-1} and 1470 cm^{-1} is usually consistent with that of carbonate ions in amorphous calcium phosphate^{110,111,118}; while peaks around 1415, 1447 and ~1492 cm^{-1} are characteristic of carbonate ions occupying two anionic sites of the apatitic

structure (trivalent anionic sites or type B carbonate; monovalent anionic sites or type A)^{108,119}.

$\nu_4(\text{CO}_3^{2-})$ region: Carbonate apatites show at least five weak bands in the ν_4 domain⁹⁷: 757, 740, 718, 692 and 670 cm^{-1} . The spectrum of pure type A carbonate shows two weak bands⁹⁷ at 766 and 675 cm^{-1} . It was reported that the bands in this region are probably due to the presence of ions other than carbonate (such as OH^- or $\text{P}_2\text{O}_7^{4-}$ that have infrared absorptions in the same region), combinations or overtone bands of phosphate groups or to calcium carbonate impurities. Thus, the band at 740 cm^{-1} can be assigned to both OH^- ions and CO_3^{2-} ions.

Hydroxide ions (OH^-):

Crystalline apatites generally show OH^- bands in their infrared spectra (OH stretch around 3570 cm^{-1} , OH libration at 630 cm^{-1} and OH translation at 343 cm^{-1})^{96,111}, although some infrared data indicated that both native rat bone mineral and also synthetic apatites formed at physiological pH were shown to have a high degree of structural imperfection. These were extensively deficient in hydroxide ion content. It was thus hypothesised that hydroxides ions were sensitive to the presence of impurities that distort the trigonal symmetry of the OH^- position such as a small amount of carbonate that would have a depressing effect on the intensity of the OH^- bands¹⁷ and it was reported that if some OH ions were present, they would exist in varied local atomic environment, resulting in a broadening and marked decrease in intensity of their infrared absorption bands¹¹¹. The detection of hydroxide ions in infrared spectra was also reported to depend on the sample preparation methodology employed. For example, it has been reported that when low-temperature and non-aqueous deproteinisation is used to decrease the organic matrix background spectrum by isolating the CaP crystals of both young and mature bone mineral, as well as the early deposits of enamel mineral^{120,121}, no OH bands (stretching mode at 3570 cm^{-1} or the librational mode band at 630 cm^{-1}) were observed in the corresponding FTIR spectra¹²². These reported observations do not however preclude the presence of OH^- ions as hydrogen bonding with adsorbed water molecules could reduce the intensity (extreme broadening) of infrared OH bands¹²³. Furthermore, some convincing evidence that OH groups can be present although they do not give rise to OH bands in the infrared spectrum was reported¹²⁴. It was assumed that a similar absence of

OH peaks in the spectrum of bone does not preclude the presence of hydroxide ions¹⁷. The failure to detect OH bands by FTIR has also been reported to represent an actual and extensive OH⁻ ion deficiency in the mineral^{111,125}. It is interesting to note that OH⁻ or halide deficiencies have been reported not to be that uncommon in apatites¹²⁶. This was also considered to indicate an inorganic apatite-like mineral phase with cationic and/or anionic vacancies¹¹¹. Indeed, it was reported that the presence of type A and B carbonates in bone apatite may contribute to the low concentration or even the absence of hydroxyl ions in bone mineral^{111,127}. In contrast, the spectra from hydroxyapatite that has been heated (it is usually the case for coatings of hydroxyapatite with implant material applications) show very acute OH bands⁵¹.

3.2.6 Raman spectroscopy

3.2.6.1 Theory:

Raman spectroscopy has become an important and widely used method for studying macromolecules¹²⁸ since the first experimental observation of Raman scattering in 1928 by C.V. Raman and his associates. They discovered that the wavelength of a small fraction of the radiation scattered by certain molecules differs from that of the incident beam and that the shifts in wavelength depend upon the chemical structure of the molecules responsible for the scattering. Raman spectroscopy does not involve absorption or emission from the energy levels directly, but rather implicates intermediate virtual energy states. Unlike in infrared spectroscopy, a vibrational mode is Raman active when there is a change in the polarisability during the vibration. A dispersive Raman spectrometer consists of a source of monochromatic radiation (represented in red in figure 3.4), a dispersing system and a detection device. The scattered radiation (including both Rayleigh and Raman scattering) is collected at 90° with respect to the incident radiation (see figure 3.4 below).

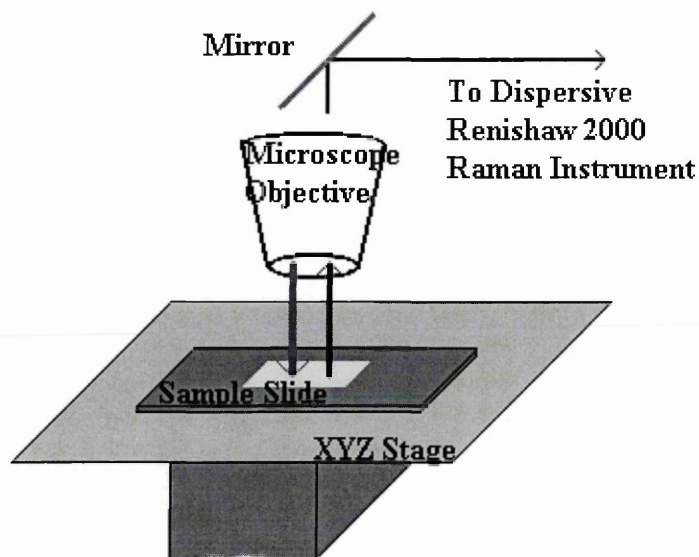


Figure 3.4: Dispersive Raman (Renishaw, Wotton-under-Edge, UK) experimental set-up (simplified)

At the very most, the intensities of the Raman scattered light is low (0.001% of the laser source intensity) and as a consequence the Raman line detection and measurement can be difficult. However, Raman spectroscopy is applicable to a wide variety of samples yielding high levels of structural information. The optical microscope of the Raman system used for these studies provides a spatial resolution of $\sim 1\mu\text{m}^2$ ¹²⁹ and this system also provides a good spectral resolution (ca. 2 cm^{-1}) across a wide range, with full wavenumber scans ($100\text{-}7000\text{cm}^{-1}$). The collection of Raman spectra, (using a dispersive instrument), from most polymers, including some biological ones, is usually precluded because of the presence of traces of strongly fluorescent impurities. This represents the major drawback of Raman spectroscopy. However, it can usually be overcome by the use of a “Fourier-transform” in Fourier-transform- (FT-) Raman instruments¹³⁰. FT-Raman spectrometers are now starting to be superseded by monochromators (dispersive instruments) equipped with CCD detectors (charge coupled device array detector, which has the characteristic of low noise and high detection efficiency) and low power lasers, which can thus also allow measurements of certain polymers, including biological ones. For further insight into the theory, the reader is invited to refer to publications by Skoog et al and Griffiths and Urban^{56,131}.

3.2.6.2 Applications related to this study:

3.2.6.2.1 Analysis of model compounds:

The application of Raman spectroscopy to the study of biological systems (amino acids, peptides and proteins) has been extensively reported in the literature over the last few decades^{132,133}. More particularly, the analysis of proteins of relevance to these studies, such as poly-L-lysine¹³⁴⁻¹³⁷, lysosyme¹³⁸⁻¹⁴² and reconstituted collagen¹⁴¹, can be found. In addition, Raman spectroscopy of an amino acid of interest (lysine) has been reported¹⁴³. The use of this technique to study tissue has been an area of particular interest, frequently using Raman microscopy¹⁴⁴ and a near-infrared laser to avoid sample damage^{145,146}. Human skin (mainly constituted of collagen) has also been the subject of a study using FT-Raman, which resulted in a method to assess the changes induced by chemicals and drugs⁶⁴. All this is of direct relevance to our study, as it has already been emphasised in section 3.2.5.2.1 of this chapter.

3.2.6.2.2 Analysis of the calcification of valve tissue:

The use of FT-Raman has been reported in the literature for the study of vascular tissue components^{145,147,148}, in particular elastin, collagen, lipids and calcium deposits. One of the main advantages of the FT-Raman technique over conventional dispersive Raman spectroscopy is the use of 1064 nm near-infrared excitation, which precludes electronic absorption of the excitation radiation, leading to the elimination of fluorescence, which is usually a major problem in Raman spectroscopy when analysing biomaterials. However, over the past decade, many authors pointed out some limitations of FT-Raman spectroscopy and stated that fluorescence may still cause problems¹⁴⁹. This is especially the case when analysing some (but not all¹⁵⁰) calcium minerals such as dicalcium phosphate dihydrate and hydroxyapatite¹⁵⁰. Nevertheless, human coronary artery composition and atherosclerotic calcified plaques were successfully identified using near-infrared FT-Raman spectroscopy^{151,152}, where a small satellite band in the calcified plaque spectrum at 1070 cm⁻¹ was attributed to carbonated apatite. Raman spectroscopy was also used for the analysis of kidney stones, where hydroxyapatite is the most common component⁴⁷.

The (dispersive) Raman spectra of the cortex of the ox tibia have been obtained by reflection from the surface of a whole piece of ox tibia, which was defatted with acetone and chloroform and dried¹⁴¹. The resulting Raman lines of the calcified tissue originated from the phosphate modes (955 cm^{-1}), and from the inorganic carbonate bands (1451 cm^{-1} and 1417 cm^{-1}). This led to the suggestion therefore that the strong Raman scattering associated with calcium phosphate would allow the possible detection of calcium phosphate in normal and pathological calcified tissue. Many Raman spectra of various inorganic salts were also obtained by conventional Raman spectroscopy and reported¹⁵³.

The dispersive Raman spectra of hydroxyapatite (HAP)^{154,155}, β -tricalcium phosphate (β -TCP)¹⁵⁶ and other calcium phosphates have also been reported^{79,157,158} and appear similar, although minor differences exist. For instance, due to their structural differences, Raman scattering was reported to successfully differentiate between HAP and β -TCP, not only through the detection of vibrational modes associated with the OH⁻ group of hydroxyapatite but also by comparing the bands arising from internal tetrahedral¹⁵⁹ PO₄²⁻ modes¹⁶⁰. In HAP the ν_2 and ν_4 bands are separated by $\sim 55\text{ cm}^{-1}$, while with β -TCP the gap is of $\sim 120\text{ cm}^{-1}$. This represents a characteristic spectral feature that can easily be used to distinguish between β -TCP and HAP. The spectra of octacalcium phosphate (OCP) are quite similar to the ones of apatite structure and a complete assignment of the Raman bands, obtained with a dispersive Raman instrument, can be found in the literature⁹⁴.

3.2.6.2.3 Major vibrational spectroscopic domains of inorganic CaP-rich phases:

Because the calcific deposits, found in calcified human explanted valves, are composed of calcium phosphates closely related to physiologic bone mineral (see chapter 1 in sections 1.4.2 and 1.7) and also because no review yet exists, the following paragraphs present the major vibrational spectroscopic domains encountered in the analysis of calcific deposits, bone and enamel by Raman spectroscopy.

Phosphate (PO₄³⁻) ions:

The most interesting portions of the spectra of calcium phosphate minerals are the phosphate bands, with the four modes being active in Raman spectroscopy.

$\nu_1(\text{PO}_4^{3-})$ region: A strong $\nu_1(\text{PO}_4^{3-})$ band, corresponding to the symmetric stretching vibration of the P-O bonds (A_1 symmetry), occurs as a single Raman band at 960 cm^{-1} and is exhibited by hydroxyapatite and some other calcium phosphate minerals, although it occurs as two peaks and a shoulder with β -TCP¹⁶⁰.

$\nu_2(\text{PO}_4^{3-})$ region: $\nu_2(\text{PO}_4^{3-})$ band corresponding to the doubly degenerate O-P-O bending mode (E symmetry) is observed at 435 cm^{-1} ($400\text{-}490\text{ cm}^{-1}$ for HAP) and ($370\text{-}505\text{ cm}^{-1}$ for β -TCP).

$\nu_3(\text{PO}_4^{3-})$ region: A $\nu_3(\text{PO}_4^{3-})$ band arises from the triply degenerate T_2 mode involving anti-symmetric P-O stretching and also P motion at 1073 cm^{-1} ($1020\text{-}1095\text{ cm}^{-1}$).

$\nu_4(\text{PO}_4^{3-})$ region: A $\nu_4(\text{PO}_4^{3-})$ band due to the triply degenerate T_2 modes of mainly O-P-O bending character is seen at 590 cm^{-1} ($570\text{-}625\text{ cm}^{-1}$ for HAP) and ($530\text{-}645\text{ cm}^{-1}$ for β -TCP¹⁶⁰).

These internal PO_4^{3-} bands are centred at frequencies, between 20 to 25 cm^{-1} , higher than those of the corresponding free-tetrahedron normal modes. The corresponding values for the normal Raman mode frequencies of the phosphate tetrahedron obtained in aqueous solution are the following: $\nu_1\ 938\text{ cm}^{-1}$, $\nu_2\ 420\text{ cm}^{-1}$, $\nu_3\ 1017\text{ cm}^{-1}$, $\nu_4\ 567\text{ cm}^{-1}$ ¹⁶¹. In addition to the internal PO_4^{3-} bands, several peaks are detected between 50 and 320 cm^{-1} , which are due to translational modes of the Ca^{2+} and PO_4^{3-} sub-lattices and rotational modes of the PO_4^{3-} group^{154,162}. The bond-stretching mode associated with the OH^- group was also reported in highly crystalline samples (difficult to detect in samples with poor crystallinity¹⁶⁰) as a sharp peak around 3576 cm^{-1} , whereas the translational modes associated with the OH^- sub-lattice yielded a Raman peak at 335 cm^{-1} ^{154,155}. The detection of this latter peak above the noise level is however difficult in samples with poor crystallinity¹⁶⁰. The resolution of the $\nu_4(\text{PO}_4^{3-})$ band was reported as being used to assess the degree of crystallinity of calcific crystals^{98,163} but the relationship was complex and did not always correlate with indices of crystallinity given by the line-broadening from the XRD data⁸⁰ of the same crystals. The $\nu_4(\text{PO}_4^{3-})$ domain has been previously shown to be suitable for deconvolution procedures⁴⁶, with three main bands around 560 , 575 and 600 cm^{-1} assigned to phosphate ions in an apatitic configuration and environment⁸⁴, a strong shoulder at 610 cm^{-1} that was assigned to a labile non-apatitic environment of

phosphate ions, which tend to disappear during maturation of the mineral phase in-vivo⁴⁶, and another shoulder of weak intensity at 620 cm⁻¹ attributed to phosphate ions in an extremely labile environment⁹⁸.

Carbonate (CO₃²⁻) ions:

Carbonate theoretically possesses four vibrational modes (ν_1 - ν_4), only two of which (ν_1 (CO₃²⁻) and ν_4 (CO₃²⁻)) have strong vibrational bands in the Raman spectra⁹².

Specific features of CaP-rich structures analysed by Raman spectroscopy:

Other specific features can also be found in the Raman spectra of CaP-containing crystals. For example, a band at 545 cm⁻¹ is found to be present in all HPO₄-containing apatites as well as in octacalcium phosphate (OCP). Additionally, a band at 530 cm⁻¹ can be found in the early stages of mineralisation of both bone and calcified cartilage^{46,98} and appears to be related to the 620 cm⁻¹ band. It has also been found in dicalcium phosphate dihydrate (DCPD) and OCP but not in HPO₄⁻-containing apatites¹⁶⁴.

3.2.7 The complementarity of FTIR and Raman spectroscopy

Raman and infrared are said to be complementary techniques and the two are usually necessary to completely measure the vibrational modes of molecules. The two forms of spectroscopy arise from different physical processes governed by specific selection rules. The information content for the two is a function of the molecular symmetry and, in a broad sense, of polarity.

3.2.8 Nuclear magnetic resonance (NMR) spectroscopy

3.2.8.1 Theory:

Since the observation of NMR signals in 1945, the technique has evolved to become an analytical tool that is used regularly for structural analysis. Although the applications have changed, the basic principles remain the same. The presence of a nuclear spin (i) in some nuclei leads to a characteristic magnetic moment. When an external magnetic field of sufficient strength is applied to atomic nuclei the interaction of the magnetic field leads to the nuclei orientating themselves in $2i + 1$ ways. Atomic nuclei can have a spin number of 1/2, 1, 3/2, etc. They both have a spin value of 1/2 and consequently can orientate in one of two ways, one of higher

energy state than the other. The difference in the energy is given by $\Delta E = h \gamma B_0 / 2\pi$, where h is the Planck constant, γ is the magnetogyric ratio and B_0 is the applied magnetic field. Boltzmann distribution governs the distribution of nuclei in the two energy states. A radio frequency is applied to the nuclei and when the radio frequency matches that at which the nuclei magnetic fields are precessing, nuclei from the lower energy state are excited to the higher state. This promotion in energy level leads to some absorption of the applied radio frequency, which can be measured. By varying the radio frequency of the magnetic field, a receiving coil can measure absorption against frequency.

The NMR instrumentation consists of a spinning tube containing the sample, placed between the receiver coils to allow measurement of absorption. Field sweep and Shim coils surround the transmitter coils, all of which are ultimately surrounded by a super-conducting magnet (cooled by liquid nitrogen). In this study, FT-NMR was used, which involves the application of a single pulse of the radio frequency that encompasses the range being studied. The pulse disrupts the precession of the nuclei and oscillation in the orientation of the magnetic field occurs. This is free induction decay (FID), which is recorded during the acquisition period to build up Fourier transform, which is in the time domain. The data are then converted into the frequency domain. Commonly in NMR spectroscopy, when the signal to noise ratio is not good, the FID signal is multiplied by an exponentially decaying function in order to remove the noise at longer acquisition times. However, this post-acquisition treatment of the data also tends to increase the rate at which the signal decays, thus increasing the line width of the signal. Hence this type of data treatment is referred to as line broadening. A profile of the coupling within the sample can also be achieved. By pulsing the sample with a radio frequency in a single experiment, the data are then displayed in a contour plot called a COSY spectrum. For further insight into the theory of NMR, the reader is invited to refer to publications by Nordon et al¹⁶⁵, Fifield and Kealey¹⁶⁶ and Abraham et al¹⁶⁷.

3.2.8.2 Applications related to this study:

NMR spectroscopy is a widely used analytical technique for structural elucidation and identification of chemical species in the analysis of many different materials including organic chemicals, inorganic complexes and large biological molecules¹⁶⁵.

A few reports found in the literature are of particular relevance to the work undergone in this thesis and the major findings are depicted thereafter.

An early ^1H NMR study of commercial aqueous solution of glutaraldehyde and of freeze-dried glutaraldehyde re-dissolved in deuterated water, demonstrated that glutaraldehyde is largely polymeric and contains significant amounts of α,β -unsaturated aldehydes resulting from the loss of water from aldol condensation adducts¹⁶⁸. Another ^1H NMR study of commercial aqueous solution of glutaraldehyde by Hardy et al¹⁶⁹ showed that glutaraldehyde consists of its monomer and of its hydrates and acetal-like structures, but not unsaturated polymer as suggested in the previous study. The effect of temperature on various commercial glutaraldehyde solutions was also assessed by ^1H NMR¹⁷⁰ and the glutaraldehyde was reported to consist mostly of monomeric glutaraldehyde, hydrates and oligomers of hydrates of glutaraldehyde, but of only a small amount of polymeric forms as suggested by Richards and Knowles¹⁶⁸. Whipple and Ruta¹⁷¹ reported both ^1H and ^{13}C NMR of a purified 25% v/v glutaraldehyde solution, which was shown to consist primarily of the cyclic hemiacetal, in equilibrium with monomeric glutaraldehyde and linear hemihydrate and the dihydrate, while higher order oligomers were reported to contribute very little to the equilibrium mixture. Monsan et al⁶⁸ analysed glutaraldehyde solution in deuterated chloroform or carbon tetrachloride and concluded that glutaraldehyde consists essentially of unstable hydrates of glutaraldehyde, but apparently no significant amounts of α,β -unsaturated aldehydes. The most recent ^1H NMR study of glutaraldehyde was reported by Holmquist and Lewin¹⁷², who failed to characterise five isolated fractions obtained after chromatography of glutaraldehyde at pH 8. Therefore it appears that the actual content of aqueous glutaraldehyde solutions has not yet been elucidated, as concluded from the review chapter on glutaraldehyde (see chapter 2).

The study of the reaction products of glutaraldehyde with proteins was also investigated by both ^1H and ^{13}C NMR, but it also led to many contradictory results and it too still needs to be further elucidated. Monsan et al⁶⁸ analysed the products of the reaction of crotonaldehyde with various amino acids by ^1H NMR and postulated the formation of aldol condensation products stabilised by resonance with the ethylenic bonds, but which did not undergo Michael-type addition reactions. Hardy et al^{69,173} investigated the reactions of glutaraldehyde with the model compounds

(that are of relevance to these studies) 6-aminohexanoic acid and N-acetyl-L-lysine in unbuffered aqueous solution, but also with protein such as ovalbumin by ^1H NMR, from which they suggested the presence of reaction products of quaternary pyridinium type. They later isolated and characterised by ^1H and ^{13}C NMR one of these reaction products of quaternary pyridinium type, baptised anabilysine^{174,175}. The latest reported data from ^{13}C NMR, recently evidenced the formation of an ethylenic double bond in the chitosan-glutaraldehyde interaction⁶⁶.

3.2.9 Electrospray ionisation mass spectrometry (ESI-MS)

3.2.9.1 Theory:

In the electrospray ionisation process, a solution of the analyte (sample) is slowly pumped through a short piece of capillary tubing. This narrow-bore metal capillary is held at approximately 3 kV relative to a counter electrode. The strong electric field at the end of the capillary pulls the solution into a Taylor cone and at the tip of the cone the solution is nebulised into small charged droplets. As the charged droplets travel towards the counter electrode, they pass through a drying gas that aids evaporation of the solvent and decreases the size of these charged droplets until they become unstable and explode (Coulomb explosion) to form a number of smaller droplets with greater charge density. Finally, the field due to the excess charge is large enough to cause desorption of an ionised sample molecule to ultimately yield molecular ions under atmospheric pressure. The ions are passed through a skimmer arrangement and sucked into the vacuum chamber through a small aperture or another piece of capillary tubing (which is usually heated to ensure that the ions are completely desolvated) for mass analysis. The mass spectrometer determines the molecular weight of compounds by separating molecular ions according to their mass-to-charge ratio (m/z). This is achieved by inducing either the loss or gain of a charge to generate the ions, which are separated according to their m/z and finally detected. Electrospray is a very mild ionisation technique, resulting in only limited fragmentation of large and thermally fragile biomolecules. A main feature of electrospray ionisation is that the molecular ions recorded are multiply charged (e.g. $(M+n\text{H})^{n+}$ in the positive ion mode). On average, one charge is added per 1000 Da in mass. Therefore, an ion of mass 10000 Da, which carried 10 charges would actually be recorded at m/z 1000. Consequently the m/z range covered by the mass analyser can be smaller than with other ionisation methods¹⁷⁶. This means that the m/z values

are small enough to make them detectable with a quadrupole instrument with a mass range of 1500 or less. For further insight into the theory, the reader is invited to refer to the publication by Skoog et al¹⁷⁷.

3.2.9.2 Applications related to this study:

ESI-MS is used routinely in the biomedical sciences¹⁷⁸ and it has become one of the most important techniques for analysing biomolecules such as peptides, proteins and oligonucleotides^{179,180}. The only analysis of glutaraldehyde and both glutaraldehyde-treated amino acid and tissue, by reverse phase high performance liquid chromatography coupled with ESI-MS, was recently reported by colleagues from Sheffield University¹⁸¹. Their analysis of hydrolysates of glutaraldehyde-treated pericardium tissue revealed only two peaks (m/z 421 and 411 respectively assigned to anabilsine and a di- α,β unsaturated aldehyde product of glutaraldehyde via a Michael-type addition. Their mass spectral data obtained from reaction of glutaraldehyde with 6-aminohexanoic acid (an amino acid relevant to these studies) showed many peaks, from which only nine have been assigned to a compound and their corresponding structures given, although a larger panel of techniques than solely ESI-MS was used. Nevertheless, apart from this study, a successful elucidation of other molecular structures, in relation to glutaraldehyde in solution or glutaraldehyde-treated model compounds, from their study by ESI-MS have not yet been reported.

However, mass spectrometric analysis of glutaraldehyde has been carried out in the past by double-focusing mass spectrometry⁶⁸, from which only two molecular structures with m/z 182 and m/z 264 were identified, corresponding respectively to the following formula $C_{10}H_{14}O_3$ (aldol condensation dimer product) and $C_{15}H_{20}O_4$ (aldol condensation trimer product). Alkaline solutions of glutaraldehyde have been also analysed by chemical-ionisation using a gas chromatograph-mass spectrometer system^{71,72}. Trioxane-type glutaraldehyde oligomers (m/z 318, m/z 518 corresponding respectively to trimer and pentamer) have thus been assigned, along with the characterisation of dimer (m/z 183) and trimer (m/z 264) produced by aldol condensation of glutaraldehyde molecules followed by dehydration.

3.2.10 MALDI-TOF MS (matrix assisted laser desorption ionisation time of flight mass spectrometry)

3.2.10.1 Theory:

MALDI-TOF mass spectrometry was developed in the late 1980s¹⁸². The sample solution (analyte) is incorporated into a solid organic matrix to co-crystallise and the mixture is placed on a sample holder that is irradiated with UV laser pulses (e.g. N₂ laser, $\lambda=337$ nm, pulse width 5 ns). The matrix strongly absorbs the laser radiation, thus the laser energy is absorbed by the matrix and then transferred to the analyte. This absorption by the matrix controls the energy subsequently deposited in the sample molecules and it results in the vaporisation of both the matrix and the embedded sample, which thus become desorbed and ionised. The charged molecules are then attracted into the TOF mass analyser. Although MALDI is considered to be a soft ionisation technique, a substantial amount of energy is involved. The analysis of small molecules is usually limited to $M_w > 500$ Da, because the matrix also tends to decompose upon absorption of the laser radiation. Thus MALDI is generally well-suited and applied to the analysis of medium to high molecular weight compounds such as proteins, although it has been reported to be suitable for the quantitative analysis of low molecular weight antibiotics with a M_w of less than 500 Da¹⁸³. The major disadvantage of MALDI MS is therefore background interference from the matrix. It has been reported that one of the most important aspects of MALDI MS is the preparation of a good, homogeneous sample^{184,185}. Thus, it is important to select the matrix carefully for a given compound because the intensity of the resulting signal varies greatly with the matrix. This was not a significant problem in this study of glutaraldehyde-treated proteins, which are mostly outside this critical mass range. However, when analysing glutaraldehyde in solution, care was taken when assigning peaks belonging to the matrix and those belonging to the sample since the molecular weight of the monomeric glutaraldehyde molecule as a simple di-aldehyde is 100.

The MALDI technique involves pulsed ionisation, making it suited for time-of-flight mass analysis. In a time-of-flight (TOF) mass spectrometer, positive ions are produced by bombardment of the sample with brief pulses of electrons, secondary ions or laser-generated photons. The ions produced are then accelerated into a field-free drift analyser tube by an electric field pulse (10^3 - 10^4 V). Based on the relationship between mass and velocity at a given kinetic energy, the instrument

measures the time taken by each ion of specific mass to travel the length of the field-free analyser tube¹⁸⁶. The resolution is related to the duration of the ionisation pulse, to the initial energy distribution of the ions and to the precision with which the time-of-flight can be measured. However, a reflectron can also be used to increase the resolution achieved, by compensating for kinetic energy distributions. In the reflectron (acting as an electrostatic mirror), ions with higher velocities (i.e. higher energies) will penetrate deeper into the zone of the electric field than low energy ions, which allow ions of the same mass with different energy distributions to be collected at the same time. The separation of ions is thus based on their relative mass and occurs during their transit to the detector located at the end of the tube, with the lighter ions reaching the detector before the heavier ones¹⁷⁷. For further insight into the theory, the reader is invited to refer to the publication by Skoog et al¹⁷⁷.

3.2.10.2 Applications related to this study:

Analysis of proteins and non-covalent protein complexes by MALDI-TOF MS have been reported^{187,188}. However, because the matrix environment and laser irradiation tend to usually dissociate most non-covalent complexes, chemical cross-linking have been successfully investigated to solve this problem^{189,190}. Nevertheless, the cross-linking agent (usually glutaraldehyde) was reported to contribute in complicating the analyses of the masses obtained, especially when highly multimeric proteins are studied. By investigating this matter, proteins of known multimericity as standards (for example lysosyme, which is of direct relevance for this study) were analysed by MALDI-TOF MS to determine the effects of glutaraldehyde and protein concentration on the stabilisation, aggregation and mass determination of the complexes¹⁹¹. Horse heart cytochrome C, (which is also a protein of interest in the scope of these studies), reacted with glutaraldehyde and analysed by TOF mass spectrometry was reported by Ohno and Kurusu^{192,193}. These authors were interested in the electron transfer of the glutaraldehyde-treated protein in poly(ethylene oxide) oligomers rather than in the actual cross-linking issue associated with the protein and glutaraldehyde, which is of direct interest in these studies. Therefore, no actual conclusions were drawn regarding the resulting cross-linking of the protein with glutaraldehyde. Furthermore, no analysis of glutaraldehyde by MALDI mass spectrometry has been reported so far.

Additionally, the direct analysis of thin layer chromatography (TLC) by MALDI MS was previously reported^{194,195}, however their preparation methodology was different from the one reported in this study (primarily results can be found in appendix II), and the transfer was accomplished by pressing the matrix onto a previously wetted (spraying of extraction solution) TLC plate. The method of matrix deposition into a TLC plate by electrospray deposition, that is used in this study, was developed by others from Sheffield Hallam University¹⁹⁶ and was found suitable to allow chromatographic information to be obtained from a TLC plate analysed by MALDI-TOF-MS¹⁹⁷. The application of such a methodology on the samples used in this thesis is presently also unreported.

1. Curtil A, Pegg DE, Wilson A. Freeze-drying of cardiac valves in preparation for cellular repopulation. *Cryobiology*. 1997;34:13-22.
2. Danilatos GD. Foundations of environmental scanning electron microscopy. In: Hawkes PW, ed. *Advances in Electronic and Electron Physics*. Boston: Academic Press; 1988:109-250.
3. Danilatos GD. A gaseous detector device for an environmental SEM. *Micron Microscopica Acta*. 1983;14:307-319.
4. Danilatos GD. Introduction to the ESEM instrument. *Microscopy Research and Technique*. 1993;25:354-361.
5. Danilatos GD. Mechanisms of detection and imaging in the ESEM. *Journal of Microscopy*. 1990;160:9-19.
6. Danilatos GD. Bibliography of environmental scanning electron microscopy. *Microscopy Research and Technique*. 1993;25:529-534.
7. Phillips MR, Toth M. Charge neutralisation of insulators in an ESEM. *Institute Physics Conference Series number 165 Symposium 7 (abstract)*. 2000:273-274.
8. Nuttall HE, Kale R. Application of ESEM to environmental colloids. *Microscopy Research and Technique*. 1993;25:439-446.
9. Geiger SL, Ross TJ, Barton LL. Environmental scanning electron microscope: evaluation of crystal and plaque formation associated with biocorrosion. *Microscopy Research and Technique*. 1993;25:429-433.
10. Keyser LF, Leu MT. Morphology of nitric acid and water ice films. *Microscopy Research and Technique*. 1993;25:434-438.
11. Rask JH, Flood JE, Borchardt JK, York GA. The ESEM used to image crystalline structures of polymers and to image ink on paper. *Microscopy Research and Technique*. 1993;25:384-392.
12. Messier P, Vitale T. Cracking in albumen photographs: an ESEM investigation. *Microscopy Research and Technique*. 1993;25:374-383.
13. Cowan AJ, Wilson NHF, Wilson MA, Watts DC. The application of ESEM in dental materials research. *Journal of Dentistry*. 1996;24:375-377.
14. Collins SP, Pope RK, Scheetz RW, Ray RI, Wagner PA, Little BJ. Advantages of environmental scanning electron microscopy in studies of microorganisms. *Microscopy Research and Technique*. 1993;25:398-405.
15. Frasca P, Buchanan JW, Soriano RZ, Dunn JM, Marmon L, Melbin J, Buchanan SJ, Golumb EE, Shapiro IM. Morphological observations of mineralising pericardium-cardiac grafts. *Scanning Electron Microscopy*. 1985;3:1253-1258.
16. Nelson AC, Schoen FJ, Levy RJ. Scanning electron microscopy methodology for study of the pathophysiology of calcification in bioprosthetic heart valves. *Scanning Electron Microscopy*. 1985;1:209-213.
17. Brown WE, Chow LC. Chemical properties of bone mineral. *Annual Review of Materials Science*. 1976;6:213-236.

18. Fulmer MT, Martin RI, Brown PW. Formation of calcium deficient hydroxyapatite at near-physiological temperature. *Journal of Materials Science. Materials in Medicine*. 1992;3:299-305.
19. Huaxia JI, Ponton CB, Marquis PM. Microstructural characterisation of hydroxyapatite coating on titanium. *Journal of Materials Science. Materials in Medicine*. 1992;3:283-287.
20. Sodian R, Hoerstrup SP, Sperling JS, Daebritz SH, Martin DP, Mayer JE, Vacanti JP. Evaluation of biodegradable, three dimensional matrices for tissue engineering of heart valves. *American Society Artificial Internal Organs Journal*. 2000;46:107-110.
21. Sodian R, Hoerstrup SP, Sperling JS, Daebritz SH, Martin DP, Schoen FJ, Vacanti JP, Mayer JE. Tissue engineering of heart valves: in-vitro experiences. *Annals of Thoracic Surgery*. 2000;70:140-144.
22. Sodian R, Hoerstrup SP, Sperling JS, Daebritz SH, Martin DP, Moran AM, Kim BS, Schoen FJ, Vacanti JP, Mayer JE. Early in-vivo experience with tissue-engineered trileaflet heart valves. *Circulation*. 2000;102:III22-III29.
23. Hoerstrup SP, Sodian R, Daebritz SH, Wang J, Bacha EA, Martin DP, Moran AM, Guleserian KJ, Sperling JS, Kaushal S, Vacanti JP, Schoen FJ, Mayer JE. Functional living trileaflet heart valves grown in-vitro. *Circulation*. 2000;102:III44-III49.
24. Greenfield S, Jones LI, Berry CT. High pressure plasma as spectroscopic emission source. *Analyst*. 1964;89:713.
25. Wendt RH, Fassel VA. Induction-coupled plasma spectrometric excitation source. *Analytical Chemistry*. 1965;37:920.
26. Thompson M, Walsh JN. In: *Handbook of Inductively Coupled Plasma Spectrometry*. 2nd ed. New York: Blackie; 1989.
27. Skoog DA, Holler FJ, Nieman TA. In: *Principles of Instrumental Analysis*. 5th ed. London: Saunders College Publishing; 1992:230-251.
28. Fifield FW, Kealey D. In: *Principles and Practice of Analytical Chemistry*. 4th ed. London: Blackie Academic and Professional; 1995:296-317.
29. Murthy GK, Rhea U, Teeler JT. Quantitative determination of calcium by atomic absorption. *Environmental Science Technology*. 1971;5:436-442.
30. Willis JB. The determination of metals in blood serum by atomic spectroscopy I. Calcium. *Spectrochimica Acta*. 1960;6:259-272.
31. Bartlett GD. Phosphorus assay in column chromatography. *Journal of Biological Chemistry*. 1959;234:466-468.
32. Chen PS, Toribara TY, Warner H. Microdetermination of phosphorus. *Analytical Chemistry*. 1956;28:1756-1758.
33. Lee WK, Park KD, Kim YH, Suh H, Park JC, Lee JE, Sun K, Baek MJ, Kim HM, Kim SH. Improved calcification resistance and biocompatibility of tissue patch grafted with sulphonated PEO or heparin after glutaraldehyde fixation. *Journal of Biomedical Materials Research. Applied Biomaterials*. 2001;58:27-35.
34. Park JC, Hwang YS, Han DW, Suh H. A novel in-vitro assessment of tissue valve calcification by a continuous flow type method. *Artificial Organs*. 2000;24:156-164.
35. Berlyne GM, Caruso C. Measurement of silicon in biological fluids in man using flameless furnace atomic absorption spectrometry. *Clinica Chimica Acta*. 1983;129:239-244.
36. Roberts NB, Williams P. Silicon measurement in serum and urine by direct current plasma emission spectrometry. *Clinical Chemistry*. 1990;36:1460-1465.
37. Skoog DA, Holler FJ, Nieman TA. In: *Principles of Instrumental Analysis*. 5th ed. London: Saunders College Publishing; 1992:294-296.
38. Moore DM, Reynolds RC. In: *XRD and the Identification and Analysis of Clay Minerals*. Oxford: University Press; 1997.
39. Zhang Q, Ren L, Liu L, Wang C. Structure investigation of polyvinylalcohol-collagen composite. *Journal of Materials Science Technology*. 1997;13:179-183.
40. Bigi A, Gandolfi M, Koch MHJ, Roveri N. X-ray diffraction study of in-vitro calcification of tendon collagen. *Biomaterials*. 1996;17:1195-1201.
41. Pettenazzo E, Deiwick M, Thiene G, Molin G, Glasmacher B, Martignano F, Bottio T, Reul H, Valente M. Dynamic in-vitro calcification of bioprosthetic porcine valves: evidence of apatite crystallisation. *Journal of Thoracic Cardiovascular Surgery*. 2001;121:500-508.
42. Glimcher MJ. The nature of the mineral phase in bone: biological and clinical applications. In: Alvioli L, Crane S, eds. *Metabolic Bone Disease*. New York: Academic Press; 1998:23-50.

43. Kuhn-Spearing LT, Rey C, Kim HM, Glimcher MJ. Carbonated apatite nanocrystals from bone. In: Bourell DL, ed. *Synthesis and Processing Nanocrystalline Powder*. Warendale: The Mineral, Metal and Materials Society; 1996:57-68.
44. Kim HM, Rey C, Glimcher MJ. Isolation of calcium-phosphate crystals of bone by non-aqueous methods at low temperature. *Journal of Bone Mineral Research*. 1995;10:1589-1601.
45. Grynblas MD, Bonar LC, Glimcher MJ. Failure to detect amorphous calcium phosphate solid phase in bone mineral: a radial distribution function study. *Calcified Tissue International*. 1984;36:291-309.
46. Rey C, Shimizu M, Collins B, Glimcher MJ. Resolution enhanced Fourier-transform infrared spectroscopy study of the environment of phosphate ions in the early deposits of a solid phase of calcium phosphate in bone and enamel, and their evolution with age I. Investigations in the ν_4 PO₄ domain. *Calcified Tissue International*. 1990;46:384-394.
47. Kontoyannis CG, Bouropoulos NC, Koutsoukos PG. Raman spectroscopy: a tool for the quantitative analysis of mineral components of solid mixtures. The case of calcium oxalate monohydrate and hydroxyapatite. *Vibrational Spectroscopy*. 1997;15:53-60.
48. Nancollas GH, Tomazic B. Growth of calcium phosphate on hydroxyapatite crystals. Effect of supersaturation and ionic medium. *Journal of Physical Chemistry*. 1974;78:2218.
49. Vetter U, Eanes ED, Kopp JB, Termine JD, Robey PG. Changes in apatite crystal size in bones of patients with osteogenesis imperfecta. *Calcified Tissue International*. 1991;49:248-250.
50. Tomazic BB, Mayer I, Brown WE. Ion incorporation into octacalcium phosphate hydrolysates. *Journal of Crystal Growth*. 1991;108:670-682.
51. Huang LY, Xu KW, Lu J. A study of the process and kinetics of electrochemical deposition and the hydrothermal synthesis of hydroxyapatite coatings. *Journal of Materials Science. Materials in Medicine*. 2000;11:667-673.
52. Boudeville P, Serraj S, Leloup JM, Marguerit J, Pauvert B, Terol A. Physical properties and self-setting mechanism of calcium phosphate cements from calcium bis-dihydrogenophosphate monohydrate and calcium oxide. *Journal of Materials Science. Materials in Medicine*. 1999;10:99-109.
53. Brown WE, Eidelman N, Tomazic B. Octacalcium phosphate as a precursor in biomineral formation. *Advances in Dental Research*. 1987;1:306-313.
54. Chittur KK. FTIR/ATR for protein adsorption to biomaterials surfaces. *Biomaterials*. 1998;19:357-369.
55. Buffeteau T, Desbat B, D. E. ATR-FTIR: theory and application to polymer samples. *Vibrational Spectroscopy*. 1996;11:29-36.
56. Griffiths PR, Urban MW. FTIR and Raman spectroscopy of polymers. *American Chemical Society Symposium Series*. 1995;598:2-7.
57. Yarwood J. Fourier-transform infrared reflection spectroscopy for surface analysis. *Analytical Proceedings*. 1993;30:13-18.
58. Hollas JM. In: *Modern Spectroscopy*. 2nd ed. New York: Wiley and Sons; 1992:60-61.
59. In: Clark RJH, Hester RE, eds. *Advances in Spectroscopy. Biomedical Applications of Spectroscopy*. Chichester: Wiley; 1996:185-216.
60. Putzig CL, Leugers MA, McKelvy ML, Mitchell GE, Nyquist RA, Papenfuss RR, Yurga L. Infrared Spectroscopy. *Analytical Chemistry*. 1994;66:26R-66R.
61. Jackson M, Mantsch H. The use and misuse of FTIR spectroscopy in the determination of protein structure. *Critical Reviews in Biochemistry and Molecular Biology*. 1995;30:95-120.
62. Moss D, Navedryk E, Breton J, Mantele W. Redox-linked conformational changes in proteins detected by a combination of IR spectroscopy and protein electrochemistry. Evaluation of the technique with cytochrome C. *European Journal of Biochemistry*. 1990;187:565-572.
63. Miller B. Infrared spectroscopy of human skin. *Laboratory News*. 1998;583:22-24.
64. Barry BW, Edwards HGM, Williams AC. Fourier-transform Raman and infrared vibrational study of human skin: assignment of spectral bands. *Journal of Raman spectroscopy*. 1992;23:641-645.
65. Yang CQ, Wei W, McIlwaine DB. Evaluating glutaraldehyde as a non formaldehyde durable press finishing agent for cotton fabrics. *Textile Research Journal*. 2000;70:230-236.
66. Monteiro Jr OAC, Airoidi C. Some studies of crosslinking chitosan-glutaraldehyde interactions in a homogeneous system. *International Journal of Biological Macromolecules*. 1999;26:119-128.

67. Chatterji PR. Gelatin with hydrophylic/hydrophobic grafts and glutaraldehyde crosslinks. *Journal of Applied Polymer Science*. 1989;37:2203-2212.
68. Monsan P, Puzo G, Mazarguil H. Etude du mecanisme d' etablissement des liaisons glutaraldehyde-proteines. *Biochimie*. 1975;57:1281-1292.
69. Hardy PM, Nicholls AC, Rydon HN. The nature of the crosslinking of proteins by glutaraldehyde I. Interaction of glutaraldehyde with the amino-groups of 6-aminohexanoic acid and N-acetyl-L-lysine. *Journal of the Chemical Society Perkin Transaction I*. 1976:958-962.
70. Margel S, Rembaum A. Synthesis and characterisation of polyglutaraldehyde. A potential reagent for protein immobilisation and cell separation. *Macromolecules*. 1980;13:19-24.
71. Tashima T, Kawakami U, Harada M, Imai M, Satoh N, Nakagawa T, Tanaka H. Polymerisation reaction in aqueous solution of glutaraldehyde containing trioxane-type oligomers under sterilising conditions. *Chemical Pharmaceutical Bulletin*. 1989;37:377-381.
72. Tashima T, Imai M. Structure of a new oligomer of glutaraldehyde produced by aldol condensation reaction. *Journal of Organic Chemistry*. 1991;56:694-697.
73. Joshi RR, Frautschi JR, Phillips RE, Levy RJ. Phosphonated polyurethanes that resist calcification. *Journal of Applied Biomaterials*. 1994;5:65-77.
74. Lee CH, Vyavahare N, Zand R, Kruth H, Schoen FJ, Bianco R, Levy RJ. Inhibition of aortic wall calcification in bioprosthetic heart valves by ethanol pretreatment: biochemical and biophysical mechanisms. *Journal of Biomedical Materials Research*. 1998;42:30-37.
75. Vyavahare NR, Hirsch D, Lerner E, Baskin JZ, Zand R, Schoen FJ, Levy RJ. Prevention of calcification of glutaraldehyde-crosslinked porcine aortic cusps by ethanol preincubation: Mechanistic studies of protein structure and water-biomaterials relationship. *Journal of Biomedical Materials Research*. 1998;40:577-585.
76. Pleshko N, Boskey AL, Mendelsohn R. Novel infrared spectroscopic method for the determination of crystallinity of hydroxyapatite minerals. *Biophysical Journal*. 1991;60:786-793.
77. Mendelsohn R, Hasankhani A, DiCarlo E, Boskey AL. FTIR microscopy of endochondral ossification at 20 micron spatial resolution. *Calcified Tissue International*. 1989;44:20-29.
78. Boskey AL, Pleshko N, Binderman I, Mendelsohn R. Mineralisation during in-vitro calcification: an FTIR microscopic mapping of early mineralisation in chick limb bud mesenchymal cell cultures. *Calcified Tissue International*. 1992;51:443-448.
79. Gadaleta SJ, Camacho NP, Mendelsohn R, Boskey AL. Application of FTIR microspectroscopy to mineralised turkey tendon. *Calcified Tissue International*. 1996;58:17-23.
80. Termine JD, Posner AS. Infrared determination of the percentage of crystallinity in apatic calcium phosphates. *Nature*. 1966;211:268-270.
81. Miller FA, Wilkins CH. Infrared spectra and characteristic frequencies of inorganic ions. *Analytical Chemistry*. 1952;24:1253-1294.
82. Pschalis EP, Jacenko O, Olsen B, Mendelsohn R, Boskey AL. FTIR microspectroscopic analysis identifies alterations in mineral properties in bones from mice transgenic for type X collagen. *Bone*. 1996;19:151-156.
83. Tagaki S, Chow LC, Markovic M, Friedman CD, Costantino PD. Morphological and phase characterisations of retrieved calcium phosphate cement implants. *Journal of Biomedical Materials Research. Applied Biomaterials*. 2001;58:36-41.
84. Rey C, Kim HM, Gerstenfeld L, Glimcher MJ. Structural and chemical characteristics and maturation of the calcium-phosphate crystals formed during the calcification of the organic matrix synthesised by chicken osteoblasts in cell culture. *Journal of Bone Mineral Research*. 1995;10:1577-1588.
85. Rey C, Kim HM, Gerstenfeld L, Glimcher MJ. Characterisation of the apatite crystals of bone and their maturation in osteoblast cell culture: comparison with native bone crystals. *Connective Tissue Research*. 1996;35:343-349.
86. Rey C, Shimuzu M, Collins B, Glimcher MJ. Resolution enhanced Fourier-transform infrared spectroscopy study of the environment of phosphate ions in the early deposits of a solid phase of calcium phosphate in bone and enamel and their evolution with age II. Investigations in the ν_3 PO₄ domain. *Calcified Tissue Research*. 1991;49:383-388.
87. Rey C, Renuopalakrishnan V, Collins B, Glimcher MJ. Fourier-transform infrared spectroscopic study of the carbonate ions in bone mineral during aging. *Calcified Tissue International*. 1991;49:251-258.

88. Posner AS. Bone mineral and the mineralisation process. *Bone Mineral Research*. 1987;5:65-116.
89. Termine JD, Eanes ED. Comparative chemistry of amorphous and apatitic calcium phosphate preparations. *Calcified Tissue Research*. 1972;10:171-197.
90. Eanes ED, Posner AS. In: Schraer H, ed. *Biological Calcification*. New York: Appleton-Century-Crofts; 1970:1-26.
91. Gibson IR, Rehman I, Best SM, Bonfield W. Characterisation of the transformation from calcium deficient apatite to beta-tricalcium phosphate. *Journal of Materials Science. Materials in Medicine*. 2000;11:533-539.
92. Nelson DGA, Featherstone JDB. Preparation, analysis, and characterisation of carbonated apatites. *Calcified Tissue International*. 1982;34:S69-S81.
93. Berry EE. The structure and composition of some calcium-deficient apatites. *Journal of Inorganic Nucleation Chemistry*. 1967;29:317-327.
94. Fowler BO, Markovic M, Brown WE. Octacalcium phosphate 3. Infrared and Raman vibrational spectra. *Chemistry and Materials*. 1993;5:1417-1423.
95. Brown WE. Crystal structure of octacalcium phosphate. *Nature*. 1962;196:1048-1050.
96. Fowler BO, Moreno EC, Brown WE. Infrared spectra of hydroxyapatite, octacalcium phosphate and pyrolysed octacalcium phosphate. *Archives of Oral Biology*. 1966;11:477-492.
97. Feki HE, Rey C, Vignoles M. Carbonate ions in apatites: infrared investigations in the nu₄ carbonate domain. *Calcified Tissue International*. 1991;49:269-274.
98. Rey C, Bshah K, Griffin R, Glimcher MJ. Structural studies of the mineral phase of calcifying cartilage. *Journal of Bone Mineral Research*. 1991;6:515-525.
99. Hallworth AS, Wheatherell JA, Robinson B. *Caries Research*. 1965;7:345.
100. Biltz RM, Pellegrino ED, Letteri JM. Skeletal carbonates and acid-base regulation. *Mineral and Electrolyte Metabolism*. 1981;5:1-7.
101. LeGeros RZ, LeGeros JP, Trautz OR, Klein E. Carbonate substitution in the apatite structure. *Bulletin Societe Chimie Francaise*. 1968;2nd trim:1712-1718.
102. Baxter JD, Biltz RM, Pellegrino ED. The physical state of bone carbonate: a comparative infrared study in several mineralised tissues. *Yale Journal of Biology and Medicine*. 1966;3:456-470.
103. Nelson DGA, Williamson BE. Low-temperature laser Raman spectroscopy of synthetic carbonated patites and dental enamel. *Australian Journal of Chemistry*. 1982;35:715-727.
104. Beshah K, Rey C, Glimcher MJ, Shimizu M, Griffin RG. Carbon-13 and proton solid state NMR studies of carbonate-containing calcium phosphates and enamel. *Journal of Solid State Chemistry*. 1990;84:71-81.
105. Elliott JC. The crystallographic structure of dental enamel and related apatites. In: London: University of London; 1964.
106. McDonnell D. The problem of the carbonate apatites IV. Structural substitutions involving carbonate and hydroxide. *Bulletin Societe Francaise Mineral Crystallography*. 1952;75:428-445.
107. Rey C, Renugopalakrishnan V, Shimizu M, Collins B, Glimcher MJ. A resolution enhanced Fourier transform infrared spectroscopic study of the environment of the carbonate ion in the mineral phase of enamel during its formation and maturation. *Calcified Tissue International*. 1991;49:259-268.
108. Vignoles M, Bonel G, Holcomb DW, Young RA. Influence of preparation conditions on the composition of type B carbonated hydroxyapatite and on the localisation of the carbonate ions. *Calcified Tissue International*. 1988;43:33-40.
109. Bonel G, Labarthe JC, Vignoles C. Contribution a l' etude des apatites carbonates de type B. *Colloque International CNRS (Paris) Physico-Chimie et Crystallographie des Apatites d' Interet Biologique*. 1973;230:117-125.
110. Rey C, Collins B, Goehl T, Dickson IR, Glimcher MJ. The carbonate environnement in bone mineral. A resolution enhanced Fourier transform infrared spectroscopy study. *Calcified Tissue International*. 1989;45:157-164.
111. Termine JD, Lundy DR. Hydroxide and carbonate in rat bone mineral and its synthetic analogues. *Calcified Tissue Research*. 1973;13:73-82.
112. Bonel G, Montel G. Sur une nouvelle apatite carbonatee synthetique. *Comptes Rendus de l' Academie des Sciences de Paris*. 1964;258:923-926.
113. Bonel G, Montel G. Sur l' introduction des ions carbonates dans le reseau des apatites calciques. *Comptes Rendus de l' Academie des Sciences de Paris*. 1966;263:1010-1013.

114. Elliott JC. In: Stack MW, Fearnhead RW, eds. *The interpretation of the infrared absorption spectra of some carbonate-structure*. Bristol: John Wright and Sons; 1965:20-58.
115. Elliott JC, Holcomb DW, Young RA. Infrared determination of the degree of substitution of hydroxyl by carbonate ions in human dental enamel. *Calcified Tissue International*. 1985;37:372-375.
116. Abergas T, Bleiwas H, Legeros JP. CO₃-for OH (type A) and CO₃-for PO₄ (type B) substitutions in precipitated carbonate-apatites. *Journal of Dental Research*. 1987;66:190.
117. Termine JD, Eanes ED, Greenfield DJ, Nylen MU. Hydrazine deproteinized bone mineral: physical and chemical properties. *Calcified Tissue Research*. 1973;12:73-90.
118. Emerson WH, Fischer EE. The infrared absorption spectra of carbonate in calcified tissues. *Archives of Oral Biology*. 1962;7:671-683.
119. Vignoles M. Contribution a l'etude des apatites carbonates de type B. In: Toulouse: Institut National Polytechnique de Toulouse; 1984.
120. Rey C, Miquel JL, Facchini L, Legrand AP, Glimcher MJ. Hydroxyl groups in bone mineral. *Bone*. 1995;16:583-586.
121. Bonar LC, Shimizu M, Roberts JE, Griffin RG, Glimcher MJ. Structural and composition studies on the mineral of newly formed dental enamel: a chemical, X-ray diffraction, and P and H NMR study. *Journal of Bone Mineral Research*. 1991;6:1167-1176.
122. Kuhn LT, Wu Y, Rey C, Gerstenfeld LC, Grynpas MD, Ackerman JL, Kim HM, Glimcher MJ. Structure, composition, and maturation of newly deposited calcium phosphates crystals in chicken osteoblast cell cultures. *Journal of Bone Mineral Research*. 2000;15:1301-1309.
123. Blumenthal NC, Posner AS. Hydroxyapatite: mechanism of formation and properties. *Calcified Tissue Research*. 1973;13:135-243.
124. Posner AS, Blumenthal NC, Boskey AL, Betts F. Synthetic analogue of bone mineral formation. *Journal of Dental Research*. 1975;54:B88-B93.
125. Pellegrino ED, Biltz RM. Mineralisation in the chick embryo I. Monohydrogen phosphate and carbonate relationship during maturation of the bone crystal complex. *Calcified Tissue Research*. 1972;10:128-135.
126. Wondratschek H. Other compounds with the apatite structure. In: Young RA, Brown WE, eds. *International Symposium on Structural Properties of Hydroxyapatite and Related Compounds*. New York: Gordon and Breach; 1968:Chapter 3.
127. Biltz RM, Pellegrino ED. The hydroxyl content of calcified tissue mineral. *Calcified Tissue Research*. 1971;7:259-263.
128. Grasselli JG, Snavely MK, Bulkin BJ. In: *Chemical Applications of Raman Spectroscopy*. New York: John Wiley and Sons; 1981:1-11.
129. Dhamelincourt P, Wallart F, Leclercq M, N'Guyen AT, Landon DO. Laser Raman molecular microprobe. *Analytical Chemistry*. 1984;56:1429-1437.
130. Parker SF, Conroy N, Patel V. Some consequences of the Fourier-transform in Fourier-transform Raman spectroscopy. *Spectrochimica Acta*. 1993;49A:657-666.
131. Skoog DA, Holler FJ, Nieman TA. In: *Principles of Instrumental Analysis*. 5th ed. London: Saunders College Publishing; 1992:429-444.
132. Carey PR. In: *Biochemical Applications of Raman and Resonance Raman Spectroscopy*. New York: Academic Press; 1982.
133. Huong PV. In: Grasselli JG, Bulkin BJ, eds. *Analytical Raman Spectroscopy*. New York: Wiley; 1991:chapter 11.
134. Wen ZQ, Hecht L, Barron LD. Alpha-helix and associated loop signatures in vibrational Raman optical activity spectra of proteins. *Journal of the American Chemical Society*. 1994;116:443-445.
135. Laroche G, Dufour EJ, Pezolet M, Dufourcq J. A proton NMR and Raman study of polylysine-phosphatidic acid systems. *Biochemistry Journal*. 1990;29:6460-6465.
136. Yu TJ, Lippert JL, Peticolas WL. Laser Raman studies of conformational variations of poly-L-lysine. *Biopolymers*. 1973;12:2161-2176.
137. Koenig JL, Sutton PL. Raman spectra of poly-L-lysine. *Biopolymers*. 1970;9:1229-1237.
138. Wilson G, Ford SJ, Cooper A, Hecht L, Wen ZQ, Barron LD. Vibrational Raman optical activity of alpha-lactalbumin: comparison with lysosyme, and evidence for native tertiary folds in molten globules states. *Journal of Molecular Biology*. 1995;254:747-760.
139. Ford SJ, Cooper A, Hecht L, Wilson G, Barron LD. Vibrational Raman optical activity of lysosyme: hydrogen-deuterium exchange, unfolding and ligand binding. *Journal of the Chemical Society Faraday Transaction*. 1995;91:2087-2093.

140. Barron LD, Cooper A, Ford SJ, Hecht L, Wen ZQ. Vibrational Raman optical activity of enzymes. *Faraday Discussion*. 1992;93:259-268.
141. Koenig JL. Raman spectroscopy of biological molecules: a review. *Journal of Polymer Science*. 1972;D:59-177.
142. Lord RC, Yu NT. Laser-excited Raman spectroscopy of biomolecules I. Native lysosyme and its constituents amino acids. *Journal of Molecular Biology*. 1970;50:509-524.
143. Lewis A, Scheraga HA. Laser Raman spectroscopy of polypeptides I: water-soluble block copolymers of L-alanine and D,L-lysine. *Macromolecules*. 1971;4:539-543.
144. Greve J, Puppels GJ, Otto C. Raman microspectroscopy of living cells: new developments. *Special Publication of the Royal Society of Chemistry: Spectroscopy of Biological Molecules*. 1991;94:293-296.
145. Baraga JJ, Feld MS, Rava RP. In-situ optical histochemistry of human artery using near IR FT-Raman spectroscopy. *Proceedings of the National Academy of Sciences of the U.S.A.* 1992;89:3473-3477.
146. Osaki Y, Mizuno AK, Fujii M, Tsuki M, Muraishi S. Non-destructive structural analysis of biological tissues by near-infrared FT-Raman spectroscopy. *Proceedings SPIE. The International Society for Optical Engineering*. 1992;1575:449-451.
147. Rava RP, Baraga JJ, Feld MS. Near-infrared Fourier-transform Raman spectroscopy of human artery. *Spectrochimica Acta*. 1991;47A:509-512.
148. Liu CH, Sha Glassman WL, Zhu HR, Akins DL, Deckelbaum LI, Stetz ML, O'Brien K, Scott J, Alfano RR. Near-infrared Fourier-transform Raman spectroscopy of normal and atherosclerotic human aorta. *Lasers Life Science*. 1992;4:257-264.
149. Schrabar B. In: Durig JR, Sullivan JF, eds. *Proceedings 12th International Conference Raman Spectroscopy*. Chichester: Wiley; 1990:890.
150. Aminzadeh A. Fluorescence bands in the FT-Raman spectra of some calcium minerals. *Spectrochimica Acta*. 1997;53:693-697.
151. Manoharan R, Baraga JJ, Feld MS, Rava RP. Quantitative histochemical analysis of human artery using Raman spectroscopy. *Journal of Photochemistry and Photobiology B: Biology*. 1992;16:211-233.
152. Brennan JF, Romer TJ, Lees RS, Tercyak AM, Kramer JR, Feld MS. Determination of human coronary artery composition by Raman spectroscopy. *Circulation*. 1997;96:99-105.
153. Degen IA, Newman GA. Raman spectra of inorganic ions. *Spectrochimica Acta*. 1993;49A:859-887.
154. Iqbal Z, Tomaselli VP, Farhenfeld O, Moller KD, Ruzsala FA, Kostiner E. Polarised Raman scattering and low frequency infrared study of hydroxyapatite. *Journal of Physics and Chemistry of Solids*. 1977;38:923-927.
155. De Aza PN, Guitian F, Santos C, De Aza S, Cusco R, Artus L. Vibrational properties of calcium phosphate compounds II. Comparison between hydroxyapatite and beta-tricalcium phosphate. *Chemistry and Materials*. 1997;9:916-922.
156. De Aza PN, Santos C, Pazo A, De Aza S, Cusco R, Artus L. Vibrational properties of calcium phosphate compounds I. Raman spectrum of beta-tricalcium phosphate. *Chemistry and Materials*. 1997;9:912-915.
157. Gerstenfeld LC, Kelly CM, Von Deck M, Lian JB. Comparative morphological and biochemical analysis of hypertrophic, nonhypertrophic and 1,25-dihydroxyvitamin D3 treated nonhypertrophic chondrocytes. *Connective Tissue Research*. 1990;24:29-39.
158. Gerstenfeld LC, Kelly CM, Von Deck M, Lian JB. Effect of 1,25-dihydroxyvitamin D3 on induction of chondrocyte maturation in culture: extracellular matrix gene expression and morphology. *Endocrinology*. 1990;126:1599-1609.
159. Kravitz LC, Kingsley JD, Elkin EL. Raman and infrared studies of coupled phosphate vibrations. *Journal of Chemical Physics*. 1968;49:4600-4610.
160. Cusco R, Guitian F, De Aza S, Artus L. Differentiation between hydroxyapatite and beta-tricalcium phosphate by means of micro Raman spectroscopy. *Journal of European Ceramic Society*. 1998;18:1301-1305.
161. Nakamoto K. In: *Infrared and Raman Spectra of Inorganic Coordination Compounds*. New York: John Wiley and Sons; 1986:138.
162. Fowler BO. Infrared studies of apatites I. Vibrational assignments for calcium, strontium, and barium hydroxyapatites utilising isotopic substitution. *Inorganic Chemistry*. 1973;13:194-207.

163. Rovira A, Bareille R, Lopez I, Rouais F, Bordenave L, Rey C, Rabaud M. Preliminary report on a new composite material made of calcium phosphate, elastin peptides and collagen. *Journal of Materials Science. Materials in Medicine*. 1993;4:372-380.
164. Royer P, Rey C. Calcium phosphate coatings for orthopaedic prosthesis. *Surface Coating Technology*. 1991;45:171-177.
165. Nordon A, McGill CA, Littlejohn D. Process NMR spectrometry. *The Analyst*. 2001;126:260-272.
166. Fifield FW, Kealey D. In: *Principles and Practice of Analytical Chemistry*. 4th ed. London: Blackie Academic and Professional; 1995:393-425.
167. Abraham RJ, Fisher J, Loftus P. In: *Introduction to NMR Spectroscopy*. Chichester: John Wiley and Sons; 1994:1-240.
168. Richards FM, Knowles JR. Glutaraldehyde as a protein crosslinking reagent. *Journal of Molecular Biology*. 1968;37:231-233.
169. Hardy PM, Nicholls AC, Rydon HN. The nature of glutaraldehyde in aqueous solution. *Journal of Chemical Society Chemical Communications*. 1969;10:565-566.
170. Korn AH, Fearheller SH, Filachione EM. Glutaraldehyde: nature of the reagent. *Journal of Molecular Biology*. 1972;65:525-529.
171. Whipple EB, Ruta M. Structure of aqueous glutaraldehyde. *Journal of Organic Chemistry*. 1974;39:1666-1668.
172. Holmquist L, Lewin M. Separation of glutaraldehyde and some of its aldol condensation products by hydroxyl-aldehyde group affinity chromatography. *Journal of Biochemical and Biophysical Methods*. 1991;22:321-329.
173. Hardy PM, Hughes GJ, Rydon HN. Formation of quaternary pyridinium compounds by the action of glutaraldehyde on proteins. *Journal of Chemical Society Chemical Communications*. 1976;5:157-158.
174. Hardy PM, Hughes GJ, Rydon HN. Identification of a 3-(2-piperidyl) pyridinium derivative (anabylisine) as a crosslinking entity in a glutaraldehyde-treated protein. *Journal of Chemical Society Chemical Communications*. 1977;21:759-760.
175. Hardy PM, Hughes GJ, Rydon HN. The nature of the crosslinking of proteins by glutaraldehyde II. The formation of quaternary pyridinium compounds by the action of glutaraldehyde on proteins and the identification of a 3-(2-piperidyl)-pyridinium derivative, anabylisine, as a crosslinking entity. *Journal of the Chemical Society Perkin Transaction I*. 1979;9:2282-2288.
176. In: Chapman JR, ed. *Protein and Peptide Analysis by Mass Spectrometry. Methods in Molecular Biology*; 1989:199-200.
177. Skoog DA, Holler FJ, Nieman TA. In: *Principles of Instrumental Analysis*. 5th ed. London: Saunders College Publishing; 1992:508-528.
178. Fenn JB, Mann M, Meng CK, Wong SF, Whitehouse CM. Electrospray Ionisation for Mass Spectrometry of Large Biomolecules. *Science*. 1989;246:64-71.
179. Hop CECA, Bakhtiar R. Electrospray ionisation mass spectrometry: Applications in inorganic chemistry and synthetic polymer chemistry. Topics in chemical instrumentation. *Journal of Chemical Education*. 1996;73:A162-A169.
180. Covey TR, Bonner RF, Shushan BI. The determination of protein, oligonucleotide and peptide molecular weights by ion-spray mass spectrometry. *Rapid Communications in Mass Spectrometry*. 1988;2:11.
181. Southern LJ, Hughes H, Lawford PV, Clench MR, Manning NJ. Glutaraldehyde-induced cross-links: a study of model compounds and commercial bioprosthetic valves. *Journal of Heart Valve Disease*. 2000;9:241-249.
182. Karas M, Bachman D, Bahr U, Hillenkamp F. Matrix assisted ultraviolet laser desorption of non volatile compounds. *International Journal of Mass Spectrometry*. 1987;78:53-68.
183. Ling YC, Lin L, Chen YT. Quantitative analysis of antibiotics by MALDI TOF MS. *Rapid communication in Mass Spectrometry*. 1998;12:317-327.
184. Cohen SL, Chait BT. Influence of matrix solution conditions on the MALDI-MS analysis of peptides and proteins. *Analytical Chemistry*. 1996;68:31-37.
185. Beavis RC, Chait BT. MALDI-MS of proteins. *Methods in Enzymology*. 1996;270:519-551.
186. Rouessac F, Rouessac A. In: *Chemical Analysis: Modern Instrumentation Methods and Techniques*. New York: Wiley and Sons; 2000:297-311.
187. Beavis RC, Chait BT. High accuracy molecular mass determination of proteins using matrix-assisted laser desorption mass spectrometry. *Analytical Chemistry*. 1990;62:1836-1840.

188. Farmer TB, Caprioli RM. Determination of protein-protein interactions by matrix-assisted laser desorption/ionisation mass spectrometry. *Journal of Mass Spectrometry*. 1998;33:697-704.
189. Farmer TB, Caprioli RM. Assessing the multimeric states of proteins-studies using laser desorption mass-spectrometry. *Biological Mass Spectrometry*. 1991;20:796-800.
190. Evans JT, Rohrmann GF. The baculovirus single-stranded DNA binding protein, LEF-3, forms a homotrimer in solution. *Journal of Virology*. 1997;71:3574-3579.
191. Helin J, Caldentey J, Kalkkinen N, Bamford DH. Analysis of the multimeric state of proteins by matrix assisted laser desorption/ionisation mass spectrometry after crosslinking with glutaraldehyde. *Rapid Communications in Mass Spectrometry*. 1999;13:185-190.
192. Ohno H, Kurusu F. Cytochrome C crosslinked with glutaraldehyde I. Electrochemical response in polyethylene oxide oligomers. *Chemistry Letters*. 1996;8:693-694.
193. Kurusu F, Ohno H. Electrochemical response of glutaraldehyde-crosslinked cytochrome C in PEO oligomers. *Solid State Ionics*. 1998;113/115:173-177.
194. Gusev AI, Vasseur OJ, Proctor A, Sharkey AG, Hercules DM. Imaging of TLC using MALDI MS. *Analytical Chemistry*. 1995;67:4565-4570.
195. Nicola AJ, Gusev AI, Hercules DM. Direct quantitative analysis from thin-layer chromatography plates using MALDI MS. *Applied Spectroscopy*. 1996;50:1479-1482.
196. Mowthorpe S, Clench MR, Crecelius A, Richards DS, Tetler LW. Matrix-assisted laser desorption ionisation/time of flight/thin layer chromatography/mass spectrometry: a rapid method for impurity testing. *Rapid Communications in Mass Spectrometry*. 1999;13:264-270.
197. Crecelius A, Clench MR, Richards DS, Mather J, Parr V. Analysis of UK-224,671 and related substances by TLC-MALDI-TOF MS. *Journal of Planar Chromatography*. 2000;13:76-81.

Chapter 4

4 Investigation of the behaviour of glutaraldehyde in solution, at various pH values.

Abstract

Objectives: The mechanism of glutaraldehyde fixation is complex and incompletely understood. A potent reason is that the behaviour of glutaraldehyde in aqueous solution and the exact content of commonly used glutaraldehyde solutions are presently unknown. The objectives were to investigate the behaviour of glutaraldehyde in solution at various pH values to further our understanding of the nature of this compound and to determine the structures present in aqueous solution of glutaraldehyde. Additionally, the application of the techniques used for this study for the analysis of glutaraldehyde over a large range of pH remains unreported to date.

Methods: Aqueous glutaraldehyde solutions at various pH values (pH 1-11 range) were subjected to analysis by electrospray ionisation (ESI-MS) and matrix assisted laser desorption ionisation-time of flight (MALDI-TOF MS) mass spectrometry, nuclear magnetic resonance (NMR), Fourier-transform infrared (FTIR) and Raman spectroscopy.

Results: The common structures found at all pH range in relative quantity were mostly the glutaraldehyde hydrates, hemiacetal, acetal cyclic polymer form, mono- and di-acid form of glutaraldehyde, various trioxane-type glutaraldehyde oligomers, dimers produced by aldol condensation of two glutaraldehyde molecules and their cyclic acetal when applicable and oligomers of glutaraldehyde consisting of the α -oxypyran ring. The aldol condensation and aldol/Michael addition products,

however, were found in larger quantity at extreme pH values (pH 1 and 11) along with higher polymer chains of some of the above-mentioned oligomeric molecules (see appendix III for details).

Conclusion: Glutaraldehyde in solution has been shown to be strongly pH-dependent. It is hypothesised that glutaraldehyde, at all analysed pH values, contains some similar structures (likely in their hydrated forms) but under extreme pH conditions, certain species, containing unsaturated groups, become more prevalent. Contrary to a widely held belief, monomeric glutaraldehyde is therefore not the major reactive species found in unbuffered commercial glutaraldehyde solutions, and commercial glutaraldehyde solution thus contain a complex mixture of structures. It is hoped that these results would provide a better insight into the chemistry of glutaraldehyde and clarify the existing knowledge. It is believed that an understanding of the behaviour of glutaraldehyde in solution is essential if the interaction of glutaraldehyde with proteins, and more so with implants such as bioprosthetic heart valves, is to be predicted.

4.1 Introduction

Glutaraldehyde is an important chemical reagent used routinely in many fields such as the biomedical field where it is extensively used as a cross-linking agent for the preparation of bioprostheses, immobilising enzymes, etc. Glutaraldehyde can react readily with a large number of the amino groups available in proteins and can span various distances between tissue protein molecules. However, the specific chemistry of the reaction of glutaraldehyde with proteins is still not fully understood. One area of its chemistry that is still at the centre of much debate is the nature of glutaraldehyde in solution. The extensive review of the literature that can be found in the chapter 2 of this thesis indicates that there is still much disagreement as to the structures present in solutions of glutaraldehyde. Aqueous solutions of glutaraldehyde were shown by different authors to mostly contain a complex mixture of free aldehydes, mono and di-hydrates, monomeric and polymeric cyclic hemiacetals and various unsaturated condensation products (see chapter 2 and cross-referenced structures found in appendix III). Others attempted to elucidate the exact chemical nature of polyglutaraldehyde in solutions by UV, IR and ^{13}C NMR

spectroscopy, but the nature could not be decided and their results only indicated a mixture of oligomers of up to six glutaraldehyde units¹. Aqueous solutions of glutaraldehyde are thus complex, capable of undergoing many types of reactions. All such reactions, that glutaraldehyde can undergo, may contribute to variation in the quality of fixation. More fundamental studies on the chemistry of cross-linking using glutaraldehyde are therefore needed to elucidate the nature of reactions. This may also aid our understanding of some of the problems presently believed to be due to this reagent, such as the causes of failure of tissue valves including their calcification.

Thus, the aim of this part of the study was to determine the structures present in aqueous solutions of glutaraldehyde, using mass spectrometry (ESI-MS, MALDI-TOF MS), NMR, FTIR-ATR and Raman spectroscopy, to provide a better insight into the chemistry of glutaraldehyde on its own and to clarify the existing knowledge. An understanding of the behaviour of glutaraldehyde in solution is essential if the interaction of glutaraldehyde with bioprosthetic heart valves is to be predicted.

4.2 Materials and methods

4.2.1 Materials

All chemicals and consumables used were of the best commercially available grade.

From BDH, UK: Glutaraldehyde 25%v/v EM grade, potassium dihydrogen orthophosphate.

From Sigma-Aldrich, UK: Glutaric acid, methanol, glacial acetic acid, sinapinic acid (3,5-dimethoxy-4-hydroxycinnamic acid), 2,5-dihydroxybenzoic acid (DHB), α -cyano-4-hydroxycinnamic acid (α -CHCA), angiotensin, dipotassium hydrogen orthophosphate.

From Fisher, UK: Buffer pH 4 (potassium hydrogen phthalate) 0.05M, buffer pH 9.2 (disodium tetraborate) 0.01M, hydrochloric acid, sodium hydroxide.

Prepared when required: Buffer pH 7.4 (phosphate) 0.03 M: 4.1 g KH_2PO_4 in 1 L water (stock A); 6.9 g K_2HPO_4 in 1 L water (stock B); mix 300 mL of stock A with

700 mL of stock B. pH was adjusted to pH 7.4 with either stock solution, depending on resultant pH.

Ultra pure water: MilliQ50 (Millipore, UK) packed with USF liquid pure cartridges. The conductivity achieved was $18 \text{ M}\Omega/\text{cm}^3$.

4.2.2 Sample preparation

Glutaraldehyde solution (electron microscopy grade, 25% v/v in water, BDH, UK) was used in these experiments as received. (The glutaraldehyde solution provided was said by the supplier to be stable when maintained for a relatively long time at refrigeration temperature (4°C)).

Solutions of 0.6% v/v glutaraldehyde (0.6 mL, 6.36×10^{-3} moles) were prepared using distilled water and various pH buffers (pH 4, 7.4, 9.2). Unbuffered commercial glutaraldehyde solutions of 0.6% v/v (pH 3.8) were also prepared by dilution with water. Additionally, solutions of 0.6% v/v glutaraldehyde at pH 1 and pH 11 were prepared in water, using respectively dilute hydrochloric acid and sodium hydroxide to adjust the pH.

4.2.3 Freeze-drier

A laboratory-built freeze-drier was used and is illustrated in figure 4.1 below. It consisted of a rotary vacuum pump (two-stage pump, Edwards, Crawley, UK), which achieved a sample chamber pressure of 0.005 mmHg. The condensing chamber (or cold trap) was cooled by liquid nitrogen to prevent damage to the vacuum pump due to cavitation. The sample chamber could be changed: from a round-bottomed flask for large amounts of aqueous samples (up to ~ 100 mL), to a desiccator chamber that was used for smaller samples, especially for Raman slides or the FTIR-ATR horizontal cell. Samples were first frozen at -20°C overnight and then left to freeze-dry for 10 hours minimum regardless of the type of sample.

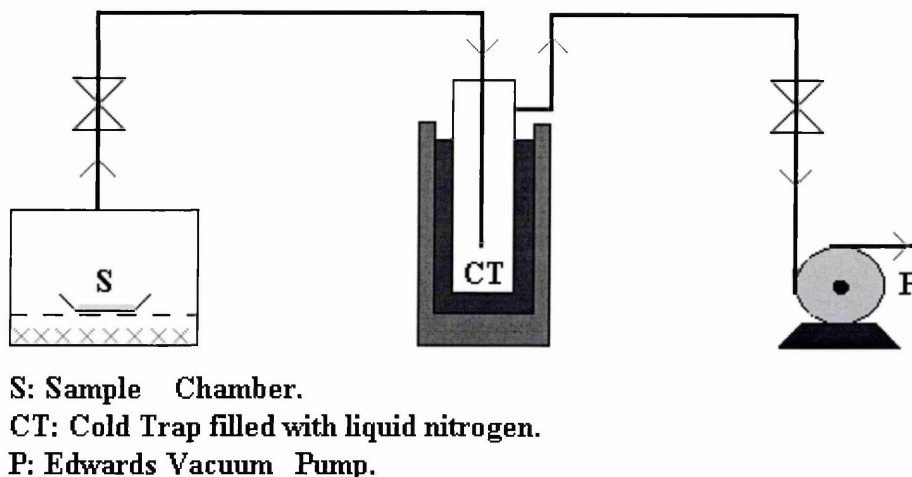


Figure 4.1: “Laboratory-built” freeze-drier set up.

4.2.4 FTIR-ATR analyses

Glutaraldehyde was studied as a solution (commercial 25% v/v solution), and also freeze-dried (commercial 25% v/v solution, 0.6% v/v and 0.2% v/v diluted in distilled water and in buffers pH 4, pH 7.4, pH 9.2, or in distilled water with adjustment of pH to pH 1 and 11 by addition of HCl or NaOH respectively). All spectra were recorded with a Mattson Polaris FTIR spectrometer (ThermoNicolet Co, Lanham, MA, USA) with an MCT detector, a KBr beam splitter, and scanned between 4000 and 400 cm^{-1} . The apodisation function was triangular and there was a Mertz phase correction. All spectra were obtained by accumulation of 1000 scans, at a resolution of 4 cm^{-1} and 45° angle of incidence, after subtracting from the spectra of the ZnSe crystal. All spectra were recorded under similar conditions (constant temperature) and were corrected for atmospheric water vapour and carbon dioxide by subtraction of the appropriate reference spectrum, even though the instrument was purged constantly with dried water vapour-free air. The spectra of freeze-dried buffer solutions (pH 4, 7.4, 9.2) were subtracted from the spectra of the corresponding freeze-dried glutaraldehyde solutions. The ATR device was a horizontal multiple reflection ATR (Graseby Specac, St Mary Cray, UK) with a ZnSe crystal. This crystal allowed easy sample preparation by pouring a few millilitres of the sample into the “pool” of the ATR cell, followed by freeze-drying.

4.2.5 Raman analyses

The Raman spectra were collected using a Renishaw system 2000 Ramascope (Renishaw, Wotton-under-edge, UK). Glutaraldehyde was studied as a solution (25% v/v) in a quartz cuvette, and freeze-dried (25% v/v, 0.6% v/v, and 0.2% v/v) on a quartz slide. A laser (helium-neon 632 nm) with a power of 25 mW (~3.4 mW at the sample) was used, with a typical scan time of 50 s with 25 accumulations, over a wavelength range of 400-4000 cm^{-1} at a spectral resolution of ~2 cm^{-1} . These conditions were chosen to allow examination of the weaker features, whilst still maintaining stability to laser excitation. The software was Galactic[®] Grams (Thermo Galactic Industries Co, Salem, NH, USA). The Raman spectra were not corrected or smoothed.

4.2.6 ESI-MS analyses

A sample (3 x 25 mL) of 0.6% v/v glutaraldehyde in distilled water was freeze-dried and re-dissolved in 3 mL of methanol. One drop of glacial acetic acid was added and the sample run on a VG Quattro (VG Micromass, Manchester, UK) instrument with a quadrupole analyser and operating in electrospray ionisation mode. The samples were run almost immediately after their dilution in methanol to avoid any possible esterification of free carboxyl groups². The inlet direct infusion of the sample was carried out at a rate of 5 $\mu\text{L} \cdot \text{min}^{-1}$ using a Harvard pump11 (Harvard apparatus, Holliston, MA, USA). The m/z range was 50-550.

4.2.7 MALDI-TOF MS analyses

Samples dissolved in (3 x 25 mL) of 0.6% v/v glutaraldehyde in distilled water and in pH 4, pH 7.4 and pH 9.2 buffers were freeze-dried and re-dissolved in 3 mL methanol. Several matrices were studied to evaluate their potential to desorb and ionise the samples. Thus, the matrix used was DHB (2,5-dihydroxybenzoic acid), although other matrices were tried (sinapinic acid (3,5-dimethoxy-4-hydroxycinnamic acid), α -CHCA (α -cyano-4-hydroxycinnamic acid)), but DHB yielded the best overall spectra and is known to exclude impurities during crystallisation³. Matrices such as CHCA and DHB were tested first because they are popular and have been shown to be useful matrices for low molecular weight compounds⁴⁻⁶. The matrix was selected according to the solubility of the matrix and analyte in similar solvents, the relative absence of interfering peaks in the spectral

regions of interest and reproducible analyte signal intensity from laser spot over the target (i.e. good crystal homogeneity). DHB was prepared as a 7 mg.mL^{-1} solution in methanol. Samples re-diluted in methanol were mixed with the matrix solution at a ratio of 1:1. The samples were run almost immediately after their dilution in methanol and mixing with the matrix, to avoid any possible esterification of free carboxyl groups². The sample/matrix mixtures were spotted ($\sim 1 \text{ }\mu\text{L}$ droplet) onto a stainless steel modified 25-well MALDI target and left to air dry. The instrument used was a fully automated LaserToF 1500 (Scientific Analytical Instrument, Manchester, UK), fitted with a N_2 laser and a linear time-of-flight mass analyser linked to a dedicated PC for data acquisition and manipulation of results. The accelerating voltage was 10 kV. The instrument was calibrated using angiotensin (Mw 1047, Sigma, UK). Only the positive mode was used in these investigations. The m/z range was generally 0-1000.

4.2.8 NMR analyses

Samples of glutaraldehyde (in distilled water, various pH buffers and at pH 1 and 11) were prepared by freeze-drying 3 x 25 mL of solution (0.6% v/v or 6% v/v glutaraldehyde solutions) and re-dissolved in 3 mL D_2O . A commercial unbuffered 25% v/v solution of glutaraldehyde in water (BDH, UK) was also analysed, without further preparation. When freeze-dried, the samples were immediately re-dissolved in D_2O and analysed. A Bruker (Bruker Biospin, USA) AC250 NMR spectrometer with an E field of 58000 Gauss was used to run ^1H (250 MHz), and ^{13}C (63 MHz) NMR analyses, whilst a Bruker (Bruker Biospin, USA) 400 spectrometer, with an E field of 92800 Gauss was used to run ^1H (400 MHz) and ^{13}C (100 MHz) NMR analyses.

4.3 Results and Discussion

4.3.1 ESI-MS

The analysis of an aqueous commercial solution of glutaraldehyde by ESI-MS yielded a complex mass spectrum that can be found in figure 4.2. The peaks appear as M and $[\text{M}+\text{H}]^+$ ions. Also, many structures appear with the addition of a sodium (Mw 23) or potassium (Mw 39) cation, for example $[\text{M}+\text{Na}]^+$, $[\text{M}+\text{K}]^+$, $[\text{M}+\text{Na}+\text{H}]^+$

and $[M+K+H]^+$. All possible molecules (based on prediction reaction pathways discussed in chapter 2), thought to be present in glutaraldehyde solutions can be found in appendix III, where the few molecules that have already been proposed in the literature are cross-referenced. The results obtained for the ESI-MS analysis of an aqueous commercial solution of glutaraldehyde (pH 3.8) are summarised in table 4.1 where only the m/z peak values are given beside their possible assignments and the corresponding molecular weight (the reader is invited to refer to the appendix III for structural details).

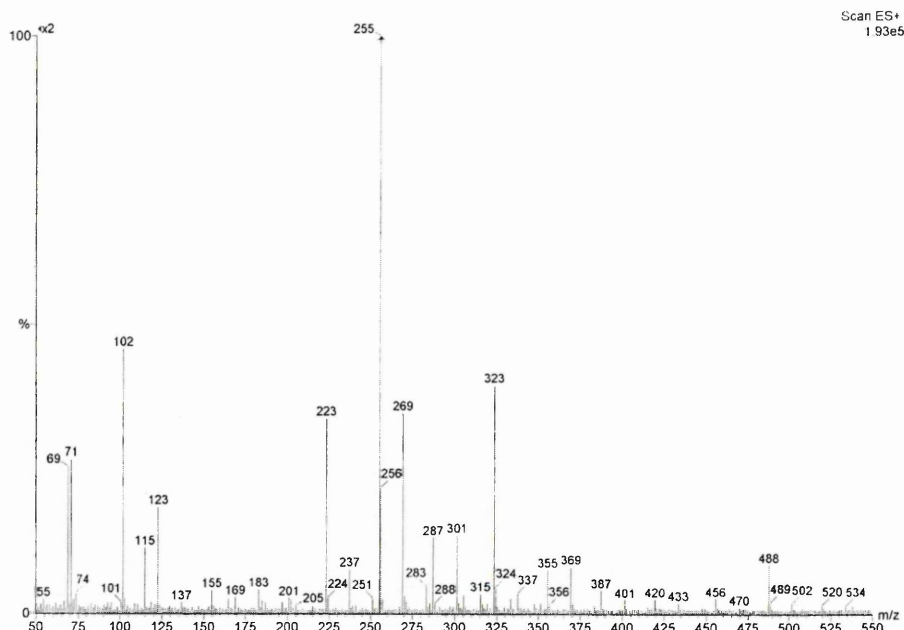


Figure 4.2: ESI-MS spectrum of unbuffered commercial aqueous solution of glutaraldehyde (pH 3.8), freeze-dried and re-dissolved in methanol. The inlet direct infusion of the sample was carried out at a rate of $5 \mu\text{L} \cdot \text{min}^{-1}$. The m/z range was 50-550.

The spectrum shows the likely presence of various molecules as shown in table 4.1. While, other hydrated forms of some of the proposed structures may also exist, but are not presented in table 4.1.

m/z	Proposed Assignment (Mw)	m/z	Proposed Assignment (Mw)
101/102	Mol I (100)	301	Mol IX (301); Mol XII (300); Mol XVIb (300); Mol XVIIb (300)
115	Mol XI (116)	305	Mol XVI (264+K); Mol XVIa (282+Na); Mol XVII (264+K); Mol XVIIa (282+Na); Mol XX (264+K); Mol XXXIII (282+Na); Mol XLV (264+K)

123	Mol I (100+Na)	323/324	Mol IX (301+Na); Mol XII (300+Na); Mol XVIa (282+K); Mol XVIb (300+Na); Mol XVIIa (282+K); Mol XVIIb (300+Na); Mol XXXIII (282+K)
137	Mol III (136)	333	Mol XXVII (310+Na)
155	Mol X (132+Na); Mol XI (116+K)	369/370	Mol XVIII (346+Na); Mol XXVI (328+K); Mol XLVII (346+Na); Mol L (328+K)
165	Mol XXIII (163)	387	Mol XVIII (346+K); Mol XVIIIa (364+Na); Mol XXXIV (364+Na); Mol XXXVII (364+Na); Mol XLVI (364+Na); Mol XLVII (346+K)
183/185	Mol XV (182); Mol XXXI (182); Mol XXXII (182)	401	Mol XVIIIc (400)
201/202	Mol VIIa (202); Mol VIII (202); Mol XVa (200); Mol XXIII (163+K)	420	Mol VII (418)
205	Mol XV (182+Na); Mol XXXI (182+Na); Mol XXXII (182+Na)	433	Mol XXVIII (410+Na); Mol XXIX (392+K)
223/224	Mol XV (182+K); Mol XVa (200+Na); Mol XXXI (182+K); Mol XXXII (182+K)	456/457	Mol VII (418+K)
251	Mol XXV (228+Na)	470	Mol XIXa (446+Na)
255/256	Mol V (218+K)	488/489	Mol XIXb (464+Na); Mol XXXV (464+Na); Mol XXXVI (464+Na); Mol XXXVIIIa (464+Na)
269	Mol XXIV (246+Na); Mol XXV (228+K)	502/503	Mol XIII (500); Mol XIXb (464+K); Mol XXXVI (464+K); Mol XIXd (500); Mol XXXV (464+K); Mol XXXVIIIa (464+K)
283	Mol XVIa (282); Mol XVIIa (282); Mol XXXIII (282)	520/521	Mol XXXVIIIb (482+K)
287/288	Mol XVI (264+Na); Mol XVII (264+Na); Mol XX (264+Na); Mol XXIV (246+K); Mol XLV (264+Na)		

Table 4.1: Proposed structures for the observed ions for the analysis of an aqueous solution of unbuffered glutaraldehyde in water (pH3.8) by ESI-MS.

The spectrum from the analysis of glutaraldehyde at pH 1 and at pH 11 can be found below respectively in figures 4.3 and 4.3. Some m/z values exhibited are similar to those seen in the spectrum of commercial glutaraldehyde (pH 3.8) (see figure 4.1).

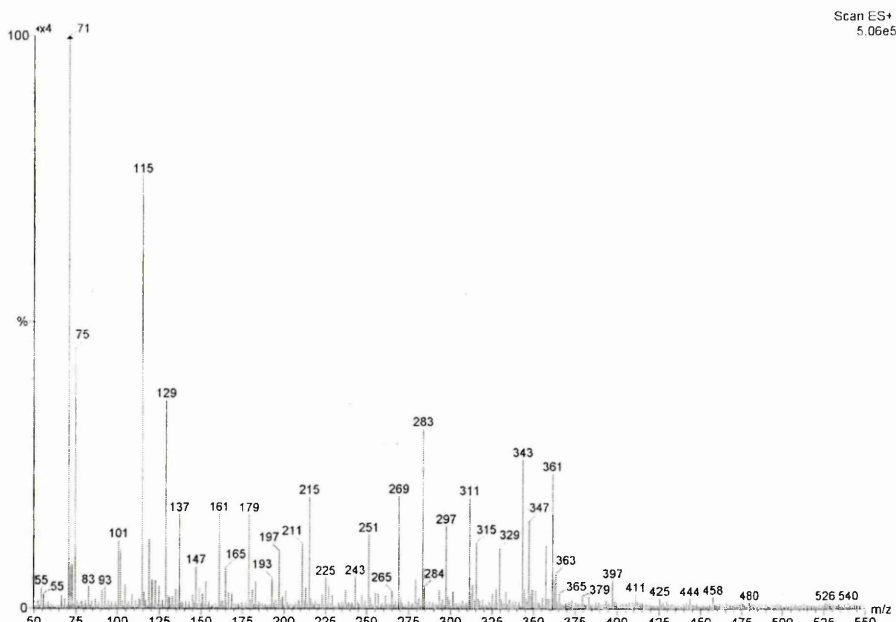


Figure 4.3: ESI-MS spectra of glutaraldehyde at pH 1 freeze-dried and re-dissolved in methanol. The inlet direct infusion of the sample was carried out at a rate of $5 \mu\text{L} \cdot \text{min}^{-1}$. The m/z range was 50-550.

There are corresponding peaks between the spectrum of glutaraldehyde at pH 1 and the one at pH 3.8 (water), but there are exceptions. The main exceptions are the presence, at pH 1, of new m/z peaks, corresponding to the possible presence of the following molecules (see appendix III):

Molecule II which is a mono-hydrated monomeric glutaraldehyde (mol I), the latter being present at pH 3.8; Molecule IV which is a cyclic hemiacetal monomer (dehydrated molecule III, being present at pH 3.8); Molecule VI which is a hemiacetal trimer, whilst its corresponding dimer (mol V) and monomer (mol IV) are both present at pH 3.8; Molecule XVIIIb which is a partially-hydrated aldol tetramer, whilst other corresponding hydrated tetramers products are present at pH 3.8 such as mol XVIII, XVIIIa and XVIIIc; Molecule XXX which is a fully-cyclised aldol pentamer, whilst its corresponding partially cyclised product is present at pH 3.8 (mol XXIX); Molecule XXXIVa which is a fully-hydrated aldol/Michael tetramer, whilst its corresponding non-hydrated product is present at pH 3.8 (mol XXXIV); Molecule XXXVIIa which is a fully-hydrated aldol/Michael tetramer, whose corresponding non-hydrated product (mol XXXVII) is present at pH 3.8 and mol XXXVIIa which is also an isomer of XXXIVa.

It thus appears that these above molecules, which are thought not to be present at pH 3.8 because of the absence of their corresponding m/z values in the spectrum, are in fact products formed by hydration/dehydration and/or cyclisation that are originating from parent compounds, whose presence was corroborated by mass spectrometric results of glutaraldehyde at pH 3.8. Thus, this does not rule out that the additional molecules, believed to be present at pH 1, could not also be formed at pH 3.8.

Another exception between the spectrum of glutaraldehyde at pH 1 and the one at pH 3.8 (water) is the absence of ions corresponding to the following molecules (see appendix III):

Molecule X (glutaric acid); Molecule XIII which is a trioxane-type pentamer, whilst its corresponding trimer (mol XII) exists at both pH 1 and 3.8; Molecule XIXb which is a partially-hydrated aldol pentamer; Molecule XIXd which is a fully-hydrated aldol pentamer; Molecule XXIX which is a partially-cyclised aldol pentamer, whilst its corresponding fully-cyclised product is present at pH 1; Molecule XXXV which is an aldol/Michael pentamer product; Molecule XXXVI which is an isomer of mol XXXV; Molecule XXXVIIIa which is a partially hydrated aldol/Michael pentamer product; Molecule XXXVIIIb which is a fully-hydrated aldol/Michael pentamer product.

It thus appears, from the above-list, that at pH 1 the formation of large aldol condensation products (with more than 4 glutaraldehyde monomers) and the formation of Michael addition products of aldol products seems to be inhibited in comparison to reactions taking place at pH 3.8.

M/z	Proposed assignment (Mw)	m/z	Proposed assignment (Mw)
101/102	Mol I (Mw 100)	302	Mol IX (301); Mol XII (300); Mol XVIb (300); Mol XVIIb (300)
118	Mol II (118); Mol IV (118); Mol XI (116)	311/313	Mol XXVII (310)
123/125	Mol I (100+Na)	325/327/ 329/333	Mol IX (301+Na); Mol XII (300+Na); Mol XVIb (300+Na); Mol XVIIb (300+Na); Mol XXVI (328); Mol XXVII (310+Na); Mol L (328)

136	Mol III (136)	343	Mol VI (318+Na)
161	Mol III (136+Na)	347/349	Mol XVIII (346); Mol XXVII (310+K); Mol XLVII (346)
163	Mol XXIII (163)	358	Mol VI (264+K)
184	Mol XV (182); Mol XXXI (182); Mol XXXII (182)	365	Mol XVIIIa (364); Mol XXXIV (364); Mol XXXVII (364); Mol XLVI (364)
201	Mol XVa (200)	384	Mol XXXVIIa (382); Mol XVIIIb (382); Mol XXXIVa (382)
223/225 /227	Mol VIIa (202+Na); Mol VIII (202+Na); Mol XVa (200+Na); Mol XV (182+K); Mol XXXII (182+K)	397	Mol XXX (374+Na)
243	Mol V (218+Na); Mol VIIa (202+K); Mol VIII (202+K)	411	Mol XXVIII (410)
251	Mol XXV (228+Na)	425	Mol XVIIIc (400+Na)
265	Mol XVI (264); Mol XVII (264); Mol XX (264); Mol XLV (264)	444	Mol VII (418+Na)
269	Mol XXIV (246+Na); Mol XXV (228+K)	458	Mol VII (418+K)
283	Mol XXXIII (282); Mol XVIa (282); Mol XVIIa (282)		

Table 4.2: Proposed structures for the observed ions for the analysis by ESI-MS of an aqueous solution of glutaraldehyde with an adjustment of pH to pH 1 by addition of HCl (see appendix III for details of structures).

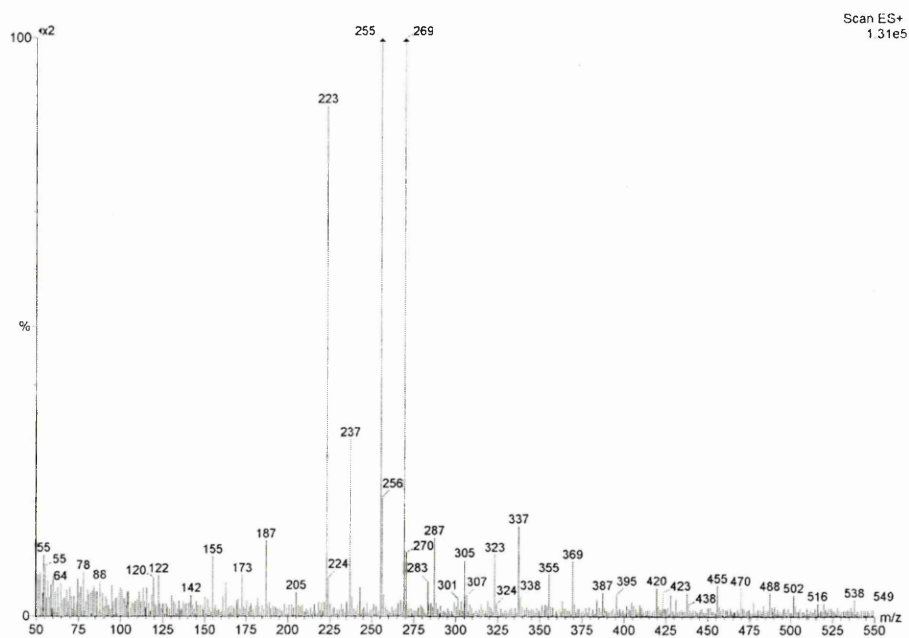


Figure 4.4: ESI-MS spectrum of glutaraldehyde at pH 11, freeze-dried and re-dissolved in methanol. The inlet direct infusion of the sample was carried out at a rate of $5 \mu\text{L}\cdot\text{min}^{-1}$. The m/z range was 50-550.

From figure 4.4 and table 4.3, one can see that the solution of glutaraldehyde at pH 11 contains many chemical structures that are similar to those found at pH 3.8. However there are some molecules that are apparently present at pH 11 which were not seen in the analysis of glutaraldehyde at pH 3.8. These include the following molecules:

Molecules II which is a glutaraldehyde monohydrate being also present at pH 1; Molecule IV which is a cyclic hemiacetal being also present at pH 1, whilst the corresponding dihydrate (mol III) can be found at pH 1, pH 3.8 and pH 11; Molecule VI which is a hemiacetal trimer being also present at pH 1, whilst both corresponding dimer (mol V) and tetramer (mol VII) are present at pH 1, pH 3.8 and pH 11; Molecule XVIIIb which is a partially hydrated tetramer aldol product being also present at pH 1, whilst the same aldol product -more or less hydrated- (mol XVIIIa and XVIIIc) can be found at pH 1, pH 3.8 and pH 11; Molecule XIXc which is a partially hydrated pentamer aldol product, whilst the same aldol product -more or less hydrated- (mol XIXb and mol XIXd) can be found at pH 3.8 and pH 11; Molecule XXXIVa which is a fully hydrated aldol/Michael pentamer being also present at pH 1, whilst the corresponding non-hydrated product (XXXIV) is present at pH 1, pH 3.8 and pH 11; Molecule XXXVIIa which is a fully hydrated aldol/Michael pentamer being also present at pH 1, whilst the corresponding non-hydrated product (XXXVII) is present at pH 1, pH 3.8 and pH 11; Molecule XXXVIII which is an aldol/Michael pentamer, whilst the corresponding hydrated product (mol XXXVIIIa) is present at pH 3.8 and pH 11; Molecule XLVIII which is an aldol/Michael cyclised hexamer and Molecule LI which is an aldol/Michael cyclised hexamer.

It thus appears that these above molecules, which are thought not to be present at pH 11 because of the absence of their corresponding m/z values in the spectrum, are in fact products formed by either hydration/dehydration and/or further reaction (particularly through Michael addition) that are originating from parent compounds, whose presence was corroborated by mass spectrometric results of glutaraldehyde at

pH 11. Thus, this does not rule out the possibility that these molecules could not also be formed at pH 11.

In contrast, some molecular structures appear not to be present at pH 11 in comparison to pH 3.8, for example molecules XXVII which is an aldol tetramer fully cyclised whilst the corresponding partially cyclised product (mol XXVI) is present at pH 1, pH 3.8 and pH 11; Molecule XXVIII which is an aldol pentamer partially cyclised whilst the corresponding further-cyclised molecule (mol XXIX) is present at pH 3.8 and pH 11.

In addition, it is worth noting that at high pH (and particularly in the presence of sodium hydroxide) there is a great likelihood that Cannizzaro reactions would take place^{7,8}, affecting the resultant spectra by turning the pendant aldehyde groups into primary alcohol and carboxyl groups. Such Cannizzaro products are not represented below in table 4.3, except by molecules XXI and XXII (see appendix III for detailed structures).

M/z	Proposed assignment (Mw)	M/z	Proposed assignment (Mw)
100/101	Mol I (Mw 100)	305/307	Mol XVI (264+K); Mol XVIa (282+Na); Mol XVII (264+K); Mol XVIIa (282+Na); Mol XX (264+K); Mol XXI (266+K); Mol XXXIII (282+Na); Mol XLV (264+K)
120/122	Mol II (118); Mol IV (118)	319	Mol VI (318)
132	Mol X (132)	323/324	Mol IX (301+Na); Mol XII (300+Na); Mol XVIa (282+K); Mol XVIIb (300+Na); Mol XVIIa (282+K); Mol XVIIb (382+Na); Mol XXXIII (282+K)
142	Mol II (118); Mol IV (118+Na)	353/355	Mol L (328+Na); Mol XXVI (328+Na)
155	Mol XI (116+K); Mol X (132+Na)	369/370	Mol XVIII (346+Na); Mol XXXIV (364+K); Mol XLVII (346+Na); Mol L (328+K)
161/163	Mol III (136+Na); Mol XXIII (163)	383	Mol XVIIIb (382); Mol XXXIVa (382); Mol XXXVIIa (382)
173	Mol X (132+K)	387	Mol XVIII (346+K); Mol XVIIIa (364+Na); Mol XXXIV (364+Na); Mol XXXVII (364+Na); Mol XLVI (364+Na); Mol XLVII (346+K)

183	Mol XV (182); Mol XXXI (182); Mol XXXII (182)	395	Mol XXIX (392)
187	Mol XXIII (163+Na)	402	Mol XVIIIc (400)
205	Mol XV (182+Na); Mol XXXI (182+Na); Mol XXXII (182+Na)	404/406	Mol XVIIIa (364+K); Mol XVIIIb (382+Na); Mol XXXIV (364+K); Mol XXXIVa (382+Na); Mol XXXVII (364+K); Mol XXXVIIa (382+Na); Mol XLVI (364+K)
223/224	Mol XV (182+K); Mol XVa (200+Na); Mol XXXI (182+K)	420	Mol VII (418)
243	Mol V (218+Na); Mol VIIa (202+K); Mol VIII (202+K)	423	Mol XVIIIb (382+K); Mol XVIIIc (400+Na); Mol XXXIVa (382+K); Mol XXXVIIa (382+K)
255/257	Mol V (218+K)	455/457	Mol VII (418+K)
269	Mol XXIV (246+Na); Mol XXV (228+K)	470	Mol XIXa (446+Na); Mol XXXVIII (446+Na); Mol XLVIII (446+Na); Mol LI (428+K)
283	Mol XVIa (282); Mol VIIa (282); Mol XXXIII (282)	483	Mol XIXc (482); Mol XXXVIIIb (482)
287	Mol XVI (264+Na); Mol XVII (264+Na); Mol XX (264+Na); Mol XXIV (246+K); Mol XLV (264+Na)	488/489	Mol XIXa (446+K); Mol XIXb (464+Na); XXXV (464+Na); Mol XXXVI (464+Na); Mol XXXVIII (446+K); Mol XXXVIIIa (464+Na); Mol XLVIII (446+K)
301/303	Mol IX (301); Mol XII (300); Mol XVIb (300); Mol XVIIb (300); Mol XXII (302)	502	Mol XIII (500); Mol XIXd (500)

Table 4.3: Proposed structures for the observed ions for the analysis by ESI-MS of an aqueous solution of glutaraldehyde with an adjustment of pH to pH 11 by addition of NaOH (detailed structures can be found in appendix III).

4.3.2 MALDI-TOF MS

The MALDI-TOF MS data obtained from the glutaraldehyde solutions at various pH values (pH 3.8-9.2) exhibited spectra very similar to each other and are shown below in figure 4.5. The characteristic ions were quite similar to those shown in table 4.1 (above) with the ions being mostly attributable to protonated molecules such as $[M+H]^+$ and adduct ions such as $[M+Na]^+$, $[M+K]^+$, $[M+Na+H]^+$ and $[M+K+H]^+$. However, although the use of MALDI also allowed the analysis of solutions containing buffers (pH 4, 7.4, and 9.2), the spectral quality was less than that obtained with ESI-MS, which was to be expected.

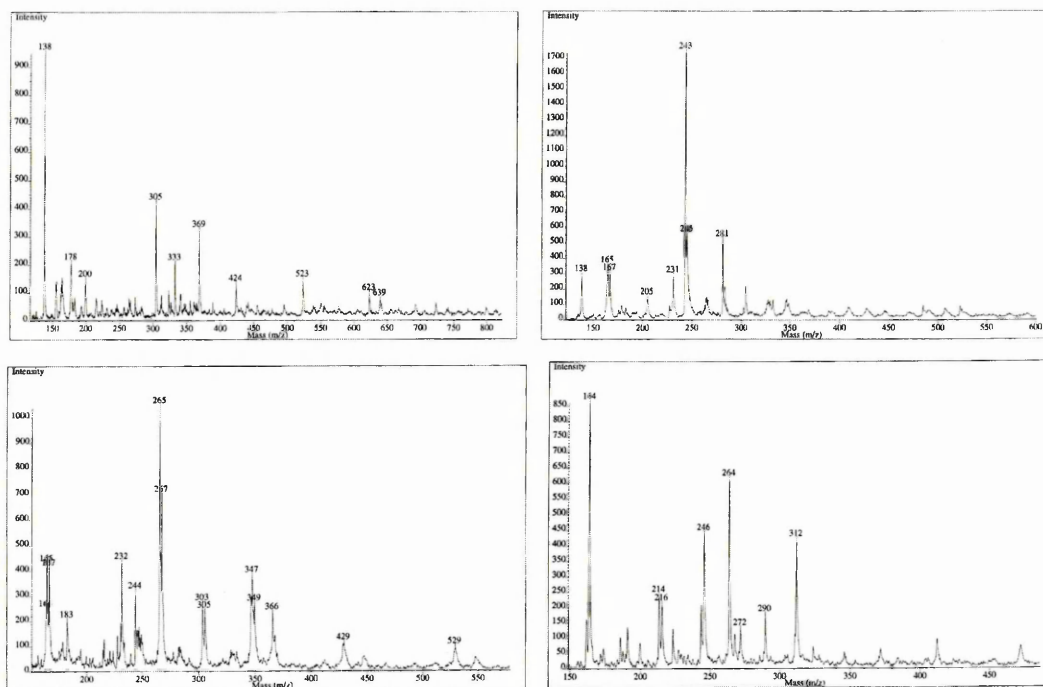


Figure 4.5: Examples of MALDI-TOF MS spectra obtained from the analysis of glutaraldehyde at various pH values: unbuffered commercial glutaraldehyde solution at pH 3.8 (*top left*), glutaraldehyde at pH 4 (*top right*), glutaraldehyde at pH 7.4 (*bottom left*) and glutaraldehyde at pH 9.2 (*bottom right*). All solutions were freeze-dried and re-dissolved in methanol. The matrix (DHB) was prepared as a 7 mg.mL^{-1} solution in methanol. Samples re-diluted in methanol were mixed with the matrix solution at a ratio of 1:1.

The MALDI-TOF MS results (see figure 4.5) show that there is some differences in spectra, which implies that glutaraldehyde is affected by pH. Nonetheless, it seems that the m/z values of the ions seen in the spectra from glutaraldehyde at various pH values (3.8-9.2) appear virtually identical, which indicates that similar molecules are formed in this pH range. The summary of such results obtained from the analysis of glutaraldehyde in pH range 3.8-9.2 by MALDI-TOF MS can be found below in table 4.4 (please refer to appendix III for the structures of the various molecules). These findings do not, however, rule out the possibility that different molecules, not yet assigned in this work, with very similar molecular weights may form at different pH values.

The MALDI-TOF MS results from glutaraldehyde in solution (over a wide pH range) indicate that species containing a maximum of eight molecules of

glutaraldehyde could be found in solution possibly in the form of an aldol condensation/Michael addition reaction product (see molecule XLIII with Mw 728 in appendix III). The largest aldol condensation product of glutaraldehyde detected involved a maximum of five molecules of glutaraldehyde (see molecule XIX with Mw 428 in appendix III). The presence of cyclic hemiacetals was also detected with a maximum of four glutaraldehyde molecules (see molecule VII with Mw 418 in appendix III).

The absence of molecule I (monomeric glutaraldehyde with Mw 100) in the MALDI data is in agreement with others who stated that no monoaldehyde was identified in the analysis of aqueous unbuffered glutaraldehyde by GC-MS⁹. However, the other conclusion to be drawn is that the MALDI-TOF MS methodology does not allow the correct analysis of molecules with a molecular weight in the vicinity of m/z 100, since its presence was detected by ESI-MS analysis of aqueous unbuffered glutaraldehyde.

Molecules	H ₂ O	pH 4	pH 7.4	pH 9.2	Molecules	H ₂ O	pH 4	pH 7.4	pH 9.2
Mol I				x	Mol XIXb		x		
Mol II	x	x	x	x	Mol XIXc	x	x		x
Mol III	x	x		x	Mol XIXd	x	x		x
Mol IV	x	x	x	x	Mol XX	x	x	x	x
Mol V	x	x	x	x	Mol XXIII	x	x	x	
Mol VI	x			x	Mol XXIV	x	x	x	x
Mol VII	x				Mol XXV	x	x	x	
Mol VIIa	x	x	x	x	Mol XXVI	x	x	x	x
Mol VIII	x	x	x	x	Mol XXVII	x	x	x	x
Mol IX	x		x	x	Mol XXXI	x	x	x	x

Mol X	x	x	x	x	Mol XXXII	x	x	x	x
Mol XI	x	x	x	x	Mol XXXIII	x	x	x	x
Mol XII	x			x	Mol XXXIV	x		x	
Mol XIII	x	x		x	Mol XXXV		x		
Mol XV	x	x	x	x	Mol XXXVI		x		
Mol XVa	x	x	x	x	Mol XXXVII	x		x	
Mol XVI	x	x	x	x	Mol XXXVIII		x	x	
Mol XVIa	x	x	x	x	Mol XXXVIIIa		x		
Mol XVIb	x			x	Mol XXXVIIIb	x	x		x
Mol XVII	x	x	x	x	Mol XLI			x	
Mol XVIIa	x	x	x	x	Mol XLV	x	x	x	x
Mol XVIIb	x			x	Mol XLVI	x		x	
Mol XVIII	x	x	x	x	Mol XLVII	x	x	x	x
Mol XVIIIa	x		x		Mol XLIX	x		x	
Mol XVIIIc	x				Mol L	x	x	x	x
Mol XIX		x	x		Mol LI		x	x	
Mol XIXa		x	x		Mol LII			x	

Table 4.4: Proposed structures for the observed ions for the analysis of an aqueous solution of glutaraldehyde solution at various pH values (pH 3.8, pH 4, pH 7.4 and pH 9.2) by MALDI-TOF MS. The data given only indicates the presence or not (represented by a cross) of molecules according to their m/z found present in relevant spectra. The structure of the molecules referred to can be found in appendix III.

4.3.3 NMR

4.3.3.1 ^1H NMR:

Some researchers have already analysed glutaraldehyde in D_2O using ^1H NMR^{10,11}. A similar experimental procedure was followed because glutaraldehyde is supplied as an aqueous solution and cross-linking with proteins is also carried out in aqueous media. As the use of anhydrous solvents might shift or change the equilibrium of the species present in glutaraldehyde solutions, freeze-drying followed by reconstitution in D_2O was used in virtually all our studies. The exception was an initial experiment where a proton NMR spectrum was measured on the sample as it was obtained in unbuffered aqueous solution, even though the water absorption obscured a part of the spectrum (50% D_2O and 50% aqueous glutaraldehyde solution). There were two main reasons for doing this. First it was our desire to examine the reagent without any alteration to it, and secondly, it was felt that changing the solvent to deuterium oxide might not only cause an exchange of deuterium for hydrogen bonded to oxygen but also for hydrogen bonded to carbon in the α -positions of glutaraldehyde. In fact, after having freeze-dried and re-dissolved the commercial solution of glutaraldehyde in a few millilitres of D_2O , the ^1H NMR spectrum obtained was the same (results not shown) and no such effects as the ones cited above seemed to have altered the spectrum. The freeze-drying process thus did not alter the spectra obtained.

The proton NMR spectrum of a commercial unbuffered glutaraldehyde solution (pH 3.8) in water (see figure 4.6 below) exhibited some well-defined peaks and also some very broad unresolved and overlapping peaks. The latter are characteristic of the abundance of molecular structures containing similarities, which result in the broad aspect of the major regions.

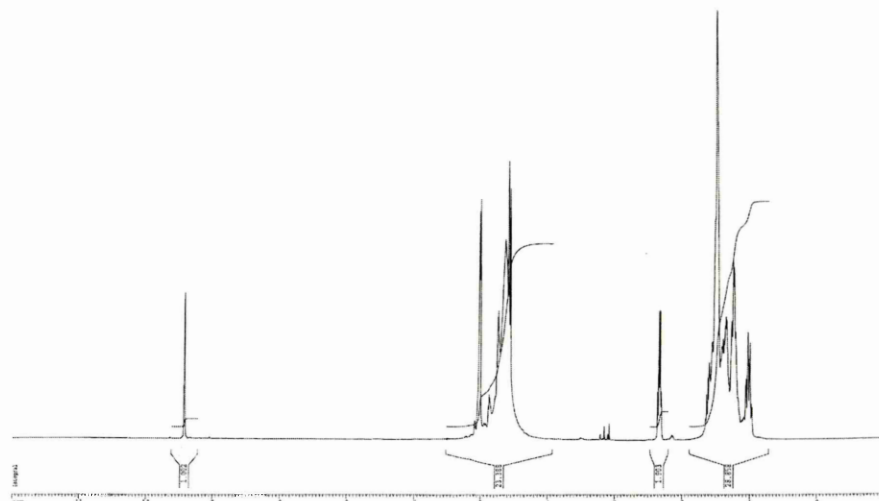


Figure 4.6: ^1H NMR of a commercial unbuffered glutaraldehyde solution (0.6% v/v) in water (pH 3.8), freeze-dried and re-dissolved in D_2O .

The broad peaks rendered a tentative assignment of the peaks extremely difficult and the ^1H NMR spectra obtained were mostly used to support the findings obtained by ^{13}C NMR. However, some conclusions could be drawn and the major finding, from the above spectrum, was the absence of aldol condensation products (α,β -unsaturated structures) expected in the 6-8 ppm region. This is in agreement with Kawahara et al¹², who stated that the concentration of these unsaturated structures was negligible between pH 2 and 8, which is almost the pH range studied here. Their presence at low concentrations is not fully precluded, however, as they might be below the level of detection of the NMR instrument. Furthermore, the mass spectrometric data (presented in sections 4.3.1 and 4.3.2) exhibit the possible presence of such unsaturated molecular structures, based on their m/z values.

The spectrum also shows the likely presence of exchangeable hydroxyl protons, along with methylene and central methylene protons represented by the broad absorption centred at 1.6 ppm, with some partially separated multiplets on both the down- and up-field sides. We can also identify the possible presence of groups (with α -methylene) such as $-\text{C}-\underline{\text{CH}}_2-\text{C}=\text{C}-$, $-\text{C}-\underline{\text{CH}}_2-\text{CO}-\text{R}$, $-\text{C}-\underline{\text{CH}}_2-\text{C}=\text{C}-\text{CO}$, $-\text{C}=\text{C}(\underline{\text{CH}}_2)-\text{CO}$ around 2.4 ppm, other groups such as $-\text{C}-\underline{\text{CH}}_2-\text{OH}$ and $-\text{C}-\underline{\text{CH}}_2-\text{OR}$ around 3.1-3.3 ppm, along with $-\text{C}=\underline{\text{CH}}-$, $-\underline{\text{CH}}=\text{CO}$, hydroxyl and hydrated aldehyde protons¹³ in the 4.5-5.2 ppm region. The strong doublet signal at ca. 5.00 ppm can be assigned¹⁴

to acetol and acetal protons absorbing at different places because of the different chemical species involved, along with the possible existence of cis and trans geometrical acetal isomerism¹⁵ and aldehyde protons around 9.4 ppm. The ¹H NMR spectra obtained from the same unbuffered commercial (25% v/v) solution of glutaraldehyde at pH 3.8, freeze-dried and re-dissolved in D₂O, confirmed the above results.

NMR spectra obtained from glutaraldehyde at pH 4, pH 7.4 and pH 9.2 appear different (see figure 4.7 below) to each another indicating a pH dependence. It would appear, however, that a similar class of material is producing a NMR pattern at the same position, thus indicating that structures with similar reacting groups are formed over this pH range (4-9.2). It is believed that many molecules assigned for the analysis of unbuffered glutaraldehyde at pH 3.8 would also be present in glutaraldehyde solutions under the pH range analysed (pH 4-9.2), which is backing up our data obtained from MALDI-TOF MS analysis of glutaraldehyde solutions under a similar pH range.

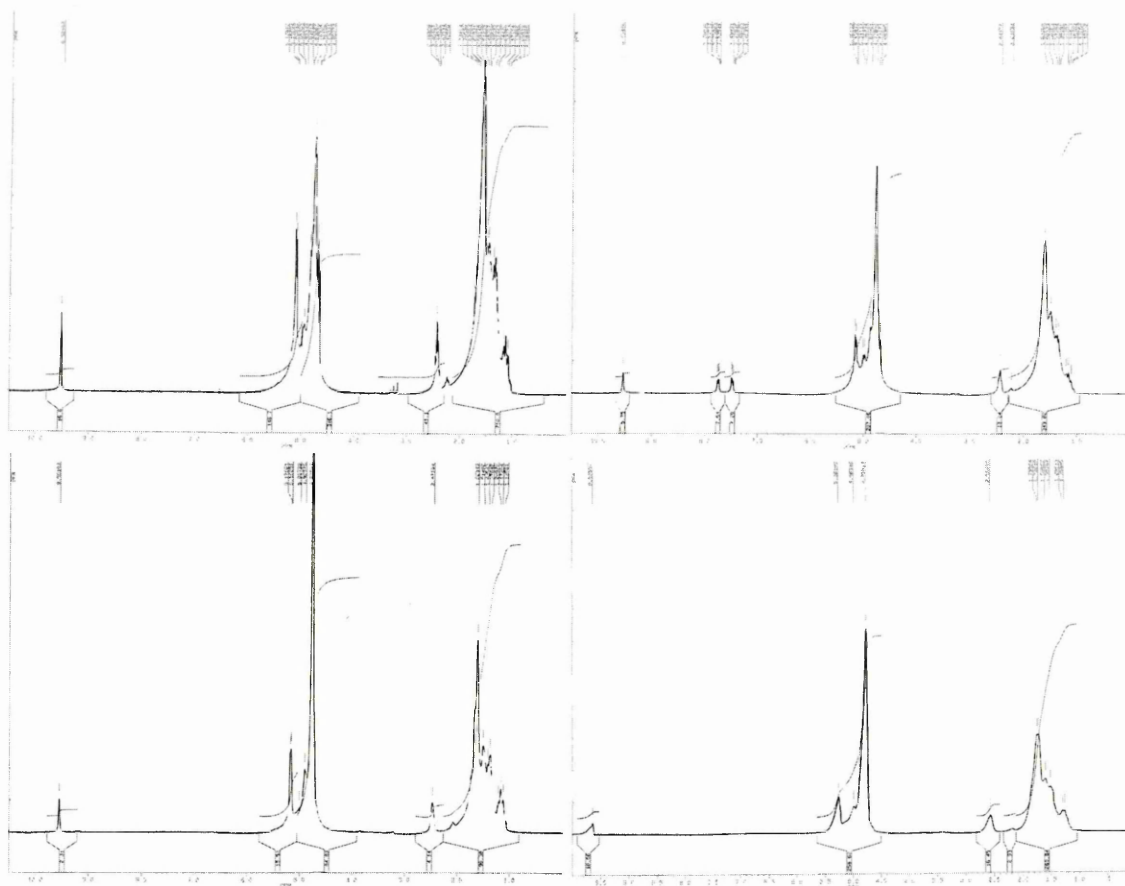


Figure 4.7: ^1H NMR of glutaraldehyde at various pH values: unbuffered commercial glutaraldehyde solution at pH 3.8 (*top left*), glutaraldehyde at pH 4 (*top right*), glutaraldehyde at pH 7.4 (*bottom left*) and glutaraldehyde at pH 9.2 (*bottom right*). All solutions were freeze-dried and re-dissolved in D_2O .

The ^1H NMR spectra obtained from glutaraldehyde at pH 1 and pH 11 are of greater interest (see figures 4.8 and 4.9 below). Both spectra obtained at pH 1 and 11 are extremely different from each other, more so when compared to the spectra obtained at pH 3.8-9.2, especially in the 8-10 ppm region. This reveals a strong influence of pH on the behaviour of glutaraldehyde solution, especially at extreme pH values.

The spectra both show some alkene protons ($\text{C}=\underline{\text{CH}}-\text{CO}$, $\underline{\text{CH}}=\text{C}-\text{CO}$) around 6.4-6.8 ppm, while no traces of alkenes were apparently visible in the ^1H NMR spectra obtained from glutaraldehyde at the pH range 3.8-9.2. The spectrum at pH 1 shows an intense peak at 8.1 ppm, which could be assigned to the presence of $-\underline{\text{CH}}(\text{OH})-\text{O}-\text{C}$ or $-\underline{\text{CH}}(=\text{O})-\text{O}-\text{C}-$, along with many aldehyde bands, indicating the presence of many different environments of these carbonyl protons. The spectrum obtained at pH 11 is quite similar to the one obtained at pH 3.8 in the 0.8-1.8 ppm and 4.4-5.4 ppm regions, while major changes occur in the 2.0-4.0 ppm region where extra peaks appear such as the triplet around 2 ppm and more intense and resolved peaks between 3.2-4.0 ppm. It is also worth noting that the signals of hydrated aldehyde protons and of the olefinic protons of hypothetical aldol condensates can be hidden behind the water/OH signal¹⁶. In addition, more intense and resolved aldehyde peaks appear in the 9.10-9.93 ppm region. These peaks were barely noticeable in the spectrum obtained at pH 3.8. Overall, this could indicate that the formation of similar chemical structures took place at these extreme pH values but with different ratios.

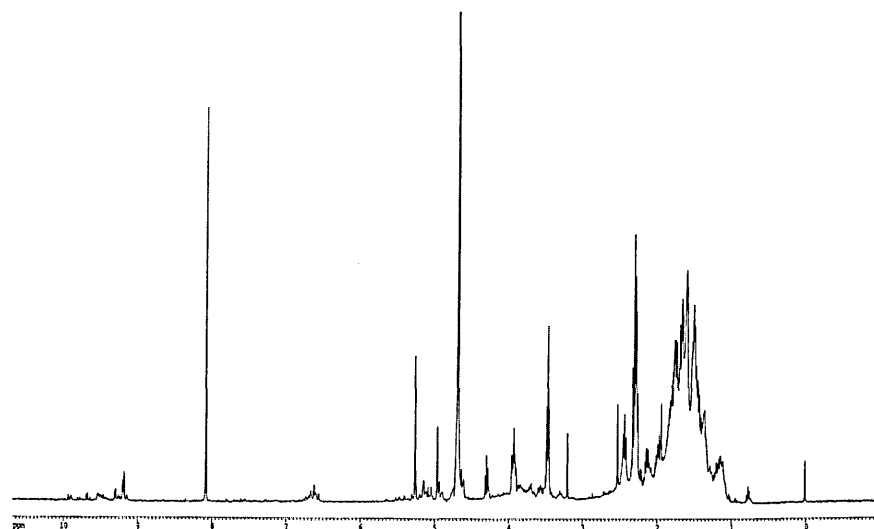


Figure 4.8: ^1H NMR spectra of glutaraldehyde solution at pH 1, freeze-dried and re-dissolved in D_2O .

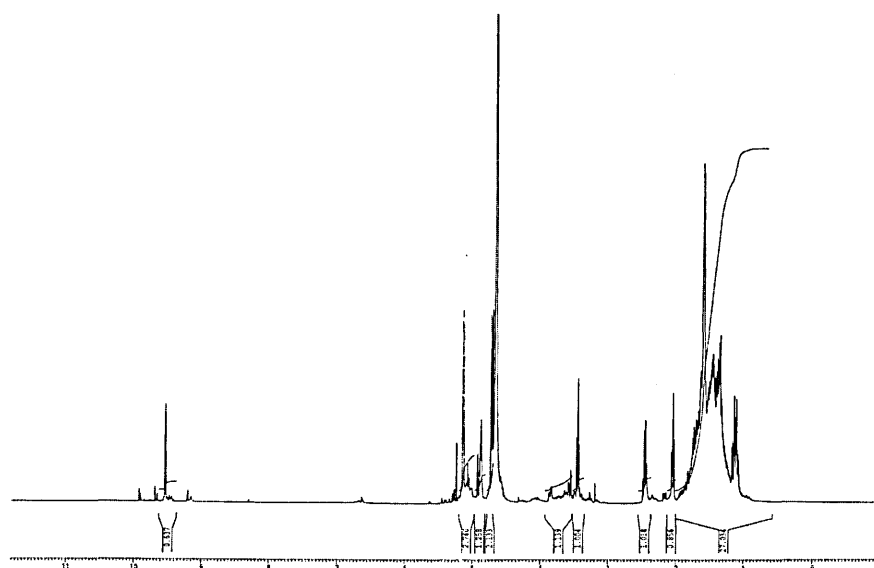


Figure 4.9: ^1H NMR spectra of glutaraldehyde solution at pH 11, freeze-dried and re-dissolved in D_2O .

4.3.3.2 ^{13}C NMR:

4.3.3.2.1 ^{13}C NMR analyses of glutaraldehyde at pH 3.8-9.2 range:

It has been reported that direct comparison of the peak intensities is not quantitative in ^{13}C NMR¹⁷. No quantification was carried out in this study, although others have attempted this¹⁴, and found that an aqueous glutaraldehyde solution (pH 3.5-4)

contained approximately 4% monomeric glutaraldehyde (mol I), 16% of the monohydrate (mol II), 9% of the dihydrate (mol III) and around 71% of the monomeric hemiacetal (cis (mol IVa) and trans (mol IVb) isomers). They also tried to assign the ^{13}C NMR (22.63 MHz) spectrum by considering only the presence of the above-cited compounds. In this work, detailed correlation tables and CS CHEMNMR prediction software (Upstream solution GmbH scientific software engineering, Hergiswil, Switzerland), which has been tested with known standards, were used to tentatively assign some of the ^{13}C NMR peaks by considering a much wider variety of possible molecular structures (see appendix III) that are thought to be present in glutaraldehyde solutions rather than those reported previously in the literature.

The ^{13}C NMR spectra of glutaraldehyde in the range of pH 3.8-9.2 appear very similar, although their corresponding ^1H NMR spectra appeared different one to another. Typical ^{13}C spectra of glutaraldehyde at various pH values, representative of the spectra obtained in this pH range, can be found in figure 4.10 below.

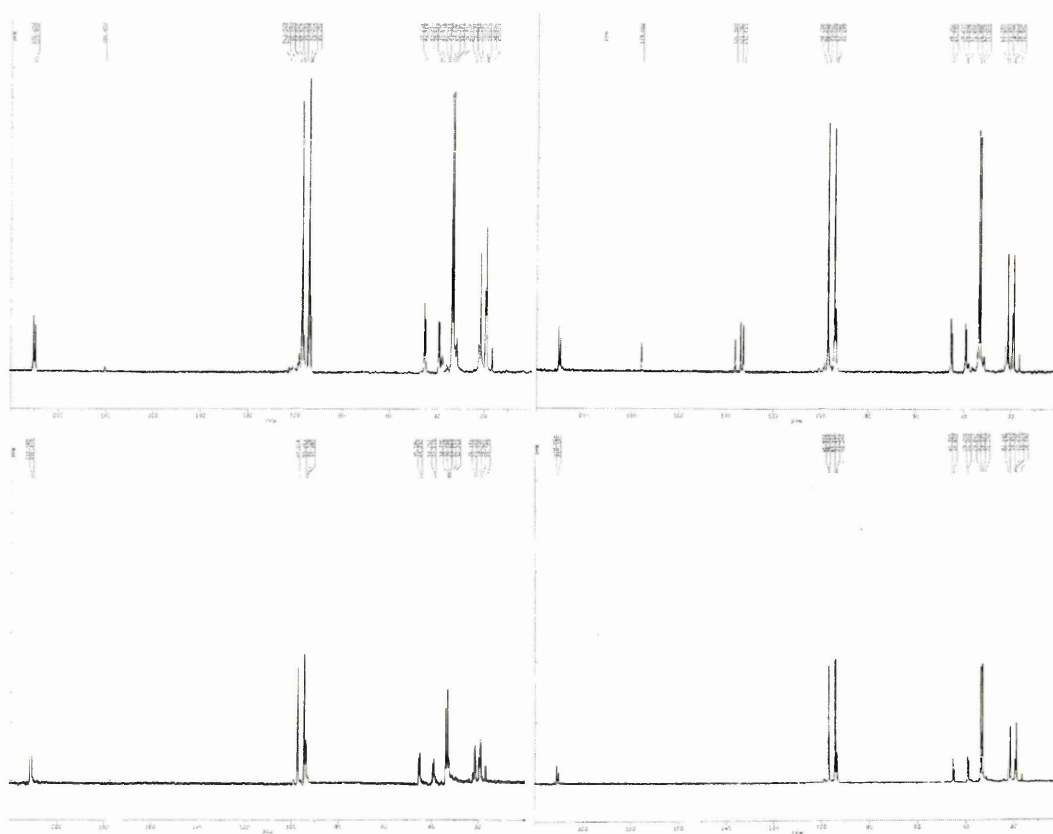


Figure 4.10: ^{13}C NMR of glutaraldehyde at various pH values: unbuffered commercial glutaraldehyde solution at pH 3.8 (*top left*), glutaraldehyde at pH 4 (*top*

right), glutaraldehyde at pH 7.4 (bottom left) and glutaraldehyde at pH 9.2 (bottom right). All solutions were freeze-dried and re-dissolved in D₂O.

The line assignment is shown below in table 4.5, with the structure of the molecules referred to being found in appendix III.

Peak position (ppm)	Proposed assignment
1 signal at 13.43	Molecules I; XII; XIII; XIV
4 signals at 15.81-16.35	Molecules II; III; IVa; V; VI; VII
5 signals at 17.91-19.11	Molecules IVb; V; VI
9 signals at 28.01, 28.04, 28.27, 28.43, 29.16, 29.50, 29.83, 30.34 and 30.53	Molecules IVa; IVb; V; VI; XIII; XIV
5 signals at 34.17, 34.68, 35.18, 35.78 and 36.18	Molecules II; III; VII; XII; XIII; XIV
2 signals at 41.67 and 42.18	Molecules I; II; XII; XIII; XIV
5 signals 90.14, 90.39, 90.56, 90.63 and 90.89	Molecules II; III; IVb; V; VI; VII
10 signals at 91.13, 91.36, 91.64, 93.26, 93.71, 94.06, 94.12, 95.12, 95.81 and 97.52	Molecules IVb; V; VI; XII; XIII; XIV
3 signals at 206.56, 207.18 and 207.32	Molecules I; II; XII; XIII; XIV

Table 4.5: Line assignment along with the proposed corresponding assignment of a ¹³C NMR spectrum of an aqueous commercial solution of glutaraldehyde (pH 3.8) (structure of the molecules referred to being found in appendix III).

Some studies have reported the ¹³C chemical shifts for the carbonyl carbon in a variety of organic compounds, such as aldehydes and carboxylic acids¹⁸, and hence it is possible to differentiate between the resonance of carbonyl carbons of conjugated aldehydes and non-conjugated aldehydes. The resonances of conjugated aldehydes are shifted by ca. 10 ppm to higher field than those in the saturated compounds and this shielding effect is comparable for α,β -unsaturated and aromatic systems¹⁹. Additionally, free carboxylic acids exhibit the carboxyl carbon resonance peak at a somewhat higher field than aldehydes (i.e. 9-20 ppm). Therefore, in the spectrum of glutaraldehyde in water at pH 3.8, only some saturated aldehyde carbon peaks seem to appear (see above table 4.5). No unsaturated aldehyde carbons or carboxylic acid carbons can be noticed in the spectrum, although their presence can not be precluded since their characteristic signals may be below the level of detection of the instrument.

The presence of aldol condensation products (for example, molecules XV, XVI, XVII, XVIII, XIX and XX) and also the aldol/Michael condensation products containing double bonds (such as molecules XXXIV, XXXVII, XXXVIII, XXXIX and XLI), are also excluded because of the absence of signal around 100-160 ppm, which is characteristic of alkenes or deshielded carbon in the neighbourhood of carbonyl (~50 ppm) in the ^{13}C NMR spectrum. This is supported by the absence of signal in the appropriate region of the ^1H NMR spectrum.

The results also indicate the absence of some unsaturated aldol and some unsaturated aldol/Michael condensation products that have not undergone a systematic dehydration step (for example, molecules XVIa, XVIIa, XVIIIa, XVIIIb, XIXa, XIXb, XIXc, XXXVIIIa, XLIa, XLIIb and XLIIa) because of the absence of deshielded carbons in the 55-65 ppm region and of ethylenic carbons. The presence of similar saturated structures (all dehydration steps of the aldol condensations did not take place) is also not confirmed due to the absence of deshielded carbons signals. Such structures would have been for example molecules XVa, XVIb, XVIIb, XVIIIc, XIXd, XXXIVa, XXXVIIa, XXXVIIIb, XXXIXa, XLIIc and XLIIa.

The presence of dimers (e.g. molecules XXXI and XXXII), formed by a dimolecular aldol condensation, is excluded because of the absence of signal due to conjugated aldehyde (around 190 ppm) and especially because of the absence of signal from the conjugated ethylenic bonds in the 120-150 ppm region. To corroborate this, the ^1H NMR spectrum does not show any signal between 1.75 and 1.95 ppm corresponding to the deshielded proton near the OH for molecule XXXI (or near the C-O-C for molecule XXXII) and the conjugated double bonds of the molecule, whilst the proton characteristic of the ethylenic double bond (~6.50 ppm) is also absent.

The presence of cyclised aldol condensation products, (such as molecules XXIII, XXIV, XXV, XXVI, XXVII, XXVIII, XXIX, XXX, XLV, XLVII, XLVIII, L), along with partially cyclised aldol condensation unsaturated products having carried out Michael addition (such as molecules LI, LII) is also unlikely because of the absence of signal from the conjugated ethylenic double bond in the 140-150 ppm region and around 45-55 ppm in the ^{13}C spectra. This is also supported by the absence, in the ^1H spectra, of signals around 1.75-1.95 ppm. Saturated partially

cyclised aldol condensation products having carried out Michael additions (e.g. molecules XLVI, XLIX) are also deemed to be absent because of the absence of signal around 45-55 ppm, in the ^{13}C spectra and to the absence of signals around 1.70-1.90 ppm, in the ^1H spectra.

The presence of (saturated) molecules formed by Michael addition on aldol condensation products (for example, molecules XXXIII, XXXV and XXXVI) is also excluded because of the absence of characteristic signals around 50-55 ppm.

Furthermore, molecules such as VIIa, VIII and IX are thought not to be present because of the absence of NMR signals at 62-67 ppm (deshielded carbon $\text{C}-\underline{\text{C}}-\text{OH}$ and/or $\text{C}-\underline{\text{C}}-\text{O}-$). This is supported by the absence of signal around 170 ppm corresponding to $-\text{O}-\underline{\text{C}}(=\text{O})-\text{C}-$, in the ^{13}C NMR spectra, along with the absence of signals in the ^1H NMR spectra at 4 ppm ($\text{CH}_2-\underline{\text{CH}}_2-\text{O}-$), which are expected to be seen from molecules VIII and IX.

Additionally, the presence of glutaric acid (molecule X) and the monoacid form of glutaraldehyde (molecule XI) are also rather excluded because of the absence of signal from carboxylic carbon in the 165-185 ppm region. However the ^1H NMR spectrum alone could not provide enough information regarding their non-existence.

One must, however, keep in mind that the presence of all the above-mentioned structures cannot be categorically ruled out, as they may be present at very low concentrations and hence be below the detection limit of the NMR instrument. Furthermore, the majority of these structures have been suggested from the presence of their corresponding ions in the mass spectrometric spectra (see sections 4.3.1 and 4.3.2).

To conclude, it seems that only molecules I, II, III, IVa, IVb, V, VI, VII, XII, XIII and XIV would appear to be present (in large enough quantities to be detected) solely according to both ^1H and ^{13}C NMR data from the analysis of glutaraldehyde solutions under the pH range 3.8-9.2.

4.3.3.2.2 ^{13}C NMR analyses of glutaraldehyde at pH 1 and at pH 11:

The presence of a solid light-yellow precipitate in the solution of glutaraldehyde at pH 1 made it impossible to obtain a ^{13}C NMR spectrum. Assignment of the compounds present in such a sample solely on the ^1H NMR analysis was therefore

quite difficult. However, the ^{13}C NMR analysis of glutaraldehyde in solution at pH 11 was carried out (no precipitates formed) and a tentative assignment of the signals seen is given below.

The signals obtained at pH 11 agree with a previously reported ^{13}C NMR spectrum from the study of a polymeric glutaraldehyde preparation in D_2O , although no attempts were made in that study to assign their signals¹. The only conclusion drawn were that their combined ^{13}C and elemental analysis results seemed to indicate the presence of a mixture of oligomers of up to six glutaraldehyde units but the absence of any free di-aldehyde. Indeed, the complex pattern seen in the ^{13}C spectrum obtained is essentially thought to be mostly due to the presence of oligomeric structures or condensation products of higher order compared to the data obtained from glutaraldehyde at pH 3.8-9.2. Unfortunately, the signal to noise ratio was not optimum enough to allow full determination of all the ^{13}C signals found in our spectra. Nevertheless, about at least one hundred and one ^{13}C signals can be clearly identified above the signal to noise level. Many others are thought to be present but their intensities are not sufficient to be characterised.

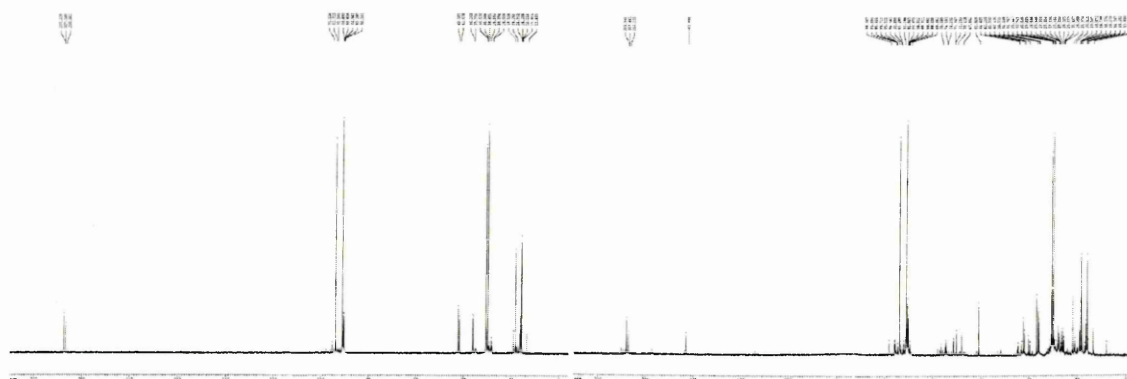


Figure 4.11: ^{13}C NMR spectra of an aqueous glutaraldehyde solution at pH 3.8 (unbuffered-*left*) and pH 11 (pH adjusted with NaOH-*right*), freeze-dried and re-dissolved in D_2O .

An interesting observation is that some similar signals to those found in the ^{13}C NMR spectrum of glutaraldehyde in water (pH 3.8) can be observed (see figure 4.11 above for a direct comparison) in the spectrum of glutaraldehyde at pH 11. This would underline the possible presence of similar chemical structures to those previously described and tentatively assigned to molecules such as molecules I, II, III, IVa, IVb, V, VI, VII, XII, XIII and XIV.

However, other signals can also be observed in the spectrum of glutaraldehyde at pH 11 in comparison to the ones obtained at pH 3.8-9.2. These signals are found below in table 4.6. This indicates one more time the strong pH dependence of the behaviour of glutaraldehyde in solution.

Peak position (ppm)	Proposed assignment
20-28ppm	Deshielded aliphatic carbons
50-80 ppm	Deshielded aliphatic carbons
139 and 154 ppm	Carbon signals in the alkene region (120-160 ppm)
183-184 ppm	Presence of unsaturated aldehydic carbons
196-197, 207-208, 209 and 210 ppm	Weak signals of some likely saturated aldehydic carbons

Table 4.6: Line assignment of a ^{13}C NMR spectrum of glutaraldehyde at pH 11.

Our findings indicate the likely presence of chemical structures containing typical alkene bonds, such as aldol condensation products (molecules XV, XVI, XVII, XVIII and XIX) and also aldol condensation/Michael-type addition products (molecules XXXIII, XXXIV, XXXV, XXXVI, XXXVII, XXXVIII, XXXIX, XL, XLI, XLII and XLIII), in addition to dimers formed by a di-molecular aldol condensation (molecules XXXI and XXXII), along with partially cyclised aldol/aldol-Michael structures (molecules XXIII, XXIV, XXV, XXVI, XXVII, XXVIII, XXIX, XXX, XLV, XLVI, XLVII, XLVIII, XLIX, L, LI, LII and LIII).

Nevertheless, only two signals can be identified in the alkene region (at 139 and 154 ppm). This led us to the hypothesis that some aldol condensation and some aldol/Michael-type addition condensation reaction products may contain other characteristic functions than only the ethylenic bonds. The aldol condensation might have not fully involved the proper dehydration step usually occurring at every consecutive step, which is yielding ethylene linkages conjugated with aldehyde functions. Some “fully hydrated” molecules containing hydroxyl pendant groups, (such as molecular structures XVa, XVIb, XVIIb, XVIIIc, XIXd, XXXIVa and XXXVIIa, XXXVIIIb, XXXIXa, XLIC and XLIIa), would exhibit carbon signals around 55-80 ppm instead of the ethylenic characteristic signals around 140-150 ppm. In addition, the corresponding ^1H NMR of glutaraldehyde at pH 11 also corroborates this hypothesis with the signals around 3.45 ppm and 2.45 ppm, meaning that most of the structures enumerated above might be predominantly in their “hydrated” form. Thus the presence of partially hydrated structures, still

containing alkene groups could also be present, although it is less likely than their fully hydrated counter parts. Such partially hydrated species would include molecules XVIa, XVIIa, XVIIIa, XVIIIb, XIXa, XIXb, XIXc, XX, XXXVIIIa, XLIa, XLIIb and XLIIa.

An even better fit for the two carbon signals at 139 and 154 ppm is the presence of unsaturated aldol condensation products that have carried out a Cannizzaro reaction at high pH (e.g. molecules XXI and XXII), more so in the presence of NaOH. Such species involve the formation of primary hydroxyl and carboxylate groups, leading to the alkene signals being slightly shifted to values very close to the ones found in our spectrum.

The NMR signals observed from the analysis of glutaraldehyde at pH 11 also corroborate the potential presence of trioxane-type glutaraldehyde species, including molecules XII, XIII and XIV, because of the presence of the characteristic signal around 95ppm ($-\text{CH}_2-\text{CH}_2-\underline{\text{CH}}(-\text{O}-\text{CH}-)-\text{O}-\text{CH}-$).

Additionally, we can conclude that molecule VIIa is likely to be present because of the ^{13}C NMR signals about 65-70 ppm ($\text{C}-\underline{\text{C}}-\text{O}-$) and because of the ^1H NMR signals around 3-4 ppm ($-\text{CH}_2-\underline{\text{CH}}_2-\text{O}-$), while molecules VIII and IX are unlikely to be present because of the absence of the characteristic NMR signal of these molecules at about 170 ppm ($\text{C}-\underline{\text{C}}(=\text{O})-\text{O}-$) from the ^{13}C NMR spectrum. Molecules X and XI (mono and di-acid forms of glutaraldehyde) are also unlikely to be present because of the absence of a characteristic signal of the carboxylic acid from the ^{13}C NMR spectrum.

4.3.4 Raman and FTIR-ATR analyses

4.3.4.1 Analysis of an aqueous commercial unbuffered solution of glutaraldehyde (pH 3.8):

The Raman spectrum obtained from a commercial solution of glutaraldehyde (25% v/v) revealed a fairly similar pattern to that seen in the corresponding infrared spectrum (see below figure 4.12 and table 4.7).

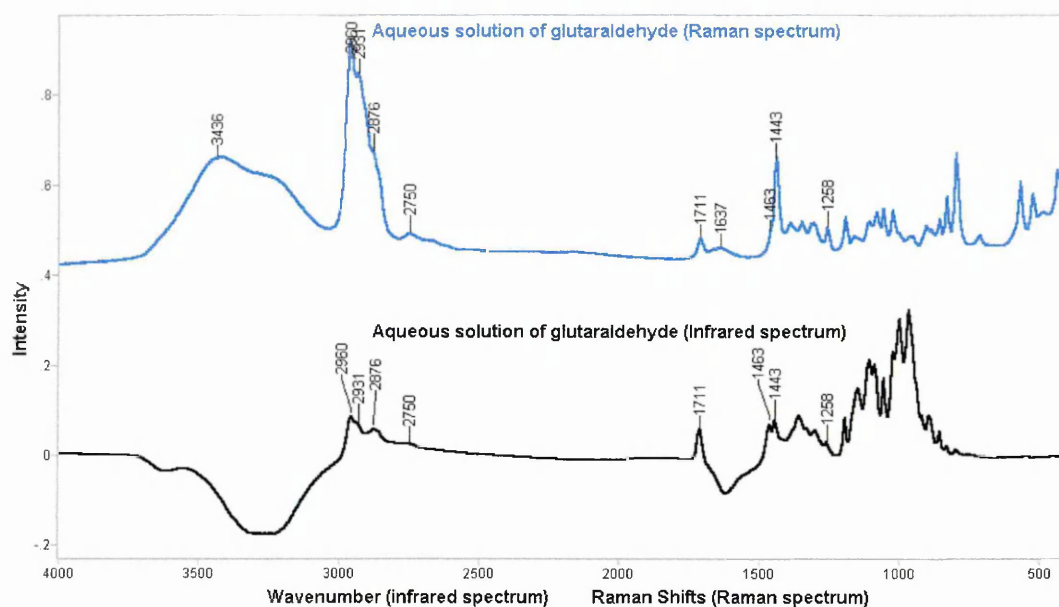


Figure 4.12: Raman (top) and FTIR-ATR (bottom) spectra obtained from an unbuffered commercial aqueous glutaraldehyde solution (25% v/v).

Peak positions (Raman spectrum)	Peak positions (Infrared spectrum)	Assignment
3436 cm ⁻¹	-	Broad and intense doublet with a maximum at 3436 cm ⁻¹ , most likely to be due to water environment but may also be due to the presence of OH groups
2960, 2931 and 2876 cm ⁻¹	2960, 2931 and 2876 cm ⁻¹	CH stretching region
2750 cm ⁻¹	2750 cm ⁻¹	Weak absorption assigned to CH stretching of an aldehyde group
1711 cm ⁻¹	1711 cm ⁻¹	Absorption arising from a C=O stretching vibration
1637 cm ⁻¹	-	Most likely due to water environment
1463, 1443, 1350 and 1258 cm ⁻¹	1463, 1443, 1350 and 1258 cm ⁻¹	Possibly due to various deformation vibrations of the CH ₂ or CH groups
1200-800 cm ⁻¹	1200-800 cm ⁻¹	Unresolved absorption bands possibly assigned to the presence of polymeric “impurities” in the commercial glutaraldehyde solution

Table 4.7: Major peak positions and corresponding vibrational spectroscopic assignment (Raman and infrared) from the analysis of an unbuffered commercial aqueous glutaraldehyde solution (25% v/v).

4.3.4.2 Analysis of freeze-dried aqueous solutions of glutaraldehyde at a range of pH values:

The infrared spectroscopic data obtained from freeze-dried solutions of glutaraldehyde (0.6% v/v and 0.2% v/v) were the same as one another. And hence, only the results obtained from solutions of 0.6% v/v glutaraldehyde are shown here. For doing so, solutions of glutaraldehyde were firstly diluted, (in distilled water or in pH 4, pH 7.4, pH 9.2 buffers, or even in distilled water with adjustment of pH to pH 1 and 11 by addition of HCl or NaOH respectively), and then subjected to freeze-dried and immediately analysed.

Figure 4.13 shows the various infrared spectra obtained from freeze-dried glutaraldehyde solutions at a range of pH values, while figure 4.14 shows an expansion of the 1230-1850 cm^{-1} spectral region.

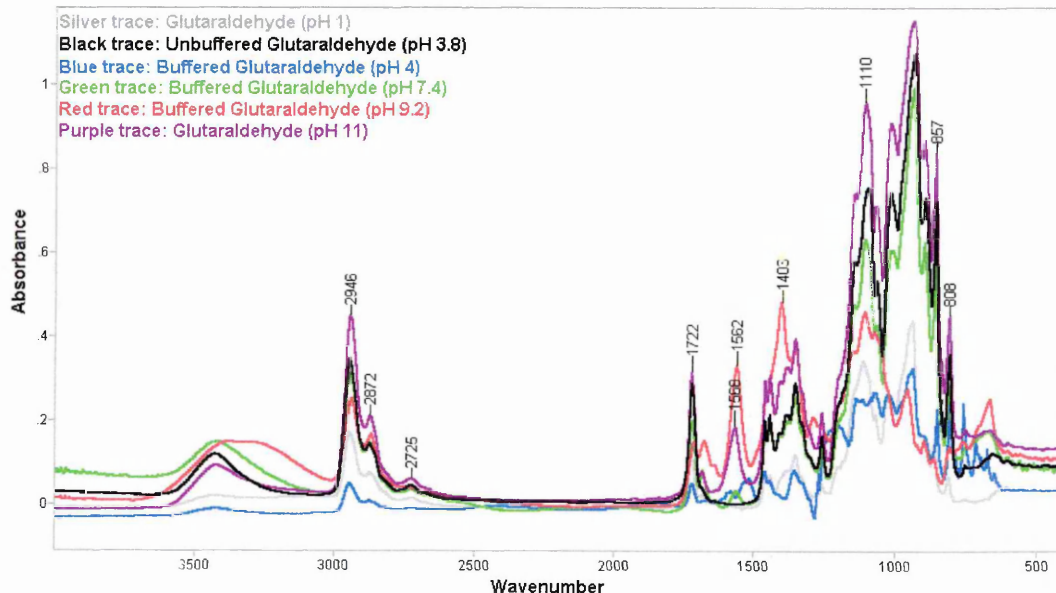


Figure 4.13: FTIR-ATR spectra of freeze-dried glutaraldehyde solutions at various pH values (unbuffered glutaraldehyde at pH 3.8, 1 and 11; and buffered glutaraldehyde at pH 4, 7.4 and 9.2).

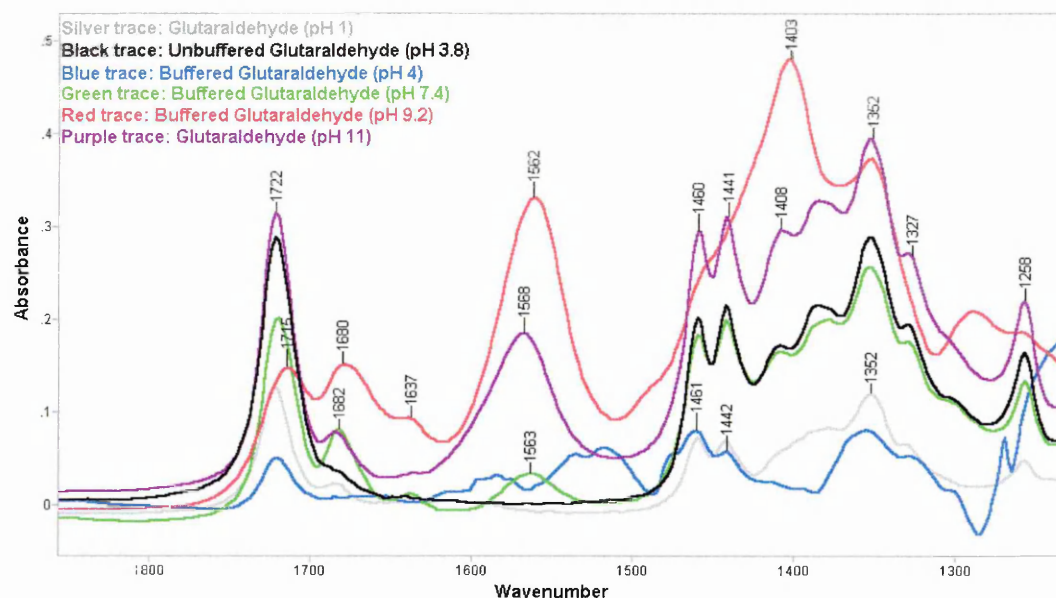


Figure 4.14: FTIR-ATR spectra of freeze-dried glutaraldehyde solutions at various pH values (expansion of the 1230–1850 cm^{-1} spectral region).

The major bands along with their corresponding assignments are found below in table 4.8.

Peaks found at pH 1 (cm^{-1})	Peaks found at pH 3.8 (cm^{-1})	Peaks found at pH 4 (cm^{-1})	Peaks found at pH 7.4 (cm^{-1})	Peaks found at pH 9.2 (cm^{-1})	Peaks found at pH 11 (cm^{-1})	Assignment
3426b	3426b	3426b	3426b	3426b	3426b	OH stretching due to water, a carboxylic group (due to oxidation of the glutaraldehyde molecules) or an alcoholic hydroxyl group due to the presence of hydrated structures, aldol condensation products which did not undergo all the dehydration steps, or even due to the enol forms of the aldehyde moieties in the glutaraldehyde structures
2947i	2947i	2947i	2944i	2941i	2946i	Antisymmetric stretching of the CH_2
2873i	2872i	2874i	2874i	2871i	2872i	Symmetric stretching of the CH_2
2724i	2725m	2723m	2724m	2725vw	2725m	Antisymmetric stretching of the CH of the aldehyde group

1723i	1722i	1721i	1721i	1715bm (band shifted)	1722i	Stretching of the C=O groups of non-conjugated aldehydes and/or carboxylic acids overlapping each other
1683m	1683w	1683w	1683m	1680bm	1682m	Stretching of the C=O group of conjugated aldehydes
-	-	-	1637w	1636m	1635m	Assigned to stretching of the C=C ethylenic linkage group conjugated with an aldehyde, formed from the dehydration step of an aldol condensation
1611bw	-	-	-	-	-	May be due to the presence of undetermined polymers formed specifically at very acidic pH
-	-	-	1563bm	1562bi	1568ib	Assigned to the antisymmetric stretching of the COO of the carboxylate group, possibly due to the presence of carboxyl functions in the form of sodium salts ²⁰ . The carboxylic acid groups possibly being formed by Cannizzaro reactions
Various bands at 1500-1200	Various bands at 1500-1200	Various bands at 1500-1200	Various bands at 1500-1200	Various bands at 1500-1200	Various bands at 1500-1200	Various bands at 1500-1200 including the main ones at ~1460, 1441, 1352, 1327 and 1258 cm ⁻¹ can be assigned to the deformation vibrations of the CH ₂ or CH groups
1411shv w	1410vw	-	1410m	1410w sh / 1403bi	1408m	May be assigned to the symmetric stretching of the COO of the carboxylate group (sodium salt)
Various bands at 1200-900	Various bands at 1200-900	Various bands at 1200-900	Various bands at 1200-900	Various bands at 1200-900	Various bands at 1200-900	Some strong, unresolved absorption bands around 1200-900 cm ⁻¹ may be assigned to ether bonds (different C-O bendings), which may, indicate the presence of "impurities" in the aqueous commercial solution consisting most likely of polymers with ether linkages
1113m	1111m	1111w	1111m	1109m	1110m	Secondary alcohol (C-O bend)
1067m	1067m	1067 vw	1067m	1067w	1067m	Primary alcohol (C-O bend)

858i and 808m	857i and 808i	857m sh and 806i	857i and 808i	858w and 808i	857i and 808m	The two bands fit with previous findings ²¹ of the possible presence of molecules such as molecule VIIa. The authors assigned two bands at 805 and 855 cm ⁻¹ as corresponding to the 811 and 872 cm ⁻¹ bands of 2-ethoxycyclohexane, which indicated the presence of molecule VIIa (see appendix III for details)
---------------------	---------------------	------------------------	---------------------	---------------------	---------------------	--

Table 4.8: Assignment of the major peaks found from the infrared spectra (see figure 4.10 and 4.11) of freeze-dried glutaraldehyde solutions at various pH values (pH range 1-11). Note: vw: very weak; w: weak; m: medium; i: intense; b: broad; sh: shoulder.

The spectra shown in figures 4.13 and 4.14 are quite different. However, from the summary of results presented above in table 4.8, it appears that a similar class of material is absorbing at the same frequency and thus many similarities can be observed. This reveals that there are similar groups (and likely similar molecules) present over a large pH range. This would agree with our previous findings (mass spectrometry, nuclear magnetic resonance).

The spectra from both samples (unbuffered glutaraldehyde at pH 3.8 and buffered at pH 4) are very similar and show the same pattern, considering the presence of buffer. This behaviour was expected since the unbuffered commercial glutaraldehyde has a pH value (3.8) close to pH 4. The infrared spectrum obtained from glutaraldehyde at pH 7.4 is also similar to that of glutaraldehyde at pH 4. However, some new bands in the 1800-1400 cm⁻¹ region seem to differ and might be due to the presence of polymers of glutaraldehyde. It is thought that at physiological pH, a considerable amount of glutaraldehyde is polymerised through the aldol condensation mechanism (see chapter 2). The spectra obtained from freeze-dried solutions of glutaraldehyde at pH 9.2 did not reveal new bands in comparison to the spectra of glutaraldehyde at pH 7.4, except that their intensities differ, indicating that similar polymeric species are formed at these pH values (pH 4-9.2). The spectrum obtained from glutaraldehyde at pH 11 also shows a similar pattern to the one obtained at pH 9.2.

For example, the presence of a broad band at 3426cm⁻¹ (stretching of the OH due to water, carboxylic groups, or alcoholic hydroxyl groups) can be partly explained because glutaraldehyde and its impurities (polymers of glutaraldehyde) have been

reported to always contain variable amounts of water, even after drying under high vacuum²². It seems that a similar statement can be made from our data obtained with freeze-dried samples. Comparison of the spectra from freeze-dried samples of glutaraldehyde with that from glutaric acid (not shown here), revealed that there was apparently no great presence of glutaric acid (molecule X, di-acid form of glutaraldehyde) as an impurity formed by oxidation, as has been hypothesised previously²³. The spectrum does not however rule out the hypothetical presence of the mono-acid form of glutaraldehyde (mol XI). Thus, it is most likely that the band at 3426 cm^{-1} , is due to the presence of hydroxyl groups and/or the presence of water. However, and especially at high pH, this band may also be due to the presence of polymers containing some carboxylic groups (e.g. molecules that might have undergone Cannizzaro reactions).

Some strong, unresolved absorption bands, around $1200\text{-}900\text{ cm}^{-1}$, may be assigned to ether C-O bonds, which may, for example indicate the presence of impurities in the aqueous commercial solution consisting of polymers with ether linkages. In addition, the presence of alcohol groups might be indicated by a band at 1067 cm^{-1} , which is thought to be due to primary alcohol, and another one at 1115 cm^{-1} , which may be due to secondary alcohol.

However, some dissimilarities can also be spotted, especially in spectra of glutaraldehyde at extreme pH values (pH 1 and 11) in comparison to other spectra. The weak, broad band found at 1611 cm^{-1} may be due to the presence of undetermined polymers formed specifically at very acidic pH (e.g. pH 1). No molecular structures of such underdetermined polymers could be deduced from the analysis of glutaraldehyde at pH 1 because no ^{13}C NMR data were available.

Additionally, a weak band at $\sim 1635\text{ cm}^{-1}$ and another band at $\sim 1568\text{ cm}^{-1}$ were not present in the spectra of glutaraldehyde at pH of less than 7.4. The band at $\sim 1568\text{ cm}^{-1}$ is possibly due to the presence of carboxyl functions in the form of sodium salts²⁰ (see figure 4.15 below proposing a likely mechanism), the carboxylic acid groups possibly being formed by Cannizzaro reactions. A band at 1410 cm^{-1} can also be better observed with spectra at pH values above 7.4 and may thus be assigned to the symmetric stretching of the COO of the carboxylate group (sodium salt).

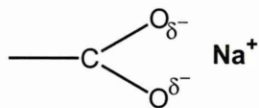


Figure 4.15: Mechanism of uptake of sodium cations by carboxylic acid

Also, the presence of some insoluble white glassy solid precipitates at high pH²⁴ has been previously reported, although no precipitates were observed with our samples under these conditions. Such precipitates have been identified as trioxane-type glutaraldehyde oligomers also existing in glutaraldehyde solution as an impurity. Such copolymers existence was supported, in a later study by the same authors, by the existence of two absorptions at 1720 cm⁻¹ and 1680 cm⁻¹, assignable to C=O of saturated and unsaturated aldehydes²⁵. Although no glassy solids were observed in our samples, the presence of such polymers is not totally precluded since it has already been reported that both insoluble and soluble polymers can coexist²² and one might be in the presence of the soluble type in our samples. It is also widely held that when the pH of glutaraldehyde solutions is increased to an alkaline value, the formation of polymers is likely favoured through aldol condensation reactions^{22,26} (see chapter 2). Our spectra indeed corroborate the finding of such polymers (both aldol condensation and trioxane-type ones) with the presence of a weak band at ~2725 cm⁻¹ corresponding to a conjugated aldehyde (but not typical of the presence of such polymers), a band at ~1722 cm⁻¹ and two others that are more typical of the presence of such polymers. These were an intense band at 1683 cm⁻¹ and a weaker band at 1635 cm⁻¹, both of which are in agreement with the findings of Monsan et al²⁶.

4.3.5 Overall discussion of data obtained

Despite the impressive amount of literature available regarding the use of glutaraldehyde as a fixative for cells and tissues, there is still no definitive agreement about the main reactive species present in glutaraldehyde solutions during the cross-linking process. It is now generally agreed that commercially available aqueous solutions of glutaraldehyde are complex mixtures of the free aldehyde (reported no more than 4%¹⁴), mono- and di-hydrated glutaraldehyde, monomeric and polymeric cyclic hemiacetals and various α,β -unsaturated polymers; in addition, impurities can be detected in small quantities such as ethanol, methanol, acrolein, butyraldehyde, glutaraldoxime and glutaric acid²⁷⁻³⁰. Furthermore, other structures, such as cyclic

glutaraldehyde oligomers with trioxane-type skeletons, have been reported²⁴. However, the exact composition of glutaraldehyde in solution is still a matter for discussion, despite the publication of many reports over the last three decades (see chapter 2 for a complete review).

The ESI-MS results in this study from the analysis of a commercial unbuffered glutaraldehyde solution (pH 3.8) appear quite similar to those reported recently elsewhere³¹. However, our more detailed investigation of the mass spectral data allowed the determination of the hypothetical presence of other molecular structures, additional to the ones already reported by Southern et al³¹, such as monomeric and polymeric cyclic hemiacetal products, as well as aldol, di-aldol and single aldol/Michael condensation products. The analysis by ESI-MS of glutaraldehyde solutions at extreme pH values (pH 1 and 11) revealed different spectra to the one obtained from commercial glutaraldehyde solution (at pH 3.8), indicating the great influence of pH on the behaviour of glutaraldehyde in solution. A similar conclusion was derived from the data obtained using MALDI-TOF MS, along with the finding of the presence of many similar products formed in the pH range 4-9. This suggested that, in the pH range 4-9, some identical products are formed disregarding of the pH, while other structures seem to be more dependent on the pH of the solution. Our data suggest that the molecular weight of the largest molecules of glutaraldehyde oligomers does not exceed 700 (molecule XIV), which is similar to what was suggested by others based on gel permeation chromatographic data³², but different from what was reported by Southern³¹.

Despite the fact that it has recently been reported that no polyaldol condensation products of glutaraldehyde in solution were detected by NMR or even mass spectrometry³³, some m/z values were found corresponding to some polyaldol condensation products in both our ESI-MS and MALDI-TOF MS data (glutaraldehyde analysed under a pH 1-11 range). Our results suggest a large number of different aldol and aldol/Michael addition products, the majority of which detected involving the equivalent of a maximum of five units of monomeric glutaraldehyde and in various hydrated states. However, some weaker signals corresponding to aldol and aldol/Michael products with an equivalent of a maximum of eight units of monomeric glutaraldehyde were also rarely detected. The formation of aldol condensation products is in agreement with some authors^{10,26} but in contrast

to others³⁴ who do not believe that such structures exist in unbuffered aqueous solutions of glutaraldehyde under the conditions studied. This conclusion may also differ from the findings of Southern³¹, who studied a similar unbuffered commercial glutaraldehyde solution solely by ESI-MS, reporting no long chain polymers of glutaraldehyde but who did not further confirm their findings with data from complementary techniques such as NMR and FTIR.

Our NMR data did not necessarily corroborate the mass spectrometric results, which agrees with Kawahara et al³⁴. However, the low sensitivity of the NMR technique in comparison to that of mass spectrometry may account for the lack of signal attributable to aldol and aldol/Michael condensation products when glutaraldehyde was analysed over the pH range 3.8-9.2. The possible existence of aldol and aldol/Michael addition products was however corroborated by NMR when glutaraldehyde at extreme pH values (pH 1 and 11) was analysed. Therefore it has been hypothesised that at extreme pH values, aldol and aldol/Michael addition products are formed in higher ratios than when under the pH range 3.8-9.2. Despite, these possible discrepancies, our results agreed with earlier NMR studies (¹H NMR¹¹ and ¹³C NMR¹⁴) and suggest the definite presence of the monohydrate, di-hydrates and cyclic hemiacetals which is also in accordance with various other authors^{15,35,36}. Our data also indicate the possible presence of glutaraldehyde oligomers such as trioxane derivatives^{24,37} and other types of dimers³⁸.

It is known that the polymerisation of glutaraldehyde is pH-dependent, with increasing polymerisation at higher pH. Our study clearly showed that glutaraldehyde solutions were prone to strong pH dependence. As the pH is increased in the range 4-8 and above, the free aldehyde is said to undergo base-catalysed aldol condensation followed by dehydration to form α,β -unsaturated oligomers. The more basic the solution, the more susceptible will be the aldehyde to condensation²⁶. At physiological and higher pH, the likely polyglutaraldehyde structures are thus aldol condensation reaction products (non-conjugated and conjugated aldehydes both identified from the infrared data), along with the possibility of additional Cannizzaro reactions at high pH leading to aldehyde pendants groups being replaced by hydroxyl and/or carboxyl groups³⁹.

Our data showed that these statements are not necessarily applicable to glutaraldehyde in solution. It appears from our mass spectrometric but especially from our NMR data, that glutaraldehyde has a strong tendency to polymerise at extreme pH values such as pH 11 but also at pH 1, comprising α,β -unsaturated oligomers. The presence of possible Cannizzaro reaction products has also been identified in infrared and mass spectrometric data in this study. It is worth noting that air oxidation of the aldehyde groups of glutaraldehyde at relatively high pH values may also yield additional carboxyl groups.

At pH range 4-8, the presence of polymers is not as prevalent as at extreme pH values (NMR data), but many polymers of glutaraldehyde are thought to exist in solution (FTIR, MS data). The aldol condensation mechanism yielding ethylene linkages conjugated with aldehydes, along with the possible Cannizzaro reactions appear to be the best mechanism to explain the occurrence of these polymers of glutaraldehyde in the physiological pH range. This conclusion is supported by the possible presence of primary hydroxyl and carboxyl groups (infrared results) that can be explained by the occurrence of a Cannizzaro reaction. However, the results do also seem to indicate that the dehydration step of the typical aldol condensation reaction does not always occur at every consecutive step. This is supported by the lack of double bonds conjugated with aldehyde functions (seen from the NMR and FTIR data) and also the possible presence of secondary hydroxyl groups (seen in the FTIR data) that would be explained by this incomplete aldol condensation. Our findings thus agree with a previous report, where it was suggested from infrared and ultraviolet spectroscopic results that polyglutaraldehyde formed in the pH range 7-13.5, could be of this hydrated aldol form²². Mass spectrometric data revealed the possible presence of such aldol and/or aldol/Michael polymeric structures in their hydrated states.

The MS results also show that the dimer is not the only polymer mainly present in commercial solutions of glutaraldehyde, as was previously reported⁴⁰, but that many different molecular structures involving many glutaraldehyde molecules (possibly up to seven glutaraldehyde monomers) coexist in aqueous solution over a large pH range. Despite the possible formation of Cannizzaro products in solution at high pH (pH 11), the polymeric molecules of glutaraldehyde formed under a wide pH range (pH 1-11) would still remain reactive to further cross-linking and thus monomeric

glutaraldehyde is not the only species capable of reacting at acidic or neutral pH in the cross-linking of proteins, as widely held and as stated by others⁴¹.

At acidic pH, a previous report³⁴ stated that dilute glutaraldehyde solutions at acidic pH were almost monomeric, the major portion (~76%) taking the cyclic hemiacetal structure (the rest being monomeric glutaraldehyde (10.8%), mono- and di-hydrate glutaraldehyde (10.4% and 2.5% respectively)). Our mass spectrometric data did not corroborated these statements because, although some monomeric glutaraldehyde was found along with its hydrates, many other compounds are thought to be present in higher quantities. Additionally despite the fact that it has been mentioned³⁴ that monomeric glutaraldehyde can only be converted to polymeric forms by the action of amino groups, species thought to correspond to some aldol/Michael addition and aldol condensation-like products were found (without any presence of amino groups to catalyse the reaction as it is believed³⁴) at pH 4-9, using ESI-MS, MALDI-TOF MS and FTIR spectroscopy. These species were also identified on analysis of glutaraldehyde at pH 1 (ESI-MS results), with the findings being corroborated by the ¹H NMR and FTIR spectroscopic results.

4.4 Conclusion

Glutaraldehyde solution studied in a wide pH range was found to be extremely dependent on pH. Overall, the aqueous glutaraldehyde solutions (in the pH range 3.8-9.2) appear to be extremely complex but also to contain similar molecular species. These consist essentially of glutaraldehyde hydrates, monomeric and polymeric cyclic hemiacetal products, and trioxane-type oligomers (molecules I, II, III, IVa, IVb, V, VI, VII, XII, XIII and XIV), but apparently do not contain large amounts of aldol, di-aldol, aldol/Michael condensation products or their corresponding hydration products, if one considers the NMR results as a determinant factor. The solutions of glutaraldehyde at extreme pH (pH 11 and also possibly at pH 1) tend to behave differently, although the reactions may yield similar species but with different relative concentrations. At pH 1 and 11, the NMR data indicated the presence of similar structures as for glutaraldehyde solutions in the pH range 3.8-9.2, but also the greater prominence of species containing alkene unsaturated groups.

Thus we can infer the likely presence of aldol and aldol/Michael condensation products, the majority of which would have undergone complete dehydration.

It therefore appears that the glutaraldehyde used in these experiments contains various amounts of a range of species, which are different from the "pure" monomeric glutaraldehyde form. This is in agreement with a previous report by Gillet and Gull²³, where the relative glutaraldehyde polymer content of commercial unbuffered glutaraldehyde solutions was ascertained by spectrophotometric analysis. They found that many "high quality" commercial glutaraldehyde solutions (electron microscopy grade) contained large amounts of impurities that absorb at 234 nm and that they were under the specified standard of quality claimed by the suppliers⁴². The complexity of glutaraldehyde solutions should not however discourage its wide application, because all characterised forms of glutaraldehyde present in solution, including those identified in this study, seem to exhibit the ability to readily react and cross-link proteins.

It is believed that these results will provide a better insight into the chemistry of glutaraldehyde and to clarify the existing knowledge. Additionally, an understanding of the behaviour of glutaraldehyde in solution is thought to be essential if the interaction of glutaraldehyde with tissue such as bioprosthetic heart valves is to be predicted. In this respect, an entire chapter (chapter 5) will be dedicated to the investigation of the chemistry of the reactions of glutaraldehyde with proteins and more specifically bioprosthetic heart valves.

1. Kirkeby S, Moe D, Kakobsen P, Romert P, Matthiessen ME. Polymeric aldehyde preparations: their chemistry and fixation capacity. *Micron and Microscopica Acta*. 1989;20:217-221.
2. Chvapil M, Gibeault D, Wang TF. Use of chemically purified and crosslinked bovine pericardium as a ligament substitute. *Journal of Biomedical Materials Research*. 1987;21:1383-1393.
3. Gusev AI, Vasseur OJ, Proctor A, Sharkey AG, Hercules DM. Imaging of TLC using MALDI MS. *Analytical Chemistry*. 1995;67:4565-4570.
4. Duncan MW, Matanovic G, Poljak AC. Quantitative analysis of low molecular weight compounds of biological interest by matrix-assisted-laser desorption ionisation. *Rapid communication in Mass Spectrometry*. 1993;7:1090-1094.
5. Pergantis SA, Emond CA, Madilao LL, Cullen WR, Eigendorf GK. Accurate measurement of positive ions in the desorption chemical ionisation mode. *Organic Mass Spectrometry*. 1994;29:439-444.
6. Lidgard R, Duncan MW. Utility of MALDI-TOF mass spectrometry for the analysis of low-molecular weight compounds. *Rapid communication in Mass Spectrometry*. 1995;9:128-132.

7. Sabatini DD, Miller F, Barnett RJ. Aldehyde fixation for morphological and enzyme histochemical studies with the electron microscope. *Journal of Histochemistry and Cytochemistry*. 1964;12:57-71.
8. Geissman TA. In: Adams R, Bachman WE, Fieser LF, Johnson JR, Snyder HR, eds. *The Cannizzaro Reaction*. New York: John Wiley and Sons; 1944:94-103.
9. Tsai SW, Que Hee SS. A new passive sampler for regulated workplace aldehydes. *Applied Occupational and Environmental Hygiene*. 1999;14:255-262.
10. Richards FM, Knowles JR. Glutaraldehyde as a protein crosslinking reagent. *Journal of Molecular Biology*. 1968;37:231-233.
11. Hardy PM, Nicholls AC, Rydon HN. The nature of glutaraldehyde in aqueous solution. *Journal of Chemical Society Chemical Communications*. 1969;10:565-566.
12. Kawahara JI, Ishikawa K, Uchimarui T, Takayama H. Crosslinking mechanism of glutaraldehyde between amino groups. *Polymer Materials Science Engineering*. 1996;75:149-150.
13. Maeda K, Kawamura K, Kondo SI, Aoyagi T, Takeuchi T, Umezawa H. The structure and activity of leupeptins and related analogs. *Journal of Antibiotics*. 1971;24:402-404.
14. Whipple EB, Ruta M. Structure of aqueous glutaraldehyde. *Journal of Organic Chemistry*. 1974;39:1666-1668.
15. Korn AH, Fairheller SH, Filachione EM. Glutaraldehyde: nature of the reagent. *Journal of Molecular Biology*. 1972;65:525-529.
16. Holmquist L, Lewin M. Separation of glutaraldehyde and some of its aldol condensation products by hydroxyl-aldehyde group affinity chromatography. *Journal of Biochemical and Biophysical Methods*. 1991;22:321-329.
17. Silverstein RM, Bassler GC, Morrill TC. In: *Spectrometric Identification of Organic Compounds*. 4th ed. New York: Wiley; 1981:249-303.
18. Stothers JB, Lauterbur PC. ¹³C chemical shifts in organic carbonyl groups. *Canadian Journal of Chemistry*. 1964;42:1563-1576.
19. Lauterbur PC. In: Nachod FC, Phillips WD, eds. *Determination of Organic Structures by Physical Methods*. New York: Academic Press; 1962.
20. Silverstein RM, Bassler GC. In: *Spectrometric Identification of Organic Compounds*. New York: Wiley; 1968.
21. Aso C, Aito Y. Studies on the polymerisation of bifunctional monomers II: Polymerisation of glutaraldehyde. *Makromolekulare Chemie*. 1962;58:195-203.
22. Margel S, Rembaum A. Synthesis and characterisation of polyglutaraldehyde. A potential reagent for protein immobilisation and cell separation. *Macromolecules*. 1980;13:19-24.
23. Gillett R, Gull K. Glutaraldehyde: Its purity and stability. *Histochemie*. 1972;30:162-167.
24. Tashima T, Kawakami U, Harada M, Sakata T, Satoh N, Nakagawa T, Tanaka H. Isolation and identification of new oligomers in aqueous solution of glutaraldehyde. *Chemical Pharmaceutical Bulletin*. 1987;35:4169-4180.
25. Tashima T, Kawakami U, Harada M, Satoh N, Nakagawa T, Tanaka H. Purification of aqueous solution of glutaraldehyde using hydrocarbonaceous silica adsorbents. *Journal of Antibacterial and Antifungal Agents*. 1988;16:121-130.
26. Monsan P, Puzo G, Mazarguil H. Etude du mechanisme d'etablissement des liaisons glutaraldehyde-proteines. *Biochimie*. 1975;57:1281-1292.
27. Scobbie E, Groves JA. An investigation of the composition of the vapour evolved from aqueous glutaraldehyde solutions. *Annals of Occupational Hygiene*. 1995;39:63-78.
28. Ruijgrok JM, Boon ME, De Wijn JR. The effect of heating by microwave irradiation and by conventional heating on the aldehyde concentration in aqueous glutaraldehyde solutions. *Histochemical Journal*. 1990;22:389-393.
29. Bovallius A, Anas P. Surface decontamination action of glutaraldehyde in the gas-aerosol phase. *Applied Environmental Microbiology*. 1977;34:129-134.
30. Anderson PJ. Purification and quantitation of glutaraldehyde and its effect on several enzyme activities in skeletal muscle. *Journal of Histochemistry and Cytochemistry*. 1967;15:652-661.
31. Southern LJ. Identification of glutaraldehyde-induced structures in bioprosthetic heart valves using mass spectrometry: an insight into valve failure. In: Sheffield: University of Sheffield; 2001.
32. Kuznetsova NP, Mishaeva RN, Gudkin LR. Oligomerisation of glutaraldehyde in the course of its condensation with glycine. *Russian Journal of Applied Chemistry*. 1999;72:1236-1241.

33. McClurg WM, Lawford PV, Hughes H, Rogers S. Formaldehyde replaces glutaraldehyde in porcine bioprosthetic heart valves. *Journal of Heart Valve Disease*. 1996;5:343-347.
34. Kawahara JI, Ohmori T, Ohkubo T, Hattori S, Kawamura M. The structure of glutaraldehyde in aqueous solution determined by ultraviolet absorption and light scattering. *Analytical Biochemistry*. 1992;201:94-98.
35. Holloway CE, Dean FH. ^{13}C NMR study of aqueous glutaraldehyde equilibria. *Journal of Pharmaceutical Science*. 1975;64:1078-1079.
36. Rasmussen KE, Albrechtsen J. Glutaraldehyde: the influence of pH, temperature, and buffering on the polymerisation rate. *Histochemistry*. 1974;38:19-26.
37. Tashima T, Kawakami U, Satoh N, Nakagawa T, Tanaka H. Detection of impurities in aqueous solution of glutaraldehyde by HPLC with a multichannel photodiode array UV detector. *Journal of Electron Microscopy*. 1987;36:136.
38. Tashima T, Kawakami U, Harada M, Imai M, Satoh N, Nakagawa T, Tanaka H. Polymerisation reaction in aqueous solution of glutaraldehyde containing trioxane-type oligomers under sterilising conditions. *Chemical Pharmaceutical Bulletin*. 1989;37:377-381.
39. Okubo M, Takahashi M. Production of submicron size monodisperse polymer particles having aldehyde groups by the seeded aldol condensation polymerisation of glutaraldehyde II. *Colloid and Polymer Science*. 1994;272:422-426.
40. Robertson EA, Schultz L. The impurities of commercial glutaraldehyde and their effect on the fixation of the brain. *Journal of Histochemistry and Cytochemistry*. 1970;15:652-661.
41. Hayat MA. Aldehydes. In: Thubrican M, ed. *Fixation for Electron Microscopy*. New York: Academic Press; 1981:64-129.
42. Preto P. Glutaraldehyde for electron microscopy: a practical investigation of commercial glutaraldehydes and glutaraldehyde-storage conditions. *Histochemical Journal*. 1995;27:906-913.

Chapter 5

5 Investigation of the cross-linking occurring in glutaraldehyde-treated valve tissue.

Abstract

Objectives: A number of studies have investigated the reactions of glutaraldehyde with a range of model compounds, from the simplest amino acids to complex collagenous tissue. A number of structures for reaction products have been proposed but at present there is no definitive understanding of the process that take place. An understanding of the interactions between glutaraldehyde and tissue is thought to be essential in order to comprehend why bioprostheses calcify and ultimately fail. Furthermore, the exact mechanism of in-vivo calcification of glutaraldehyde-treated bioprostheses is unknown, although a great deal of effort has been directed at various aspects of the problem. Much of the work has been approached in an empirical fashion, due to the lack of specific knowledge regarding the mechanism of calcification. It is likely that the mechanism involves, amongst other factors, a contribution from the collagenous tissue itself and aldehyde fixative (glutaraldehyde) used routinely in the manufacture of bioprosthetic valves. Thus the objectives of this study were to investigate the reactions between glutaraldehyde and amines, peptides and proteins, to determine the molecular structures of the likely reaction products, and to extrapolate these to those occurring during the glutaraldehyde pre-treatment of bioprosthetic valves.

Methods: The reactions between glutaraldehyde and amines, peptides and proteins were investigated at a range of pH values (4-9.2) and subjected to analysis by matrix assisted laser desorption ionisation-time of flight mass spectrometry (MALDI-TOF

MS), nuclear magnetic resonance (NMR), Fourier-transform infrared (FTIR) and Raman spectroscopy.

Results: Our results indicate that glutaraldehyde reacts with the amino groups in a wide range of pH (pH 4-9.2). The mass spectral, along with the NMR and FTIR data obtained for the products of the reaction between glutaraldehyde and small amines and peptides showed the presence of a rich palette of compounds such as aldol and aldol/Michael condensation products of glutaraldehyde, Schiff base moieties (including cross-links) and various cyclisation products incorporating pyridinium and dihydropyridine ring structures (see appendix IV for structural details). The results indicate the likely presence of 29 stable mono-bound structures along with 25 stable multi-bound (cross-linking) entities including the anabilysine-like compounds, which is the only stable cross-linking entity reported so far in the literature. In addition, although the presence of stable structures was shown, other less-stable chemical entities were also characterised, which brought the hypothesis of their role in the tissue failure of bioprostheses (likely from in-vivo degradation of cross-linked tissue) but also of their potential role in the initiation of mineralisation from the presence of many free pendant electronegative groups.

Conclusion: The molecular structures of the likely reaction products formed between glutaraldehyde and amino groups are quite complex. Many new structures were proposed in addition to those already reported in the literature. Successful characterisation of some possible chemical structures involved in the reaction of glutaraldehyde and proteins, and their cross-linking is hoped to bring new insights into the complex model that represent the cross-linking of collagenous tissue used in many biomaterial applications. In addition, characterisation of unstable cross-links entities is also believed to give some reasonable hints as to why cross-linked bioprosthetic valves fail when implanted in-vivo.

5.1 Introduction

Commercial bioprosthetic heart valves fabricated from porcine aortic valves are usually treated with a low concentration glutaraldehyde solution (typically around 0.5 %) for more than 24 hours to ensure optimum fixation¹. Despite its wide use over

the last three decades, the mode of action of glutaraldehyde has been the focus of many investigations²⁻⁴ (see chapter 2) and is still of concern these days. Although many physical factors influencing the cross-linking reactions have been elucidated, the chemical aspect of the actual cross-linking process is unknown. The discrepancies in the literature and the uncertainties in the chemical mechanism of the reaction of glutaraldehyde with proteins seem to be due to the complexity of the reaction. Isolation and characterisation of the reactions products would seem to be the most direct approach to understanding the mechanism, but the complex nature of the reaction suggests the difficulty of this approach. The problems encountered in determining the course of the reaction and the difficult characterisation of the products formed have thus impeded the complete elucidation of the reaction mechanism involved^{5,6}.

Calcification is the predominant cause in the failure of valve bioprostheses and although it is thought to be caused by a number of factors (see chapter 1), the mineralisation process has been attributed to the glutaraldehyde cross-linking process⁷⁻¹⁰. It is thought to occur as a result of the formation of molecular species, which are believed to play a significant role by creating potential points that can trap foreign particles that may lead to nucleation centres for calcium and other ions involved in the mineralisation process.

The reaction of glutaraldehyde with the collagenous tissue of bioprosthetic tissue valves is heterogeneous and therefore difficult to study. Glutaraldehyde has been shown to react with a number of amino acids^{11,12} but in proteins, amino acid analysis has shown that only the 6-amino functions of lysine react to any significant extent¹³. Small amines and peptides that mimic the lysine residues of proteins have therefore been chosen to model the reaction of glutaraldehyde with the 6-amino functions of lysine present in collagen. 6-amino-n-caproic acid was chosen, as its structure is similar to lysine but without the α -amino function. For the same reason N- α -acetyl lysine was chosen because the α -amino group is blocked. Additionally, the peptides (N-acetyl Gly Lys methyl ester acetate salt and N-acetyl Phe Lys) both contain a lysine moiety but with the α -amino function blocked leaving only the ϵ -amino (6-amino) group to potentially react. The study was also extended to include proteins that contain several lysine residues, for example lysozyme (containing six lysine

residues) and cytochrome C (containing nineteen lysine residues), to determine the reaction products formed with glutaraldehyde in a more complex system.

5.2 Materials and methods

5.2.1 Materials

All chemicals and consumables used were of the best commercially available grade.

From BDH, UK: Glutaraldehyde 25% EM grade, pure ethanol, potassium dihydrogen orthophosphate.

From Sigma-Aldrich, UK: 6-amino-n-caproic acid (also called amino-hexanoic acid) (Mw 131.2), N- α -acetyl lysine (Mw 188.2), N-acetyl Gly Lys methyl ester acetate salt (total Mw 319.4), N-acetyl Phe Lys (Mw 335), cytochrome C, lysozyme.

Methanol, trifluoroacetic acid, sinapinic acid (3,5-dimethoxy-4-hydroxycinnamic acid), 2,5-dihydroxybenzoic acid (DHB), α -cyano-4-hydroxycinnamic acid (α -CHCA), dipotassium hydrogen orthophosphate.

From Fisher, UK: Buffer pH 4 (potassium hydrogen phthalate) 0.05M, buffer pH 9.2 (disodium tetraborate) 0.01M.

Prepared when required: Buffer pH 7.4 (phosphate) 0.03 M: 4.1 g KH_2PO_4 in 1 L water (stock A); 6.9 g K_2HPO_4 in 1 L water (stock B); mix 300 mL of stock A with 700 mL of stock B. pH was adjusted to pH 7.4 with either stock solution, depending on resultant pH.

Ultra pure water: MilliQ50 (Millipore, UK) packed with USF liquid pure cartridges. The conductivity achieved was 18 $\text{M}\Omega/\text{cm}^3$.

5.2.2 Sample preparation

The various model compounds used in this study (see figure 5.1 below for the corresponding structures) were fixed using an unbuffered solution of 0.6% v/v glutaraldehyde in water and in various aqueous pH buffers (pH 4, 7.4 and 9.2) for 14 days in the dark at 37°C (see table 5.1 for details). Unbuffered commercial glutaraldehyde (0.6% v/v) in water was used as a control and was left under similar conditions for 14 days prior to being analysed. It has already been reported that the

reactions of glutaraldehyde with proteins are complete after 7 days¹⁴. The solution of glutaraldehyde was diluted immediately before use from a 25% v/v commercial glutaraldehyde solution.

Model compound names (0.1% w/v)	Glutaraldehyde (0.6% v/v)	Solvents
6-amino-n-caproic acid (0.025 g, 1.90×10^{-4} moles)	(0.6 mL, 6.36×10^{-3} moles)	In buffers pH 4, 7.4, 9.2 and unbuffered in H ₂ O
N- α -acetyl lysine (0.025 g, 1.33×10^{-4} moles)	(0.6 mL, 6.36×10^{-3} moles)	In buffers pH 4, 7.4, 9.2 and unbuffered in H ₂ O
N-acetyl Phe Lys (0.025 g, 7.46×10^{-5} moles)	(0.6 mL, 6.36×10^{-3} moles)	In buffers pH 4, 7.4, 9.2 and unbuffered in H ₂ O
N-acetyl Gly Lys methyl ester (0.025 g, 9.65×10^{-5} moles)	(0.6 mL, 6.36×10^{-3} moles)	In buffers pH 4, 7.4, 9.2 and unbuffered in H ₂ O
Cytochrome C (0.025 g, 2.02×10^{-6} moles)	(0.6 mL, 6.36×10^{-3} moles)	Unbuffered in H ₂ O
Lysozyme (0.025 g, 1.75×10^{-6} moles)	(0.6 mL, 6.36×10^{-3} moles)	Unbuffered in H ₂ O

Table 5.1: Model compounds fixation methodology.

The optimum molar ratio for the reaction of 0.1% w/v (0.025 g , 1.90×10^{-4} moles) 6-amino-n-caproic acid and glutaraldehyde reacted in water for 14 days was also investigated using FTIR-ATR. The molar ratio was changed by increasing the glutaraldehyde molar concentration as follows: (1:2), (1:4), (1:8), (1:11) and (1:33).

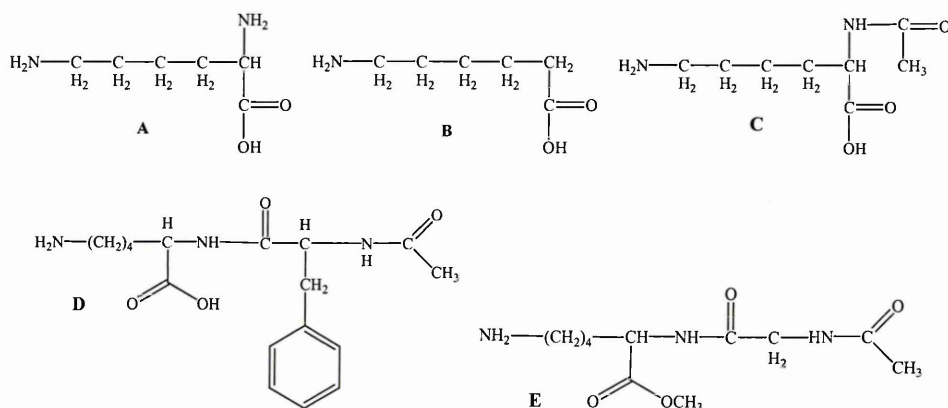


Figure 5.1: Molecular structures of some of the model compounds used in this study compared to lysine. (A) lysine; (B) 6-amino-n-caproic acid; (C) n-acetyl-l-lysine; (D) n-acetyl phenylalanine lysine; (E) n-acetyl glycine lysine methyl ester.

5.2.3 Freeze-drier

The freeze-drier used and the procedure employed were the same as the one stated previously in chapter 4 (section 4.2.3).

5.2.4 FTIR-ATR analyses

The methodology employed in this study was as described in chapter 4 (section 4.2.4).

5.2.5 Raman analyses

The samples were freeze-dried on a quartz slide and analysed directly under the microscope of the Raman instrument. The instrument and methodology employed in this study were as described in chapter 4 (section 4.2.5).

5.2.6 NMR analyses

For the study of amino acids and peptides reacted or not with glutaraldehyde in water and in various pH buffers, the samples were prepared by freeze-drying 3 x 25 mL of solution (0.1% w/v solution of amino-containing compounds, reacted or not with 0.6% v/v glutaraldehyde). The samples were immediately re-dissolved in 3 mL of D₂O and analysed. ¹H (250 MHz) and ¹³C (63 MHz) NMR were then run on these samples. The NMR spectrometer used was a Bruker AC250 (Bruker Biospin, USA). The E field was of 58000 Gauss.

For the study of proteins (lysosyme and cytochrome C), reacted or not with glutaraldehyde in water and in various pH buffers, the samples were prepared the same way as for amino acids and peptides (see above). ¹H (400 MHz) and ¹³C (100MHz) NMR were then run on these samples. The NMR spectrometer used was a Bruker 400 (Bruker Biospin, USA). The E field was of 92800 Gauss.

5.2.7. ESI-MS analyses

The instrument and methodology employed in this study were as described in chapter 4 (section 4.2.6).

5.2.8 MALDI-TOF MS analyses

For the analysis of amino acids (6-amino-n-caproic acid, N- α -acetyl lysine) and peptides (N-acetyl Phe Lys, N-acetyl Gly Lys methyl ester), samples (3 x 25 mL) of 0.6% v/v glutaraldehyde-treated compounds in distilled water and in pH 4, pH 7.4

and pH 9.2 buffers were freeze-dried and re-dissolved in 3 mL methanol. The instrument and methodology used in the amino acids and peptides study were as described in chapter 4 (section 4.2.7).

For the analysis of the proteins (lysosyme and cytochrome C), the matrix solution (DHB) was prepared as a 7 mg/mL solution in ethanol. A volume of 2 μ L of the proteins samples (0.1% w/v) reacted or not with glutaraldehyde (0.6% v/v) was mixed with 20 μ L of the DHB matrix solution. One drop of trifluoro-acetic acid (0.1% v/v TFA) was added to facilitate the formation of a protonated molecular ion. The sample/matrix mixtures were spotted (\sim 1 μ L droplet) onto a stainless steel modified 25-well MALDI target and left to air dry. The instrument used was a Finnigan Vision 2000 Reflectron MALDI-TOF MS (Finnigan Mat Ltd., Hemel Hempstead, Herts, UK) with a N₂ (λ =337 nm) laser and a linear time-of-flight mass analyser linked to a dedicated PC for data acquisition and manipulation of results. Only the positive mode was used in these investigations.

5.3 Results and discussion

5.3.1 Determination of optimum molar ratio

The optimum ratio for the reaction of ACA (6-amino-n-caproic acid, an aliphatic amine mimicking the behaviour of lysine/hydroxylysine residues in tissue) with glutaraldehyde in solution was investigated by FTIR spectroscopy, altering the molar ratio by increasing the amount of glutaraldehyde in solution and keeping the amount of the aliphatic amine constant. The results obtained can be seen in figures 5.2 and 5.3 below. Figure 5.2 shows the various infrared spectra (expansion of the 3600-2000 cm^{-1} region) obtained from freeze-dried glutaraldehyde-treated 6-amino-n-caproic acid solutions at a range of molar ratios, while figure 5.3 shows an expansion of the 1800-600 cm^{-1} spectral region.

In figure 5.2, one can notice the presence of aromatics (band at 3060 cm^{-1}) due to reaction products appearing at the 1:4 ratio (blue trace) but the intensity of the peak clearly increases at the 1:8 ratio (green trace). The position of the 2929 cm^{-1} band (CH₂ anti-symmetric stretch) characteristic of ACA (6-amino-n-caproic acid) found in the silver trace is shifted slowly through the various increasing ratios until

reaching 2932 cm^{-1} at the 1:33 ratio (brown trace). The ACA characteristic peak at 2895 cm^{-1} disappears fairly quickly with increasing ratios: it is still observed at the 1:2 ratio (black trace) but is barely seen at the 1:4 ratio (blue trace). The ACA band at 2856 cm^{-1} (CH_2 symmetric stretch) is gradually shifted as the ratio increases, for example it is seen at 2860 cm^{-1} at the ratio 1:2 (black trace) and at 2868 cm^{-1} at the 1:33 ratio (brown trace), which are still thought to correspond to the symmetric stretching of CH_2 . Many other peaks characteristic of the presence of 6-amino-n-caproic acid (e.g. 2849 , 2768 , 2703 , 2653 , 2560 and 2496 cm^{-1}) tend to disappear as the amount of glutaraldehyde is increased, i.e. these peak are still observed at the 1:2 ratio (black trace), are barely observed at the 1:4 ratio (blue trace) and can not be seen at ratios of 1:8 (green trace) and above. However, a band at 2724 cm^{-1} (anti-symmetric stretching of the CH of an aldehyde group) looks present at the 1:11 ratio (red trace) and is definitely present at the 1:33 ratio (brown trace), which would indicate a large excess of glutaraldehyde at these ratios since this band is characteristic of glutaraldehyde (pink trace). In addition, the NH_3^+ stretch band at 2211 cm^{-1} disappears gradually with increasing ratio, being weaker at the 1:2 ratio (black trace), just observed at the 1:4 ratio (blue trace), but not observed at ratios of 1:8 (green trace) and above. This indicates uptake of the amino group in the reaction with glutaraldehyde.

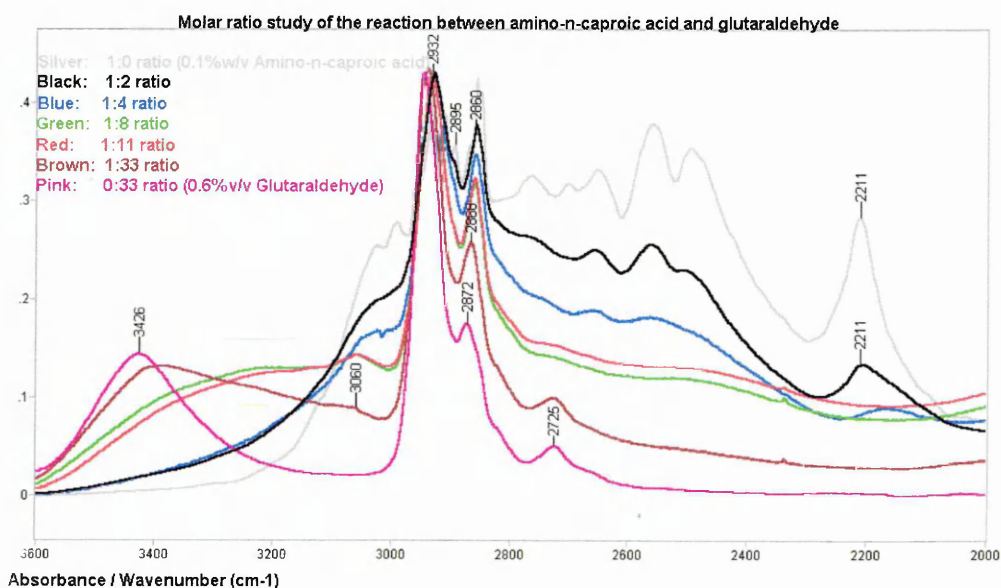


Figure 5.2: FTIR-ATR spectrum (expansion of the 3600-2000 cm^{-1} region) obtained from the molar ratio study of the reaction between 6-amino-n-caproic acid and glutaraldehyde (freeze-dried unbuffered aqueous solutions).

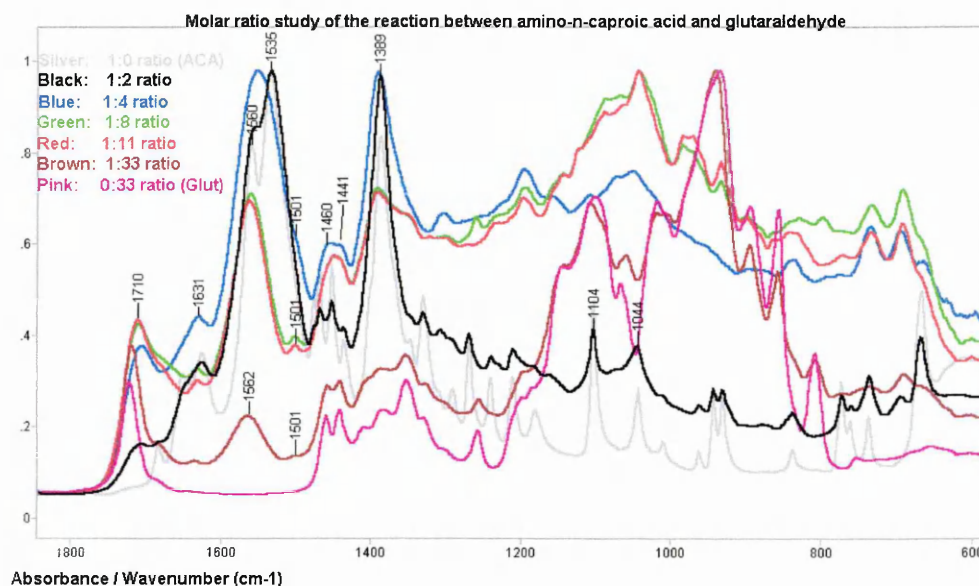


Figure 5.3: FTIR-ATR spectrum (expansion of the 1800-600 cm^{-1} region) obtained from the molar ratio study of the reaction between 6-amino-n-caproic acid and glutaraldehyde (freeze-dried unbuffered aqueous solutions).

In figure 5.3 above, as soon as glutaraldehyde reacts with the aliphatic amine, the characteristic ACA band at 1683 cm^{-1} (possibly assigned to a $\nu(\text{C}=\text{O})$ acid mode) disappears, along with bands at 1651 and 1624 cm^{-1} (NH bending of the amine) and the ones at 1103 cm^{-1} (NH_3^+ rock/ NH_2 twist) and 1043 cm^{-1} (C-N stretch). These losses are expected because of the reaction of glutaraldehyde with the amino group of the aliphatic amine. Instead, other peaks appear in the region indicative of the reaction of the aliphatic amine with glutaraldehyde. For example, a band at 1710 cm^{-1} appears weak as early as at the ratio 1:2 (black trace) and gets more intense with increasing ratio (from 1:2 to 1:11 ratios). However, this peak becomes a shoulder at the 1:33 ratio since another band at 1721 cm^{-1} (stretching of the CO groups of non-conjugated aldehydes and possibly carboxylic acids) becomes more prominent from the 1:4 ratio to the 1:33 ratio. This seems to be indicative of the presence of excess of glutaraldehyde since this band is also present in the glutaraldehyde spectrum (pink trace). A new band at 1631 cm^{-1} can also be observed clearly at the 1:11 ratio (red

trace) and could possibly be assigned to the formation of pyridinium ions, while the two characteristic peaks of the aliphatic amines at 1651 and 1624 cm^{-1} slowly disappear (see the 1:2 ratio, black trace). The characteristic doublet (1536 and 1560 cm^{-1}) assigned to the $\nu(\text{COO}^-)$ anti-symmetric mode that can be observed in the ACA spectrum (silver trace), disappears as soon as glutaraldehyde is introduced (see the 1:2 ratio, black trace), while a single unassigned band at 1562 cm^{-1} appears as early as at the 1:4 ratio (blue trace). A shoulder appears also at 1501 cm^{-1} at the 1:4 ratio (blue trace). The three characteristic peaks of ACA at 1469, 1452 and 1436 cm^{-1} (assigned to $\delta(\text{CH}_2)$ mode) disappear slowly with an increasing ratio but can be still observed at the 1:2 ratio (black trace). However, two bands at 1460 and 1441 cm^{-1} appear as a partially separated broad band (ratio 1:4, blue trace) and appear sharper with increasing ratio (ratio 1:33, brown trace). These bands can thus be assigned to the deformation of CH_2 and CH groups, due to an excess of glutaraldehyde since bands at the same frequency are found in the spectrum of glutaraldehyde (pink trace). The sharp and intense characteristic band of ACA at 1388 cm^{-1} also disappears slowly (see ratio 1:2 black trace and ratio 1:4 blue trace), until it has disappeared completely at the ratio 1:8 (green trace) leaving new bands that appear to belong to the reaction products (see appendix IV).

The overall results suggest an optimum molar ratio between about 1:2 and 1:4, with a preference for the 1:4 ratio. It would appear therefore that a molecule of an amino compound reacts with two to four molecules of glutaraldehyde, though this stoichiometric relationship may well vary depending on the amino compound used for the reaction study. Our data (molar ratio between about 1:2 and 1:4) agree with others who also tried to clarify the stoichiometric factor of the reaction between an aliphatic amine and glutaraldehyde in aqueous solution and who proposed the following molar ratio: 1 mole of amino residue: 3 moles of glutaraldehyde⁶, 2 moles of amino residues: 3 moles of glutaraldehyde⁵, 1 mole of amino residue: 4 moles of glutaraldehyde^{3,15,16}.

5.3.2 General characteristics of the reactions of model compounds with glutaraldehyde

The products of the reaction of glutaraldehyde with amino compounds exhibit a yellow colour in solution at any pH studied. However, this colouration becomes

more intense with an increasing pH. The extent of this colour production with lysine has been reported to be proportional to the glutaraldehyde concentration, when measured by UV absorbance at 460 nm, when reaction times were kept constant¹⁷. In this study, we observed a dark amber colouration at basic pH, and a yellow and pale whitish-yellow colour at physiologic and acidic pH respectively, which is in agreement with the statements of others⁷. Other likely explanation is that the colour is due to conjugated condensation products of glutaraldehyde or to oxidation products of pyridinium compounds and more probably the former because of the presence of double ethlenic bonds.

Monitoring the pH before and after combining glutaraldehyde and amino-model compounds in solution showed that immediately after combining them, the pH of all the reaction mixtures decreased slightly (the pH drop being more pronounced in the absence of buffer), a fact that was already underlined by others^{18,19}. This can be partly explained by the uptake of basic amino groups in the reaction with glutaraldehyde. Alternatively, the solutions become more acidic because of deprotonation of the amino groups¹⁹. The reaction of glutaraldehyde with free amino groups causes the following dissociation equilibrium to be shifted to the right⁷ and thus neutral or basic pHs enhance this reaction^{20,21}:



This release of hydrogen ions contributes to the pH change in the tissue/model compounds during fixation with glutaraldehyde. One can consider that the isoelectric state (zwitterion) of the model compounds studied in this study would be observed over a wide pH range (4-8) similarly to glycine¹⁹. Since the amino groups, in order to react with glutaraldehyde, need to be deprotonated, this can explain the change in colour between pH 4-9 (more intense at high pH) because it would be easier for the reaction to take place at higher pH rather than at lower pH levels. Also, in order to explain this drop in pH, it has been previously documented that purified glutaraldehyde contains about 0.002 equivalents of hydrogen ions per mole of glutaraldehyde, the total amount of hydrogen ions released when added to amines/proteins solutions being proportional to the concentration of primary amines²². This could explain the slight drop in pH observed with all our samples (amino-containing compounds reacted with glutaraldehyde).

5.3.3 Study of the reaction of glutaraldehyde with small amines and peptides

5.3.3.1 6-amino-n-caproic acid reacted with glutaraldehyde:

5.3.3.1.1 ESI-MS:

A typical mass spectrum of the products of the reaction between 0.1% w/v 6-amino-n-caproic acid and unbuffered 0.6% v/v glutaraldehyde in water (resulting pH of 4.76) after 14 days is shown in figure 5.4 below. It appears that the reaction yields quite a complex palette of products, more complicated than what was previously reported²³, where the mixture was found to be composed of at least 12 unidentified compounds. A recent mass spectrometric study of the reaction products of 6-amino-n-caproic acid and glutaraldehyde allowed the determination of ten molecular structures^{24,25}, which represent only a few out of the ones depicted in this study (see table 5.1 and appendix IV for details of the m/z values and corresponding molecular structures, including references for some structures that have previously been assigned by others).

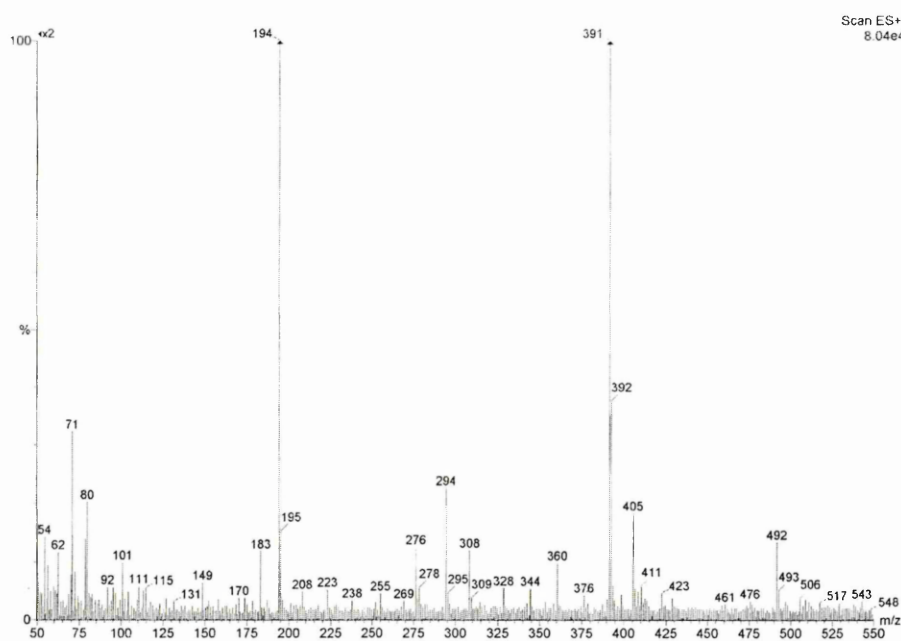


Figure 5.4: ESI-MS spectrum of an unbuffered aqueous solution of glutaraldehyde-treated 6-amino-n-caproic acid (resulting pH of 4.76). The inlet direct infusion of the sample was carried out at a rate of $5 \mu\text{L} \cdot \text{min}^{-1}$. The m/z range was 50-550.

For the sake of clarity, the characteristic ions in the mass spectrum obtained are summarised in table 5.2 (see appendices III and IV for details). The ions include

protonated molecules $[M+H]^+$ and $[M+Na]^+$, and $[M+K]^+$ adduct ions. Most spectra are dominated by intense $[M+H]^+$ ions.

m/z	Proposed assignment (Mw)	m/z	Proposed assignment (Mw)	m/z	Proposed assignment (Mw)
101	Mol I (100)	308/309	Mol XVIa (282+Na), mol XVIIa (282+Na), mol XXXIII (282+Na)	423	Mol XVIIIb (382+K), mol XVIIIc (400+Na), mol XXXIVa (382+K); mol XXXVIIa (382+K)
183	Mol XV (182), mol XXXI (182), mol XXXII (182)	328	Mol LXI (326), mol XXVI (328), mol L (328)	429	Mol XIX (428), mol LI (428), mol XCVII (390+K), mol XCVIII (389+K), mol CXVI (390+K)
194/195	Mol LXV (195), mol LXVI (194)	342	Mol VI (318+Na), mol IX (301+K)	461	Mol CXIV (459), mol CLV (460), mol CLIX (459)
223	Mol XV (182+K), mol XVa (200+Na), mol XXXI (182+K), mol XXXII (182+K)	344	Mol LXXIII (344)	477	Mol CLXIX (477), mol CLXX (477)
238	Mol LX (223+Na), mol CLXXIII (214+Na)	360	Mol VI (318+K)	492/493	Mol CVIII (490), mol CXII (490), mol CXXIII (490), mol CXXIX (490), mol CXLVII (490), mol CLXVIII (490)
255	Mol LXII (231+Na), mol LXVII (231+Na), mol LXXII (231+Na), mol CLXXIII (214+K)	376/377/378	Mol CVI (377), mol CVII (377), mol CVIIa (377), mol CXI (377), mol CXXII (377), mol CXLIX (377), mol CXLIXa (376), mol CL (377), mol CLXVI (377), mol CLXXIV (378) mol CLXXV (376)	506	Mol XIXc (482+Na), mol XXXVIIIb (482+Na)
269	Mol XXIV (246+Na), mol XXV (228+K)	391/392/395	Mol XXIX (392), mol XCVII (390), mol XCVIII (389), mol CXVI (390), mol CXLI (395), mol CXLVIII (395), mol CLXIV (395)	509	Mol CXLII (508), mol CXLV (507), mol CXLVI (508), mol CLI (508), mol CLXV (508)

276/278	Mol CXV (277)	405	Mol XVIIIa (364+K), mol XVIIIb (382+Na), mol XXXIV (364+K), mol XXXIVa (382+Na), mol XXXVII (364+K), mol XXXVIIa (382+Na), mol XLVI (364+K)	543	Mol CI (520+Na)
294/295	Mol XCII (295), mol CIII (295), mol CIV (295), mol CV (295), mol CXIX (295), mol CXXXVII (295), mol CXXXIX (295)	410/411/ 413/414	Mol XXVIII (410), mol LXIX (414), mol LXXVI (414), mol LXXX (413), mol XCIII (408), mol XCVI (408), mol CXVII (408), mol CXXXVIII (408)		

Table 5.2: Proposed structures for the observed ions (see spectrum in figure 5.4) for the analysis by ESI-MS of an unbuffered aqueous solution of glutaraldehyde-treated 6-amino-n-caproic acid. The molecule numbers refer to the molecular structures found in appendices III and IV (molecules in blue are due to excess glutaraldehyde, while the ones in black belong to the reaction products formed between glutaraldehyde and 6-amino-n-caproic acid).

From the ESI-MS spectrum, one can assume that all the 6-amino-n-caproic acid has totally undergone reaction with glutaraldehyde since no protonated molecular ion is observed (expected at $\sim m/z$ 132). The spectrum indicates the presence of various molecular structures, including the reaction products of the amino-compound with glutaraldehyde (in black in table 5.1) and also the presence of excess glutaraldehyde (in blue in table 5.2). The most intense ions that can be observed in figure 5.4 are discussed below, however a more complete account of all the molecules present in the spectrum according to their m/z values and structures can be found in table 5.2 and appendices III and IV, respectively.

The intense ions detected at m/z 194/195 could indicate the presence of molecule LXVI (quaternary pyridinium compound: 5-(pyridin-1-yl) caproic acid with Mw 194), and the corresponding dihydropyridine (molecule LXV with Mw 195).

The intense signal of ions at m/z 391/392/395 could be due to the anabilysine-like compound (molecule XCVII with Mw 390 and molecule XCVIII with Mw 389) or an aldol dimer of glutaraldehyde that underwent two Schiff base reactions (molecule

CXVI with Mw 390). They could also be indicative of a trialdol condensation product which underwent a Michael-type addition of the amine (molecule CXLI with Mw 395); a dialdol condensation product of glutaraldehyde that underwent a Schiff base addition and a Michael addition (molecule CXLVIII with Mw 395, or a dialdol condensation product that underwent a Mannich-type reaction forming a stable secondary amine (molecule CLXIV with Mw 395). These ions could also be due to the presence of an aldol condensation pentamer product of glutaraldehyde partially cyclised (molecule XXIX with Mw 392).

The molecule CXLVIII is also an intermediate in the formation of molecule CXLIXa with Mw 376 and the corresponding dihydropyridine molecule CXLIX (Mw 377), with m/z 376/377/378).

Relatively intense ions seen at m/z 276/278 may correspond to molecule CXV with Mw 277 (glutaraldehyde aldol dimer that underwent a Schiff base reaction).

The intense peaks at m/z 294/295 could indicate the presence of molecule XCII with Mw 295 (Schiff base on an dialdol condensation product), molecule CIII with Mw 295 (Michael-type addition on a dialdol condensation product with a subsequent cyclisation), molecule CIV with Mw 295 (isomer of CIII with a different cyclisation), molecule CV with Mw 295 (isomer of CIII with a different cyclisation), molecule CXIX with Mw 295 (Michael-type addition on an aldol dimer of glutaraldehyde), molecule CXXXVII with Mw 295 (Schiff base addition on an aldol condensation product) or molecule CXXXIX with Mw 295 (dehydrated product of CXXXVII).

The intense signals at m/z 492/493 may be indicative of molecules CVIII with Mw 490 (di-Schiff base addition on an aldol trimer), molecule CXII with Mw 490 (same as CVIII but with a subsequent cyclisation step), molecule CXXIII with Mw 490 (di-Michael-type addition on an aldol trimer), molecule CXXIX with Mw 490 (Michael-type addition and Schiff base on an aldol trimer), molecule CXLVII with Mw 490 (di-Michael-type addition on an aldol trimer with a subsequent cyclisation step) or molecule CLXVIII with Mw 490 (Mannich-type addition followed by a cyclisation step and a Schiff base addition).

Overall, there was also evidence of various Schiff base cross-links involving between two and five molecules of glutaraldehyde, along with more complicated structures (see table 5.1 and appendix IV).

5.3.3.1.2 MALDI-TOF MS:

The characteristic ions in the MALDI-TOF mass spectra (a typical MALDI spectrum is shown below in figure 5.5) of 6-amino-n-caproic acid reacted with glutaraldehyde, buffered at pH 4, 7.4 and 9.2 for 14 days (see table 5.3 for summary of results) appeared to present many similarities in comparison to the ones obtained with glutaraldehyde-treated 6-amino-n-caproic acid reacted in water (both ESI and MALDI mass spectra), suggesting the formation of similar reaction products. For instance, the two most intense peaks observed in the ESI-MS spectrum of unbuffered glutaraldehyde-treated 6-amino-n-caproic acid (see above figure 5.4) also correspond to the most intense peaks in the MALDI-TOF spectrum (see below figure 5.5). These intense ions detected at m/z 194/195 could indicate the presence of molecule LXVI (quaternary pyridinium compound: 5-(pyridin-1-yl) caproic acid with Mw 194), and the corresponding dihydropyridine (molecule LXV with Mw 195). The intense peaks at m/z 391/392 could correspond to the anabilysine-like compound (molecule XCVII with Mw 390 and molecule XCVIII with Mw 389) or an aldol dimer of glutaraldehyde that underwent two Schiff base reactions (molecule CXVI with Mw 390). These ions could also be due to the presence of an aldol condensation pentamer product of glutaraldehyde partially cyclised (molecule XXIX with Mw 392).

The spectra included protonated molecules i.e. $[M+H]^+$ and $[M+Na]^+$ and $[M+K]^+$ adduct ions, with most being dominated by intense $[M+H]^+$ ions. Similar m/z values to those discussed above (section 5.3.3.1.1) were observed allowing the conclusion that similar molecules to the ones already mentioned were present.

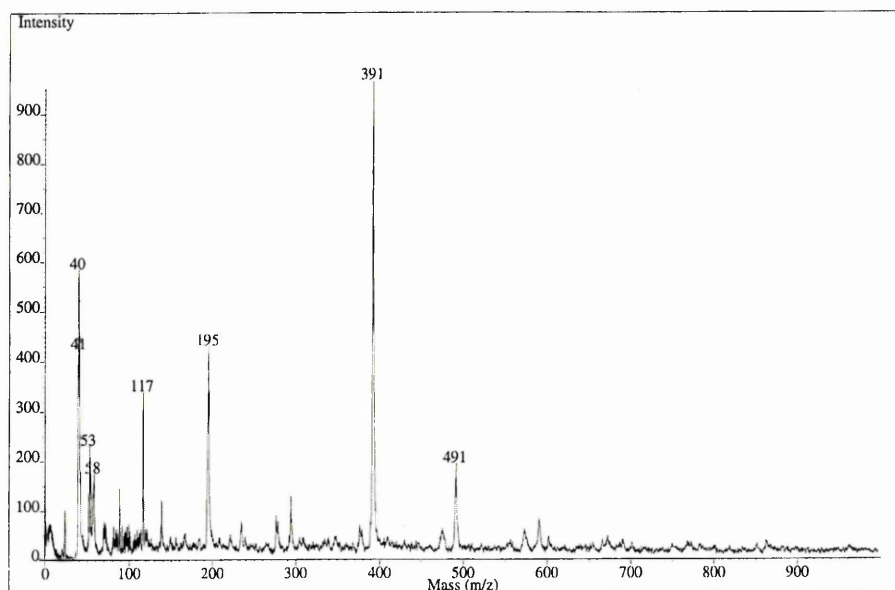


Figure 5.5: Typical MALDI-TOF mass spectrum obtained from the analysis of 0.1% w/v 6-amino-n-caproic acid reacted with 0.6% v/v unbuffered glutaraldehyde. Samples were freeze-dried and re-dissolved in methanol. The matrix (DHB) was prepared as a 7 mg.mL⁻¹ solution in methanol. Samples rediluted in methanol were mixed with the matrix solution at a ratio of 1:1.

The MALDI-TOF MS analyses also allowed the investigation of the effect of pH on the reaction products of glutaraldehyde-treated 6-amino-n-caproic acid. The effect of pH on the reaction of glutaraldehyde with 6-amino-n-caproic acid has already been reported by Ishii et al²⁶. They observed that after being reacted for 60 minutes, only 40.2%, 88.1% and 86.1% of 6-amino-n-caproic acid reacted with glutaraldehyde at pH 4, 7, and 10 respectively, and that the reaction products at pH 4 behaved differently (dye affinity assay) in comparison with the reaction products at pH 7 and 10. However, when the reaction was continued further, the reaction products at pH 4 bound the dye in a similar fashion to those at other pHs. We believed that, immediately after mixing chemicals together (glutaraldehyde and amino acid for example), the observed dark amber colouration at basic pH, the yellow and pale whitish-yellow colour at physiologic and acidic pH respectively are due to the extent of reactions taking place in solution. In fact, all solutions at any kind of pH were recorded to exhibit a similar dark amber colour after being left for 14 days to react. Thus, our results agree undirectly with the findings of Ishii et al, since after the reaction has been allowed to proceed for 14 days, the reaction products would appear to be similar disregarding the pH (see below table 5.3). This led to the hypothesis of

a time dependence of the reaction kinetics of the reactions involving glutaraldehyde and amino acids in solution at a pH range 4-9.

M/z (reactions products formed in H ₂ O)	m/z (reactions products formed at pH 4)	m/z (reactions products formed at pH 7.4)	m/z (reactions products formed at pH 9.2)	Proposed Assignment (Mw)
23/24	23	23/24	23/24	Sodium (Na) cation
40/41	39/41	39/41	39/41	Potassium (K) cation
117	116/117	-	116/117/118	Mol XI (116)
-	120	119	120/122	Mol II (118); mol Iva and Ivb (118)
130	132/133	132	132/133	Mol X (132)
138	138	137	138	Mol III (136)
-	142/144	144	141/144/145	Mol I (100+K); mol II (118+Na); mol IV (118+Na); mol XI (116+Na)
-	156/157	157/158/159	154/155/156	Mol II (118+K); mol III (136+Na); mol IVa and IVb (118+K); mol X (132+Na); mol XI (116+K)
-	168/169	164/166/168	161/163	Mol XXIII (163)
-	177	175/177	177/178	Mol III (136+K)
-	-	-	187/188/189	Mol XXIII (163+Na)
194/195/196	193/194/195	193/195	192/193	Mol LXV (195); mol LXVI (194)
-	-	197/199	198/199/200	Mol XVa (200)
206	204/205	-	204/205	Mol VIIa (202); mol VIII (202); mol XV (182+Na); mol XXIII (163+K); mol XXXI (182+Na); mol XXXII (182+Na)
-	212/215/217/218	212/214/215	212/213/215/216/217	Mol LX (213); mol LXV (195+Na); mol LXVI (194+Na); mol CLXXIII (214); mol V (218)
221	223	-	220/221	Mol LXV (195+Na); mol V (218); mol XV (182+K); mol XVa (200+Na); mol XXXI (182+K); mol XXXII (182+K)
226	-	-	225/227	Mol VIIa (202+Na); mol VIII (202+Na); mol XVa (200+Na)
-	228/229	-	228/229	Mol XXV (228)
234	234	231/233	-	Mol LXII (231); Mol LXV (195+K); mol LXVI (194+K); mol LXVII (231); mol LXXII (231);
240	240/243	240/241	240/243	Mol V (218+Na); mol VIIa (202+K); mol VIII (202+K); Mol XVa (200+K)
-	-	-	245/246/247	Mol XXIV (246)
-	252	-	252/256	Mol LX (213+K); mol LXXII (231+Na); mol XXV (228+Na)
-	265	266	264	Mol XVI (264); mol XVII (264); mol XX (264); mol XLV (264)
-	-	-	271/272	Mol LXII (231+K); mol LXVII (231+K); mol LXXII (231+K); mol XXIV (246+Na)
276/278	277/279	276/278	-	Mol CXV (277)
283	281/283	281/283	283/284	Mol XVIa (282); mol XVIIa (282); mol XXXIII (282)
-	-	-	289	Mol XVI (264+Na); mol XVII (264+Na); mol XX (264+Na); mol XLV (264+Na)

294	294/295	294	-	Mol XCII (295); mol CIII (295); mol CIV (295); mol CV (295); mol CXIX (295); mol CXXXVII (295); mol CXXXIX (295)
304	304/305/306	305/306	303/304	Mol IX (301); mol XVI (264+K); mol XVIa (282+Na); mol XVII (264+K); mol XVIIa (282+Na); mol XVIa (282+Na); mol XX (264+K); mol XXXIII (282+Na); mol XLV (264+K)
309/311	308/312	-	311/312	Mol XXVII (310)
320	-	-	-	Mol XCII (295+Na); mol CIV (295+Na); mol CV (295+Na); mol CXIX (295+Na); mol CXXXVII (295+Na) mol CXXXIX (295+Na); mol VI (318)
323/324	-	-	324	Mol IX (301+Na); mol XII (300+Na); mol XVIa (282+K); mol XVIb (300+Na); mol XVIIa (282+K); mol XVIIb (300+Na); mol XXXIII (282+K)
332	332	332/333	332	Mol LXIII (332); mol LXXIV (331); mol XXVII (310+Na)
-	336/337	336	-	Mol LXVIII (314+Na); mol XCII (295+K); mol CII (313+Na); mol CIII (295+K); mol CIV (295+K); mol CV (295+K); mol CXIX (295+K); mol CXXXIV (313+Na); mol CXXXV (313+Na); mol CXXXVII (295+K); mol CXXXIX (295+K); mol CXL (313+Na); mol CLXIII (313+Na)
339	340/341	342	-	Mol LXVIII (314+Na); mol VI (318+Na); mol IX (301+K); mol XII (300+K); mol XVIb (300+K); mol XVIIb (300+K)
349	-	348	-	Mol XVIII (346); XXVII (310+K)
368	-	368	368/371	Mol LXXIII (344+Na); mol XXVI (328+K); mol L (328+K)
376/377/378	377/379	377/379	378	Mol CVI (377); mol CVII and CVIIa (377); mol CXI (377); mol CXXII (377); mol CXLIX (377); CXLIXa (376); mol CL (377); mol CLXVI (377); mol CLXXIV (378); mol CLXXV (376)
-	-	-	383/385	Mol LXXIII (344+K); mol XVIII (346+K); mol XVIIIb (382); mol XXXIVa (382); mol XXXVIIa (382); mol XLVII (346+K)
391/393	392/394	391/393	-	Mol XCVII (390); mol XCVIII (389); mol CXVI (390); mol XXIX (392)
-	-	394/395	-	Mol CXLI (395); mol CXLVIII (395); mol CLXIV (395)

-	-	-	398/400/402	Mol CVI (377+Na); mol CVII and CVIIa (377+Na); mol CXI (377+Na); mol CXXII (377+Na); mol CXLIX (377+Na); mol CL (377+Na); mol CLXVI (377+Na); mol CLXXIV (378+Na); mol CLXXV (376+Na); mol XVIIIc (400); mol XXX (374+Na)
-	-	-	406/407	Mol XVIIIb (382+Na); mol XXXIVa (382+Na); mol XXXVIIa (382+Na)
-	410	-	411	Mol XCIII (408); mol XCVI (408); mol CXVII (408); mol CXXXVIII (408); mol XXVIII (410)
-	-	-	422/424	Mol XVIIIb (382+K); mol XVIIIc (400+Na); mol XXXIVa (382+K); mol XXXVIIa (382+K)
-	430	429	430	Mol XCVII (390+K); mol XCVIII (389+K); mol CXVI (390+K); mol XIX (428); mol LI (428)
-	-	-	440/442	Mol LXIX (414+Na); mol LXXVI (414+Na); mol VII (418+Na); mol XVIIIc (400+K)
-	-	-	453	Mol LXIX (414+K); mol LXXVI (414+K); mol LXXX (413+K); mol XIX (428+Na); mol LI (428+Na)
-	472	-	471/472	Mol LXXV (431+K); mol CLII (472); mol CLXVII (472); mol XIXa (446+Na); mol XLVIII (446+Na)
475/478	477	478	477	Mol CXXVIII (455+Na); mol CLII (472); mol CLXIX (477); mol CLXX (477)
-	-	482	-	Mol CXIV (459+Na); mol CLIX (459+Na); mol XIXc (482); mol XXXVIIIb (482)
491/493	491	-	-	Mol CVIII (490); mol CXII (490); mol CXXIII (490); mol CXXIX (490); mol CXLVII (490); mol CLXVIII (490)
-	-	-	506	Mol XIXc (482+Na); mol XXXVIIIb (482+Na)
522	-	-	-	Mol XCIV (521); mol C (521); mol CI (520); mol CXVIII (521); mol XIXc (482+K); mol XXXVIIIb (482+K)
575	-	574/576	-	Mol CLXXVIII (574)
603	-	-	-	Mol CIX (603); mol CXXVI (603); mol CXXX (603); mol XXXIXa (564+K); mol XLb (564+K)
638	-	-	-	Mol LXXXIII (613+Na)
667	-	-	-	Mol XLII (628+K); mol LIII (628+K)
672	-	-	-	Mol CLVII (672)

Table 5.3: Proposed structures for the observed ions for the analysis by MALDI-TOF MS of aqueous solutions of glutaraldehyde-treated 6-amino-n-caproic acid unbuffered in water and buffered at pH 4, 7.4 and 9.2. The molecule numbers refer to the molecular structures found in appendices III and IV (molecules in blue are due

to excess glutaraldehyde, while the ones in black belong to the reaction products formed between glutaraldehyde and 6-amino-n-caproic acid).

5.3.3.1.3 NMR:

The ^1H NMR spectra of glutaraldehyde-treated 6-amino-n-caproic acid obtained at various pH values can be found in figure 5.6 below.

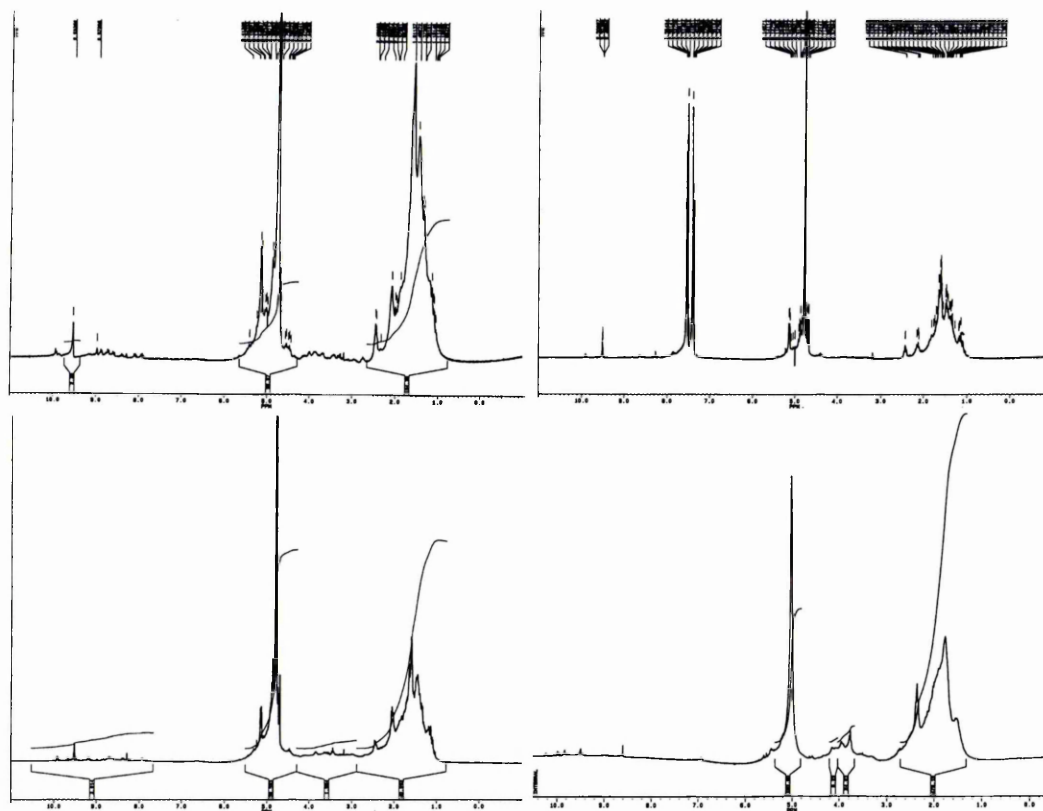


Figure 5.6: ^1H NMR spectra of unbuffered aqueous solution of glutaraldehyde-treated 6-amino-n-caproic acid at pH 4.76 (*top left*), buffered at pH 4 (*top right*), buffered at pH 7.4 (*bottom left*) and buffered at pH 9.2 (*bottom right*). The samples were freeze-dried, re-dissolved in D_2O and then analysed. Note that the strong extra bands (7.30-7.60 ppm) found in the spectrum at pH 4 correspond to the buffer (potassium hydrogen phthalate).

The proton NMR spectra, shown above in figure 5.6, although different to one another, exhibit many similar features. The broad peaks rendered the assignment of the peaks extremely difficult and the data obtained were mostly used to support the findings obtained by ^{13}C NMR. Nevertheless, a rough tentative assignment was made and is shown below in table 5.4.

Peak positions	Proposed assignments
Broad absorption (1-2.2 ppm) centered at 1.6 ppm	Assigned to exchangeable hydroxyl proton, methylene and central methylene protons
Signals between 2.2-2.5 ppm	Assigned to $-C-CH_2-CO-N-R$, $-C-CH_2-C=C-$, $-C-CH_2-CO-R$, $-C-CH_2-C=C-CO-$, $-C=C(CH_2-)-CO$ or $-C-CH_2-N$
Multiple weak signals between 2.6-4.3 ppm	Assigned to $-C-CH_2-OH$, $-C-CH_2-OR$, $-CH_2-N=$, $-CH_2-C=O$ or $=CH-N=$
Complex broad absorption between 4.3-5.6 ppm	Assigned to $-C=CH-$, $-CH=CO$, hydroxyl, hydrated aldehyde protons and olefinic protons of aldol condensates
Signals at 7.4-8.5 ppm	Assigned to aromatic protons and these of imine functions
Protons signals at 8.5-10 ppm	Assigned to aldehyde bands indicating the presence of many different environments of these carbonyl protons

Table 5.4: Line assignment of 1H NMR spectra (spectra found in figure 5.6) of aqueous solutions of glutaraldehyde-treated 6-amino-n-caproic acid at various pH values (pH 4-9.2). The samples were freeze-dried, re-dissolved in D_2O and then analysed.

The NMR data corroborate the mass spectral results since it appears that all the 6-amino-n-caproic acid has undergone reaction with glutaraldehyde (signals characteristic of the NMR analysis of 6-amino-n-caproic acid (spectrum not shown) can not be found), whilst signal attributable to excess glutaraldehyde was also seen. Additionally, the presence of pyridinium compounds could be inferred from some characteristic peaks, for example the unresolved band at ~ 1.2 (inside the broad band centered at 1.6 ppm) could be considered as diagnostic for aromatic protons. Additionally, a band at ~ 5.4 can be assigned to the CH_2 groups adjacent to N^+ , since the corresponding protons in cross-linking structures found in elastin (desmosine and isodesmosine) were reported to absorb at 5.5 and 5.45 respectively²⁷. Peaks at 8-9 ppm support the presence of substituted- and poly-substituted pyridine. However, our high-resolution NMR data failed to demonstrate the definite presence of polyaldol condensation products with almost no peaks detected at 6-8 ppm, but since these seem to be present from the MS data, they may be present at levels below the detection limit of this NMR experiment.

The ^{13}C NMR spectra of glutaraldehyde-treated 6-amino-n-caproic acid obtained at various pH values can be found in figure 5.7 below. Note that the extra bands

(131.89, 133.25, 137.09 and 176.69 ppm) found in the spectrum at pH 4 correspond to the buffer (potassium hydrogen phthalate).

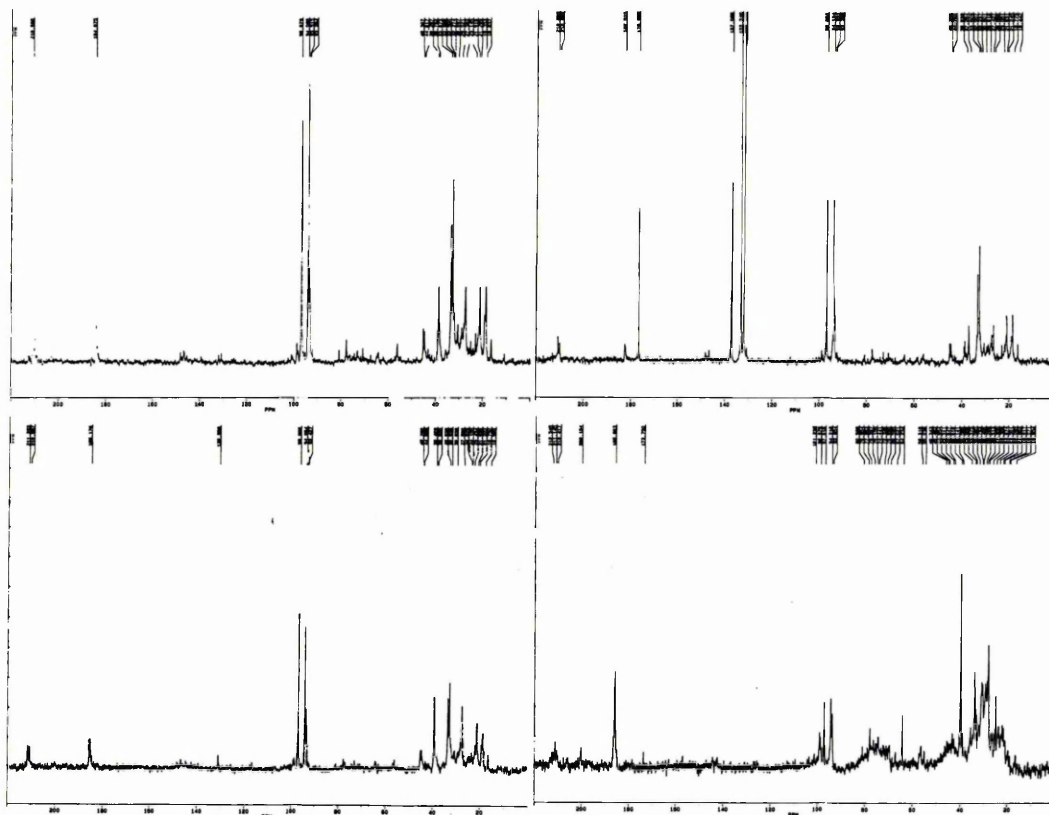


Figure 5.7: ^{13}C NMR spectra of unbuffered aqueous solution of glutaraldehyde-treated 6-amino-n-caproic acid at pH 4.76 (*top left*), buffered at pH 4 (*top right*), buffered at pH 7.4 (*bottom left*) and buffered at pH 9.2 (*bottom right*). The samples were freeze-dried, re-dissolved in D_2O and then analysed. Note the presence of the organic phthalate buffer in the spectrum at pH 4.

The ^{13}C NMR spectra shown in figure 5.7 appear different to each another indicating a pH dependence. It would appear, however, that a similar class of material is producing a NMR pattern at the same position, thus indicating that structures with similar reacting groups are formed over this pH range (4-9.2). The major difference between the spectra is the peak intensities. There has been limited ^{13}C NMR data related to the reaction between amino-containing compounds and glutaraldehyde reported in the literature, except for the spectrum of anabilysine²⁸, which is thought to be one likely cross-linking chemical structure. In an attempt to identify the chemical structures of the cross-links between hyaluronic acid and glutaraldehyde,

^{13}C NMR spectra in the hydrated state were also measured but no convincing evidence for the nature of the cross-link was found²⁹. Our ^{13}C NMR data however contain evidence for the molecular structures already proposed from the mass spectral data in this study. The chemical shifts of alkanes³⁰, heterocyclic compounds³¹ and alcohols³² have already been reported and were of some use in assigning some of the signals and identifying the various organic compounds present in solution. Unfortunately, the signal to noise ratio was not optimum enough to allow full determination of all the ^{13}C signals found in our spectra. Nevertheless, about at least fifty two ^{13}C signals can be clearly identified above the signal to noise level. Many others are thought to be present but their intensities are not sufficient to be characterised. A tentative assignment was performed, the results of which are shown in table 5.5 below.

Peak positions	Number of signals	Proposed assignments
0-20 ppm	4 signals	possibly assigned to $-\text{CH}_2-\text{CH}_2-\text{CH}(\text{CHO})-\text{CH}=\text{}$, $\text{CH}_2-\text{CH}_2-\text{CH}_2-\text{CH}(\text{CHO})=\text{CH}-$, $-\text{CH}_2-\text{CH}_2-\text{CH}_2-$, $-\text{CH}_2-\text{CH}_2-\text{CH}=\text{}$ or $-\text{CH}_2-\text{CH}_2-\text{C}$
20-32 ppm	10 signals	possibly assigned to $=\text{CH}-\text{CH}_2-\text{CH}(\text{CH}=\text{})-\text{CHO}$, $-\text{CH}_2-\text{CH}_2-\text{CH}_2-$, $-\text{CH}_2(=\text{CH})-\text{CH}-\text{CH}_2-$, $-\text{CH}_2-\text{CH}_2-\text{CH}=\text{}$, $=\text{CH}-\text{CH}_2-\text{C}(-\text{CH}=\text{})=\text{CH}-$, $-\text{CH}_2-\text{CH}_2-\text{CH}=\text{N}-$, $-\text{CH}_2-\text{CH}_2-\text{C}(-\text{CH}=\text{})=\text{CH}-$, $-\text{CH}_2-\text{CH}_2-\text{CH}(-\text{CH}=\text{})-\text{O}-$, $-\text{CH}_2-\text{CH}_2-\text{CH}(-\text{CH}=\text{})-\text{N}=\text{}$ or $=\text{CH}-\text{CH}_2-\text{CH}=\text{}$
32-40 ppm	7 signals	possibly assigned to $-\text{CH}_2-\text{CH}_2-\text{CH}(\text{O}-)-\text{O}-$, $-\text{CH}_2-\text{CH}_2-\text{C}(=\text{O})-\text{O}-$, $-\text{CH}_2-\text{CH}_2-\text{CH}(\text{C}\equiv\text{N})=\text{}$, $-\text{CH}_2-\text{CH}_2-\text{CH}(\text{O}-)-\text{NH}-$, $-\text{CH}_2-\text{CH}_2-\text{CH}(\text{OH})-\text{O}-$, $\text{C}-\text{CH}-\text{CH}_2-\text{C}$, $=\text{CH}-\text{CH}(-\text{CH}_2-)-\text{CH}=\text{}$, $-\text{CH}_2-\text{CH}(\text{CH}=\text{})-\text{CH}_2-$, $-\text{CH}_2-\text{CH}_2-\text{CH}(\text{OH})-\text{N}=\text{}$, $-\text{CH}_2-\text{CH}_2-\text{CH}(\text{OH})-\text{NH}-$ or $\text{CH}_2-\text{CH}_2-\text{N}=\text{}$
40-70 ppm	7 signals	possibly assigned to $-\text{CH}_2-\text{CH}_2-\text{NH}-$, $-\text{CH}_2-\text{CH}_2-\text{CHO}$, $-\text{CH}_2-\text{CH}=\text{CH}-\text{N}=\text{}$, $-\text{CH}_2-\text{CH}(\text{N}=\text{})-\text{CH}=\text{}$, $-\text{CH}_2-\text{CH}(\text{CHO})-\text{CH}=\text{}$, $-\text{CH}_2-\text{CH}_2-\text{NH}-$, $=\text{CH}-\text{CH}(-\text{CH}_2-)-\text{N}=\text{}$, $-\text{CH}_2-\text{CH}_2-\text{N}^+ \equiv \text{NH}(-\text{CH}_2-)-\text{CH}-\text{C}(-\text{CH}=\text{})=\text{CH}-$, $-\text{CH}_2(=\text{CH})-\text{C}-\text{CH}(-\text{CH}=\text{})-\text{N}=\text{}$, $-\text{CH}_2-\text{CH}(\text{C})-\text{N}=\text{}$, $-\text{CH}_2-\text{CH}=\text{CH}(-\text{CH}_2-)-\text{CH}=\text{}$, $-\text{CH}_2-\text{CH}_2-\text{OH}$ or $-\text{CH}_2-\text{CH}_2-\text{O}-$
70-90 ppm	5 signals	possibly assigned to $-\text{CH}_2-\text{CH}(-\text{CH}=\text{})-\text{O}-$, $-\text{CH}_2(-\text{OH})-\text{CH}-\text{CH}=\text{}$, $-\text{NH}-\text{CH}(-\text{CH}_2-)-\text{O}-$, $-\text{CH}_2-\text{CH}(\text{OH})-\text{NH}$ or $-\text{O}-\text{CH}(-\text{CH}_2-)-\text{OH}$
90-130 ppm	9 signals	possibly assigned to $-\text{O}-\text{CH}(-\text{CH}_2-)-\text{O}-$, $-\text{CH}_2(-\text{OH})-\text{CH}-\text{N}^+$, $-\text{CH}_2-\text{CH}=\text{CH}-\text{N}=\text{}$, $=\text{C}=\text{CH}-\text{N}=\text{}$, $-\text{CH}_2-\text{CH}=\text{C}=\text{}$, $-\text{CH}_2-\text{C}(=\text{CH})-\text{CH}=\text{}$, $=\text{N}-\text{CH}=\text{C}(-\text{CH}_2-)-\text{CH}=\text{}$, $=\text{N}-\text{CH}=\text{CH}-$ or $-\text{CH}=\text{CH}-\text{CH}=\text{}$
130-150 ppm	5 signals	possibly assigned to $-\text{CH}_2-\text{CH}=\text{CH}-\text{NH}-$, $-\text{CH}_2-\text{CH}=\text{CH}-\text{N}=\text{}$, $-\text{CH}_2-\text{CH}=\text{CH}-\text{N}^+ \equiv \text{C}(-\text{CH}_2-)-\text{C}-\text{N}^+ \equiv \text{CH}_2(=\text{CH})-\text{C}=\text{CH}-$, $-\text{CH}_2-\text{CH}=\text{C}(-\text{CHO})-\text{CH}_2-$, $=\text{CH}-\text{CH}=\text{CH}-$ or $-\text{CH}=\text{C}(-\text{CHO})-\text{CH}_2-$
150-200 ppm	1 signal	possibly assigned to $-\text{N}=\text{CH}-\text{CH}_2-$, $-\text{N}=\text{CH}-\text{CH}=\text{}$, $-\text{N}=\text{CH}-\text{C}$, $-\text{O}-\text{C}(=\text{O})-\text{CH}_2-$, $-\text{CH}_2-\text{COOH}$ or $-\text{CH}_2-\text{CH}(\text{CH}=\text{})-\text{CH}=\text{O}$
200-220 ppm	4 signals	possibly assigned to $-\text{CH}_2-\text{CH}_2-\text{CH}=\text{O}$ or $=\text{CH}(-\text{CH}_2-)-\text{CH}-\text{CH}=\text{O}$

Table 5.5: Line assignment of ^{13}C NMR spectra of aqueous solutions of glutaraldehyde-treated 6-amino-n-caproic acid (spectra found in figure 5.7). The samples were freeze-dried, re-dissolved in D_2O and then analysed.

These results suggest that probably not only the double imine bond ($\text{C}=\text{N}$) characteristic of the Schiff base is formed, but also a double ethylenic bond ($\text{C}=\text{C}$) characteristic of unsaturated structures such as aldol polymers. In addition, the NMR results corroborate the findings obtained by mass spectrometry, providing further evidence for the proposed structures of the molecules. Our data also seem to show the presence of some aldol polymers of glutaraldehyde involved in cross-linking and possibly in their free form, since glutaraldehyde is found in excess. This may disagree with previous work⁶, where only a low amount of aldol polymers was reported to be formed in the solution during cross-linking, which suggested only a small contribution of these molecules to the cross-linking. Nevertheless, the presence of such aldol polymers formed in glutaraldehyde aqueous solution was shown in chapter 4 (according to the NMR data) to represent apparently a small contribution to the overall content of the glutaraldehyde solution (in the pH range 4-9), and they thus could only account for a small amount of cross-linking structures when reacted with the amino-compound, except if one assumes that the presence of the amino compound could catalyse a further formation of glutaraldehyde polymers. This has been suggested by others³³ who reported that monomeric glutaraldehyde can only be converted to polymeric forms by the action of amino groups. But this is hard to confirm because the data obtained were not quantitative.

5.3.3.1.4 Raman spectroscopy:

The use of the dispersive Raman instrument was of limited value. All the samples reacted with glutaraldehyde (amino acids, peptides and proteins) showed a high degree of fluorescence, which totally masked the presence of Raman bands. Despite the use of a CCD camera and the known potential of the near-infrared laser to minimise fluorescence, successful analysis of the glutaraldehyde-reacted samples was not achieved. However, the spectra of all unreacted samples were recorded and kept for comparison with the infrared spectra of untreated samples. They were also used in the assignment of the infrared spectra of the freeze-dried glutaraldehyde-treated samples.

5.3.3.1.5 Fourier-transform infrared spectroscopy:

The spectra of 6-amino-n-caproic acid reacted with glutaraldehyde at various pH values (pH 4-9) are quite complex, but show very similar peaks (see figure 5.8 below for an example spectrum).

The bands at 2941 and 2868 cm^{-1} are CH stretching vibrations bands. Regarding the bands in the 1720-1600 region, previous authors³⁴ reported some infrared bands in this region that were characteristic of the reaction of glutaraldehyde with aliphatic amino compounds (isopropylamine). They showed that an imine (Schiff base) was formed, by condensation between the amine and the aldehyde function. A band at 1621 cm^{-1} was assigned to a conjugated imine, a shoulder at 1625 cm^{-1} was assigned to an alkene C=C bond or a conjugated imine, a broad peak at 1655 cm^{-1} was assigned to a double C=N bond (imine) and the band at 1720 cm^{-1} was assigned to a non-conjugated aldehyde function. The bands at 1625 and 1655 cm^{-1} were reported to be conjugated with each other³⁵.

Our spectra also show the presence of aromatic groups (3057 cm^{-1}), which could be assigned to the presence of pyridinium compounds, that are known to exhibit some characteristic bands at $\sim 3050 \text{ cm}^{-1}$ ($\nu \text{ CH}$), 1637-1630 cm^{-1} or 1538-1528 cm^{-1} ($\nu \text{ ring}$). Thus the band at 1635 cm^{-1} can be tentatively assigned to pyridinium compounds, while the band at 1665 cm^{-1} can be attributed to an ethylenic bond (C=C). The presence of many peaks in the 1800-1400 cm^{-1} region did not facilitate their assignment, since they are generally broad and overlap each other. Nevertheless, the main peaks present in this region can definitely be assigned to the reaction products since they do not appear in the spectra of the starting materials (not shown here). Additionally, the peak at 1460 cm^{-1} may be due to the absorption of an aldimine³⁶. The complex pattern between 1200-800 cm^{-1} is reminiscent of the infrared spectrum found with glutaraldehyde (see chapter 4), which was attributed to polymeric forms of glutaraldehyde. This indicates the contribution of the glutaraldehyde in the protein-glutaraldehyde reaction and supports the theory that glutaraldehyde is present in excess.

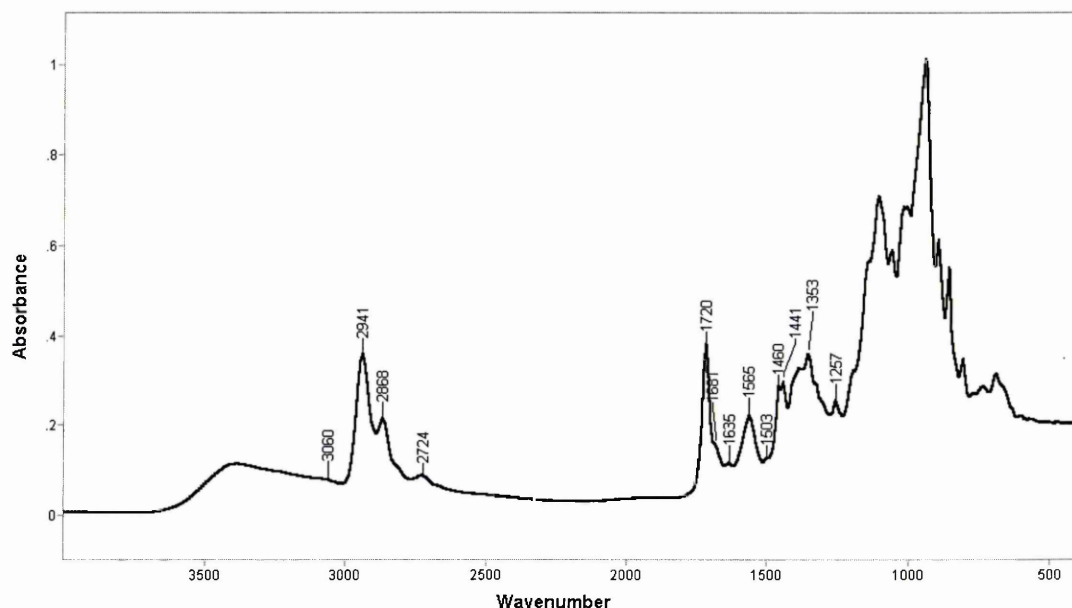


Figure 5.8: FTIR-ATR spectrum of a freeze-dried unbuffered aqueous solution of 6-amino-n-caproic acid (0.1% w/v) reacted with 0.6% v/v glutaraldehyde (resulting pH of 4.76).

5.3.3.2 N-acetyl-L-lysine and glutaraldehyde:

There was a general similarity between the reactions of the various model compounds (N- α -acetyl lysine and 6-amino-n-caproic acid) with glutaraldehyde, a fact that had been observed previously by others²³. The same reactions seemed to occur between glutaraldehyde and 6-amino-n-caproic acid or N- α -acetyl lysine, however, the final structures formed differed due to differences in the radical groups (R) of the two compounds (see appendix IV).

5.3.3.2.1 ESI-MS:

The results can be seen in figure 5.9 and table 5.6 below.

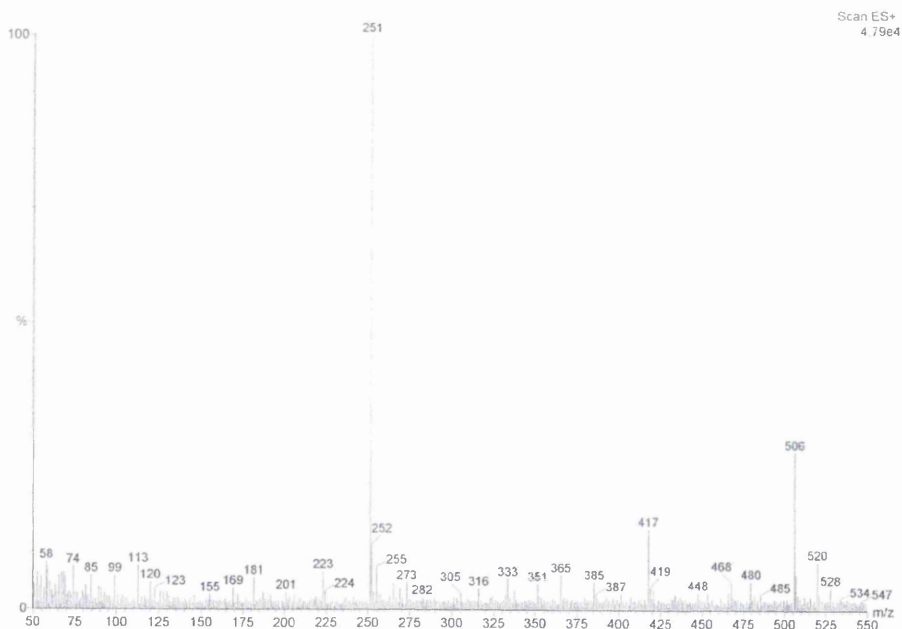


Figure 5.9: ESI-MS spectrum of a freeze-dried unbuffered glutaraldehyde-treated N-acetyl-L-lysine solution in water (resulting pH 3.96). The inlet direct infusion of the sample was carried out at a rate of $5 \mu\text{L} \cdot \text{min}^{-1}$. The m/z range was 50-550.

m/z	Proposed assignment (Mw)	m/z	Proposed assignment (Mw)	m/z	Proposed assignment (Mw)
120/ 123	Mol I (100+Na), mol II (118), mol IVa and IVb (118)	324	Mol IX (301+Na), mol XII (300+Na), mol XVIb (300+Na), mol XVIIb (300+Na)	448	Mol XIXa (446), mol XXXVIII (446), mol XLVIII (446)
155	Mol X (132+Na), mol XI (116+K)	333	Mol XXVII (310+Na)	453	Mol XIX (428+Na), mol LI (428+Na), mol CXLI (452), mol CXLVIII (452), mol CLXIV (452)
201	Mol XVa (200)	336	Mol CXV (334)	466/ 468	Mol XIX (428+K), mol XIXb (464), mol XXXV (464), mol XXXVI (464), mol XXXVIIIa (464), mol LI (428+K)
206	Mol XV (182+Na), mol XXXI (182+Na), mol XXXII (182+Na)	351/ 352	Mol XXVI (328+Na), mol XXVII (310+K), mol L (328+Na), mol XCII (352), mol CIII (352), mol CIV (352), mol CV (352), mol CXIX (352), mol CXXXVII (352), mol CXXXIX (352)	480	Mol LXI (440+K)

223/ 224	Mol XV (182+K), mol XVa (200+Na), mol XXXI (182+K), mol XXXII (182+K)	365	Mol XVIIIa (364), mol XXXIV (364), mol XXXVII (364), mol XLVI (364)	485	Mol XIXa (446+K), mol XIXc (482), mol XXXVIII (446+K), mol XLVIII (446+K), mol LXIII (446+K)
251/ 252	Mol XXV (228+Na), mol LXV (252), mol LXVI (251)	385/ 387	Mol XVIII (346+K), mol XVIIIa (364+Na), mol XXXIV (364+Na), mol XXXVII (364+Na), mol XLVI (364+Na), mol XLVII (346+K)	506/ 507	Mol XIXc (482+Na), mol XXXVIIIa (464+K), mol XXXVIIIb (482+Na), mol XCVII (504), mol CXVI (504)
273	Mol LX (270), mol CLXXIII (271)	401	Mol XVIIIc (400)	520	Mol CLV (517)
282	Mol XVIa (282), mol XVIIa (282), mol XXXIII (282)	417/ 419	Mol VII (418), mol XXIX (392+Na)	528	Mol XLI (528), mol LII (528), mol LXXV (488+K), mol XCVII (504+Na), mol XCVIII (503+Na), mol CXVI (504+Na)
305	Mol XVI (264+K), mol XVIa (282+Na), mol XVII (264+K), mol XVIIa (282+Na), mol XX (264+K), mol XXXIII (282+Na), mol XLV (264+K)	433/ 434	Mol XXVIII (410+Na), mol XXIX (392+K), mol CVI (434), mol CVII (434), mol CVIIa (434), mol CXI (434), mol CXXII (434), mol CXLIX (434), mol CXLIXa (433), mol CLXVI (434), mol CLXXV (433)		

Table 5.6: Proposed structures for the observed ions (see spectrum in figure 5.9) for the analysis by ESI-MS of a freeze-dried unbuffered solution of glutaraldehyde-treated N-acetyl-L-lysine (molecules in blue are due to excess glutaraldehyde, while the ones in black belong to the reaction products formed between glutaraldehyde and 6-amino-n-caproic acid). The molecule numbers refer to the molecular structures found in appendices III and IV.

The mass spectral results obtained from the products of the reaction of glutaraldehyde with N-acetyl-L-lysine are very much like the ones already described (see section 5.3.3.1) for the reaction between glutaraldehyde and 6-amino-n-caproic acid. The major ions detected, at m/z 251/252, again indicated the presence of molecule LXVI (a quaternary pyridinium compound with Mw 251), the corresponding dihydropyridine structure (molecule LXV with Mw 252) and possibly the presence of the glutaraldehyde-based aldol trimer molecule XXV (Mw 228 + sodium adduct). The other most intense peaks, at m/z 506/507, could be assigned to the presence of molecule XCVII (an anabylisine-like compound with Mw 504) and an aldol dimer of glutaraldehyde that underwent two Schiff base reactions (molecule

CXVI with Mw 504), along with the presence of glutaraldehyde molecules in excess in solution, such as molecules XIXc (fully hydrated aldol condensation pentamer product with Mw 482 + sodium adduct), XXXVIIIa (partially hydrated aldol condensation/Michael pentamer product with Mw 464 + potassium adduct) and XXXVIIIb (fully hydrated aldol/Michael pentamer product with Mw 482 + sodium adduct).

5.3.3.2.2 MALDI-TOF MS:

The characteristic ions seen in the MALDI-TOF mass spectra of the reaction mixtures at various pH values (pH range 4- 9.2) were virtually the same as the ones observed by ESI-MS for the analysis of unbuffered glutaraldehyde-treated N-acetyl-L-lysine (pH 3.96). The spectra included protonated molecules i.e. $[M+H]^+$, along with $[M+Na]^+$ and $[M+K]^+$ adduct ions. Most spectra were also dominated by intense $[M+H]^+$ ions and exhibited peaks with similar m/z values to those seen in table 5.5 (e.g. very intense peaks at m/z 252 or m/z 506). This therefore led to the conclusion that species to those identified from the reaction between glutaraldehyde and 6-amino-n-caproic acid were present. These Maldi-TOF MS data were quite identical to those observed for the MALDI analysis of glutaraldehyde-treated 6-amino-n-caproic acid (e.g. the intense peak observed below at m/z 607 in figure 5.10 correspond to the peak at m/z 491 found in figure 5.5). A typical MALDI-TOF mass spectrum obtained from the analysis of unbuffered glutaraldehyde-treated N-acetyl-L-lysine is shown below in figure 5.10.

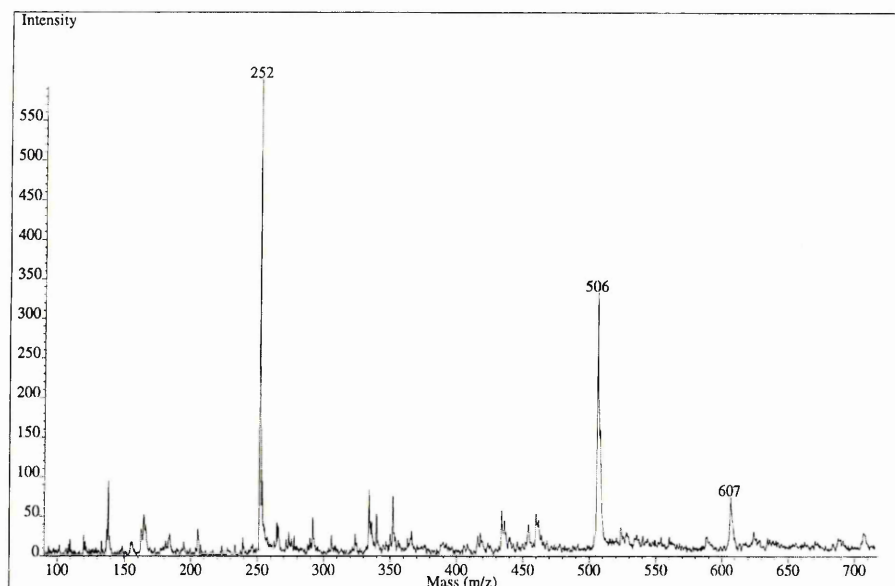


Figure 5.10: Typical MALDI-TOF mass spectrum obtained from the analysis of 0.1% w/v N-acetyl-L-lysine reacted with 0.6% v/v unbuffered glutaraldehyde. Samples were freeze-dried and re-dissolved in methanol. The matrix (DHB) was prepared as a 7 mg.mL⁻¹ solution in methanol. Samples re-diluted in methanol were mixed with the matrix solution at a ratio of 1:1.

5.3.3.2.3 NMR:

The NMR data obtained in the study of glutaraldehyde-treated N-acetyl-L-lysine revealed similar peak patterns to those found in the study of 6-amino-n-caproic acid. Typical ¹³C NMR spectra of glutaraldehyde-treated N-acetyl-L-lysine, obtained at various pH values, can be found in figure 5.11 below.

There was a general similarity between the NMR spectra (¹H and ¹³C) from reactions of glutaraldehyde-treated N-α-acetyl lysine and those from the analysis of glutaraldehyde-treated 6-amino-n-caproic acid (see figures 5.6 and 5.7 in section 5.3.3.1.3). All four NMR spectra are different from one another, revealing the pH dependence of the reactions of glutaraldehyde with amino acids. However they contain many similarities in their pattern, indicating the presence of similar reactive groups in reaction products. The assignment of the ¹³C signals were found very similar to those proposed for the analysis of glutaraldehyde-treated 6-amino-n-caproic acid (found in table 5.4 in section 5.3.3.1.3). This suggests that the NMR results also corroborate the findings obtained by mass spectrometry, providing further evidence for similar structures of the molecules to those proposed for the

analysis of the reaction products of glutaraldehyde-treated 6-amino-n-caproic acid. The same reactions therefore seemed to occur between glutaraldehyde and lysino group-containing model compounds such as 6-amino-n-caproic acid and N-acetyl-L-lysine.

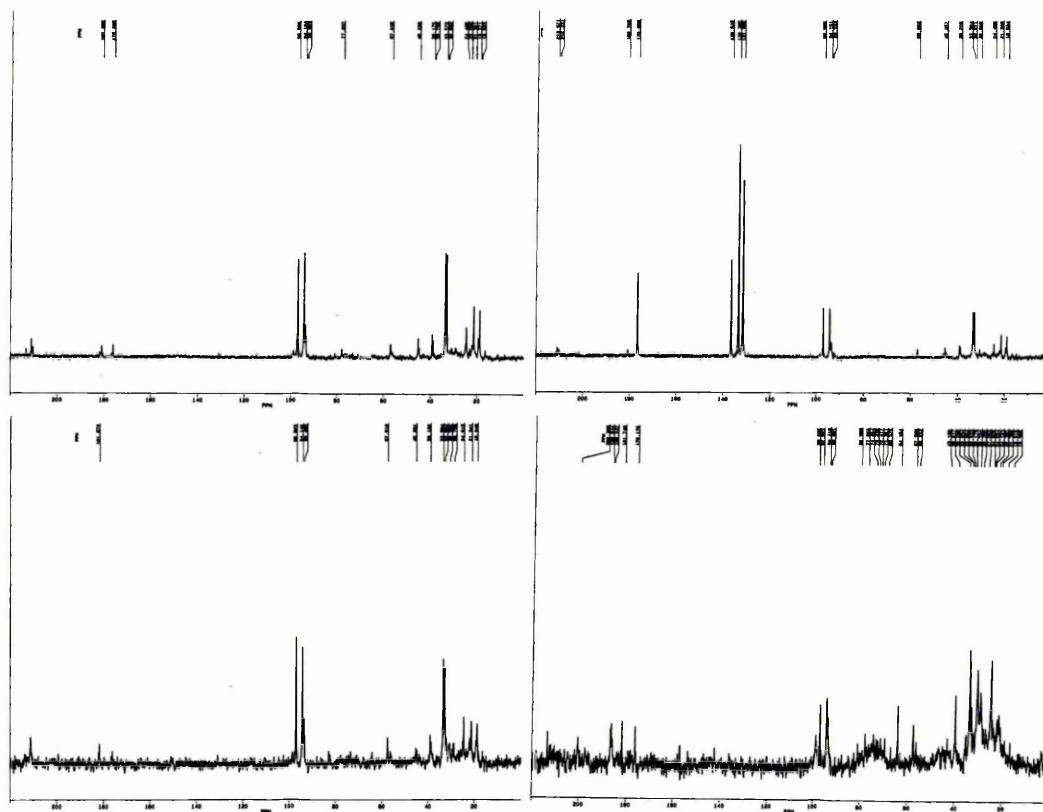


Figure 5.11: ^{13}C NMR spectra of unbuffered glutaraldehyde-treated N-acetyl-L-lysine at pH 3.96 (*top left*), buffered at pH 4 (*top right*), buffered at pH 7.4 (*bottom left*), buffered at pH 9.2 (*bottom right*). Note that the extra bands (at ca. 132, 133, 137 and 177 ppm) found in the spectrum at pH 4 correspond to the buffer (potassium hydrogen phthalate). The samples were freeze-dried, re-dissolved in D_2O and then analysed.

5.3.3.2.4 Fourier-transform infrared spectroscopy:

The infrared spectra obtained from the products of the reaction of N-acetyl-L-lysine with glutaraldehyde at various pH values (pH 4-9) are quite complex, but appear to display similar peak patterns to one another. Figure 5.12 shows an example spectrum. In addition, this pattern appears to be almost identical to the one described previously for the analysis of glutaraldehyde-treated 6-amino-n-caproic acid. This therefore allows the hypothesis that similar chemical structures species are formed

during the reaction between glutaraldehyde and N-acetyl-L-lysine, as seen been glutaraldehyde and 6-amino-n-caproic acid.

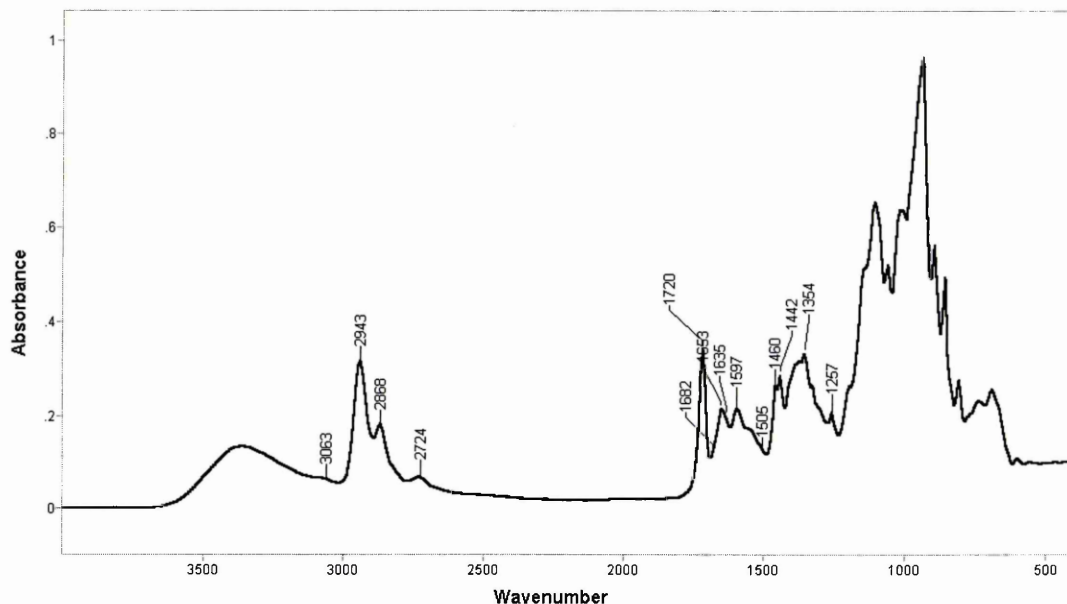


Figure 5.12: FTIR-ATR spectrum of a freeze-dried unbuffered aqueous solution of 0.1% w/v N-acetyl-L-lysine reacted with 0.6% v/v glutaraldehyde (resulting pH 3.96).

5.3.3.3 Peptides (N-acetyl glycine lysine methyl ester, N-acetyl phenylalanine lysine) and glutaraldehyde:

The data obtained from the analyses of the reaction of two peptides with glutaraldehyde were similar to those reported in sections 5.3.3.1 and 5.3.3.2 and hence are not shown here. It can however be concluded that similar compounds to those reported for the reactions of 6-amino-n-caproic acid and N-acetyl-L-lysine with glutaraldehyde are formed.

5.3.4 Study of the reaction of glutaraldehyde with proteins (cytochrome C and lysosyme)

5.3.4.1 MALDI-TOF MS results and discussion from the study of proteins:

5.3.4.1.1 MALDI-TOF MS data from the study of lysosyme:

The first of the two proteins studied was lysosyme; it contains 7 primary amino groups (6 lysines and one amino terminus). The results obtained from the MALDI-TOF MS analyses showed some interesting features and indicate the suitability of

MALDI-TOF MS in the determination and analysis of the multimericity of proteins after cross-linking with glutaraldehyde. Both non-cross-linked and glutaraldehyde-cross-linked proteins were analysed (see figure 5.13 below).

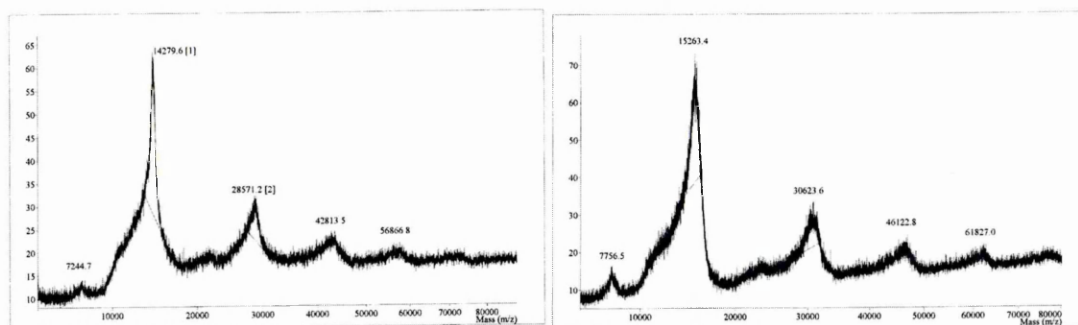


Figure 5.13: MALDI-TOF mass spectra of (*on the left*) non-cross-linked lysosyme (1.75 μmol), and (*on the right*) 1.75 μmol lysosyme cross-linked with 0.6% v/v glutaraldehyde (6.36 mmol). All samples were freeze-dried, re-dissolved in pure ethanol and mixed with DHB matrix solution in the ratio 1:10. One drop of TFA was added to facilitate the formation of a protonated molecular ion.

The non-cross-linked lysosyme spectrum shows signals at m/z 7244 corresponding to $[M+2H]^{2+}$ and m/z 14279 corresponding to $[M+H]^+$. There are also some laser-induced multimers at m/z 28571 ($[2M+H]^+$), m/z 42813 ($[3M+H]^+$), m/z 56866 ($[4M+H]^+$), along with a weaker signal at ca. m/z 70000 which corresponds to $[5M+H]^+$. Thus, the MALDI-TOF MS results may show that the proteins can undergo dimerisation, possibly due to attractive interaction between specific charged groups, similar to other protein behaviour already reported in the literature¹³. Since after treatment with glutaraldehyde, the standard peaks obtained for lysosyme were no longer present, it was inferred that all the protein had undergone reaction with glutaraldehyde. The peaks obtained from glutaraldehyde-treated lysosyme indicate the addition of about 12 or 15 glutaraldehyde molecules if we consider (disregarding the likely presence of oligomers of glutaraldehyde) its monomer mass to be 82 Da or 64 Da by assuming that one or both of the aldehyde groups have reacted. Peaks are observed at m/z 7756 ($[M+2H]^{2+} + 512$ Da); m/z 15263 ($[M+H]^+ + 983$ Da, which corresponds to either ~12 or ~15 glutaraldehyde molecules); m/z 30623 ($[2M+H]^+ + 2064$); m/z 46122 ($[3M+H]^+ + 3286$ Da); m/z 61827 ($[4M+H]^+ + 4709$ Da); and a small weak hump possibly corresponding to $[5M+H]^+ +$ glutaraldehyde molecules. The mass increase is almost linear, which is to be expected. The observed multimers

that are thought to be laser-induced, could also be seen as possible intermolecular cross-links, since mono-, di-, tri- and tetramers of glutaraldehyde-treated lysosyme have already been hypothesised by others³⁷ who used chemical cross-linking with glutaraldehyde to study crystallizing lysosyme solutions by gel electrophoresis (SDS-PAGE). This does, however, it seems unlikely in our work since some multimers are also observed in the MALDI-TOF mass spectrum of the untreated protein. The number of bound glutaraldehyde molecules observed by Wang et al³⁷ somewhat exceeded the number of amino groups present, and hence they suggested that some of the amino groups reacted with previously formed glutaraldehyde oligomers. Our data agree with this statement because the number of bound glutaraldehyde molecules somewhat exceeded the number of amino groups.

If we consider that theoretically all 6 lysine groups are available to react with glutaraldehyde, then it would appear that about 2-3 glutaraldehyde molecules reacted per lysine residue. Our results are thus in agreement with some work from previous authors³⁸ who reported the successful application of MALDI-TOF MS for studying cross-linked proteins, emphasizing the main advantages of the method i.e. its rapidity, simplicity and relative accuracy. By studying various proteins, including egg white lysosyme, Helin et al thus reported that there was no observable protein concentration dependence on the binding of glutaraldehyde (over the lysosyme concentration range 5-80 μM), however, they did not study lysosyme at the low concentration (1.75 μM) used in this study. In addition, no laser-induced multimers in either untreated or glutaraldehyde-treated lysosyme were observed in their mass spectra. Nevertheless, although the exact value was not given, the major signal obtained at their lowest lysosyme concentration (5 μM) reacted with 0.6% v/v glutaraldehyde appeared to be in the vicinity of our data (~ 15225 m/z by interpolation, which corresponds to $[\text{M}+\text{H}]^+$ with in addition ~ 14 glutaraldehyde molecules). Therefore, it would appear that at such a low concentration of lysosyme, there is also no protein concentration dependence in the binding of glutaraldehyde since the m/z value for the major peak found in this study appears to corroborate the work of Helin et al.

5.3.4.1.2 MALDI-TOF MS data from the study of cytochrome C:

The second of the two proteins studied was cytochrome C; it contains 19 lysine groups. Both non-cross-linked and glutaraldehyde-cross-linked proteins were analysed (see figure 5.14 below).

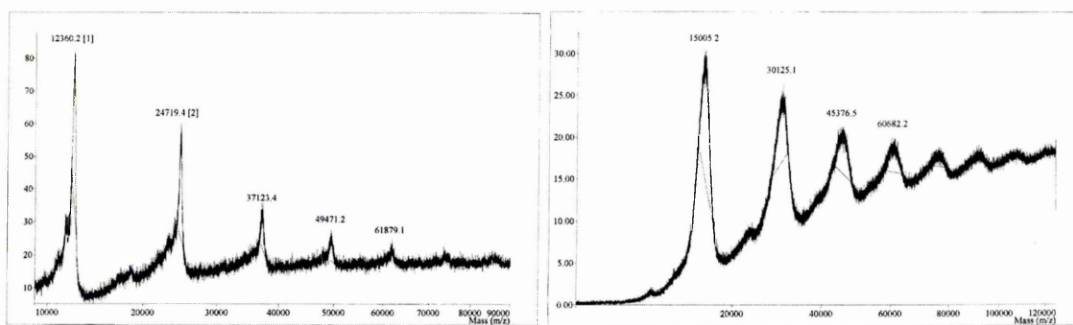


Figure 5.14: MALDI-TOF mass spectra of (*on the left*) non-cross-linked cytochrome C (2.02 μmol), and (*on the right*) 2.02 μmol cytochrome C cross-linked with 0.6% v/v glutaraldehyde (6.36 mmol). All samples were freeze-dried, re-dissolved in pure ethanol and mixed with the DHB matrix solution in the ratio 1:10. One drop of TFA was added to facilitate the formation of a protonated molecular ion.

The non-cross-linked cytochrome C spectrum shows main signals at m/z 12360 corresponding to $[\text{M}+\text{H}]^+$, followed by some laser-induced multimers at m/z 24719 ($[2\text{M}+\text{H}]^+$), m/z 37123 ($[3\text{M}+\text{H}]^+$), m/z 49471 ($[4\text{M}+\text{H}]^+$) and at m/z 61879 ($[5\text{M}+\text{H}]^+$), along with other weaker signals, which probably correspond to $[6\text{M}+\text{H}]^+$ and $[7\text{M}+\text{H}]^+$. Since after treatment with glutaraldehyde, the standard peaks obtained for cytochrome C were no longer present, this indicated that all the protein had undergone reaction with glutaraldehyde. After cross-linking, the mass spectra exhibit broadening of the peaks (a decrease in resolution), which may imply a more heterogeneous sample. This could be seen as various reaction products around the same m/z and the addition of different numbers of glutaraldehyde molecules but resulting in a relatively similar m/z . The peaks obtained from glutaraldehyde-treated cytochrome C indicate the addition of about 32 or 41 glutaraldehyde molecules if we consider (disregarding the likely presence of oligomers of glutaraldehyde) its monomer mass to be 82 Da or 64 Da by assuming that one or both of the aldehyde groups have reacted. Peaks are observed at m/z 15005 ($[\text{M}+\text{H}]^+ + 2645$ Da, which corresponds to either ~ 32 or ~ 41 glutaraldehyde molecules); m/z 30125 ($[2\text{M}+\text{H}]^+ + 5406$ Da); m/z 45376 ($[3\text{M}+\text{H}]^+ + 8253$ Da); m/z 60682 ($[4\text{M}+\text{H}]^+ + 11211$ Da); m/z 76092 ($[5\text{M}+\text{H}]^+ + 14292$ Da); and some small weaker humps possibly

corresponding to $[6M+H]^+$ and $[7M+H]^+$ with a corresponding molecular mass increase. The general mass increase is almost linear. The number of bound glutaraldehyde molecules somewhat exceeded the number of amino groups (similarly to what was found with glutaraldehyde-cross-linked lysosyme), and this suggests that some of the amino groups reacted with previously-formed glutaraldehyde oligomers incorporating several glutaraldehyde monomeric moieties. If we consider that theoretically all 19 lysines groups of the protein are available to react with glutaraldehyde, then it would appear that about 2 glutaraldehyde molecules reacted per lysine residues.

Our data disagree with the results reported by Ohno and Kurusu^{39,40}, who studied the electrochemical response of cross-linked cytochrome C in PEO oligomers with the same concentration of cytochrome as the one used in this study (0.1 g.L⁻¹). Their results do not reveal any laser-induced multimers and only show the $[M+2H]^{2+}$ and $[M+H]^+$ signals at m/z 6203 and 12413 for untreated cytochrome C and at m/z 6289 and 12561 for treated-cytochrome C, which involves an increase in molecular mass of only 86 and 148 Da respectively for the $[M+H]^+$ and $[M+2H]^{2+}$ signals. From these results, they only concluded the presence of a specific intramolecular cross-linking, involving only the mass equivalent of two glutaraldehyde monomeric molecules per cytochrome C. In contrast, our results clearly suggest a mean of about 36 glutaraldehyde monomeric molecules involved in intramolecular cross-linking, which corresponds to about 2 glutaraldehyde molecules per lysine residue of the cytochrome C. Furthermore, the multimers observed could also be seen as possible intermolecular cross-linking, although this seems unlikely since some multimers are also observed with the untreated proteins and are attributed to a laser-induced effect. Nevertheless, if one of the aldehyde groups of a monomeric glutaraldehyde theoretically binds to a lysine on one protein molecule and the other aldehyde binds to a lysine on another protein molecule, then the two proteins are linked together by one glutaraldehyde, forming an intermolecular cross-link and roughly doubling the molecular weight. Also, if the protein contains many more than two lysines, another glutaraldehyde molecule can propagate a branch to a third protein molecule and this can branch yet again, resulting in a star-shaped polymer, still by inter-molecular cross-linking. Such inter-molecular cross-links have already been deliberately

produced with another protein (bovine serum albumin) for use as molecular weight markers to calibrate electrophoresis gels⁴¹.

5.3.4.2 NMR results and discussion from the study of proteins:

The NMR spectra (^1H and ^{13}C) of glutaraldehyde-treated proteins, (see figure 5.15 below, where only the NMR spectra from the analysis of glutaraldehyde-treated lysosyme are shown), were observed to be very different to those from unreacted proteins (results not shown here), indicating that a reaction took place and that the majority of the protein (if not all) may have reacted with glutaraldehyde. Generally, however, the spectra from the glutaraldehyde-treated proteins were quite weak and unfortunately did not allow proper discrimination of all the peaks. Nevertheless, some interesting features can be outlined.

Due to the large excess of glutaraldehyde present in the reaction mixture of glutaraldehyde-treated lysosyme (molar ratio of 1:3634), both ^{13}C and ^1H NMR spectra (observed below in figure 5.15) exhibit mostly the characteristic signals of glutaraldehyde (see chapter 4). There are, however, some very weak signals that indicate that a reaction between glutaraldehyde and the protein may have taken place. For example, the signal observed at 3-4 ppm in the proton NMR spectrum may possibly be assigned to $-\text{CH}_2-\text{N}=\text{}$ or $=\text{CH}-\text{N}=\text{}$, whilst the presence of weak signals in the 50-70 ppm region of the ^{13}C NMR spectrum may also possibly be assigned to $-\text{CH}_2-\text{N}=\text{}$ or $=\text{CH}-\text{N}=\text{}$, which would point to the likely presence of Schiff base species. A similar conclusion could be drawn from the data obtained from the analysis of glutaraldehyde-treated cytochrome C.

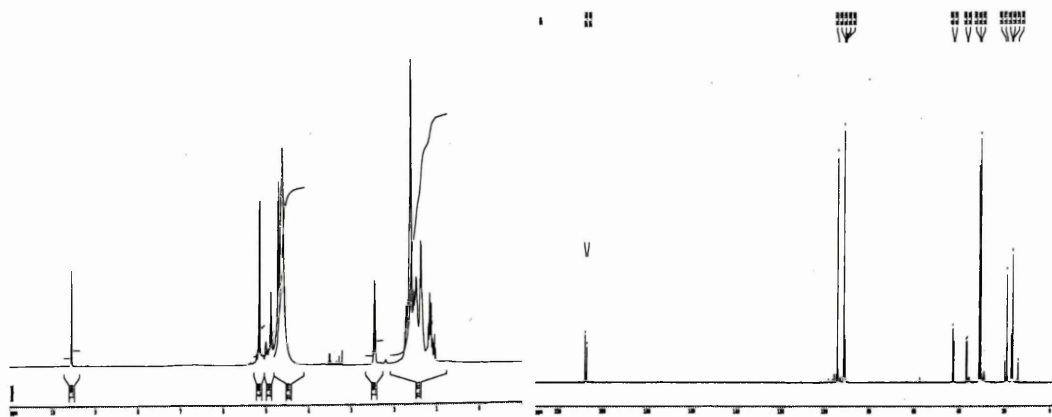


Figure 5.15: ^1H (left) and ^{13}C (right) NMR spectra of unbuffered aqueous solution of lysosyme (0.1% w/v) unbuffered aqueous solution. The samples were freeze-dried, re-dissolved in D_2O and then analysed.

5.3.4.3 Infrared results and discussion from the study of proteins:

The infrared spectra obtained from lysosyme or cytochrome C reacted with glutaraldehyde are very different from the spectra of the original proteins⁴², indicating that the proteins have reacted with glutaraldehyde (see below figure 5.16). This observation is in contrast to the findings for various films (e.g. glycosaminoglycan (hyaluronic acid), alginic acid, amylopectin, PVA) treated with glutaraldehyde, where no appreciable IR spectral changes were observed after cross-linking with glutaraldehyde²⁹.

The spectra obtained from the reacted proteins were virtually identical, indicating the formation of similar reaction products with the same IR absorption pattern. Comparison with the corresponding spectra from the unreacted proteins showed that major new bands appeared, such as the band at 1721 cm^{-1} related to a free aldehydic group, the one at 1656 cm^{-1} , which can be attributed to an imine bond ($\text{C}=\text{N}$), the peak at 1636 cm^{-1} (possibly associated with an imine) and the peak at 1460 cm^{-1} , which can be assigned to an aldimine absorption. The complex pattern observed between $1200\text{--}800\text{ cm}^{-1}$ is similar to the infrared pattern found with glutaraldehyde (see chapter 4), which can be explained by the large excess of glutaraldehyde in comparison to the proteins.

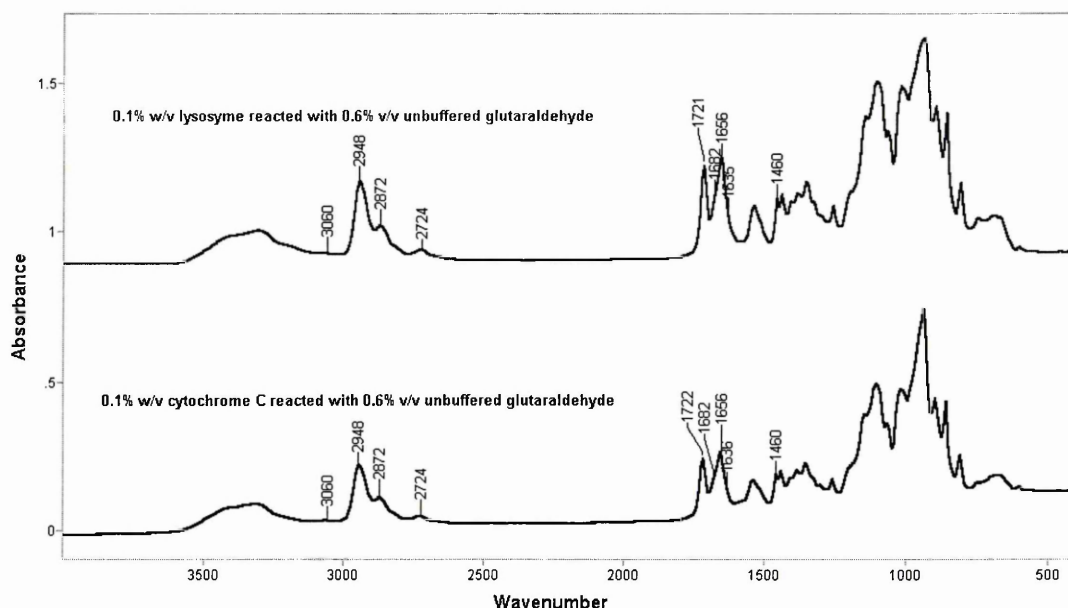


Figure 5.16: FTIR-ATR spectra of freeze-dried unbuffered aqueous solutions of 0.1% w/v lysosyme and cytochrome C reacted with 0.6% v/v glutaraldehyde.

5.3.5 Overall discussion of data obtained

One can quote the following “the success of glutaraldehyde as a cross-linking agent is based on the large number of different types of molecules present simultaneously in the reagent solution”⁴³, in order to express the fact that the chemistry of glutaraldehyde reacted with model compounds in aqueous solutions is more than, or at least, as complex as the chemistry of glutaraldehyde itself in solution (see chapter 4). Although glutaraldehyde has been used extensively as a fixative for many applications, the way solutions of glutaraldehyde react with proteins and the nature of the reagent are still under debate. In addition, many reported reactions of glutaraldehyde with proteins are actually assuming reactions of the monomeric form (molecule I in appendix III), despite the definite presence of polymers in glutaraldehyde solutions, as concluded in chapter 4. Also, many authors disagree whether the reactive species are the monomeric form of glutaraldehyde or its polymers. However, it does appear that “polyglutaraldehyde” is more efficient in cross-linking proteins than with purified (monomeric) glutaraldehyde⁴⁴. The amount of polymeric structures was reported to be less than 0.05% of that of glutaraldehyde⁵, and is thought not to be responsible for the reactivity of glutaraldehyde as has been indicated by others^{16,45}, a fact that we strongly disagree with because our results provided evidence for the presence of many polymeric structures in both glutaraldehyde solutions (see chapter 4) and also in glutaraldehyde-treated amino compounds solutions.

Our data on the elucidation of the chemical structures present in glutaraldehyde solutions (see chapter 4), in addition to those reported in this chapter, lead to the general conclusion that glutaraldehyde (under many different forms more complex than the simple monomeric form) reacts primarily with amino groups forming Schiff bases. These are known to be unstable in aqueous solutions, but more stable structures involving one or more amino compounds also occur (some of them originating from Schiff base moieties). These have the ability to form more stable cross-links through electronic resonance effects, additional Michael-type reactions or cyclisation steps.

In contrast to previous findings, where it was stated that the anabylysine compound (molecule XCVIII m/z 391) was the only detectable stable cross-link found by mass spectrometry from the analysis of glutaraldehyde-treated 6-amino-n-caproic acid²⁵, there is evidence from our mass spectral data of other types of stable cross-linking structures involving at least two amino acid residues. For example, major mass spectrometric peaks have been attributed to molecules (see appendix IV for structural details) such as CXII (di-Schiff base addition on an aldol trimer with a subsequent cyclisation step), CXXVIII (di-Michael-type addition on an aldol glutaraldehyde trimer), CXLVII (di-Michael-type addition on an aldol trimer with a subsequent cyclisation step), CLII (cyclised dialdol condensation product that underwent a Michael addition and two Schiff base additions), CLVII (1,3,4,5 tetrasubstituted pyridinium structure that underwent aldol, Michael and a Schiff base reaction) and CXVII (aldol dimer that underwent a Schiff base and a Michael-type addition). Our FTIR and NMR data are consistent with the presence of such cross-linking structures. However, we have seen no evidence for the formation of the larger complex stable cross-links proposed by Hardy's group^{23,46}, or those proposed by Johnson⁴⁷ (see figures 2.25 and 2.26 in section 2.2.4.5 of chapter 2 for detailed structures). Our results would therefore seem to indicate that the formation of cross-links may consist of several steps including reversible and multi-molecular steps involving several moieties, with the composition of the reaction products being distributed slightly heterogeneously, depending on reaction conditions.

Our data also show that glutaraldehyde (in its multivariate structural forms) reacts with amino groups over a wide range of pH, which is in agreement with the statement of others⁵ who reported that glutaraldehyde reacts with amino groups at pH 3 and above. This is worth mentioning because some authors have claimed that a low pH interferes with the reaction of glutaraldehyde with amino groups and have concluded that the best reaction conditions are at neutral or basic pH³⁴. In our work, the reactions of glutaraldehyde with model compounds do not seem to be very much affected by pH in the range pH 4-9, which is consistent with literature statements⁶. The fact that the various model compounds seem to yield similar species when reacted with glutaraldehyde across the pH range (4-9) could simply come from the fact that the 6-amino group of lysine (known to react primarily with glutaraldehyde), modelled in this study by various analogous molecules, has a pK_a ⁴⁸ of about 10.

Thus a change in pH in this range should have little effect on the reactivity of lysine-like molecules with glutaraldehyde¹³.

The polymers of pyridine-like structures are proposed as important cross-linkers in glutaraldehyde-treated proteins since such formation of branched polymer products is thought to provide the flexibility required for intra-molecular cross-linking^{23,46} and such cross-linking entities are found with elastin (e.g. desmosine, isodesmosine^{27,49}). In contrast, the monomeric pyridine-like structures are not functional cross-linkers since only one amine group is incorporated into the monomer. Our data suggest the presence of both polymers and monomers of pyridine-like and dihydropyridine-like structures that represent some kind of stable reaction products (e.g. molecules LXV and XCVII). This is partially in agreement with the data of Hardy et al²³ who found that the reaction of glutaraldehyde with aliphatic amines yielded a mixture of at least 12 chemical entities including postulated stable quaternary pyridinium derivatives, although these were not fully characterised. In addition, our results are in agreement with previous work, which reported the presence of a mono-bound (molecule CXLI, tri-aldol condensation product which underwent a Michael-type addition of the amine) and a cross-linked chemical structure (molecule XCVIII, anabilysine compound) from the analysis of glutaraldehyde-treated bovine pericardium tissue²⁵. They also indicated the likely differences that would be observed between the studies of model compounds and tissue because of the greater constraints present in the tissue reaction (stereochemical effects).

Our results also provide a multiplicity of evidence for the formation of mono-Schiff base compounds, di-Schiff base (and also a few tri-Schiff base) cross-linking structures involving glutaraldehyde and its condensation products, along with many other structures involving Schiff base addition, aldol condensation, Michael and Michael-type addition products (see appendix IV for details of structures). In contrast to other work²⁵, some of the cross-links proposed by Richards and Knowles⁵⁰ involving Michael-type additions of the amine to aldol condensation products (molecules CXXII (di-Schiff base addition on an aldol trimer with a subsequent cyclisation step), CXXIII (di-Michael-type addition on an aldol trimer) and CXLV (Schiff base and Michael-type addition on a glutaraldehyde aldol trimer)) were found in this study. Additionally, other structures based on Michael-type addition with various aldol condensation products of glutaraldehyde were also found,

such as the molecules proposed by Walt and Agayn⁵¹ CXXXIV, CXXXV and CXXXVI, along with other molecules such as CII, CXIX, CXL, CXLI and CXLVI. In addition, the data obtained showed that stable cross-links could also be formed from Michael-type addition reactions, for example molecules CXX and CXXIII (di-Michael-type addition on an aldol dimer and trimer respectively).

The largest cross-link observed involved a total of five molecules of glutaraldehyde (molecule CLVII). The largest glutaraldehyde-based molecules present in the glutaraldehyde-treated amino compound mixtures mostly involved a total of five molecules of glutaraldehyde (e.g. molecules XIX, XIXc, XXVIII, XXIX, XXXVIIIb and LI), which is similar to what was reported for the analysis of glutaraldehyde solutions (see chapter 4).

Similar glutaraldehyde structures were found from the analysis of glutaraldehyde-treated amino compounds as from the analysis of pure glutaraldehyde solution (see chapter 4) over a similar pH range (pH 4-9), although no quantitative data have been retrieved. Our data showed that glutaraldehyde species in presence of amino groups do not seem to evolve further through the formation of polymers and the amino groups do not seem to play a catalytic role for the formation of such polymers, as was hypothesised by Kawahara et al³³.

No long chain polymers of glutaraldehyde were present in the reaction solutions over the range of pH conditions employed from our MS data. This is in disagreement with the hypothesis of Cheung et al^{3,4}, who stated that very high molecular weight glutaraldehyde polymers were formed in the presence of excess aldehyde and that these long polymeric glutaraldehyde chains were generating inter-molecular cross-links.

Although some unsaturated chromophoric products, such as the 1,3,4,5-substituted pyridinium salt, that represent some of the possible cross-linking structures²³, have been reported not to affect either tissue stability or its calcification⁷ (pericardium tissue calcification was found to occur at the same levels despite a borohydride reduction), we believe that many structures characterised in this study are likely to induce calcification, simply due to the presence of carbonyl groups or other reactive groups in their backbones (a study of the calcification potential of the chemical groups of glutaraldehyde, model compounds and glutaraldehyde-treated model

compounds is presented in chapter 6). Such pendant carbonyl groups can form a potential initiation site for mineralisation for example. In addition, despite the presence of some stable cross-linking structures, the existence of other chemical structures involving Schiff bases that are readily hydrolysed may give a reasonable explanation for a gradual reduction through time in tissue stability towards stress and enzymatic attack in-vivo, thus being potentially responsible for cross-linked bioprosthetic valves failure in-vivo. Furthermore, the in-vivo oxidation of pendant aldehyde groups within glutaraldehyde-treated tissue can also form potential binding sites for initialising tissue calcification and this issue is discussed in a dedicated study in chapter 6.

5.4 Conclusion:

Our results indicate that glutaraldehyde reacts with amino groups over a wide pH range and the results from studies of the reaction of glutaraldehyde with 6-amino-n-caproic acid, N- α -acetyl-L-lysine and peptides broadly agrees with previous work of various authors^{6,23,25,33,50,51}, although some differences are brought forward. The mass spectral data, along with the results of the NMR and FTIR analyses, obtained for the products of the reaction between glutaraldehyde and small amines and peptides showed the presence of a rich palette of compounds. These compounds included aldol and aldol/Michael condensation products of glutaraldehyde, Schiff base moieties (including cross-links) and various cyclisation products incorporating pyridinium and dihydropyridine ring structures. The results (found in appendix IV) indicated the likely presence of about 25 stable cross-linking (multi-bound) entities including an anabilysine-like compound, along with about 29 stable mono-bound entities. The stability of which is mainly due to the presence of cycles, Michael-type additions-resulting products or electronic resonance effects. However, our data also showed the presence of other less stable types of mono- and multi-bound structures, essentially due to the presence of Schiff bases.

Despite the presence of many stable structures, other less stable chemical entities were also characterised, which brought about the hypothesis of their role in the initiation of mineralisation because these less stable entities could break up easily in-vivo and lead to failure and calcification of cross-linked-tissue used in bioprostheses

manufacture. This led to the study found in the chapter 6, where the potential of glutaraldehyde, but also its oxidised forms (e.g. glutaric acid), to initiate the mineralisation was investigated, along with the possible uptake of calcium (calcification) by amino acids and other molecular compounds, mimicking the behaviour of collagenous tissue, will be studied by attenuated-total reflectance infrared spectroscopy (FTIR-ATR). In addition, the role of the cross-linker and tissue factors in the mineralisation process of cardiac bioprostheses will be further discussed in chapter 6. Furthermore, the use of FTIR-ATR microscopy was thought to able us to see chemical differences between glutaraldehyde-treated and untreated collagen, by allowing us to investigate the surface grouping and to find any relations between chemical groups of the valve tissue (essentially made of collagen type I) and their calcification potential. These preliminary results can be found in the appendix I.

The study of glutaraldehyde-treated proteins showed the suitability of MALDI-TOF MS in the determination and analysis of the multimericity of proteins after cross-linking with glutaraldehyde. A further study of the reaction products of glutaraldehyde with the model compounds was performed using TLC-MALDI-TOF MS. The data are included in appendix II, however, we can conclude that the application of TLC-MALDI-TOF MS is shown successful for the study of the separated reactions products from complex reactions involving small amino acids or peptides with glutaraldehyde.

In conclusion, the successful characterisation in this study of some possible chemical structures involved in the reaction of glutaraldehyde with proteins and their cross-linking has led to new insights into the complex model that represents the cross-linking of collagenous tissue (see chapter 2) and its application for cardiac bioprostheses.

1. Khor E. Methods for the treatment of collagenous tissues for bioprostheses. *Biomaterials*. 1997;18:95-105.
2. Cheung DT, Nimni ME. Mechanism of crosslinking of proteins by glutaraldehyde I. Reaction with model compounds. *Connective Tissue Research*. 1982;10:187-199.
3. Cheung DT, Nimni ME. Mechanism of crosslinking of proteins by glutaraldehyde II. Reaction with monomeric and polymeric collagen. *Connective Tissue Research*. 1982;10:201-216.

4. Cheung DT, Perelman N, Ko EC, Nimni ME. Mechanism of crosslinking of proteins by glutaraldehyde III. Reactions with collagen in tissues. *Connective Tissue Research*. 1985;13:109-115.
5. Okuda K, Urabe I, Yamada Y, Okada H. Reaction of glutaraldehyde with amino and thiol compounds. *Journal of Fermentation and Bioengineering*. 1991;71:100-105.
6. Olde Damink LHH, Dijkstra PJ, Van Luyn MJA, Van Wachem PB, Nieuwenhuis P, Feijen J. Glutaraldehyde as a crosslinking agent for collagen-based biomaterials. *Journal of Materials Science. Materials in Medicine*. 1995;6:460-472.
7. Golomb G, Schoen FJ, Smith MS, Linden J, Dixon M, Levy RJ. The role of glutaraldehyde-induced cross-links in calcification of bovine pericardium used in cardiac valve bioprostheses. *American Journal of Pathology*. 1987;127:122-130.
8. Levy RJ, Schoen FJ, Golomb G. Bioprosthetic heart valve calcification: clinical features, pathobiology and prospects for prevention. In: William DF, ed. *Critical Reviews in Biocompatibility*: CRC Press; 1986:147-187.
9. Thubrikar MJ, Deck JD, Aouad J, Nolan SP. Role of mechanical stress in calcification of aortic bioprosthetic valves. *Journal of Thoracic Cardiovascular Surgery*. 1983;86:115-125.
10. Girardot MN, Torrianni M, Dillehay D, Girardot JM. Role of glutaraldehyde in calcification of porcine heart valves: comparing cusp and wall. *Journal of Biomedical Materials Research*. 1995;29:793-801.
11. Bowes JH, Cater CW. The reaction of glutaraldehyde with proteins and other biological materials. *Journal of the Royal Microscopical Society*. 1966;85:193-200.
12. Bowes JH, Cater CW. The interaction of aldehydes with collagen. *Biochimica et Biophysica Acta*. 1968;168:341-352.
13. Tomimatsu Y, Jansen EF, Gaffield W, Olson AC. Physical chemical observations on the alpha-chymotrypsin glutaraldehyde system during formation of an insoluble derivative. *Journal of Colloid and Interface Science*. 1971;36:51-64.
14. Woodroof EA. Use of glutaraldehyde and formaldehyde to process tissue heart valves. *Journal of Bioengineering*. 1978;2:1-9.
15. Happich WF, Taylor MH, Fairheller SH. Amino acid composition of glutaraldehyde-stabilised wool. *Textile Research Journal*. 1970;40:768-769.
16. Korn AH, Fairheller SH, Filachione EM. Glutaraldehyde: nature of the reagent. *Journal of Molecular Biology*. 1972;65:525-529.
17. Munton TJ, Russell AD. Aspects of the action of glutaraldehyde on Escherichia Coli. *Journal of Applied Bacteriology*. 1970;33:410-419.
18. Holloway CE, Dean FH. ¹³C NMR study of aqueous glutaraldehyde equilibria. *Journal of Pharmaceutical Science*. 1975;64:1078-1079.
19. Kuznetsova NP, Mishaeva RN, Gudkin LR. Oligomerisation of glutaraldehyde in the course of its condensation with glycine. *Russian Journal of Applied Chemistry*. 1999;72:1236-1241.
20. Hopwood D. Theoretical and practical aspects of glutaraldehyde fixation. *Histochemistry*. 1972;4:267-303.
21. Lubig R, Kusch P, Roper K, Zahn H. On the mechanism of protein crosslinking with glutaraldehyde. *Monatshefte fur Chemie*. 1981;112:1313-1323.
22. Johnson TJA. Aldehyde fixatives: quantification of acid producing reactions. *Journal of Electron Microscopy Techniques*. 1985;2:129-138.
23. Hardy PM, Nicholls AC, Rydon HN. The nature of the crosslinking of proteins by glutaraldehyde I. Interaction of glutaraldehyde with the amino-groups of 6-aminohexanoic acid and N-acetyl-L-lysine. *Journal of the Chemical Society Perkin Transaction I*. 1976:958-962.
24. Southern LJ. Identification of glutaraldehyde-induced structures in bioprosthetic heart valves using mass spectrometry: an insight into valve failure. In. Sheffield: University of Sheffield; 2001.
25. Southern LJ, Hughes H, Lawford PV, Clench MR, Manning NJ. Glutaraldehyde-induced cross-links: a study of model compounds and commercial bioprosthetic valves. *Journal of Heart Valve Disease*. 2000;9:241-249.
26. Ishii T, Sorita A, Sawamura M, Kusunose H, Ukeda H. Determination of the reaction product of glutaraldehyde and amine based on the binding ability of coomassie brilliant blue. *Analytical Sciences*. 1997;13:5-9.
27. Thomas J, D.F. E, Partridge SM. Degradation products from elastin. *Nature*. 1963;200:651-652.

28. Hardy PM, Hughes GJ, Rydon HN. The nature of the crosslinking of proteins by glutaraldehyde II. The formation of quaternary pyridinium compounds by the action of glutaraldehyde on proteins and the identification of a 3-(2-piperidyl)-pyridinium derivative, anabylisine, as a crosslinking entity. *Journal of the Chemical Society Perkin Transaction I*. 1979;9:2282-2288.
29. Tomihata K, Ikada Y. Crosslinking of hyaluronic acid with glutaraldehyde. *Journal of Polymer Science Part A-1*. 1997;35:3553-3559.
30. Grant DM, Paul EG. ¹³C magnetic resonance II: Chemical shift data for the alkanes. *Journal of the American Chemical Society*. 1964;86:2984-2990.
31. Maciel GE, Savitsky GB. ¹³C magnetic resonance study of some saturated heterocyclic compounds. *Journal of Physical Chemistry*. 1965;69:3925-3929.
32. Roberts JD, Weigert FJ, Kroshwitz JI, Reich HJ. Nuclear magnetic resonance spectroscopy: ¹³C chemical shifts in acyclic and alicyclic alcohols. *Journal of the American Chemical Society*. 1970;92:1338-1347.
33. Kawahara JI, Ohmori T, Ohkubo T, Hattori S, Kawamura M. The structure of glutaraldehyde in aqueous solution determined by ultraviolet absorption and light scattering. *Analytical Biochemistry*. 1992;201:94-98.
34. Monsan P, Puzo G, Mazarguil H. Etude du mecanisme d' etablissement des liaisons glutaraldehyde-proteines. *Biochimie*. 1975;57:1281-1292.
35. Blout ER, Fields M, Karplus R. Absorption spectra VI. The infrared spectra of certain compounds containing conjugated double bonds. *Journal of the American Chemical Society*. 1948;70:194-198.
36. Chatterji PR. Gelatin with hydrophylic/hydrophobic grafts and glutaraldehyde crosslinks. *Journal of Applied Polymer Science*. 1989;37:2203-2212.
37. Wang F, Hayter J, Wilson LJ. Salt-induced aggregation of lysosyme studied by crosslinking with glutaraldehyde: implications for crystal growth. *Acta Crystallographica Section D Biological Crystallography*. 1996;52:901-908.
38. Helin J, Caldentey J, Kalkkinen N, Bamford DH. Analysis of the multimeric state of proteins by matrix assisted laser desorption/ionisation mass spectrometry after crosslinking with glutaraldehyde. *Rapid Communications in Mass Spectrometry*. 1999;13:185-190.
39. Ohno H, Kurusu F. Cytochrome C crosslinked with glutaraldehyde I. Electrochemical response in polyethylene oxide oligomers. *Chemistry Letters*. 1996;8:693-694.
40. Kurusu F, Ohno H. Electrochemical response of glutaraldehyde-crosslinked cytochrome C in PEO oligomers. *Solid State Ionics*. 1998;113/115:173-177.
41. Payne J. Polymerisation of proteins with glutaraldehyde. Soluble molecular-weight markers. *Biochemistry Journal*. 1973;135:867-873.
42. Lord RC, Yu NT. Laser-excited Raman spectroscopy of biomolecules I. Native lysosyme and its constituents amino acids. *Journal of Molecular Biology*. 1970;50:509-524.
43. Peters K, Richards FM. Chemical crosslinking: reagents and problems in studies of membrane structure. *Annual Review of Biochemistry*. 1977;46:523-551.
44. Rembaum A, Levy J, Gupta A, Margel S. Reactions of polyglutaraldehyde with proteins. *Polymer Preparation American Chemical Society Division Polymers*. 1978;19:648-650.
45. Hardy PM, Nicholls AC, Rydon HN. The nature of glutaraldehyde in aqueous solution. *Journal of Chemical Society Chemical Communications*. 1969;10:565-566.
46. Hardy PM, Hughes GJ, Rydon HN. Formation of quaternary pyridinium compounds by the action of glutaraldehyde on proteins. *Journal of Chemical Society Chemical Communications*. 1976;5:157-158.
47. Johnson TJA. Glutaraldehyde fixation chemistry: oxygen-consuming reactions. *European Journal of Cell Biology*. 1987;45:160-169.
48. Greenberg DM. In: Greenberg DM, ed. *Amino Acids and Proteins*. Springfield: Thomas; 1951:423.
49. Anwar RA. Comparison of elastins from various sources. *Canadian Journal of Biochemistry*. 1966;44:725.
50. Richards FM, Knowles JR. Glutaraldehyde as a protein crosslinking reagent. *Journal of Molecular Biology*. 1968;37:231-233.
51. Walt DR, Agayn VI. The chemistry of enzyme and protein immobilisation with glutaraldehyde. *Trends in Analytical Chemistry*. 1994;13:425-430.

Chapter 6

6 Infrared spectroscopy in the evaluation of the calcification potential of molecular models.

Abstract

Objectives: Glutaraldehyde is the only chemical cross-linker exclusively used in the bioprosthetic valve industry today. It also has many other important applications in various fields. However, there is evidence to suggest that glutaraldehyde plays a critical role in tissue calcification^{1,2} and subsequent mechanical degeneration of bioprosthetic heart valves in-vivo³. The specific mechanisms by which glutaraldehyde fixation facilitates calcification, however, are not fully understood⁴. In addition, collagenous valve tissue is believed to have the potential to initiate the mineralisation process because it has been reported that both collagen and bovine pericardium can take up calcium and phosphate in-vitro in the absence of host factors⁵⁻⁷. Furthermore, it has been reported that glutaraldehyde-treated collagen has potential calcium-binding sites (e.g. amino, carbonyl and/or carboxylic groups) and therefore may have a natural tendency to calcify⁸; these sites being normally protected by glycosaminoglycans and proteoglycans that are lost during the glutaraldehyde treatment process. One of the main objective was thus to investigate the potential of glutaraldehyde, along with its di-acid form (glutaric acid), to initiate mineralisation by complexing some relevant ions such as calcium. Other objectives were to investigate the possible uptake of calcium (calcification) by amino acids and other molecules that can mimic the behaviour of collagenous tissue and also to comment on the role of the cross-linker and tissue factors in the mineralisation process of cardiac bioprostheses.

Methods: The possible uptake of calcium (calcification) by model compounds was investigated using Fourier-transform infrared-attenuated total reflectance (FTIR-ATR) spectroscopy. Any significant binding of a metal ion such as calcium to a specific functional group of a molecule might be detected, either by a shift in wavenumber of the relevant peak or by a variation in the relative size of the peak. Hence, binding sites relevant to calcification should be identified. Additionally, the formation of a salt could be discriminated by infrared bands from the different groups (COOH, COO⁻ and C=O) involved in such a salt formation.

Results: Glutaraldehyde and oxidised glutaraldehyde (glutaric acid) have been shown to have the potential to induce mineralisation by attracting cations (potentially calcium) from a metastable calcifying solution, although the two compounds seem to behave differently. It is ironic that the glutaraldehyde treatment itself, presently used in commercial valve processing, might be a calcification initiator. The FTIR spectra of glutaraldehyde-treated model compounds, incubated in a calcifying solution, were very complex and hence could not be interpreted. It was therefore not possible to identify the amino or carbonyl groups of the molecules backbone as binding sites for phosphate and calcium respectively. Nevertheless, the spectra do not rule out the likely possibility that glutaraldehyde-treated model compounds mimicking glutaraldehyde-treated tissue would also attract calcium ions. Model compounds not reacted with glutaraldehyde were shown to bind calcium, probably via the carbonyl oxygen atoms of their backbones.

Conclusion: The ability of glutaraldehyde to cross-link is unfortunately opposed to its increasingly believed potential to intrinsically facilitate tissue mineralisation, which was demonstrated in-vitro by the results from this study. Results from the analysis of glutaraldehyde and oxidised forms of glutaraldehyde (e.g. glutaric acid) demonstrated a strong potential for their involvement in the mineralisation process of glutaraldehyde-treated tissues. Whilst amino acid residues of collagenous tissue could also have a role to play in the mineralisation process, further studies would be required to confirm this hypothesis. Nevertheless, the overall results bring forward some new insights into the hypothetical primary processes of mineralisation of tissue and may help to clarify the involvement of the tissue and cross-linking reagent in calcification.

6.1 Introduction

Collagen has been reported to be implicated in the mechanisms of calcification^{2,9} and to be a major site for the calcification of glutaraldehyde-treated cardiac bioprotheses⁸. According to Glimcher et al¹⁰ collagen fibrils are potential nucleation sites for calcium crystal formation. Early mineral deposits are predominantly localised to transplanted connective tissue cells and their remnants, found in the collagen/elastin matrix. However mineral deposits also involve extracellular collagen fibres¹¹.

Another predominant site for calcification in aortic tissue is elastin¹². The concept of “neutral binding site/charge neutralisation” has been proposed from studying the calcification of aortic elastin. Long et al¹³ bound calcium to neutral purified elastin and studied the distribution of calcification throughout the bulk, upon exposure to solutions containing phosphorus. The carbonyl oxygen sites of the peptide backbone were thus hypothesised to bind positively charged calcium and subsequently to attract phosphate to maintain the overall charge neutrality. This can act as a potential initiation site for the mineralisation of tissue and, theoretically, a similar process could be expected with collagen, as reported by Urry¹⁴.

A likely candidate for a general calcification mechanism therefore is cation-chelation by groups present in the material containing lone pairs of electrons susceptible to interacting with electron-deficient species. Such a process of cation-chelation in the sorption of metals by polyurethanes has been proposed by Hamon et al¹⁵. Their hypothesis was that phosphate was carried along in this process as the accompanying anion to maintain charge neutrality and the polyether segments of the polyurethanes provided binding sites for the complexation of cations such as calcium. This calcium complexation mechanism associated with polyurethanes has been investigated using the analysis of model compounds^{16,17} but so far no equivalent study has been carried out using model compounds of collagenous tissue.

Phosphate moieties can also bind at the N-termini of helices in proteins, corresponding to an optimal interaction of the helix dipole and the charged phosphate¹⁸. This brings another factor to the puzzle of mineralisation i.e. proteins

could also bind phosphate, which could eventually trigger the subsequent attraction of calcium ions. X-ray and neutron diffraction investigations of calcifying turkey leg tendons have shown that apatite crystal formation was initiated in the gap zones of the collagen type I fibres. This suggests that the N-termini telopeptides (forming the gap zones) or substances adsorbed to these sites were actively involved in crystal nucleation and growth¹⁹.

Previous studies have already presumed that glutaraldehyde pre-treatment of bioprosthetic heart valves is a critical determinant in their calcification^{20,21}. Schoen et al²² have also reported a significant correlation between the glutaraldehyde treatment of tissue materials used in bioprosthetic heart valves and in-vivo calcification. The presence of reactive aldehydes has also been shown to be essential for bioprosthetic tissue calcification in subcutaneous implants in rats^{2,23}. Golomb et al²⁴ determined the minimum amount of glutaraldehyde in valve tissue required to initiate calcium deposition in a subdermal model, to be 100 nM/mg. The amount of glutaraldehyde in bovine pericardium rat implants has also been shown to have a quantitative relationship with calcific deposits. The hypothesis that glutaraldehyde could be a nucleating site for calcium ions has also been proposed to account for the in-vivo dystrophic calcification of bioprosthetic tissue²⁵.

Aqueous glutaraldehyde solutions in the pH range 3.8 - 9.2 were shown in chapter 4 to consist essentially of glutaraldehyde hydrates, hemiacetals, acetal cyclic polymers, mono- and di-acid forms of glutaraldehyde and various glutaraldehyde oligomers. Figure 6.1 below shows such molecular structures. These primarily include trioxane-type oligomers, dimers produced by aldol condensation of two glutaraldehyde molecules and their cyclic acetal, oligomers of glutaraldehyde consisting of the α -oxypyran ring, some (apparently much smaller amounts of) different unsaturated aldol condensation products and aldol/Michael addition products. All these structures (see chapter 4 and appendix III for further details) exhibit many carbonyl pendant groups that could act as theoretical nucleating sites, in a similar way to polyether segments of polyurethanes that were found to instigate calcium complexation^{25,26}. Calcium complexation may lead to site-specific increases in calcium ion concentration that can then initiate a sequence leading to the formation of calcium phosphate salts and the subsequent crystallisation of mineral²⁷.

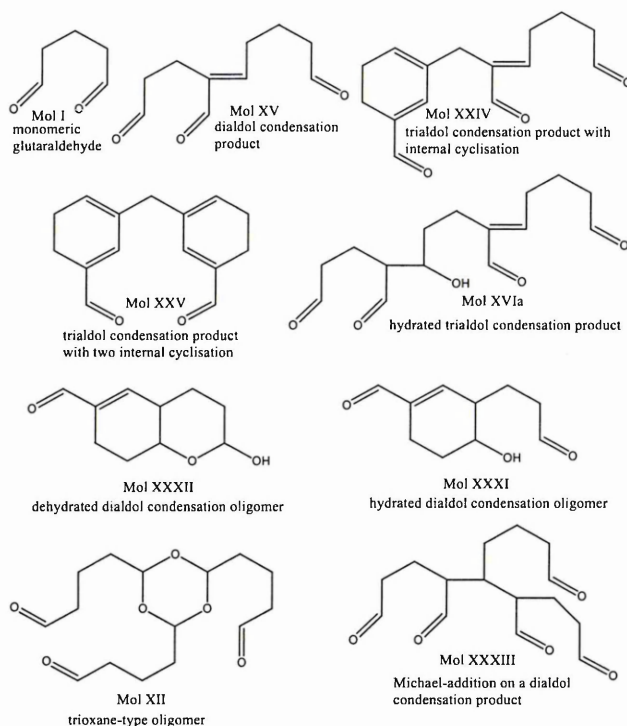


Figure 6.1: Structures of molecules thought to be predominant in aqueous glutaraldehyde solutions (pH 3.8 – 9.2). (Extracted from the results found in chapter 4 and appendix III). Structure numbers correspond to those used in appendix III.

The reaction of glutaraldehyde with valve collagenous tissue and other matrix components was also assumed by Cheung, Nimni et al to yield products with functional groups that were hypothesised to be correlated with the calcification process of valve tissue. That is, the final form of the cross-linked tissue tends to contain nucleophilic residues such as carbonyl oxygens²⁸⁻³¹. In a more recent study, tissue valve calcification has also been hypothesised to correlate with the calcium-binding ability of glutaraldehyde polymers that are present on the surface of treated tissue²⁵. Furthermore, it has been suggested that the reaction of glutaraldehyde with lysine side chains (lysyl and hydroxylysyl residues of collagenous tissue) may lead to an impaired balance between positively and negatively charged functional groups in the collagenous tissue, thus favouring calcium ion deposition³²⁻³⁵. Many reports have indicated a role for aldehyde-induced intra- and inter-molecular collagen cross-links in initiating tissue mineralisation³⁶⁻³⁹. For instance, it has been reported that the treatment of tissue by glutaraldehyde would result in the formation of Schiff bases which are likely to be susceptible to hydrolysis⁴⁰ under physiological conditions and could generate free formyl groups that could in turn be readily oxidised to form

carboxyl groups⁴¹ (probably as carboxylate anions). To corroborate this statement, Southern et al investigated the presence of oxidation products in hydrolysed cross-linked collagenous tissue⁴² Various oxidation products (including carboxylic acids) were found and were hypothesised to play a role in the calcification of the tissue, as previously suggested by Urist et al³¹. Our study of model compounds reacted with glutaraldehyde (see chapter 5 and appendix IV for further details), suggested the presence of many different molecular structures. These included Michael-addition products, Schiff base moieties (including cross-links) associated with various aldol/Michael condensation products of glutaraldehyde and some cyclisation products incorporating pyridinium and dihydropyridine ring structures. All these structures contain free pendant carbonyls that can form carboxylic groups under physiological conditions⁴³. Some of the major structures identified from the analysis of the products of the reaction between glutaraldehyde and model compounds similar to the lysine residue (chapter 5 and in appendix IV) are reproduced below in figure 6.2.

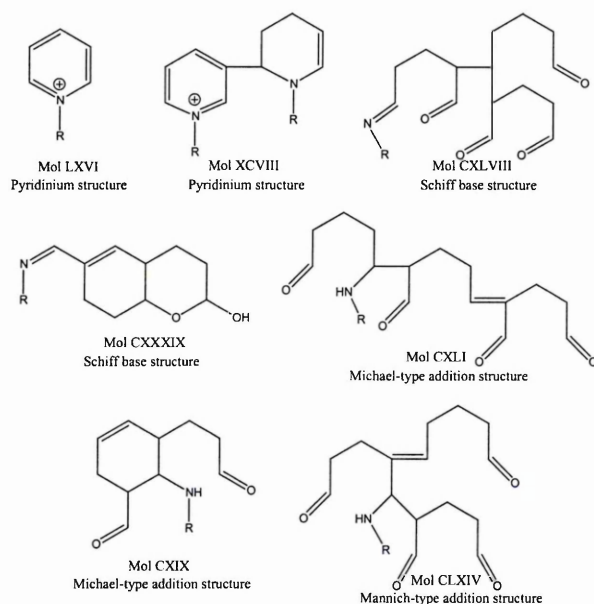


Figure 6.2: Some chemical structures from the reaction between the 6-amino group of lysine and glutaraldehyde thought predominantly present under the pH range 3.8 - 9.2. (Extracted from the results found in chapter 5 and appendix IV). Structure numbers correspond to those used in appendix IV.

The pyridinium structures identified, being quaternary amines, could potentially attract phosphate ions because of the positive charge on the structures⁴⁴ and also

because compounds similar to pyridinium were found in bone-derived collagen⁴⁵. For example, quaternary pyridinium-type cross-links found in both elastin and collagen are thought to serve as a nucleation point for calcification⁴⁶. Moreover, a dipyridine structure has been suggested to be involved in calcification of glutaraldehyde cross-linked collagen as well as accounting for the high stability of the cross-links⁴⁷. This hypothesis was also confirmed by Van Luyn et al⁴⁸, who showed the possible involvement of cyclic cross-links as nucleation point for calcification.

The air oxidation of aldehydes has also been well documented^{49,50} and glutaraldehyde can be hypothesised to behave similarly, forming 4-formylbutanoic acid or glutaric acid. This was confirmed by our findings reported in chapter 4 of this thesis, where traces of mono- and possibly di-acid (glutaric acid) forms of glutaraldehyde were both found in aqueous glutaraldehyde solutions under physiological conditions. Bioprosthetic valves (during their manufacture) are floating in large pools, containing glutaraldehyde that can be readily oxidised because of the large surface area in contact with air. Additionally, despite the presence of isotonic phosphate buffer in these pools (to avoid any swelling or shrinkage of tissue due to osmotic effects), if one makes the assumption of the large size of these pools and the natural acidity of glutaraldehyde, a buffer of about 0.2 M (currently used in valve manufacture) would probably not be enough to maintain the pH at a neutral physiological value. Additionally, it can be hypothesised that a resulting drop of pH, such as the one observed in-vitro from the reaction between glutaraldehyde and proteins (see chapter 5), could affect the overall pH of these pools and favour the formation of acid forms of glutaraldehyde such as glutaric acid. Unfortunately, this can only be a hypothetical statement because of the lack of communication with the different valves manufacturing companies on this potential matter.

Carboxylate anions formed from the oxidation of aldehyde groups can readily bind cations such as calcium by electrostatic interaction forming salts, which could act as an initiation site for subsequent mineralisation⁴¹. (Theoretically, a calcium ion (radius of about 100 pm⁵¹) can be bound by carbonyl groups, similarly to magnesium ion that was shown favoring oxygen donor ligands, especially the phosphate groups⁵²). Computer modelling of the calcification of polyurethane valves (calcium complexation providing initiation sites for the ultimate formation of calcific

deposits) has been successfully demonstrated²⁵. The authors of the study proposed that the potential exists for similar calcium complexation of glutaraldehyde-treated tissue valves, driven by the formation of a crown-like complex of polymeric forms of glutaraldehyde with calcium. Their data support the hypothesis that a key initiator in mineral formation is the presence of binding sites within the bulk and at the blood/material surface.

The aim of this study therefore was to determine spectroscopically whether glutaraldehyde and its di-acid form, glutaric acid, have the potential to initiate mineralisation by complexing some relevant ions such as calcium. Additionally, the possible uptake of calcium by amino acids and other molecules mimicking the behaviour of collagenous tissue was investigated using Fourier-transform infrared-attenuated total reflectance (FTIR-ATR) spectroscopy.

6.2 Materials and Methods

6.2.1 Calcification studies

The chemicals and consumables used were the following:

From BDH, UK: Glutaraldehyde 25% EM grade.

From Sigma, UK: Glutaric acid, 6-amino-n-caproic acid, N-acetyl-L-lysine, N-acetyl-Phe Lys.

Calcification solution preparation: Sodium chloride (BDH, UK) 7.9 g, calcium chloride dihydrate (BDH, UK) 0.294 g, potassium dihydrogen orthophosphate (BDH, UK) 0.163 g, MOPS buffer (3-N-morpholinopropanesulfonic acid) (Sigma, UK) 0.010 g, in 1 L of distilled water.

Experiments were carried out in sterile closed sample vials, kept in the dark at 37° C and shaken in a Gallenkamp orbital incubator at 100 rev/min.

Glutaraldehyde (0.2% v/v and 0.6% v/v in water) was incubated in a calcification solution (pH 7.4). A similar protocol was carried out with 0.1% w/v glutaric acid in a calcification solution in order to study the possibility that oxidised glutaraldehyde

(glutaric acid is the di-acid structure of glutaraldehyde, as can be seen in figure 6.3 below) might attract calcium ions.

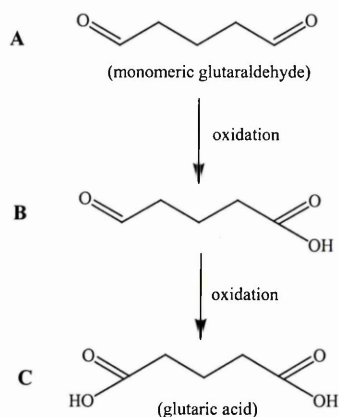


Figure 6.3: the oxidation of monomeric glutaraldehyde (A) into the mono-acid form (B) and the di-acid form (glutaric acid) of glutaraldehyde (C).

In order to model the behaviour of collagen towards a calcification solution, the same type of experiment was carried out using amino acids and a peptide. This would indicate whether the collagen itself can be considered responsible for initiating calcification. Thus, 6-amino-n-caproic acid, N-acetyl-L-lysine and N-acetyl phenylalanine lysine (unreacted and reacted with glutaraldehyde) were studied by Fourier-transform infrared spectroscopy. The structures of these model compounds can be found in figure 6.4 below.

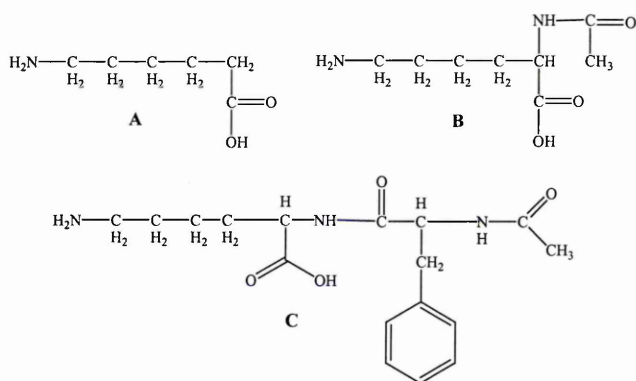


Figure 6.4: Chemical structures of 6-amino-n-caproic acid (also called aminohexanoic acid) (A), N-acetyl-L-lysine (B), and N-acetyl phenylalanine lysine (C).

6.2.2 Freeze-drier

The freeze-drying procedure was similar to the one described previously in chapter 4 section 4.2.3.

6.2.3 Infrared spectroscopy

All spectra were recorded with a Mattson Polaris FTIR spectrometer (ThermoNicolet Co, Lanham, MA, USA) with an MCT detector, a KBr beam splitter, and scanned between 4000 and 400 cm^{-1} . The apodisation function was triangular and there was a Mertz phase correction. All spectra were obtained by accumulation of 1000 scans, at a resolution of 4 cm^{-1} and 45° angle of incidence, after subtracting the spectra of the ZnSe crystal. All spectra were recorded under similar conditions (constant temperature) and were corrected for atmospheric water vapour and carbon dioxide by subtraction of the appropriate reference spectrum, even though the instrument was purged constantly with dried, water vapour-free air. The ATR device was a horizontal multiple reflection ATR (Graseby Specac, St Mary Cray, UK) with a ZnSe crystal. This crystal allowed easy sample preparation by pouring a few millilitres of the sample into the “pool” of the ATR cell, followed by freeze-drying.

6.3 Results and discussion

6.3.1 Calcification of glutaraldehyde

Glutaraldehyde is usually considered as a monomeric dialdehyde molecule of molecular weight 100. However, we showed in chapter 4 that commercial glutaraldehyde solutions contain many more chemical species than just monomeric glutaraldehyde (see appendix III for detailed chemical structures). The FTIR-ATR results obtained from a time dependent study of glutaraldehyde (0.6% v/v or 0.2% v/v) incubated in a calcifying solution showed a singular pattern in the 1850-1550 cm^{-1} region. The overall spectra can be seen in figure 6.5, while figure 6.6 shows expansions of the 1850-1250 cm^{-1} spectral region.

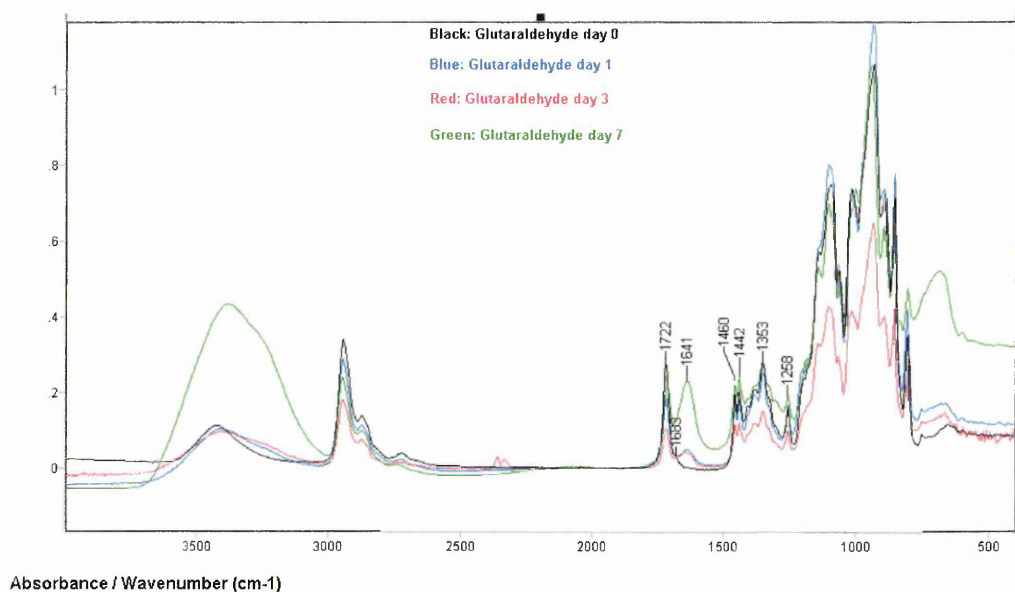


Figure 6.5: FTIR-ATR spectra from the calcification of glutaraldehyde (0.6% v/v glutaraldehyde solution plus calcifying solution, freeze-dried).

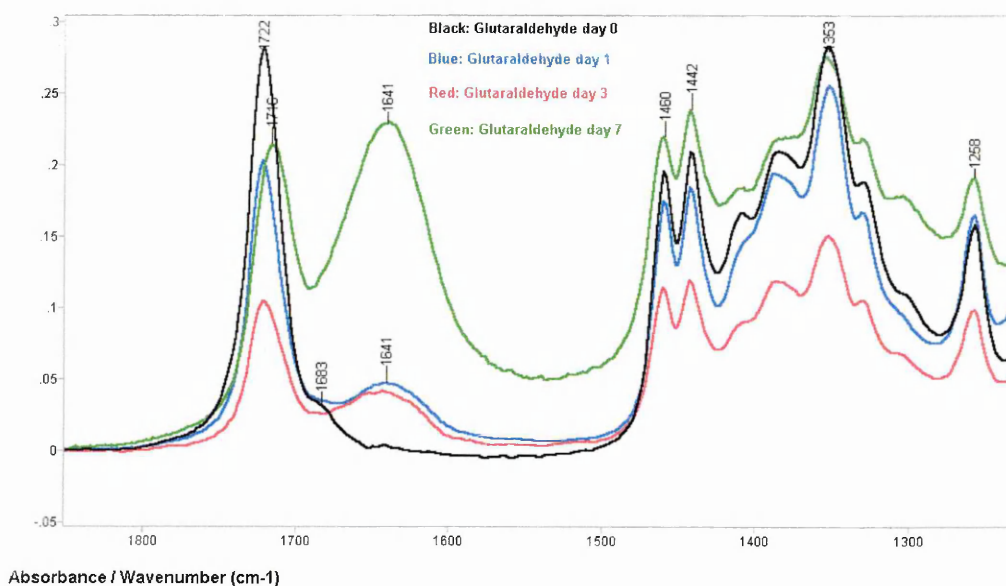


Figure 6.6: Expansion of the 1850-1250 cm⁻¹ spectral region of the FTIR-ATR spectra from the calcification of glutaraldehyde (0.6% v/v glutaraldehyde solution plus calcifying solution, freeze-dried).

At day 0 (non-incubated glutaraldehyde in aqueous solution), the interpretation of the infrared spectra is as shown in table 6.1 below, although a fuller account can be found in chapter 4.

Peak position (cm ⁻¹)	Assignment
3426	Assigned to the presence of bulk water (although the sample was freeze-dried) but also possibly to the presence of alcohol (hydrated oligomers of glutaraldehyde) or acid groups due to the oxidation of the aldehydes of the glutaraldehyde molecules
2947	Assigned to anti-symmetric stretching of the CH ₂ group
2872	Assigned to symmetric stretching of the CH ₂ group
2725	Weak band assigned to anti-symmetric stretching of the CH of the aldehyde group
1722	Main sharp and intense peak assigned to stretching of the C=O groups of non-conjugated aldehydes and carboxylic acids overlapping with each other
1683	Very weak band assigned to stretching of the CO group of conjugated aldehyde due to the presence of some polymeric glutaraldehyde structures (see chapters 2 and 4 for detailed account of the structures). However this band is also observed in the spectrum of glutaric acid assigned for the C=O of the carboxyl group and could therefore be due to the presence of the mono- or di-acid form (glutaric acid) of glutaraldehyde

Table 6.1: FTIR peaks and their corresponding assignments, from the analysis of glutaraldehyde in aqueous solution (not incubated in calcification solution). See also figures 6.5 and 6.6.

As early as day one of incubation, one can observe some major changes in the 1800-1500 cm⁻¹ region, while no other changes take place in the rest of the spectrum. The band at 1722 cm⁻¹ (stretching of the C=O groups of non-conjugated aldehydes and carboxylic acids overlapping with each other) is still present (though perhaps reduced in size) but the band at 1683 cm⁻¹ has disappeared while a broad band at 1641 cm⁻¹ has appeared (possibly assigned to stretching of the C=O group of a carboxylic acid).

After 3 days incubation, the peak at 1722 cm⁻¹ broadened, possibly indicating an uptake of a cation such as calcium from the calcifying solution and the broad peak at 1641 cm⁻¹ was still present.

After 1 week of incubation, the peak assigned to the stretching of the C=O groups of non-conjugated aldehydes was shifted to 1716 cm⁻¹ and was broader than that observed at day 0 or 1. The broad, weak peak at 1641 cm⁻¹ (observed from day 1 of incubation) appears now as a definite intense, but broad, peak.

These results with glutaraldehyde thus bring the hypothesis of a possible uptake of cation (e.g. calcium) through a likely mechanism such as the one shown in figure 6.7 below.

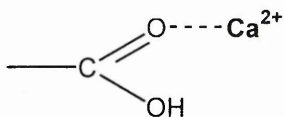


Figure 6.7: Mechanism of uptake of calcium by a carboxylic acid.

6.3.2 Calcification of glutaric acid

The FTIR-ATR spectra of glutaric acid mixed with a calcifying solution are shown in figure 6.8 below; only the 1850-1000 cm^{-1} region is shown as this is where the spectral changes take place. When carboxylic acids are converted to alkaline salts, the bands of the carboxylic acid group vanish and tend to be replaced by two bands of the COO^- group at lower wavenumbers. However, since the nature of the cation has little effect on the frequency of the bands, it is usually difficult to assess whether a calcium salt or another cation is present⁵³.

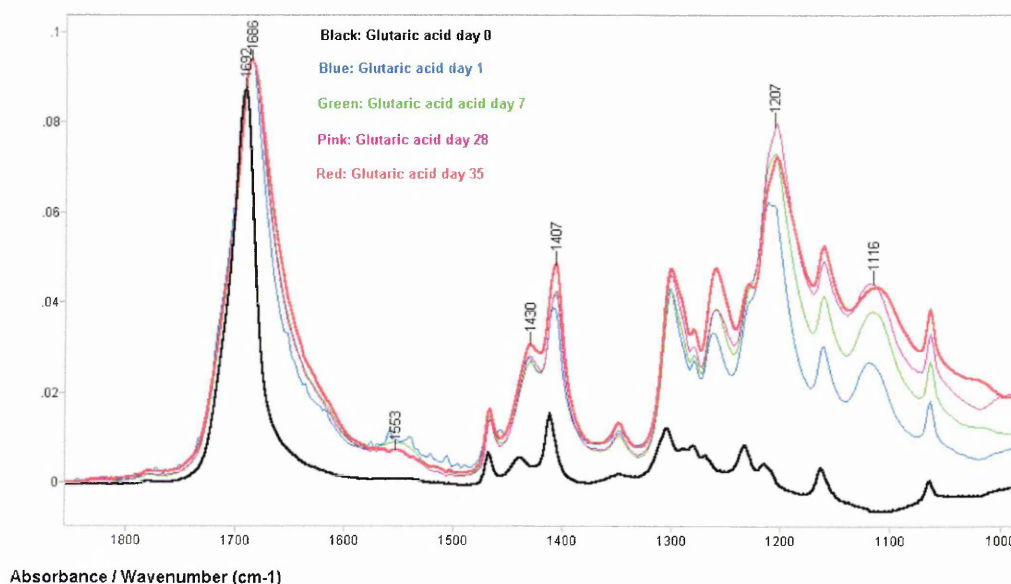


Figure 6.8: FTIR-ATR spectra from the in-vitro calcification of 0.1% w/v glutaric acid (expansion of the 1850-1000 cm^{-1} spectral region).

At day 0 (non-incubated glutaric acid in aqueous solution), the interpretation of the infrared spectra is as shown in table 6.2 below.

Peak position (cm ⁻¹)	Assignment
1692	Most intense and sharp peak of the spectrum. Assigned to stretching of the C=O mode of the carboxylic acid
1464	Corresponds to the scissoring absorption mode of the “intermediate” CH ₂ group found in the middle of the glutaric acid molecule
1441 and 1305	Assigned to the coupling of the OH in plane deformation and to the C-O stretching vibration occurring in the plane of the ring formed by the dimeric carboxyl groups ⁵³
1407	Can be due to the strong scissoring mode of the CH ₂ group close to the carboxylic group

Table 6.2: FTIR peaks and their corresponding assignments, from the analysis of 0.1% w/v glutaric acid in aqueous solution (not incubated in calcification solution). See also figure 6.8.

After 1 day of incubation, the peak at 1692 cm⁻¹ became broader and shifted to a lower wavenumber (1686 cm⁻¹). This shifting is possibly due to the uptake of a cation such as calcium from the calcifying solution because the width of the peak at half height is doubled. This leads to the hypothesis of the uptake of a cation (calcium) by the mechanism shown in figure 6.9:

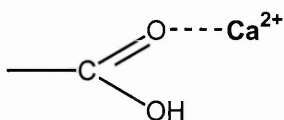


Figure 6.9: Mechanism of uptake of calcium by carboxylic acid.

A weak but broad band at ~1553 cm⁻¹ also appeared (anti-symmetric stretching of the COO⁻ of the carboxylate group) and is likely to be due to the presence of carboxyl functions in the form of salts⁵⁴, while the slight shift of the band at 1430 cm⁻¹ (formerly 1441 cm⁻¹ at day 0 of implantation) could be due to a symmetric stretching of the COO⁻ of the carboxylate group (salt), which leads to another hypothetical mechanism, as shown in figure 6.10 below.

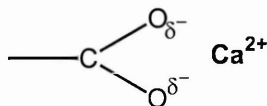


Figure 6.10: Mechanism of uptake of calcium by carboxylate anion by electrostatic interaction, forming a salt.

It is however rather difficult to be sure about the presence of the COO⁻ group symmetric stretch at 1430 cm⁻¹ because of the large number of bands occurring in this region. The peaks at 1430 cm⁻¹ and 1302 cm⁻¹ could correspond to the former

bands at 1441 cm^{-1} and 1305 cm^{-1} shifted because of a chelate formation. Intense peaks at 1207 and 1116 cm^{-1} were the only bands observed due to the absorption of the calcifying solution in this region (spectrum not shown).

At day 7, and up to 35 days of incubation, the peak at 1686 cm^{-1} became slightly broader and the peak at $\sim 1553\text{ cm}^{-1}$ was still present. No other changes in the spectra could be observed.

The spectra thus show the possible uptake of cations such as calcium from the surrounding calcifying metastable solution. Hence, it can be concluded that glutaric acid (the di-acid form of glutaraldehyde) is capable of attracting cations (such as calcium) and forming some sort of complex.

6.3.3 Calcification of an amino acid and peptide

Any significant binding of a metal ion such as calcium to a specific functional group of an amino acid or peptide might be detected, either by a shift in wavenumber of the relevant peak or by a variation in the relative size of the peak, hence binding sites relevant to calcification could thus be identified. Additionally, the formation of a salt can be discriminated by infrared bands from the different groups involved in such a salt formation (COOH , COO^- and C=O). It has been reported that a shift of up to 100 cm^{-1} between the carboxylic band and the corresponding carboxylic anion band involved in complex formation, may be observed in the case of complex formation between a metal ion and the carboxylate residue of the amino acid glycine^{55,56}. The most reactive amino acids available in valve tissue are lysine residues, which have only limited α -amino groups available to react (most are involved in peptide bonds), in comparison to their ϵ -amino (or 6-amino) groups (see chapter 2). A typical FTIR series of spectra of an amino acid (6-amino-n-caproic acid, mimicking a lysine group of collagenous tissue but without an α -amino group), incubated in a calcifying solution is shown in figure 6.11 below. The region $1850\text{-}1000\text{ cm}^{-1}$ only is shown as this included the major peaks of interest.

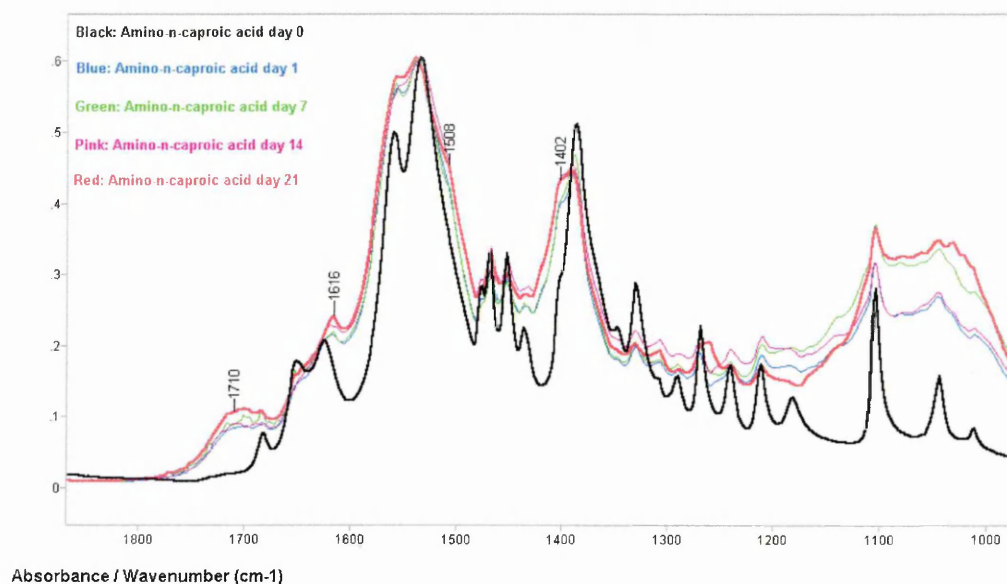


Figure 6.11: FTIR-ATR spectra from the in-vitro calcification of 0.1% w/v 6-amino-n-caproic acid (expansion of the 1850-1000 cm^{-1} spectral region).

An interpretation of the major bands found in the spectrum (not fully shown in figure 6.10 above) of non-incubated 6-amino-n-caproic acid (day 0 of incubation) follows in table 6.3, below.

Peak position (cm^{-1})	Assignment
2211	The amino acid appeared to be predominantly in its zwitterionic form, because of the presence of the characteristic NH_3^+ symmetric stretching band (part of the spectrum not shown here)
1683	C=O acid group stretch mode
1651	Possibly assigned to a NH bending mode (amine group)
1624	Possibly assigned to a NH bending mode (amine group)
1560 and 1534	Doublet assigned to C=O anti-symmetric stretching mode (COO^- group)
1469, 1452 and 1436	Possibly CH_2 group scissoring modes
1388	Possibly a C=O group symmetric stretching mode
1330, 1309 and 1291	Possibly CH_2 groups wagging modes
1103	Assigned to a NH_3^+ group rocking mode/ NH_2 group twisting mode
1043	Possibly a C-N group stretching mode.

Table 6.3: FTIR peaks and their corresponding assignments, from the analysis of 6-amino-n-caproic acid in aqueous solution (not incubated in calcification solution). See also figure 6.11.

As early as day one of incubation in the calcium-containing solution, many changes were seen in the FTIR spectrum. The appearance of a broad and relatively weak peak around 1710 cm^{-1} could be assigned to the presence of chelation mechanism between

acid groups of the molecule and a cation such as calcium from the calcifying solution. The structure of the complex formed is likely to be shown below in figure 6.12. Such a metal complex structure is expected to exhibit a characteristic C=O infrared absorption frequency around about 1700 cm^{-1} , as it was suggested in the literature⁵⁵.

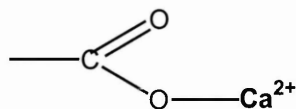


Figure 6.12: Chelation mechanism of a carboxylic acid and a metal cation such as calcium.

The appearance of a peak at 1616 cm^{-1} is most likely to be due to the infrared absorption of the calcifying solution in this region (spectrum not shown), but could also be assigned to a NH bending mode (or a deformation mode of the NH_3^+ group), which could also be involved with the chelation of phosphate. The appearance of a shoulder at $\sim 1508\text{ cm}^{-1}$, which became more prominent with increasing incubation time is likely to be due to the presence of carboxyl functions in the form of salts⁵⁴ (anti-symmetric stretching mode of the C=O of the carboxylate group), while the appearance of an intense band around 1402 cm^{-1} could be due to the symmetric stretching mode of the C=O of the carboxylate group (salt)⁵⁶. These findings could also suggest the hypothetic presence of another mechanism for the attraction of cations by amino acids, as is shown in figure 6.13 below.

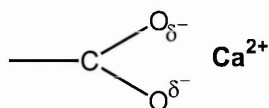


Figure 6.13: Mechanism of uptake of calcium by carboxylate group, forming a salt.

The peak at $\sim 1508\text{ cm}^{-1}$ could also be assigned as the second peak of the NH bending mode indicating the presence of an amino group ($\text{NH}_2/\text{NH}_3^+$), which could possibly also be involved in a chelation mechanism with phosphate. It is more likely however that this peak is covered by the COO^- anti-symmetric vibration mode peak.

Other model compounds studied were also incubated in-vitro in a calcifying solution. (i.e. N-acetyl-L-lysine and N-acetyl phenylalanine lysine). Despite the complexity of the spectra obtained (results not shown), especially the one of the

peptide, they appeared to behave similarly and exhibited similar features such as the broad, weak band around $1710\text{-}1730\text{ cm}^{-1}$, the presence of carboxylic acid salts (deduced from the presence of the anti-symmetric stretch around $1500\text{-}1580\text{ cm}^{-1}$) and also the hypothetical presence of some protonated amino groups. All of these assignments suggest the possibility of uptake of cations such as calcium but possibly also phosphate anions from the incubation medium.

6.3.4 Calcification of glutaraldehyde-treated amino acids and peptide

FTIR spectra of glutaraldehyde-treated model compounds (6-amino-n-caproic acid, N-acetyl-L-lysine and N-acetyl-phenylalanine lysine) were extremely complex and hence could not be fully interpreted. It has not been possible therefore to identify a possible interaction of the amino or carbonyl/carboxyl groups of the molecules backbones as binding sites for phosphate and calcium respectively. However, since the attraction of calcium by both glutaraldehyde and model compounds on their own was observed using FTIR-ATR spectroscopy, it can be strongly hypothesised that glutaraldehyde-treated model compounds would behave similarly.

6.3.5 Overall discussion of data obtained

Glutaraldehyde in solution was shown in chapter 4 to consist of various molecular entities, comprising essentially of glutaraldehyde monomers, acetals, hydrated structures, aldol polymers, Michael-addition polymers and also some possible acid forms of glutaraldehyde. The infrared spectroscopic study of glutaraldehyde, incubated in a calcification solution, revealed the potential character of glutaraldehyde to uptake a cation (calcium or potassium from the metastable calcifying solution) from its carboxylic acid. This cation uptake could well be an initiator for the mineralisation process. It was also shown in chapter 4, however, that the amount of carboxylic acid forms of glutaraldehyde oligomers was small. Therefore the mechanism of cation uptake by carboxylic acid groups cannot be considered to be the only one to account for the potential of glutaraldehyde to attract cations such as calcium and hence to be an initiator of the mineralisation process. Thus, other mechanisms involving carbonyl groups are likely to be alternatives to the cation uptake observed by FTIR spectroscopy in this study, although this mechanism could be valid in-vivo.

Our data would agree with the suggestions of Thoma et al²⁵, who proposed from a theoretical molecular modelling study that some glutaraldehyde polymers in glutaraldehyde-treated tissue valves could have the potential to form a crown-like complex with calcium. The pendant carbonyl groups would act as binding sites, assuming that the most likely form of polyglutaraldehyde in solution would be based on hemiacetal polymerisation. Formation of such a complex could be one key initiator for mineral formation in glutaraldehyde-treated valve tissue. The presence of such hemiacetal glutaraldehyde structures was also observed in our study (see chapter 4) and this mechanism could well be considered valid. Furthermore, it can be hypothesised that other glutaraldehyde species present in solution could form similar complexes with a cation such as calcium. This is because of the presence of electronegative sites due to the oxygen-rich environment of the polyglutaraldehyde structures, such as the ones found in our study (see chapter 4). It is expected that such complex formation, would exhibit similar behaviour to that seen in the infrared spectroscopic analysis of the calcified glutaraldehyde solution and would thus represent further candidates to explain the potential of glutaraldehyde to attract cations.

The mechanism of cation uptake by chemical groups in glutaraldehyde-treated valve tissue (essentially those containing lone pairs of electrons, such as carbonyl, carboxyl and amino groups) is a likely candidate for the initiation of mineralisation of valve tissue, according to the results of this study. Those groups are readily available in the collagen backbone, especially the carbonyl oxygens that are very susceptible to interactions with cations such as calcium. It is suggested that phosphate ions could be attracted by this micro-electric field because of the unbalanced charge. This would help to maintain overall charge neutrality and thus create the potential for hydroxyapatite formation (hydroxyapatite $[\text{Ca}_5(\text{PO}_4)_3\text{OH}]$ being the main inorganic phase observed in heavily calcified tissues). It could also facilitate formation of other precursors of the calcification process containing essentially calcium and phosphorus.

The cytotoxic effect of the glutaraldehyde fixation treatment has been implicated in an extrinsic form of calcification where the cytotoxicity of glutaraldehyde causes cell death and formation of extrinsic calcific nodes. However, the most significant tissue failure mechanism relates to intrinsic calcification⁴, where the calcific deposits form

deep within the tissue matrix. The various cation chelation mechanisms proposed in this study give a reasonable explanation why both intrinsic (calcification directly associated with the material) and extrinsic calcification (in association with debris and located at the surface of the material) may be observed. The material components (such as elastin and predominantly collagen, in the case of valve tissue) are probably the main cause of intrinsic calcification, while debris on the surface of the material could have identical properties and hence possess similar possible binding sites. This mechanism could therefore affect the fragile equilibrium of the metastable state of the ions involved in mineralisation, by shifting the equilibrium towards the spontaneous precipitation of calcium phosphate. The cation chelation mechanism induces a slight local increase in the calcium phosphate product, taking it above the critical level needed for precipitation, allowing growth of crystal structures once precipitation is initiated. Once crystals are formed, the reaction would be irreversible since the products tend to be insoluble and the mineralisation mechanism would certainly continue.

6.4 Conclusion

Glutaraldehyde and oxidised glutaraldehyde (glutaric acid) have been shown to have the potential to induce mineralisation by attracting cations (potentially calcium) from a metastable calcifying solution. The two species do, however, seem to behave differently.

The FTIR spectra from glutaraldehyde-treated model compounds, were extremely complex and hence too difficult to fully interpret. Therefore identification of possible interactions of the amino or carbonyl groups as binding sites for phosphate and calcium respectively was not possible but could not be ruled out. However, the same model compounds not reacted with glutaraldehyde were shown to bind calcium. It is most likely that the carbonyl oxygen atoms contained in their backbones facilitate binding, although other chemical groups, such as the protonated amino groups, could also be involved in the mineralisation process by potentially binding phosphate. Collagen is thought to have the potential to behave similarly. A study of type I collagen films and their subsequent calcification was thus carried out and the early results, including the successful methodology, can be found in the appendix I.

Overall, the data shown in this chapter bring forward some new insights into the hypothetical primary processes of mineralisation of tissue. They may also help to explain the involvement of glutaraldehyde and tissue in the calcification process of valve bioprostheses.

1. Grabenwoger M, Grimm M, Eybl E. New aspects of the degeneration of bioprosthetic heart valve failure: pathology and pathogenesis. *Cardiology Clinics*. 1984;2:717-739.
2. Levy RJ, Schoen FJ, Sherman FS, Nichols J, Hawley MA, Lund SA. Calcification of subcutaneously implanted type I collagen sponges: effects of glutaraldehyde and formaldehyde pretreatments. *American Journal of Pathology*. 1986;122:71-82.
3. Liao K, Frater RWM, LaPietra A, Ciuffo G, Ilardi CF, Seifter E. Time-dependent effect of glutaraldehyde on the tendency to calcify of both autografts and xenografts. *Annals of Thoracic Surgery*. 1995;60:S343-S347.
4. Schoen FJ, Tsao JW, Levy RJ. Calcification of bovine pericardium used in cardiac valve bioprostheses. Implications for the mechanism of bioprosthetic tissue mineralisation. *American Journal of Pathology*. 1986;123:134-145.
5. Wadkins CL, Luben RA. Effects of fluoride on in-vitro calcification of tendon matrix. *Calcified Tissue Research*. 1978;26:51-59.
6. Anderson HC. Normal and abnormal mineralisation in mammals. *American Society Artificial Internal Organs Transaction*. 1981;27:702-708.
7. Bernacca GM, Fisher AC, Mackay TG, Wheatley DJ. A dynamic in-vitro method for studying bioprosthetic heart valve calcification. *Journal of Materials Science. Materials in Medicine*. 1992;3:293-298.
8. Ferrans VJ, Boyce SW, Billingham ME, Jones M, Ishihara T, Roberts WC. Calcific deposits in porcine bioprostheses: structure and pathogenesis. *American Journal of Cardiology*. 1980;46:721-734.
9. Fleisch H, Neuman WF. Mechanisms of calcification: role of collagen, polyphosphonates and phosphatase. *Journal of the American Chemical Society*. 1960;82:1296-1300.
10. Glimcher MJ. Mechanism of calcification: role of collagen fibrils and collagen-phosphoprotein complexes in-vitro and in-vivo. *The Anatomical Record*. 1989;224:139-153.
11. Valente M, Bortolotti U, Thiene G. Ultrastructural substrates of dystrophic calcification in porcine bioprosthetic valve failure. *American Journal of Pathology*. 1985;119:12-21.
12. Webb CL, Nguyen NM, Schoen FJ, Levy RJ. Calcification of allograft aortic wall in a rat subdermal model: pathophysiology and inhibition by aluminium and aminodiphosphonate preincubations. *American Journal of Pathology*. 1992;141:487-496.
13. Long MM, Urry DW. On the molecular mechanism of elastic fiber calcification. *American Society Artificial Internal Organs Transaction*. 1981;27:690-696.
14. Urry DW. Neutral sites for calcium ion binding to elastin and collagen: a charge neutralisation theory for calcification and its relationship to atherosclerosis. *Proceedings of the National Academy of Science of the USA*. 1971;68:810-814.
15. Hamon RF, Khan AS, Chow A. The cation-chelation mechanism of metal-ion sorption by polyurethanes. *Talanta*. 1982;29:313-326.
16. Benson RS, Wong RP. The dynamic mechanical properties of the blood diaphragm of the JARVIK-70 TAH. *Transaction of the 3rd World Biomaterials Congress*. 1988;(abstract):124.
17. Chinn JA, Frautschi JR, Phillips RE. Calcification in-vitro: a comparison between mineralisation of unstrained and cyclically strained polymers. *Transaction of the 4th World Biomaterials Congress*. 1992;(abstract):81.
18. Hol WGH, Van Duijnen PTV, Berendsen HJC. The α -helix dipole and the properties of proteins. *Nature*. 1978;273:443-446.
19. Miller A. Collagen: the organic matrix of bone. *Philosophical Transaction of the Royal Society of Chemistry London Series B*. 1984;304:455.
20. Girardot MN, Torrianni M, Dillehay D, Girardot JM. Role of glutaraldehyde in calcification of porcine heart valves: comparing cusp and wall. *Journal of Biomedical Materials Research*. 1995;29:793-801.

21. Sherman FS, Schoen FJ, Hawley MA, Nichols J, Levy RJ. Collagen crosslinks: a critical determinant of bioprosthetic heart valve calcification. *American Society Artificial Internal Organs Transaction*. 1984;30:577-581.
22. Schoen FJ, Levy RJ. Bioprosthetic heart valve failure: pathology and pathogenesis. *Cardiology Clinics*. 1984;2:717-739.
23. Grimm M, Eybl E, Grabenwoger M, Bock P, Muller M, Wolner E. Glutaraldehyde affects biocompatibility of bioprosthetic heart valves. *Surgery*. 1992;111:74-78.
24. Golomb G, Schoen FJ, Smith MS, Linden J, Dixon M, Levy RJ. The role of glutaraldehyde-induced cross-links in calcification of bovine pericardium used in cardiac valve bioprostheses. *American Journal of Pathology*. 1987;127:122-130.
25. Thoma RJ, Phillips RE. The role of material surface chemistry in implant device calcification: a hypothesis. *Journal of Heart Valve Disease*. 1995;4:214-221.
26. Thoma RJ. Poly(ether)urethane reactivity with metal-ion in calcification and environmental stress cracking. *Journal of Biomaterials Applications*. 1987;90:449-486.
27. Pollack E, Andrews EJ, Lentz DJ, Sheikh D. Tissue ingrowth and porosity of biomer. *American Society Artificial Internal Organs Transaction*. 1981:405-409.
28. Cheung DT, Nimni ME. Mechanism of crosslinking of proteins by glutaraldehyde I. Reaction with model compounds. *Connective Tissue Research*. 1982;10:187-199.
29. Cheung DT, Nimni ME. Mechanism of crosslinking of proteins by glutaraldehyde II. Reaction with monomeric and polymeric collagen. *Connective Tissue Research*. 1982;10:201-216.
30. Nimni ME, Bernick S, Cheung DT, Ertl DC, Nishimoto SK, Paule WJ, Salka C, Strates BS. Biochemical differences between dystrophic calcification of cross-linked collagen implants and mineralisation during bone induction. *Calcified Tissue International*. 1988;42:313-320.
31. Urist MR, Adams JM. Effects of various blocking reagents upon local mechanism of calcification. *Archives of Pathology*. 1966;81:325-342.
32. Bowes JH, Cater CW. The reaction of glutaraldehyde with proteins and other biological materials. *Journal of the Royal Microscopical Society*. 1966;85:193-200.
33. Bowes JH, Cater CW. The interaction of aldehydes with collagen. *Biochimica et Biophysica Acta*. 1968;168:341-352.
34. Chvapil M. Reconstituted collagen. In: Viidik A, Vuust J, eds. *Biology of Collagen*. London: Academic; 1980:313-324.
35. Golomb G, Ezra V. Prevention of bioprosthetic heart valve tissue calcification by charge modification: effects of protamine binding by formaldehyde. *Journal of Biomedical Materials Research*. 1991;25:85-98.
36. Angell WW, Angell JD, Kosek JC. Twelve-year experience with glutaraldehyde-preserved porcine xenografts. *Journal of Thoracic and Cardiovascular Surgery*. 1982;83:493-502.
37. Schoen FJ, Collins JJ, Cohn LH. Long-term failure rate and morphologic correlations in porcine bioprosthetic heart valves. *American Journal of Cardiology*. 1983;51:957-966.
38. Imamura E, Sawatani O, Koyanagi H, Noishiki Y, Miyaya T. Epoxy compounds as a new crosslinking agent for porcine aortic leaflets: subcutaneous implant studies in rats. *Journal of Cardiac Surgery*. 1989;4:50-57.
39. Bernacca GM, Dimitri WR, Fischer AC, Mackay TG, Wheatley DJ. Chemical modification of bovine pericardium and its effect on calcification in the rat subdermal model. *Biomaterials*. 1992;13:345-352.
40. Tomimatsu Y, Jansen EF, Gaffield W, Olson AC. Physical chemical observations on the alpha-chymotrypsin glutaraldehyde system during formation of an insoluble derivative. *Journal of Colloid and Interface Science*. 1971;36:51-64.
41. Chanda J. Prevention of calcification of heart valve bioprostheses: an experimental study in rat. *Annals of Thoracic Surgery*. 1995;60:S339-S342.
42. Southern LJ, Hughes H, Lawford PV, Clench MR, Manning NJ. Glutaraldehyde-induced cross-links: a study of model compounds and commercial bioprosthetic valves. *Journal of Heart Valve Disease*. 2000;9:241-249.
43. Chaubey GS, Susngi A, Das S, Mahanti MK. Kinetic features of the oxidation of aliphatic dialdehydes by quinolinium dichromate. *Kinetics and Catalysis*. 2002;43:789-793.
44. Levy RJ, Schoen FJ, Levy JT, Nelson AC, Howard SL, Oshry LJ. Biological determinants of dystrophic calcification and osteocalcin deposition in glutaraldehyde-preserved porcine aortic valve leaflets implanted subcutaneously in rats. *American Journal of Pathology*. 1983;113:143-155.

45. Eyre DE, Oguchi H. The hydroxypyridinium crosslinks of skeletal collagens. *Biochemica et Biophysica Research Communication*. 1980;92:403-410.
46. Olde Damink LHH. Structure and properties of crosslinked dermal sheep collagen. In: Twente, The Netherlands: University of Twente; 1992:93-111.
47. Nimni ME, Cheung DT, Strates BS, Kodama M, Sheikh K. Chemically modified collagen: a natural biomaterial for tissue replacement. *Journal of Biomedical Materials Research*. 1987;21:741-771.
48. Van Luyn MJA, Van Wachem PB, Dijkstra PJ, Olde Damink LHH, Feijen J. Calcification of subcutaneously implanted collagens in relation to cytotoxicity, cellular interactions and crosslinking. *Journal of Materials Science. Materials in Medicine*. 1995;6:288-296.
49. Larkin DR. The role of catalysts in the air oxidation of aliphatic aldehydes. *Journal of Organic Chemistry*. 1990;55:1563-1568.
50. Niclause M, Lemaire J, Letort M. The kinetics and mechanism of photochemical oxidation of aldehydes by molecular oxygen. In: *Advances in Photochemistry*. New York: Wiley and Sons; 1966:25-48.
51. Martin RB. Bioinorganic chemistry of metal ion toxicity. *Metals Ions Biological System*. 1986;20:21-65.
52. Martin RB. Bioinorganic chemistry of magnesium. *Metal Ions Biological System*. 1990;26:1-13.
53. Avram M, Mateescu GHD. Infrared Spectroscopy. In: *Applications in Organic Chemistry*. London: Wiley Interscience; 1972.
54. Silverstein RM, Bassler GC. In: *Spectrometric Identification of Organic Compounds*. New York: Wiley; 1968.
55. Mizushima SI, Quagliano JV. Structure of ligands in inorganic coordination compounds by infrared spectra. *Journal of American Chemical Society*. 1953;75:4870.
56. Sen DN, Mizushima SI, Curran C, Quagliano JV. Infrared absorption spectra of inorganic coordination complexes I: the nature of chelation bonding in bis-(glycino)-copper(II) monohydrate and bis-(glycino)-nickel(II) dihydrate. *Journal of American Chemical Society*. 1955;77:211-212.

Chapter 7

7 Characterisation of the calcification of cardiac valve bioprotheses by environmental scanning electron microscopy, x-ray diffraction and vibrational spectroscopy.

Abstract

Objectives: Cardiovascular implant mineralisation involving bioprosthetic materials such as glutaraldehyde cross-linked tissue valves is an important clinical problem. The objectives of this part of the study, therefore, were to develop methodology to investigate heart valve tissue and associated calcification in its natural state, using environmental scanning electron microscopy (ESEM) and to comment on future applications of ESEM in tissue bioprotheses research. The use of energy dispersive X-ray (EDS), X-ray diffraction (XRD), Fourier-transform infrared (FTIR) and Raman spectroscopy were sought to characterise the various calcific deposits observed with ESEM. Additionally, the application of EDS via the ESEM remains unreported for microanalytical studies of explanted heart valve tissue to date. The major elements present in calcified valves were analysed by inductively coupled plasma-optical emission spectroscopy (ICP-OES). In order to better understand the precursors formation of the calcific deposits, these results from the elemental analyses were statistically correlated.

Methods: The surface morphology of unimplanted and explanted cardiac bioprotheses was observed using ESEM. Each valve was also subjected to EDS analysis, which focused mainly on the calcification of the valves. The nature of the crystal phases of the calcific deposits was also investigated using XRD, FTIR and

Raman spectroscopy. Calcified explanted valves were subjected to a quantitative study using ICP-OES.

Results: Analysis of valve tissue by ESEM gives valuable results. However some problems may be encountered with the EDS analysis. The water environment can reduce the EDS signal intensity and there is an apparent signal from the water, preventing semi-quantification using the oxygen peak. A predictable skirting effect can also be present. Despite these problems, ESEM revealed the presence of four broad types of calcium phosphate crystal morphology. These were classified according to their size as sub-microns crystals, aggregates ranging from sub-micron up to 5 μm , micronodules of 5-10 μm and large aggregates (found on heavily calcified valves) that can grow up to 100 μm in size and cover the entire collagen matrix. The crystals were found attached to the dense collagen bundles, following their orientation throughout the tissue and within the fibrils. Additionally, two main patterns of organisation of calcific deposits were observed associated with the collagen fibres: spherical aggregates (1-10 μm) found along collagen fibrils and in interfibrillar spaces, and needle-like crystal structures (sub-micron, micron scale). The EDS microanalysis identified the crystals observed by ESEM as salts containing mainly calcium and phosphate with varying ratios from 1.340 (possibly octacalcium phosphate (OCP) which has a Ca/P ratio of 1.336) to 2.045 (possibly hydroxyapatite (HAP) with incorporation of carbonate and metal ion contaminants, such as silicon and magnesium, in the crystal lattice). The presence of silicon and magnesium in the EDS spectra confirmed this view and raised the possibility of the presence of precursor phases associated with the embryonic stages of calcification. The crystalline calcium phosphate salts found on heavily calcified valves had a mean Ca/P ratio of 1.676, which is very close to crystalline hydroxyapatite with a Ca/P ratio of 1.670. XRD patterns from these same calcium deposits showed a poorly crystalline hydroxyapatite-like pattern. Raman and FTIR spectroscopy also identified the presence of carbonate and the analyses showed spectral features very similar to a crystalline hydroxyapatite spectrum, thus refuting the presence of precursor phases such as β -tricalcium phosphate (β -TCP), OCP and dicalcium phosphate dihydrate (DCPD). However, it is still possible that these precursor mineral phases might have been formed but transformed too quickly into other phases to be detected by these techniques.

Conclusion: ESEM allows the imaging of hydrated heart valve bioprostheses with minimal manipulation and without the need for conducting coatings. It may also play an important role in developing our understanding of the calcification of heart valve bioprostheses and a similar methodology to the one described here is thought to be appropriate for the study of new tissue-engineered heart valves.

7.1 Introduction

The ESEM is an instrument that enables the examination of the surfaces of hydrated, unfixed specimens with a depth of field, resolution and magnification equivalent to that typically afforded by scanning electron microscopy (SEM)^{1,2}. With the conventional scanning electron microscope, the electron beam is brought to a focus on the surface of the sample. The beam is scanned across the sample and a detector picks up the signal of secondary electrons that emerge from the surface, this signal being used to build up an image of the sample. The sample chamber, in addition to the electron optics, is held at high vacuum. Analysis of insulating specimens has always been something of a challenge because surface charging generated by the impinging electron beam has to be continually neutralised to prevent any distortion of the image. Specimen charging is usually overcome by the deposition of a thin metallic coating on the specimen to provide a conducting path to ground. Typically, imaging insulating materials such as valve tissue requires special coatings (C, Au or Pt) or the use of very low accelerating voltages (0.3 kV to 1.5 kV). Unfortunately, under these conditions, elemental micro-analysis via characteristic X-ray emission (EDS) is quite restricted. For example, peaks from the coatings may mask or overlap certain spectral features, while although X-ray generation is theoretically possible at low accelerating voltages, it is rather difficult to generate peaks at all.

The development and principles of ESEM were first described by Danilatos^{3,4}. The ESEM operates under similar principles to conventional SEM but allows samples to be viewed in their natural states, at high accelerating voltages, without the need for coating or other specimen preparation. The ESEM differs from conventional SEM in two major ways: the use of differential pumping allows the specimen chamber to be at a low pressure while the electron gun chamber still achieves a very high vacuum environment; and the mode of secondary electron detection. The ESEM employs a

two-stage differential pumping system (the ESEM-field electron gun (ESEM-FEG) employs a three-stage system) by which the gun chamber remains at high vacuum while the specimen chamber pressure can be as high as 30 Torr (1 Torr = 133 Pa)⁵. At pressures of 1-30 Torr, the scattering of the primary electron beam by the gas adds a broad skirt to the central beam but does not alter the Gaussian distribution of the remaining focused beam. Thus high quality images can be produced without any interference from the skirting effect and, under optimum conditions, a resolution of 5 nm can sometimes be achieved. Detection of the secondary electron signal is achieved with the help of a gaseous secondary electron detector (GSED). A moderate electric field is applied to the detector, causing secondary electrons to be drawn towards it. As the secondary electrons move towards the GSED, they collide with neutral gas molecules and ionise them, creating a cascade multiplication of the secondary signal. The surface charging of the specimen under study is effectively neutralised by the positive ions created in the gas. Consequently, specimens may be viewed at any accelerating voltage without coating or sample preparation. The ESEM is particularly suited to the use of energy dispersive X-ray analysis systems (EDS), especially to identify high atomic number elements in insulators. The X-ray signal is relatively unaffected by the gas present in the sample chamber, although it can be affected by gas pressure and ESEM mode conditions. Thus, quantitative as well as qualitative data can be obtained using EDS coupled to the ESEM.

In term of tissue preparation for both light and electron microscopy, soft tissues are often freeze-dried, frozen in liquid nitrogen, freeze-fractured or embedded in acrylic blocks and sectioned into micron-thick slides before being scanned. Bone samples might be demineralised and dried, or broken via freeze-fracturing techniques. Most of these steps can alter the results, the interpretations and thus the understanding of the scientific evidence. In fact, there is no simple way to determine whether the structures of interest are altered or masked by the preparation process. However, by comparing the data obtained from studies using SEM and ESEM, it was reported that sample preparation had altered the structure of the samples⁶⁻⁸. All these findings agree with the warning given by other scientists against the sample preparation of biological tissues⁹⁻¹¹.

Although some detailed histopathological studies¹²⁻¹⁶ and some ultrastructural studies by SEM¹⁷⁻²⁰, TEM²¹⁻²³ and high resolution SEM²⁴ carried out on

bioprosthetic valves, revealed that calcification involved sub-cellular organelles, cell membrane debris and extracellular connective tissue (particularly collagen fibres), the pathogenetic mechanisms of calcium deposition in the bioprosthetic valve tissues are still poorly understood. Thus, the main objectives of this part of the study were to determine appropriate methodology to allow ESEM analysis of tissue samples and later to apply this to bioprosthetic heart valves and their calcification. The data produced were compared with those from earlier studies using conventional scanning electron microscopy (SEM). It was hoped that the information obtained from the ESEM analyses would provide a new insight into the understanding of biological calcification. The nature of the crystal phases associated with the calcific deposits was also investigated using ICP-OES, XRD, FTIR and Raman spectroscopy.

7.2 Materials and Methods

7.2.1 Materials

Explanted calcified valves, explanted non-calcified valves and unimplanted valves were kindly provided by Dr P. Lawford from the Royal Hallamshire Hospital, Sheffield. Leaflet samples were retrieved from the clinical bioprosthetic explants. The calcified areas of some heavily calcified valves were often even visible to the unaided eye.

Standards of what were thought to be potential precursor phases of calcification (β -tricalcium phosphate standard (97%+) and hydroxyapatite standard (99%+)) were obtained from Rose Chemicals Ltd. (Sheffield, UK), and Fluka (Gillingham, UK). Saline water was phosphate buffer saline (PBS, Baxter, USA) and ultra pure water was obtained from a MilliQ50 (Millipore, UK) packed with USF liquid pure cartridges. The conductivity achieved was $18 \text{ M}\Omega/\text{cm}^3$. Acids (HCL and HNO_3) used for the hydrolysis of samples prior to ICP-OES analysis were both Aristar grade and obtained from BDH, UK.

7.2.2 Low Energy Radiography

After retrieval at re-operation or at post-mortem, the bioprosthetic valves studied were examined radiographically for shadowing caused by calcification. Gross visualisation of mineral deposition was carried out using low energy radiography with a Hewlett Packard 43855A Faxitron machine (Faxitron, Hewlett Packard, Birmingham, UK). The tube voltage was set at 25 kV and the diagnostic film was exposed for 3 seconds with an intensity of 3 mA. The Kodak Industrex M films were developed using a Kodak RP X-OMAT processor (Kodak, Eastman Chemical Co. Kingsport, TN, USA). The data obtained from low energy radiography helped in the selection of the area where the calcification was the most obvious to be analysed by ESEM, although other areas, not showing any apparent signs of calcification, were analysed too.

7.2.3 Electron Microscopy

ESEM was used to observe the surface morphology of explants. Much effort was placed on describing the morphology in as quantitative a manner as possible, to give an objective interpretation of our findings. Predominantly, the external surfaces of explants were analysed. ESEM was also used in combination with energy-dispersive X-ray microanalysis (EDS) to compare the structure and chemical nature of both embryonic and advanced calcific deposits in these tissues in their native hydrated state, with minimal sample preparation after micro-dissection. The presence and distribution of calcium, phosphorus and other metal ions were thus assessed. For comparison, some calcified human explants were analysed by conventional SEM (work performed with courtesy of the Royal Hallamshire Hospital, Sheffield), and additionally, some synthetic CaP materials (hydroxyapatite and β -tricalcium phosphate) were analysed under the same conditions as tissue samples using the ESEM. These synthetic standards are two of the CaP species that have been suggested as the initial CaP solid mineral phases deposited during bone and tooth formation and possibly during the dystrophic calcification of tissue (see chapter 1 section 1.6).

7.2.3.1 SEM analyses and sample preparation:

The SEM was a Philips 501 (Philips, The Netherlands), operated at an accelerating voltage of 15 kV. The processing protocol for tissue preparation was as follows. The

sample was first washed with 0.1 M sodium cacodylate buffer. The tissue was then subjected to treatment with 1% osmium tetroxide in 0.1 M sodium cacodylate buffer, followed by dehydration with a series of ethanol:acetone solutions and culminating in dehydration in 100% acetone. The sample was then transferred into a Polaron 3000 Critical Point Drier (Quorum Technologies, Newhaven, UK) through acetone. Finally, it was mounted on an aluminium stub using double-sided carbon adhesive disks and sputter-coated with gold (sputter-coating unit Edwards S150, analyses typically operated at 50 mA for 1 min).

7.2.3.2 ESEM analyses:

The ESEM was a FEI Philips (Philips, The Netherlands) XL30 ESEM-FEG (environmental scanning electron microscope-field electron gun). An accelerating voltage of 20 kV was selected because it is a common voltage for coated specimen work in SEM and ESEM and it provided sufficient penetration of the primary electron beam into the bulk of the samples. In addition, this accelerating voltage gave good results with the X-ray analysis (good signal and a reduced skirting effect under the hydrated condition used). Samples required no sample preparation and were kept wet in a saline solution until the time of analysis, when they were rinsed several times with deionised water. The ESEM imaging gas was water vapour, at a pressure of 3.9-5.0 Torr. At these pressures, and by cooling the sample surface to around 5°C by means of a Peltier stage, fully hydrated conditions were established in the ESEM chamber. The samples were then controlled for dehydration during the analysis.

An EDAX Oxford Instrument (Oxford Instrument, High Wycombe, UK) was used to perform a semi-quantitative analysis of the samples studied. The operating programme identified peaks by position in the spectrum and shape of the count distribution, matching these to a stored reference library of elemental peak spectra and their derivatives. Accurate quantification depended on the identification of every peak present in the spectrum: count data was collected for all detected peaks and calcium and phosphorus quantified as their proportions present in the region of interest relative to the other elemental species present. Data were automatically corrected for atomic number (software ISIS 300, Oxford Instrument, High Wycombe, UK), absorption and fluorescence, and provided atomic compositions of

data points, allowing comparative examination of spectra. Raw count data were checked for anomalies which were then rejected, such as in the case of low count rates due to the sample topography which can sometimes shield the detector from the generated X-rays (shadowing effect).

The major parameters requiring optimisation in order to obtain decent quality secondary electron images are the gaseous pressure, the working distance (also called the beam gas pathlength), gas type and composition, the primary beam voltage and the detector voltage.

The gaseous secondary electron differential voltage (detector voltage) was of high setting and varied between 200 and 500 eV (by changing the contrast, the voltage on the GSED was changed, while the brightness corresponds to the gain after the signal has been detected). The primary electron beam voltage was varied between 15 and 25 kV, with a mean value of 20 kV. The gas type was water vapour whilst the working distance was 8-16 mm. The most demanding part of the instrument set-up was the control of the gas (water) pressure in order to control the dehydration of the samples. The hydrated sample was placed on a Peltier cooling stage, allowing the stage temperature to be regulated in the sample chamber. The sample chamber can be seen in figure 7.1 below. The vacuum pump was activated until the chamber pressure reached 10 Torr. The sample chamber was then subjected to three or four floodings by decreasing the water pressure to 4 Torr and then increasing it to 10 Torr. During this process, the CCD camera was used to check the state of the sample, particularly whether it tilted because of the surrounding water pressure. The pressure was then decreased to 4 Torr and the GSED switched on instead of the CCD camera. The sample was then slowly dehydrated by carefully and progressively lowering the gas chamber pressure, thus slowly removing the water layers covering the sample, until its complete disclosure. Using an electronic pressure-servo system, the chamber pressure was kept steady at the desired level with an accuracy of 0.1 Torr. The final working pressure was usually around 4 Torr, although it varied between samples from 4 to 2 Torr.

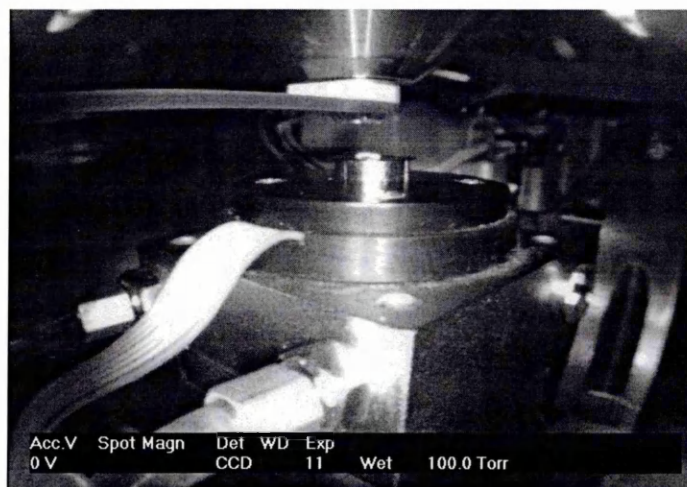


Figure 7.1: ESEM sample chamber of a FEI Philips XL30 ESEM-FEG instrument. This picture obtained with a CCD camera shows the sample (center of the picture) kept cool by means of a Peltier stage. The GSED can be observed right above the sample.

7.2.3 X-ray diffraction (XRD)

The tissue samples were analysed in a freeze-dried state and the calcified deposits were also extracted from the freeze-dried organic matrix with the help of a magnifying lens and a scalpel. The resulting isolated crystals were turned into fine powder using a pestle and mortar and were analysed as pressed powders on a quartz slide. Usually, samples that are to be examined with XRD are turned into ashes so that the organic matrix is removed and the resulting spectrum essentially shows inorganic diffraction peaks without any organic amorphous background. However, it was decided not to do so for this study simply because at the temperatures needed to turn the samples into ashes (calcination temperatures), the apatite-like crystals (calcific deposits) may transform to the low temperature polymorph of tricalcium phosphate (β -TCP) at around 740°C, with a loss of water²⁵. This is the same reaction as described by the following equation for the formation of TCP-ceramics²⁶: $\text{Ca}_9(\text{HPO}_4)_5(\text{OH}) \rightarrow 3\text{Ca}_3(\text{PO}_4)_2 + \text{H}_2\text{O}$. The high temperatures could also lead to the transformation into the high temperature polymorph, α -TCP, at around 1100°C²⁵.

The analyses were undertaken at room temperature with a Philips (Philips, The Netherlands) PW1710 X-ray diffractometer operating with Bragg-Brentano geometry. Experimental conditions were 40 kV and 40 mA, with Cu-K $\alpha_{1,2}$ radiation. The diffraction patterns were recorded with an angle range of 5 to 100° 2θ and using

the step-by-step method with a step width of 0.02 degrees and a counting time of 10 seconds per step. The comparison analyses were performed against synthetic mineral standards.

7.2.4 Fourier-transform infrared (FTIR) spectroscopy

All spectra were recorded with a Magna IR 860 Nicolet FTIR spectrometer (Nicolet, Warwick, UK) at a resolution of 4 cm^{-1} , 1000 scans, with a horizontal ATR device ("Golden Gate" apparatus) from Graseby Specac (St Mary Cray, UK) and a single reflection diamond ATR crystal with a 45° angle of incidence, scanned between 4000 and 400 cm^{-1} . The apodisation function was Happ-Genzel and there was a Mertz phase correction. All spectra were recorded under similar conditions and were corrected for atmospheric water vapor and carbon dioxide transmittance by subtraction of the appropriate reference spectrum.

The freeze-dried calcified tissues were analysed as they were and, similarly to the samples used for XRD, the calcified deposits were also extracted from the freeze-dried organic matrix with the help of a magnifying lens and a scalpel, and the resulting isolated crystals were turned into fine powder using a pestle and mortar. The analyses were also performed against synthetic mineral standards (such as hydroxyapatite and β -tricalcium phosphate).

7.2.5 Raman spectroscopy

In this study, (dispersive) Raman spectroscopy was used to characterise the type of calcium phosphate phase formed in the samples and to identify the presence of carbonate or other inorganic species such as hydrogenophosphate or hydroxide ions. The Raman instrument used was a Renishaw Ramascope 2000 (Renishaw, Wotton-under-edge, UK), with a red laser (633 nm). Spectra were scanned between 4000 and 100 cm^{-1} at a resolution of 4 cm^{-1} .

7.2.6 Inductively coupled plasma-optical emission spectroscopy (ICP-OES)

Glutaraldehyde-treated explanted calcified valves were subjected to a quantitative study using ICP-OES. Prior to be analysed, the valves were washed five times, each for a period of 5 minutes in phosphate-buffered saline and then distilled water. All the samples were lyophilised with a Cold trap 1000 freeze-drier (achieving a pressure of 75 mbar (0.35 atm) with a temperature of approximately -40°C),

weighed and subsequently hydrolysed with a mixture of 3 mL of HCl (Aristar grade, BDH, UK) and 1 mL of HNO₃ (Aristar grade, BDH, UK) simmering/boiling for 5 hours. A final sample volume of 10 mL was made up using de-ionised water. The samples were then submitted for ICP-OES using a FC1400 Spectro analytical instrument (Spectro, Germany). The presence of silicon, calcium and magnesium was thus estimated quantitatively. It was decided not to analyse the phosphorus content because of the phosphate-buffered saline solution (PBS, Baxter, USA) used to store the bioprosthetic valves prior to analysis.

7.3 Results and discussion

7.3.1 ESEM imaging

The ESEM imaging methodology described in section 7.2.3.2 was successfully applied to valve analysis. Figure 7.2 (*left*) represents a valve sample totally covered by water, before it was slowly dehydrated by carefully and progressively lowering the gas chamber pressure until complete disclosure of the sample was achieved. The typical appearance of collagenous valve tissue obtained finally by ESEM imaging can be seen in figure 7.2 (*right*).

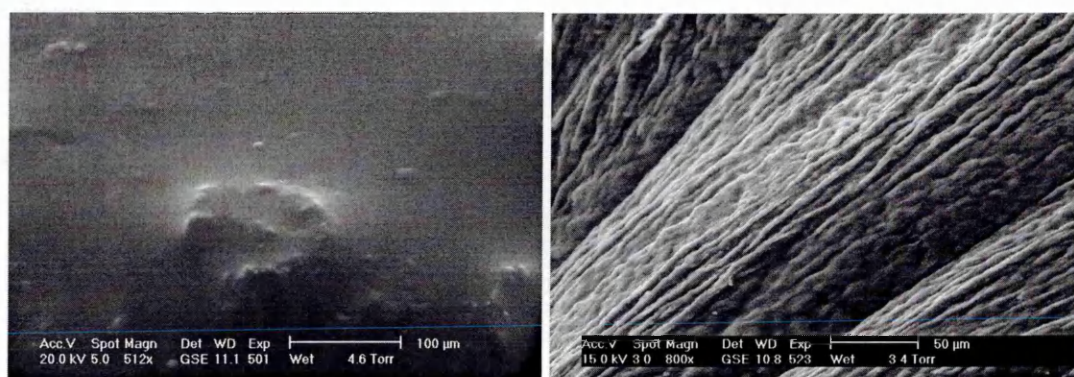


Figure 7.2: *Left*: ESEM secondary electron image of a tissue valve totally covered by a thin layer of water, prior to dehydration. *Right*: ESEM secondary electron image of a hydrated unimplanted bioprosthetic valve.

The intrinsic low atomic number of biological valve samples provided little resistance to transmission of signal from underlying materials since heavy metal coatings were absent. ESEM imaging of uncoated biological specimens has already been reported to provide good information about internal or overlapping structures²⁷.

Heavier elements appear brighter than elements of low atomic number. For instance, calcium phosphate crystals appear brighter than the collagen background of the valve.

The valve structure, when analysed by ESEM, is essentially undisturbed and the samples appear to be stable during prolonged exposure to the electron beam. A major difference can be observed between the secondary electron images obtained from similar valve sample using ESEM (see figure 7.2 above) and conventional SEM (see figure 7.3 below). The net difference lies in the arrangement of the collagen bundles that appear totally collapsed when analysed with the conventional SEM. A similar ESEM image to the one obtained with SEM could be obtained when a sample was dried out extensively by decreasing the sample chamber pressure of the ESEM instrument.

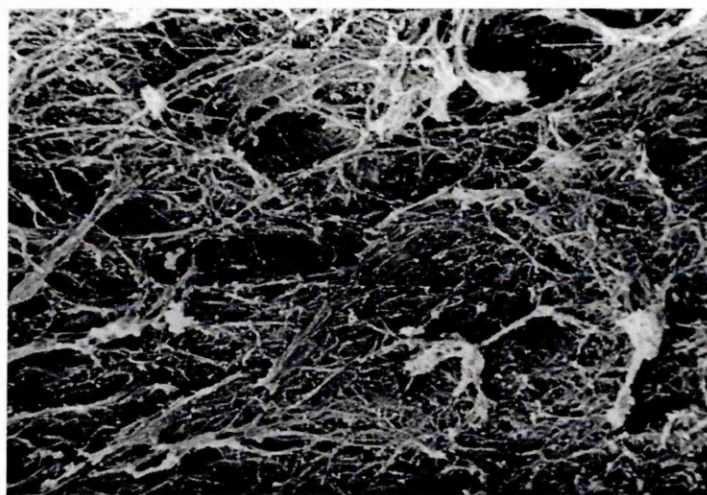


Figure 7.3: SEM secondary electron image of a calcified bioprosthetic heart valve (x2500, accelerating voltage of 15 kV, sample critically point dried and sputter coated with gold). The dried collagen mesh appears to be collapsed.

Secondary electron imaging along with EDS analysis with the ESEM revealed several forms of accumulated calcium phosphate mineralisation on explanted calcified bioprosthetic valves. The figures 7.4-7.17 show various characteristic forms of calcification. These forms include the ordered growth of crystals of 0.2-2 μm size distributed along collagen fibrils and also within the collagen structure (figures 7.4, 7.5, 7.6).

Other crystalline structures were also often found arranged into discrete aggregates of 1-10 μm (see figures 7.7, 7.8 and figure 7.9), large nodules of 20-30 μm (see figures 7.10-7.14), or even forming sheets (see figure 7.15). Crystals were observed either underneath the collagen surface (see figure 7.5), attached to the surface of individual collagen fibres (and possibly sometimes elastin), (see figures 7.7, 7.8 and 7.15), or in the interfibrillar space. Calcific crystals were seen to form parallel arrays following the longitudinal axis of the collagen fibrils (see figure 7.15).

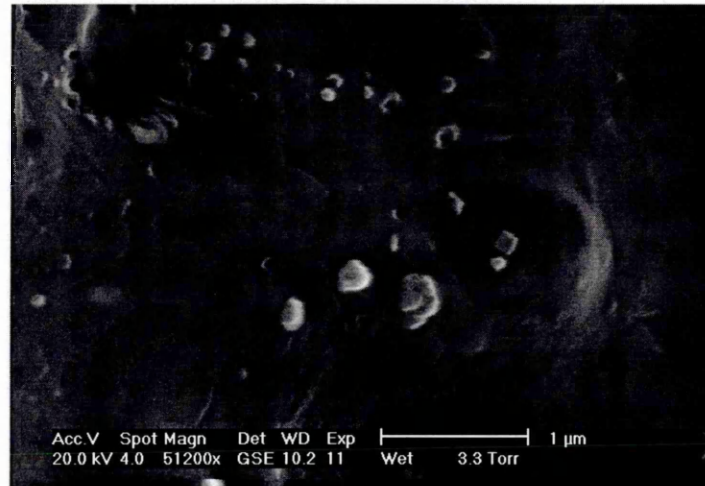


Figure 7.4: ESEM secondary electron image of an explanted calcified valve, showing formation of small particles of 100-500 nm in size that seem to grow from the inside of the collagen surface.

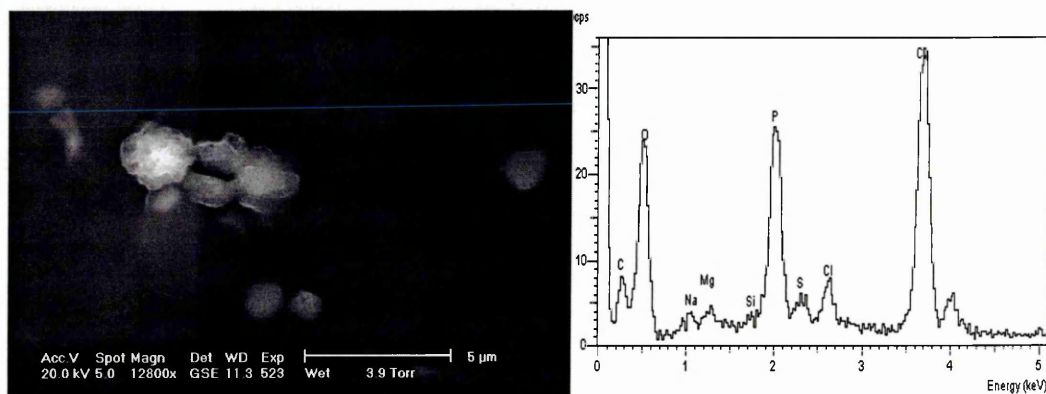


Figure 7.5: ESEM secondary electron image of an explanted calcified valve (*left*), showing inorganic growth occurring underneath the collagenous valve surface. The crystals are about 1-3 μm in size. The corresponding EDS trace (*right*) indicates the

presence of Ca, P, Mg, and possibly Si in the crystal, in addition to the organic matrix components (C, O and S). Note: Na and Cl are from the saline solution, used to store the valves.

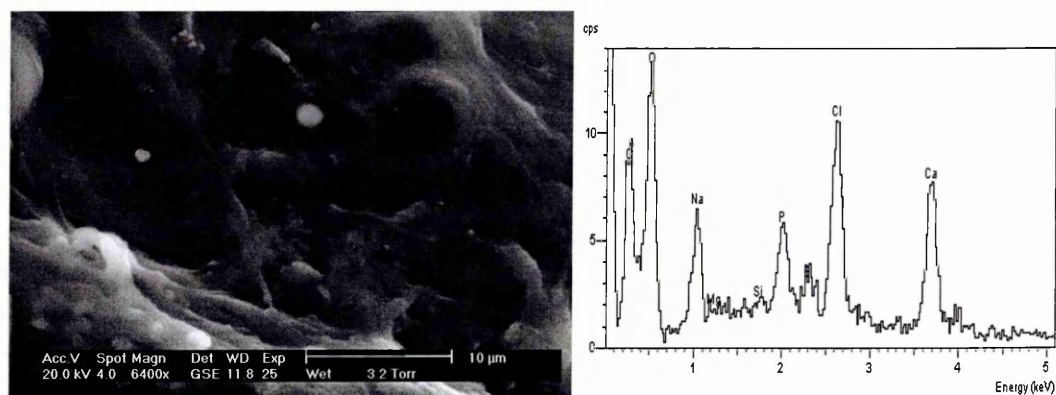


Figure 7.6: A particle of about 2 μm in size can be seen on the secondary electron image (*left*) with a poor contrast that indicates that it is located underneath the tissue surface. The EDS spectrum (*right*) shows it is rich in Ca and P with some trace of Si.

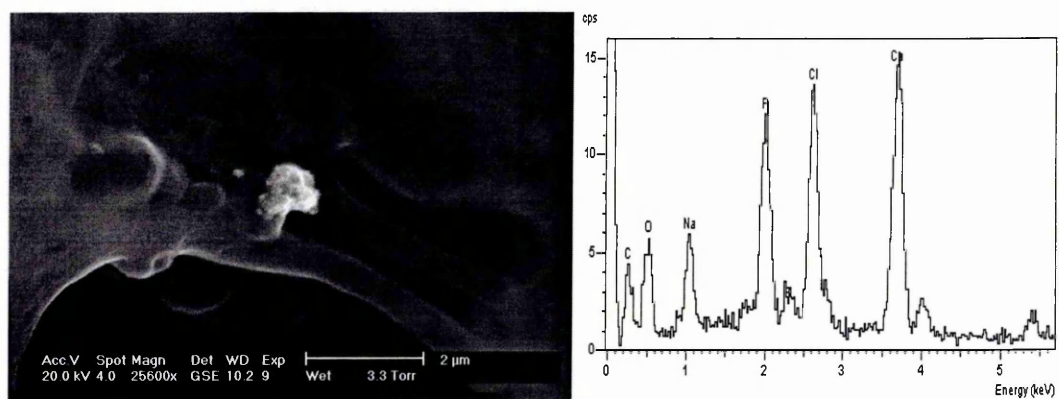


Figure 7.7: ESEM secondary electron image of an explanted calcified valve (*left*), showing a crystal growth of less than 1 μm in size on a collagen bundle (possibly an elastin bundle). The corresponding EDS spectrum (*right*) shows it is rich in Ca and P.

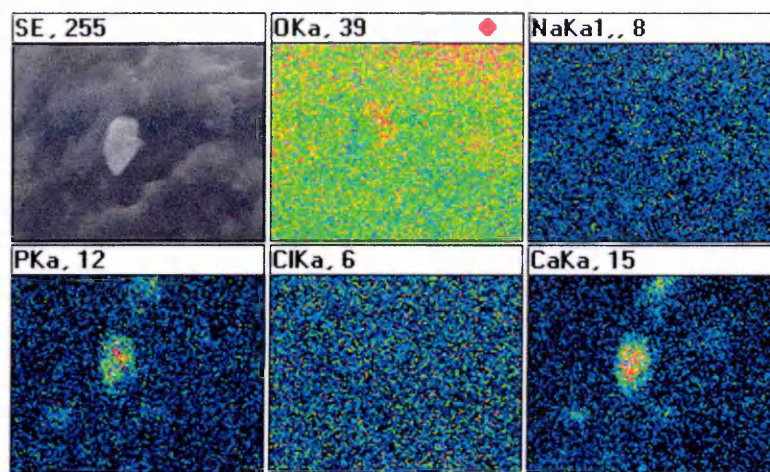


Figure 7.8: ESEM secondary electron image of an explanted calcified valve (*top left*), showing a particle of about 10 μm in size and rich in Ca and P. Other smaller areas also rich in Ca and P can be observed underneath the surface thanks to the EDS mapping, although unnoticed with the secondary electron imaging. The brighter the colour, the more present an element. The elements analysed were oxygen, sodium, phosphorus, chlorine and calcium.

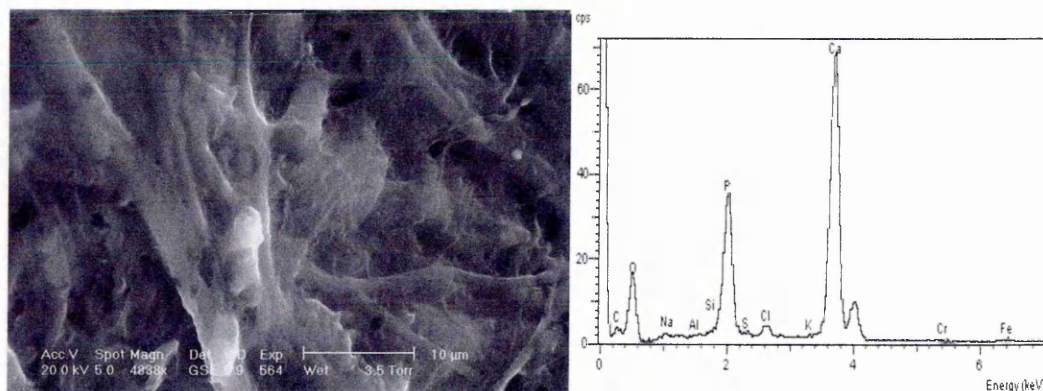


Figure 7.9: ESEM secondary electron image of an explanted calcified valve (*left*), showing a calcific nodule (up to 10 μm) rich in Ca and P growing off a collagen bundle and its corresponding EDS spectrum (*right*). The crystal growth seems to follow the collagen plane formed by the bundle.

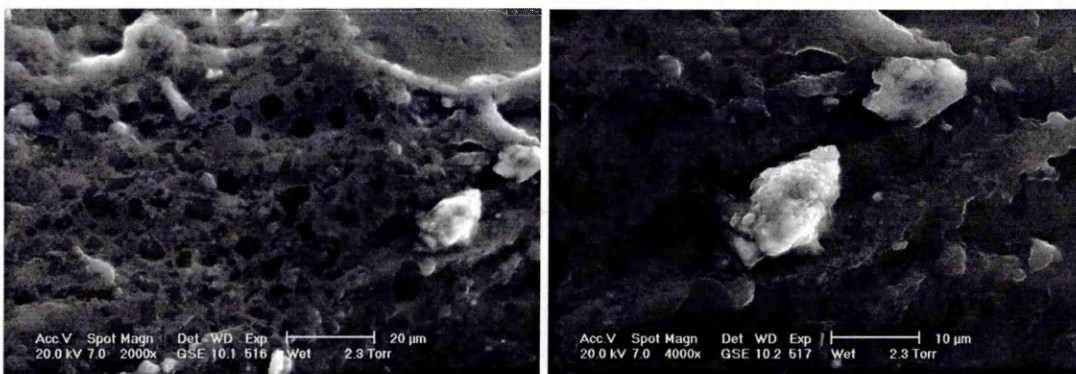


Figure 7.10: ESEM secondary electron image of an explanted calcified valve with a low (*left*) and higher (*right*) magnification of an inorganic particle of about 10 μm in size rich in Ca and P (EDS trace not shown here). The crystal growth is seen growing off the collagen bundles (partially covered with a film of water, which appears as small black pools), along smaller calcific nodules of micron size.

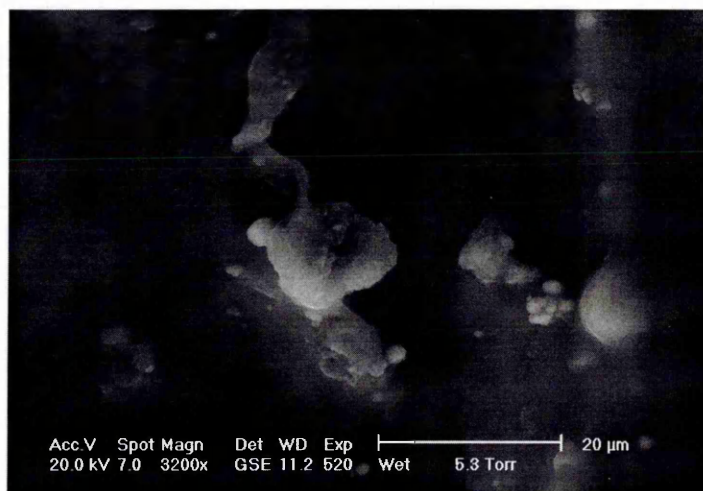


Figure 7.11: The secondary electron image of a calcified valve shows the simultaneous presence of particles (rich in Ca and P-EDS spectrum not shown here) ranging from 1-20 μm in size.

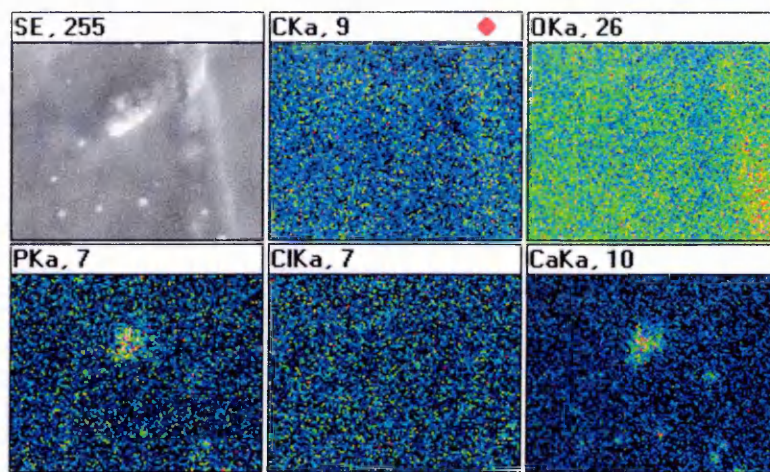


Figure 7.12: ESEM secondary electron image of an explanted calcified valve (*top left*), along with the corresponding EDS map, showing various nodules rich in Ca and P on and underneath the collagen surface with a particle size of less than 1 micron and a large calcific aggregate of up to 20 μm in size. Note the pool of water (rich in oxygen) located on the right hand side.

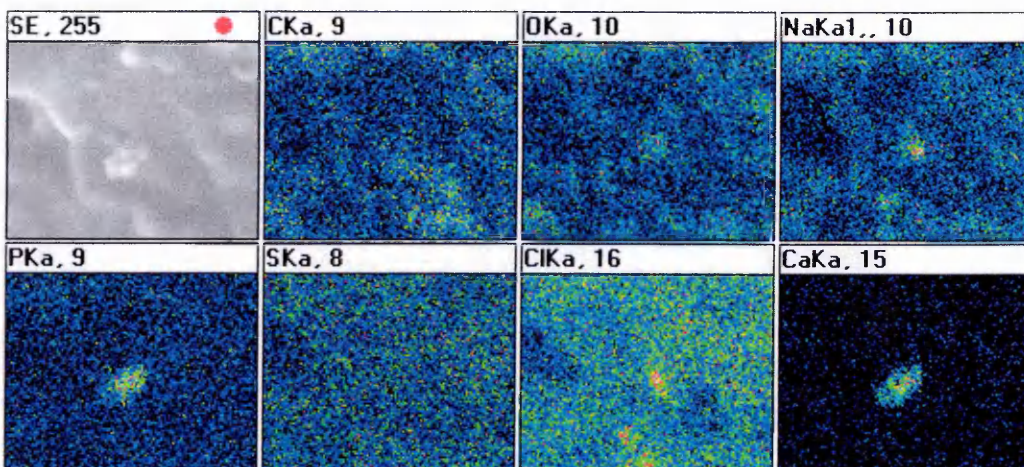


Figure 7.13: ESEM secondary electron image of an explanted calcified valve (*top left*), along with the corresponding EDS elemental mapping, showing a calcified nodule of about 10-20 μm in size rich in Ca and P.

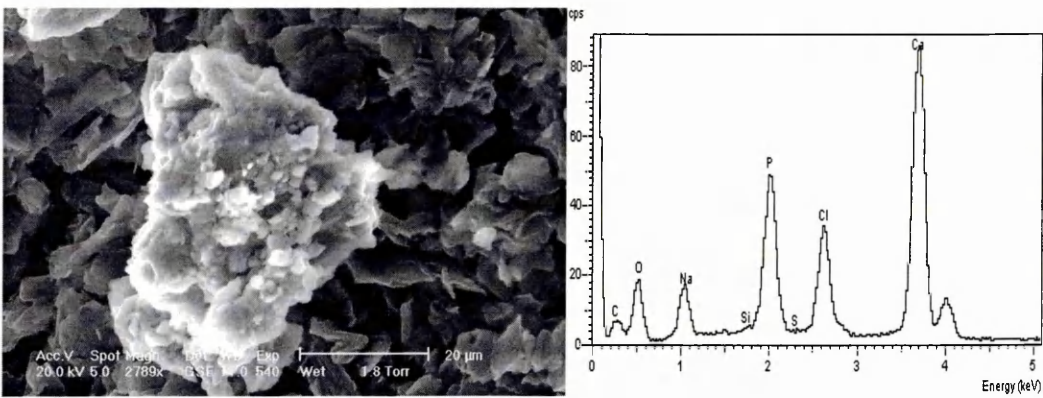


Figure 7.14: ESEM secondary electron image of an explanted calcified valve showing an aggregate of 30 μm on the collagen surface. Its corresponding EDS spectrum shows it is rich in Ca and P.

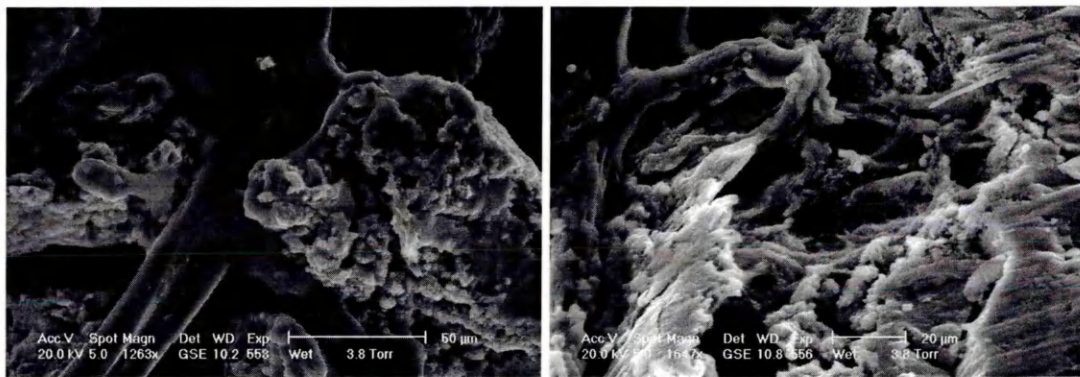


Figure 7.15: ESEM secondary electron images of an explanted calcified valve, showing that the valve calcification extends onto and along collagen and elastin fibrils (*left*), by following their planes. The valve calcification is also found to occur in the interfibrillar spaces (*right*) and eventually to form large plaques rich in Ca and P (EDS spectrum not shown here).

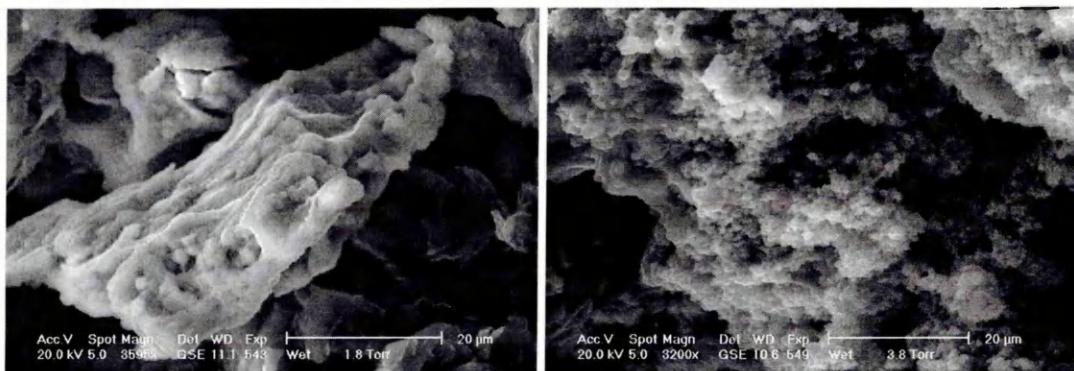


Figure 7.16: ESEM secondary electron images of an explanted calcified valve, showing different inorganic growth structures that can be differentiated. Some plate-like aggregate structures with a typical crystal growth very similar to bone growth morphology (*left*), and one with a fluffy aspect (*right*), which is very similar to the appearance of a crystalline hydroxyapatite standard run under the same experimental conditions.

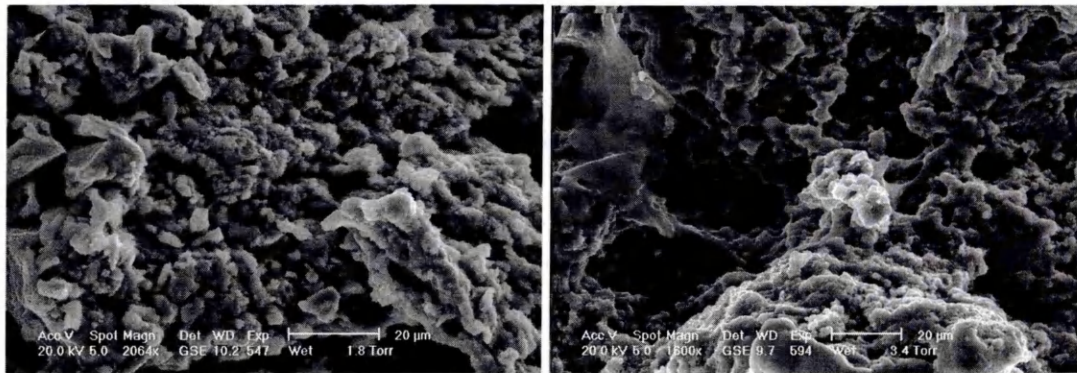


Figure 7.17: ESEM secondary electron images of a heavily calcified explanted valve, showing the valve surface extensively calcified. Large aggregates are covering the entire collagenous surface of the valve.

Calcium-rich calcific deposits have been previously described in bioprosthetic valves in association with collagen, especially sites of collagen disorganisation and/or disintegration^{21,28}. Our photomicrographs confirmed that calcification was initiated within the tissue of the valves, with calcium-containing crystals often present just underneath the disrupted surface and then propagated towards the outer surface of the tissue as calcification proceeded. The most common form of crystal morphology present were as spherical shapes, found mainly in the collagen interstitium, similar to that reported previously with high-resolution electron microscopy²⁴. Less commonly, the calcific deposits were also observed as needle-like (fluffy aspect) or plate-like structures, showing well-developed basal pinacoids (a clear-cut morphologic finding consistent with the hexagonal nature of apatite). The observed arrangement of plate-shaped crystals (assigned to apatite structure) and their predominant association with the interfibrillar spaces are similar to the findings of a study of calcifying turkey leg tendons²⁹, and have been reported in an SEM study of bioprosthetic heart valve

tissue²². The needle-like morphology of some of the calcific deposits observed in calcified explanted valves was similar to that reported for in-vitro synthesised deficient hydroxyapatite observed by ESEM, where both plate-like and needle-like structures were seen³⁰. In addition, the morphology of standard hydroxyapatite, observed under similar conditions to those which the explanted valves were analysed under, also appeared as needle-like crystals. This suggested that explanted calcified valves, based strictly on morphology, seem to contain poorly crystalline apatite crystals, amongst others. Moreover, the observed irregular morphology of many calcific deposits and the abutting of small and large crystals tend to support the hypothesis that a hydrolytic process could occur during the calcification^{30,31} (a precursor phase could be fully or partially hydrolysed for the benefit of the formation of another until the morphology and Ca/P ratio approach those of apatite-like material, almost those of hydroxyapatite). The varied morphology of the calcific crystals observed in our study shows similarities with that of DCPD³¹, hydrolysed OCP³²⁻³⁴ or possibly more likely a morphological variation of the apatite structure³⁵. The calcification process is thought to involve phase transformations of thermodynamically unstable calcium-phosphate salts to more stable ones^{34,36-38}, hence the likelihood of seeing several different morphological structures.

7.3.2 Energy dispersive X-ray (EDS) analysis

It has been reported that the semiquantitative EDS analysis of hydrated biological materials can be undertaken when EDS is coupled with an ESEM³⁹. The surface geometry of the samples, the heterogeneity of the distribution of elements in biological valve samples and the semiquantitative nature of EDS, tend to limit the elemental analysis of samples using ESEM-EDS. However, in this study, it was possible to obtain maps, which revealed the presence of accumulated calcium phosphate mineralisation, showing different Ca/P ratios. The EDS results were processed so that the software gave the atomic Ca/P ratios. No calculations of the Ca/PO₄ ratios were made because of the use of water vapour in the sample chamber, would affect the observed oxygen content. The stoichiometric atomic Ca/P ratios (see table 7.1 below) were used to identify the crystal phases present.

Inorganic CaP Phases commonly encountered	Atomic Ca/P ratios (as usually reported in the literature)
Hydroxyapatite (HAP) $\text{Ca}_{10}(\text{PO}_4)_6(\text{OH})_2$	1.670
B-Tricalcium Phosphate (β -TCP) $\text{Ca}_3(\text{PO}_4)_2$	1.500
Octacalcium Phosphate (OCP) $\text{Ca}_8\text{H}_2(\text{PO}_4)_6 \cdot 5\text{H}_2\text{O}$	1.330
Dicalcium Phosphate Dihydrate (DCPD) $\text{CaHPO}_4 \cdot 2\text{H}_2\text{O}$	1.000

Table 7.1: Common inorganic CaP-rich phases and their corresponding atomic Ca/P ratios

In the case of heavily calcified valves, EDS analysis identified the components of calcification as calcium and phosphorus in an atomic ratio typical of hydroxyapatite. The spectra obtained were comparable to those collected in an extensive EDS analysis of a crystalline hydroxyapatite standard, run under the same conditions (see figure 7.18 below). The atomic Ca/P ratio of an heavily calcified tissue valve obtained from the corresponding EDS trace (figure 7.18 left) appears very similar to the one (Ca/P: 1.675) of a pure crystalline hydroxyapatite standard run under the same conditions (figure 7.18 right). The results are in agreement with the theoretical calculated data (Ca/P: 1.670).

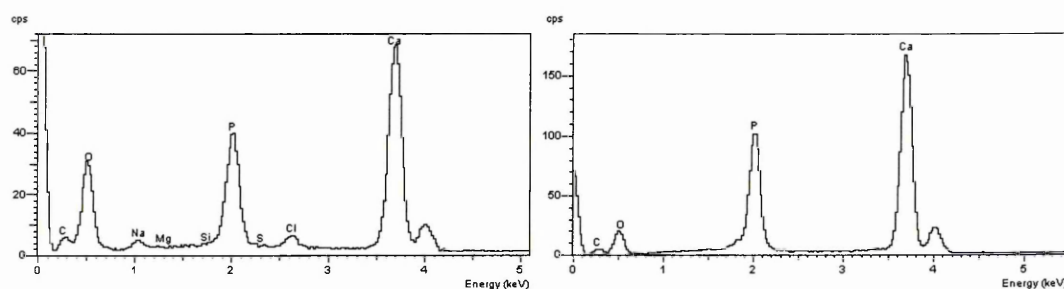


Figure 7.18: (left) EDS spectrum obtained from a heavily calcified tissue valve. (right) EDS spectrum obtained from a pure crystalline hydroxyapatite standard analysed under the same conditions.

The high values of the atomic molar ratios of Ca/P, obtained for the various mineral deposits on the valves analysed in this study (see figure 7.19 below) ranging from 1.340 to 2.115 with a mean value of 1.676, may be attributed to the substitution of the calcium and phosphate ions by other ions⁴⁰ (e.g.: sodium, magnesium, carbonate and silicon). Unfortunately, substitutions of calcium and phosphate lattice ions, with

nonmetallic (carbonate, acidic phosphate) and metallic (Na, Mg, Si) components, render the simple stoichiometric analysis of isolated calcific deposits difficult to provide conclusive evidence for the nature of different calcium phosphate phases coexisting at each stage of the calcification process. However, the EDS analysis of an hydroxyapatite standard, analysed under the same conditions as the valve samples, showed that reasonably accurate Ca/P ratio data could be obtained, which was in agreement with the theoretical calculated data (see figure 7.18 above). This suggests that the EDS analyses, although prone to complications because of the water vapour environment, do yield reliable results.

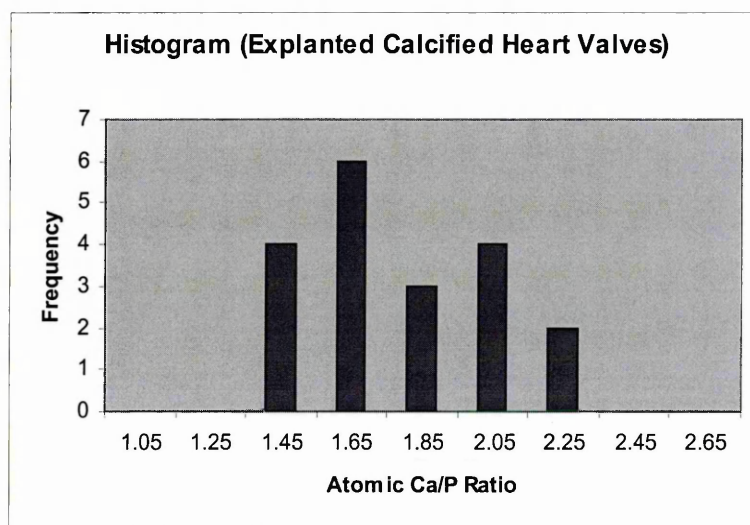


Figure 7.19: Histogram showing the frequency of occurrence versus the atomic Ca/P ratios from the EDS analyses of calcific deposits found on various calcified tissue valves analysed by ESEM.

EDS analysis of the calcium phosphate deposits also showed the substantial incorporation of silicon and magnesium in calcified tissue valves. Many EDS traces of calcific deposits reported in this chapter corroborate this statement. However, the hypothetical presence of sodium (its incorporation in the inorganic calcific phases) could not be confirmed because the valves were stored in saline solution prior to analysis.

The presence of Si appears to be in agreement with the above-hypothesis, which states that substitutions of calcium and phosphate lattice ions with metallic components can occur. The presence of Si is also in agreement with various

reports⁴¹⁻⁴⁴, where it has been shown that a reduced weight gain and pathological changes to bone and connective tissue in rats and chickens (maintained on silicon-depleted diets) could be reversed by silicon (silicate) supplementation in their diet. It was thus reported that silicon was required as an essential trace element in bone and connective tissue formation, and that it also participated in many other important metabolic processes^{45,46}. A role for silicon in osteogenesis had already been suggested by observing that silicon was uniquely localised at the mineralisation front in bones of young rats⁴⁷. Silicon was found specifically in connective tissue cells and in isolated osteocytes of young rats⁴⁸. It was thus suggested that silicon has a physiological role in bone calcification and that it is involved in the early stages of mineralisation, where a direct relationship appears between silicon and calcium. Silicic acid ($\text{Si}(\text{OH})_4$) is the physiologically active species that was reported to be capable of binding calcium in-vitro⁴⁹, with a plasma concentration in humans ranging from 5 to 20 mM. However this concentration can rise to above 100 mM in renal diseases⁵⁰, in which calcification of the patient's valves is thought to be particularly acute (see chapter 1 sections 1.3 and 1.7). Calcium and silicon have also been found co-deposited in senile plaques^{50,51}. Whether there is a direct correlation between silicon and calcification remains to be proven. Silicon can be observed in the EDS spectra of calcified valves in a paper by Glasmacher et al¹⁸. However, no explanation for its presence was given. It was reported that at later stages of mineralisation, where the Ca/P ratio tends towards the value of mature hydroxyapatite, the relationship between calcium and silica falls markedly or that as the calcium content increases the silicon content becomes less important. The fact that silicon might play a part in the initiation of mineralisation was also demonstrated in-vitro by Damen et al⁵² and in-vivo using a rat subcutaneous implantation model⁵³. In our study, the significance of silicon in the initial calcification of tissue valve bioprostheses was investigated. It was personally hypothesised that silicon does play a role in the calcification of bioprosthetic heart valves, most likely being incorporated into a mineralisation precursor phase⁵⁴.

Magnesium, in this study, was also found in the early stages of calcification of bioprosthetic valves. This is in agreement with earlier work which reported that magnesium may substitute for calcium within the crystalline matrix of hydroxyapatite⁵⁵. This would therefore explain the levels of magnesium seen here.

Magnesium can also be observed in the EDS spectra of calcified valves analysed by SEM in the literature²⁴, although no explanation for its presence was given. However, Suh et al^{56,57} stated its presence in their EDS spectra and reported that Ca/P ratios indicating a higher calcium content composition than that of crystalline hydroxyapatite can be explained by the formation of calcium phosphate crystals incorporating magnesium and possibly sodium and carbonate⁵⁸. They believed that these species, following crystal aggregation, grow to form the calcified nodules that result in valve dysfunction and failure. In addition, others think that in the very early stages of calcification, magnesium stabilises amorphous calcium phosphate in the vesicles (where the process of mineralisation is thought by some authors to be initiated)⁵⁹. Hence, nucleation of hydroxyapatite would not occur until the membrane of the vesicles was ruptured, releasing the magnesium and exposing the complex to the extracellular fluid. For this reason, we also hypothesised that there might be a correlation between phosphate and magnesium in the early stages of calcification but, because of the presence of phosphate in saline solutions, the phosphate level was not assessed in this study and therefore this hypothesis is strictly theoretical. The possible incorporation of sodium in the calcific deposits was also impossible to study because the valves had been stored in phosphate buffered saline prior to being analysed.

7.3.3 X-ray diffraction (XRD) analysis

Freeze-dried explanted calcified valve samples, analysed without any further sample preparation, showed a pattern in keeping with hydroxyapatite ($\text{Ca}_{10}(\text{PO}_4)_6(\text{OH})_2$). However, because of the large amount of organic tissue, the background radiation was particularly high. This can be seen in figure 7.20 below, which shows the diffraction pattern of an intact explanted calcified valve along with the hydroxyapatite pattern given by the Philips XRD library. Also, included is the diffraction pattern of a crystalline hydroxyapatite standard unground and spread unevenly over the quartz slide (to mimic the tissue sample).

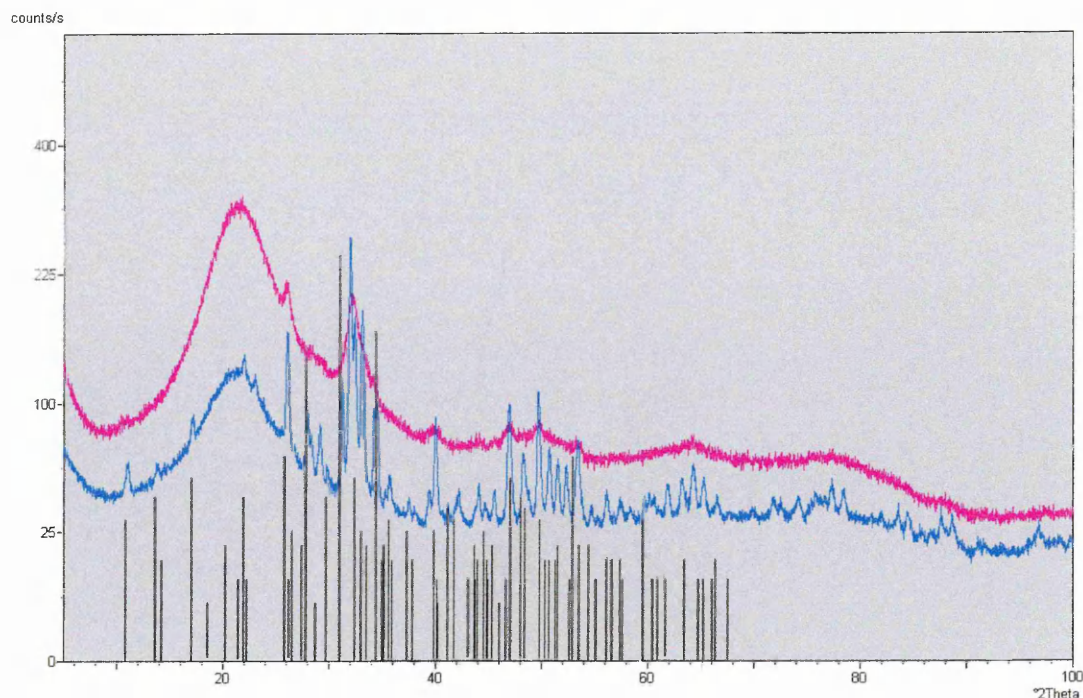


Figure 7.20: XRD data from an “intact” freeze-dried calcified valve showing a diffraction pattern consistent with hydroxyapatite. Calcified valve (*magenta*); hydroxyapatite standard (*blue*); hydroxyapatite library pattern (*black*). Diffractions patterns recorded with a 40 kV voltage and 40 mA intensity, an angle range of 5 to 100° 2θ using a step-by-step method with a step width of 0.02° and a counting time of 10 seconds per steps.

It was decided therefore to extract the calcific deposits from the organic collagen matrix and the resulting isolated crystals were powdered. As a result of this, the XRD spectrum showed sharp peaks, which is in keeping with well-crystallised apatite precipitates. Figure 7.21 shows the diffraction pattern of the extracted calcific deposits of the same valve as analysed previously (figure 7.20), along with the diffraction pattern of a crystalline hydroxyapatite standard prepared in the same way as the sample. The presence of octacalcium phosphate (OCP, $\text{Ca}_8\text{H}_2(\text{PO}_4)_6 \cdot 5\text{H}_2\text{O}$) in the valve sample is rather excluded because of the absence of the most prominent (100) OCP reflection ($d=18.6\text{\AA}$ around 4.75° 2θ) and of other peaks. However the pattern shows some similarities with the pattern of the hydrolytic OCP product OCPH³³. The pattern does not however show the coexistence of tricalcium phosphate (β-TCP, $\text{Ca}_3(\text{PO}_4)_2$), since some typical reflections, such as (214) $d=3.21\text{\AA}$ at 27.77° 2θ and (220) $d=2.607\text{\AA}$ at 34.38° 2θ, are absent.

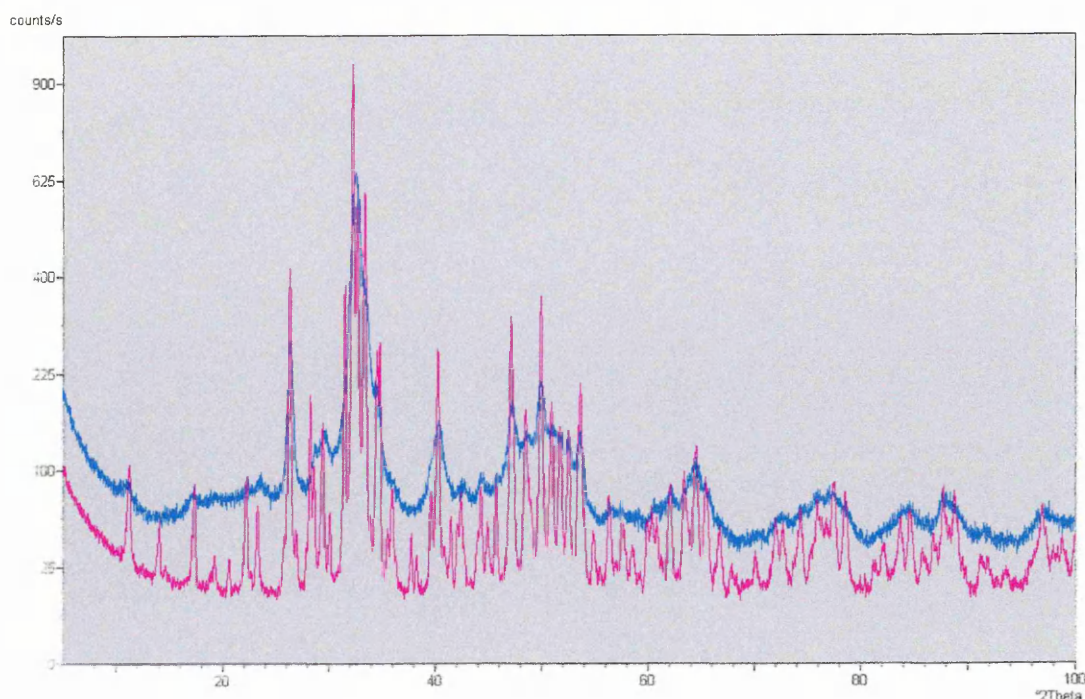


Figure 7.21: XRD data from extracted calcific deposits from a calcified valve (*blue*) showing a diffraction pattern very similar to the hydroxyapatite standard run under the same conditions (*magenta*). Diffractions patterns recorded with a 40 kV voltage and 40 mA intensity, an angle range of 5 to 100° 2 θ using a step-by-step method with a step width of 0.02° and a counting time of 10 seconds per steps.

7.3.4 FTIR-ATR and Raman analyses

7.3.4.1 FTIR-ATR analyses:

A typical FTIR-ATR spectrum from an explanted calcified valve can be observed below in figure 7.22. The peak positions and their assignments are reported in table 7.2.

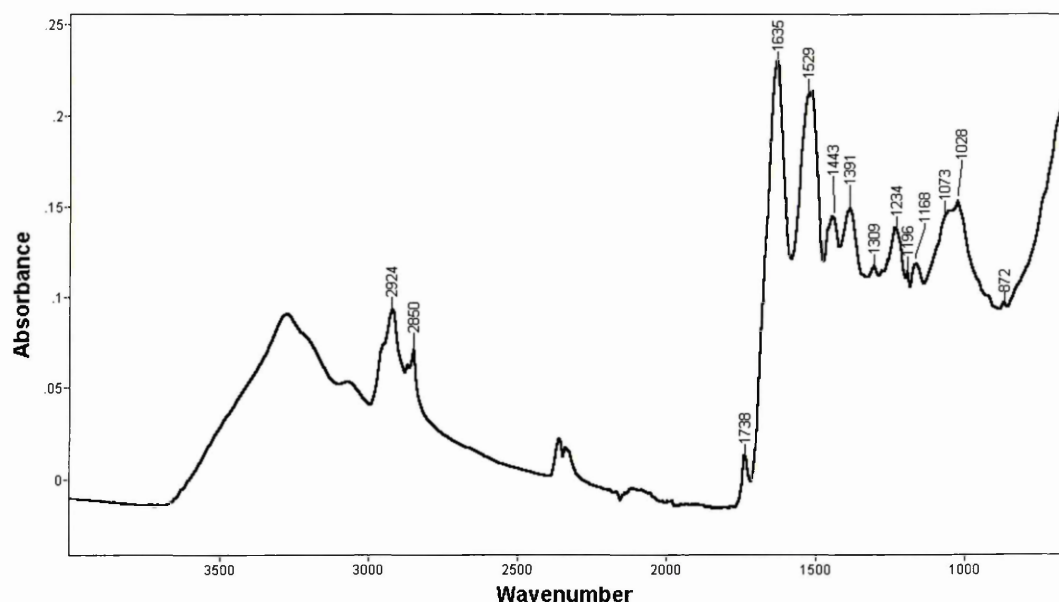


Figure 7.22: A typical FTIR-ATR spectrum from an “intact” calcified bioprosthetic valve, exhibiting a major contribution from the organic matrix. (1000 scans, resolution of 4 cm^{-1} , horizontal ATR device with a single reflection diamond ATR crystal with a 45° angle of incidence).

Peak position (cm^{-1})	Assignment
$\sim 3400\text{-}3100$	NH stretching
2924	Anti-symmetric stretching of the CH_2 group
2850	Symmetric stretching of the CH_2 group
1738	C=O stretching mode typical of phospholipids
1635	Amide I (C=O stretching)
1529	Amide II (N-H stretching)
1443	CH_2 group scissoring modes
1391	C=O symmetric stretching mode
1309	CH_2 group wagging modes
1028	P-O stretching in the $\nu_3(\text{PO}_4^{3-})$ domain
872	Out-of-plane band of the $\nu_2(\text{CO}_3^{2-})$ domain

Table 7.2: FTIR peak positions and their corresponding assignments from an “intact” explanted calcified bioprosthetic valve (freeze-dried). (see figure 7.22 for spectrum). (1000 scans, resolution of 4 cm^{-1} , horizontal ATR device with a single reflection diamond ATR crystal with a 45° angle of incidence).

The spectrum shown in figure 7.22 demonstrates that infrared spectroscopy of an “intact” (“intact”, in this case, denotes no further sample preparation) calcified valve

can detect the presence of calcium phosphate with a band of absorption at 1028 cm^{-1} (P-O stretching in the $\nu_3(\text{PO}_4^{3-})$), as was reported by Shen et al⁶⁰. The assignment of the inorganic bands is however rendered difficult because of the strong absorption of the organic matrix. Unfortunately, other typical bands of the $\nu_4(\text{PO}_4^{3-})$ region expected at $\sim 602\text{ cm}^{-1}$ (bending) and $\sim 561\text{ cm}^{-1}$ (bending), cannot be determined from our FTIR data because of the detector and beam splitter limits. However, the presence of lipids can be identified by the appearance of a band at 1738 cm^{-1} , while the presence of proteins can be detected from the absorbance of the amide I (C=O stretching) at 1635 cm^{-1} and from the amide II (N-H stretching) at 1529 cm^{-1} . The sharp peak at 872 cm^{-1} could be due to the ν_2 vibrational band of the carbonate ion (expected at $850\text{--}880\text{ cm}^{-1}$), which is usually relatively free of absorption by organic substituents. However, other carbonate peaks are difficult to assign because they are unresolved from other broad absorption bands. The absence of a band at 910 cm^{-1} , which is usually considered characteristic of OCP, refutes the theoretical presence of an OCP phase in the calcified valve.

The FTIR-ATR spectrum of the extracted calcific deposits from calcified explanted valves allows a much better assignment of the inorganic peaks, although there is still some evidence of the organic matrix. Such a spectrum can be found in figure 7.23 below.

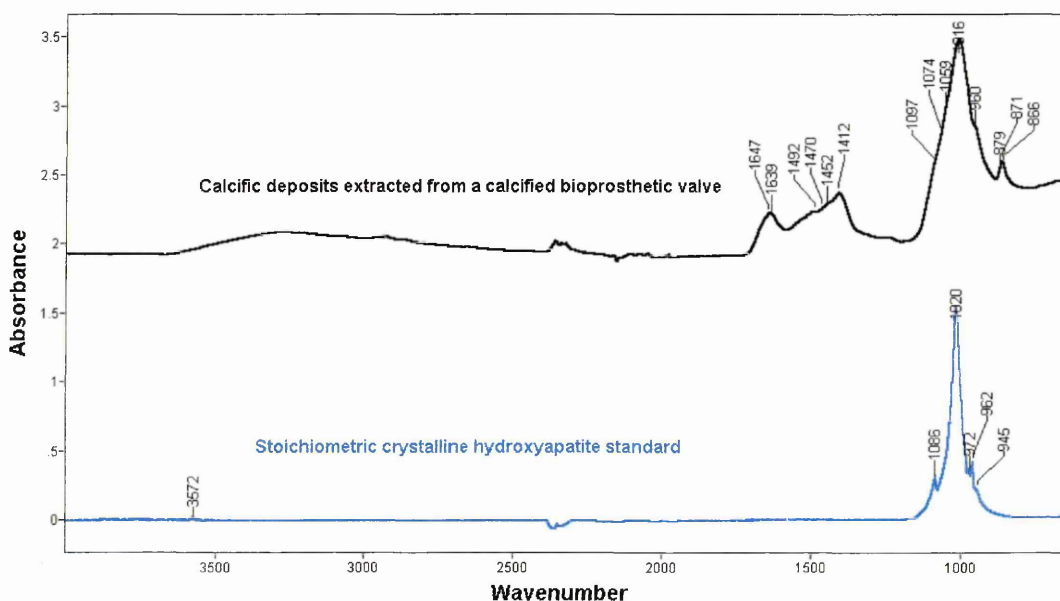


Figure 7.23: FTIR-ATR spectrum of extracted calcific deposits from a calcified explanted valve (black trace), along with the spectrum of a stoichiometric crystalline hydroxyapatite standard (blue trace). (1000 scans, resolution of 4 cm^{-1} , horizontal ATR device with a single reflection diamond ATR crystal with a 45° angle of incidence).

Apatitic structure:

Of interest when analysing the mineralised tissue or the calcific minerals themselves by FTIR are the ν_1 and ν_3 phosphate peaks ($900\text{--}1200\text{ cm}^{-1}$), as it is the only accessible area with the spectrometer used for this study (mercury cadmium telluride (MCT) detector and KBr beamsplitter, cutting the signal at 650 cm^{-1} , preventing the analysis of the $\nu_4(\text{PO}_4^{3-})$ region). To resolve underlying bands, second derivative spectra can be calculated, facilitating the determination of peak positions⁶¹⁻⁶³, which in turn may be used to identify the presence of acid phosphates or non-stoichiometric apatites⁶⁴. Comparison of the FTIR spectra obtained from calcific deposits extracted from explanted calcified valves with the spectra of standards such as β -TCP, OCP, brushite (DCPD) and HAP, raised some interesting points. First of all, the theoretical presence (see chapter 1 section 1.6.4) of β -TCP, brushite and OCP is refuted because of the differences in the spectra. For example, the characteristic β -TCP band at 970 cm^{-1} ⁶⁴ is absent, as is the brushite band at 1128 cm^{-1} ⁶⁴, the OCP band (HPO_4^{2-} ion of OCP) at 1138 cm^{-1} ⁶⁴ and another specific band for the OCP structure at $913\text{--}917\text{ cm}^{-1}$ ⁶⁵. The presence of HPO_4^{2-} -containing apatite is also refuted because of the absence of the typical absorption band at 1143 cm^{-1} , which has generally been assigned to HPO_4^{2-} ions⁶⁶. Nevertheless, the spectra from the explanted calcified valves do contain some similarities with that from pure crystalline hydroxyapatite, suggesting the presence of an apatic phase (see figure 7.23). However, the hydroxyl stretch observed at 3572 cm^{-1} in the spectrum from the hydroxyapatite standard is not observed in the spectrum of the calcified valve. The stoichiometric hydroxyapatite standard shows well known sharp absorption bands exhibiting maxima in the $\nu_3(\text{PO}_4^{3-})$ region at 1020 and 1086 cm^{-1} , while a non-stoichiometric apatite-like structure usually shows bands at 1110 and 1125 cm^{-1} that are considered as representative of phosphate environments in poorly crystalline apatitic calcium phosphates⁶⁴. For instance, a clear band can be observed at 1125 cm^{-1} in the spectrum of the mineral of young enamel⁶⁴, while a shoulder would indicate lability

of crystals. Despite the presence of a relatively broad phosphate band at $\sim 1020\text{ cm}^{-1}$ in the spectrum of the explanted calcified valve (such a band has also been interpreted as an indication of the persistence of vacancies in non-stoichiometric apatites containing impurity ions⁶⁴), the absence of bands around $1100\text{--}1125\text{ cm}^{-1}$ indicates the possible presence of a mixture of stoichiometric and non-stoichiometric apatite structures. Additionally, other bands, such as the peaks at 1647 cm^{-1} , at 1452 and 1412 cm^{-1} (carbonate $\nu_3(\text{CO}_3^{2-})$ bands) that are assigned to non-stoichiometric apatites, lead to the conclusion that calcium-deficient apatite is present. The band at 960 cm^{-1} can be assigned to the $\nu_1(\text{PO}_4^{3-})$ band, the rest of the ν_1 domain being hidden behind the intense $\nu_3(\text{PO}_4^{3-})$ bands. The bands of calcium-deficient apatite (or non-stoichiometric apatite) are quite similar in fact to the ones of stoichiometric apatite but they are generally characterised by additional bands similar to those found in most biological apatites⁶⁴ (around 1020 and 1100 cm^{-1}). Such bands can be identified, using second derivatives, at 1016 , 1059 , 1074 and 1097 cm^{-1} in the FTIR spectrum obtained from the calcific deposits of explanted valves. This leads to the general conclusion therefore that the calcific deposits consist of calcium-deficient apatites.

Carbonate and hydroxyl-containing apatite:

The FTIR-ATR spectra from extracted calcific deposits found in valves (see figure 7.23) indicate the presence of carbonate. For example, bands are observed in the $\nu_3(\text{CO}_3^{2-})$ domain (two main ones at 1639 cm^{-1} and 1412 cm^{-1} , along with others around 1492 cm^{-1} , 1470 cm^{-1} and 1452 cm^{-1}). Bands are also seen in the $\nu_2(\text{CO}_3^{2-})$ region, which is composed of three main FTIR shifts at 871 cm^{-1} , a shoulder at 866 cm^{-1} (corresponding to a labile carbonate environment) and another at 879 cm^{-1} . Most of these carbonate bands observed in our spectrum, also substantiate the fact that lattice-bound carbonates can substitute for phosphates, as it has already been reported in the literature^{67,68}. Thus, the calcific deposits of calcified valves appear to be of a B-type carbonated-apatite⁶⁹ (carbonate ions substituting for phosphate ions in the apatic structure). However, the presence of the shoulder at 879 cm^{-1} may also indicate the possible presence of some type A carbonate, a fact that could be corroborated by the presence of other typical peaks in the $\nu_3(\text{CO}_3^{2-})$ domain assigned to type A carbonate⁷⁰ (carbonate ions substituting for the OH^- ions in the apatic structure). This leads to the conclusion that, as with bone, the environment of

carbonate ions in the calcified valves might be a mixture of type A and type B-carbonate. Unfortunately, the infrared spectral range scanned in this study does not allow the definite determination of the apatite carbonate-type that would have been facilitated by assignment of bands in the $\nu_4(\text{PO}_4^{3-})$ domain (500-650 cm^{-1}). Although no quantitative data are available, the main carbonate location appears to be in the phosphate sites (type B), with minor amounts in the monovalent anionic sites (type A). The fact that some carbonate was found to be present in the calcific deposits is not surprising as the incorporation of carbonate in calcified valves, analysed as KBr pellets, has been previously reported³⁴.

The presence of type A and B carbonates in the calcific deposits of calcified valves may contribute to the absence or very low concentration of hydroxyl ions observed in the spectra. Again, this is quite similar to what is observed with bone mineral^{71,72}. However, the absence of bands indicative of the OH group in our spectra does not preclude the presence of hydroxide ions, as it was previously reported^{73,74}. Some convincing evidence that OH groups can be present although they do not give rise to OH bands in the infrared spectrum was reported⁷⁵. Also, hydrogen bonding with adsorbed water molecules could reduce the intensity (extreme broadening) of infrared OH bands⁷⁶.

7.3.4.2 Raman analyses:

The Raman spectra obtained from “intact” calcified valves showed a strong fluorescent background, masking the entire pattern. This is thought to be due to a yellow colouration of the tissue caused by the glutaraldehyde treatment. A typical spectrum of such a calcified valve can be found in figure 7.24. Only the expected relatively strong vibrations can be seen above the fluorescence background (as assigned in table 7.3).

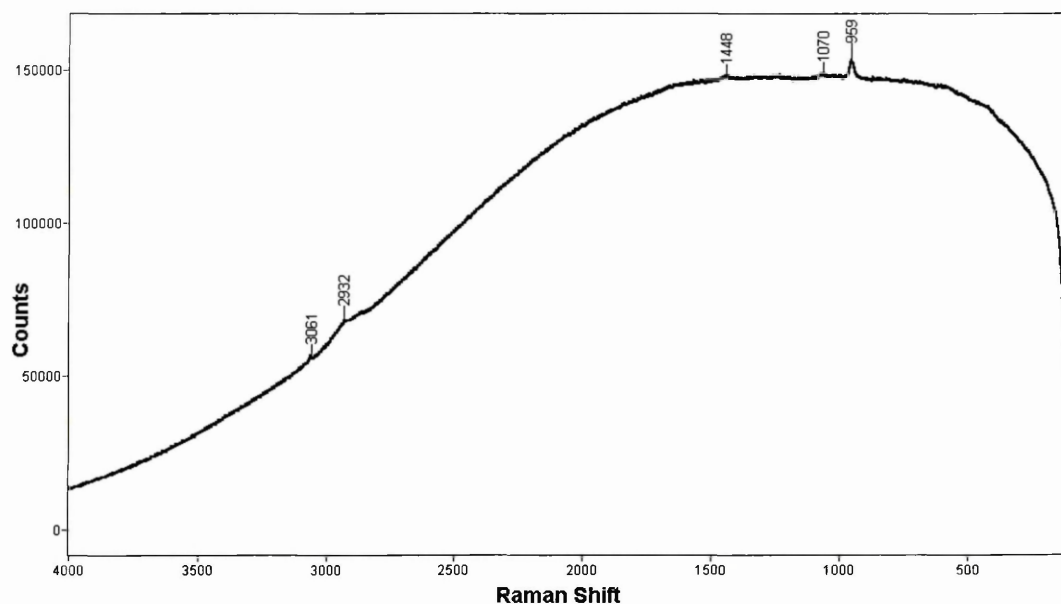


Figure 7.24: Raman spectrum of an “intact” explanted calcified bioprosthetic valve. Spectrum scanned between 4000 and 100 cm^{-1} at a resolution of 4 cm^{-1} , with a red laser (633nm).

Peak position (cm^{-1})	Assignment
3061	Amide B (contribution from the organic matrix)
2932	CH stretching (contribution from the organic matrix)
1448	Possible carbonate band $\nu_3(\text{CO}_3^{2-})$
1070	Anti-symmetric P-O stretching $\nu_3(\text{PO}_4^{3-})$
959	Symmetric stretching vibration of the P-O bonds $\nu_1(\text{PO}_4^{3-})$ band

Table 7.3: Peaks positions and their corresponding assignments from the Raman spectrum (see figure 7.24) of an “intact” explanted calcified bioprosthetic valve (freeze-dried). Spectrum scanned between 4000 and 100 cm^{-1} at a resolution of 4 cm^{-1} , with a red laser (633nm).

Extraction of the calcific deposits from the calcified valves by removing the majority of the collagen matrix yielded much better spectra with minimal fluorescent background (see figure 7.25 below). In addition, and in comparison to the FTIR study that did not allow bands to be characterised below 650 cm^{-1} , the Raman spectra were collected over a wider spectral range. The $\nu_4(\text{PO}_4^{3-})$ region was therefore visible and able to reveal interesting features, which were not visible in the FTIR spectra. In addition, $\nu_4(\text{CO}_3^{2-})$ bands, which have very low intensities and are seldom seen in infrared spectra⁷⁷ (no peaks were observed in this study in this region), have strong vibrational bands in Raman spectra and hence could be observed. Similarly,

the $\nu_1(\text{CO}_3^{2-})$ region is not observable in the FTIR spectra as this region is obscured by strong phosphate absorption bands⁷⁷, however the $\nu_1(\text{CO}_3^{2-})$ vibrational mode have also strong vibrational bands in the Raman spectra⁷⁸ and hence can be observed. A typical spectrum of extracted calcific deposits from a calcified valve can be seen in figure 7.25 below. The presence of some traces of the organic matrix is easily observed. For example, the broad band around 3300 cm^{-1} is attributable to NH whilst bands at 3061 and 2932 cm^{-1} can be assigned to the amide B and CH stretching, respectively.

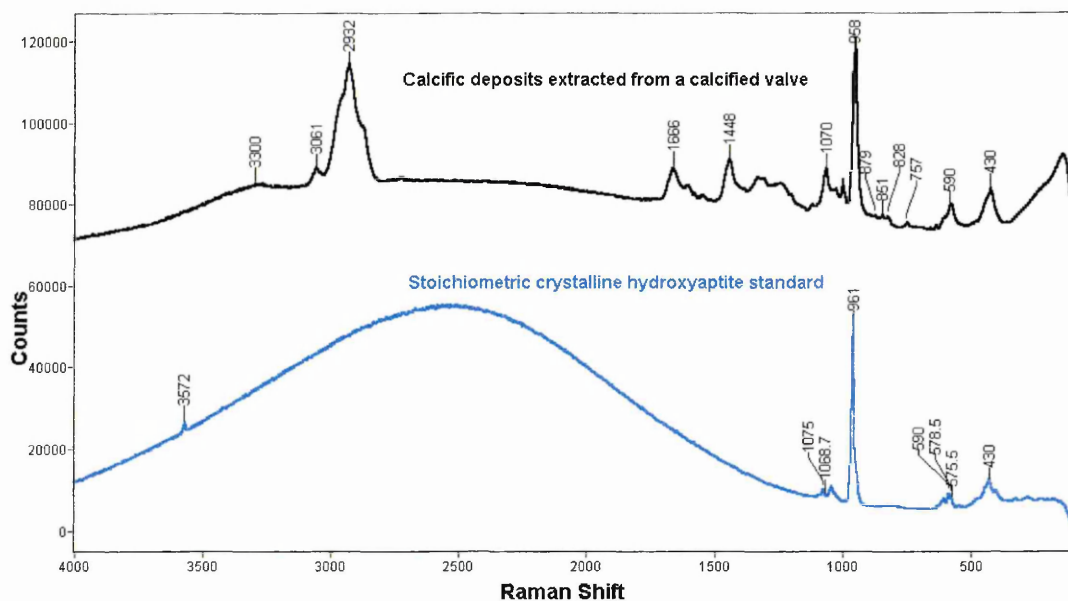


Figure 7.25: Raman spectra of extracted calcific deposits of a calcified explanted valve (black trace) and of hydroxyapatite standard (blue trace). Spectra scanned between 4000 and 100 cm^{-1} at a resolution of 4 cm^{-1} , with a red laser (633 nm).

Apatitic structure:

The intense, and single band at 958 cm^{-1} corresponds to the symmetric stretching vibration of the P-O bonds ($\nu_1(\text{PO}_4^{3-})$) and hence refutes the hypothetical presence of β -TCP, which exhibits two peaks and a shoulder instead of a single peak. A similar single, intense peak at 961 cm^{-1} can be found in the hydroxyapatite standard spectrum.

The single band at 430 cm^{-1} is assigned to the doubly degenerate O-P-O bending mode ($\nu_2(\text{PO}_4^{3-})$). This band appears very much similar to the hydroxyapatite $\nu_2(\text{PO}_4^{3-})$ mode.

The single but quite broad band with a maximum at 1070 cm^{-1} may be assigned to anti-symmetric P-O stretching ($\nu_3(\text{PO}_4^{3-})$). In the same region, the hydroxyapatite standard exhibits a sharp, intense peak at 1075 cm^{-1} and a shoulder at 1068 cm^{-1} , which might explain the width of the band observed in the spectrum from the calcific deposits. In another region of the $\nu_3(\text{PO}_4^{3-})$ mode (between 1055 and 1020 cm^{-1}), hydroxyapatite standard peaks at 1046 , 1028 and a shoulder at 1038 cm^{-1} can be compared to the broad, weak bands observed in the same region of the spectrum of the extracted calcific deposits (peaks not annotated in spectra for sake of clarity).

The broad singlet (with possible splitting) around 590 cm^{-1} ($\nu_4(\text{PO}_4^{3-})$) can be assigned predominantly to the anti-symmetric O-P-O bending frequency. It corresponds roughly to an “advanced” amorphous calcium phosphate form, since the conversion of amorphous calcium phosphate to a fully crystalline solid is usually accompanied by a gradual splitting of the Raman band into a well-defined doublet for the fully crystalline material⁷⁹. In fact, the crystalline stoichiometric hydroxyapatite standard shows a doublet (590 and 578 cm^{-1}) with a shoulder at 575 cm^{-1} in this region. The presence of such an “advanced” amorphous calcium phosphate phase in the calcific deposits is corroborated by the absence of a band at 530 cm^{-1} , which is usually found in the early stages of mineralisation of bone and enamel^{80,81}.

Carbonate and hydroxyl-containing apatite:

The strong band at 1448 cm^{-1} may be assigned to a carbonate band $\nu_3(\text{CO}_3^{2-})$. Some bands at 879 , 851 and 828 cm^{-1} can be assigned to the out-of-plane bending $\nu_2(\text{CO}_3^{2-})$ mode, which is not obscured by the organic matrix or by any phosphate absorption bands⁷⁰. No band corresponding to an HPO_4 -containing apatite can be observed (expected at 545 cm^{-1}), which excludes the hypothetical presence of OCP. Thus, we can conclude that the calcific deposits are made up of calcium-deficient apatite containing CO_3^{2-} ions but no HPO_4^{2-} . The band at 757 cm^{-1} can be assigned to a $\nu_4(\text{CO}_3^{2-})$ mode. The stretching mode of OH^- found with crystalline samples is present at 3572 cm^{-1} in the spectrum of the hydroxyapatite standard. This band is known to be difficult to detect in poorly crystalline samples⁸²⁻⁸⁴ and is absent from the Raman spectrum of the calcific deposits from the calcified valve, thus indicating the presence of a poorly crystalline apatite phase in the calcific deposits. Hence, the

calcific deposits from the calcified valve are more likely to be assigned to carbonate apatite, although the absence of OH peaks in the spectrum does not preclude the presence of hydroxide ions as it was previously reported for bone analysis⁷⁴.

7.3.5 ICP-OES analysis

The results obtained with the in-vivo study can be found in the table 7.2 below.

Valve / elements analysed	Silicon ($\mu\text{mol/g}$)	Magnesium ($\mu\text{mol/g}$)	Calcium ($\mu\text{mol/g}$)
Cardiac Valve 1	0.098	0.552	29.042
Cardiac Valve 2	0.046	0.302	17.415
Cardiac Valve 3	0.210	1.491	65.494
Cardiac Valve 4	0.045	0.320	18.189
Cardiac Valve 5	0.066	0.784	39.122
Cardiac Valve 6	0.039	0.251	13.223
Cardiac Valve 7	0.114	1.490	85.903

Table 7.2: Elemental analyses (silicon, magnesium and calcium) of explanted calcified human bioprosthetic heart valves by ICP-OES.

The correlation of the elements analysed was calculated and a two-tailed statistical test carried out for each pair of elements to be correlated. The corresponding results can be found in table 7.3 below.

Pair of elements to be correlated	r value (estimator of the population correlation coefficient)	t value (statistic for the test of significance for the correlation coefficients)	Conclusion of the statistic under the null hypothesis
Ca/Si	0.73899	2.45273	poor evidence for correlation only at 10% level of significance
Mg/Si	0.85287	3.65260	evidence for correlation at 2% level of significance
Mg/Ca	0.97636	10.09951	Strong evidence for correlation at 0.02% level of significance

Table 7.3: Correlation data from the elemental analyses (Ca, Si and Mg) of explanted calcified human bioprosthetic heart valves by ICP-OES.

From these results, it appears that silicon is somehow correlated to magnesium, both being possibly involved as important precursors in the calcification of bioprosthetic

tissue valves. Furthermore, magnesium definitely appears to correlate with calcium, indicating the strong role that magnesium might play during the calcification of tissue valves. Unfortunately, no published data on levels of Ca/Mg/Si in calcified material is available for comparison. Nevertheless, one may suggest the hypothesis therefore that magnesium is involved with both the early precursors and the later stages of calcification. No strong correlation was found between calcium and silicon. The use of ICP-OES was only recently reported for quantitative analysis of calcium and phosphorous deposits on valve leaflets in a canine in-vivo model⁸⁵ and an in-vitro model⁸⁶, but not on explanted human calcified valves as in this study, which renders a direct comparison extremely difficult.

7.4 Conclusion

The ESEM study revealed different patterns of calcification in explanted cardiac valves that can be considered as a sequence of events in the calcification process. In the first stage, the calcific deposits were located either within or on the surface of the collagen fibrils. Such deposits were found to have various morphologies and sizes with various Ca/P ratios. It is hypothesised therefore that they might represent some calcium phosphate-rich precursor phases (possibly containing silicon and magnesium based on the results obtained with EDS and ICP-OES analyses), explaining their wide range of morphologies, sizes and Ca/P ratios. In the second stage, the calcific deposits (poorly crystalline apatite containing carbonate and possibly hydroxyl ions based on the XRD, infrared and Raman data) were found to be more likely to occur along the collagen bundles and also to be distributed in the interfibrillar spaces, where they accumulate. This gave, on secondary electron images, the morphological appearance of some electron-dense homogeneous phases corresponding to localised patches of calcification, which appeared (in the case of heavily calcified valves) to be like mature hydroxyapatite crystal sheet from the EDS analyses. From this study, it is thus hypothesised that calcification in the collagen interstitium proceeds via the formation of small particulates rich in calcium phosphate. These have a range of Ca/P ratios hence indicating the involvement of a number of precursors. These particulates subsequently aggregate to form larger nodules, which are then transformed into the apatite crystal structure.

This study has demonstrated the application of the ESEM technique to the investigation of complex and delicate samples (the imaging of hydrated or dehydrated biological samples) with minimal manipulation and without the need for the sample preparation associated with conventional SEM. ESEM coupled to EDS is thought to be useful in the investigation of the pathogenesis and prevention of bioprosthetic heart valve calcification. However, because studying calcification of bioprosthetic tissue valves explanted from patients or retrieved at post-mortem is difficult, the use of tissue samples subdermally implanted into rats (in-vivo) and also calcified in-vitro, may constitute the basis for further studies (see chapter 8 of this thesis).

1. Agar AW, Alderson RH, Chescoe D. In: *Principles and practice of electron microscope operation*. Oxford: North-Holland Biomedical; 1974.
2. Danilatos GD. Introduction to the ESEM instrument. *Microscopy Research and Technique*. 1993;25:354-361.
3. Danilatos GD. A gaseous detector device for an environmental SEM. *Micron Microscopica Acta*. 1983;14:307-319.
4. Danilatos GD. Foundations of environmental scanning electron microscopy. In: Hawkes PW, ed. *Advances in Electronic and Electron Physics*. Boston: Academic Press; 1988:109-250.
5. Taylor F, Hardt T. ESEM adds new dimension to research. *Ceramic Industry*. 1991;137:37-40.
6. Bolon RB, Robertson CD, Lifshin E. The environmental SEM: a new way to look at insulators. *Microbeam Analysis*. 1989:449-452.
7. Gilbert LC, Doherty RE. Using ESEM and SEM to compare the performance of dentin conditioners. *Microscopy Research and Technique*. 1993;25:419-423.
8. Uwins PJR, Murray M, Gould RJ. Effects of four different processing techniques on the microstructure of potatoes: comparison with fresh samples in the ESEM. *Microscopy Research and Technique*. 1993;25:412-418.
9. Hardy JP, Anderson VJ, Gardner JS. Stomatal characterisation of grass leaves by four preparation techniques. *Microscopy: The Key Research Tool*. 1992;22:87-90.
10. Haggis GH. Sample preparation for electron microscopy of internal cell structure. *Microscopy Research and Technique*. 1992;22:151-159.
11. Peters KR, Pohl R. Freeze-substitution of chemically stabilised samples for biological field emission scanning electron microscopy. *Microscopy Research and Technique*. 1992;22:170-184.
12. Ferrans VJ, Tomita Y, Hilbert SC, Jones M, Roberts WC. Pathology of bioprosthetic cardiac valves. *Human Pathology*. 1987;18:586-595.
13. Schoen FJ, Levy RJ, Nelson AC, Bernhard WF, Nashef A, Hawley M. Onset and progression of experimental bioprosthetic heart valve calcification. *Laboratory Investigation*. 1985;52:523-532.
14. Valente M, Bortolotti U, Thiene G. Ultrastructural substrates of dystrophic calcification in porcine bioprosthetic valve failure. *American Journal of Pathology*. 1985;119:12-21.
15. Valente M, Bortolotti U, Arbustini E, Talenti E, Thiene G, Gallucci V. Glutaraldehyde-preserved porcine bioprosthesis. Factors influencing performance as determined by pathologic studies. *Chest*. 1983;83:607-611.
16. Cipriano PR, Billingham ME, Oyer PE, Kutsche LM, Stinson EB. Calcification of porcine bioprosthetic heart valves. A radiographic and light microscopic study. *Circulation*. 1982;66:1100-1104.
17. Datta D, Kundu PK, Bandyopadhyay BN. Bioprosthetic heart valves-replacing order with chaos: electron microscopic study. *Artificial Organs*. 1999;23:372-376.

18. Glasmacher B, Deiwick M, Reul H, Knesch H, Keus D, Rau G. A new in-vitro test method for calcification of bioprosthetic heart valves. *The International Journal of Artificial Organs*. 1997;20:267-271.
19. Pathak YV, Boyd J, Johnston TP, Levy JT, Golomb G, Schoen FJ, Levy RJ. Scanning electron microscopy studies of the prevention of bioprosthetic heart valve calcification with controlled release polymeric matrices. *Cells and Materials*. 1991;1:65-72.
20. Gliozzi A, Morchio R, Ciferri A. In: Endre A, Balaz S, eds. *Chemistry and Molecular Biology of the Intercellular Matrix*. London: Academic Press; 1970:315.
21. Ferrans VJ, Spray TC, Billingham ME, Roberts WC. Structural changes in glutaraldehyde-treated porcine heterografts used as substitute cardiac valves. Transmission and scanning electron microscopy observation in 12 patients. *American Journal of Cardiology*. 1978;41:1159-1184.
22. Grabenwoger M, Grimm M, Eybl E, Leukauf C, Muller MM, Plenck HJ, Bock P. Decreased tissue reaction to bioprosthetic heart valve material after L-glutamic acid treatment: a morphological study. *Journal of Biomedical Materials Research*. 1992;26:1231-1240.
23. Chung SW, Kin JW, Lee HR, Kim YD, Chung HK. Calcification of experimental valve bioprostheses. *Asian Cardiovascular and Thoracic Annals*. 2001;9:19-23.
24. Lee YS. Morphogenesis of calcification in porcine bioprosthesis: insight from high resolution electron microscopic investigation at molecular and atomic resolution. *Journal of Electron Microscopy*. 1993;42:156-165.
25. Kreidler ER, Hummel FA. Phase relationships in the system SrO-P2O5 and the influence of water vapour on the formation of Sr4P2O9. *Inorganic Chemistry*. 1967;6:884.
26. Gibson IR, Rehman I, Best SM, Bonfield W. Characterisation of the transformation from calcium deficient apatite to beta-tricalcium phosphate. *Journal of Materials Science. Materials in Medicine*. 2000;11:533-539.
27. Collins SP, Pope RK, Scheetz RW, Ray RI, Wagner PA, Little BJ. Advantages of environmental scanning electron microscopy in studies of microorganisms. *Microscopy Research and Technique*. 1993;25:398-405.
28. Ferrans VJ, Boyce SW, Billingham ME, Jones M, Ishihara T, Roberts WC. Calcific deposits in porcine bioprostheses: structure and pathogenesis. *American Journal of Cardiology*. 1980;46:721-734.
29. Traub W, Arad T, Weiner S. Three dimensional ordered distribution of crystals in turkey tendon collagen fibers. *Proceeding of the National Academy of Science*. 1989;86:9822-9826.
30. Fulmer MT, Martin RI, Brown PW. Formation of calcium deficient hydroxyapatite at near-physiological temperature. *Journal of Materials Science. Materials in Medicine*. 1992;3:299-305.
31. Mavrilas D, Apostolaki A, Kapalos J, Koutsoukos PG, Melachrinou M, Zolota V, Dougenis D. Development of bioprosthetic heart valve calcification in-vitro and in animal models: morphology and composition. *Journal of Crystal Growth*. 1999;205:554-562.
32. Brown WE, Eidelman N, Tomazic B. Octacalcium phosphate as a precursor in biomineral formation. *Advances in Dental Research*. 1987;1:306-313.
33. Tomazic BB, Tung MS, Gregory TM, Brown WE. Mechanism of hydrolysis of octacalcium phosphate. *Scanning Microscopy*. 1989;3:119-127.
34. Tomazic BB, Brown WE, Schoen FJ. Physicochemical properties of calcific deposits isolated from porcine bioprosthetic heart valves removed from patients following 2-13 years function. *Journal of Biomedical Materials Research*. 1994;28:35-47.
35. Pettenazzo E, Deiwick M, Thiene G, Molin G, Glasmacher B, Martignano F, Bottio T, Reul H, Valente M. Dynamic in-vitro calcification of bioprosthetic porcine valves: evidence of apatite crystallisation. *Journal of Thoracic Cardiovascular Surgery*. 2001;121:500-508.
36. Perez L, Shyu LJ, Nancollas GH. The phase-transformation of calcium-phosphate dihydrate into octacalcium phosphate in aqueous suspensions. *Colloids and Surfaces*. 1989;38:295-304.
37. Ten Huysen KS, Brown PW. Variations in solution chemistry during calcium-deficient and stoichiometric hydroxyapatite formation from CaHPO4 center dot 2H(2)O and Ca-4(PO4)(2)O. *Journal of Biomedical Materials Research*. 1997;36:233-241.
38. Tomazic BB, Brown WE, Eanes ED. A critical evaluation of the purification of biominerals by hypochlorite treatment. *Journal of Biomedical Materials Research*. 1993;27:217-225.
39. Egerton-Warburton LM, Griffin BJ, Kuo J. Microanalytical studies of metal localisation in biological tissues by environmental SEM. *Microscopy Research and Technique*. 1993;25:406-411.

40. Koutsoukos PG. In: Amjad Z, ed. *Calcium Phosphates in Biological and Industrial Systems*. Boston: Kluwer Academic Publishers; 1998:145-171.
41. Schwarz K, Milne DB. Growth promoting effects of silicon in rats. *Nature*. 1972;239:333-334.
42. Carlisle EM. Biochemistry of essential ultra trace elements. *Biochemical Elements*. 1984;3:257-291.
43. Carlisle EM. Silicon: a requirement in bone formation independent of vitamin D1. *Calcified Tissue International*. 1981;33:27-34.
44. Carlisle EM. Silicon as an essential trace element in animal nutrition. In: *Silicon Biochemistry*. Chester: Ciba Foundation Symposium; 1986:123-139.
45. Berlyne GM, Adler AJ, Ferran N, Bennett S, Holt J. Silicon metabolism I. Some aspects of renal silicon handling in normal man. *Nephron*. 1986;43:5-9.
46. Alder AJ, Berlyne GM. Silicon metabolism II. Renal handling in chronic renal failure patients. *Nephron*. 1986;44:36-39.
47. Carlisle EM. Silicon: a possible factor in bone calcification. *Science*. 1970;167:179-180.
48. Carlisle EM. The nutritional essentiality of silicon. *Nutrition Reviews*. 1982;40:193-198.
49. Wiegand KE. Modulation of adenylate cyclase response. In; 1990.
50. Birchall JD. The interrelationship between silicon and aluminium in the biological effects of aluminium. In: *Aluminium in Biology and Medicine*. Chichester; 1992:50-68.
51. Garruto RM, Swyt C, Yanagihara R, Fiori CE, Gajdusek DC. Intraneuronal colocalisation of silicon with calcium and aluminium in amyotrophic lateral sclerosis and parkinsonism with dementia of guam. *Northern England Journal of Medicine*. 1986;315:711-712.
52. Damen JJM, Ten Cate JM. The effect of silicic acid on calcium phosphate precipitation. *Journal of Dental Research*. 1989;68:1355-1359.
53. Shen M, Farge D, Daudon M, Carpentier S, Pellerin M, Lacour B, Chen L, Martinet B, Carpentier A. Proteins and bioprosthetic calcification in the rat model. *Journal of Heart Valve Disease*. 1996;5:50-57.
54. Hughes H. Personal Communication. In; 2001.
55. Landis WJ, Lee DD, Brenna JT, Chandra S, Morrison GH. Detection and localisation of silicon and associated elements in vertebrate bone tissue by imaging ion microscopy. *Calcified Tissue International*. 1986;38:52-59.
56. Suh H, Park JC. Evaluation of calcification in porcine valves treated by ultraviolet ray and glutaraldehyde. *Materials Science and Engineering C*. 2000;13:65-73.
57. Suh H, Hwang YS, Park JC, Cho BK. Calcification of leaflets from porcine aortic valves cross-linked by ultraviolet irradiation. *Artificial Organs*. 2000;24:555-563.
58. Huang-Lee LHH, Cheung DT, Nimni ME. Biochemical changes and cytotoxicity associated with the degradation of polymeric glutaraldehyde derived cross-links. *Journal of Biomedical Materials Research*. 1990;24:1185-1201.
59. Bernacca GM, Mackay TG, Wheatley DJ. In-vitro calcification of bioprosthetic heart valves: report of a novel method and review of the biochemical factors involved. *Journal of Heart Valve Disease*. 1992;1:115-130.
60. Shen M, Lajos PS, Farge D, Daudon M, Carpentier SM, Chen L, Martinet B, Carpentier AF. Infrared spectroscopy in the evaluation of the process of calcification of valvular bioprostheses. *Annals of Thoracic Surgery*. 1998;66:S236-S239.
61. Boskey AL, Pleshko N, Doty SB, Mendelsohn R. Applications of FTIR microscopy to the study of mineralisation in bone and cartilage. *Cells and Materials*. 1992;2:209-220.
62. Gadaleta SJ, Paschalis EP, Betts F, Mendelsohn R, Boskey AL. FTIR of the solution mediated conversion of amorphous calcium phosphate to hydroxyapatite: new correlations between X-ray diffraction and infrared data. *Calcified Tissue International*. 1996;58:9-16.
63. Pleshko N, Boskey AL, Mendelsohn R. Novel infrared spectroscopic method for the determination of crystallinity of hydroxyapatite minerals. *Biophysical Journal*. 1991;60:786-793.
64. Rey C, Shimizu M, Collins B, Glimcher MJ. Resolution enhanced Fourier-transform infrared spectroscopy study of the environment of phosphate ions in the early deposits of a solid phase of calcium phosphate in bone and enamel and their evolution with age II. Investigations in the ν_3 PO₄ domain. *Calcified Tissue Research*. 1991;49:383-388.
65. Fowler BO, Markovic M, Brown WE. Octacalcium phosphate 3. Infrared and Raman vibrational spectra. *Chemistry and Materials*. 1993;5:1417-1423.
66. Berry EE. The structure and composition of some calcium-deficient apatites. *Journal of Inorganic Nucleation Chemistry*. 1967;29:317-327.

67. Etz ES, Tomazic BB, Brown WE. Micro-Raman characterisation of atherosclerotic and bioprothetic calcification. In: Romig ADJ, Chambers WF, eds. *Microbeam Analysis*. San Francisco: San Francisco Press; 1986:39-46.
68. Tomazic BB, Brown WE, Queral LA, Sadovnik M. Physicochemical characterisation of cardiovascular calcified deposits. *Atherosclerosis*. 1988;69:5-19.
69. Tomazic BB, Mayer I, Brown WE. Ion incorporation into octacalcium phosphate hydrolysates. *Journal of Crystal Growth*. 1991;108:670-682.
70. Rey C, Collins B, Goehl T, Dickson IR, Glimcher MJ. The carbonate environment in bone mineral. A resolution enhanced Fourier transform infrared spectroscopy study. *Calcified Tissue International*. 1989;45:157-164.
71. Termine JD, Lundy DR. Hydroxide and carbonate in rat bone mineral and its synthetic analogues. *Calcified Tissue Research*. 1973;13:73-82.
72. Biltz RM, Pellegrino ED. The hydroxyl content of calcified tissue mineral. *Calcified Tissue Research*. 1971;7:259-263.
73. Tannenbaum PJ, Posner AS, Mandel ID. Formation of calcium phosphates in saliva and dental plaque. *Journal of Dental Research*. 1976;55:997-1000.
74. Brown WE, Chow LC. Chemical properties of bone mineral. *Annual Review of Materials Science*. 1976;6:213-236.
75. Posner AS, Blumenthal NC, Boskey AL, Betts F. Synthetic analogue of bone mineral formation. *Journal of Dental Research*. 1975;54:B88-B93.
76. Blumenthal NC, Posner AS. Hydroxyapatite: mechanism of formation and properties. *Calcified Tissue Research*. 1973;13:135-243.
77. Feki HE, Rey C, Vignoles M. Carbonate ions in apatites: infrared investigations in the ν_4 carbonate domain. *Calcified Tissue International*. 1991;49:269-274.
78. Nelson DGA, Featherstone JDB. Preparation, analysis, and characterisation of carbonated apatites. *Calcified Tissue International*. 1982;34:S69-S81.
79. Termine JD, Posner AS. Infrared determination of the percentage of crystallinity in apatic calcium phosphates. *Nature*. 1966;211:268-270.
80. Rey C, Shimizu M, Collins B, Glimcher MJ. Resolution enhanced Fourier-transform infrared spectroscopy study of the environment of phosphate ions in the early deposits of a solid phase of calcium phosphate in bone and enamel, and their evolution with age I. Investigations in the ν_4 PO_4 domain. *Calcified Tissue International*. 1990;46:384-394.
81. Rey C, Bshah K, Griffin R, Glimcher MJ. Structural studies of the mineral phase of calcifying cartilage. *Journal of Bone Mineral Research*. 1991;6:515-525.
82. Rey C, Miquel JL, Facchini L, Legrand AP, Glimcher MJ. Hydroxyl groups in bone mineral. *Bone*. 1995;16:583-586.
83. Bonar LC, Shimizu M, Roberts JE, Griffin RG, Glimcher MJ. Structural and composition studies on the mineral of newly formed dental enamel: a chemical, X-ray diffraction, and P and H NMR study. *Journal of Bone Mineral Research*. 1991;6:1167-1176.
84. Kuhn LT, Wu Y, Rey C, Gerstenfeld LC, Grynpas MD, Ackerman JL, Kim HM, Glimcher MJ. Structure, composition, and maturation of newly deposited calcium phosphates crystals in chicken osteoblast cell cultures. *Journal of Bone Mineral Research*. 2000;15:1301-1309.
85. Lee WK, Park KD, Kim YH, Suh H, Park JC, Lee JE, Sun K, Baek MJ, Kim HM, Kim SH. Improved calcification resistance and biocompatibility of tissue patch grafted with sulphonated PEO or heparin after glutaraldehyde fixation. *Journal of Biomedical Materials Research. Applied Biomaterials*. 2001;58:27-35.
86. Park JC, Hwang YS, Han DW, Suh H. A novel in-vitro assessment of tissue valve calcification by a continuous flow type method. *Artificial Organs*. 2000;24:156-164.

Chapter 8

8 In-vitro and in-vivo calcification of pericardial tissue characterised by environmental scanning electron microscopy.

Abstract

Background and objectives: While the calcification of bioprosthetic valves presents a well-known major clinical problem, the mechanism of calcification remains unclear. Host factors can influence both the extent of the calcification and its progression. The calcification process can also be observed in-vitro that is without the interaction of these host factors. It is not certain however, whether these in-vitro calcific deposits are similar to those found in-vivo. Therefore the objectives of this study were to define the progressive chemical and morphologic sequence of mineralisation in glutaraldehyde-treated pericardial tissue, implanted subcutaneously in rats and incubated in-vitro in a metastable calcifying solution.

Methods: Calcification obtained in a static in-vitro model was compared with that produced in-vivo (subcutaneous animal model). Each sample underwent gross and X-ray examination, histology (Von Kossa staining) and predominantly analysis by environmental scanning electron microscopy (ESEM) coupled with energy dispersive X-ray analysis (EDS). The semi-quantitative data obtained by ESEM-EDS were compared with those obtained by inductively coupled plasma-optical emission spectroscopy (ICP-OES).

Results: Secondary electron photomicrographs from pericardial tissue calcified in-vivo confirmed that calcification initiated in the internal region of the tissue and then extended, with time of implantation, towards the outer surface. The calcific crystals

were found to occur preferentially by following the collagen fibril bundles arrangement and also in the sub-surface collagen structure. The ESEM-EDS analyses confirmed progressive calcification, beginning in the early specimens (7 days minimum) with progressive multifocal inter- and intra-fibrillar collagen calcification (nodules of 2 μm). Larger deposits (up to 10 μm) and then confluent nodular regions became more and more prominent until covering the majority of the collagen matrix at day 100.

ESEM micrographs of in-vitro calcified tissues revealed several forms of accumulated calcium on the tissue surface with different sizes (ranging from <1 up to 30 μm) of crystal phases. Some were in contact with collagen tissue fibres and possibly some with elastin. However the micrographs did not reveal any calcification inside the tissue, with calcific deposits only seen on the surface of the tissue in relation to the collagen structure.

Calcification was thus found to involve mostly collagen fibres and interfibrillar spaces in both the in-vitro and in-vivo models. EDS confirmed the presence of calcium phosphate-rich deposits with various Ca/P ratios in both models. A picture of the onset of tissue mineralisation in-vivo was hypothesised involving precursors containing various amounts of calcium and phosphate, along with silicon and magnesium. These evolved with the time of implantation, to a poorly crystalline form of hydroxyapatite (as found in late stage calcification). Calcification in the static in-vitro model was however mostly composed of calcium associated with low amounts of phosphorus and often potassium.

Conclusion: Intrinsic calcification of glutaraldehyde-treated pericardial tissue was induced both in-vivo and in-vitro. ESEM-EDS analysis in both models showed the presence of hydroxyapatite-like crystallisation with a similar morphology to that observed in explanted valves analysed under the same conditions. Analyses of the static in-vitro calcification model gave a low Ca/P ratio and calcification was limited even after 100 days of incubation. This meant that the calcific deposits could not be studied using techniques such as FTIR, Raman and XRD because the amounts present were below the limit of detection. The relative heterogeneity of the tissue calcification also made analysis difficult, bringing into question the reliability of the in-vitro model.

8.1 Introduction

A large number of bioprosthetic valves implanted into humans for a period of at least 4 years become calcified¹. The current rather limited knowledge of the causes and mechanisms of the formation of calcific deposits in implanted cardiac bioprostheses makes its prevention a difficult task for manufacturers. Calcification is a multi-parametric process and many chemical, biological and mechanical factors seem to be involved and might play a significant role (see chapter 1 section 1.7).

Although the extent and progression of calcification depends on host factors such as age, renal function, pregnancy and other determinants, the host-tissue graft relationship is not essential for tissue mineralisation. Indeed, calcification can be reproduced in-vitro statically or using pulsatile testing apparatus (dynamically) with an appropriate calcium-containing solution^{2,3}. The formation of calcium phosphate mineral is thought to proceed, provided there is a stimulus to initiate calcification, since the plasma medium in contact with the tissue contains levels of salts sufficient to propagate the salts formation.

Since the various calcium phosphate phases thought to be present in valve calcification have markedly different solubilities, precipitation is hypothesised to proceed through the formation of unstable precursor phases. The identity of these calcification precursors is still a matter for discussion, despite many relevant studies in the literature (see chapter 1 section 1.6.4). Elucidation of the calcification mechanism and the identification of its precursors is important in order to successfully design the right prevention strategy. As studying the early phases of calcification in explanted calcified valves is difficult, in-vivo and in-vitro calcification models can be used as alternatives.

Over recent years, a number of experimental in-vivo and in-vitro models have been proposed (see chapter 1 section 1.6.5). It is known that the biochemical and morphologic features of extensive intrinsic tissue calcification in subcutaneous implants are analogous to those seen in clinical explants⁴⁻⁶. This is despite the fact that calcium and phosphorus are accumulated at a clearly accelerated rate in the former⁷⁻⁹. Generally, in-vivo models are relatively expensive in comparison to in-

vitro models but it is not certain whether the latter are as reliable and fast as we might wish. Furthermore, although both types of model appear to give relatively similar calcification end products, whether the mineral deposition is the same and involves similar precursors is also unknown.

The aim of this research was to study the process of calcification by comparing in-vivo and in-vitro models. ESEM-EDS, optical microscopy and ICP-OES were used to achieve both qualitative and quantitative data and also to compare the mineral deposits formed.

8.2 Materials and methods

8.2.1 Materials

Bovine pericardium tissue was obtained from a local abattoir (Doncaster, UK).

Glutaraldehyde 25% v/v EM grade, formaldehyde, along with Analar grade sodium chloride, calcium chloride dihydrate, potassium dihydrogen orthophosphate, Aristar grade nitric acid and hydrochloric acid, paraffin wax, ethanol, silver nitrate, sodium thiosulphate, picric acid and acid fuchsin were obtained from BDH, UK.

MOPS Buffer (morpholino propanesulphonic acid) and methanol were obtained from Sigma, UK.

Xylene was obtained from Fisher Scientific, UK.

β -Tricalcium phosphate standard (97%) was obtained from Rose Chemicals Ltd, UK.

Hydroxyapatite standard (99%) was obtained from Fluka, UK.

Buffer pH 7.4 (phosphate) 0.03M (see chapter 4 section 4.2.1) and the calcification solution were prepared when required. The calcification solution was based on work from Wadkins and Luben¹⁰ and Bernacca¹¹ and was prepared as follows. Sodium chloride 7.9g (135mmol.L⁻¹), calcium chloride dihydrate 0.294g (2mmol.L⁻¹), potassium dihydrogen orthophosphate 0.163g (1.2mmol.L⁻¹), MOPS buffer 0.010g (0.05mmol.L⁻¹) were dissolved in 1 litre of distilled water. The atomic Ca/P ratio was thus 1.670, as in pure stoichiometric crystalline hydroxyapatite.

Ultra pure water was obtained using a MilliQ50 (Millipore, UK) packed with liquid pure cartridges (USF). The conductivity achieved was 18 MΩ/cm. Saline was a phosphate buffer saline (PBS, Baxter, USA).

8.2.2 Tissue fixation

The bovine pericardial tissue used in this study was prepared similarly to the standard process used by Carpentier-Edwards for their clinical glutaraldehyde-fixed valves. It was fixed using a solution of 0.2% v/v glutaraldehyde in 0.1 mol.L⁻¹ phosphate buffer at pH 7.4, for 48 hours at room temperature. The solution of glutaraldehyde was diluted immediately before use from 25% v/v glutaraldehyde. After fixation, the tissue was rinsed in cold PBS (phosphate buffered saline, Baxter, USA) and then sterilised using a solution of 4% v/v formaldehyde for an hour, followed by three saline washes (each of 10 minutes). Pieces of bovine pericardial tissue (density around 1.75) were cut (20 x 7.5 x 4 mm), and rinsed three times, for 2 minutes each, in saline and then used for in-vitro or in-vivo studies.

8.2.3 In-Vitro Calcification Study

Static in-vitro calcification of tissue samples was carried out in clean, sterile screw-top sample vials. Small samples of tissue (similar in size to the ones implanted subcutaneously in rats) were first washed in 0.9% saline solution and then placed in individual vials in the calcification solution buffered to pH 7.4^{10,11}. The tests were carried out at 37°C and the vials were shaken slightly in a Gallenkamp orbital incubator at 100 rev/min. The calcifying solution was not changed during this period, nor was the vial opened before the end of the test. This test protocol avoided the addition of antibacterial or antifungal agents that might affect the calcification process. On completion of the tests, samples were washed in three changes of distilled water to remove traces of unbound inorganic material. The retrieved samples (at 0, 14, 21, 28, 90 and 100 days) were then processed for analysis.

8.2.4 In-vivo Calcification Studies

Calcification of glutaraldehyde-treated pericardial tissue was evaluated using the rat subdermal model because it is a convenient model that mirrors human calcification¹². The rat subcutaneous static in-vivo model has mainly been used to determine the propensity for in-vivo calcification. Despite its simplicity the effectiveness of the

subdermal implantation model for investigating calcification is accepted even in the absence of or minimal contact with blood¹³. This procedure was conducted at the Royal Hallamshire Hospital, Sheffield, complying with Home Office Regulations. Five-week-old male Wistar rats (35 days old on arrival) were used for this study. Individual rats were assigned a unique number and those considered suitable for use in the study were also identified by cage tags and tail tattoos. Within 2 days of receipt, the animals were examined by a clinical veterinarian and representative animals were subjected to a pre-test health screen that included full necropsy, an examination for intestinal parasites, histology of selected tissues, clinical pathology and serum viral antibodies. Prior to subcutaneous implantation, the remaining rats were anaesthetised using Halothane (Mallinkrodt, UK) gas. Halothane was applied initially at a concentration of 5 mol.L⁻¹ at a rate of 4 L.min⁻¹ as the sleep-inducing dose, then at 2 mol.L⁻¹ at 2 L.min⁻¹ as the maintenance dose. There were no deaths. After the animals were anaesthetised, their dorsum was shaved using clippers and swabbed with 70% alcohol. Using an aseptic technique, up to four incisions per rat were made through the epidermis and dermis of the skin (see figure 8.1 below). Subcutaneous pouches were created between the skin and muscle layers using blunt dissection and a sample of treated tissue (7.5 x 20 mm) was placed inside each one, well away from the incisions. Dorsal implantation was preferred as it has been reported that it is much more difficult for the animals to disturb the implant sites and the incisions, and that dorsal implantation results in greater mineralisation than abdominal implantation¹⁴. The location of the different types of test sample was rotated in each consecutive animal to ensure that the results were not influenced by site-specific reactions. Each animal contained one control and three test tissues. The incisions were closed using Ethibond 5/0 braided polyester sutures (Ethicon, UK). During acclimation, the rats were allowed free access to food and water *ad libitum*. Water was delivered by Nalgene water bottles with stainless steel sipper tubes. Food was ground certified rodent chow. The rats were sacrificed by cervical dislocation, complying with Home Office Regulations, at various time intervals post-operatively (at days 7, 14, 21, 28, 35 and 100) and the tissue specimens were then excised for analysis.

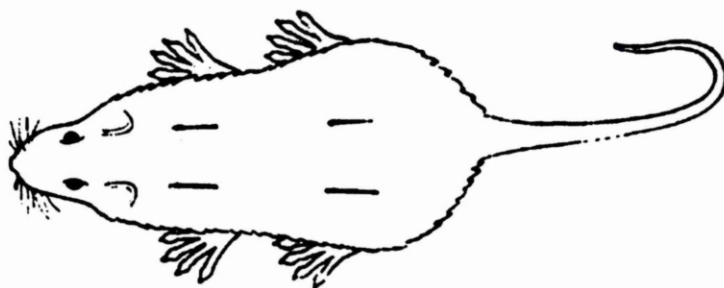


Figure 8.1: The positions of incisions in the dorsum of the rat.

8.2.5 Low Energy Radiography

At the end of the in-vivo and in-vitro calcification tests, pericardial tissues were examined radiographically for shadowing caused by calcification. Gross visualisation of mineral deposition was carried out on the excised tissue samples using low energy radiography with a Hewlett Packard 43855A Faxitron machine, Hewlett Packard, Birmingham, UK. For the in-vivo study samples, the tube voltage was set at 25 kV and the diagnostic film was exposed for 3 seconds with an intensity of 3 mA. For the in-vitro study samples, the tube voltage was set at 18 kV and the diagnostic film was exposed for 3 seconds with an intensity of 3 mA. The Kodak Industrex M films (Kodak, Eastman Chemical Co. Kingsport, TN, USA) were developed using a Kodak RP X-OMAT processor (Kodak, Eastman Chemical Co. Kingsport, TN, USA).

8.2.6 ICP-OES (Inductively Coupled Plasma-Optical Emission Spectroscopy)

For the quantitative study, the glutaraldehyde-treated and non-treated tissues from the in-vitro study were retrieved at 0 and at 100 days of incubation. Prior to analysis, the samples were washed five times for 2 minutes each time in distilled water.

In parallel, sample implants from the in-vivo study were retrieved at 0, 7, 14, 28, 35 and 100 days. The surrounding tissue was carefully removed and the samples were washed five times for 2 minutes each time in saline and distilled water. Pieces of untreated unimplanted pericardial tissue were also subjected to ICP analysis.

All samples were lyophilised with a Cold Trap 1000 freeze-drier, achieving a pressure of 75 mbar (0.35 atm) with a temperature of approximately -40°C and weighed. They were then hydrolysed with a mixture of 3 mL HCl and 1 mL HNO_3 , simmering/boiling for 5 hours. A final volume of 10 mL was made up using

deionised water. The samples were then submitted to ICP analysis. The presence of silicon, calcium, magnesium and potassium was thus determined quantitatively by ICP-OES. The phosphorus content was not determined because of the use of the phosphate-buffered saline solution to store the tissues prior to being analysed. It was believed that the phosphorus content of the buffer might possibly interfere with the results despite the washes carried out. The ICP-OES was a FC1400 Spectro analytical instrument (Spectro, Germany).

8.2.7 Histological study

For the histology study, pericardium tissue samples from the in-vitro calcification study were retrieved after 14, 28, 90 and 100 days. The samples (glutaraldehyde-fixed ones only) were then processed for examination by light microscopy using Von Kossa's silver method for calcium deposits, as reported elsewhere¹⁵. Specimens were embedded in paraffin wax and sections were cut as slices of 5 μm thickness. These were then stained using a silver Von Kossa test, which stains calcium phosphate to brown-black, osteoid, cell nuclei and collagenous tissue in red, muscle will appear in yellow and cytoplasm in pink¹⁶.

The methodology was as follows. The sections were dewaxed in two consecutive baths of xylene for 5 min each, rehydrated through 100%, 96% and 70% alcohol for 5 min each, transferred to distilled water, placed in 1% aqueous silver nitrate solution and exposed to strong light (e.g. anglepoise lamp) for 60 min. They were then washed in 3 changes of distilled water, treated with 2.5% aqueous sodium thiosulphate for 5 min, washed in distilled water, counterstained with Van Gieson stain for 5 min (Van Gieson is composed of 90 mL aqueous picric acid and 10 mL 1% aqueous acid fuchsin), dehydrated in alcohol, immersed in xylene for 5 min and mounted. The stained sections were then examined under a light microscope. The Von Kossa method is in fact a silver reduction technique, which demonstrates phosphates and carbonates, but since the demonstrable forms of these anions are almost invariably found combined with calcium, it is usually regarded as a method for calcium.

8.2.8 ESEM

ESEM was used to observe the surface morphology of in-vitro and in-vivo calcified pericardial tissue samples. The samples were analysed on both external and internal

sides. Samples were cut longitudinally, following the collagen planes, prior to the analysis in order to access and examine internal tissues. Much effort was placed on describing the morphologic observation in as quantitative a manner as possible for an objective interpretation of our findings. The presence and distribution of calcium, phosphorus and other metal ions were assessed using energy dispersive X-ray analysis (EDS) coupled to ESEM. For comparison, some synthetic CaP materials (hydroxyapatite and β -tricalcium phosphate) were run under the same conditions in the ESEM. The ESEM was a FEI Philips (Philips, The Netherlands) XL30 ESEM-FEG (environmental scanning electron microscope-field electron gun), operating at an accelerating voltage of 20 kV. Samples required no preparation and were kept wet in saline solution, until the time of analysis when they were rinsed several times with deionised water. The sample preparation and technical parameters were as already described in chapter 7 (sections 7.2.2.2 and 7.2.2.3).

The EDS results were processed so that the software gave the atomic Ca/P ratios as described in chapter 7 (section 7.3.2) and the stoichiometric atomic Ca/P ratios were used to identify the crystal phases present. It has been shown, by extensive analysis of standards of stoichiometric hydroxyapatite (chapter 7), that ESEM-EDS gives reliable data concerning the Ca/P ratio with the practical Ca/P ratio obtained being similar to the theoretical one.

8.2.9 XRD

Analyses were undertaken at room temperature with a Philips (Philips, The Netherlands) PW1710 X-ray diffractometer operating with Bragg-Brentano geometry. Experimental conditions were 40 kV and 40 mA, with Cu-K $\alpha_{1,2}$ radiation. The diffraction patterns were recorded with an angle range of 5 to 100° 2 θ and using the step-by-step method with a step width of 0.02 degrees and a counting time of 10 seconds per step. The samples were freeze-dried prior to analysis.

8.3 Results and Discussion

8.3.1 Low energy radiography

Soft X-ray analysis of in-vitro calcified samples showed no sign of calcification, probably because the degree of calcification was below the limit of detection of the

technique. However, radiography of the in-vivo calcified samples showed some signs of calcification after 28 and 100 days of implantation.

8.3.2 ESEM analysis

8.3.2.1 In-vivo samples:

Secondary electron photomicrographs of pericardial tissue calcified in-vivo indicated that calcification initiated in the internal region and then extended with time of implantation towards the outer surface of the tissue. This is in opposition to the findings of Tinghei et al¹⁷, who implied that calcification started from the surface of tissue samples implanted subcutaneously. ESEM-EDS analyses of the early samples calcified in-vivo showed that calcium phosphate deposits were present at various, random locations inside the tissues examined. Generally relatively large, medium and small size crystals co-existed in the neighbourhood of the calcification sites. ESEM micrographs showed the existence of different sizes (less than 1 and up to 30 μm) of crystal phases in contact with collagen tissue fibres and possibly sometimes with elastin fibres. The calcification seemed to be limited to the collagen mesh itself, as already reported by others¹⁸.

At day 7 of implantation, particles of a few microns (figure 8.2) were identified attached to the collagen matrix. These were rich in phosphorus and silicon, but apparently lacked calcium. Other crystal growth was also observed associated with collagen and was found to be rich in phosphorus and magnesium (see figure 8.3).

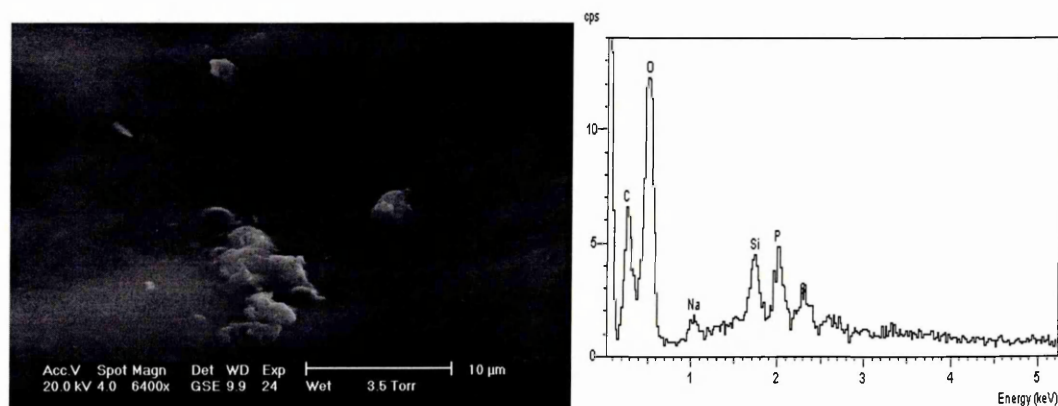


Figure 8.2: Secondary electron micrograph (*left*) and the corresponding EDS spectrum from the inside of an in-vivo sample implanted for 7 days (*right*) showing

particles of a few microns attached to the collagen matrix. The particles are rich in phosphorus, silicon and possibly sodium (the latter might come from the saline solution). Note: the carbon, oxygen and sulfur content come from the collagen matrix.

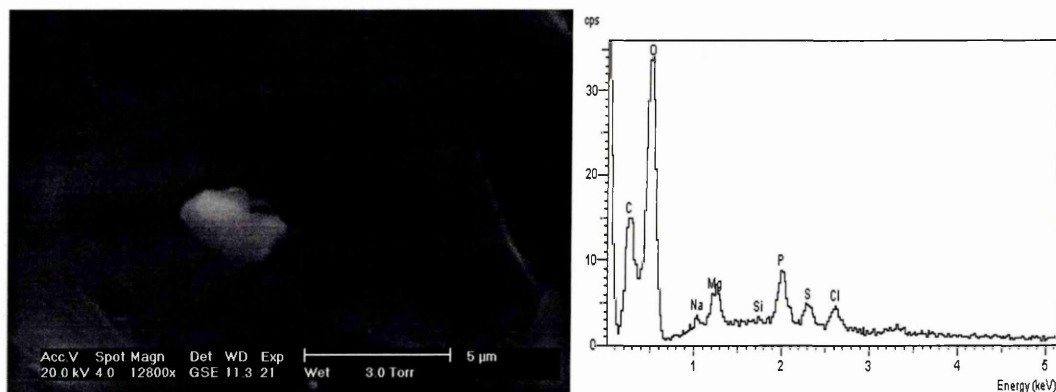


Figure 8.3: Secondary electron micrograph (*left*) and the corresponding EDS spectrum from the inside of an in-vivo sample implanted for 7 days (*right*) showing particles of a few microns in size attached to the collagen matrix. The particles are rich in phosphorus and magnesium. Note sodium and chlorine are likely to arise from the saline solution.

At day 14, particles of a few microns in size and with an irregular morphology were observed (see figure 8.4). These were quite rich in calcium but contained much less phosphorus and silicon than the day particles. Some crystal growth of less than 10 μm in size, with a different morphology, can also be seen (see figure 8.5). These also contained silicon but also with a higher calcium and phosphorus content. Such a high Ca/P ratio may be explained if one takes into account the presence of silicon and possibly other ions in the lattice that tend to increase the Ca/P ratio.

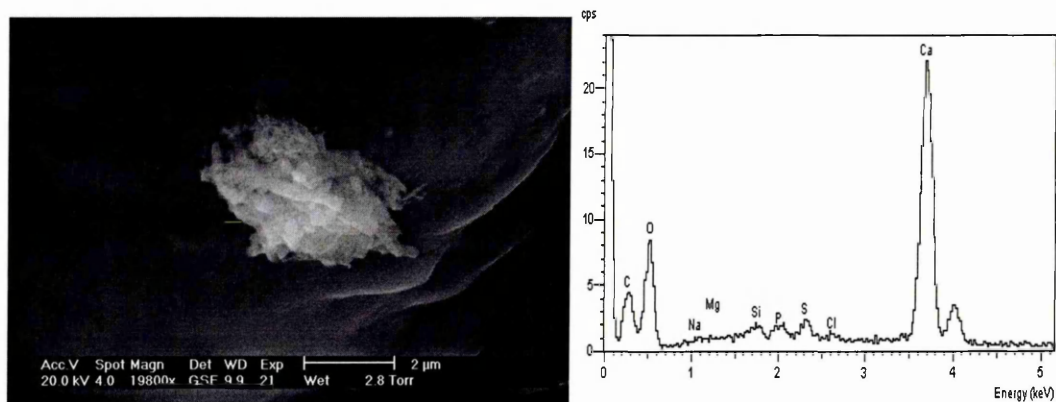


Figure 8.4: Secondary electron micrograph (*left*) and the corresponding EDS spectrum from the inside of an in-vivo sample implanted for 14 days (*right*) showing a particle with an irregular contour morphology of a couple of microns in size, rich in Ca with traces of phosphorus and silicon.

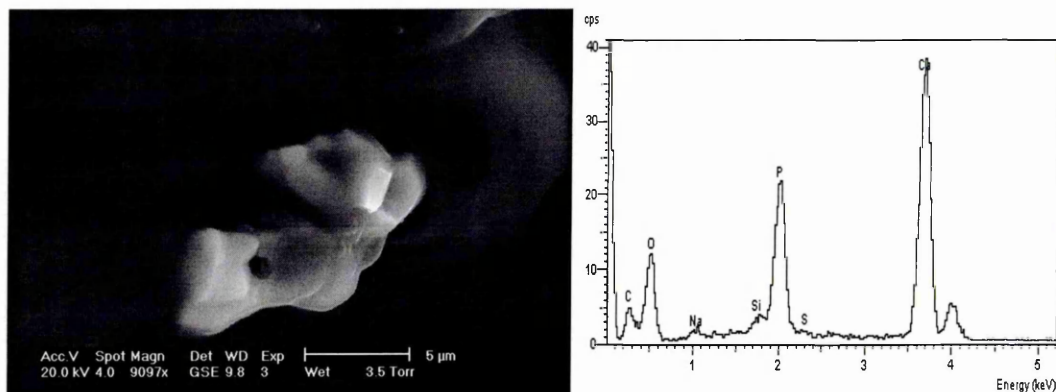


Figure 8.5: Secondary electron micrograph (*left*) and the corresponding EDS spectrum from the inside of an in-vivo sample implanted for 14 days (*right*) showing a particle of less than 10 μ m in size associated with the collagen matrix, rich in calcium, phosphorus, with traces of silicon and possibly sodium.

At day 28, crystals ranging from 5 to 10 μ m in size were observed growing on collagen bundles. These contained low but significant amounts of calcium and phosphorus (see figures 8.6 and 8.7).

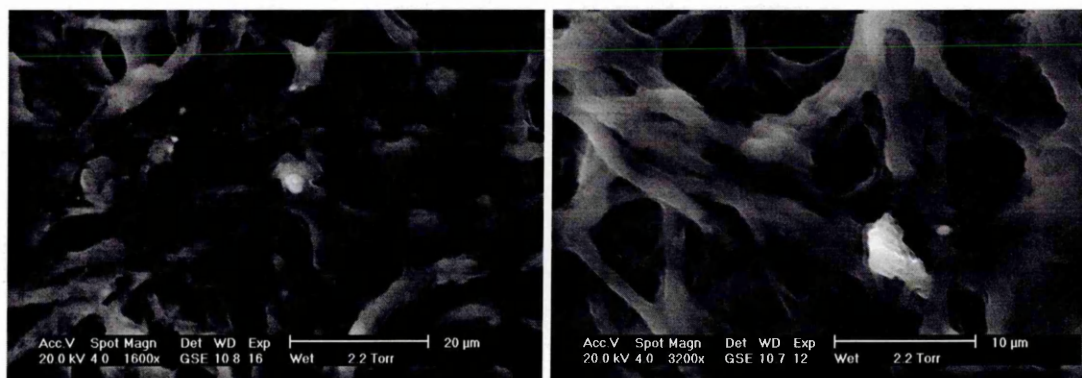


Figure 8.6: Secondary electron micrographs from the inside of an in-vivo sample implanted for 28 days showing particles of 5-10 μ m in size associated with collagen bundles.

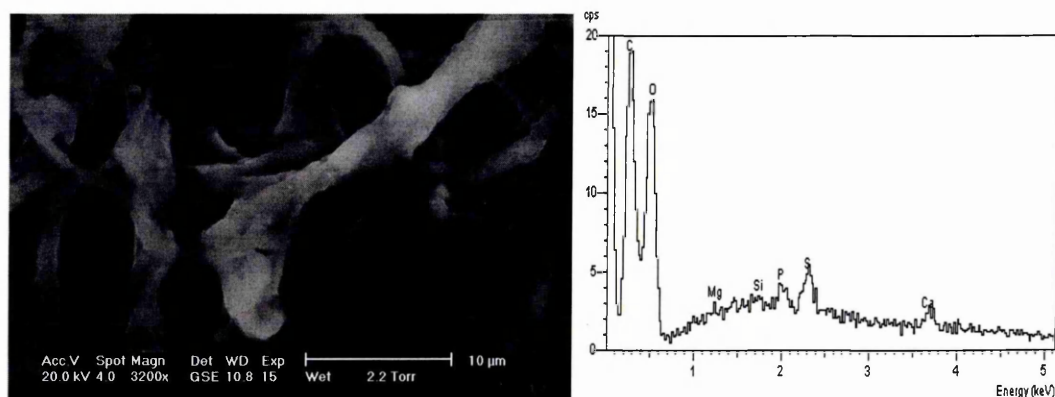


Figure 8.7: Secondary electron micrograph (*left*) and the corresponding EDS spectrum from the inside of an in-vivo sample implanted for 28 days (*right*) showing particles of about 5-10 μ m in size forming along the collagen fibres, rich in calcium, phosphorus, silicon and possibly magnesium.

At day 100, the morphology of the majority of crystals was similar to that of the crystals obtained from explanted calcified bioprosthetic valves (see chapter 7). The calcific deposits had Ca/P ratios ranging between 1.609 and 1.943, with a mean of 1.702, which is very similar to the theoretical Ca/P ratio for a crystalline hydroxyapatite standard (1.670) analysed under the same conditions. The histogram of frequency vs. the atomic Ca/P ratios obtained from samples at day 100 of implantation (see figure 8.8 below) was however different to the one obtained from explanted calcified valves (see chapter 7 section 7.3.2). In the case of the explanted valves, the Ca/P ratios showed a greater range, revealing the existence of phases probably resulting from the incorporation of impurities in the crystals. These impurities, such as sodium, carbonate, magnesium and silicon, come from the diet of the individuals^{19,20}. The diet of the rats is more controlled and thus the narrower range of Ca/P ratio values obtained may be explained. However, the relatively high Ca/P ratios obtained in the rat experiment also suggest the incorporation of impurities in the apatite crystals, although the mean value (1.702) indicates the predominance of an apatite phase similar to crystalline hydroxyapatite in relation to its Ca/P ratio (1.670).

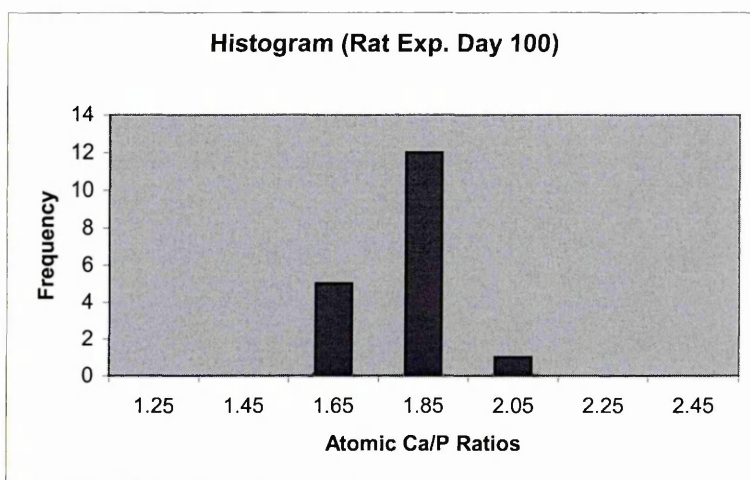


Figure 8.8: Histogram representing the frequency versus the atomic Ca/P ratios obtained from the EDS analyses of calcific deposits from an in-vivo rat calcification experiment (at day 100st implantation).

The typical morphology of crystals found at day 100 was a tabular hexagonal shape, growing from collagen, which was also consistent with apatite (see figure 8.9 below).

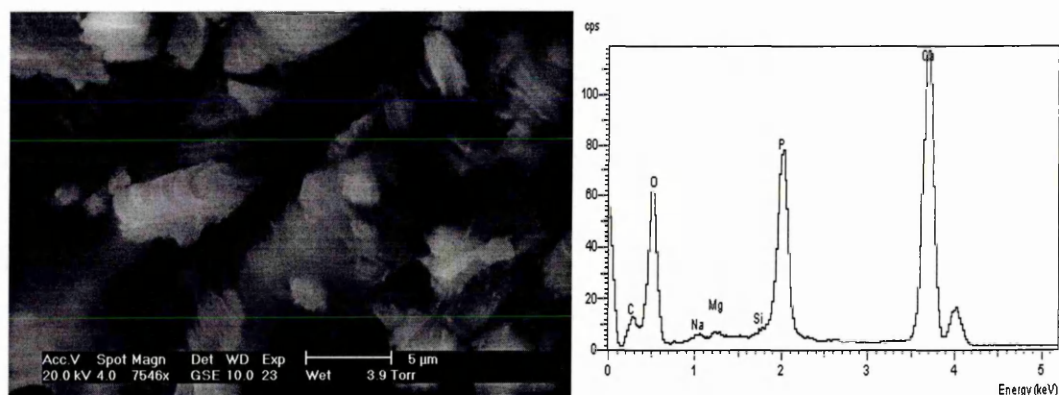


Figure 8.9: ESEM secondary electron micrograph of the inside of a day 100 of implantation sample (*left*), showing the tabular hexagonal-shape crystal growth found on collagen fibrils, which is consistent with apatite morphology. Its corresponding EDS spectrum (*right*) shows the presence of Ca, P, Mg and Na, whilst exhibiting a Ca/P ratio of 1.657, which is very close to that of hydroxyapatite.

These data led to the hypothesis that early precursor phases, containing essentially silicon, magnesium and phosphorus, tend to accumulate and attract calcium. They then form other larger precursor phases with an irregular morphology, all leading to

the final apatite-like structure. It has been reported recently that magnesium and sodium may participate in the calcification process²¹, which partially agrees with our findings. In the later stages of in-vivo calcification, calcific deposits were observed to form in parallel arrays following the longitudinal axis of the fibrils, possibly indicating the significance of the molecular structure of the collagen fibrils on the arrangement of calcific crystals.

The Ca/P ratios for the majority of calcific deposits found in the in-vivo samples (particularly at 100 days of implantation) were usually relatively high compared to the theoretical values for pure calcium phosphate phases. These high values may be attributed to non-stoichiometric apatite and the substitution of the calcium and phosphate ions by other ions²², such as carbonate, magnesium and/or silicon, as discussed in chapter 7. Alternatively, the Ca/P ratios could be explained in terms of rapid co-precipitation of the two main calcium phosphate compounds: apatite and the metastable octacalcium phosphate (OCP)²³. The hypothetical presence of OCP would agree with the *de novo* precipitation of hydroxyapatite and with the mechanism of the non-energy requiring calcium trap by phospholipids, as described in cartilage mineralisation²⁴. Although no OCP was found when analysing calcified explanted valves (see chapter 7), which are likely to represent the later stages of calcification, this does not rule out the absence of such a phase in earlier stages of calcification. Additionally, it would be quite difficult to differentiate early OCP from a hydroxyapatite phase solely from atomic Ca/P ratios. However, whether OCP could be present in earlier stages of valve calcification is strictly hypothetical and remains to be observed experimentally.

8.3.2.1.1 Pattern of in-vivo mineralisation stages (subcutaneous model):

When focusing our attention on the day 100 samples, a calcification model was postulated by creating virtual contour lines (concentric circles labelled from 1 to 10) starting from the obvious calcified area of a sample (identified by X-ray radiography and labelled contour line 1) and moving away from it (see figure 8.10 below). A summary of the observations at each contour line is given in table 8.1.

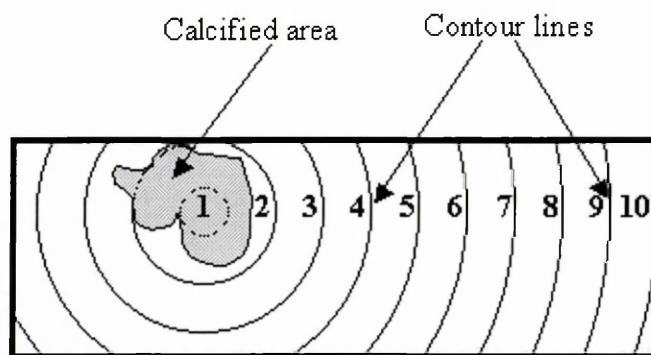


Figure 8.10: Sketch representing a calcified glutaraldehyde-treated pericardium sample after 100 days of subcutaneous implantation, showing the only calcific area identified by X-ray radiography and the corresponding theoretical contour lines moving away from that area and labelled 1-10.

Contour	Observations from ESEM and EDS analyses
10/9/8/7/6	Collagen was not found to be calcified
5/4	Sub- μm particles forming on collagen bundles/in the interfibrillar spaces. 1-2 μm particles embedded in the collagen matrix. EDS showed the presence of Ca and P, along with traces of Si.
3	Aggregates of a few μm with particular morphology (tabular hexagonal, plate-like, spherical-shaped) erupting from the collagen matrix and growing along collagen bundles. EDS showed the presence of high levels of Ca and P, along with traces of Mg.
2	Spherical nodules and needle-like particles accumulating in the interfibrillar space, following collagen bundle arrangements. EDS showed the presence of high levels of Ca and P. Ca/P ratios suggested incorporation of "impurity" ions in the crystal structure.
1	Accumulating calcific deposits are filling gaps between collagen bundles, covering most of the surface. EDS exhibited Ca/P ratios very close to that of crystalline hydroxyapatite.

Table 8.1: Summary of observations from the ESEM analysis of a calcified glutaraldehyde-treated pericardium sample after 100 days of subcutaneous implantation.

The ESEM data (summarised in table 8.1) showed that soft X-ray radiography failed to detect minor calcification sites, indicating the difficulty in definitely detecting calcification in-vitro and at early in-vivo calcification stages using this technique. They also showed that the calcification distribution is not uniform within the tissue, which is in agreement with Suh et al²¹.

Ten major contour lines were drawn theoretically (as shown in figure 8.10) and the inside of tissue samples were analysed from these regions. Although no dynamic analysis was performed, a pattern of the calcification process was set up as follows from the static pictures and EDS analyses.

Contours 10/9/8: The collagen is seen uncalcified or “intact” (see figure 8.11 (*left*), which also shows a cross section of the sample).

Contours 7/6: The collagen is still found “intact” (see figure 8.11 (*right*)). No traces of calcification were observed in these contours from the ESEM-EDS analyses.

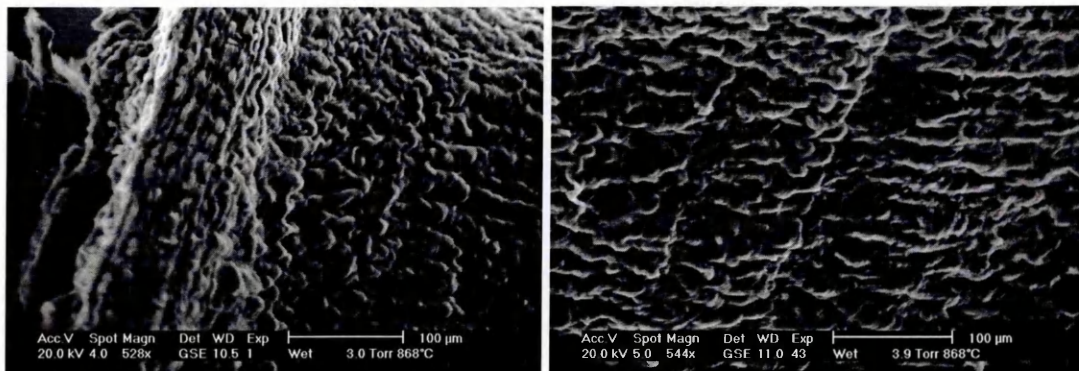


Figure 8.11: ESEM secondary electron micrographs showing the intact collagen inner surface from a day 100 of implantation sample. Micrograph (*left*) corresponds to contours 10/9/8 (see figure 8.10), whilst the other (*right*) corresponds to contours 7/6.

Contours 5/4: Collagen is seen with sub-micron particles forming on the collagen bundles and in the interfibrillar spaces. These particles are characterised by a weak EDS spectrum containing some traces of silicon, phosphorus and calcium (see figure 8.12). In association with these sub-micron particles, other particles of about 1-2 μm and containing calcium, phosphorus and silicon traces are found partially embedded inside the collagen matrix, with a Ca/P ratio of 1.609 (see figure 8.13).

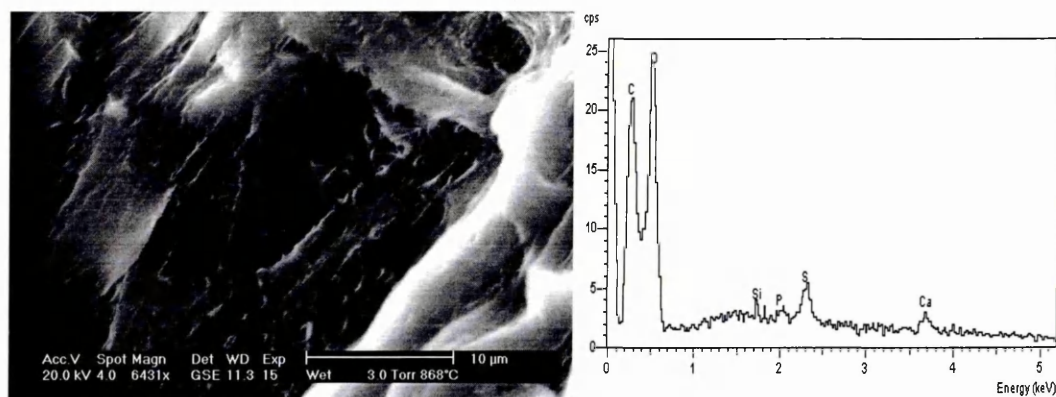


Figure 8.12: ESEM secondary electron micrograph (*left*) corresponding to contours 5/4, showing sub-microns particles on the collagen bundles and in the interfibrillar space (center of the micrograph) from the inside of a day 100 of implantation sample. Corresponding EDS spectrum (*right*) showing the presence of calcium, phosphorus and silicon.

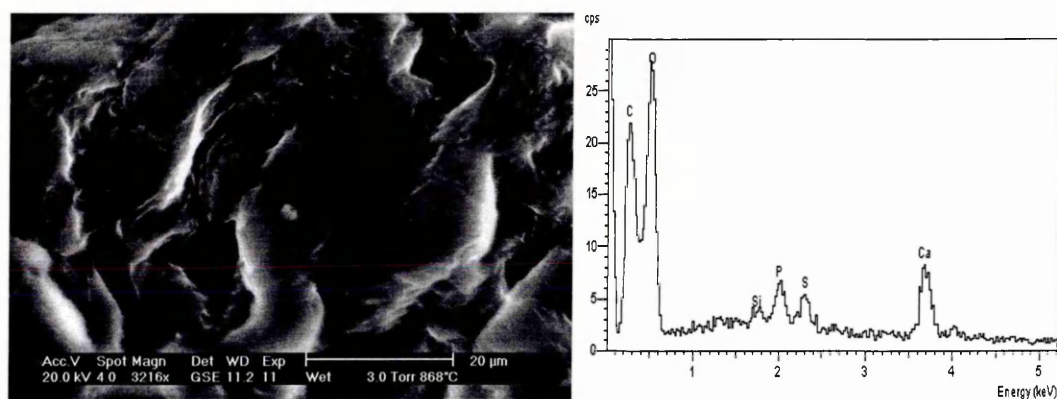


Figure 8.13: ESEM secondary electron micrograph (*left*) corresponding to contours 5/4, showing 1-2 µm particles (center of the micrograph) embedded inside the collagen matrix from the inside of a day 100 of implantation sample. Corresponding EDS spectrum (*right*) showing the presence of calcium, phosphorus and silicon. The spectrum exhibits a Ca/P ratio of 1.609.

Contour 3: The secondary electron micrograph (see figure 8.14) shows a typical repartition of particles growing from the collagen matrix surface and along collagen bundles, with a Ca/P ratio ranging from 1.654 to 1.685. These crystals are rich in calcium and phosphate, whilst possibly incorporating silicon and magnesium (see figure 8.15). The morphology observed (see figure 8.16) is mostly of a tabular hexagonal or plate-like shape, along with some spherical-shaped aggregates of a few

microns. The plate-like morphology of the calcific crystals may be comparable to hydrolysed octacalcium phosphate (OCPH), and they can be seen in the neighbourhood of small-sized-crystals that are probably of apatitic structure (although the exact nature of the calcium phosphate crystals formed cannot be established by morphological examination alone). Furthermore, the abutting of small and large crystals tends to confirm the hypothesis that a hydrolytic process occurs during the calcification. Indeed, the calcification process is thought to involve various precursor phases such as OCP that has been previously proposed for calcium phosphate formation, although the formation of dicalcium phosphate dihydrate (DCPD) was not precluded²⁵.

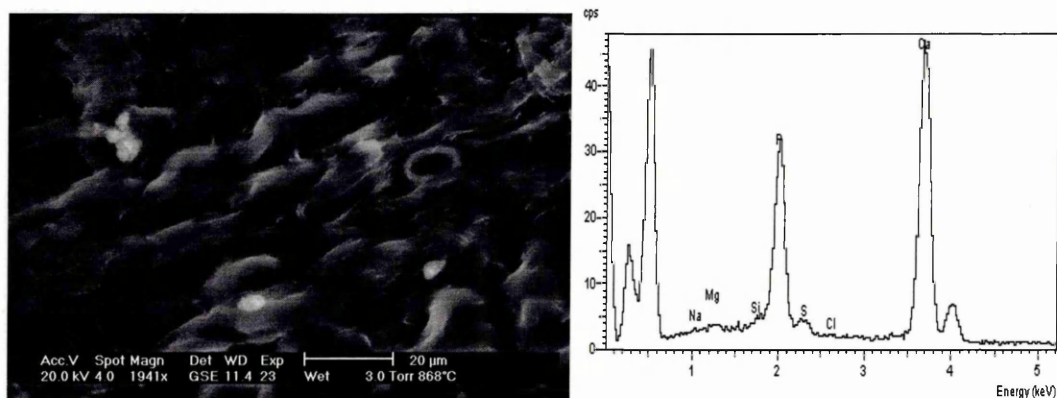


Figure 8.14: ESEM secondary electron micrograph (*left*) corresponding to contour 3, showing a typical particles distribution growing from the collagen matrix along the collagen bundles from the inside of a day 100 of implantation sample. Corresponding EDS spectrum (*right*) showing a large presence of calcium and phosphorus with a Ca/P ratio of 1.680.

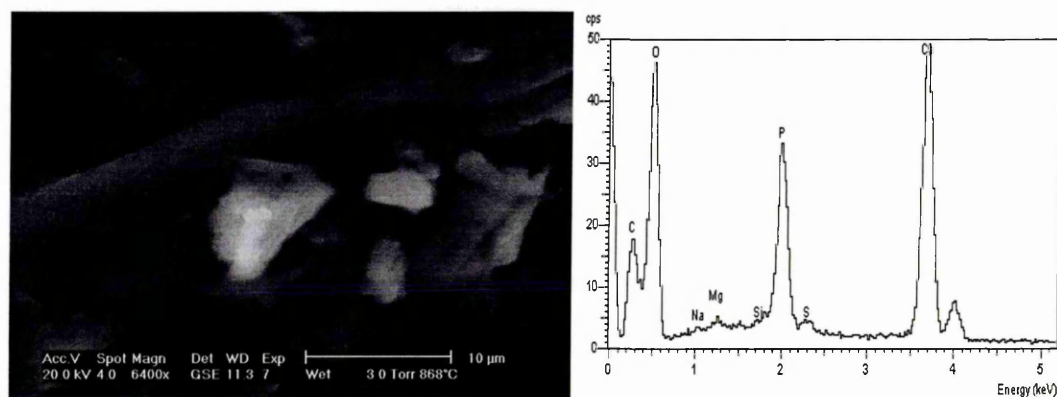


Figure 8.15: ESEM secondary electron micrograph (*left*) corresponding to contour 3, showing crystals growing off collagen bundles from the inside of a day 100 of

implantation sample. Corresponding EDS spectrum (*right*) showing the presence of calcium, phosphorus along with traces of magnesium and silicon with a Ca/P ratio of 1.654.

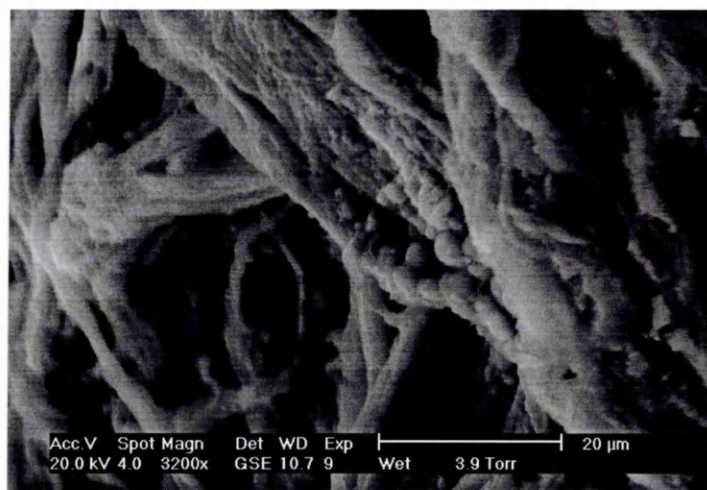


Figure 8.16: ESEM secondary electron micrograph corresponding to contour 3, showing a typical morphology of tabular-hexagonal shape or plate-like shape (top left), along with some spherical-shaped aggregates of a few microns in size (center of the picture) from the inside of a day 100 of implantation sample.

Contour 2: The calcific deposits growing along collagen tend to accumulate in the interfibrillar space, disrupting the collagen bundles (see figure 8.17 (*left*)). It also appears that the arrangement of the collagen bundles seems to partially control the formation of calcification (see figure 8.17 (*right*)). The morphology of the calcific deposits appeared to be homogeneous at low magnification, although at high magnification it is seen to be composed of a mixture of small spherical nodules and needle-like particles (see figure 8.18 (*left*)), the needle-like morphology being quite similar to the morphology of crystalline hydroxyapatite (see figure 8.18 (*right*)). EDS analyses of the various deposits demonstrates the presence of essentially calcium and phosphorus, while magnesium and silicon are not observed, however their presence is not precluded because of ICP-OES data obtained on these samples (see section 8.3.3). Although the morphologies are different, the Ca/P ratios of the various deposits are quite similar and typically between 1.622 and 1.943. This high ratio, along with the morphology of the calcific deposits, may be explained by the incorporation of non-metallic and metallic impurities in the crystal lattice, similar to

that thought to occur in the calcific deposits found in explanted valves (see chapter 7).

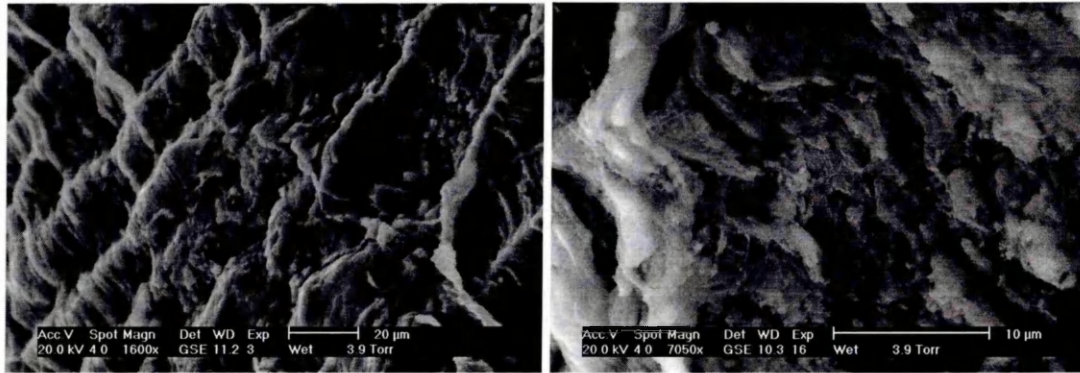


Figure 8.17: ESEM secondary electron micrographs corresponding to contour 2, showing collagen bundles disrupted by the accumulation of calcific deposits in the interfibrillar spaces (*left*), and collagen bundles that seem to control the accumulation of calcific deposits that form parallel arrays by following the longitudinal orientation of the collagen fibrils (*right*), from the inside of a day 100 of implantation sample.

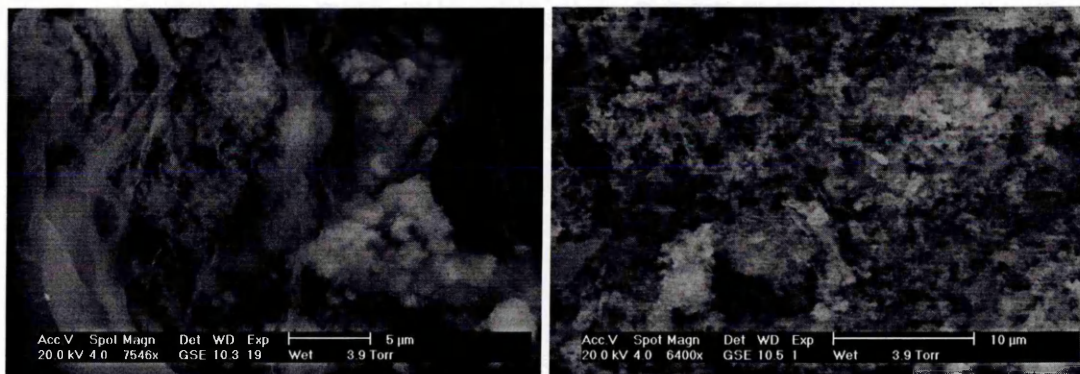


Figure 8.18: ESEM secondary electron micrographs corresponding to contour 2, showing calcific deposits (*left*) showing various morphologies (needle-like particles with a fluffy aspect and spherical nodules), and the morphology of highly crystalline hydroxyapatite standard (*right*) which appears essentially as a fluffy aspect composed of needle-like crystals, from the inside of a day 100 of implantation sample.

Contour 1: The accumulating calcific deposits are filling gaps between the collagen bundles (see figure 8.19). They eventually aggregate to such an extent that they cover the collagen matrix by forming a sort of “crust” (see figure 8.20), with a Ca/P

ratio of 1.692 (see figure 8.20), which is very close to that of crystalline hydroxyapatite.

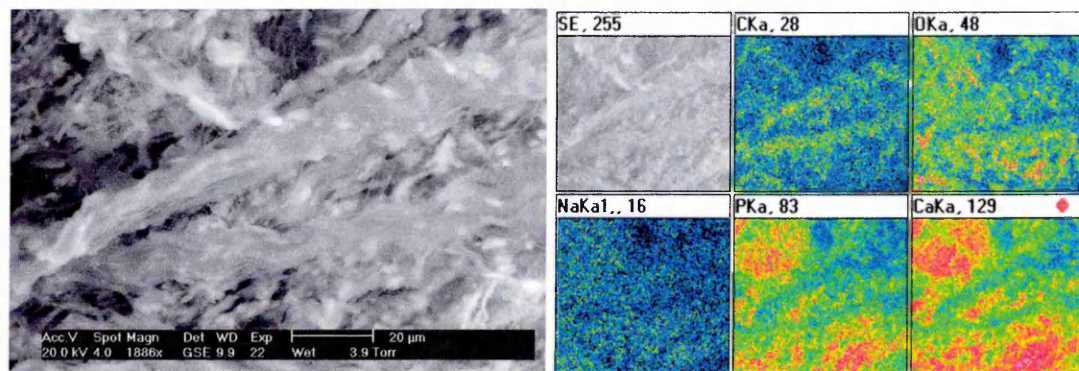


Figure 8.19: ESEM secondary electron image corresponding to contour 1 from the inside of a day 100 of implantation sample (*left*), showing accumulating calcific deposits between collagen bundles. Corresponding EDS mapping (*right*) shows collagen bundle, identified by their rich content in carbon, while the inorganic calcific deposits are richer in calcium, phosphorus and oxygen.

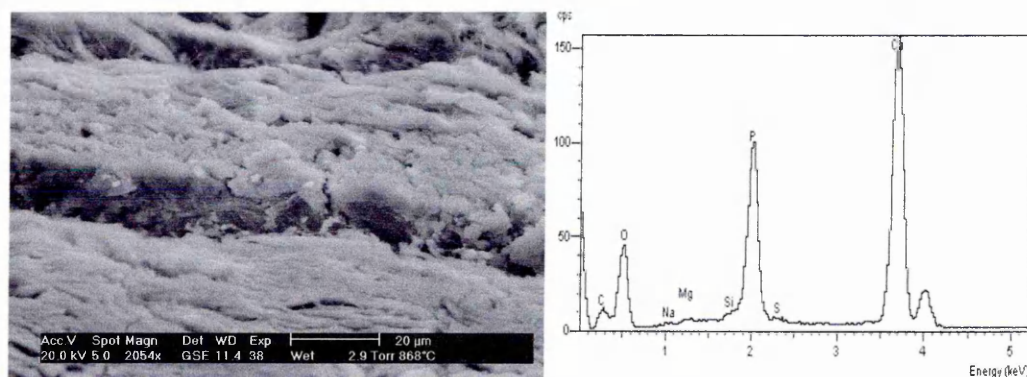


Figure 8.20: ESEM secondary electron micrograph (*left*) corresponding to contour 1, showing calcific deposits totally covering the collagen matrix from the inside of a day 100 of implantation sample. Corresponding EDS spectrum (*right*) shows the large presence of calcium and phosphorus with a Ca/P ratio of 1.692, which is very close to that of crystalline hydroxyapatite.

The observations from ESEM and EDS analyses (summary given in table 8.1) of a calcified glutaraldehyde-treated pericardium sample after 100 days of subcutaneous implantation revealed that mineralisation is not so heterogeneous after all, as generally held, and a pattern could be drawn from the data. These observations

specifically revealed the significant role of collagen in the orientation of calcific deposits, along with its potential role as being an important factor in the formation of early crystals. The presence of calcific deposits with various morphologies and different Ca/P ratios shows that calcification is a complex process involving many inorganic precursor phases that lead inevitably to a phase that resembles that of hydroxyapatite (similar morphology and Ca/P ratio).

8.3.2.2 In-vitro samples:

Calcific deposits were only found on the surface of the pericardial tissue subjected to the in-vitro experiment. Mavrilas et al²⁶ have previously studied in-vitro calcified porcine valve tissue (static in-vitro model) using SEM, reporting some evidence of calcific deposits on the surface and in the central region of the collagen tissue (mainly in fibrosa). The main difference in their static in-vitro set up was the fact that they used a computer-controlled pump to restore the consumed ions (potassium, sodium, calcium and phosphate) throughout the experiment, thus maintaining the initial physiological concentrations, which can have a great influence on the formation and propagation of Ca-rich deposits. The fact that in our study calcific crystals were essentially found on the external surface of the pericardial tissue leads to the conclusion that calcification in this type of static in-vitro model is essentially a deposition process and that calcification is intrinsic (i.e. it occurred selectively on the valve tissue, which is the same statement as Mavrilas et al from their in-vitro calcification study of porcine tissue valves).

No samples were analysed by ESEM prior to day 21 of the in-vitro experiment, except for the treated and untreated tissue samples (day 0) used as a reference.

8.3.2.2.1 Glutaraldehyde-treated pericardial tissue:

After incubation of the pericardial tissue with the calcifying solution for 21 days, ESEM-EDS analyses detected very thin accumulated crystals of a few microns (see figure 8.21 (*left*)) in association with collagen or aggregates of several microns in size (up to 5 μm) attached to collagen (see figure 8.21 (*right*) and figure 8.22). All were essentially rich in calcium with only weak traces of phosphorus from day 21 of implantation. This could lead to the hypothesis that the calcium is bound to some

negatively-charged components of the collagenous matrix, such as phospholipids (as proposed by Irving et al in a study of the mineralisation of cartilage²⁴.) Unfortunately, samples were not analysed prior to day 21 and hence one can only hypothesise that calcification started to occur before this time.



Figure 8.21: ESEM secondary electron micrographs, showing crystals of a few microns in size accumulating in association with collagen matrix (*left*) and calcific crystals clearly attached to the collagen matrix (*right*), from the analysis of the outside surface of a calcified glutaraldehyde-treated pericardial tissue sample after 21 days of incubation in-vitro.

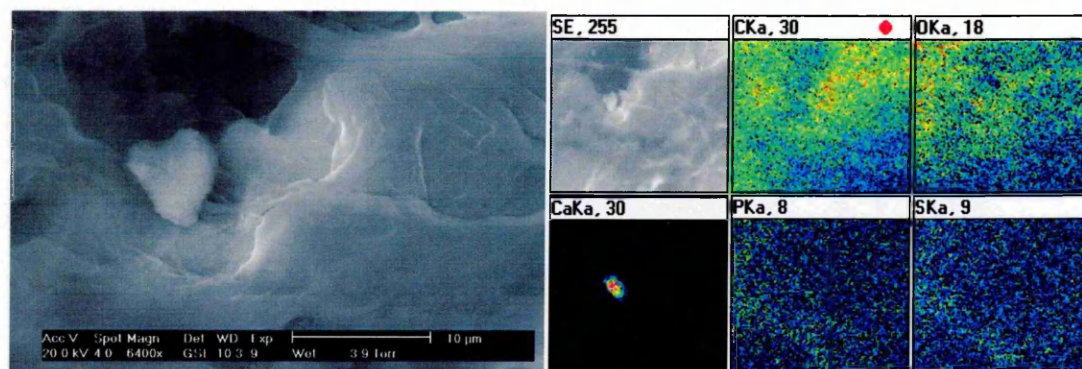


Figure 8.22: ESEM secondary electron micrograph from the analysis of the outside surface of a calcified glutaraldehyde-treated pericardial tissue sample after 21 days of incubation in-vitro, showing calcific crystals associated with the collagen matrix (*left*) and corresponding EDS mapping (*right*) showing collagen matrix rich in carbon and oxygen while the calcific deposits is richer in calcium.

At day 100, plate-like (see figure 8.23 (*left*)) and needle-shaped (see figure 8.23 (*right*)) aggregates were found on the tissue samples. These calcific deposits were

larger in size ($20\text{ }\mu\text{m}$) than those seen at day 21, but they were still characterised by a very high calcium content and very low phosphorus content (see figure 8.24). In addition, the samples exhibited calcium phosphate-rich particles growing along collagen and elastin (see figure 8.25), ranging in size from less than $1\text{ }\mu\text{m}$ up to $10\text{ }\mu\text{m}$, and showing uptake of potassium (see figure 8.24), probably from the calcification medium. This could indicate the growth of various unrelated phases or the presence of some crystal growth phases which eventually form an ultimate crystal phase containing essentially calcium and phosphate (as yet undetermined). The range of morphologies seen includes needle-like and plate-like crystal growth, sometimes with a sort of tabular hexagonal shape or even a fluffy aspect. All this suggests gradual development of the crystals through precursors towards a final phase. During the experiments, the vials were not opened and thus the content of calcium and other constituents of the medium have not been replenished. This may have impeded the crystals' growth and development. Nevertheless, the fact that after 100 days of incubation the deposits are richer in calcium than they are in phosphorus, may lead to the hypothesis that calcium deposition firstly involve the negatively-charged components of the organic matrix, followed by the progressive accumulation of phosphorus. Phosphoproteins, for example, have already been reported as being implicated in the calcification of glutaraldehyde-treated cardiac bioprostheses²⁷ and could possibly account for the observed phenomenon in this study.

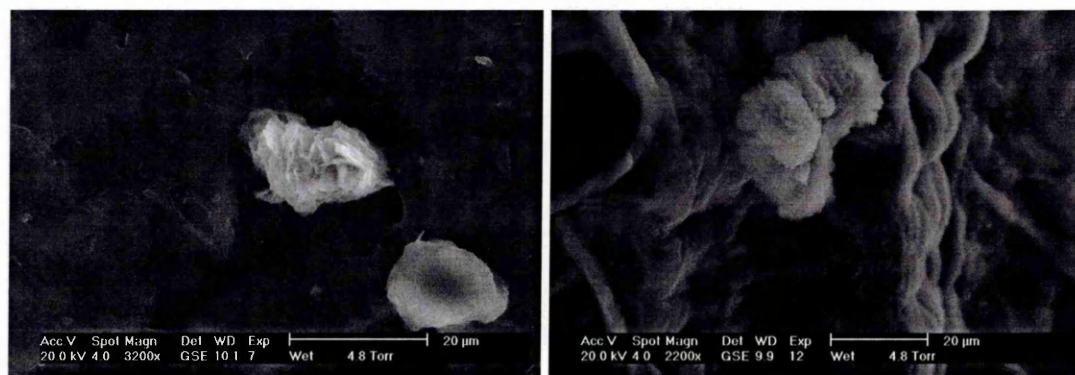


Figure 8.23: ESEM secondary electron micrographs, showing plate-like aggregated calcific crystals (aggregate of $20\text{ }\mu\text{m}$ in size) (*left*), and needle-shaped-like aggregated crystals (aggregate of $20\text{ }\mu\text{m}$ in size) (*right*), from the analysis of the outside surface of a calcified glutaraldehyde-treated pericardial tissue sample after 100 days of incubation in-vitro.

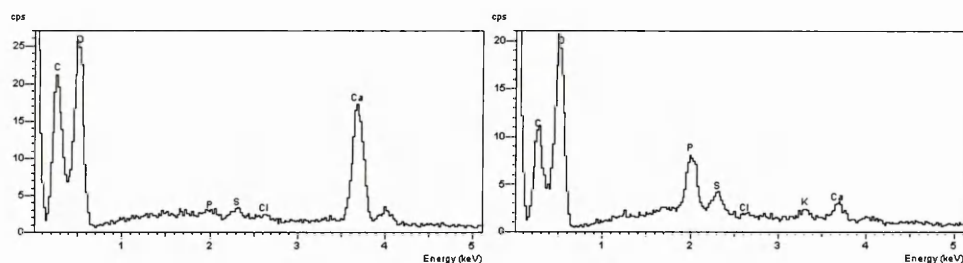


Figure 8.24: Typical EDS spectra from calcific crystals from the analysis of the outside surface of a calcified glutaraldehyde-treated pericardial tissue sample after 100 days of incubation in-vitro, showing the presence of various amounts of essentially Ca and P.

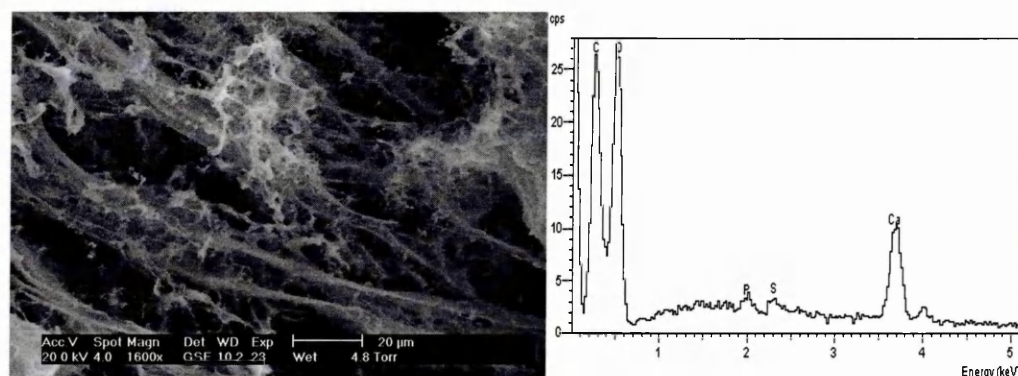


Figure 8.25: ESEM secondary electron micrograph (*left*), showing particles (from sub- μm up to $10\ \mu\text{m}$ in size) growing along collagen and larger fibrils (possibly elastin), from the analysis of the outside surface of a calcified glutaraldehyde-treated pericardial tissue sample after 100 days of incubation in-vitro. Corresponding EDS spectrum (*right*) shows the presence of calcium and phosphorus.

8.3.2.2.2 Untreated pericardial tissue:

Unexpectedly, untreated pericardial tissue incubated for 100 days in-vitro was found to calcify. This can be explained if one considers that the in-vitro calcification process involved here does not involve any host-immune response (see chapter 1 section 1.8.1.5) that would part of the generally observed in-vivo tissue degradation. It has indeed been reported that untreated valve tissue does not undergo calcification in the rat subdermal (in-vivo) model, but undergoes necrosis²⁸. Mineral growths of a micron in size were found all along collagen fibrils, sometimes forming large aggregates of $10\ \mu\text{m}$ in size (see figure 8.26 below). The elemental composition differed from one aggregate to another and the Ca/P ratio was not constant, probably reflecting the presence of amorphous calcium deposits. The EDS spectra did,

however, show some consistency, as they were rich in calcium and phosphorus, with traces of potassium and chlorine (see figure 8.27 below). The morphology of the crystal aggregates was comparable to that found with treated pericardial tissue at day 100. The larger crystals also exhibited morphology that had some similarities with that of some structures observed in the in-vivo model and explanted calcified valves (see chapter 7), although their elemental composition differed markedly. Calcium phosphate precipitation in-vitro is random in comparison to pathological calcification in-vivo and this may explain the observed differences between in-vitro calcification and the in-vivo calcification crystal phases.

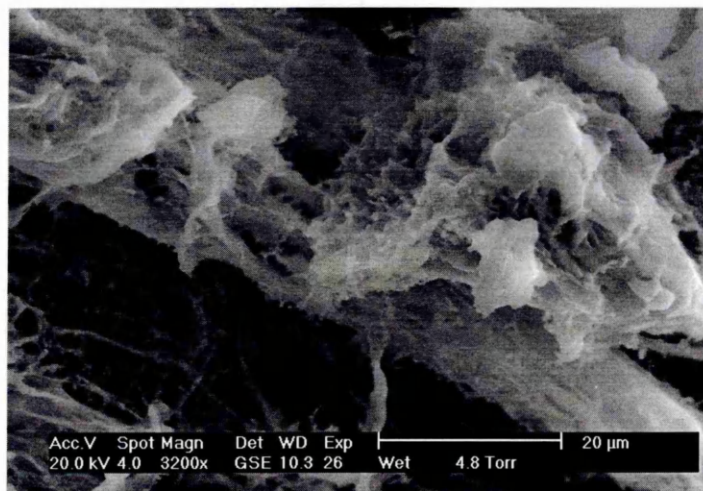


Figure 8.26: ESEM secondary electron micrograph, showing mineral growth along collagen bundles forming large aggregates up to 10 μm in size, from the analysis of the outside surface of a calcified untreated pericardial tissue sample after 100 days of incubation in-vitro.

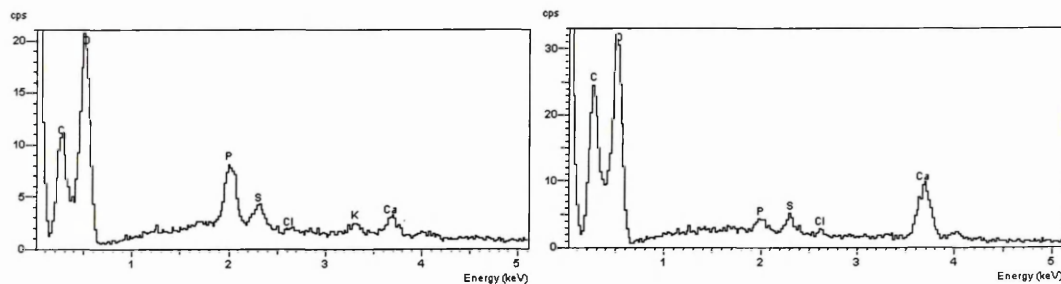


Figure 8.27: Typical EDS spectra from calcific crystals from the analysis of the outside surface of a calcified untreated pericardial tissue sample after 100 days of incubation in-vitro, showing the presence of various amounts of essentially Ca and P, along with traces of potassium and chlorine (the presence of C, O and S is attributed to the collagen matrix).

8.3.2.2.3 Comparison between *in-vitro* and *in-vivo* calcification studies:

ESEM micrographs of *in-vitro* calcified tissue showed the existence of different sizes of crystal phases, ranging from less than 1 μm up to 30 μm , in contact with collagen tissue fibres. The extent of calcification *in-vitro* was not comparable to that found *in-vivo* (rat subcutaneous model). Some studies¹⁷ already reported a poor correlation between the results of *in-vitro* and *in-vivo* calcification methods. Besides, whether mineral deposits obtained by *in-vitro* models are similar to the ones with *in-vivo* models is not particularly known. It should be emphasised also, that no *in-vitro* study up to now has reproduced the morphologies of both *in-vivo* and clinical explants.

However, with this *in-vitro* model, both untreated and glutaraldehyde-treated pericardial tissue were found to calcify. Although untreated pericardial tissue is reported not to calcify *in-vivo* but to be degraded by the host immune response, one can hypothesise that untreated collagen also has the capacity to calcify but that its degradation could be too fast *in-vivo* for calcification to be observed. All the above-presented results indicate that pericardial tissue can calcify *in-vitro* (static *in-vitro* model) but it does not involve the same process of calcification as *in-vivo*, although similar products might be formed subsequently.

There are many limitations to this *in-vitro* calcification model when compared to *in-vivo* conditions. The calcification is mostly restricted to the surface (see ESEM data in section 8.3.2.2 and histological results in section 8.3.4) and the available amount of calcium phosphate precipitated in the *in-vitro* system is limited. Furthermore calcification depends upon the initial working concentrations, while in contrast the body homeostasis generates unlimited amounts of calcium and phosphate. Although this static *in-vitro* system used in our study was reported to be highly reproducible²⁹, it does not seem to be of great value in mimicking the calcification behaviour of tissue bioprostheses since the morphology and composition of the calcific deposits was rather different from those in the *in-vivo* study. In previous studies, researchers who used a similar static *in-vitro* test methodology^{29,30}, considered the tissue to be calcified as long as calcium was detected by atomic absorption spectroscopy, even in small quantities. However, they made no comment on the morphology observed nor reported the full elemental composition, along with the Ca/P ratio, of their calcific

deposits. An alternative to the static in-vitro methodology used in this study would be to replace the calcification solution as often as possible so that the availability of calcium and phosphorus would be much higher than in our present study, although the outcome of such a procedure is unknown.

A possible advantage of in-vitro studies over in-vivo studies is the ability to study the early stages of the calcification process more easily. In-vivo studies generally quickly produce relatively heavily calcified material. However, in contrast to the in-vivo models, in-vitro models do not take into consideration the possible plasma insudation mechanism or the possible role of host immune response in calcification. Hence the early stages of calcification observed might not be representative of the true tissue calcification.

The validity of the static in-vitro model used in this study is therefore questioned, essentially because it does not produce a pathologic morphology of dystrophic calcification consistent with that seen in both circulatory models and clinical explants^{5,31}. Although static in-vitro test systems can be used to study large numbers of small samples of materials relatively quickly, they cannot give information regarding the response of the material to mechanical stress, unlike dynamic in-vitro test systems (see chapter 1 section 1.7.5.2). An improvement on the model may be the use of dynamic in-vitro testing. It is postulated that ESEM might be useful in such a study, which has been reported to reproduce successfully the calcification occurring in bioprostheses implanted in-vivo³².

8.3.2.2.4 Collagen structure:

A detailed structural assessment of pericardial tissue in its native state using ESEM has not yet been reported. Our studies of pericardial tissue, which is essentially made of collagen, revealed the following structural features. The pericardial tissue was composed of bundles of parallel collagen fibres, with a certain definite periodicity of the bundles. This is similar to reported findings by SEM examination³³ and to Normarski micrographs of wet collagenous tissue³⁴. In cross-section (see figure 8.11), the pericardial tissue used in this study was found to have around twenty clearly stacked collagen bundles, which were very well organised without any located area of surface voids. The two surfaces of the pericardium were easily differentiated: the smooth pericardium was characterised by parallel collagen

bundles, whilst the rough surface showed a random collagen structure without a definite pattern. Furthermore, while micrographs of untreated pericardium showed a “loose” collagen structure with a well-defined crimp and thicker elastin fibres, micrographs of glutaraldehyde cross-linked pericardium revealed a tightened crimp structure and a greater compactness of the collagen bundles into a ribbon-like morphology.

8.3.3 ICP-OES analysis

The digestion of untreated pericardial tissue was readily achieved in acid, however the complete digestion of glutaraldehyde-treated pericardial tissue was much more difficult. Although the samples were left in acid for 5 hours at boiling temperature, digestion was not complete and the solid remnants of the samples were removed by filtration before analysis. Such a procedure has recently been mentioned to be necessary when digesting glutaraldehyde-treated tissues³⁵.

8.3.3.1 In-vivo study:

The results obtained from the in-vivo study can be found in table 8.2 below. The maximum calcium content determined was 642 $\mu\text{g/g}$ of dry tissue in the day 100 sample. The calcium values found seem to be lower than the average reported by other authors³⁶. It is accepted, however, that calcification is affected by various host factors that can result in different values in each test. It is therefore important to compare results obtained using the same methodology and employing similar parameters (rat strain, age, sex, implantation place etc).

Implantation time/elements analysed	Silicon ($\mu\text{g/g}$ of tissue)	Magnesium ($\mu\text{g/g}$ of tissue)	Calcium ($\mu\text{g/g}$ of tissue)
Day 0	29.67	6.16	68.63
Day 7	18.84	11.16	317.28
Day 14	141.01	23.99	252.74
Day 28	200.51	34.80	254.59
Day 35	209.65	29.09	272.73
Day 100	242.90	26.46	642.08

Table 8.2: Implantation time in the rat model against elemental data from analyses (silicon, magnesium and calcium) by ICP-OES of glutaraldehyde-treated pericardial

tissue samples subdermally implanted in the rat model (number of samples that were averaged at each implantation time was n=6).

The correlation of the elements analysed was calculated and a two-tailed statistical test carried out for each pair of elements to be correlated. The corresponding results can be found in table 8.3 below.

Pair of elements to be correlated	r value (estimator of the population correlation coefficient)	t value (statistic for the test of significance for the correlation coefficients)	Conclusion of the statistic under the null hypothesis
Ca/Mg	0.7185	2.0661	poor evidence for correlation only at 10% level of significance
Ca/K	0.8641	3.4336	Poor evidence for correlation at 5% level of significance
Ca/Si	0.9087	4.3551	evidence for correlation at 2% level of significance
Mg/K	0.9295	5.0414	evidence for correlation at 1% level of significance
Mg/Si	0.9178	4.6235	evidence for correlation at 1% level of significance
Si/K	0.9736	8.5365	strong evidence for correlation at the 0.2% level of significance

Table 8.3: The correlation calculations of the elements analysed by ICP-OES from analyses (silicon, magnesium and calcium) of glutaraldehyde-treated pericardial tissue samples subdermally implanted in the rat model.

From these results, it appears that potassium is somehow strongly correlated to silicon, as is magnesium with potassium and silicon. This is similar to the results obtained for calcified heart valves (see chapter 7), where the silicon appeared to be correlated with magnesium. The data however do not suggest significant correlation between magnesium and calcium, as might have been expected. As only a small number of samples were considered in this statistical analysis, the data cannot be said to preclude the involvement of magnesium in the calcific precursors of tissue calcification. Further experiments, using many more samples, would have to be performed to obtain reliable statistical correlations.

8.3.3.2 In-vitro study:

The determination of calcium in the day 100 sample gave the following results: 141 $\mu\text{g/g}$ of dry tissue for the untreated pericardial tissue and 243 $\mu\text{g/g}$ of dry tissue for the glutaraldehyde-treated pericardial tissue. It is extremely difficult to compare our data with those from other studies because chemical analysis from other static in-vitro experiments are generally excluded²⁶ as the low mineral content of the tissues calcified in-vitro preclude accurate chemical analysis.

8.3.4 Light microscopy analysis

Histologic examination (Von Kossa staining) confirmed that all in-vitro test samples showed varying degrees of calcification, with intrinsic Von Kossa stain-positive deposits, and thus that the observed minerals formed in-vitro were calcium phosphate salts. This was in agreement with the ESEM-EDS data. The calcification was observed only on the outside/external surface of the in-vitro calcified pericardial tissue despite a long period of incubation. Because of the absence of any host immune response, no infiltration neither foreign body giant cells nor phagocytotic activity were observed with the in-vitro calcified tissue, as expected.

Although no histologic examination of in-vivo samples was carried out in this study, the presence of such infiltration, phagocytic activity and foreign body giant cells has been reported from the study of in-vivo calcified tissue^{26,37}. Additionally, light microscopy examinations of in-vivo calcified samples reported in the literature indicated that mineral deposits were found located in the centre of the implants³⁷. This is particularly interesting because this is in agreement with our study by ESEM-EDS.

8.3.5 XRD analysis

The limited quantities of sample and the low mineral content formed by nucleation and crystal growth in-vitro and in-vivo, resulted in insufficient material to be reliably analysed by X-ray diffraction methods. Therefore results from the in-vivo and in-vitro experiments were excluded.

8.4 Conclusion

In both in-vitro and in-vivo models, it was shown that calcification was intrinsic (i.e. it occurred selectively on the surface and inside of the in-vivo samples and on the surface of the tissue calcified in-vitro). This study also provided further evidence for the similarity of intrinsic calcific deposits in the rat models and in explanted valves (see chapter 7). However, the calcification obtained in the in-vitro model, although also observed as being intrinsic, is somehow different from in-vivo mineralisation (rat experiment or explants). Nevertheless, it is of interest that calcification can be induced in tissue even in the absence of cellular mechanisms and despite the lack of elements present in live biologic systems.

Overall, this study again demonstrated the broad ranging applicability of the ESEM technique, which allows investigation of wet, unstable biomaterials with minimal sample preparation.

1. Schoen FJ, Kujovich JL, Webb CL, Levy RJ. Chemically determined mineral content of explanted porcine aortic valve bioprostheses: correlation with radiographic assessment of calcification and clinical data. *Circulation*. 1987;76:1061-1066.
2. Glasmacher B, Deiwick M, Reul H, Knesch H, Keus D, Rau G. A new in-vitro test method for calcification of bioprosthetic heart valves. *The International Journal of Artificial Organs*. 1997;20:267-271.
3. Deiwick M, Glasmacher B, Zarubin AM, Reul H, Geiger A, Von Bally G. Quality control of bioprosthetic heart valves by means of holographic interferometry. *Journal of Heart Valve Disease*. 1996;5:441-447.
4. Schoen FJ, Golomb G, Levy RJ. Calcification of bioprosthetic heart valves: a perspective on models. *Journal of Heart Valve Disease*. 1992;1:110-114.
5. Schoen FJ, Levy RJ. Heart valve bioprostheses: antimineralisation. *European Journal of Cardiothoracic Surgery*. 1992;6:S91-S94.
6. Dewanjee MK, Solis E, Mackey ST, Lenker J, Edwards WD, Didisheim P. Quantification of regional platelet and calcium deposition on pericardial tissue valve prostheses in calves and effect of hydroxyethylene diphosphonate. *Journal of Thoracic and Cardiovascular Surgery*. 1986;92:337-348.
7. Fishbein MC, Levy RJ, Ferrans VJ, Dearden LC, Nashef A, Goodman AP, Carpentier A. Calcification of cardiac valve bioprostheses: biochemical, histological, and ultrastructural observations in a subcutaneous implantation model system. *Journal of Thoracic Cardiovascular Surgery*. 1982;83:602-609.
8. Levy RJ, Schoen FJ, Levy JT, Nelson AC, Howard SL, Oshry LJ. Biological determinants of dystrophic calcification and osteocalcin deposition in glutaraldehyde-preserved porcine aortic valve leaflets implanted subcutaneously in rats. *American Journal of Pathology*. 1983;113:143-155.
9. Schoen FJ, Levy RJ. Bioprosthetic heart valve failure: pathology and pathogenesis. *Cardiology Clinics*. 1984;2:717-739.
10. Wadkins CL, Luben RA. Effects of fluoride on in-vitro calcification of tendon matrix. *Calcified Tissue Research*. 1978;26:51-59.

11. Bernacca GM. Calcification in pericardial and polyurethane biomaterials used to fabricate prosthetic heart valve leaflets. In: PhD Thesis. Glasgow: University of Strathclyde; 1991.
12. Schoen FJ, Tsao JW, Levy RJ. Calcification of bovine pericardium used in cardiac valve bioprostheses. Implications for the mechanism of bioprosthetic tissue mineralisation. *American Journal of Pathology*. 1986;123:134-145.
13. Schoen FJ, Levy RJ. Tissue heart valves: current challenges and future research perspectives. *Journal of Biomedical Materials Research*. 1999;47:439-465.
14. Mako WJ, Shah A, Vesely I. Mineralisation of glutaraldehyde-fixed porcine aortic valve cusps in the subcutaneous rat model: analysis of variations in implant site and cuspal quadrants. *Journal of Biomedical Materials Research*. 1999;45:209-213.
15. Bock P. In: *Romeis-MikroKopische Technik*. Wien-Munchen-Baltimore: Urban and Schwarzenberg; 1989.
16. In: Sheenan DC, Hrapchak BB, eds. *Theory and Practice of Histotechnology*. Detroit: Lipshaw; 1980:227.
17. Tingfei X, Jiazhen M, Wenhua T, Xuehui L, Shuhui L, Baoshu X. Prevention of tissue calcification on bioprosthetic heart valve by using epoxy compounds: a study of calcification tests in-vitro and in-vivo. *Journal of Biomedical Materials Research*. 1992;26:1241-1251.
18. Sherman FS, Schoen FJ, Hawley MA, Nichols J, Levy RJ. Collagen crosslinks: a critical determinant of bioprosthetic heart valve calcification. *American Society Artificial Internal Organs Transaction*. 1984;30:577-581.
19. Rude RK, Singer FR. Magnesium deficiency and excess. *Revistica de Medicina/Revistica Medica*. 1981;32:245-259.
20. Nagano M, Nakamura T, Kokubo T, Tanashi M, Ogawa M. Differences of bone bonding ability and degradation behaviour in-vivo between amorphous calcium phosphate and highly crystalline hydroxyapatite coating. *Biomaterials*. 1996;17:1771-1777.
21. Suh H, Hwang YS, Park JC, Cho BK. Calcification of leaflets from porcine aortic valves cross-linked by ultraviolet irradiation. *Artificial Organs*. 2000;24:555-563.
22. Koutsoukos PG. In: Amjad Z, ed. *Calcium Phosphates in Biological and Industrial Systems*. Boston: Kluwer Academic Publishers; 1998:145-171.
23. Cheng PT. Formation of octacalcium phosphate and subsequent transformation to hydroxyapatite at low supersaturation: a model for cartilage calcification. *Calcified Tissue International*. 1987;40:339-343.
24. Irving JT, Wuthier RE. Histochemistry and biochemistry of calcification with special reference to the role of lipids. *Clinical Orthopaedics*. 1968;56:237-260.
25. Tomazic BB, Chow LC, Carey CM, Shapiro AJ. An in-vitro diffusion model for the study of calcification of bovine pericardium tissue. *Journal of Pharmaceutical Sciences*. 1997;86:1432-1438.
26. Mavrilas D, Apostolaki A, Kapolos J, Koutsoukos PG, Melachrinou M, Zolota V, Dougenis D. Development of bioprosthetic heart valve calcification in-vitro and in animal models: morphology and composition. *Journal of Crystal Growth*. 1999;205:554-562.
27. Gura TA, Wright KL, Veis A, Webb CL. Identification of specific calcium binding noncollagenous proteins associated with glutaraldehyde preserved bovine pericardium in the rat subdermal model. *Journal of Biomedical Materials Research*. 1997;35:483-495.
28. Webb CL, Schoen FJ, Levy RJ. Covalent binding of aminopropanehydroxydiphosphonate to glutaraldehyde residues in pericardial bioprosthetic tissue: stability and calcification inhibition studies. *Experimental and Molecular Pathology*. 1989;50:291-302.
29. Mako WJ, Vesely I. In-vivo and in-vitro models of calcification in porcine aortic valve cusps. *Journal of Heart Valve Disease*. 1997;6:316-323.
30. Bernacca GM, Mackay TG, Wheatley DJ. In-vitro calcification of bioprosthetic heart valves: report of a novel method and review of the biochemical factors involved. *Journal of Heart Valve Disease*. 1992;1:115-130.
31. Schoen FJ, Hirsch D, Bianco RW, Levy RJ. Onset and progression of calcification in porcine aortic bioprosthetic valves implanted as orthotopic mitral valve replacements in juvenile sheep. *Journal of Thoracic Cardiovascular Surgery*. 1994;108:880-887.
32. Pettenazzo E, Deiwick M, Thiene G, Molin G, Glasmacher B, Martignano F, Bottio T, Reul H, Valente M. Dynamic in-vitro calcification of bioprosthetic porcine valves: evidence of apatite crystallisation. *Journal of Thoracic Cardiovascular Surgery*. 2001;121:500-508.
33. Datta D, Kundu PK, Bandyopadhyay BN. Bioprosthetic heart valves-replacing order with chaos: electron microscopic study. *Artificial Organs*. 1999;23:372-376.

34. Broom ND, Thomson FJ. Influence of fixation conditions on the performance of glutaraldehyde-treated porcine aortic valves: towards a more scientific basis. *Thorax*. 1979;34:166-176.
35. Suh H, Park JC. Evaluation of calcification in porcine valves treated by ultraviolet ray and glutaraldehyde. *Materials Science and Engineering C*. 2000;13:65-73.
36. Schoen FJ, Levy RJ. Pathophysiology of bioprosthetic heart valve calcification in biologic and bioprosthetic valves. In: Bodnar E, Yacoub M, eds. *Biologic and Bioprosthetic Valves*. New York: Yorke Medical Books; 1986:418-429.
37. Grabenwoger M, Grimm M, Eybl E, Leukauf C, Muller MM, Plenck HJ, Bock P. Decreased tissue reaction to bioprosthetic heart valve material after L-glutamic acid treatment: a morphological study. *Journal of Biomedical Materials Research*. 1992;26:1231-1240.

Chapter 9

9 General conclusion and suggested future work.

9.1 General Conclusion

Little is known of the mechanism of pathological calcification which leads to the failure of bioprosthetic heart valves and, until this is rectified, strategies for its prevention will remain elusive. Unfortunately, valve companies and research groups receiving commercial sponsorship are governed by strict codes of commercial confidentiality. These limit the release of information into the public domain. Without free access to the results of all relevant research, progress is greatly hindered. This is reflected in the fact that, to date, there have been no clear reports of the factors influencing the valves pathological calcification, no consensus on the chemistry behind the cross-linking process and no proven successful anticalcification treatments developed.

The deterioration of collagenous tissue used in clinical devices must be prevented and hence there is a need to stabilise it by glutaraldehyde cross-linking. However, glutaraldehyde (the chemical used to treat all commercially available bioprosthetic valves) has been cited as being likely to be implicated in the process of their failure and calcification. In addition, naturally occurring cross-links break down during implantation. Failures of bioprosthetic heart valves are thus mostly due either to structural and mechanical degeneration or to calcification.

In structural and mechanical degeneration, the chemical cross-linking might not be sufficient or chemical bonds, created through the cross-linking process, may break up with time in-vivo. Glutaraldehyde-treated bioprostheses are known to slowly release glutaraldehyde over time (see chapter 1 section 1.7.2), possibly by the partial hydrolytic degradation and reversibility of some cross-links (for example, Schiff

bases possess a N=CH group which represents a hydrolysis-sensitive site). The degradation of these cross-links can cause a lack of structural and mechanical integrity, which in turn can be responsible for failure of the valves. In the process of calcification, it is thought that free carbonyl groups of the molecules resulting from the cross-linking process can be oxidised in-vivo to carboxyl groups (see chapter 1 and 6). These, may have the ability to bind host plasma calcium and contribute toward initiating calcification during implantation. Also, the hypothesis that the slow release of glutaraldehyde within tissue may be a potential initiator for calcification is supported by the fact that mineralisation is prevented by the use of binding agents that react with residual or free glutaraldehyde moieties. Additionally, many reports have suggested a role for aldehyde-induced cross-links in initiating tissue mineralisation (see chapter 1 and 6). For example, quaternary pyridinium-type cross-links found in both elastin and collagen are thought to serve as a nucleation point for calcification, while cyclic cross-links (dipyridine structure) have been suggested to account for the high stability of the cross-links as well as being possibly involved in the calcification of glutaraldehyde-treated collagen.

Despite its wide use in many commercial applications, including manufacturing of bioprostheses, the chemistry of glutaraldehyde remains to be fully elucidated. An understanding of the interactions between glutaraldehyde and tissue is essential if we are to comprehend why bioprostheses calcify and ultimately fail. This represents the main aim of this thesis.

Many studies have investigated the reactions of glutaraldehyde with a range of model compounds, from the simplest amino acids to complex collagenous tissue (see chapter 2 section 2.2.4). A number of structures have been proposed for reactions products (see chapter 2 and appendices III and IV) but at present there is no definitive understanding of the processes that take place. Many contradictions can be found in the literature regarding the nature of glutaraldehyde in solution and also the nature of the products of the reactions between proteins and glutaraldehyde. An earlier study by colleagues within this research group, investigating the cross-linking of valve tissue by glutaraldehyde, showed promise. They subjected the reaction products of 6-amino-n-caproic acid and glutaraldehyde to analysis by electrospray ionisation-mass spectrometry (ESI-MS) and successfully characterised ten molecular structures that had previously been reported by others using different techniques.

This previous study was the starting point for the present thesis since the application of mass spectrometry along with other analytical techniques was expected to produce data that would lead to a better comprehension of the cross-linking process of valve tissue by glutaraldehyde.

Initially, methodology was developed to analyse glutaraldehyde solutions at various pH values by mass spectrometry, nuclear magnetic resonance, infrared and Raman spectroscopy (see chapter 4). This methodology was first used to determine the presence and nature of other molecular structures of glutaraldehyde than those already reported in the literature. Consideration of the theoretical chemistry that can take place under the conditions of analysis was used in the elucidation of possible structures. A summary of these findings can be found in appendix III.

The methodology was then used to determine the structures of species present in glutaraldehyde-treated tissue (see chapter 5). The reactions between glutaraldehyde and amines, peptides and proteins were investigated in order to determine possible molecular structures of the reaction products and to extrapolate these to those occurring during the glutaraldehyde-treatment of bioprosthetic valves. Twenty nine stable mono-bound structures along with twenty five stable multi-bound (cross-linking) entities, including anabilysine-like compounds (the only stable cross-linking entity reported so far in the literature) were determined. All these structures were in agreement with the theoretical chemistry that takes place under the conditions of analysis (Schiff base formation, aldol, aldol-type, Mannich-type, Michael and Michael-type additions). A summary of results can be found in appendix IV. In addition to the stable structures, other less-stable chemical entities were also characterised. It was hypothesised that these could play a role in the tissue failure of bioprostheses (probably via in-vivo degradation of cross-linked tissue). All the chemical structures determined may also have a potential role in the initiation of mineralisation due to the presence of many free pendant electronegative groups.

These hypotheses prompted an investigation of the potential of glutaraldehyde, along with its oxidised form (di-acid, glutaric acid), to initiate mineralisation by complexing ions such as calcium (see chapter 6). A similar investigation dealt with the possible uptake of calcium (calcification) by amino acids and other molecules that can mimic the behaviour of collagenous tissue (see chapter 6 and appendix I).

Glutaraldehyde and glutaric acid have thus been shown to have the potential to induce mineralisation by attracting cations (potentially calcium) from a metastable calcifying solution, although the two compounds seemed to behave differently. Model compounds not reacted with glutaraldehyde were also shown to bind calcium, probably via the carbonyl oxygen atoms of their backbones.

It is ironic that the glutaraldehyde treatment itself, presently used in commercial valve processing, might be an initiator of calcification. Results from the analysis of glutaraldehyde and glutaric acid demonstrated a strong potential for their involvement in the mineralisation process of glutaraldehyde-treated tissues. The ability of glutaraldehyde to cross-link is thus unfortunately opposed to its potential to intrinsically facilitate tissue mineralisation, which was demonstrated in-vitro by this study. Overall, the data bring forward some new insights into the hypothetical primary processes of mineralisation of tissue. The data may also help to explain the involvement of glutaraldehyde and tissue factors in the calcification process of valve bioprostheses.

In an attempt to gain a better understanding of the mineralisation process of bioprosthetic heart valves, the next step was to analyse calcified heart valve tissue. The objectives of the first part of this study were to develop methodology to investigate heart valve tissue and associated calcification in its natural state, using environmental scanning electron microscopy (ESEM) and to comment on future applications of ESEM in tissue bioprostheses research (see chapter 7). ESEM was found to allow the imaging of hydrated heart valve bioprostheses with minimal manipulation and without the need for conducting coatings. It is thought that ESEM will be useful in the study of new tissue-engineered heart valves. It may also play an important role in further developing our understanding of the calcification of heart valve bioprostheses.

Energy dispersive X-ray analysis (EDS coupled to the ESEM), X-ray diffraction (XRD), Fourier-transform infrared (FTIR) and Raman spectroscopy were used to characterise the various calcific deposits observed with ESEM, while the major elements present in calcified valves were analysed by inductively coupled plasma-optical emission spectroscopy (ICP-OES). The calcific crystals observed by ESEM were found attached to dense collagen bundles, following their orientation

throughout the tissue and within the fibrils, and possibly also attached to elastin. The role of elastin in heart valves has been largely ignored in the past due to its low content. However, the importance of elastin (even when present as a minor component) in proper mechanical function indicates that any disruption of elastin through disease or other means could be the reason for mechanical failure of a valve. Thus the potential mineralisation of elastin could play a significant role in the failure of these valves and it has already been demonstrated in the literature that elastin fibres might be the principal site of calcification of biological vascular grafts when implanted in animals. Additionally, these results suggest the potential role that collagen can play in valve mineralisation. Furthermore, although not reported, it is conceivable that similarly to collagen, the natural cross-linking of elastin may be strengthened by the glutaraldehyde cross-linking process and that the new cross-linking entities would be involved in the mineralisation process.

The likelihood of involvement of the tissue factor in the mineralisation of bioprosthetic heart valves is thus strongly believed by our group. However, no conclusive evidence for this was found in this work from a study of glutaraldehyde-treated model compounds by infrared (FTIR-ATR) spectroscopy. It has not been possible to identify interactions of the amino or carbonyl/carboxyl groups of the molecules backbones as binding sites for phosphate and calcium respectively. Yet, since the attraction of calcium by both glutaraldehyde and model compounds on their own was observed using infrared spectroscopy, it can be strongly hypothesised that glutaraldehyde-treated model compounds would behave similarly. After all, it has already been reported that collagen has potential calcium-binding sites and therefore may have a natural tendency to calcify, while elastin has been reported as a predominant site of calcification in aortic tissue (see chapters 1 and 6, sections 1.7.2 and 6.1 respectively).

From a study of human explanted calcified valve tissue by ESEM, two main patterns of organisation of calcific deposits were observed: spherical aggregates (1-10 μm) found along collagen fibrils and in inter-fibrillar spaces, and needle-like crystal structures (sub-micron, micron scale). EDS microanalysis identified the crystals observed by ESEM as salts containing mainly calcium and phosphate with Ca/P ratios varying from 1.340 (possibly octacalcium phosphate (OCP), which has a Ca/P ratio of 1.336) to 2.045 (possibly hydroxyapatite (HAP) with incorporation of

carbonate and metal ion contaminants, such as silicon and magnesium, in the crystal lattice). The presence of peaks attributable to silicon and magnesium in the EDS spectra confirmed this view and raised the possibility of the presence of precursor phases associated with the embryonic stages of calcification. The crystalline calcium phosphate salts found on heavily calcified valves had a mean Ca/P ratio of 1.676, which is very close to crystalline hydroxyapatite with a Ca/P ratio of 1.670. XRD patterns from these same calcium deposits showed a poorly crystalline hydroxyapatite-like pattern. Raman and FTIR spectroscopy also identified the presence of carbonate and the analyses showed spectral features very similar to a crystalline hydroxyapatite spectrum, thus refuting the presence of precursor phases such as β -tricalcium phosphate (β -TCP), OCP and dicalcium phosphate dihydrate (DCPD) at this stage in the calcification. However, it is still possible that these precursor mineral phases might have been formed but transformed too quickly into other phases to be detected by these techniques.

Other researchers have stated that there is no evidence for the presence of a precursor phase in calcific deposits with only apatite, as the single mineral component being observed. Additionally, the initiation site of valve mineralisation has not been established conclusively. Thus, the final section of this work (see chapter 8) investigated the calcification obtained in a static in-vitro model and compared it with that produced in-vivo (subcutaneous animal model) and with human explanted calcified valves, using the ESEM methodology previously developed. Explanted samples are generally extensively calcified and hence do not easily allow the determination of any possible precursor phases. Thus the use of in-vivo and in-vitro models was investigated to study the precursor phases of calcification.

A picture of the onset of tissue mineralisation in-vivo was hypothesised involving precursors containing various amounts of calcium and phosphate, along with silicon and magnesium. These evolved with the time of implantation, to a poorly crystalline form of hydroxyapatite (as found in late stage calcification of both in-vivo samples and explanted valves). Calcific deposits in the static in-vitro model were however mostly composed of calcium associated with low levels of phosphorus and often potassium. It therefore appears that in-vitro calcific deposits are not the same as those found in-vivo and from explants, bringing into question the reliability of the static in-vitro model.

This work has advanced our understanding of relevant potential factors associated with mineralisation and failure of bioprosthetic implants. There are still many areas that require a thorough investigation and it is hoped that the work presented in this thesis will bring new insights for future studies of both the cross-linking and calcification of bioprosthetic heart valves.

9.2 Suggested Future Work

The following represents some general ideas for future work continuing from the present thesis. The investigations proposed are believed to either involve new applications of the techniques or to potentially bring new insights into aspects of this study.

9.2.1 High Performance Liquid Chromatography-Matrix Assisted Laser Desorption Ionisation Mass Spectrometry (HPLC-MALDI MS)

Another approach to the analysis of the reaction products formed between glutaraldehyde and various model compounds would be to separate the reaction products by reverse-phase HPLC, collect sample fractions and then analyse the latter by MALDI-TOF MS. The early phases of this work, including some analysis of fractions by MALDI-TOF MS, has been achieved¹. The HPLC separation achieved was far from being optimal and much work is still required. It is thought that once a reproducible separation is achieved, the collected fractions could be concentrated by freeze-drying and then analysed by techniques such as FTIR and NMR spectroscopy, as well as mass spectrometry. Preliminary analyses of freeze-dried fractions using NMR proved unsuccessful due to the inherent insensitivity of the technique². Hence further work would also be required to ensure samples of adequate concentration were available.

9.2.2 Atomic Force Microscopy (AFM)

Since its invention in 1986³, AFM has evolved as a valuable imaging technique with a spatial resolution in the micrometre to subnanometre region. This could be of great value when analysing collagen films and tissues. In AFM, a sharp probe is attached

to a cantilever spring, which is scanned in close proximity to a sample surface. During scanning (or imaging), the cantilever is deflected by forces acting between the surface and the probe. AFM employs probes with a tip to produce contact areas of ca. 10 nm^2 . AFM can be also used to measure Van der Waals and electrostatic forces⁴. To produce an image, the deflections are monitored with respect to its lateral position on the sample⁵. However, care must be taken when analysing non-flat topographical samples (such as valve collagenous tissues), although some methods do exist to allow this type of analysis.

It is thought that AFM analysis could provide details about the surface topography and variations in chemical composition across glutaraldehyde-treated collagen surfaces. As an example, this would be particularly useful for mapping specific sites on a tissue surface, such as COO^- , that are thought to be involved in calcification (see chapter 6). The detection of such functional groups by AFM has been reported⁶. Carboxylic acid groups have also been covalently bound to the probe tip, which was scanned across a surface having various organic functional groups. The differences in frictional forces, between the acid groups on the tip and the surface of the sample, result in a map of the distribution of surface functional groups. The surface morphology of apatite film (calcific deposits found within calcified tissue are apatitic in nature) has also been reported using AFM⁷. It may be possible therefore to study valve calcification using AFM and it might also be particularly useful perhaps for the investigation of the very early stages of calcification or even initiation of mineralisation.

9.2.3 Scanning Tunnelling Microscopy (STM)

The use of STM to study the surface defects of heart valve bioprostheses has been reported⁸. It was used to prove the hypothesis that surface imperfections (such as surface defects or sub-surface voids) may serve as preferred sites for initiating the calcification process, as proposed for smooth polymer surfaces⁹⁻¹¹. Lee found that calcification in explanted valves was always associated with surface defects and proposed that calcification could be a result of the increased development of these surface defects, which would cause the subsequent insudation of plasma constituents and then the interaction of calcium. These constituents and the valve structure may

aid the initiation of calcification. Only “first-generation” valves (those fixed at high pressure were more prone to mechanical surface damages, in comparison to the low-pressure fixation process of the “second-generation” cardiac bioprotheses actually on the market) have been previously analysed. No data have yet been reported for the analysis of “second-generation” valves or newly tissue-engineered cardiac valves that can be considered as “third generation” valves. It is thus thought that using STM to study “second generation” bioprotheses or tissue-engineered valves may increase our understanding of the calcification process. A major difficulty when using STM, however, is the requirement that the sample surface being examined must conduct electricity.

Scanning tunnelling microscopy has also been used in the investigation of a chemical reaction involving glutaraldehyde on a nanometre scale¹². Heckl and Smith have studied the effect of a high electric field and a high current density between the STM tip and glutaraldehyde molecules covering a graphite surface, during a short voltage pulse. They reported that the resulting energy polymerised monomers of glutaraldehyde to oligomers ranging from about 5 to 15 monomeric glutaraldehyde units in size. It is thought that further work in this area might prove beneficial, since there are some doubts regarding their theory of polymerisation because commercial unbuffered glutaraldehyde solution has been shown to contain some (see chapters 2 and 4). It is possible, however, that energy in the form of heat might have accelerated and increased polymerisation of the glutaraldehyde.

9.2.4 Circular Dichroism (CD)

The use of circular dichroism in the study of metal ion binding (aluminium and calcium) on α -elastin has been reported¹³. However the application of this technique to collagen has not. It is thought that a similar study of the interaction of calcium ions and collagen could prove useful.

9.2.5 X-ray Photoelectron Spectroscopy

The study of hydroxyapatite-collagen nanocomposites cross-linked with glutaraldehyde has been recently reported¹⁴. They confirmed the covalent bond

formation between Ca^{2+} of hydroxyapatite and RCOO^- of collagen molecule, along with the assessment for bridge formation between collagen fibers. It is believed that the use of XPS for investigating bond formation between Ca^{2+} and carbonyl groups of glutaraldehyde and or of glutaraldehyde treated proteins could be carried out in a similar manner.

9.2.6 Time of Flight Secondary Ion Mass Spectrometry (TOF-SIMS)

Static secondary ion mass spectrometry (SSIMS) employs very low intensity primary ion or fast atom beams to sputter the top monolayer of a surface¹⁵. The secondary ions produced under static SIMS conditions are elemental or molecular in nature and are characteristic of the near-surface composition. Detection in the ppm-ppb region can be achieved with this technique. The advantage of such a method would be the direct analysis of solid surfaces (such as collagen or polylysine films, reacted or not with glutaraldehyde) with good sensitivity for high molecular weight species. This is thought to be possible since the study of a number of biomaterials, drugs and protein systems using this technique has been reported¹⁶. The data obtained might be correlated to the mass spectrometry results obtained from model compounds reacted with glutaraldehyde, as described in chapter 5. Furthermore, in the context of biological tissue imaging, SIMS has been used to map heterogeneous cation distribution and other secondary ions at the cellular level¹⁷. It would therefore be of interest to apply similar methodology to the study of calcified valve tissues. Samples might be analysed directly following freeze-drying, or they could be prepared in a solid organic matrix (2,5-dihydroxybenzoic acid) similar to the sample preparation used in MALDI (see chapters 4 and 5). Such a preparation technique was reported to provide a general enhancement of molecular secondary ions emitted from analyte/matrix mixtures when peptides, proteins and nucleic acids were analysed by TOF-SIMS¹⁸.

9.2.7 Surface Enhanced Raman Spectroscopy (SERS)

The Raman analysis of the reaction of glutaraldehyde and model compounds in solution was very difficult for two major reasons. Firstly, the low concentrations of

the compounds used produced spectra that were not intense enough to allow proper spectral interpretation. Secondly, the level of fluorescence was too great.

A solution could be to mix the aqueous reacted solutions with silver colloids that would generate an interaction between the sample and the silver colloids electron waves (plasmon) thus increasing considerably the intensity of the Raman signal (this is essentially the SERS technique). Additionally, the fluorescent background associated with Raman spectroscopy is decreased in SERS. Additionally, the coupling of thin layer chromatography with spectroscopic techniques such as surface enhanced resonance Raman spectroscopy (SERRS) or even Fourier-transform infrared (FTIR) may provide useful information. The possibility of coupling such spectroscopic techniques with this form of chromatography has been previously reported^{19,20}.

1. Dalle A. Development of a range of chromatographic methods for the separation of the reaction products of glutaraldehyde and various small peptides. In. Sheffield: Final Year Project Report Sheffield Hallam University; 2000.
2. Nordon A, McGill CA, Littlejohn D. Process NMR spectrometry. *The Analyst*. 2001;126:260-272.
3. Binnig G, Quate CF, Gerber C. Atomic force microscope. *Physical Review. Letters*. 1986;56:930-933.
4. Butt HJ. Measuring electrostatic, van der Waals, and hydration forces in electrolyte-solutions with an atomic force microscope. *Biophysical Journal*. 1991;60:1438-1444.
5. Allen S, Davies MC, Roberts CJ, Tendler SJB, Williams PM. Atomic force microscopy in analytical biotechnology. *Trends in Biotechnology*. 1997;15:101-105.
6. Frisbie CD, Rozsnyai LF, Noy A, Wrighton MS, Lieber CM. Functional-group imaging by chemical force microscopy. *Science*. 1994;265:2071-2074.
7. Antonov EN, Bagratashvili VN, Popov VK, Sobol EN, Davies MC, Tendler SJB, Roberts CJ, Howdle SM. Atomic force microscopic study of the surface morphology of apatite films deposited by pulsed laser ablation. *Biomaterials*. 1997;18:1043-1049.
8. Lee YS. Calcification of porcine bioprosthesis implanted into human heart: high resolution scanning electron microscopic and scanning tunnelling microscopic investigation. *Journal of Electron Microscopy*. 1994;43:131-140.
9. Schoen FJ, Harasaki H, Kim KM, Anderson C, Levy RJ. Biomaterials-associated calcification: pathology, mechanisms, and strategies for prevention. *Journal of Biomedical Materials Research: Applied Biomaterials*. 1988;22:11-36.
10. Thoma RJ, Philips RE. Calcification of poly(ether)urethanes. *Transactions of the Society of Biomaterials*. 1987;10:245.
11. Coleman D. Mineralisation of blood pump bladders. *American Society Artificial Internal Organs Transaction*. 1981;27:708-713.
12. Heckl WM, Smith DPE. Electropolymerisation of glutaraldehyde observed by scanning tunnelling microscopy and its applications for scanning tunnelling microscopy imaging of organic material. *Journal of Vacuum Science and Technology B. Microelectronics Processing and Phenomena*. 1991;9:1159-1161.
13. Vyavahare N, Ogle M, Schoen FJ, Levy RJ. Elastin calcification and its prevention with aluminium chloride pre-treatment. *American Journal of Pathology*. 1999;155:973-982.
14. Chang MC, Tanaka J. XPS study for the microstructure development of hydroxyapatite-collagen nanocomposites cross-linked using glutaraldehyde. *Biomaterials*. 2002;23:3879-3885.

- Chapter 7
15. Vickerman JC, Brown A, Reed NM. In: *Secondary Ion Mass Spectrometry: Principles and Applications*. Oxford: Clarendon Press; 1989.
 16. Todd PJ, McMahon JM, Short RT, McCandish CA. Organic SIMS of biological tissue. *Analytical Chemistry News and Features*. 1997;Sept.:529A-535A.
 17. In: Clark RJH, Hester RE, eds. *Advances in Spectroscopy. Spectroscopy for Surface Science*. Chichester: Wiley; 1998:71-120.
 18. Wu KJ, Odom RW. Matrix-enhanced secondary ion mass spectrometry: a method for molecular analysis of solid surfaces. *Analytical Chemistry*. 1996;68:873-882.
 19. Somsen GW, Morden W, Wilson ID. Review: planar chromatography coupled with spectroscopic technique. *Journal of Chromatography A*. 1995;703:613-665.
 20. Somsen GW, Coulter SK, Gooijer C, Velthorst NH, Brinkham UAT. Coupling of column liquid chromatography and surface-enhanced Raman spectroscopy via a thin-layer chromatographic plate. *Analytica Chimica Acta*. 1997;349:189-197.

Appendix I

A.1 Investigation of the in-vitro calcification potential of type I collagen films by FTIR microscopy.

1.1 Introduction

It has been demonstrated that the formation of hydroxyapatite crystals from slightly undersaturated, metastable calcium phosphate solutions can be catalysed by reconstituted collagen fibres, tendons and skin^{1,2}. Subsequently, it has also been shown that beef tendon matrix will catalyse the formation of a matrix-bound form of calcium phosphate from solutions of calcium and phosphate ions with a solubility product lower than that of normal serum³⁻⁶. Moreover, collagen was later reported to be the most important site for the calcification of cardiac bioprostheses⁷. Study of the in-vitro calcification of glutaraldehyde, model compounds (mimicking the amino residues of collagenous tissue) and glutaraldehyde-treated model compounds by FTIR spectroscopy (see chapters 4 and 5) brought about the postulate that chemical groups of the amino-residues of the collagenous tissue are likely to be involved in an ion-complex formation. Such chemical groups (likely carbonyl and/or amino groups) could act as a nidus for further calcification. Collagen is thought to have the potential to behave similarly. A preliminary study of collagen type I films and their subsequent in-vitro calcification was thus undertaken.

Infrared spectroscopy has been used in the past to study the secondary and tertiary structure of type I collagen⁸⁻¹³. FTIR spectroscopic studies of glutaraldehyde-treated type I collagen have already been reported in the solid state, showing two characteristic peaks (1658 and 1628 cm^{-1}) in the convoluted amide I region¹⁴⁻¹⁷. A

study of collagen extracted from bovine tendon (untreated and aldehyde-treated) by FTIR can be also found in the literature¹⁸.

The use of an attenuated total reflectance Fourier transform infrared (ATR-FTIR) microscope to enable us to see chemical differences on the surface of collagenous tissue was investigated. The infrared microscope can allow us to probe surface groupings. It can also indicate how calcium ions may interact with chemical groups on the surface of the collagen and hence how this may influence its in-vitro calcification.

1.2 Materials and Methods

1.2.1 Sample preparation

The preparation steps of collagen solutions can be found in the Sigma-Aldrich catalogue, or an alternative avoiding the laboratory preparation is to order a 0.1% w/v collagen solution in 0.1M acetic acid (Ref. C8919 SIGMA, UK). Collagen type I films were prepared as follows.

Spin-coating was first investigated. Five drops of 0.1% w/v collagen solution was placed on a quartz slide and spin at between 3400 and 4000 rpm for one minute. The film thickness achieved was less than the penetration depth of the infrared beam (a few μm) and the resulting spectra were essentially from the quartz. Thus, in order to achieve a reasonable but uniform thickness, one would need to repeat, at least 10 times, the previous procedure in order to achieve a thickness that would be of the order of the penetration depth of the ATR-FTIR beam (typically ca. 20 μm).

Another method to prepare the collagen films was thus thought. Acid-cleaned quartz slides were coated with a few mL of the 0.1% w/v collagen solution. Gentle rocking ensured an even coating on the quartz slide surface. The collagen was then allowed to bind for several hours at room temperature. It was planned to study the in-vitro calcification potential of untreated and glutaraldehyde-treated collagen films. The films, on quartz slides, were placed in acid-cleaned glass petri dishes that allowed treatment with glutaraldehyde to take place. After glutaraldehyde treatment took place for a defined period, the glutaraldehyde solution was removed and the film was gently washed with distilled water. The glutaraldehyde-treated and untreated films

were then subjected to an in-vitro calcification solution (see chapter 6 for details). The collagen films can be stored in sterile plastic tubes filled with this calcification solution or simply left in the glass petri dishes and the calcification solution added. Both methods can allow the calcification solution to be changed when felt necessary. After a determined period, the films can be removed from the calcification solution and gently washed with distilled water to remove any unbound inorganic ions. The films were left to air-dry and then analysed by ATR-FTIR microscopy.

Pericardium valve tissue was prepared as in chapter 8 section 8.2.2.

1.2.2 Instrument

The FTIR microscope used was a Nicolet continuum microscope with a silicon ATR objective (Spectra-Tech, UK). The data collection parameters were as follows: 1000 scans, resolution of 4 cm^{-1} , aperture of 100, MCT detector, KBr beamsplitter, spectral range of $4000\text{--}400\text{ cm}^{-1}$, Happ-Genzel apodisation and Mertz phase correction.

1.3 Results

1.3.1 Analysis of collagen films by FTIR microscopy

The first method of preparing thin films of collagen was the spin-coating technique. A typical FTIR spectrum obtained from a spin-coated film, can be found in figure A1.1 below. It appears that the film thickness achieved was too thin and the spectrum represents the underlying quartz slide.

The second method for preparation of the collagen films involved evaporation. A typical FTIR spectrum, obtained from a film prepared by evaporation, can be found in figure A1.1 below. The characteristic bands of collagen (from the second derivative) can be seen and are summarised in table A1.1.

Peak position (cm^{-1})	Assignment
$\sim 3200\text{ cm}^{-1}$	NH stretching of proteins (amide A)
$\sim 3311\text{ cm}^{-1}$	OH stretching of hydroxyl groups
2947	anti-symmetric stretching of the CH_2 group
2872	symmetric stretching of the CH_2 group
$\sim 1722\text{ cm}^{-1}$	protonated carboxyl and carbonyl groups

1695 cm ⁻¹	band resulting from amide I components
~1656 cm ⁻¹	amide I of α -helical structures
~1630 cm ⁻¹	amide I of β -pleated sheet structures
1553 cm ⁻¹	amide II band
1517 cm ⁻¹	tyrosine band
1469 cm ⁻¹	CH scissoring of methylene
1405 cm ⁻¹	symmetric CO stretching of carboxylate anion

Table A1.1: FTIR peaks and their corresponding assignments, from the analysis of collagen films (not incubated in calcification solution). See also figure A1.1.

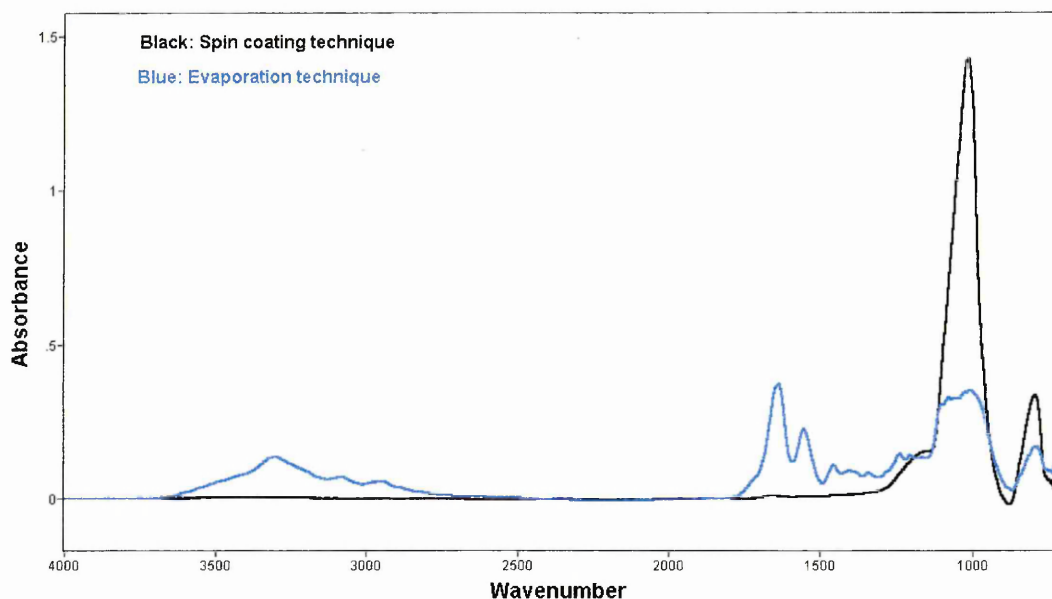


Figure A1.1: FTIR-ATR spectra of collagen films formed using two different techniques (spin coating and evaporation).

The glutaraldehyde-treated films were not analysed.

1.3.2: Analysis of pericardium valve tissue by FTIR microscopy

The FTIR microscope can also be used to study valve tissue. Tissue samples have to be frozen in liquid nitrogen and sliced, as in sample preparation for light microscopy (histological technique). This allows the sample to be flat and of a known thickness. A typical FTIR spectrum of untreated pericardium tissue, can be found in figure A1.2 below. The infrared absorption pattern is quite similar to the one found above in figure A1.1 because the pericardium tissue consists essentially of type I collagen.

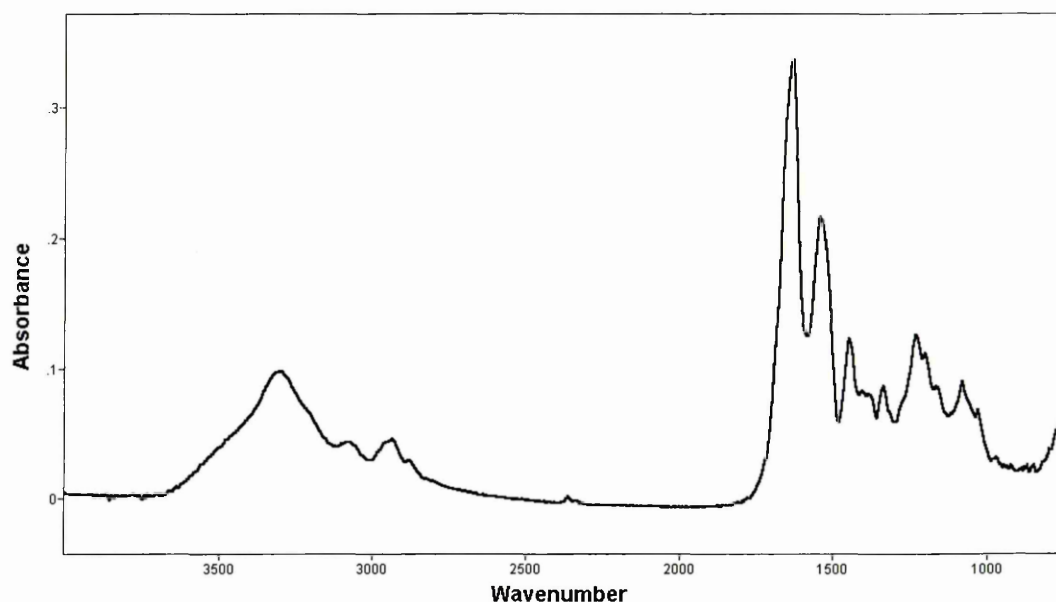


Figure A1.2: FTIR-ATR spectrum of a histological section of untreated pericardium tissue.

1.4 Overall Discussion

Due to a lack of time on the FTIR microscope, the study was not completed and only the few first steps, indicating the success of the preparation method, were carried out. The mapping of collagen film surfaces (typically $100 \times 100 \mu\text{m}$) using FTIR microscopy is nevertheless expected to give information regarding the calcification potential of collagen, especially through mapping of C=O and COO⁻ groups. Such findings have not been reported yet. Although not completed, a preliminary study of such maps has been successfully achieved with some untreated collagen films (data not shown here). A similar approach could be carried out with glutaraldehyde-treated collagen films, allowing the influence of cross-links, formed by the reaction between glutaraldehyde with protein, on collagen mineralisation to be studied. There are thirty-four amino groups in a collagen unit of molecular weight 100,000 and seventeen cross-links could be theoretically accommodated in this unit (assuming glutaraldehyde only to be a single dialdehyde molecule), while the maximum number reported, found by reaction with glutaraldehyde, was between thirteen¹⁹ and twenty five²⁰. The resulting cross-links would therefore be complex and very difficult to determine solely by FTIR spectroscopy. However, the use of FTIR

microscopy could still provide information on the role of collagen and cross-links in the mineralisation of tissue.

1.5 Conclusion

Successful methodologies for the preparation of collagen films and valve tissue sections have been carried out. Preliminary analyses by FTIR microscopy showed that such methodology could prove useful in increasing our understanding of the role of collagen and cross-links in the calcification of collagenous tissue.

1. Strates BS, Neuman WF, Levinskas GJ. The solubility of bone mineral II. Precipitation of near neutral solutions of calcium and phosphate. *Journal of Physical Chemistry*. 1957;61:279-283.
2. Strates B, Neuman WF. On the mechanism of calcification. *Proceedings of the Society for Experimental Biology and Medicine*. 1958;97:688-693.
3. Wadkins CL. Experimental factors that influence collagen calcification in-vitro. *Calcified Tissue Research*. 1968;2:214-228.
4. Jethi RK, Inlow CW, Wadkins CL. Studies on the mechanism of biological calcification I. Kinetic properties of the in-vitro calcification of collagen-containing matrices. *Calcified Tissue Research*. 1970;6:81-92.
5. Jethi RK, Mackey MG, Meredith PE, Wadkins CL. Studies of the mechanism of biological calcification III. The interaction of strontium with a calcifiable matrix from beef tendon. *Calcified Tissue Research*. 1972;9:310-324.
6. Wadkins CL, Luben RA. Effects of fluoride on in-vitro calcification of tendon matrix. *Calcified Tissue Research*. 1978;26:51-59.
7. Ferrans VJ, Boyce SW, Billingham ME, Jones M, Ishihara T, Roberts WC. Calcific deposits in porcine bioprostheses: structure and pathogenesis. *American Journal of Cardiology*. 1980;46:721-734.
8. Susi H, Ard JS, Carroll RJ. The infrared spectrum and water binding of collagen as a function of relative humidity. *Biopolymers*. 1971;10:1597-1604.
9. Jakobsen RJ, Brown LL, Hutson TB, Fink DJ, Veis A. Intermolecular interactions in collagen self-assembly as revealed by FTIR spectroscopy. *Science*. 1983;220:1288-1290.
10. Lazarev YA, Grishkovsky A, Khromova TB. Amide I band of IR spectrum and structure of collagen and related polypeptides. *Biopolymers*. 1985;24:1449-1478.
11. Payne KJ, Veis A. FTIR spectroscopy of collagen and gelatin solutions: deconvolution of the amide I band for conformational studies. *Biopolymers*. 1988;27:1749-1760.
12. Renugopalkrishnan V, Chandrakasan G, Moore S, Hutson TB, Berney CV, Bhatnagar R. Bound water in collagen. Evidence from FTIR and FTIR photoacoustic spectroscopic study. *Macromolecules*. 1989;22:4121-4124.
13. George A, Veis A. FTIRs in water demonstrates that collagen monomers undergo a conformational transition prior to thermal self-assembly in-vitro. *Biochemistry Journal*. 1991;30:2372-2377.
14. Doyle BB, Bendit EG, Blout ER. Infrared spectroscopy of collagen and collagen like peptides. *Biopolymers*. 1975;14:937-957.
15. Jackson M, Choo LP, Watson PH, Halliday WC, Mantsch HH. Beware of connective tissue proteins: assignment and implications of collagen absorptions in infrared spectra of human tissue. *Biochimica et Biophysica Acta*. 1995;1270:1-6.
16. Vyavahare N, Hirsch D, Lerner E, Baskin JZ, Schoen FJ, Bianco R, Kruth HS, Zand R, Levy RJ. Prevention of bioprosthetic heart valve calcification by ethanol preincubation: efficacy and mechanisms. *Circulation*. 1997;95:479-488.

17. Vyavahare N, Ogle M, Schoen FJ, Zand R, Gloeckner DC, Sacks M, Levy RJ. Mechanisms of bioprosthetic heart valve failure: fatigue causes collagen denaturation and glycosaminoglycan loss. *Journal of Biomedical Materials Research*. 1999;46:44-50.
18. Zhang Q, Ren L, Liu L, Wang C. Structure investigation of polyvinylalcohol-collagen composite. *Journal of Materials Science Technology*. 1997;13:179-183.
19. Cater CW. The evaluation of aldehydes and other difunctional compounds as crosslinking agents for collagen. *Journal of the Society of Leather Trades Chemists*. 1963;47:259-272.
20. Bowes JH, Cater CW. The formol titration for the determination of epsilon-amino groups substituted in modified collagens. *Biochimica et Biophysica Acta*. 1968;168:353-355.

Appendix II

A.2 Investigation of the reaction products of glutaraldehyde-treated model compounds using TLC-MALDI-TOF MS.

1.1 Introduction

The use of Matrix Assisted Laser Desorption Ionisation Time-Of-Flight Mass Spectrometry (MALDI-TOF MS) has already been described in chapters 4 and 5 of this thesis, for the analysis of the reaction of glutaraldehyde with model compounds (amino acids, peptides and proteins) at various pH values. However, another application of MALDI-TOF MS was undertaken by analysing the same reaction products of glutaraldehyde and model compounds as the ones mentioned previously but this time directly from thin layer chromatography plates (TLC MALDI-TOF MS).

There are several methodologies for combining TLC with MALDI MS. The components of a reaction mixture are initially separated on a TLC plate. In the first method, the analyte spots are then scraped off the plate, extracted into a solvent and analysed by mass spectrometry^{1,2}. This method requires an independent visualisation method to locate the analyte spots before extracting the samples. Another method involves the formation of a matrix layer on a stainless steel substrate while the TLC plate is sprayed with an extraction solvent. The matrix and the TLC plate are then placed face to face, transferring matrix to the plate and the stainless steel substrate discarded³.

Our approach was much simpler and did not require the sample to be scraped or extracted from the TLC plate, thus maintaining the integrity of the TLC plate.

Additionally, an advantage of the TLC-MALDI-TOF MS technique is the high sensitivity of MALDI and its ability to ionise low and high molecular weight compounds without fragmentation.

1.2 Materials and Methods

Please refer back to chapter 5 (sections 5.2.1 and 5.2.2) for details of chemicals and consumables used (e.g. model compounds, glutaraldehyde, etc.).

1.2.1 Sample preparation

This methodology involved the direct analysis of the intact TLC plate mounted on a modified MALDI target. The samples (3 x 25 mL of model compound reacted with glutaraldehyde were freeze-dried and re-dissolved in 3 mL of methanol (same methodology as reported previously in chapter 5). With the help of a capillary tube, a very small volume ($\sim 4 \mu\text{L}$) of the sample in methanol was spotted on a TLC plate (TLC plates (10 x 3 cm) coated with 0.2 nm layers of silica gel ref.: 60F254 from Merck, UK), backed with an aluminium support material. To achieve the best separation, the sample spot was kept as small as possible.

1.2.2 Development

The separation of each sample, using various mobile phases, was first carried out. The TLC development jars were lined with filter paper and sealed tightly to ensure that no solvent vapour evaporated. The mobile phases were thus always left to saturate for 2 hours prior to use. The TLC plates were then placed in an upright position and developed on their own in a pre-prepared jar. After separation had occurred the plates were removed and the solvent front was marked by a pencil line, in order to allow calculation of the R_f value of each spot. The TLC plates were air-dried and then visualised under UV light at 254 nm. Each TLC separation was carried out several times, whilst maintaining the experiment conditions, in order to check the reproducibility of the methodology. The following tables summarise the samples analysed (including dissolving solvent), the mobile phases used and the success of the separations^{4,5}.

1.2.2.1 Unreacted Glutaraldehyde:

Solvent used and resulting pH	Mobile Phase	Quality of separation (number of spots along with Rf values)
Water (pH 3.97)	methanol:water:acetic acid (80:15:5)	poor separation achieved with one clear spot with Rf 0.87
Buffer pH 4	methanol:water:acetic acid (80:15:5)	poor separation achieved with one clear spot with Rf 0.87
Buffer pH 7.4	methanol:water:acetic acid (80:15:5)	poor separation achieved with one clear spot with Rf 0.80
Buffer pH 9.2	methanol:water:acetic acid (80:15:5)	poor separation achieved with two spots with Rf of 0.42 and 0.78

Table A2.1: Mobile phases and the corresponding retention factors^{4,5} from the TLC separation of aqueous solutions of 0.6% v/v glutaraldehyde at various pH values (pH 4-9).

1.2.2.2 Glutaraldehyde-treated 6-Amino-n-caproic acid:

Solvent used and resulting pH	Mobile Phase	Quality of separation (number of spots along with Rf values)
Water (pH 4.76)	methanol:water:acetic acid (80:15:5)	very good separation achieved with 6 spots with Rf values of 0.034, 0.17, 0.26, 0.43, 0.60 and 0.77
Buffer pH 4	methanol:water:acetic acid (80:15:5)	very good separation achieved with 7 spots with Rf values of 0.017, 0.086, 0.17, 0.29, 0.46, 0.65 and 0.76
Buffer pH 7.4	methanol:water:acetonitrile (80:15:5)	very good separation achieved with 6 spots with Rf values of 0.016, 0.083, 0.16, 0.23, 0.42 and 0.75
Buffer pH 9.2	methanol:acetonitrile:cyclohexane (80:15:5)	very good separation achieved with 6 spots with Rf values of 0.017, 0.086, 0.21, 0.29, 0.60 and 0.72

Table A2.2: Mobile phases and the corresponding retention factors^{4,5} from the TLC separation of aqueous solutions of 0.1% w/v 6-amino-n-caproic acid reacted with 0.6% v/v glutaraldehyde at various pH values (pH 4-9).

1.2.2.3 Glutaraldehyde-treated N-Acetyl-L-lysine:

Solvent used and resulting pH	Mobile Phase	Quality of separation (number of spots along with Rf values)
Water (pH 3.96)	methanol:water:acetic acid (80:15:5)	very good separation achieved with 6 spots with Rf values of 0.030, 0.028, 0.25, 0.45, 0.62 and 0.79
Buffer pH 4	methanol:water:acetic acid (80:15:5)	very good separation achieved with 6 spots with Rf values of 0.016, 0.066, 0.15, 0.33, 0.50 and 0.75

Buffer pH 7.4	methanol:water:acetonitrile (80:15:5)	very good separation achieved with 6 spots with Rf values of 0.015, 0.07, 0.15, 0.31, 0.50 and 0.76
Buffer pH 9.2	methanol:acetonitrile:cyclohexane (80:15:5)	very good separation achieved with 5 spots with Rf values of 0.016, 0.10, 0.23, 0.50 and 0.66

Table A2.3: Mobile phases and the corresponding retention factors^{4,5} from the TLC separation of aqueous solutions of 0.1% w/v N-Acetyl-L-lysine reacted with 0.6% v/v glutaraldehyde at various pH values (pH 4-9).

1.2.2.4 Glutaraldehyde-treated N-Acetyl Glycine Lysine Methyl Ester:

Solvent used and resulting pH	Mobile Phase	Quality of separation (number of spots along with Rf values)
Water (pH 4.38)	Methanol:water:acetic acid (80:15:5)	Good separation achieved with 4 spots with Rf values of 0.06, 0.15, 0.33 and 0.70
Buffer pH 4	methanol:water:acetic acid (80:15:5)	Good separation achieved with 3 spots with Rf values of 0.19, 0.34 and 0.70
Buffer pH 7.4	methanol:water:acetonitrile (80:15:5)	Very good separation achieved with 5 spots with Rf values of 0.10, 0.26, 0.40, 0.50 and 0.75
Buffer pH 9.2	methanol:acetonitrile:cyclohexane (80:15:5)	Very good separation achieved with 5 spots with Rf values of 0.047, 0.20, 0.36 and 0.68

Table A2.4: Mobile phases and the corresponding retention factors^{4,5} from the TLC separation of aqueous solutions of 0.1% w/v N-acetyl Gly Lys Methyl Ester reacted with 0.6% v/v glutaraldehyde at various pH values (pH 4-9).

1.2.2.5 Glutaraldehyde-treated N-Acetyl Phenylalanine Lysine:

Solvent used and resulting pH	Mobile Phase	Quality of separation (number of spots)
Water (pH 3.60)	methanol:water:acetonitrile (80:15:5)	Relatively good separation achieved with 5 spots but the separation was faint and the spots were difficult to identify (no Rf values available)
Buffer pH 4	methanol:water:acetonitrile (80:15:5)	Very good separation achieved with 5 spots (no Rf values available)
Buffer pH 7.4	methanol:water:acetonitrile (80:15:5)	Very good separation achieved with 6 spots (no Rf values available)
Buffer pH 9.2	methanol:water:acetonitrile (80:15:5)	Poor separation achieved with only 2 spots (no Rf values available)

Table A2.5: Mobile phases⁴ from the separation of aqueous solutions of 0.1% w/v N-acetyl Phe Lys reacted with 0.6% v/v glutaraldehyde at various pH values (pH 4-9).

1.2.2.6 Glutaraldehyde-treated Proteins (lysosyme and cytochrome c):

Separation of glutaraldehyde-treated proteins was not carried out because of time constraints, however work on the separation of drugs reacted with glutaraldehyde has already been reported⁶. The mobile phase used consisted of methanol, ethyl acetate and acetic acid in a ratio of 85:10:5. Although this mobile phase was not found to work efficiently in the separation of both amino acids and peptides (results showed only one clear spot without any streaks), it is believed that this mobile phase might be successful for the separation of the reaction products of proteins reacted with glutaraldehyde because the separated drugs contained similar pendant groups as reactions products of glutaraldehyde-treated model compounds.

1.2.3 Matrix application

In all experiments, a 600 x 2 mm strip of the developed TLC plate, containing the spots for analysis, was attached to a modified MALDI target with double-sided tape before the matrix (2,5-dihydroxycinnamic acid, DHB) was electrosprayed onto the silica gel surface. The matrix solution (7 mg DHB/mL of methanol) was electrosprayed onto the TLC plate using an in-house modified commercial robotic x,y,z axis motion system (PROBOT, BAI, Germany). The electrospray used in this study consisted of a syringe pump fitted with a 100 μ L syringe which was connected via PTFE tubing to a HPLC zero dead volume fitting to a capillary steel needle, to which a high voltage (ca 2.5 kV) was applied. The capillary needle was further threaded to a HPLC T-piece zero dead volume fitting through which dry nitrogen could be applied to the capillary tube. The TLC plate was earthed and held horizontally during electrospraying and set to a distance of ca. 4 mm from the spray needle⁷. The syringe was filled with the matrix solution, which was electrosprayed at a rate of 150 μ L.h⁻¹, whilst the TLC plate was moving at 0.6 cm.min⁻¹. Once the TLC plate was electrosprayed, it was left to air dry for at least an hour, before placing the MALDI target into the spectrometer⁸. Letting the solvent evaporate, allowed the matrix solution to co-crystallise with the sample to be analysed on the TLC plate.

1.2.4 Mass spectrometer

Mass spectra and mass chromatograms were recorded directly from the TLC plate with a modified linear Laser TOF 1500 (Scientific Analytical Instruments, Manchester, UK), equipped with a N₂ laser (λ =337 nm). The sample holder within

this instrument has been modified to enable TLC strips of approximately 65 x 2 mm to be fitted into the recessed slot and the sample probe was adapted to allow free movement along the z (vertical) axis, while the software has also been modified to allow the construction of total ion and mass chromatograms. These modifications to the instrument and its software, for use in TLC-MALDI-MS mode, have been previously further described elsewhere⁸. Only the positive ion mode was used in these investigations.

1.3 Results

The TLC-MALDI-TOF MS method was used to identify low molecular weight compounds with masses within the matrix region (100 Da and above), a goal that is normally difficult to achieve. Low molecular weight compounds were successfully detected by almost complete suppression of the matrix peaks using a relatively low matrix concentration in comparison to the analyte. The data obtained from the TLC plates showed similarities with the same reaction mixtures analysed by simple MALDI-TOF MS (see chapter 5 of this thesis). Such correlation was expected and successfully achieved. A typical TLC-MALDI-TOF MS spectrum is shown in figure A2.1 below (glutaraldehyde-treated 6-amino-n-caproic acid at pH 9.2).

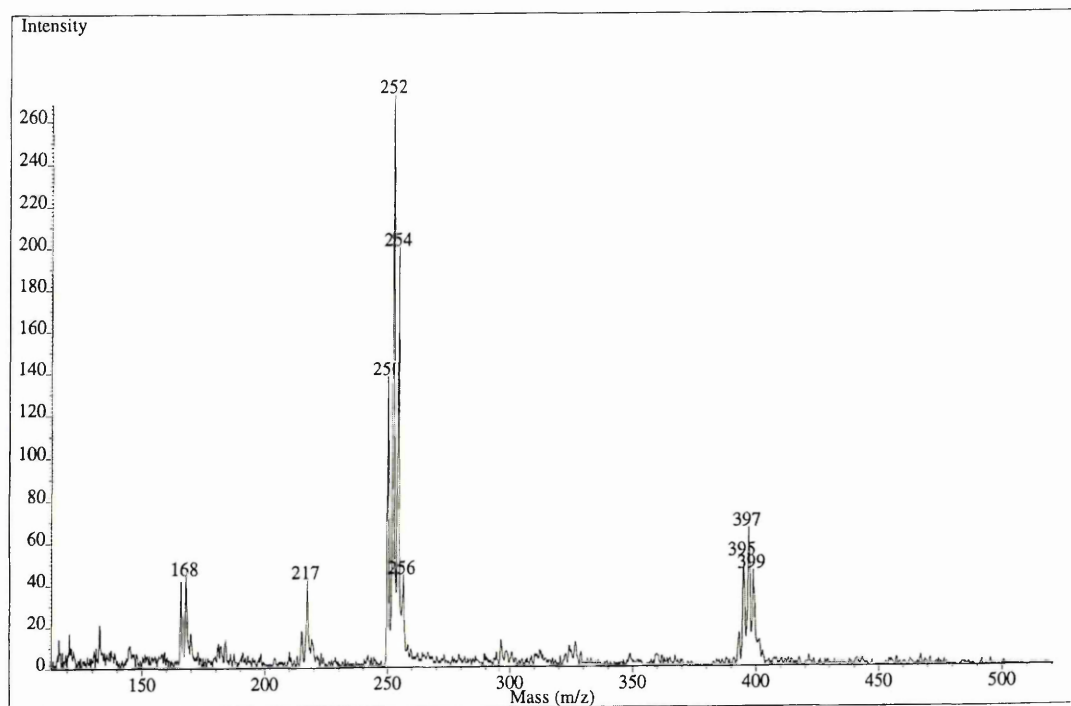


Figure A2.1: TLC-MALDI-TOF MS spectrum of a mixture of 0.1% w/v 6-amino-n-caproic acid reacted with 0.6% v/v glutaraldehyde at pH 9.2 separated using a methanol:acetonitrile:cyclohexane mobile phase with a 80:15:5 ratio (spot position on the TLC: 31.33mm from the origin).

The peaks appear as M and $[M+H]^+$ ions. In addition, many molecular structures also appear with the addition of a sodium (Mw 23) or potassium (Mw 39) cation such as $[M+Na]^+$ or $[M+K]^+$, and more rarely as $[M+Na+H]^+$ and $[M+K+H]^+$ adduct ions. A tentative assignment of the spectrum shown in figure A2.1 is given in table A2.6 below (for the molecules of glutaraldehyde please refer to the appendix III, and for those of the reaction between glutaraldehyde and 6-amino-n-caproic acid, please refer to appendix IV).

m/z (vs=very strong, s=strong, w=weak signal)	Proposed assignment for glutaraldehyde molecules (Mw)	Proposed assignment for model compound + glutaraldehyde reaction products (Mw)
165s/168s/169w	Mol XXIII (163)	
183w	Mol XV (182); Mol XXXI (182); Mol XXXII (182)	
214w/217s/218w		Mol LX (213); Mol LXV (195+Na=218); Mol LXVI (194+Na=217)
250s/252vs/254vs/256w	Mol XXV (228+Na=251); Mol V (218+K=257)	Mol LX (213+K=252); Mol LXII (231+Na=254); Mol LXVII (231+Na=254); Mol LXXII (231+Na=254)
296w/297w		Mol XCII (295); Mol CIII (295); Mol CIV (295)
324w/327w/328w	Mol IX (301+Na=324); Mol XII (300+Na=323); Mol XVIIb (300+Na=323); Mol 17b (300+Na=323)	Mol LXI (326)
395s/397s/399s		Mol CXLI (395); Mol CXLVIII (395); Mol CLXIV (395)

Table A2.6: Tentative assignment of the mass spectrometric data from the spectrum of 6-amino-n-caproic acid reacted with glutaraldehyde at pH 9.2 (see figure A2.1).

1.4 Overall Discussion

The major problem encountered was to obtain a reasonable separation of the reaction products. The TLC separation of such products has been rarely attempted, only limited TLC separations of such products have been reported^{9,10}. However, HPLC methodology has been reported for the separation of related species. For example, measurement of personal exposure to glutaraldehyde¹¹, quantify glutaraldehyde traces on medical equipment after final rinsing^{12,13} and after inactivation with sodium bisulphite¹⁴, detect glutaraldehyde into hydrolysed pericardial tissue¹⁵⁻¹⁷, but also to follow the extent of protein (cottonseed) cross-linking with glutaraldehyde¹⁸. Nevertheless, this study has shown that a relatively satisfactory TLC separation can be attained, however this was not a complete separation, as indicated by the number of different products found in the mass spectra.

The results summarised in table A2.6 obtained from the analysis of a TLC plate of a glutaraldehyde-treated model compound showed similarities with the same reaction mixtures analysed by simple MALDI-TOF MS (data shown in chapter 5). Most peaks can either be assigned for unreacted glutaraldehyde or reaction products.

The methodologies presented here offer a good basis for future experiments. It is thought that TLC-MALDI-TOF MS would be most successful once an optimum TLC separation is achieved. It was also noted that different concentrations of the matrix solution can affect the spectra. It is believed that better resolution may be achieved by altering the matrix solution or altering the ratio of sample:matrix. Also, the addition of trifluoroacetic acid (generally used to ionise the matrix) to the matrix might be beneficial. Additionally, from MALDI-TOF MS data, the analysis of glutaraldehyde-treated proteins seems to give relatively easier spectra to interpret than glutaraldehyde-treated model compounds spectra. Thus, it is postulated that if a suitable TLC separation could be found the resulting spectra may help our understanding of the reaction between glutaraldehyde and proteins.

1.5 Conclusion

It has already been shown (see chapter 5) that the analysis of a model compound reacted with glutaraldehyde at various pH values (pH 4-9) by MALDI-TOF MS can be successfully achieved. Many peaks could be assigned to different chemical

structures of varying complexity involving both reaction products and unreacted glutaraldehyde molecules. This preliminary study demonstrates that TLC-MALDI-TOF MS can also be successful in the separation and analysis of products of complex reactions involving small amino acids or peptides with glutaraldehyde.

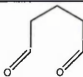
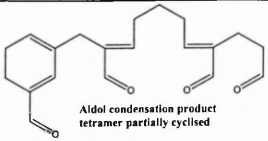
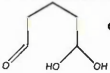
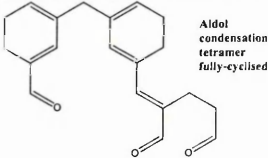
1. St Hilaire PM, Cipolla L, Tedebark U, Meldal M. Analysis of organic reactions by thin layer chromatography combined with MALDI-TOF MS. *Rapid Communications in Mass Spectrometry*. 1998;12:1475-1484.
2. Bush KL. TLC coupled with mass spectrometry. In: Sherma J, Fried B, eds. *Handbook of Thin Layer Chromatography*. New York: Dekker, M.; 1991:183-209.
3. Mehl JT, Gusev AI, Hercules DM. Coupling protocol for TLC/MALDI. *Chromatographia Journal*. 1997;46:358-364.
4. Patel H. Study of the reaction between glutaraldehyde amino acids and small peptides. In. Sheffield: Final Year Project Report Sheffield Hallam University; 2001.
5. Chollet C. A study of the products of glutaraldehyde reacted with small peptides and amino acids. In. Sheffield: Final Year Project Report Sheffield Hallam University; 2001.
6. Stead AH, Gill R, Wright JP, Gibbs JP, Moffat AC. Standardised thin layer chromatographic systems for the identification of drugs and poisons. 1982;107:1106-1168.
7. Mowthorpe S, Clench MR, Crecelius A, Richards DS, Tetler LW. Matrix-assisted laser desorption ionisation/time of flight/thin layer chromatography/mass spectrometry: a rapid method for impurity testing. *Rapid Communications in Mass Spectrometry*. 1999;13:264-270.
8. Crecelius A, Clench MR, Richards DS, Mather J, Parr V. Analysis of UK-224,671 and related substances by TLC-MALDI-TOF MS. *Journal of Planar Chromatography*. 2000;13:76-81.
9. Monsan P, Puzo G, Mazarguil H. Etude du mecanisme d'etablissement des liaisons glutaraldehyde-proteines. *Biochimie*. 1975;57:1281-1292.
10. Blass J, Verriest C, Leau A, Weiss M. Monomeric glutaraldehyde as an effective crosslinking reagent for proteins. *Journal of the American Leather Chemists Association*. 1976;71:121-132.
11. Cuthbert J, Groves JA. The measurement of airborne glutaraldehyde by HPLC. *Annals of Occupational Hygiene*. 1995;39:223-233.
12. Menet MC, Gueylard D, Fievet MH, Thuillier A. Fast specific separation and sensitive quantification of bactericidal and sporicidal aldehydes by HPLC. *Journal of Chromatography B*. 1996;692:79-86.
13. Liu FF, Li XP, Zhang LH, Lan TB, Guo SH, Wang YQ. Detection of trace glutaraldehyde in the fluid from venous circuit tube by HPLC. *Chinese Pharmaceutical Journal*. 2001;36:57-59.
14. Jordan SLP, Russo MR, Blesing RL, Theis AB. Inactivation of glutaraldehyde by reaction with sodium bisulfite. *Journal of Toxicology and Environmental Health*. 1996;47:299-309.
15. Hughes H, Lilburn S, Tipton S, Aboul-Enein HY, Duran CMG. Chemical assay of glutaraldehyde incorporation into pericardial tissue. *Journal of Heart Valve Disease*. 1994;3:105-110.
16. McClurg WM, Lawford PV, Hughes H, Rogers S. Formaldehyde replaces glutaraldehyde in porcine bioprosthetic heart valves. *Journal of Heart Valve Disease*. 1996;5:343-347.
17. McClurg WM, Rogers S, Lawford PV, Hughes H. Acid hydrolysable aldehydes in long term stored commercial bioprosthetic heart valves: implications for calcification. *Cardiovascular Pathology*. 1998;7:233-237.
18. Marquie C, Tessier AM, Aymard C, Guilbert S. HPLC determination of the reactive lysine content of cottonseed protein films to monitor the extent of crosslinking by formaldehyde, glutaraldehyde, and glyoxal. *Journal of Agricultural and Food Chemistry*. 1997;45:922-926.

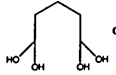
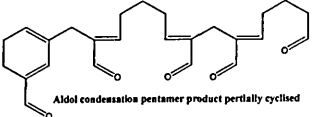
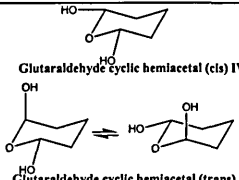
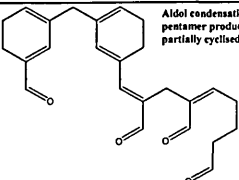
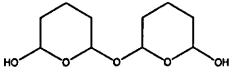
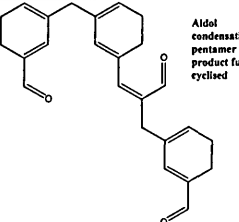
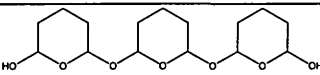
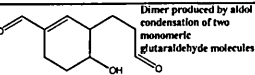
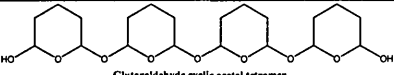
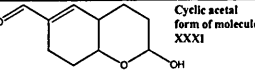
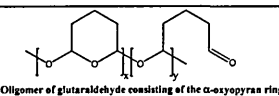
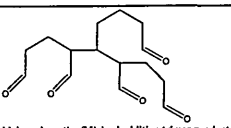
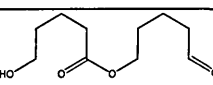
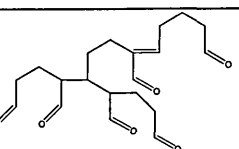
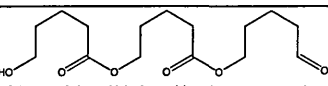
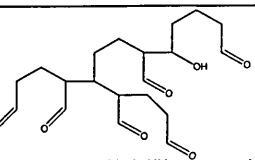
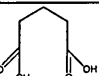
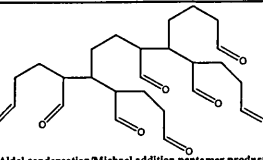
Appendix III

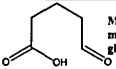
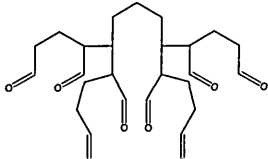
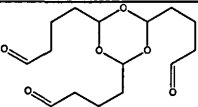
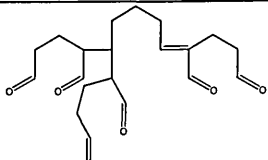
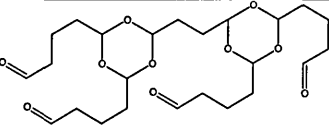
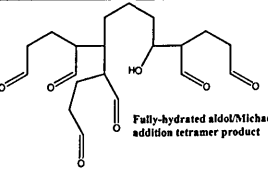
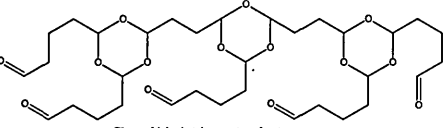
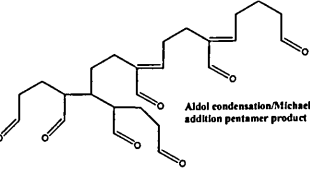
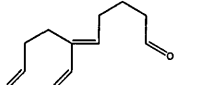
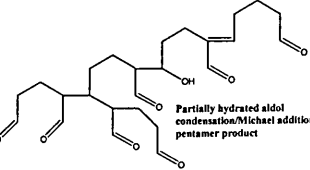
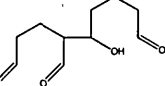
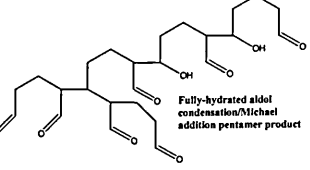
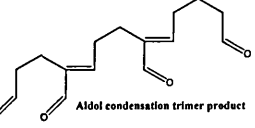
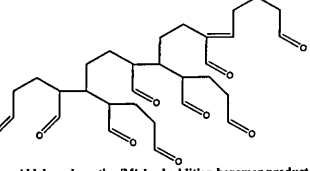
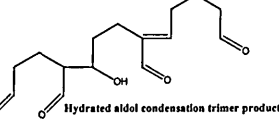
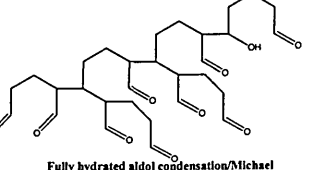
A.3 Hypothetical molecular structures present in glutaraldehyde solutions.

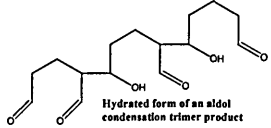
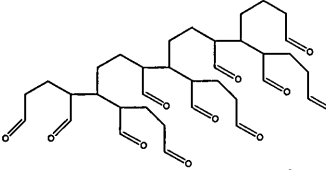
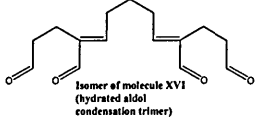
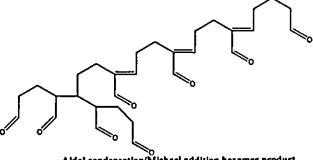
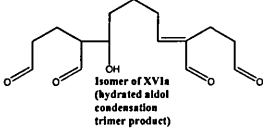
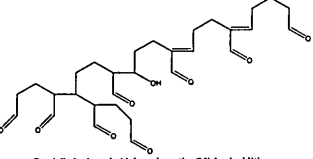
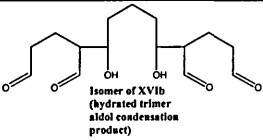
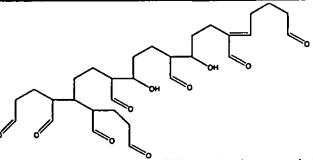
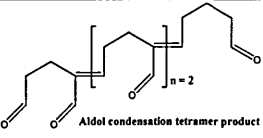
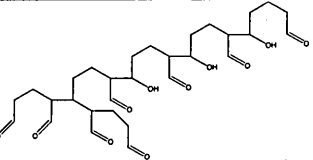
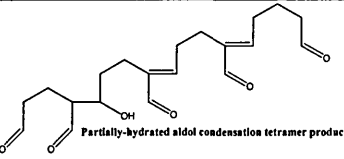
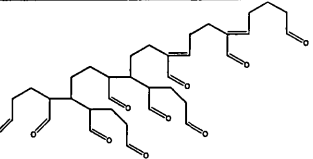
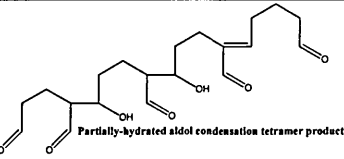
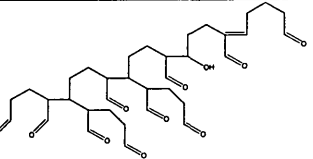
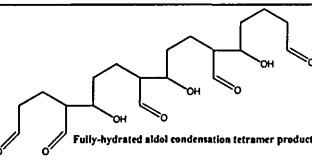
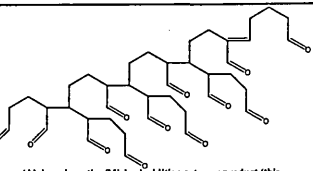
The table below summarises the possible molecular structures identified from the mass spectrometric data (see chapters 4 and 5) obtained from the analysis of glutaraldehyde and glutaraldehyde-treated compounds. The references found in association with some molecules in the table below refer to authors who reported proof of their likely presence in the literature.

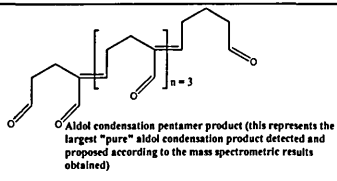
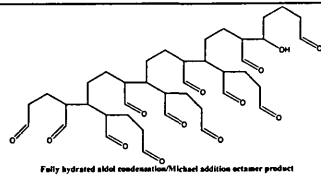
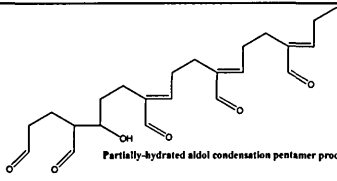
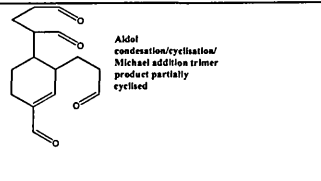
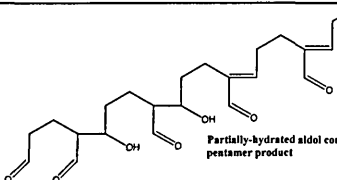
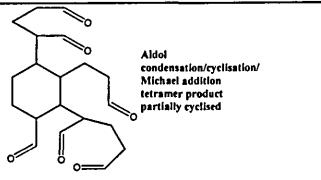
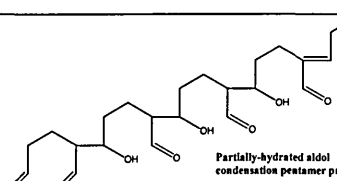
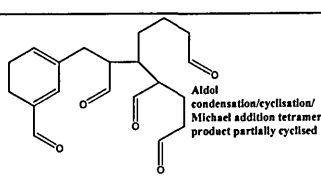
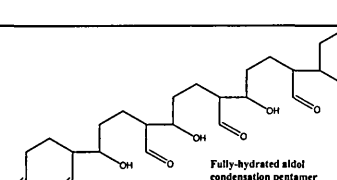
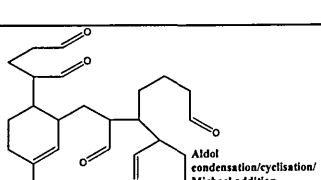
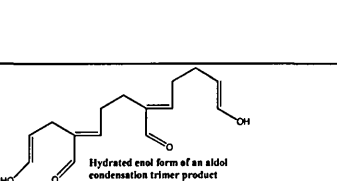
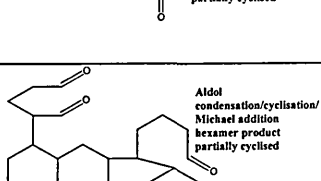
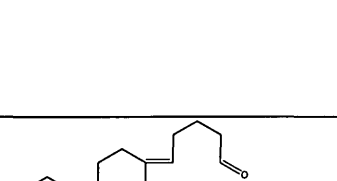
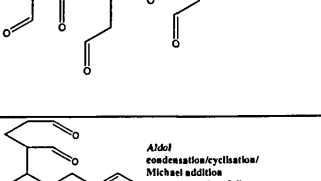
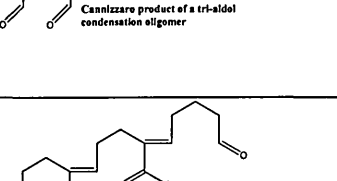
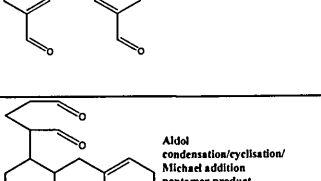
Note that the molecular structures that are not cross-referenced have not previously been reported. Only 23 molecules out of the 73 found below have previously been proposed in the literature. These represent only 31% of all the hypothetical molecular structures present in glutaraldehyde solutions proposed in this thesis, emphasising the important contribution of this study to the elucidation of the behaviour of glutaraldehyde in solution.

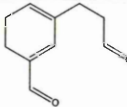
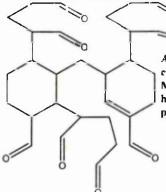
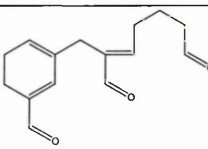
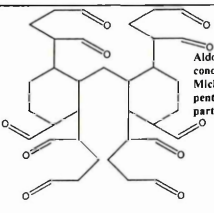
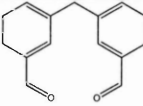
Molecule number (Molecular weight)	Molecular structure	Molecule number (Molecular weight)	Molecular structure
Mol I ¹⁻⁴ (100)	 Monomeric glutaraldehyde	Mol XXVI (328)	 Aldol condensation product tetramer partially cyclised
Mol II ¹⁻⁴ (118)	 Glutaraldehyde monohydrate	Mol XXVII (310)	 Aldol condensation tetramer fully-cyclised

Mol III ¹⁻⁴ (136)	 Glutaraldehyde dihydrate	Mol XXVIII (410)	 Aldol condensation pentamer product partially cyclised
Mol IV ¹⁻³ (118) (2 isomers ⁴ : IVa and IVb)	 Glutaraldehyde cyclic hemiacetal (cis) IVa Glutaraldehyde cyclic hemiacetal (trans) IVb	Mol XXIX (392)	 Aldol condensation pentamer product partially cyclised
Mol V ^{1,3,5} (218)	 Glutaraldehyde hemiacetal dimer	Mol XXX (374)	 Aldol condensation pentamer product fully cyclised
Mol VI ^{1,3,5} (318)	 Glutaraldehyde hemiacetal trimer	Mol XXXI ⁶ (182)	 Dimer produced by aldol condensation of two monomeric glutaraldehyde molecules
Mol VII ^{1,3,5} (418)	 Glutaraldehyde cyclic acetal tetramer	Mol XXXII ⁷ (182)	 Cyclic acetal form of molecule XXXI
Mol VIIa ⁸ (202)	 Oligomer of glutaraldehyde consisting of the α -oxopyran ring	Mol XXXIII (282)	 Aldol condensation/Michael addition trimer product
Mol VIII ⁵ (202)	 Glutaraldehyde hemiacetal-type dimer	Mol XXXIV (364)	 Aldol condensation/Michael addition tetramer product
Mol IX ⁵ (301)	 Oligomer of glutaraldehyde consisting of the α -oxopyran ring	Mol XXXIVa (382)	 Fully-hydrated aldol/Michael addition tetramer product
Mol X (132)	 Glutaric acid (di-acid form of monomeric glutaraldehyde)	Mol XXXV (464)	 Aldol condensation/Michael addition pentamer product

Mol XI (116)	 Mono-acid form of monomeric glutaraldehyde	Mol XXXVI (464)	 Isomer of XXXV. Aldol/Michael addition pentamer product
Mol XII ⁷ (300)	 Trioxane-type glutaraldehyde trimer	Mol XXXVII (364)	 Isomer of XXXIV. Aldol/Michael addition tetramer product
Mol XIII ⁸ (500)	 Glutaraldehyde trioxane-type pentamer	Mol XXXVIIa (382)	 Fully-hydrated aldol/Michael addition tetramer product
Mol XIV ⁸ (700)	 Glutaraldehyde trioxane-type heptamer	Mol XXXVIII (446)	 Aldol condensation/Michael addition pentamer product
Mol XV (182)	 Aldol condensation product consisting of two monomeric glutaraldehyde molecules	Mol XXXVIIIa (464)	 Partially hydrated aldol condensation/Michael addition pentamer product
Mol XVa (200)	 Hydrated form of molecule XV (hydrated aldol condensation dimer product)	Mol XXXVIIIb (482)	 Fully-hydrated aldol condensation/Michael addition pentamer product
Mol XVI ¹ (264)	 Aldol condensation trimer product	Mol XXXIX (546)	 Aldol condensation/Michael addition hexamer product
Mol XVIa ⁸⁻¹¹ (282)	 Hydrated aldol condensation trimer product	Mol XXXIXa (564)	 Fully hydrated aldol condensation/Michael addition hexamer product

Mol XVIIb (300)	 Hydrated form of an aldol condensation trimer product	Mol XL (646)	 Aldol condensation/Michael addition heptamer product
Mol XVII ^{1,5} (264)	 Isomer of molecule XVI (hydrated aldol condensation trimer)	Mol XLI (528)	 Aldol condensation/Michael addition hexamer product
Mol XVIIa (282)	 Isomer of XVIa (hydrated aldol condensation trimer product)	Mol XLIa (546)	 Partially hydrated aldol condensation/Michael addition hexamer product
Mol XVIIb (300)	 Isomer of XVIIb (hydrated trimer aldol condensation product)	Mol XLIb (564)	 Partially hydrated aldol condensation/Michael addition hexamer product
Mol XVIII (346)	 Aldol condensation tetramer product	Mol XLIc (582)	 Fully hydrated aldol condensation/Michael addition hexamer product
Mol XVIIIa (364)	 Partially-hydrated aldol condensation tetramer product	Mol XLII (628)	 Aldol condensation/Michael addition heptamer product
Mol XVIIIb (382)	 Partially-hydrated aldol condensation tetramer product	Mol XLIIa (646)	 Partially hydrated aldol condensation/Michael addition heptamer product
Mol XVIIIc (400)	 Fully-hydrated aldol condensation tetramer product	Mol XLIII (728)	 Aldol condensation/Michael addition octamer product (this molecule represents the largest aldol condensation/Michael addition product proposed according to the mass spectrometric data obtained)

Mol XIX (428)	 <p>Aldol condensation pentamer product (this represents the largest "pure" aldol condensation product detected and proposed according to the mass spectrometric results obtained)</p>	Mol XLIIIa (746)	 <p>Fully hydrated aldol condensation/Michael addition octamer product</p>
Mol XIXa (446)	 <p>Partially-hydrated aldol condensation pentamer product</p>	Mol XLV (264)	 <p>Aldol condensation/cyclisation/Michael addition trimer product partially cyclised</p>
Mol XIXb (464)	 <p>Partially-hydrated aldol condensation pentamer product</p>	Mol XLVI (364)	 <p>Aldol condensation/cyclisation/Michael addition tetramer product partially cyclised</p>
Mol XIXc (482)	 <p>Partially-hydrated aldol condensation pentamer product</p>	Mol XLVII (346)	 <p>Aldol condensation/cyclisation/Michael addition tetramer product partially cyclised</p>
Mol XIXd (500)	 <p>Fully-hydrated aldol condensation pentamer product</p>	Mol XLVIII (446)	 <p>Aldol condensation/cyclisation/Michael addition pentamer product partially cyclised</p>
Mol XX ^{12,13} (264)	 <p>Hydrated enol form of an aldol condensation trimer product</p>	Mol XLIX (546)	 <p>Aldol condensation/cyclisation/Michael addition hexamer product partially cyclised</p>
Mol XXI ^{9,14} (266)	 <p>Cannizzaro product of a tri-aldol condensation oligomer</p>	Mol L (328)	 <p>Aldol condensation/cyclisation/Michael addition tetramer product fully cyclised</p>
Mol XXII ⁹ (302)	 <p>Cannizzaro product of a tri-aldol condensation oligomer</p>	Mol LI (428)	 <p>Aldol condensation/cyclisation/Michael addition pentamer product partially cyclised</p>

Mol XXIII (163)	 <p>Fully cyclised dimer produced by aldol condensation of two monomeric glutaraldehyde molecules</p>	Mol LII (528)	 <p>Aldol condensation/cyclisation/ Michael addition hexamer product partially cyclised</p>
Mol XXIV ^{5,6} (246)	 <p>Partially-cyclised trimer formed by aldol condensation</p>	Mol LIII (628)	 <p>Aldol condensation/cyclisation/ Michael addition pentamer product partially cyclised</p>
Mol XXV ^{15,16} (228)	 <p>Fully-cyclised trimer of XXIV, formed by aldol condensation</p>		

- Hardy PM, Nicholls AC, Rydon HN. The nature of glutaraldehyde in aqueous solution. *Journal of Chemical Society Chemical Communications*. 1969;10:565-566.
- Munton TJ, Russell AD. Aspects of the action of glutaraldehyde on Escherichia Coli. *Journal of Applied Bacteriology*. 1970;33:410-419.
- Korn AH, Fearheller SH, Filachione EM. Glutaraldehyde: nature of the reagent. *Journal of Molecular Biology*. 1972;65:525-529.
- Whipple EB, Ruta M. Structure of aqueous glutaraldehyde. *Journal of Organic Chemistry*. 1974;39:1666-1668.
- Yokota K, Suzuki Y, Ishii Y. Temperature dependence of the polymerisation modes of glutaraldehyde. *Chemical Abstracts*. 1965;65:13835.
- Tashima T, Imai M. Structure of a new oligomer of glutaraldehyde produced by aldol condensation reaction. *Journal of Organic Chemistry*. 1991;56:694-697.
- Tashima T, Kawakami U, Harada M, Imai M, Satoh N, Nakagawa T, Tanaka H. Polymerisation reaction in aqueous solution of glutaraldehyde containing trioxane-type oligomers under sterilising conditions. *Chemical Pharmaceutical Bulletin*. 1989;37:377-381.
- Aso C, Aito Y. Studies on the polymerisation of bifunctional monomers II: Polymerisation of glutaraldehyde. *Makromolekulare Chemie*. 1962;58:195-203.
- Margel S, Rembaum A. Synthesis and characterisation of polyglutaraldehyde. A potential reagent for protein immobilisation and cell separation. *Macromolecules*. 1980;13:19-24.
- Walt DR, Agayn VI. The chemistry of enzyme and protein immobilisation with glutaraldehyde. *Trends in Analytical Chemistry*. 1994;13:425-430.
- Shan ZH. Glutaraldehyde and modified glutaraldehyde used in leather making. *Leather Science and Engineering*. 1999;9:30-33.
- Hooper DL. Nuclear magnetic measurements of equilibria involving hydration and hemiacetal formation from some carbonyl compounds. *Journal of the Chemical Society B*. 1967:169-170.
- Kawahara JI, Ohmori T, Ohkubo T, Hattori S, Kawamura M. The structure of glutaraldehyde in aqueous solution determined by ultraviolet absorption and light scattering. *Analytical Biochemistry*. 1992;201:94-98.
- Okubo M, Takahashi M. Production of submicron size monodisperse polymer particles having aldehyde groups by the seeded aldol condensation polymerisation of glutaraldehyde II. *Colloid and Polymer Science*. 1994;272:422-426.
- Richards FM, Knowles JR. Glutaraldehyde as a protein crosslinking reagent. *Journal of Molecular Biology*. 1968;37:231-233.
- Woodroof EA. Use of glutaraldehyde and formaldehyde to process tissue heart valves. *Journal of Bioengineering*. 1978;2:1-9.

Appendix IV

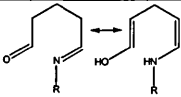
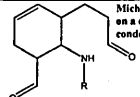
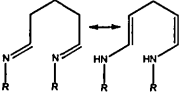
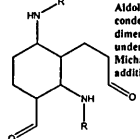
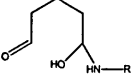
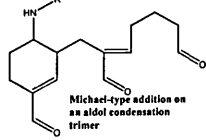
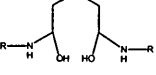
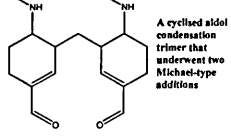
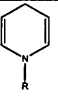
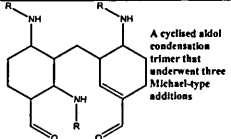
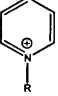
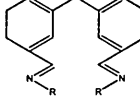
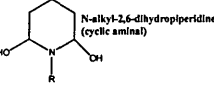
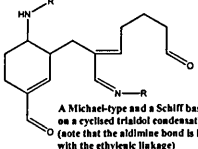
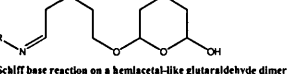
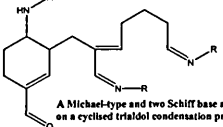
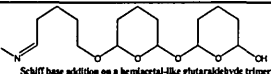
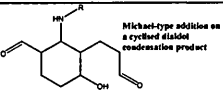
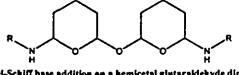
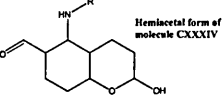
A.4 Hypothetical molecular structures present in solutions of glutaraldehyde-treated model compounds.

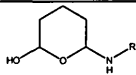
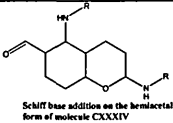
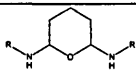
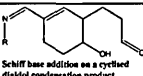
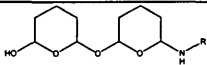
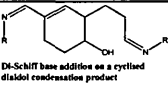
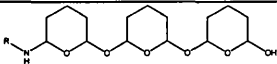
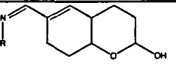
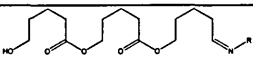
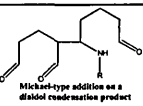
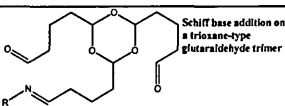
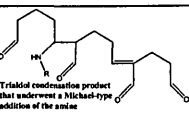
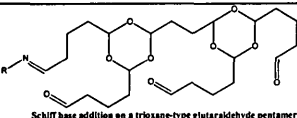
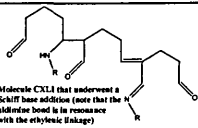
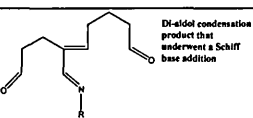
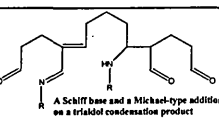
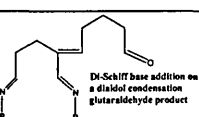
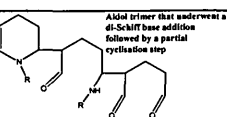
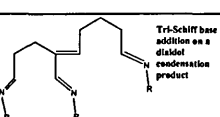
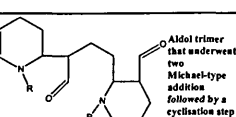
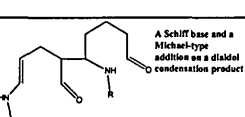
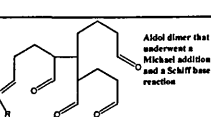
The table below summarises the possible molecular structures identified from the mass spectrometric data (see chapters 4 and 5) obtained from the analysis of glutaraldehyde-treated model compounds. The references found in association with some molecules in the table below refer to authors who reported proof of their likely presence in the literature.

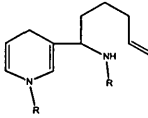
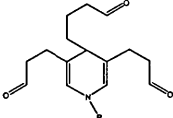
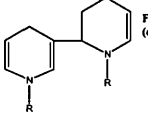
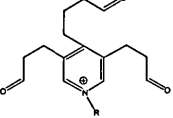
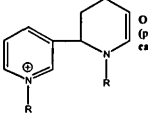
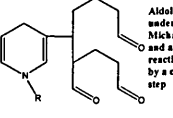
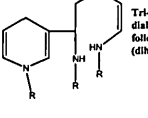
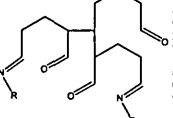
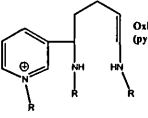
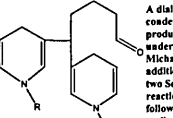
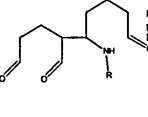
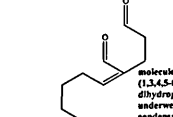
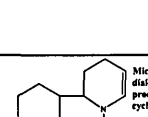
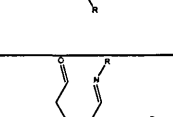

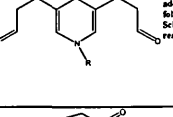
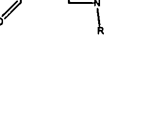
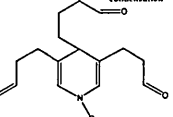
Note that the molecular structures that are not cross-referenced have not previously been reported. Only 23 molecules out of 84 have previously been proposed in the literature. These represent only ca. 27% of all the proposed molecular structures present in glutaraldehyde-treated model compounds identified in this thesis (excluding the glutaraldehyde molecules summarised in appendix III). This emphasises the complexity of the reaction of glutaraldehyde with proteins and the important contribution of this study to the elucidation of the cross-links between glutaraldehyde and lysino groups of tissue.

N. B. R stands for the radical: R=115 for 6-amino-n-caproic acid (also called 6-amino hexanoic acid); R=172 for N-acetyl-L-lysine; R=335 for N-acetyl phenylalanine lysine; R=243 for N-acetyl glycine lysine methyl ester.

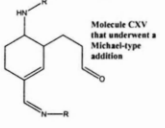
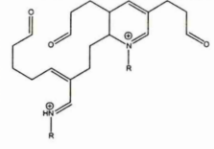
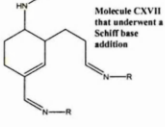
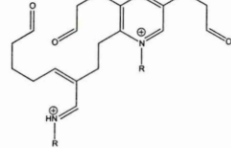
Molecule number (Molecular weight)	Molecular structure	Molecule number (Molecular weight)	Molecular structure

Mol LX ¹⁻³ (98+R)	 Mono-Schiff base addition on a monomeric glutaraldehyde molecule	Mol CXIX (180+R)	 Michael-type addition on a dialdol condensation product
Mol LXI ¹⁻³ (96+2R)	 Di-Schiff base addition on a monomeric glutaraldehyde molecule	Mol CXX (196+2R)	 Aldol condensation dimer that underwent two Michael-type additions
Mol LXII ⁴ (116+R)	 Michael-type addition on an aldol condensation trimer	Mol CXXII ⁵ (262+R)	 Michael-type addition on an aldol condensation trimer
Mol LXIII ⁶ (102+2R)	 A cyclised aldol condensation trimer that underwent two Michael-type additions	Mol CXXIII ⁷ (260+2R)	 A cyclised aldol condensation trimer that underwent three Michael-type additions
Mol LXV ^{3,7,8} (80+R)	 Schiff base addition on a monomeric glutaraldehyde followed by a cyclisation step (dihydropyridine structure)	Mol CXXVI (258+3R)	 A cyclised aldol condensation trimer that underwent three Michael-type additions
Mol LXVI ^{3,6,8} (79+R)	 Oxidised form of molecule LXV (quaternary pyridinium compound)	Mol CXXVIII (225+2R)	 Di-Schiff base on an aldol condensation trimer
Mol LXVII ^{3,9} (116+R)	 N-alkyl-2,6-dihydropiperidine (cyclic aminal)	Mol CXXIX (260+2R)	 A Michael-type and a Schiff base addition on a cyclised trialdol condensation product (note that the aldimine bond is in resonance with the ethylenic linkage)
Mol LXVIII ^{3,10} (199+R)	 Schiff base reaction on a hemiacetal-like glutaraldehyde dimer	Mol CXXX (258+3R)	 A Michael-type and two Schiff base additions on a cyclised trialdol condensation product
Mol LXIX ^{3,9} (299+R)	 Schiff base addition on a hemiacetal-like glutaraldehyde trimer	Mol CXXXIV ¹⁰ (198+R)	 Michael-type addition on a cyclised dialdol condensation product
Mol LXX (214+2R)	 Di-Schiff base addition on a hemiacetal glutaraldehyde dimer	Mol CXXXV ¹⁰ (198+R)	 Hemiacetal form of molecule CXXXIV

Mol LXXII (116+R)		Mol CXXXVI ¹⁰ (196+2R)	
Mol LXXIII (114+2R)		Mol CXXXVII (180+R)	
Mol LXXIV (216+R)		Mol CXXXVIII (178+2R)	
Mol LXXV (316+R)		Mol CXXXIX (180+R)	
Mol LXXVI (299+R)		Mol CXL (198+R)	
Mol LXXX (298+R)		Mol CXLI (280+R)	
Mol LXXXIII (498+R)		Mol CXLII (278+2R)	
Mol XCII (180+R)		Mol CXLV ⁷ (277+2R)	
Mol XCIII (178+2R)		Mol CXLVI (278+2R)	
Mol XCIV (176+3R)		Mol CXLVII (260+2R)	
Mol XCV (196+2R)		Mol CXLVIII (280+R)	

Mol XCVI (178+2R)	 Partially cyclised molecule XCV	Mol CXLIX (262+R)	 Corresponding 1,3,4,5-tetra-substituted dihydropyridine structure of molecule CXLIXa
Mol XCVII (160+2R)	 Fully cyclised molecule XCV (dihydropyridine structure)	Mol CXLIXa (261+R)	 1,3,4,5-tetra-substituted pyridinium structure
Mol XCVIII ^{3,6,8} (159+2R)	 Oxidised molecule XCVII (pyridinium structure, called anabitylsine)	Mol CL (262+R)	 Aldol dimer that underwent a Michael addition and a Schiff base reaction, followed by a cyclisation step
Mol C (176+3R)	 Tri-Schiff base addition on a dialdol condensation product, followed by a cyclisation step (dihydropyridine structure)	Mol CLI (278+2R)	 A dialdol condensation product that underwent a Michael addition and two Schiff base reactions
Mol CI (175+3R)	 Oxidised molecule C (pyridinium structure)	Mol CLII (242+2R)	 A dialdol condensation product that underwent a Michael addition and two Schiff base reactions, followed by a cyclisation step
Mol CII (198+R)	 Dialdol condensation product that underwent a Michael-type addition	Mol CLV (345+R)	 molecule CXLIX (1,3,4,5-tetra-substituted dihydropyridine) that underwent an aldol condensation
Mol CIII (180+R)	 Michael-type addition on a dialdol condensation product with a subsequent cyclisation step	Mol CLVII (442+2R)	 Molecule CLV that underwent a Michael addition, followed by a Schiff base reaction
Mol CIV (180+R)	 Isomer of molecule CIII, but with a different cyclisation	Mol CLIX (344+R)	 molecule CXLIX (1,3,4,5-tetra-substituted dihydropyridine) that underwent an aldol condensation
Mol CV (180+R)	 Isomer of molecule CIII, but with a different cyclisation	Mol CLXIII ^{11,12} (198+R)	 Michael-type addition on a dialdol glutaraldehyde product

Mol CVI ^{3,13} (262+R)	 Schiff base addition on a trialdol condensation product	Mol CLXIV (280+R)	 A trialdol condensation product that underwent a Mannich-type reaction, forming a stable secondary amine
Mol CVII ^{3,11} (262+R)	 Isomer of molecule CVI	Mol CLXV (278+2R)	 Molecule CLXIV that underwent a Schiff base reaction
Mol CVIIa ^{14,15} (262+R)	 Schiff base addition on a trialdol condensation product (resonance effect between the aldimine and ethyletic link)	Mol CLXVI (262+R)	 Cyclic molecule CLXIV
Mol CVIII (260+2R)	 Di-Schiff base addition on a trialdol condensation product (resonance effect between the aldimine and ethyletic link)	Mol CLXVII (242+2R)	 Molecule CLXIV that underwent a Schiff base addition, followed by two cyclization steps
Mol CIX (258+3R)	 Tri-Schiff base addition on a trialdol condensation product (note that only two aldimine linkages are in resonance with ethyletic link)	Mol CLXVIII (260+2R)	 Molecule CLXIV that underwent a Schiff base addition, followed by a cyclization step
Mol CXI (262+R)	 Schiff base addition on a trialdol condensation product, followed by a cyclization step	Mol CLXIX (362+R)	 A trialdol condensation product that underwent a Mannich-type addition (isomer of molecule CLXX)
Mol CXII (260+2R)	 Di-Schiff base addition on a trialdol condensation product, with two subsequent cyclization steps	Mol CLXX (362+R)	 A trialdol condensation product that underwent a Mannich-type addition (isomer of molecule CLXIX)
Mol CXIV (344+R)	 Schiff base addition on an aldol condensation tetramer (note that the aldimine is in resonance with the ethyletic linkage)	Mol CLXXIII ¹⁶ (99+R)	 A cyclic structure with a positive charge on the nitrogen atom and a hydroxyl group
Mol CXV (162+R)	 Clutaraldehyde dimer formed by aldol condensation, that underwent a Schiff base addition	Mol CLXXIV ¹⁶ (263+R)	 A cyclic structure with a positive charge on the nitrogen atom
Mol CXVI (160+2R)	 Clutaraldehyde dimer formed by aldol condensation, that underwent two Schiff base additions	Mol CLXXV ¹⁶ (261+R)	 A cyclic structure with a positive charge on the nitrogen atom

Mol CXVII (178+2R)	 <p>Molecule CXV that underwent a Michael-type addition</p>	Mol CLXXVIII (344+2R)	
Mol CXVIII (176+3R)	 <p>Molecule CXVII that underwent a Schiff base addition</p>	Mol CLXXIX (342+2R)	

1. Tramezzani JH, Chiocchio S, Wassermann GF. A technique for light and electron microscopic identification of adrenalin and noradrenaline storing cells. *Journal of Histochemistry and Cytochemistry*. 1964;12:890-899.
2. Chatterji PR. Gelatin with hydrophylic/hydrophobic grafts and glutaraldehyde crosslinks. *Journal of Applied Polymer Science*. 1989;37:2203-2212.
3. Matsuda S, Iwata H, Se N, Ikada Y. Bioadhesion of gelatin films crosslinked with glutaraldehyde. *Journal of Biomedical Materials Research*. 1999;45:20-27.
4. Shan ZH. Glutaraldehyde and modified glutaraldehyde used in leather making. *Leather Science and Engineering*. 1999;9:30-33.
5. Richards FM, Knowles JR. Glutaraldehyde as a protein crosslinking reagent. *Journal of Molecular Biology*. 1968;37:231-233.
6. Yang CQ, Wei W, McIlwaine DB. Evaluating glutaraldehyde as a non formaldehyde durable press finishing agent for cotton fabrics. *Textile Research Journal*. 2000;70:230-236.
7. Hardy PM, Hughes GJ, Rydon HN. The nature of the crosslinking of proteins by glutaraldehyde II. The formation of quaternary pyridinium compounds by the action of glutaraldehyde on proteins and the identification of a 3-(2-piperidyl)-pyridinium derivative, anabylisine, as a crosslinking entity. *Journal of the Chemical Society Perkin Transaction I*. 1979;9:2282-2288.
8. Hardy PM, Hughes GJ, Rydon HN. Identification of a 3-(2-piperidyl) pyridinium derivative (anabylisine) as a crosslinking entity in a glutaraldehyde-treated protein. *Journal of Chemical Society Chemical Communications*. 1977;21:759-760.
9. Lubig R, Kusch P, Roper K, Zahn H. On the mechanism of protein crosslinking with glutaraldehyde. *Monatshefte fur Chemie*. 1981;112:1313-1323.
10. Walt DR, Agayn VI. The chemistry of enzyme and protein immobilisation with glutaraldehyde. *Trends in Analytical Chemistry*. 1994;13:425-430.
11. Woodroof EA. Use of glutaraldehyde and formaldehyde to process tissue heart valves. *Journal of Bioengineering*. 1978;2:1-9.
12. Olde Damink LHH, Dijkstra PJ, Van Luyn MJA, Van Wachem PB, Nieuwenhuis P, Feijen J. Glutaraldehyde as a crosslinking agent for collagen-based biomaterials. *Journal of Materials Science. Materials in Medicine*. 1995;6:460-472.
13. Hardy PM, Nicholls AC, Rydon HN. The nature of glutaraldehyde in aqueous solution. *Journal of Chemical Society Chemical Communications*. 1969;10:565-566.
14. Monsan P, Puzo G, Mazarguil H. Etude du mecanisme d' etablissement des liaisons glutaraldehyde-proteines. *Biochimie*. 1975;57:1281-1292.
15. Marquie C, Tessier AM, Aymard C, Guilbert S. HPLC determination of the reactive lysine content of cottonseed protein films to monitor the extent of crosslinking by formaldehyde, glutaraldehyde, and glyoxal. *Journal of Agricultural and Food Chemistry*. 1997;45:922-926.
16. Johnson TJA. Glutaraldehyde fixation chemistry: oxygen-consuming reactions. *European Journal of Cell Biology*. 1987;45:160-169.